



HAL
open science

β -Hairpin peptidomimetics as inhibitors of hIAPP amyloid protein aggregation: design, synthesis and evaluation

Jacopo Lesma

► **To cite this version:**

Jacopo Lesma. β -Hairpin peptidomimetics as inhibitors of hIAPP amyloid protein aggregation: design, synthesis and evaluation. Medicinal Chemistry. Université Paris-Saclay, 2020. English. NNT : 2020UPASQ018 . tel-03793799

HAL Id: tel-03793799

<https://theses.hal.science/tel-03793799v1>

Submitted on 2 Oct 2022

HAL is a multi-disciplinary open access archive for the deposit and dissemination of scientific research documents, whether they are published or not. The documents may come from teaching and research institutions in France or abroad, or from public or private research centers.

L'archive ouverte pluridisciplinaire **HAL**, est destinée au dépôt et à la diffusion de documents scientifiques de niveau recherche, publiés ou non, émanant des établissements d'enseignement et de recherche français ou étrangers, des laboratoires publics ou privés.

β -Hairpin peptidomimetics as
inhibitors of hIAPP amyloid protein
aggregation: design, synthesis and
evaluation

Thèse de doctorat de l'université Paris-Saclay

École doctorale n° 569, Innovation thérapeutique : du fondamental
à l'appliqué (ITFA)

Spécialité de doctorat: Chimie Thérapeutique

Unité de recherche : Université Paris-Saclay, CNRS, BioCIS, 92290, Châtenay-Malabry,
France

Référent : Faculté de pharmacie

**Thèse présentée et soutenue à Châtenay-Malabry,
le 27 Novembre 2020, par**

Jacopo LESMA

Composition du Jury

Abdallah HAMZE Professeur, Université Paris-Saclay	Président
Sophie FAURE Chargée de Recherche CNRS, Université Clermont-Auvergne, HDR	Rapporteur
Thierry LEQUEUX Professeur, Université Caen, ENSICAEN, CNRS	Rapporteur
Philippe KAROYAN Professeur, Sorbonne Université	Examineur
Maria Luisa GELMI Professeure, Università degli Studi di Milano	Examinatrice
Sandrine ONGERI Professeure, Université Paris-Saclay	Directrice de thèse
Julia KAFFY Maîtresse de conférences, Université Paris-Saclay	Co-encadrante

Acknowledgement

As one of my PhD colleague was used to say “J'ai la tête dure” so, first of all I would like to thank my thesis supervisor Sandrine Ongeri and my co-supervisor Julia Kaffy, who patiently guided me during these three years of thesis. The whole time you dedicated to me and my project made me a better scientist. Thank you for always being there and for being a human support during the daily life. I will always bring with me all your teaching.

I would also like to thank all the members of the jury who accepted to read and judge my research work.

Work that I could not have done without collaborations with other laboratories in which I was welcomed.

For the Biophysical evaluations I would like to thank the team of Professor Miriam Taverna from the Institut Galien and the team of Professor Guillaume Van Der Rest at LCP.

The NMR conformational studies would not have been possible without the support of the team Chimie et Biologie Structurales et Analytiques CNRS, ICSN Gif sur Yvette. Thanks to Carine Van Heijenoort and Jean-François Gallard for their invaluable support and the patience for the endless request for tons of information about the theory behind the each different type of NMR analysis.

Thank you to Camille Dejean, Remi Franco and Jean Christophe Jullian for the various NMR analysis of the all synthesized compounds.

Thank to Karine Leblanc and Somia Rharrabti who made possible the purification by HPLC and the purity analysis of my compounds.

Thank you to Nicolò Tonali, our last acquisition as Maître de conférences but always available and kind since our first meeting. Probably without your advice for the bureaucracy, I would still be looking for the forms to obtain the “Carte Vitale”.

Thank to Jean-Louis Soulier for help in solving the synthesis problems but above all thanks for the long chats about our common passion: the Judo, unfortunately now it is time to say “Rei”.

I would like to thank all the members of the Fluoepit team for the great moments spent all together inside and outside the laboratory. I will always carry with me the laughter of Friday night aperitif. For all these moments, thank you: Benoît Crousse, Tap Ha-Duong and Thierry Milcent.

Along the years of the thesis I had the opportunity to meet several master students:

Thank you Valentina, Matthieu, Astaa for your contribute to this work, especially for having resynthesized all the precursors needed to continue the research.

Thank you Sharmila, Valentina, Chiara, Solene, Diego for the great moments passed all together, your company made less hard some of the worst days of the thesis.

How to not mention all the PhD students that I had the pleasure to meet: thank you Renjin, Sondes, Monika, José, Maxence, Ping, Ting-Ting, Chenghui, Davide and Nicolò. Thank you to all of you.

Special mention to Faustine and Maud, the first who welcomed me. I will always be grateful to have met you. Thank you for the friendship that has been created and for every single beautiful memory spent together. I could not have asked to find someone better than you.

I would like to thank my family who, even if from afar, have always supported and encouraged me during all my studies. If I have become what I am, it is also thanks to you who have believed in me, pushing me to go a step further every day.

Last but not least thanks is for Jessica, who has been at my side for the past seven years despite the difficulties of the distance. Thank you for being my silent listener in moments of mumbling, my support in times of discouragement and voice of reason. Thank you for having encouraged me to follow the PhD path despite the fact that this has led us to live 800 km away. I know how hard it has been for you, and I will never thank you enough for that. For all those reasons, I could not wish for a better woman by my side, thank you.

Curriculum vitae

Education

- Oct. 2017— **BioCIS, Université Paris Saclay, CNRS**
Sep. 2020 PhD student in Medicinal Chemistry
Supervisor: Prof. Ongerì Sandrine and Dr. Kaffy Julia
Research project: β -Hairpin peptidomimetics as inhibitors of hIAPP amyloid protein aggregation: design, synthesis and evaluation
- Sep. 2011— **Università degli studi di Milano**
Sep. 2017 Master degree in Medicinal Chemistry and Pharmaceutical Technology (Faculty of Pharmacy). 108/110
Final internship of 1 year at DISFARM-Sez. Chimica Generale e Organica “A. Marchesini”
Supervisor: Prof. Pellegrino Sara and Prof. Maria-Luisa Gelmi
Research topic: “Metal binding ultra-short peptides”
- Mar. 2015— **Internship: Farmacia San Giuseppe, Calolziocorte**
Sep. 2015 Supervisor: Susanna Rusconi
- Sep. 2006— **ITIS G. Natta**
Jul. 2011 High school diploma in industrial chemistry

Publications

- “Introducing sequential aza-amino acids units induces repeated β -turns and helical conformations in peptides” Nicolo Tonalì, Isabelle Correia, [Jacopo Lesma](#), Guillaume Bernadat, Sandrine Ongerì and Olivier Lequin. *Org. Biomol. Chem.*, **2020**, 18, 3452. DOI:10.1039/C9OB02654A. [Organic & Biomolecular Chemistry HOT article collection](#) and front cover.
- “ β -Hairpin peptide mimics decrease human Islet Amyloid Polypeptide (hIAPP) Aggregation” Jacopo Lesma, Faustine Bizet, Corentin Berardet, Nicolo Tonalì, Sara Pellegrino, Myriam Taverna, Lucie Khemtemourian, Jean-Louis Soulier, Carine van Heijenoort, Frédéric Halgand, Tap Ha-Duong, Julia Kaffy, and Sandrine Ongerì. *Front. Cell Dev. Biol.*

Conferences

- Oral communications
- 17^{èmes} Rencontres de Chimie Organique (RCO), Gif-sur-Yvette, Paris, 19 April 2019. “Synthesis of novel fluorinated peptidomimetics as potential protein aggregation inhibitors in amyloidoses”
 - BIOCIS Day, Chatenay Malabry, France, 20 June 2019. “Novel acyclic peptidomimetics as inhibitors for hIAPP aggregation: interest in type II diabetes”
 - Journée de la recherche (JDR), Chatenay Malabry, France, 22 January 2020. “Novel acyclic peptidomimetics as inhibitors for hIAPP aggregation: interest in type II diabetes”
- Posters
- Journées des Jeunes Chercheurs SCT, Paris, France, 20-22 February 2019.

- 21^{ème} congrès du Groupe Français des Peptides et Protéines (GFPP), Amboise, France, 12-16 May 2019.
- Journée de l'école doctorale (JED), Chatenay Malabry, France, 21 June 2019.
- ULLA Summer School, Helsinki, Finland, 30 June-5 July 2019.
- Awarded with the grant for the 36th European Peptide Symposium (EPS), Sitges (Barcelona), Spain, postponed to 2021

Table of content

Chapter 1	1
Introduction	1
1.1 Amyloidosis and amyloid	1
1.1.1 What is amyloidosis?	1
1.1.2 Amyloid's history.....	4
1.2 Diabetes	6
1.2.1 Generality.....	6
1.2.2 Type II diabetes: mechanisms and influencing factors	9
1.2.3 Type II Diabetes treatment	10
a) Biguanides:.....	11
b1) Direct secretagogues:	12
Sulfonylureas:.....	12
Glinides:	13
b2) Indirect secretagogues or incretin mimetics	13
GLP-1 agonists:.....	13
DPP4 inhibitors.....	14
α -glucosidase inhibitors	14
Gliflozins:.....	15
1.2.4 New frontiers in T2D treatment.....	16
1.3 human Islet Amyloid Polypeptide (hIAPP) and T2D	17
1.3.1 hIAPP or amylin	17
1.3.2 Physiological role of hIAPP	18
1.3.3 Pathological role of hIAPP.....	20
1.3.4 hIAPP role in another pathology: Alzheimer's Disease (AD).....	21
1.3.5 hIAPP amyloidogenicity from a structural point of view	22
Primary sequence:	22
hIAPP conformations analysis by experimental techniques	23
The power of the computational techniques in hIAPP conformations analysis:.....	26
A model to correlate hIAPP conformational change and membrane damage:.....	27
Deeper in the hIAPP fibrils structure:	28
1.3.6 Targeting hIAPP aggregation as possible T2D therapy	32

Polyphenols:.....	32
Peptidic compounds:	33
hiAPP analogues:.....	33
Short peptides derived from hiAPP amyloidogenic sequence:	34
Insulin:.....	35
HI18 β -wrapping inhibitor:.....	36
Peptidomimetics:	36
hiAPP N-methylations:	36
Short peptidomimetics derived from hiAPP amyloidogenic sequence:	37
Cyclic β -hairpins:	38
Acyclic β -hairpins:	39
α -helix:	40
Chapter 2	42
On the way for new hiAPP aggregation inhibitors	42
2.1 Research group expertise	42
2.1.1 Inhibitors of protein-protein interactions.....	42
Glycopeptidomimetics:	42
Pre-structured β -hairpins:.....	44
α -helix foldamers:	47
2.1.2 Biophysical evaluations.....	47
Thioflavin-T fluorescence spectroscopy:	48
Transmission electron microscopy (TEM).....	49
Membrane permeability assay	50
Ion mobility spectroscopy-mass spectroscopy (IMS-MS):	51
Capillary electrophoresis (CE):	53
Cell viability assay:	55
2.1.3 Conformational studies.....	56
Circular dichroism (CD):	57
Nuclear magnetic resonance (NMR):.....	58
Through-bond magnetization transfer: J coupling	59
Chemical shift analysis	59
Through-space magnetization transfer: NOE	60

Molecular dynamics (MD):.....	61
2.2 Objective of the thesis	61
2.2.1 General structure of the hairpins.....	62
2.2.2 Overview of the investigated structures.....	63
Chapter 3	65
Non-fluorinated β -hairpin mimics structure: β -hairpin mimics as protein-protein interaction inhibitors in T2D.....	65
3.1 Peptidic and aza-peptidomimetic β -hairpins.....	65
3.1.1 Choice of the sequences	65
3.1.2 β -Turn inducer synthesis.....	69
3.1.3 Draft paper	70
Chapter 4	71
Fluorinated β -hairpin mimics in T2D: new protein-protein interaction inhibitors and potential tools for early diagnosis	71
4.1 Fluorine in medicinal chemistry.....	71
4.1.1 Fluorine as bioisoster	71
4.1.2 Influence on the ADME	72
4.1.3 Fluorine in weak interactions.....	73
4.1.4 Fluorinated compounds as diagnostic tools	73
MRI:.....	73
PET:	74
4.2 Fluorinated peptidomimetics.....	76
4.2.1 β -hairpin mimics containing the 3-fluoro-5-benzamido-2-hydroxybenzohydrazide peptidomimetic.....	76
Design of the compounds bearing a blocking sequence based on the 3-fluoro-5-benzamido-2-hydroxybenzhydrazide	76
Synthesis of the compounds bearing the fluorinated benzhydrazide arm.....	82
Synthesis of the lysine-F-benzhydrazide- 4.7	82
Synthesis of the valine-F-benzhydrazide-N-benzoyl 4.8	87
Synthesis of the valine-F-benzhydrazide-N-acetyl 4.9	88
Synthesis of intermediate 4.10 : introduction of the SRE Alanine-Valine on the tosyl scaffold..	89
Synthesis of intermediate 4.11 : introduction of the SRE Alanine-Isoleucine-Leucine on the β -turn inducer	90

Synthesis of the complete hairpin mimics 4.3 bearing the lysine F-benzhydrazide and 4.6 bearing the valine F-benzhydrazide-N-benzoyl	93
Conformational studies.....	95
Biophysical evaluations.....	95
Conclusion.....	98
4.2.2 β -hairpin mimics containing the <i>N</i> -difluoromethyltriazolyl peptidomimetic arm	99
Design of the compounds bearing the <i>N</i> -difluoromethyltriazolyl peptidomimetic arm	99
Synthesis of the hairpins bearing the <i>N</i> -difluoromethyl-1,4-triazolyl peptidomimetic arms.....	101
Synthesis of the <i>N</i> -difluoromethyl-1,4-triazolyl blocking sequences 4.38 and 4.39	102
Synthesis of compounds 4.36 and 4.37 bearing the <i>N</i> -difluoromethyl-1,4-triazolyl blocking sequence	105
Conformational studies.....	106
Hairpin 4.36 bearing the Phe- <i>N</i> -difluoromethyl-1,4-triazolyl-Val-CONH ₂ blocking sequence .	107
Hairpin 4.37 bearing the Phe- <i>N</i> -difluoromethyl-1,4-triazolyl amide blocking sequence	111
Biophysical evaluations.....	116
Conclusion.....	118
4.2.3 β -hairpin mimics fluorinated on the β -turn inducer.....	119
Design of the compounds based on the fluorinated β -turn inducer	119
Synthesis of the hairpins having fluorinated β -turn inducer	120
Synthesis of the <i>N</i> -Fmoc-4-(trifluoromethyl)benzenesulfonyl-COOH β -turn 4.52	121
Synthesis of the <i>N</i> -Fmoc-(trifluoromethyl)prolyl-COOH β -turn 4.53	126
Synthesis of the hairpin 4.50 containing the 4-trifluoromethylebenzenesulfonyl scaffold	128
Conformational studies.....	129
Biophysical evaluations.....	133
Conclusion.....	134
General conclusion and perspectives	136
Annex 1: hairpins chapter 3	136
Annex 2: hairpins chapter 4	137
Experimental part	137
General experimental methods.....	137
NMR, HPLC, Mass.....	137
Fluorescence-Detected ThT Binding Assay (hIAPP)	137
Fluorescence-Detected ThT Binding Assay (A β ₁₋₄₂)	138

Transmission Electron Microscopy	139
Preparation of large unilamellar vesicles.....	139
Membrane permeability assay	140
Capillary electrophoresis protocol (hIAPP)	140
ESI-MS experiments	141
Cell viability assay	141
Compounds chapter 3.....	142
Compounds chapter 4.....	166
List of abbreviations.....	213
Bibliography	218

Chapter 1

Introduction

1.1 Amyloidosis and amyloid

1.1.1 What is amyloidosis?

Over the last decades, amyloidosis research field has gained more and more interest because of its relation with pathologies like Alzheimer's Disease (AD), Parkinson Diseases (PD), Type 2 Diabetes (T2D), Huntington's Disease, Prion Disease and many others, most of which are related with ageing or life-style. Nowadays, this group of more than 20 severe degenerative disorders are named amyloidosis. The common hallmark is the aggregation of misfolded proteins into amyloid fibrils which are the main constituent of the amyloid deposits. It has been proved that the self-assembly of protein is a relative common process among living systems but, on the other hand, only 40 proteins have been correlated with the amyloidosis.¹ Referring to this characteristic it is possible to define as amyloidosis any pathology caused by (or associated with) amyloid aggregates.² Pathologists defined amyloid deposit as any accumulation which stains when treated with Congo Red dye and, when exposed to cross-polarized light, shows green birefringence. The actual structure-related definition, describes the amyloid fibers as structures which display the cross- β fibers diffraction pattern, reported for the first time by Astbury *et al.* in 1935. Amyloid fibrils shared common features; the main ones being listed above:

- 1) Fibrils are formed by the association of only one type of proteins with a width of at least 10 nm and a length between 0.1 and 10 μ m;
- 2) The repeated β -sheets are parallel along the fibril axis, with the β -strands being perpendicular to the fiber axis;
- 3) β -sheets can be formed of parallel or anti parallel β -strands;
- 4) Along the fiber axis the β -sheets are "in register". It means that one β -strand lies exactly above the subsequent in parallel sheets or above the β -strand that is two strands beneath in antiparallel sheets. To be noted that, among the β -strands the distance due to the backbone amide hydrogen bond, is always 4.7 Å (Figure1).

5) Amino acidic side chains protrude perpendicularly to the fibril axis forming an interdigitation between mating sheet that resembles to a zipper, for that reason it is called steric zipper.^{1,3-5} Figure 2 presents 8 classes of steric zippers formed with different amyloid proteins.

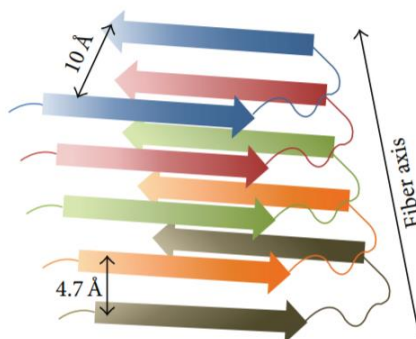


Figure 1 Disposition of the β -sheets along the fibril axis⁶

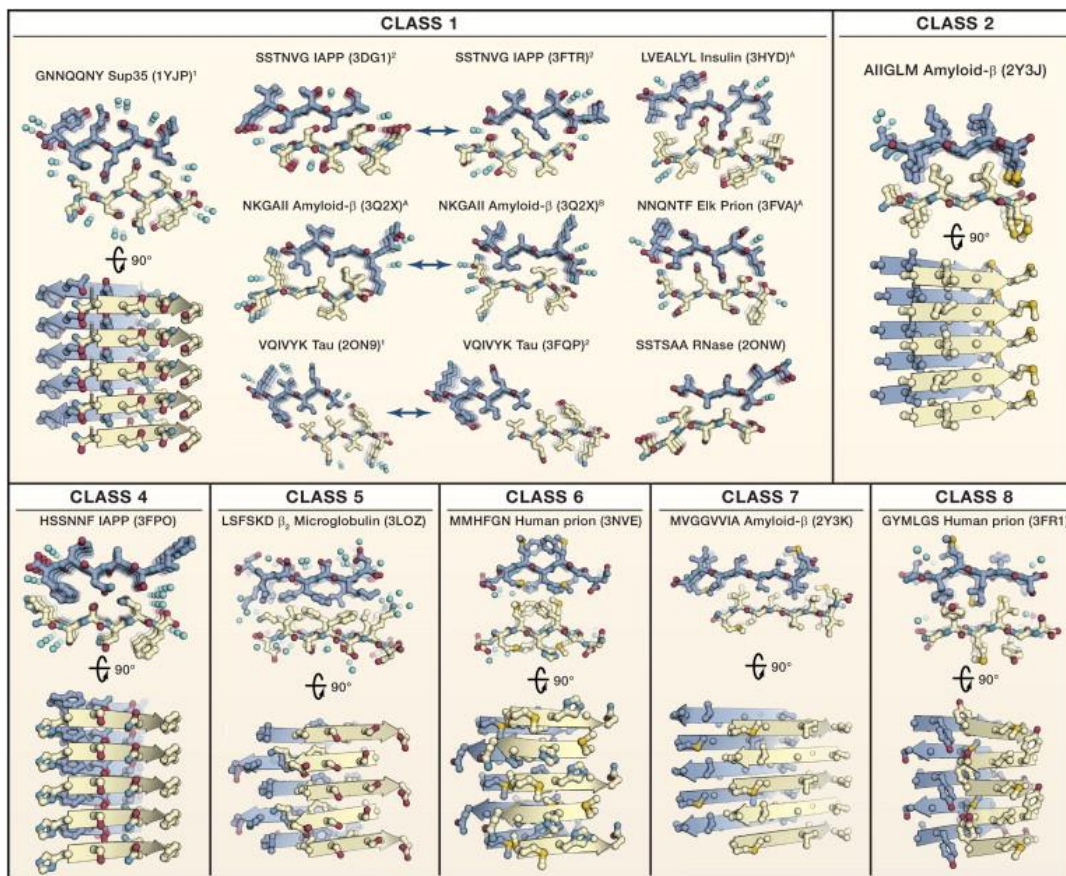


Figure 2 Representation of the 8 classes of the steric-zippers formed by some different amyloid proteins⁴

The amyloid state formation is a slow process during which a correctly folded protein gradually converts into a highly ordered aggregate state through the loss of the original folding. Although, the correctly folded proteins are in the energetically favored states,^{7,8} the aggregation takes place leading, from a thermodynamic point of view, to a product with a lower free energy surface. This implies that the correct folded proteins do not represent the global minima on the free surface energy but a metastable state, which is separated from the amyloid state only by high kinetics factor. As the system naturally tends to the lowest energetic content, the maintenance of the native state is possible only thanks to the evolution of the biological systems (Figure 3). However, under certain conditions, mostly in later life, the biological system lost the ability to avoid the aggregation process leading to the amyloidosis.^{9,10}

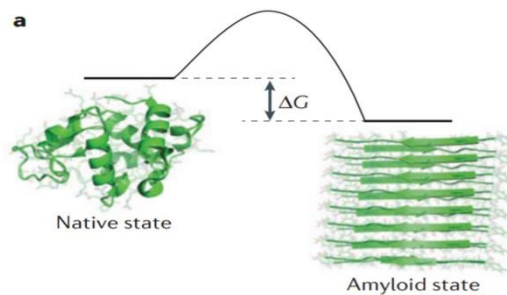


Figure 3 Graphical representation of $\Delta G_{\text{surface}}$ between native state and amyloid state of a generic protein¹¹

Since the *in vivo* aggregation process occurs over decades and the actual techniques do not allow the study of the aggregation kinetics *in vivo*, *in vitro* models have been developed. Because the *in vitro* experiment occurs on the timescale of minutes or at least hours, it has been possible to study the amyloid proteins self-assembly process.

Plotting the time versus the aggregation percentage, it is possible to draw the kinetics curve, which is represented by a sigmoidal. The advancement in the study of the curves have allowed to highlight 3 different phases (Figure 4):

- 1) Nucleation/lag phase: this process begins with monomeric proteins, in dynamic equilibrium between folded, partially folded and unfolded state which assemble to form the first oligomeric species. Such oligomers, through the oligomerization process, self-assemble into bigger and high ordered protofibrils.

- 2) Elongation phase: during this exponential phase, the protofibrils grow by addition of monomers forming the fibrils (primary nucleation). The formed fibrils can grow, fragment or promote the nucleation phase (secondary nucleation). This phase continues until all the monomers are consumed.
- 3) Saturation/stationary phase: when all the monomers are consumed, the exponential phase turn into the final saturation phase in which fibrils associate to form the amyloid plaques.^{12,13}

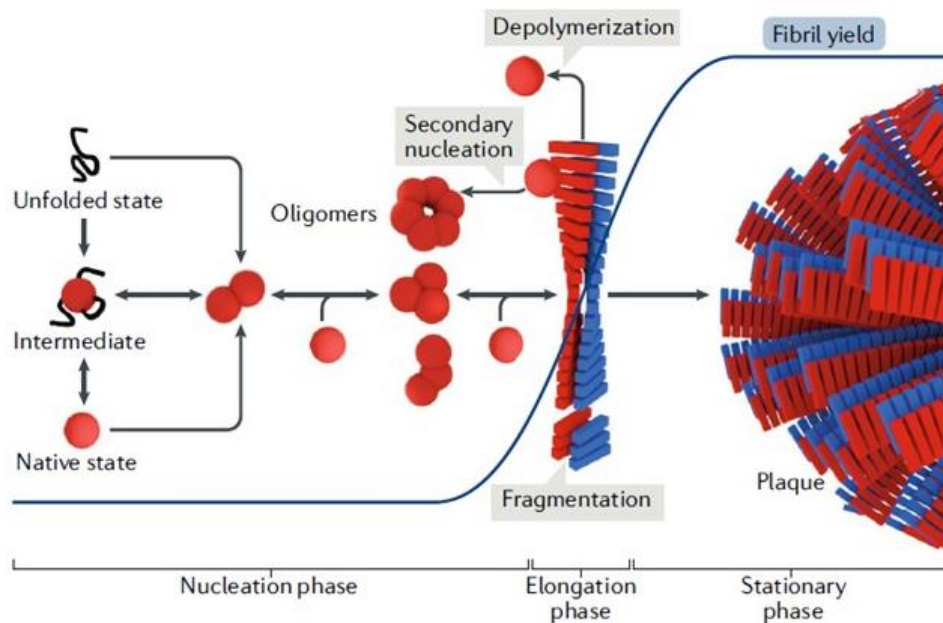


Figure 4 General kinetic of amyloid protein aggregation¹³

1.1.2 Amyloid's history

The word Amyloid is etymologically related to the Greek word *amylon* and to the Latin word *amylion*. Literally, this word means like starch.¹⁴ To understand why nowadays this word is used to describe proteinaceous deposits, often related with pathological conditions, it is necessary to go back in the time for a short story of amyloid and amyloidosis.

Since the beginning of the XVII century, localized deposits of undefined material, described as lardaceous, waxy, spongy, white stone are reported under different names (Figure 5). The absence of an univocal name for this group of deposits makes hard to define its first observation. From an

historical point of view, Rudolf Virchow can be identified as the first who employed the word amyloid to describe such aggregates. In 1854, Virchow was studying the corpora amylacea in the nervous system when he observed their feature to stain in pale blue after iodine treatment. Because the reaction was known to be characteristic of the cellulose, he concluded that the corpora was formed of carbohydrate and he named them amyloid because in that period there was not a clear distinction between starch and cellulose.^{15,16}

Just five years later, amyloid's elemental analysis performed by Friedrich and Kekulé demonstrated that Virchow was wrong; indeed, the analysis showed a high content of nitrogen incompatible with the chemical composition of carbohydrate. This new data led them to conclude that the corpora amylacea was composed predominantly of proteins, associated with proteoglycans.¹⁷ Thanks to the introduction of such nomenclature and to the clarification of the chemical composition, several amyloid were reported during the following years.

The introduction of Congo Red (CR) as histopathological dye for amyloid deposit, in 1922, with its ability to enhance the green birefringence of amyloid deposit under cross polarized light, represents the first breakthrough in the identification and the understanding of amyloid deposit structure.

The introduction of X-ray diffraction techniques as tool for the amyloid structural investigations represents the stepping stone for the amyloid molecular structure understanding. Indeed, in 1935, Astbury and Dickinson, using the X-ray, took the first "photography" of the fibrils in the amyloid deposits. Moreover, they were able to conclude that fibrils are formed of polypeptide chains which are disposed in the so-called cross- β pattern.

Since this first structural investigation by X-ray diffraction, the introduction of new techniques such as Electron Microscopy (EM), cryo-Electron Microscopy (cryo-EM), cryo-Electron Tomography (cryo-ET) and solid state NMR spectroscopy (ssNMR) allowed a progressive resolution of the atomic structure of the amyloid deposit which are strictly related to the degenerative disorders generically called amyloidosis.^{13,18}

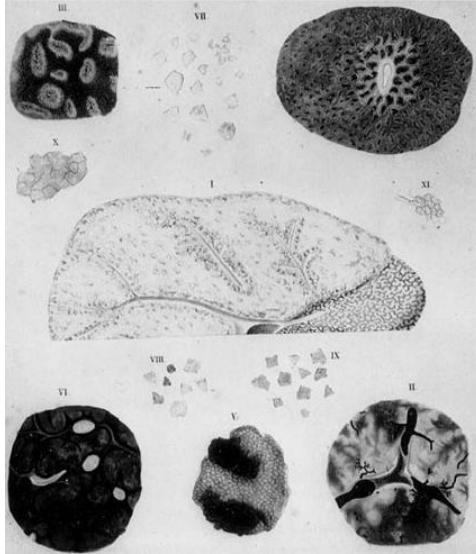


Figure 5 Image of amyloid deposits at low magnification attributed to Friedrich¹⁵

1.2 Diabetes

1.2.1 Generality

Diabetes is a chronic pathology associated with high glucose level in the blood stream. The impaired blood level is due to a lack in the insulin secretion or in its activity.

According to the last data reported by the International Diabetes Federation (IDF), in 2019, almost 463 million adults (20-79 years) were affected by diabetes. It has also been estimated that this value is expected to increase to 700 million in 2045 (Figure 6), leading diabetes to become one of the major causes of invalidity and death.

The high incidence of this pathology with its related diseases caused in 2019 almost USD 760 billion dollar in health expenditure.

Number of adults (20–79 years) with diabetes worldwide

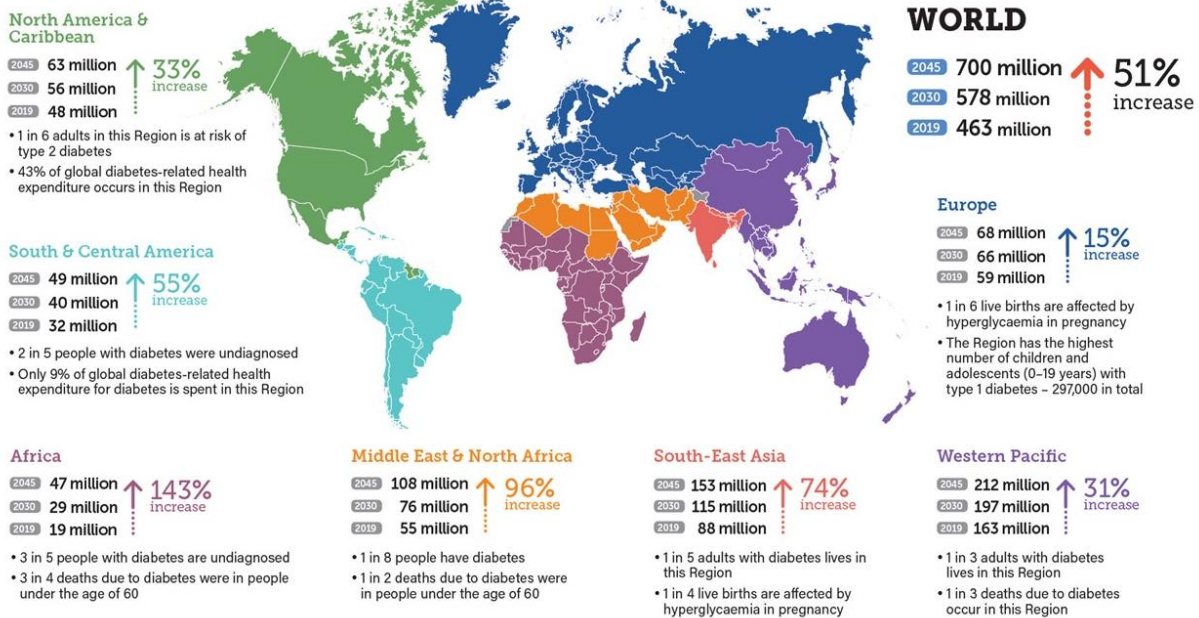


Figure 6 Actual and future estimation of diabetes global incidence¹⁹

Thanks to a simple analysis like the measure of glucose level in the blood stream it is possible to diagnose diabetes. As reported by the World Health Organization (WHO), the normal fasting glucose level is between 3.9 and 5.5 mmol/L (0.7 to 1 g/L). When this value is over 7 mmol/L (1.26 g/L) the person is diagnosed as diabetic. Moreover, to diagnose diabetes there is also a second criteria used when the measure is performed not in fasting state: 11 mmol/L (200 mg/dL).

Since the cells consume between 200 and 300 g/day of glucose as main energetic source (adenosine triphosphate production, ATP), its homeostasis regulation is crucial for the survival. This homeostasis is regulated by a complex equilibrium of hormone. While the blood's level of glucose rises during the meals, pancreatic β -cells (islets of Langerhans cells) start to secrete the insulin. This hormone, interacting with its receptors, promotes the glucose uptake through membrane transporter GLUT-4, expressed in the liver, muscles and the adipose tissue. When internalized, glucose is converted and deposited as glycogen. During fasting periods, when blood's glucose level decreases, the glucagon, through the glycogenolysis process, promotes the release of glucose from the deposits. In the case of inadequate level of glycogen, the gluconeogenesis occurs as backup process to ensure the optimal glucose level (Figure 7).^{19,20}

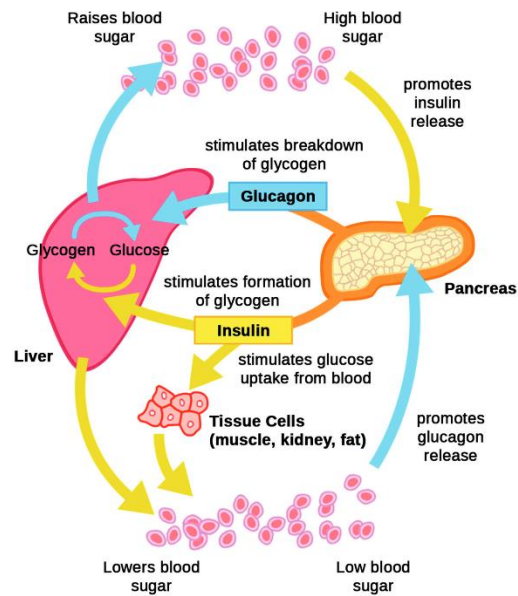


Figure 7 Glucose homeostasis regulation²¹

The word diabetes, when used generically, refers to a group of at least 3 different pathologies: type I diabetes (T1D), gestational diabetes and type II diabetes (T2D).

T1D, also called insulin-dependent diabetes, represents the majority of diabetes cases during the childhood. It is characterized by a lack of insulin due to a an autoimmune pancreatic β -cell destruction. Although pancreatic β -cells destruction begins from the birth, the pathology rudely appears mainly during the adolescence.

Gestational diabetes is the form that is affecting the women during the pregnancy. The incidence is between 1.5 and the 6.5% of the pregnancies. Moreover, it is important to monitor who is affected by gestational diabetes because it could evolve in T2D.

T2D, also called insulin-resistant diabetes, represents 90% of the diabetes cases and mainly affect people older than 40 years. In contrast with T1D, insulin is normally produced by pancreatic β -cells but the insulin receptors are unable to correctly interact with the hormone. This insulin-resistance leads to an inadequate glucose up take by the tissues. Moreover, in the late stage of the pathology, T2D is associated with a loss of pancreatic β -cells (Figure 8).

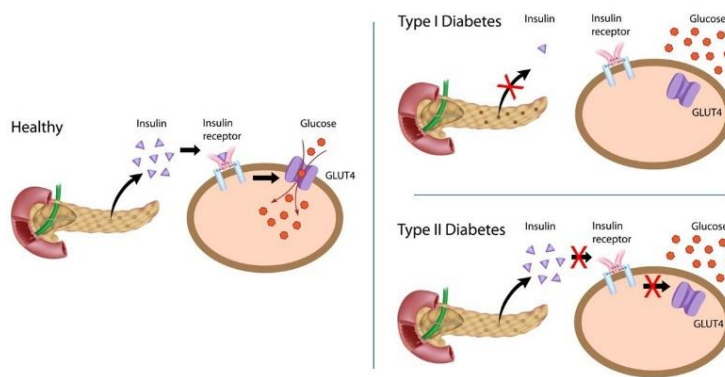


Figure 8 Mechanism of insulin action respectively in healthy, TD1 and TD2 subjects.

(From internet, author unknown)

1.2.2 Type II diabetes: mechanisms and influencing factors

Type II diabetes is a complex and multifactorial pathology characterized by hyperglycaemia. At least at the onset, the increased glucose level is due to a lack of interaction between insulin and its receptor. As a consequence, the transporter GLUT-4 is not moved into the cell membrane resulting in a reduced glucose uptake. The maintained hyperglycaemia triggers a feedback mechanism which leads to an increased demand and secretion of insulin by the pancreatic β -cells.²² On the other hand, in the long term, the hyperglycaemia is also caused by a lack in the production of insulin due to the pancreatic β -cells death.

Despite the main mechanisms involved in T2D are known, lots of the factors influencing the onset of the pathology have to be understood because of the complexity of the pathology.

Until now genetic, early life and environmental factors have been proposed.

From a genetic point of view, for example, it has been estimated that if one of the parents is affected a child has 40% of probability to develop T2D when adult and, in the case of both parents affected, the percentage rises until 70%.²³

It also seems that lots of pre-birth factors could influence the incidence of T2D in adult life. As well reviewed by Yan Liu *et al.* in 2013,²⁴ several factors like smoking, consuming alcohol or hormonal therapy during the pregnancy could increase the risk to develop T2D in the adult life. It

is also known that the same wrong behaviour during the lactation time could have the same effect on future life of the children.

Among the environmental factors it is important to cite the obesity, the sedentary life or the stress, all factors that could be present from the childhood.

Unfortunately, despite the progress in the study of this multifactorial pathology, the causes of T2D remain not completely understood and, as mentioned in the previous paragraph, the economic impact of diabetes still remains impressive, both for the direct treatment of T2D and indirectly for the treatment of the related pathologies.

The chronic hyperglycemia, in the long term, leads to a series of related pathologies linked to micro- and macrovascular complications.^{19,25}

- 1) Coronary Heart Disease (CHD): cardiovascular complications, affecting approximately 65% of the diabetes cases, represent the first cause of death for T2D patients. It has been calculated that for T2D patients the mortality related to CHD is nearly four times higher than in healthy population;
- 2) Dialysis: almost 50% of T2D patients are affected by nephropathy and 15% of them need dialysis or kidney transplant to survive;
- 3) Diabetic foot and lower limb complications: globally around 40 and 60 million patients are affected by these complications. Often, diabetic foot leads to amputation, being the first cause of amputation surgery.
- 4) Blindness: diabetic retinopathy is affecting more than 50% of diabetic patients and, with others diabetic eyes pathologies, represent the first cause of blindness for population over 65 years old.

1.2.3 Type II Diabetes treatment

As recommended by WHO, patients diagnosed with T2D should adopt optimal lifestyle to avoid or retard as long as possible the occurrence of the complications previously reported. The diabetic patients should reduce their body weight, practice sports activities and follow an healthy diet. Along with improvement of the life style, often it is necessary to associate a pharmacological treatment.

Nowadays several drugs are available on the market among which is possible to select the optimal treatment, depending on the clinical situation (Figure 9).²⁶ These drugs can be classified in four different categories according to their mechanism of action:

- a) Biguanides;
- b) Secretagogues:
 1. Direct: sulfonylureas and glinides
 2. Indirect or Incretin mimetics: GLP-1 agonist and DPP4 inhibitors
- c) α -glucosidase inhibitors;
- d) Gliflozins.

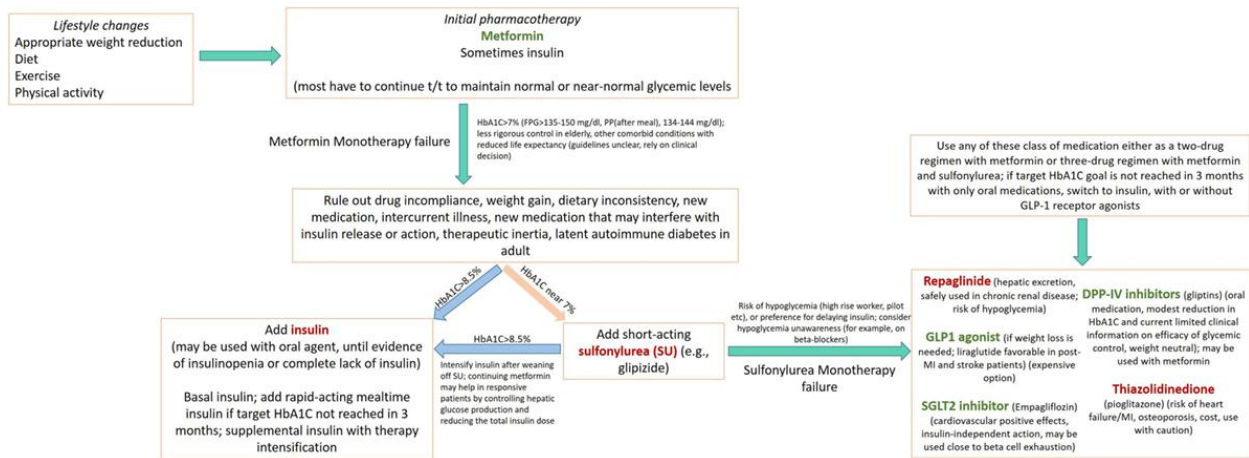
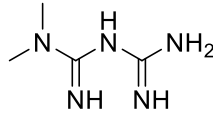


Figure 9 Flowchart of treatment in T2D considering the weight gain/loss (red and green)²⁶

a) Biguanides:

Among them, the most important is metformin (Figure 10), drug used as first-line treatment. At hepatic level, through the activation of an adenosine monophosphate-activated protein kinase, it improves the glucose uptake and inhibits the gluconeogenesis process. Moreover, it is able to increase the insulin sensitivity through the activation of insulin receptor expression. Nowadays metformin is a treatment employed on a large scale even though it can present side effects such as gastrointestinal disturbs.



Metformin

Figure 10 First-line drugs metformin

b1) Direct secretagogues:

This class includes all the drugs that are able to promote the insulin secretion by direct interaction with pancreatic β -cells.

Sulfonylureas:

The sulfonylureas, e.g. glibenclamide, glipizide and glimepiride (Figure 11) are able to block potassium channels exposed by the pancreatic β -cells and this block triggers the opening of calcium channels. The resulting influx of ions Ca^{2+} initiates a cascade signaling which lead to insulin secretion. Actually, these drugs are used as second line or add-on treatment because of their side effects (the most common is hypoglycemia). Indeed, sulfonylureas can promote a gain of weight and can induce kidney and hepatic failure. Moreover, because of the stability of their complexes with the receptors, they can cause hypoglycemia.

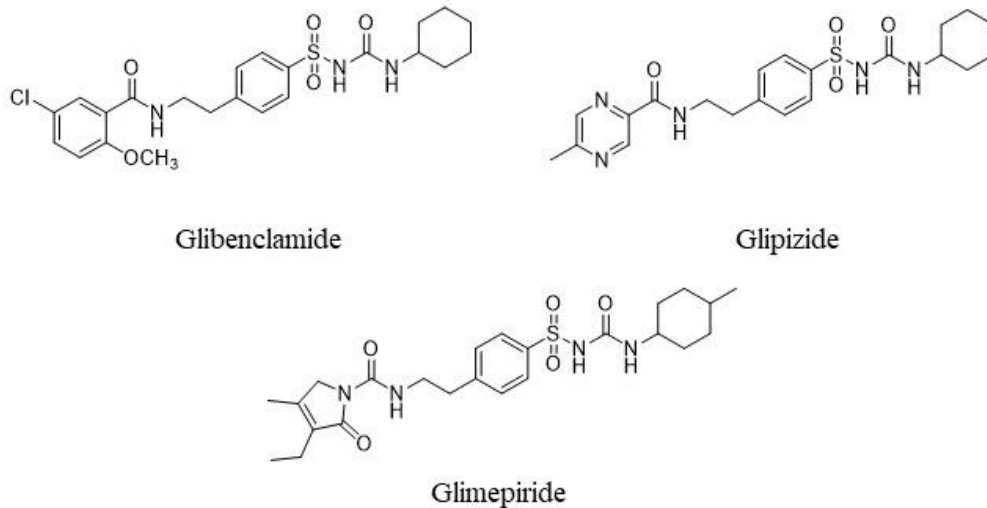


Figure 11 Examples of sulfonylureas

Glinides:

Repaglinide (Figure 12) is the only glinide on the market and it shares the same mechanism as sulfonylureas. However, its weaker binding, the necessity of higher level of glucose to trigger its activity and the rapid onset give a better pharmacological profile.

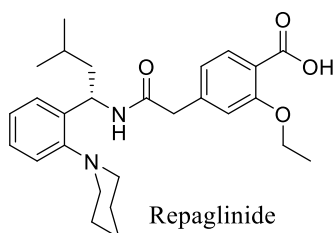


Figure 12 Representant of glinide family: Repaglinide

b2) Indirect secretagogues or incretin mimetics

This is a big family based on the two incretin hormones: GLP-1 (Glucagon Like Peptide 1) and GIP (glucose-dependent insulintropic polypeptide). These two hormones are involved in the glycaemia regulation; indeed, they stimulate insulin secretion and inhibit glucagon release when blood's glucose level rises. Usually these hormones have a short life because they are rapidly metabolized by the dipeptidyl peptidase 4 (DPP4). In patients affected by T2D the reduced concentration of these incretins results in a reduction of insulin secretion and as consequence in a hyperglycemia. Actually, two different classes of incretin mimetics are available on the market: GLP-1 receptor agonists and DPP4 inhibitors.

GLP-1 agonists:

To date, several GLP-1 agonists have been approved on the market, among them it is possible to find exenatide and liraglutide (Figure 13)^{27,28}. These two GLP-1 analogues differ from the parent compound by aminoacidic sequence. Exenatide was the first GLP-1 analogue approved for T2D treatment, it is a 39 amino acids peptide found in the salivary gland of Gila monster that shares only 53% of homology with GLP-1. Liraglutide, which shares 97% of homology with GLP-1(7-37), is a 31 amino acids synthetic derivative that is conjugated to a fatty acid through a covalent bond on the NH₂ of the Lysine34 lateral chain. In both cases the modifications enhance the metabolic stability against the DPP4 leading to an increased insulin secretion.

GLP-1	H2N-HAEGTFTSDV SSYLEGQAAK EFWLWKGR-CONH ₂
Exenatide	H2N-HGEGTFTSDL SKQMEEEAVR LFIEWLKNNGG PSSGAPPPS-CONH ₂
Liraglutide	H2N-HAEGTFTSDV SSYLEGQAAK EFWLVRGR G-CONH ₂



Figure 13 Sequence comparison of GLP-1 and its analogues exenatide and liraglutide.

In red differences in the sequences

DPP4 inhibitors

The purpose of DPP4 inhibitors is to reduce incretins metabolism. Nowadays there are several drugs of this class on the market and among them we can find: sitagliptin, saxagliptin, vildagliptin, linagliptin and alogliptin (Figure 14).²⁹ Although these drugs are widely employed, they display some side effects that must be reminded: nausea, vomiting and acute pancreatitis.

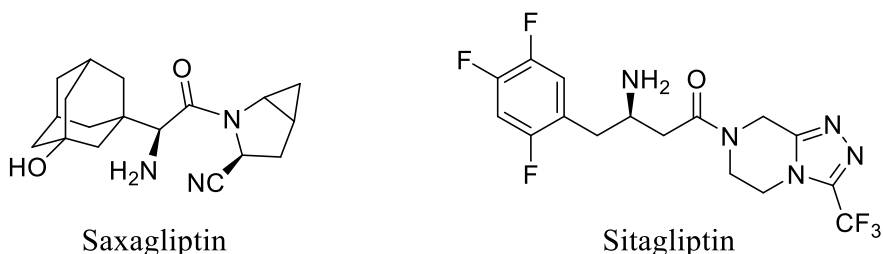


Figure 14 Two examples of incretin mimics

α -glucosidase inhibitors

The α -glucosidase is a small intestine enzyme responsible of the degradation of complex sugars in monosaccharides that can cross the intestinal barrier. An inhibition of such enzyme by acarbose or miglitol (Figure 15) reduces the glucose uptake and as consequence the post-prandial glycemic peak. Unfortunately, their glucose lowering effect in patients with mild to moderate hyperglycemia is lower than other oral antidiabetic drugs. Moreover, their assumption may cause digestive problems.

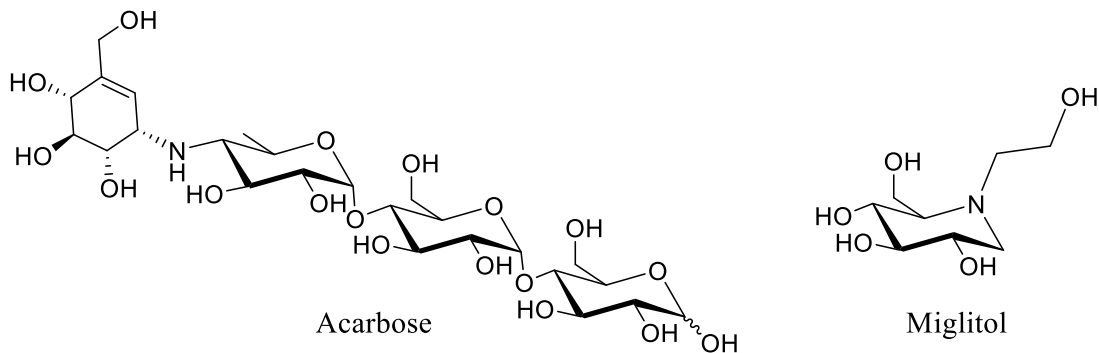


Figure 15 α -glucosidase inhibitors

Gliflozins:

Nowadays there are three different gliflozins on the market: dapagliflozin which is the only one commercialized in France, canagliflozin and empagliflozin that have been approved by the European Medicines Agency (EMA) (Figure 16). These drugs are inhibitors of the sodium-glucose cotransporter-2 (SGLT-2) that is localized at the proximal renal tubule. The inhibition of this cotransporter prevents the glucose re-uptake leading to a reduction of the blood's glucose level. Their insulin-independent mechanism of action makes them suitable also for the patients in advanced stages of T2D.

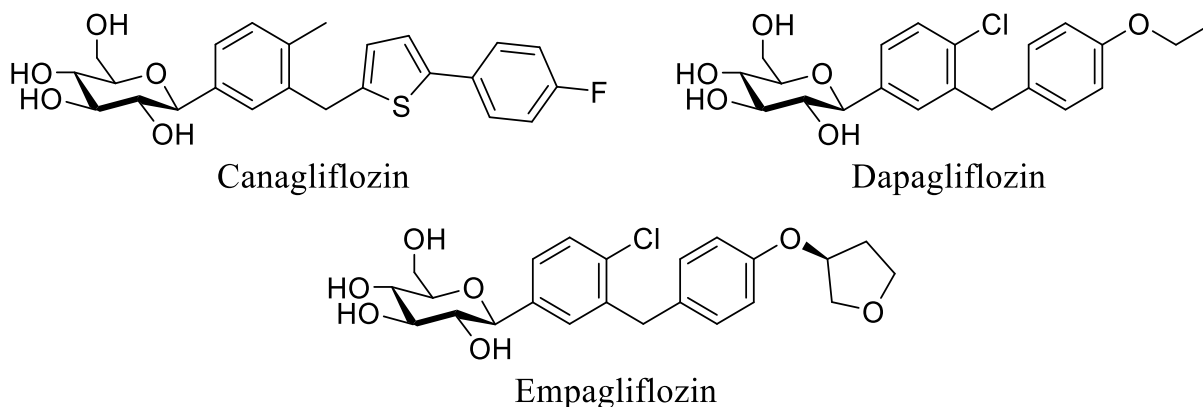


Figure 16 SGLT-2 inhibitors

Unfortunately all these treatments can only reduce the hyperglycemia and moreover not all lifelong. Indeed, with the progress of the disease and the consequent β -cells death, the patients have to progressively move to the insulin therapy.^{26,30}

1.2.4 New frontiers in T2D treatment

Despite the large number of antidiabetic drugs on the market, an optimal treatment is far; indeed all of T2D treatments available are associated with side effects. For this reason, over the last years, lots of potential drugs for old and new targets have been proposed as reviewed by Kerru *et al.* and Belete respectively in 2018 and 2020.^{31,32}

Among the new compounds, noteworthy are the protein tyrosine phosphatase 1 B (PTP1B) inhibitors. PTP1B is an enzyme involved in down regulation of insulin receptors (IR); its inhibition promotes the phosphorylation of the IR and as consequence increase the glucose uptake.

Another proposed interesting target is the free fatty acid receptor 1 (FFAR1), which under activation is able to promote an insulin secretion through a complex glucose level depending mechanism. The employment of FFAR1 agonist could be an interesting treatment for glucose regulation because it avoids the hypoglycemia risk.

As already explained, glucose deposition as glycogen in liver and muscle covers a crucial role in the glucose homeostasis, so being able to modulate this process could be an interesting treatment for T2D. Actually, some research groups are focused on the development of inhibitors for the enzyme glycogen phosphorylase (GP) which is involved in the glycogen deposit process.

As last example, it is mandatory to mention the opportunity to modulate the glucose level through the gluconeogenesis down regulation. Following this way the most relevant strategy is to employ small molecules able to inhibit the crucial enzyme fructose-1,6-bisphosphatase (FBPase).^{31,33} As clearly demonstrated, glucose homeostasis and insulin resistance are widely explored fields and, despite they represent a good way to prevent T2D complications, they remain only a management of the symptoms.

Over the last decades the role of the progressive loss of pancreatic β -cells has been extensively debated. Despite a lot remains to be understood, it is actually clear that β -cells function loss first and death after are strongly related with T2D development and progression. As emerged from the conference “Beta Cell Failure in Type 2 Diabetes” in 2013, preventing β -cells loss represents a new and interesting way of intervention for T2D treatment. In light of the β -cells death prevention, some critical issues have been proposed in order to focus the joint efforts on the finding of causative treatment through the β -cells loss prevention (Figure 17).^{30,34}

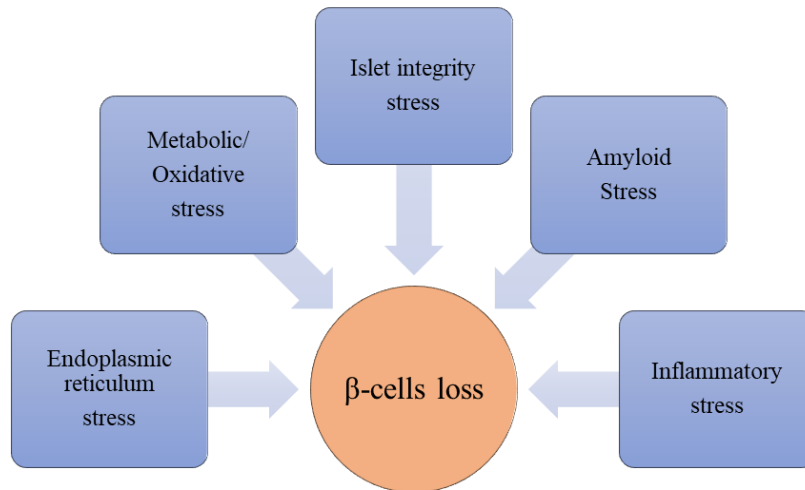


Figure 17 Main physiological stressors involved in pancreatic β -cells

1.3 human Islet Amyloid Polypeptide (hIAPP) and T2D

1.3.1 hIAPP or amylin

Because of its multifactoriality, find a causative treatment for T2D, is a challenging research. Among the new approaches, preventing the β -cells loss represents a real chance to obtain the first causative treatment. Taking into account the physiological stressors, hIAPP, also called amylin, gained lots of interest because its amyloid deposits have been found in more than 95% of T2D patients.

hIAPP is a member of the calcitonin family (CT) composed of calcitonin, α and β -calcitonin gene-related peptide, adrenomedullin and intermedin. hIAPP, a 37 amino acids peptide, was identified for the first time more than 30 years ago.^{35,36} hIAPP is physiologically expressed as 89 amino acids prepropeptide, which is converted in proIAPP (67 amino acids) in the endoplasmic reticulum. The pro hormone is then stored in the secretory vesicles, where the final conversion in hIAPP takes place. The involved enzymes are the same as for the biosynthesis of the insulin from proinsulin. ProIAPP undergoes to a double cleavage, first at the *C-terminus* and secondly at the *N-terminus* performed respectively by the prohormone convertase 1/3 (PC1/3) and the prohormone convertase 2 (PC2). Subsequently, the dipeptide KR (lysine-arginine) is removed again from the *C-terminus* by the carboxypeptidase E (CPE). The immature hormone is then processed by the bifunctional enzyme peptidylglycine- α -amidating monooxygenase (PAM) which promotes the amidation of

the carboxylic group of the glycine and the formation of the disulfide bridge between the residues 2 and 7. These last two transformations are necessary to obtain a peptide able to perform its biological function (Figure 18).^{37,38}

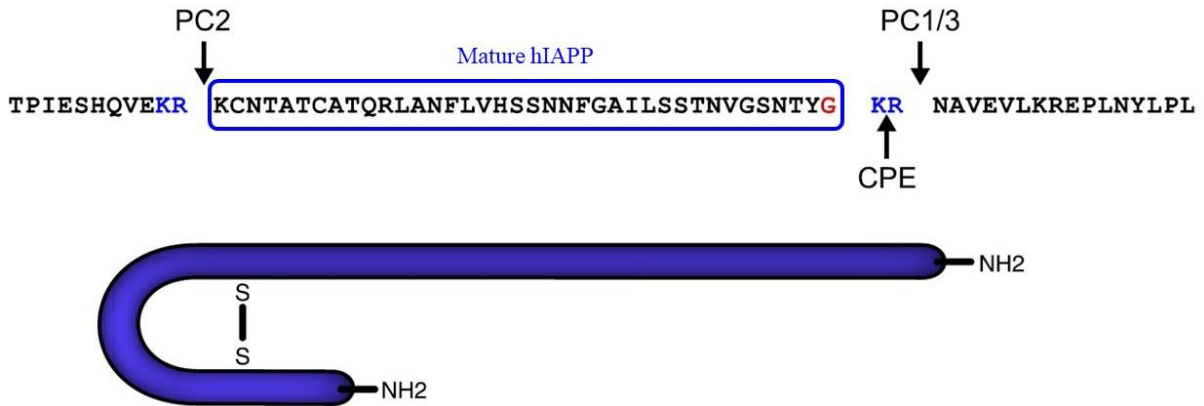


Figure 18 Conversion of proIAPP in hIAPP³⁷

1.3.2 Physiological role of hIAPP

Despite numerous evidences, the physiological role of hIAPP is not still completely clarified. Now it is reported that hIAPP action is receptor mediated but for a long time hIAPP receptors identification failed, even if specific binding sites were known (e.g. brain and renal cortex). The mystery was solved when the family of receptor activity-modifying proteins (RAMPs) was discovered. RAMPs act as receptor modifiers on the calcitonin receptors (CTR). CTR conformational variation promoted by the combination with RAMPs leads to a change in ligand affinity, generating new receptors of this class, known as Amylin Receptors Y (AMY), that are sensitive to amylin. Actually three different amylin receptors have been reported: AMY₁, AMY₂ and AMY₃ (Figure 19).^{37,39,40}

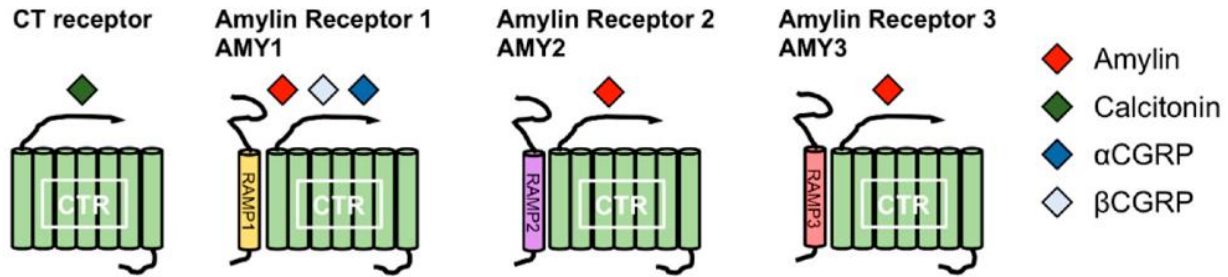


Figure 19 Conversion of CT in AMY receptor by interaction with RAMPs proteins³⁹

In contrast with the knowledge on insulin role and despite hIAPP has been identified more than 30 years ago, its physiological role is not yet fully understood. One of the main difficulties encountered is the trouble in the separation between the physiological or physio-pathological role from the pharmacological effect obtained experimentally. In addition, sometimes it is impossible to draw conclusions because the experimental data reported by different groups are totally in contrast. Despite all these issues, it is known that amylin acts in the pancreatic β -cells and in the central nervous system.³⁷

Concerning its role in the pancreatic β -cells, it has been proved that an absence of amylin results in an increased glucose mediated secretion of insulin in line with the fact that a physiological dose reduces the insulin secretion. It has also been reported that hIAPP is able to promote pancreatic β -cells proliferation at low glucose level. This results in a modulation of glucose homeostasis.^{41,42}

Experimental evidences confirmed that after a peripheral administration, it is possible to identify hIAPP in the Central Nervous System (CNS). This proves that amylin is able to cross the blood-brain barrier (BBB) in order to activate its receptors largely expressed in the CNS. The activation of amylin receptors in the CNS leads to an inhibition of the food intake (action in the area Postrema and ventral tegmental area) and to a body weight reduction (action in the ventral tegmental area). Despite the mechanism is not completely clear, it has been demonstrated that the administration of pramlintide, an amylin analogue acting on the CNS, is able to slow down the gastric emptying. This effect reduces the glucose uptake from the small intestine resulting in a lower blood glucose level during the post prandial phase.^{37,39}

It is possible to conclude that hIAPP is involved in the glucose homeostasis regulation process through several mechanisms even though these processes are not still well clarified.

1.3.3 Pathological role of hIAPP

Over the last decades, the implication of hIAPP in T2D progression has become more and more evident. Physiologically hIAPP is co-secreted with insulin at the ratio of 1/100 in favor of insulin.⁴³ When a subject is affected by T2D, this ratio is reduced to 1/20.⁴⁴ This increased quantity of amylin can be linked to the observation that more than 90% of diabetic patients present hIAPP deposits in the pancreas.⁴⁵ Beside the enhanced concentration of hIAPP, other factors like amylin mutation, modification of the pH when it is released, or presence of fiber seeds that act as catalyzer, have been proposed as factors able to contribute to the aggregation process.^{37,46}

Taking in account these data, it is easy to fall into error by deducing that the only responsible of hIAPP toxicity are the amyloidogenic deposits. Indeed, since 1999 it is known that hIAPP mature fibrils are much less toxic than the intermediate oligomers.⁴⁷ Moreover, it has been demonstrated that a freshly prepared solution of hIAPP in a nascent and non-fibrillar state is able to destabilize the membrane of the cells, inducing apoptosis and necrosis resulting in an altered production of insulin.⁴⁸ In support of this evidence, there are the results reported by Meier *et al.* according to whom inhibiting hIAPP fibrils formation, employing small molecules which do not prevent the oligomers formation, do not prevent cell toxicity.⁴⁹ Nowadays, according to these results, it is accepted that the most toxic species in hIAPP aggregation process are the oligomers, which are formed during the lag phase (see paragraph 1.1.1 page 3).

Because the hypothesis of the toxic oligomers is the more accredited, their mechanism of toxicity is widely studied. Until now the most explored is the one related to the membrane disruption, according to which hIAPP oligomers are able to promote the formation of trans-membrane pores. The formed pores act as channel for the ions; particularly it has been demonstrated that the formed flux of Ca^{2+} from the extracellular to intracellular environment can lead finally to the activation of the apoptosis process.⁵⁰

Through the membrane disruption, it seems that the oligomers, are the most involved species in the amylin toxicity but fibrils can also play a crucial role. Indeed, it has been reported that some trans membrane channels can be activated by the interaction with hIAPP fibrils, thus causing an influx of Ca^{2+} .^{51,52} In addition, fibrils could promote the formation of reactive oxygen species (ROS) also involved in the membrane damage.⁵³ As demonstrated *in vitro*, the presence of an

antioxidant like phycocyanin reduced INS-1 cells apoptosis due to the oxidative damage promoted by hIAPP.⁵⁴

To date the scientific community widely accepts the involvement of hIAPP in T2D development, nevertheless how and in which measure hIAPP exerts its toxicity on the pancreatic β -cells is still under debate and remains to be completely clarified.

1.3.4 hIAPP role in another pathology: Alzheimer's Disease (AD)

AD, like T2D, is a severe degenerative disorder characterized by the aggregation of an amyloid peptide; $A\beta_{1-42}$. Recently T2D has been proved to be a major risk factor for the development of Alzheimer's disease.^{55,56}

Several proofs of hIAPP involvement in AD have been reported but as far as efforts are made to understand the pathological mechanisms, they are still unclarified. Recent studies highlighted the colocalization of the amylin in the senile plaque of $A\beta_{1-42}$ suggesting a crucial role in the development of AD. The colocalization of amylin and $A\beta_{1-42}$ can be explained by two different mechanisms: amylin can be incorporated in pre-existing plaque or can act as seed to promote *the novo* deposition of $A\beta_{1-42}$.^{57,58}

Nearby the co-deposition of the peptides, another suggested mechanism is the receptor mediated toxicity; in fact, it has been reported that both hIAPP and $A\beta_{1-42}$ could activate some AMY receptors. The over activation of these receptors leads to an intracellular ion homeostasis disruption followed by a cellular apoptosis.⁵⁹

However, in opposition to hIAPP toxicity, other studies provided evidence for a protective role of amylin in AD. One of the most interesting evidence is the fact that systemic administration of pramlintide, an amylin analogue, is able to reduce the production of $A\beta_{1-42}$ in the CNS and it seems that this effect is due to an efflux of peptide $A\beta_{1-42}$ in the blood stream.^{60,61}

Nowadays it is clear that targeting hIAPP system could be a promising strategy also for AD treatment. However, the fact that amylin could have both positive and negative impact on the AD development underlines the needed of more efforts in the harmonization of the data in order to treat this severe and until now untreatable pathology.⁶²

1.3.5 hIAPP amyloidogenicity from a structural point of view

Primary sequence:

To understand hIAPP spontaneous tendency to the self-aggregation, it is necessary to start the investigation from its primary sequence. As previously reported, amylin is a 37 amino acids peptide and, with other hormones like calcitonin gene-related peptide (CGRP), it forms the family of the calcitonin related peptide. CGPR and hIAPP share a high homology sequence (43% and 46% respectively for CGPR1 and CGPR2) but CGPRs do not self-aggregate. A simple overlapping of their primary sequence affords the first important data: the main differences are concentrated in the region of the amino acids 20-29 (Figure 20), so it is possible to conclude that this region could be strongly involved in hIAPP aggregation process.

	1	10	20	30
Human CGRP1:	ACDTATCVT	<i>HRLAGLLSRS</i>	GGVVKNNFVP	TNVGSKAF
Human CGRP2:	ACDTATCVT	<i>HRLAGLLSRS</i>	GGMVKSNFVP	TNVGSKAF
hIAPP:	KCNTATCAT	QRLANFLVHS	SNNFGAILSS	TNVGSNTY

Figure 20 Primary sequences comparison of Human CGPR1, CGPR2 and hIAPP. In the red square the relevant sequence fragment 20-29. In Italic the aminoacidic differences³⁸

Moreover, from an evolutionary point of view IAPP primary sequence is strongly preserved in several species (Figure 21), but the small differences result to a huge variation in its self-aggregation ability.

	1	10	20	30	Amyloidogenicity
hIAPP:	KCNTATCAT	QRLANFLVHS	SNNFGAILSS	TNVGSNTY	Amyloidogenic
Rat:	KCNTATCAT	QRLANFLVRS	<i>SNNLGPVLPP</i>	TNVGSNTY	Non-Amyloidogenic
Bear:	KCNTATCAT	QRLANFLVRS	<i>GNNLGAILSP</i>	TNVGSNTY	Not investigated
Puffer fish:	KCNTATCVT	QRLADFLVRS	<i>SNTIGTVYAP</i>	TNVGSNTY	Not investigated
Monkey:	KCNTATCAT	QRLANFLVRS	<i>SNNFGTILSS</i>	TNVGSNTY	Amyloidogenic
Macaque:	KCNTATCAT	QRLANFLVRS	<i>SNNFGTILSS</i>	TNVGSNTY	Amyloidogenic
Baboon:	<i>ICNTATCAT</i>	QRLANFLVRS	<i>SNNFGTILSS</i>	TNVGSNTY	Amyloidogenic
Porcine:	KCNMATCAT	<i>QHLANFLDRS</i>	<i>RNNLGTIFSP</i>	TKVGSNTY	Less Amyloidogenic than human
Cow:	KCGTATCET	QRLANFLAPS	<i>SNKLGAIKSP</i>	TKMGSNTY	Not investigated
Cat:	KCNTATCAT	QRLANFLIRS	<i>SNNLGAILSP</i>	TNVGSNTY	Amyloidogenic
Dog:	KCNTATCAT	QRLANFLVRT	<i>SNNLGAILSP</i>	TNVGSNTY	Non-Amyloidogenic
Mouse:	KCNTATCAT	QRLANFLVRS	<i>SNNLGPVLPP</i>	TNVGSNTY	Non-Amyloidogenic

Figure 21 Primary sequences comparison of IAPP for different species. In Italic the aminoacidic differences³⁸

In figure 20, the sequences of IAPP for several mammals are shown and as widely documented in the literature, they are not all able to self-aggregate. For example, it has been reported that almost all the primate's IAPP peptides present this feature like the cat. It is interesting to note that rodents, the animal usually employed in diabetes research, do not develop amylin plaques. Again, as mentioned above for the comparison with CGRP primary sequence, the difference between amyloidogenic and non-amyloidogenic IAPP lies in the portion of the amino acids 20-29. Furthermore, the different aggregation propensity of rat IAPP (rIAPP) and hIAPP can also be ascribed to the rIAPP richness in proline (3 on 6 different amino acids are proline), an amino acid known to be able to disrupt the β -sheet formation.^{37,63,64}

hIAPP conformations analysis by experimental techniques

Until now only the differences in the primary sequence as source of amyloidogenicity have been described but it is also important to have a general overview on the three-dimensional structure of hIAPP in order to well understand its aggregation process with the aim to design compounds able to inhibit it.

hIAPP structure has been under investigation since a long time but, as demonstrated by the several models proposed through the years, it is a really challenging field. Most of the difficulties come from the self-aggregating tendency of the peptide, which leads to an equilibrium of metastable soluble and insoluble species, each characterized by a different morphology.

One of the first evidence of equilibrium among different species was published in 2000 by Higham and colleagues applying circular dichroism (CD). They found that hIAPP, incubated in for some days, adopted a soluble α -helix conformation. However, when the percentage of HFIP is reduced to 1%, in about 24h, the peptide precipitated in β -sheet conformation;⁶⁵ being the major components of hIAPP fibrils.

Shortly later, Clark *et al.* proposed an “e” model for the peptide conformation. According to which the misfolded hormone adopts a conformation with 3 β -sheets alternated by two turns among the amino acids 17-19 and 28-29.⁶⁶ This proposed model found confirmation in 2004 when Serpell and collaborators, applying X-ray, electron microscopy and cryoelectronic microscopy techniques, confirmed the same structure with an intra-sheet distance of 4.7Å.⁶⁷

The same hypothesis of 3 β -sheets was also proposed by another group just one year later but, in contrast with the founding of Serpell, Kajava's group proposed a "s" shaped model (Figure 22) in which the 3 parallel β -sheets are between the amino acids 12-17, 22-27 and 31-37.⁶⁸

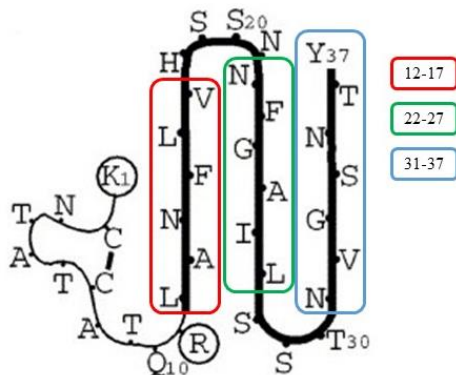


Figure 22 "s" shape model proposed by Kajava *et al.*⁶⁸

In 2007, thanks to the application of solid-state NMR, an "u" shaped structure (Figure 23) has been proposed. According to the results of this analysis the 2 β -sheets are connected by the turn between the amino acids 18-27. Moreover, in this study it has also been proposed that two monomers of hIAPP, symmetrically disposed, are the constituents of a protofibril; anyway several dispositions of the symmetry have been observed.⁶⁹ In light of the "u" shaped model, it has been proposed by Bedrood and co-workers that the distance among the β -sheets is about 15Å, which results in a left-handed twist along the fibril axis.⁷⁰

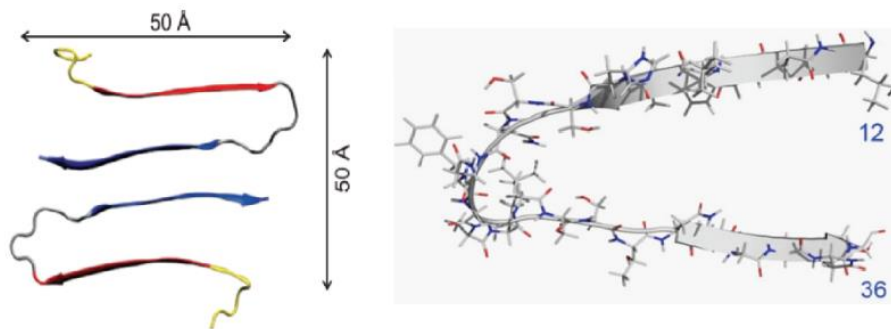


Figure 23 "u" shaped proposed by Luca *et al.* (left) and Bedrood *et al.* (Right)^{69,70}

Another structure was described by Mirecka *et al.* in 2016 studying the complex obtained by interaction between hIAPP and the aggregation inhibitor "β-wrapping" HI18 (see paragraph 1.3.6

page 36). NMR studies of this complex found the involvement in this interaction with HI18 of two sequences of hIAPP adopting β -strand structure (N₂₂FGAIL₂₇ and A₈TQRLANFLVH₁₈) connected by a turn between the amino acids 19 and 21 (Figure 24).

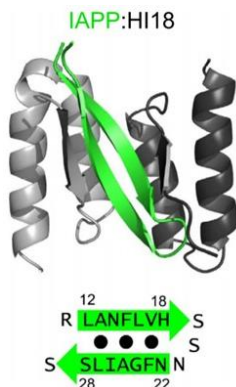


Figure 24 Structure of hIAPP:HI18 complex reported by Mirecka *et al.* hIAPP structure is highlighted in green⁷¹

Recently, Röder *et al.* investigated hIAPP conformations in different fibril polymorphs grown at pH 6. The authors identified at least 5 different fibril polymorphs of which the main polymorph PM1 was representing the 90% of the fibrillar amount.⁷² Employing the cryo-EM, the authors found that each monomer stacked in PM1 fibrils was characterized by “s” shaped structure (Figure 25), in which the *N*-terminal is highly disordered. Considering the sequence 13-37, it has been reported that the “s” shape is due to the presence of two turns between the amino acids 20-24 and 32-34.

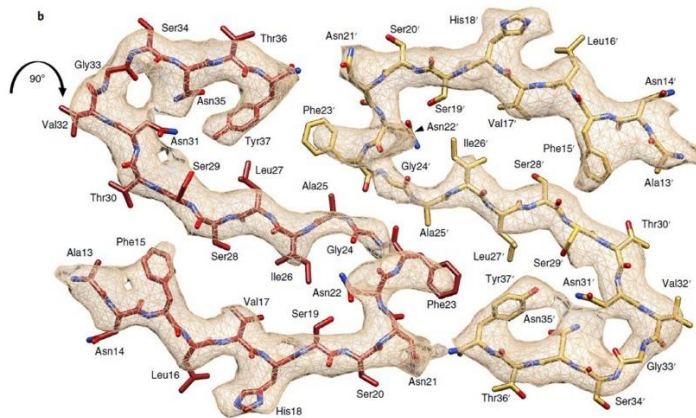


Figure 25 Atomic model of the “s” shaped structure between amino acids 13-37 observed by Röder *et al.*⁷²

The power of the computational techniques in hIAPP conformations analysis:

As seen until now, several conformations have been proposed applying different experimental techniques. Over the last decades the *in silico* analyses like Molecular Dynamics gained relevance for their versatility in the conformational study field. So, in the understanding of hIAPP structure it has been widely employed both alone or in combination with experimental data. Noteworthy, is the work proposed by Eisenberg *et al.* in 2008⁷³. They, starting from the crystallographic data of two different sequences of hIAPP, obtained an *in silico* model coherent with “u” shaped hypothesis already proposed. Two years later, the application of the two dimensions infra-red (2DIR) coupled with molecular dynamics further confirmed the same structure.⁷⁴ Interesting results were also obtained by the application of MD alone; indeed modeling experiments conducted by Zheng *et al.*⁷⁵ led to the same structure previously reported: “u” shaped β -sheets stacked in fibrils.

Beside the application in the studies about conformation of hIAPP monomers in the fibrils, MD has been employed to study also the monomeric form, in order to try to elucidate its conformational change involved in the aggregation process.

With this purpose, the application of replica exchange molecular dynamics simulations (REMD) allowed Wu and colleagues to establish that non amyloidogenic IAPP (e.g. rIAPP) preferentially adopts α -coil conformation, while the amyloidogenic hIAPP adopts both α -coil and β -sheet conformations (Figure 26).

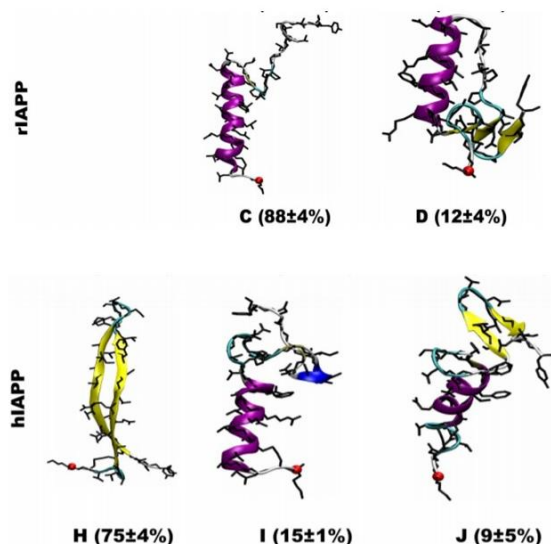


Figure 26 Conformations cluster of rIAPP and hIAPP proposed by Wu *et al.*⁷⁶

Moreover, the authors were also able to establish that the transition from the coil to the β -sheet form is the starting point of the aggregation process (Figure 27).⁷⁶ Nevertheless, it is important to remember that the conformation reported by Wu *et al.* is not univocal because differences in the experimental part, due to the peptide self-aggregation propensity, often led to get divergent models by *in silico* experiments.

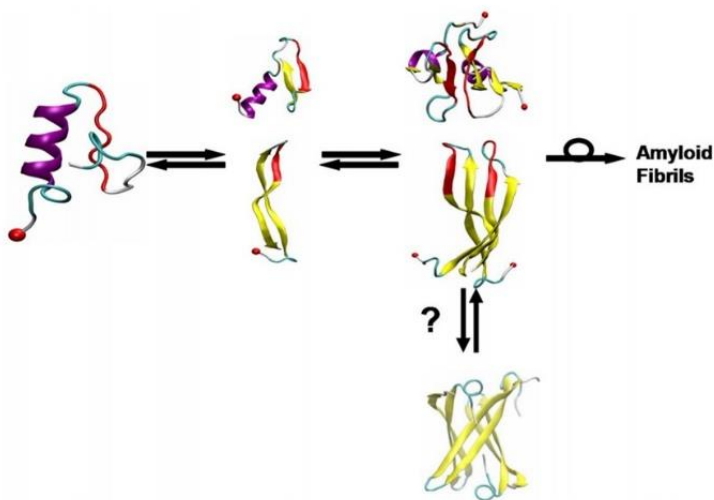


Figure 27 hIAPP conformational change involved in the aggregation process as proposed by Wu *et al.*⁷⁶

A good overview of the structural conformations of the monomers was reported by Tap Ha-Duong,⁷⁷ a Professor of our team, who in 2016 summarized the huge ensemble of data reported in the literature. His meta-analysis showed some common elements among the several proposed models like the tendency to find the helical conformation at the *N-terminus*.

A model to correlate hIAPP conformational change and membrane damage:

As already reported, hIAPP oligomers are able to disrupt cell membrane and, at the same time, the lipidic double layer has been reported to be able to catalyze the aggregation process. Thus amylin conformational changes, when in contact with the membrane, were investigated. Unfortunately, as reported by Ha-Duong *et al.* in their review, where and how monomers interact with the membrane is still to elucidate. However, some experimental data obtained by circular dichroism, suggest that intrinsically disordered amylin, when in contact with the membrane, starts to adopt an α -helix from the *N-terminal* partially inserted into the lipidic bilayer (Figure 28).⁷⁸

Knight *et al.*, in their work about hIAPP-bilayer interaction, proposed a 4 steps mechanism for aggregation catalyzed by the lipidic bilayer:

- 1) Structural conversion: amylin, interacting with the membrane, adopts an α -helix conformation;
- 2) Aggregation: a small group of α -helices linked to the bilayer aggregate into clusters;
- 3) Propagation: monomers are added to the clusters of helices;
- 4) Conversion: such clusters change their organization in fibrils rich in β -sheets.

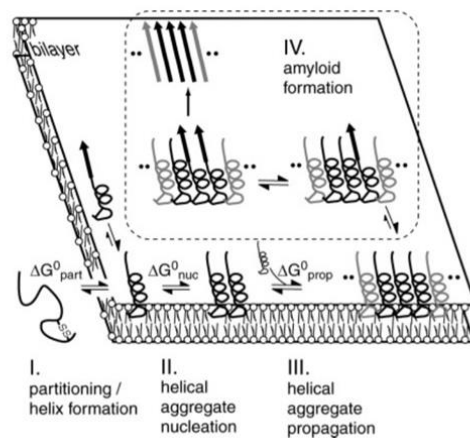


Figure 28 How membrane promote the aggregation process, model by Knight *et al.*⁷⁸

Deeper in the hIAPP fibrils structure:

Last but not less important is the aspect of hIAPP structure when it is aggregated. As seen until now, several models for the fibrils have been proposed along the time.

The application of the atomic force microscopy to the study of the fibrils structure have allowed to draw two aggregation pathways from protofibrils to fibrils, the first is called *lateral assembly*, while the second is named *coiling assembly*. The first mechanism involves the addition of protofibril by lateral stacking on the side, while the second one takes place when the fibrils assemble like a rope. Both pathways have been observed by different groups, with some divergences about the dimension of the fibrils.^{66,67}

The evolution of the Nuclear Magnetic Resonance (NMR) techniques and the development of the ssNMR allowed a deeper exploration of the fibrils structures, providing also useful data for further molecular modeling.

ssNMR data about oligomers have been employed to develop models in which different symmetries and number of oligomers have been combined. Noteworthy is the work reported by Zhao *et al.*, in which the authors explored how different layers of pentamers (from 1 to 3) can stack, generating different larger aggregates. When two layers of pentamers are stacked to form a decamer, the analysis of the results showed that only three different interactions among pentamers interfaces are allowed, each involving different amino acidic sequences (Figure 29)⁷⁹:

- 1) *C-terminus/C-terminus* (CC): amino acids 29-37 or 27-37;
- 2) *N-terminus/N-terminus* (NN): amino acids 13-17 or 11-17;
- 3) *C-terminus/N-terminus* (CN): amino acids 11-17 and 29-37.

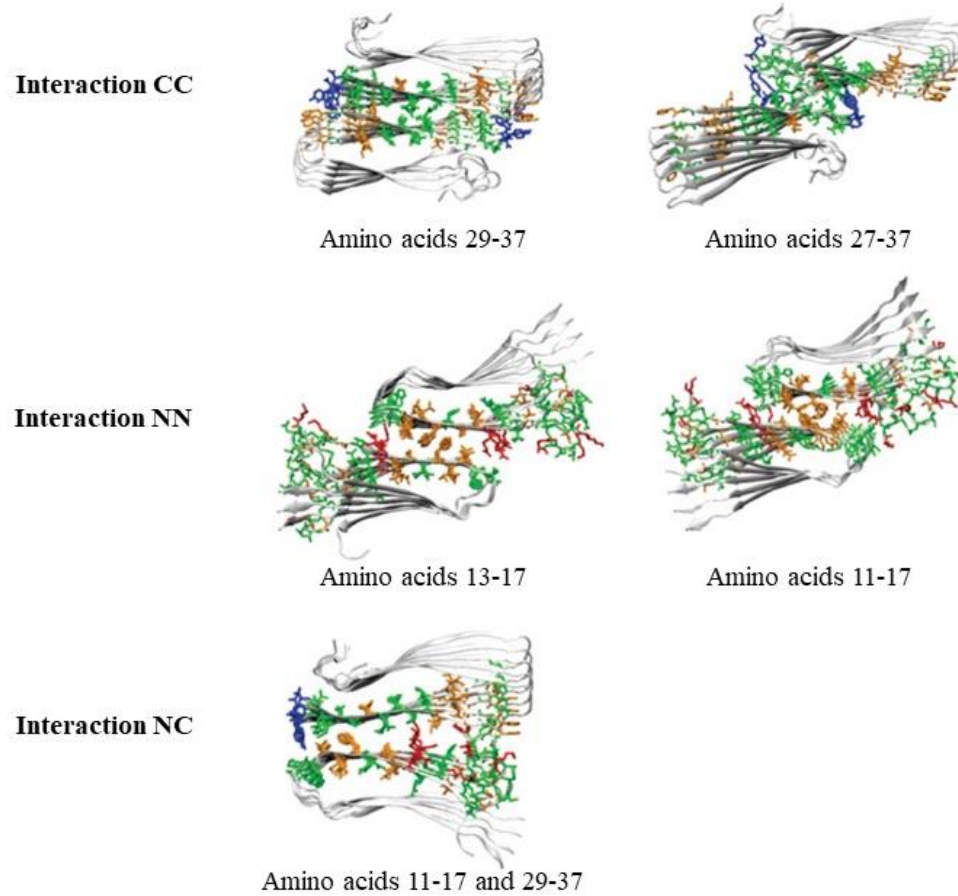


Figure 29 Possible pentamer double layer symmetry and aminoacidic sequence involved in the interface interactions by Zhao *et al.*⁷⁹

In the same paper, the authors proposed also an aggregation model in which the pentamers are consequentially assembled in accordance with the possible interfaces found for the pentamers bi-layer (Figure 30), outlying how this different assembly could be at the base of the hIAPP fibrils polymorphism.

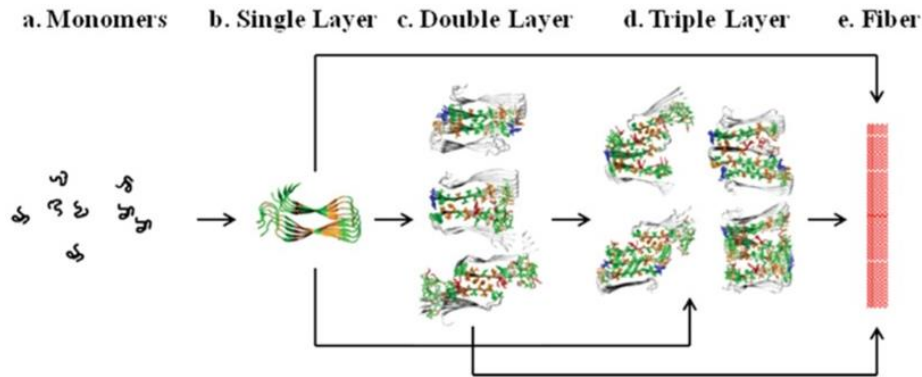


Figure 30 hIAPP aggregation model based on the pentamer double layer symmetry by Zhao⁷⁹

The same group, explored also the possibility to build fibrils overlapping layer of 3 pentamers in order to explore amylin fibril polymorphism that could explain its toxicity. From this second work, they demonstrated that assembling 3 pentamers in the same layer is possible to obtain at least 3 different stable models of fibrils (Figure 31).^{79,80}

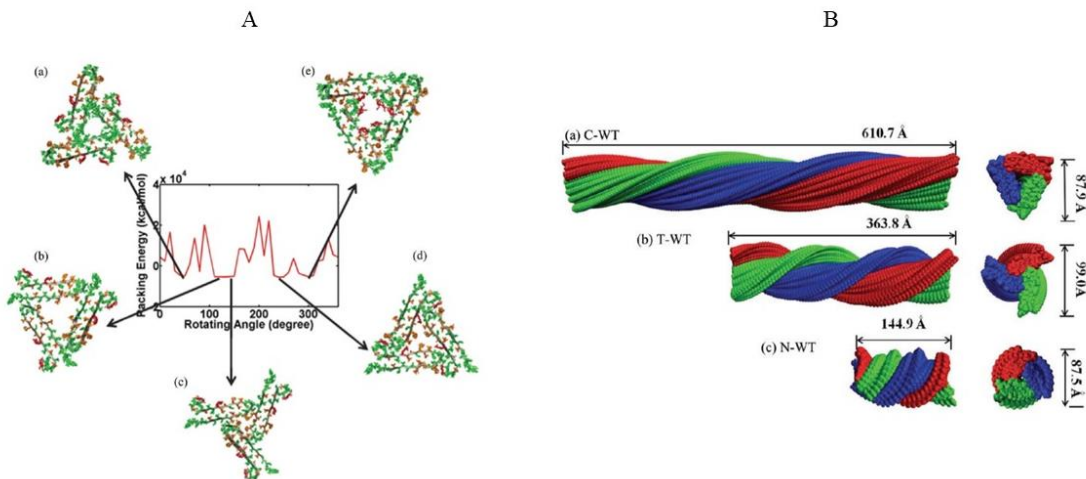


Figure 31 (A) Representation of the tri-pentamers structuration at lowest packing energy and (B) possible fibril models by Zhao *et al.*⁸⁰

It is important to underline that the reported structures are only few examples of the enormous work made in this field. However, despite the efforts in the exploration of hIAPP structure in order to elucidate the relation with its pathological role, we are still far from an exhaustive answer, mainly because high number of species, each adopting several conformations and being generally metastable, are involved in the aggregation process.

1.3.6 Targeting hIAPP aggregation as possible T2D therapy

Among the cellular stressor which lead to pancreatic β -cells death in T2D, hIAPP aggregation process represents a suitable target for the design of new possible causative treatments. As reported previously, amylin is strongly related to the pancreatic β -cells loss through different mechanisms. In the literature several compounds have been reported to be able to reduce or completely inhibit the aggregation process acting at diverse levels of the pathway. I will report here the most significative and relevant classes.

Polyphenols:

Polyphenols represent the first class of hIAPP aggregation inhibitors, of which Epigallocatechin Gallate (EGCG), Curcumin and Resveratrol are the forefathers. Polyphenols are well known to be non-selective inhibitors of the aggregation of amyloid proteins. Moreover, their mechanism of action is still under debate, despite it is known that they are able to interact with the target protein by π -stacking interactions and H-bonds.⁸¹

One of the most studied polyphenol is EGCG (Figure 32A), extracted from green tea. The EGCG, interacting with the dimer of hIAPP, is able to avoid the formation of inter- and intra-peptide interactions; moreover, it can promote a structural change in favor of the less toxic monomeric species.^{82,83} Another interesting property is the ability to promote the disaggregation of fibrils into smaller structures, however it is not able to completely reverse the process until the monomers.^{81,84} Due to its planarity EGCG carries out its activity on all the β -sheet rich steps of the aggregation so it is less active on the preliminary step in which the helices are mainly involved.⁸⁵

Resveratrol and curcumin (Figure 32B/C) extracted respectively from the curcuma and the grape, are two others well studied polyphenols. Both showed the common ability to stabilize “off-pathway” oligomers characterized by different structures and molecular weight if compared with the classical species.⁸⁶

Despite the lack of strong interactions between the amylin and the resveratrol, the polyphenol showed a marked ability to preserve the cells viability. Indeed, when its activity has been tested on the INS-1 cells, it maintained 90% of cells viability. In contrast with EGCG, curcumin is active also on the early stages of the aggregation, meaning that it is able to disrupt the α -helix aggregation catalyzed by the membrane.^{81,87}

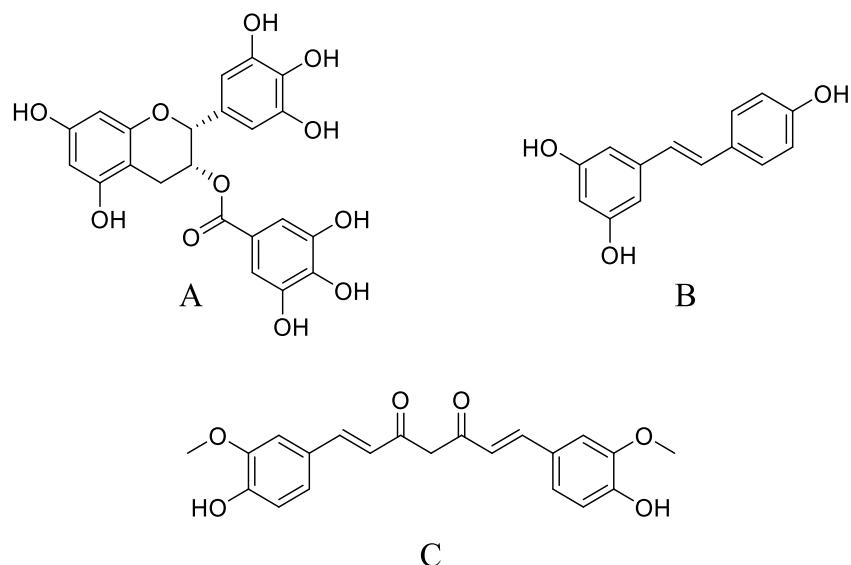


Figure 32 Structures of some natural polyphenols (A) EGCG (B) resveratrol (C) curcumin

Peptidic compounds:

hIAPP analogues:

One of the main class of inhibitors is represented by the peptidic compounds. As often happens in drug design, for these compounds the authors were inspired by the nature. IAPP is extremely preserved in the evolution and it is also known that small variations in the primary sequence have dramatic impact on the amyloidogenicity (see paragraph 1.3.5 page 22). Considering the high homology sequence among hIAPP and the non-amyloidogenic rIAPP (Figure 33A), Cao *et al.* found that a co-incubation of these two IAPP peptides led to an inhibition of the aggregation process in a dose-dependent manner from ratios 1/1 to 10/1 of rIAPP/hIAPP.⁸⁸

In order to find inhibitors for hIAPP aggregation, the researchers explored the possibility to design non amyloidogenic hIAPP homologues by replacing one or more amino acids in the primary sequence of the native peptide. An interesting example of inhibitors obtained by the replacement of a single amino acid is the work reported by Abedini and colleagues. They were able to produce a potent inhibitor by replacing the isoleucine 26 of the native amylin with a proline, an amino acid well known to be able to prevent the formation of β -sheets (Figure 33B).⁸⁹

The ability of proline to act as β -sheets disruptor, linked to the fact that the non-aggregative rIAPP differs from hIAPP by only six amino acids and among them three are prolines, led to a wide employment of the proline scan procedure in the design of inhibitors. Following this strategy,

pramlintide has been developed, a hIAPP analogue in which the native amino acids in positions 25, 28 and 29 were replaced by three prolines that are in the same positions in rIAPP.^{38,90} In 2005, this peptide has become the only amylin analogue approved on the market. Pramlintide, also called Symlin, was approved by the FDA as co-treatment for T1D and T2D in association with the administration of insulin. Pramlintide plays the same role as endogenous hIAPP; it helps the glycemic control through several mechanisms such as increasing the satiety, slowing down the gastric emptying and suppressing the postprandial glucagon level.⁹¹

Despite it is approved for another scope, pramlintide is actually the only inhibitor of hIAPP aggregation available on the market. Indeed, as demonstrated in a comparative study of 2015, pramlintide is the most effective aggregation inhibitor among the tested compounds: rIAPP, pramlintide and the two single-point pramlintide mutants H18R and F23L.⁹² The two mutants were selected in order to examine how an increased homology with rIAPP could influence the activity. The results of the study showed that, despite it is not the most potent inhibitor known, pramlintide is able to inhibit the aggregation process more efficiently than other compounds of the series. From these evidences the authors concluded that an equilibrium among the high homology with the native peptide and a non-amyloidogenicity of the final inhibitors is necessary to reach a good inhibition. (Figure 33C).⁹²

	hIAPP	H ₂ N-KCNTATCATQ RLANFLVHSS NNFGAILSS TNVGSNTY-CONH ₂
A	rIAPP	H ₂ N-KCNTATCATQ RLANFLV R SS NN L GPV L SS TNVGSNTY-CONH ₂
B	I ₂₆ →P ₂₆ hIAPP	H ₂ N-KCNTATCATQ RLANFLVHSS NNFGA P LSS TNVGSNTY-CONH ₂
C	Pramlintide	H ₂ N-KCNTATCATQ RLANFLVHSS NNFG P IL P P TNVGSNTY-CONH ₂
D	IAPP-GI	H ₂ N-KCNTATCATQ RLANFLVHSS NNFG A ILSS TNVGSNTY-CONH ₂ <div style="margin-left: 150px;"> Me-N N-Me </div>

Figure 33 Structure of hIAPP inhibitors based on its sequence

Short peptides derived from hIAPP amyloidogenic sequence:

Nowadays it is well known that several sequences of hIAPP are able to self-aggregate and among them the polypeptide constituted by the amino acids S₂₀NNFGAILSS₂₉ of amylin is one of the most studied. As reported by Tenidis *et al.*, from these 11 amino acids peptide it is possible to prepare various amyloidogenic peptides with different grades of amyloidogenicity.⁹³ It has been

demonstrated that phenylalanine of the sequence N₂₂FGAILSS₂₈ is important for the aggregation process because of its ability to form π -stacking interactions.⁹⁴ The same group also reported that a substitution of the Phe₂₃ with others amino acids can modulate the peptide ability to form aggregates, indeed its replacement with hydrophobic amino acids such as Val or Leu completely removes its aggregation propensity. More interesting is the substitution of Phe₂₃ with another aromatic amino acid like the tryptophan, which led to an aggregation prone peptide. In contrast, when Phe₂₃ is replaced by a Tyr, a non-aggregative form of the peptide is obtained. The authors explained that the inability to aggregate of NYGAILSS is due to the spatial disposition of the lateral chains of the two Tyr potentially involved in the formation of π -stacking interactions.⁹⁵ The same group, in a following work, compared the inhibitory activity of NYGAILSS with the native octapeptide NFGAILSS and the NFGAILPP in which are presents two Pro as β -sheet breaker. Interestingly, NYGAILSS showed an hIAPP aggregation inhibitory activity higher than NFGAILPP. However the sequence showed high toxicity for the pancreatic β -cells.⁹⁶

Insulin:

Based on the fact that insulin and hIAPP are co-accumulated in the secreting vesicles at high concentrations, insulin has been proved to be a stabilizer of hIAPP monomers.⁹⁷ When co-solubilized at the ratio 1/1 insulin was able to stabilize the monomers for a long time forming clusters of 3 molecules of insulin for 1 of hIAPP.⁹⁸ Further experiments were also conducted to well elucidate the role of insulin chains A and B (IAC and IBC) in the inhibition process. Gilead and co-workers reported that IBC was able to inhibit the aggregation while IAC did not; at the same time, the sequence responsible of the interaction between IBC and amylin was identified. The results were further confirmed few years later when another independent study found that the same amino acids, 8-18 of hIAPP and 11-19 of IBC, were involved in the hIAPP/IBC interaction. The authors of these two studies also proposed that the stabilization of hIAPP monomers, mediated by the IBC, was due to an helix-helix interaction (Figure 34).^{98,99}

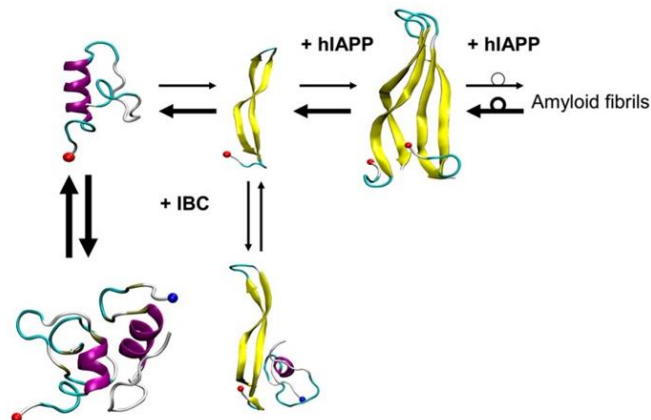


Figure 34 Proposed mechanism for hIAPP aggregation inhibition by IBC.⁹⁸ Red ball indicate hIAPP *N-terminus* while blue ball indicate IBC *N-terminus*

HI18 β -wrapping inhibitor:

In 2016, Mirecka *et al.* reported a protein able to bind and inhibit hIAPP aggregation.⁷¹ This protein, called HI18, was selected by phage display from a β -wrapping protein library.¹⁰⁰ The entire library was based on the dimeric protein ZA β 3, which bound to the β -hairpin form of A β ₁₋₄₂ peptide, inhibiting its aggregation. HI18 is a homodimer which subunits are linked through a disulfide bond between the residues Cys-28. The subunits are characterized by two α -helix connected by a β -turn (Figure 24, page 25).

Peptidomimetics:

The number of inhibitors in this group is extremely large, therefore here below only some of the more studied classes are reported.

hIAPP N-methylations:

Beside the peptidic compounds previously reported there are other pseudopeptide inhibitors, obtained by a modification of the peptidic backbone of the amylin. The pseudopeptide IAPP-GI (Figure 33D) is an inhibitor of hIAPP aggregation, characterized by the *N*-methylation of the amino acids G₂₄ and I₂₆. This non-amyloidogenic analogue is able to interact with hIAPP and prevents its aggregation. Moreover, the process can be reversed when the compound is in contact with mature fibrils. However, as reported by Yan *et al.* this pseudopeptide is not strongly selective for hIAPP, indeed it is also able to bind with A β ₁₋₄₀.¹⁰¹

Short peptidomimetics derived from hIAPP amyloidogenic sequence:

Another approach explored by the authors is the possibility to replace some amino acids by non-natural amino acids. In 2004 Gilead *et al.* designed a series of short peptidomimetics, based on hIAPP amyloidogenic sequence, in which the aliphatic amino acids Ala₁₃ and Leu₁₅ were replaced by the α -aminoisobutyric acid (Aib, Figure 34).¹⁰² Aib is an achiral non-natural amino reported to be a β -sheet breaker because of its ability to induce helical conformation when inserted in a polypeptide. Among the designed peptidomimetics, the group found that the Aib-NF-Aib-VH hexa-pseudopeptide was the most active in the inhibition of hIAPP fibrillization.

A decade later, another group exploited the same strategy by studying the influence on the aggregation process of *ortho*, *meta* and *para* aminobenzoic acids (Abz, Figure 34) when inserted into the amyloidogenic sequence NFGAIL.¹⁰³ Paul *et al.* deeply explored the effect of the replacement of G₂₄ or I₂₆ or both by Abz. Interestingly they were able to demonstrate that the differences in the position of the aromatic substituents on Abz were influencing the inhibition activity of the pseudopeptide; indeed *ortho* and *meta* were able to disrupt the fibril formation, while *para* did not.

The peptidomimetics proposed by Mishra and colleagues are based on the same amyloidogenic sequence. In the NFGAIL sequence there are two relevant amino acids for the β -sheets formation: F₂₃ and I₂₆; the authors generated a series of peptides in which these two aa were replaced singularly by an α,β -dehydrophenylalanine (Δ F, Figure 35). Δ F is a non-natural amino acid that has a dualistic effect: it is able to induce helical conformation and β -turns when inserted respectively in long and short peptide. The resulted penta- and hexa-peptidomimetics FGA Δ FL and NFGA Δ FL were able to inhibit the aggregation process. Interestingly it seems that FGA Δ FL is able to prevent the aggregation by stabilization of the helical monomeric form of hIAPP.¹⁰⁴

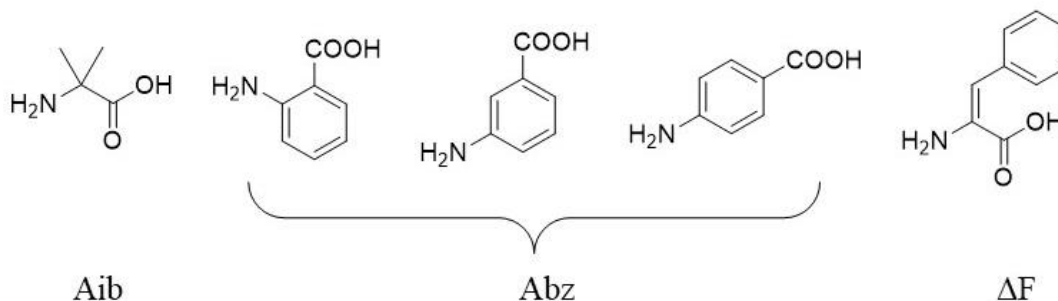


Figure 35 Structures of non-natural amino acids Aib, Abz and Δ F

In the class of the peptidomimetics, there are also conformationally restrained structures designed to mimic and target selectively the protein-protein interactions (PPI). As recently reviewed by our group, the molecules designed to target PPI of structures rich in β -sheets are a promising but not yet widely explored strategy. The lack of investigation in this field is probably to attribute to the fact that structures rich in β -sheets are mainly involved in amyloidosis, which gained more and more attention only in the recent past decades.¹⁰⁵ The most investigated restrained structures for the inhibition of hIAPP are the cyclic and acyclic hairpins.

Cyclic β -hairpins:

Nowick *et al.* were among the first to propose a macrocycle rationally designed for the modulation of hIAPP aggregation process. In their cyclic hairpin it is possible to identify different key elements:

- 1) Recognition strand: heptapeptide from the amyloidogenic sequence of hIAPP (N₂₁NFGAIL₂₇);
- 2) Blocking strand: this strand contains the non-natural amino acid Hao, which takes its name from the structure (Hydrazine, 5-Amino-2-methoxybenzoic acid and Oxalic acid). The presence of Hao imposes a β -sheet structure to the macrocycle. This is possible because its design allows the formation of 4 internal hydrogen bonds but meanwhile the external H-bonds, necessary for the aggregation, are prevented;
- 3) Linkers: two ornithines act as β -turns connecting the 2 strands.

The ensemble of the described structure generated a macrocyclic β -hairpin (Figure 36) able to disrupt the aggregation process. Indeed, when tested in Thioflavin-T fluorescence assay, the cyclic hairpin was able to extend the lag phase by 150%, while others cyclic hairpins designed with others sequences of hIAPP (R₁₁LANFLV₁₇, F₁₅LVHSSN₂₁, I₂₆LSSTNV₃₂, N₃₁VGSNTY₃₇) only accelerated the aggregation process. Noteworthy is the fact that this structure can modulate the aggregation process of several amyloidogenic peptides changing the recognition heptapeptide strand. However it is also important to denote that no proof of selectivity is available.^{106,107}

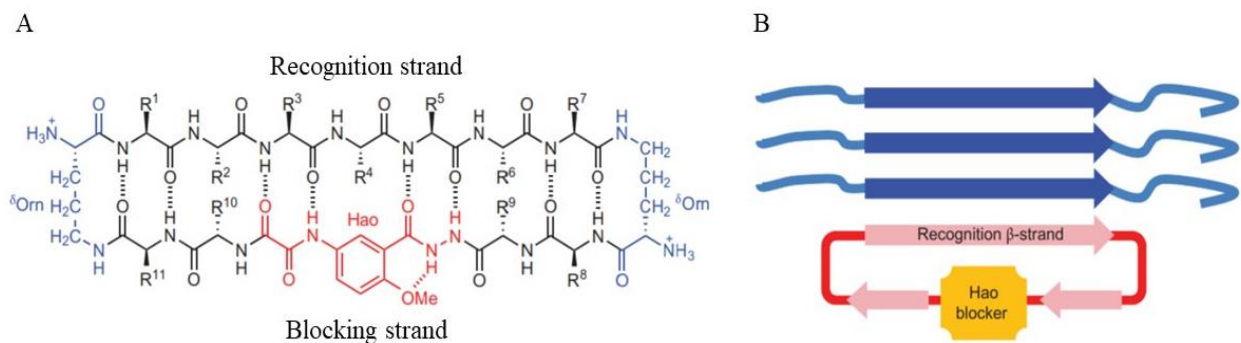


Figure 36 (A) Cyclic β -hairpin structure and (B) its interactions with hIAPP by Nowick¹⁰⁷

More recently, as reported by Spanopoulou and colleagues, it has been demonstrated that it is also possible to design cyclic hairpin able to inhibit the aggregations of both hIAPP and A β peptides.¹⁰⁸

The team, exploiting their linear inhibitor R3-GI based on hIAPP sequences involved in the hIAPP/A β_{1-42} cross interaction (A₈TQRLANFLVH₁₈ and N₂₂FGAILS₂₈),¹⁰⁹ developed cyclic dual inhibitor thank to a disulfide bridge between two cysteines added at the ends of the amino acidic sequence. Through sequential optimization steps, the group prepared an inhibitor in which the hIAPP key residues F₁₅, L₁₆, F₂₃ and I₂₆ were maintained while the others were replaced by glycines. Moreover, this peptide is characterized by the presence of several D amino acids that ensure an improved proteolytic stability (Figure 37).



Figure 37 Structures of the linear peptide R3-GI and the cyclized small dual inhibitor. In blue amino acids preserved from hIAPP sequence and in red the tripeptide spacer. D amino acids are indicated in lower case^{108,109}

Acyclic β -hairpins:

With the advancement in the knowledge of hIAPP aggregation it has become evident that this process involves several species in dynamic equilibrium. For this reason, some groups have turned

their attention to the development of small acyclic β -hairpin inhibitors, thus creating more flexible and adaptable structures. However, looking in the literature it is noticeable that this family is the least investigated. The deficiency of small acyclic β -hairpins could be ascribed to the difficulty in the design of short peptides/peptidomimetics able to maintain a stable β -hairpin folding, without the employment of stabilizing covalent bonds.

Pointing in this direction is the work proposed by Huggins *et al.* in which stable acyclic β -hairpins were prepared.¹¹⁰ The folding of these structures is due to the presence of aromatic amino acids like tryptophan that contribute to the stability by aromatic interactions. These inhibitors, in contrast with what has been reported until now, are not based on the hIAPP sequence, they are just designed to be folded in β -hairpins. Their inhibitory activity lies in the secondary structure recognition; indeed, the authors proposed that the pre-folding of the hairpin is the driving force of the inhibitory activity (Figure 38). However, the absence of a recognition sequence induces a lack of selectivity, making them active also on the aggregation of α -synuclein involved in Parkinson's disease.

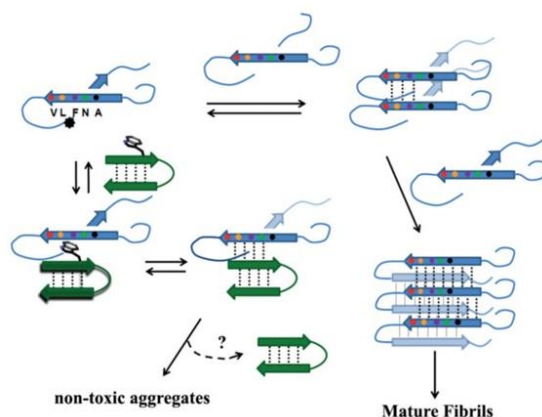


Figure 38 Inhibitory mechanism for acyclic β -hairpin by Huggins¹¹⁰

α -helix:

As previously reported, the cellular membranes acting as catalyst, are involved in the preliminary steps of the aggregation process, in which hIAPP is partially folded in a coil. Thus, some researchers envisaged the possibility to impeach the aggregation process trapping these monomeric forms by helix-helix interactions. Over the last decades, the foldamer field has come a long way in the design of well-structured molecules, so as to make possible the synthesis of helices able to target the abovementioned preliminary aggregation steps. Saraogi first and Kumar later with their

oligopyridylamide compounds (respectively five and three units, Figure 39) were able to prove that the employment of rationally designed α -helix is an useful strategy to inhibit the early stage of the oligomerization, when hIAPP monomers are still coil in contact with the membranes (Figure 40).^{111–113} Both authors built the foldamers derivatized with carboxylic lateral chain in order to engage ionic interactions with positively charged amino acids that are present at hIAPP *N*-terminal (lysine 1 and arginine 11). While Saraogi and colleagues introduced five carboxylic groups to maximize the ionic interactions, Kumar *et al.* alternated two acidic lateral chains with an ethyl group in order to create a surface complementary as much as possible to the α -helix surface adopted by hIAPP.

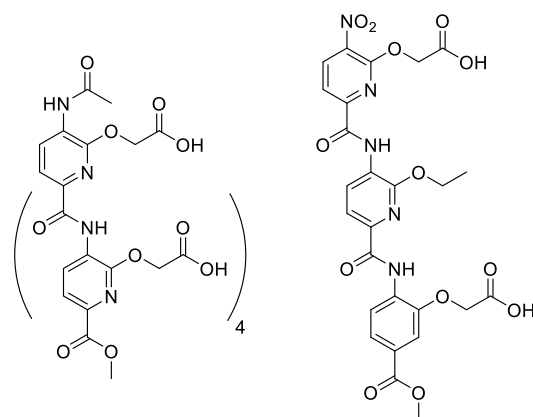


Figure 39 Structures of the oligopyridylamide compounds reported by Saraogi (left) and Kumar (right)^{111,112}

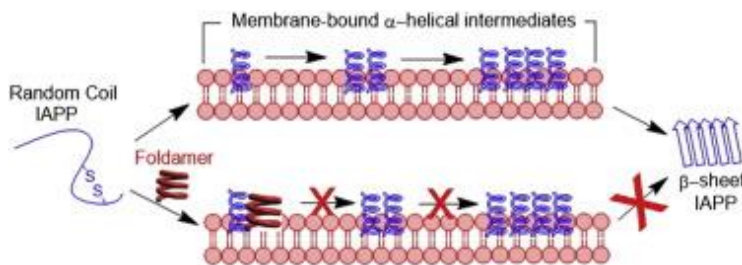


Figure 40 Helical foldamer inhibition mechanism proposed by Kumar *et al.*¹¹³

Chapter 2

On the way for new hIAPP aggregation inhibitors

2.1 Research group expertise

2.1.1 Inhibitors of protein-protein interactions

Currently it is widely proved that protein-protein interactions (PPIs) are at the base of many processes both pathological and biological. Since the first evidences of their importance, the possibility to modulate the PPIs by interfering with the processes in which they are involved has been taken into account. However, despite the efforts made in this field, the design of PPIs inhibitors is still a great challenge. Because of the absence of defined binding pocket and the extended surface involved in PPIs, it is almost impossible to use small molecules as modulators. Actually, the employment of peptides or peptidomimetics represents the main strategy to overcome small molecules drawback. Moreover, the recent advancements in the peptide and peptidomimetic field made them the most eligible class as PPIs inhibitors.^{105,114}

Over the time, our research group developed skills in the design and synthesis of compounds able to modulate the PPIs. During the last years, the projects were mainly focused on the development of peptidomimetics as modulator of amyloid aggregation. In particular, we were recently interested in developing different classes of rationally designed peptidomimetics like glycopeptidomimetic, β -hairpin and α -helix, able to modulate and inhibit the aggregation of β -amyloid peptide, that is involved in Alzheimer's disease.

Glycopeptidomimetics:

In 2011, our group proposed for the first time glycopeptidomimetic molecules as modulators of $A\beta_{1-40}$ peptide aggregation.¹¹⁵ The conception of these compounds was easy but effective: a central β -sheet breaker linked to two hydrophobic peptidic arms rationally selected to interact with the β -amyloid (Figure 41, compounds **a-d**). The presence of the two arms Ala-Val and Val-Leu ensured the reconnaissance of the target while the central D-glucopyranosyl moiety disrupted the inter-strand hydrogen bonds network formation. Their activity on the fibrillization process of $A\beta_{1-40}$ peptide, was evaluated, by thioflavin T fluorescence spectroscopy (ThT), transmission electron

microscopy (TEM), and NMR (NOE and STD). These glycopeptidomimetic compounds displayed a good inhibition on the fibrillization of A β ₁₋₄₀ peptide and were able to interact with the aggregated species through the hydrophobic amino acid arms. Since the peptide A β ₁₋₄₂ is more aggregative and neurotoxic than the shorter analogue A β ₁₋₄₀, our group also evaluated the activity of these compounds on this more amyloidogenic variant.¹¹⁶ The free amine derivative (Figure 41 compound **e**) showed a marked delay effect of the fibrillization process, while the completely protected compound (Figure 41 compound **f**) was, on the contrary, able to accelerate the process. These compounds were also tested by Capillary Electrophoresis (CE), a new methodology developed by one PhD student (Dimitri Brinet) who was in co-tutoring with our team and the team of Prof. Myriam Taverna (Institut Galien de Paris-Sud, Université Paris-Saclay) with whom our research team closely collaborates. This method allows to monitor the soluble species formed during the early stage of the aggregation process. It showed how the free amine (**e**) delayed the aggregation process by stabilizing the non-toxic monomeric and also the small and large oligomeric species, that unfortunately are known to be the most toxic species in the aggregation process. In contrast, the protected compound (**f**) showed an accelerating effect by promoting the formation of larger and insoluble aggregates, which could be considered as different but interesting strategy to prevent the toxicity of the A β ₁₋₄₂ soluble oligomers.¹¹⁶

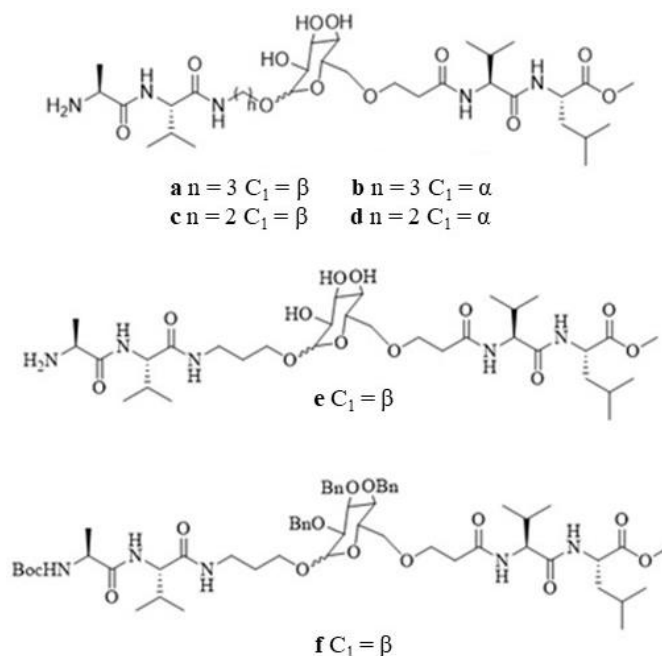


Figure 41 Structures of the glycopeptidomimetic inhibitors proposed by our team^{115,116}

Being encouraged by these results, the research team decided to further investigate the opportunity to replace one dipeptide arm with a peptidomimetic one in order to increase the inhibitory effect on the aggregation and the bioavailability by reducing the number of possible sites for proteolytic attack (Figure 42).¹¹⁷ The peptidomimetic chosen was the 5-amino-2-methoxybenzhydrazone (Amb) that is an analogue of Hao (Figure 36 chapter 1), where the oxalic acid moiety was removed. The Hao unit, when included in a peptidic macrocycle forming anti-parallel β -strands, has already showed the ability to disturb the formation of $A\beta_{1-42}$ and hIAPP β -sheets and inhibit their aggregation.^{106,107} A positively charged amino acid (Lys) was introduced next to the benzhydrazone motif in order to enhance the interaction between the amyloid target and the peptidomimetic arm by a ionic interaction. The target peptidomimetic molecule (Figure 42) led to a stronger oligomerization and fibrillization inhibitor than the peptidic analogue, as proved by a range of bio- and physicochemical assays (ThT fluorescence, capillary electrophoresis, NMR, surface plasmon resonance). Of particular interest are the results obtained with the cellular viability assay. Indeed, this inhibitor showed a marked protective effect against $A\beta_{1-42}$ toxicity on SH-SY5Y neuroblastoma cells at equimolar inhibitor/peptide ratio. This activity was maintained, although to a lesser extent, even at a sub-stoichiometric inhibitor/peptide ratio of 0.1/1.

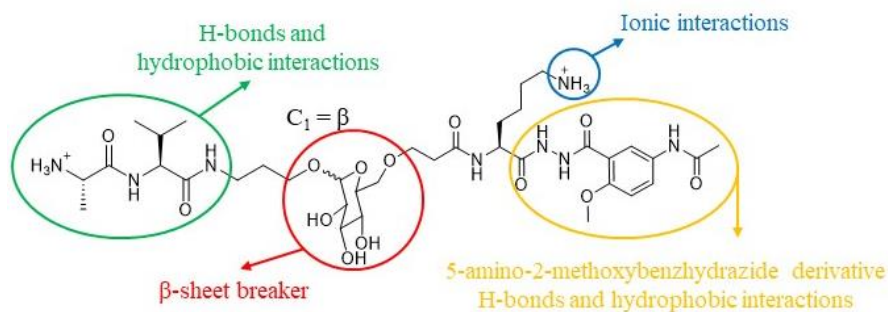


Figure 42 Structure of the glycopeptidomimetic compound bearing the 5-amino-2-methoxybenzhydrazone motif¹¹⁷

Pre-structured β -hairpins:

As reported in chapter 1, the richness in β -sheets is a common feature of all the amyloidogenic proteins so, the employment of a pre-organized β -sheet inhibitor could improve the inhibition. In light of this assumption, our research group focused its efforts on the design and the synthesis of acyclic β -hairpin mimics able to selectively bind the β -amyloid peptide and inhibit its aggregation.

In 2017, our team published the first example of acyclic β -hairpin mimics based on a rigid diketopiperazine β -turn inducer able to modulate the early oligomerization and the fibrillization of $A\beta_{1-42}$.^{118,119} Because often a strong peptidic character represents a limit for the development of a drug, one peptidic arm was kept and the second arm fixed on the hairpin was peptidomimetic (Figure 43, only *cis* derivatives are shown). As for the glycopeptidomimetic series, the peptidomimetic arm was based on the 5-amino-2-methoxybenzhydrazide moiety and the tetrapeptidic arm, which acts as self-recognition element, was derived from the C-terminal sequence G₃₈VVI₄₁ and the amyloidogenic sequence K₁₆LVF₁₉ of $A\beta_{1-42}$. The conformational studies, conducted by NMR and molecular dynamics confirmed the hairpin conformation, but only for the *cis* derivatives, while the *trans* showed an extended conformation.^{118,119} From the biophysical evaluations (ThT and CE), only the *cis* derivatives displayed activity on the oligomerization and the fibrillization, proving that the hairpin conformation is essential for the interaction with the amyloid peptide. The hairpin bearing the C-terminal sequence G₃₈VVI₄₁ instead of K₁₆LVFF₂₀ was less efficient.

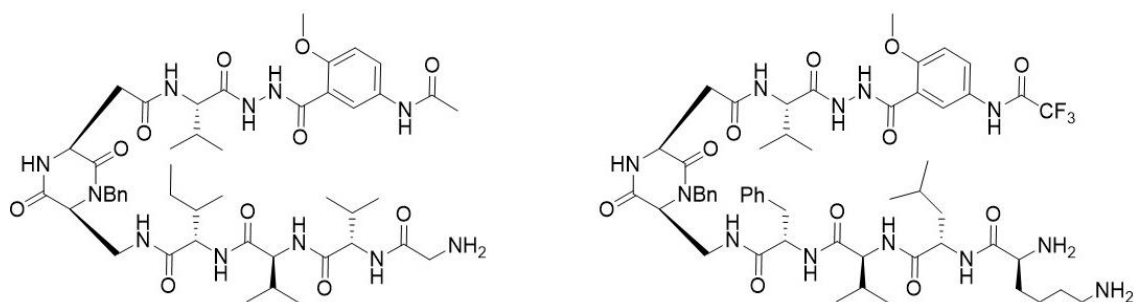


Figure 43 Structure of diketopiperazine based modulators¹¹⁹

In 2016, in collaboration with a team from the Università degli Studi di Milano, our team have also undertaken the development of another family of acyclic β -hairpin mimics. They were built on the piperidine-pyrrolidine scaffold, a semirigid β -turn inducer developed by the Italian team,¹²⁰ linked to two pentapeptidic arms.¹¹ Two groups of hairpin were developed, both characterized by the same amyloidogenic sequence K₁₆LVFF₂₀, from $A\beta_{1-42}$, faced to different pentapeptides: GLMVG (G1) and GVVIE (G2), corresponding to the sequences at the C-terminus (33-37 and 38-42 respectively) in interaction with KLVFF respectively in the oligomers or in the fibrils (Figure 44).¹²¹



Figure 44 Structure of the acyclic hairpins G1 and G2 based on the semirigid piperidine-pyrrolidine β -turn inducer¹²¹

The biophysical evaluations showed for both an excellent inhibition of the oligomerization (CE) and the fibrillization (ThT), more marked for G1. Moreover, both displayed a protective effect against $A\beta_{1-42}$ toxicity on the SH-SY5Y neuroblastoma cells, maintaining the activity even at a sub-stoichiometric ratio at which the reference compound (Resveratrol) was less effective. NMR conformational studies showed a certain flexibility degree, more pronounced for the most active G1 and in any case higher than for inhibitors based on the diketopiperazine. The evidence gathered from this work allowed us to prove our theory according to which a preorganized hairpin improve the inhibitory activity. Moreover, a certain grade of flexibility promotes the inhibitor/target interaction, by making the hairpin free to adapt itself to the dynamic environment present during the aggregation of $A\beta_{1-42}$.¹²¹ One year later structure-activity relationship studies, on hairpin based on the piperidine-pyrrolidine β -turn inducer, led to smaller acyclic β -hairpin mimics with a reduced peptidic character (one dipeptidic arm and one peptidomimetic arm) able to modulate the β -amyloid aggregation (Figure 45).¹²²

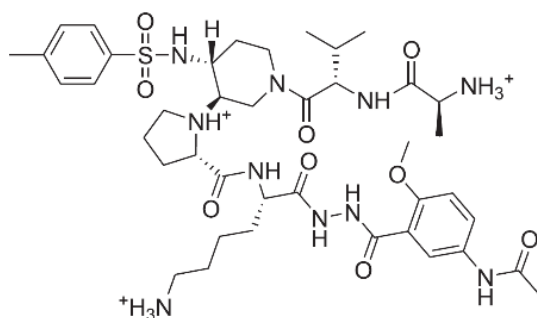


Figure 45 Structure of the smaller acyclic hairpin mimic displaying a lower peptidic character¹²²

α -helix foldamers:

As reported in chapter 1, recent evidence supports the cross link between the aggregation of hIAPP and A β_{1-42} , respectively involved in T2D and AD. In light with this theory, in collaboration with the team of Dr. Ludovic Maillard (Institut des Biomolécules Max Mousseron, Universités Montpellier, France), the research team recently explored the opportunity to stabilize the monomeric species of both amyloid peptides employing only one rationally designed inhibitor. The objective was to prevent the protein self-assembly trapping the monomer in its initial α -helix conformation preventing the conversion in β -sheet. This strategy, scarcely explored until now in the literature, has been pursued building a 9-helix foldamer based on the repetition of 6 units of γ -amino acid 4-amino(methyl)-1,3-thiazole-5-carboxylic acid (ATC).¹²³ The most active compound, the hexameric foldamer represented in figure 46, was bearing alternated 3 hydrophobic (*iso*-butyl) and 3 cationic (4-aminobutyl) side chains.¹²⁴

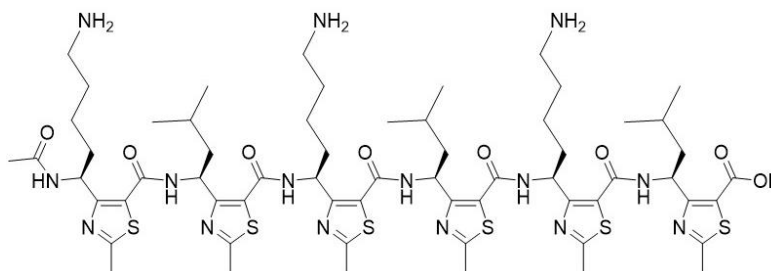


Figure 46 Structure of the most active foldamer 6-ATC¹²⁴

The fibrillization of A β_{1-42} was totally inhibited in the presence of the foldamer at foldamer/peptide ratio of 10/1 and was still significantly delayed at stoichiometric ratio. The effect on hIAPP was less marked; the hexameric foldamer significantly slowing down hIAPP fibrillization at the inhibitor/peptide ratio of 10/1 and having almost no activity at stoichiometric ratio. Further investigations by CE and MS revealed that the foldamer activity was mainly due to a stabilization of the monomeric form of both targets.

2.1.2 Biophysical evaluations

The design and the synthesis of bioactive compounds also require the capacity to test their activity. Through the time we employed several analytical techniques in order to evaluate our modulators. The biophysical evaluation that we performed range from the already available Thioflavin-T

fluorescence spectroscopy to novel more specific protocol for CE and IMS-MS, developed in collaboration with expert teams in our University.

Thioflavin-T fluorescence spectroscopy:

The Thioflavin-T fluorescence (ThT) spectroscopy can be considered as one of the oldest technique employed to evaluate the fibrillization of amyloid proteins.¹²⁵ This technique employs the ThT (Figure 47A) as fluorescent dye that structurally can be divided in two different fragments: one aniline core and a benzothiazole cycle. These two portions are bound by one single C-C covalent bond which is responsible of the change in fluorescence quantum yield. When ThT is solubilized alone, the fast rotation around this single bond quenches the excitation caused by the interaction with the photon. When the two fragments are constrained to lie on the same plane, the absence of rotation led to the fluorescence emission.^{126,127} The coplanarity of the two rings is normally obtained when ThT is intercalated in structures rich in β -sheets like the amyloid aggregates (large oligomers and fibrils) (Figure 47B), that is why ThT is the dye of first choice to monitor *in vitro* the aggregation process.

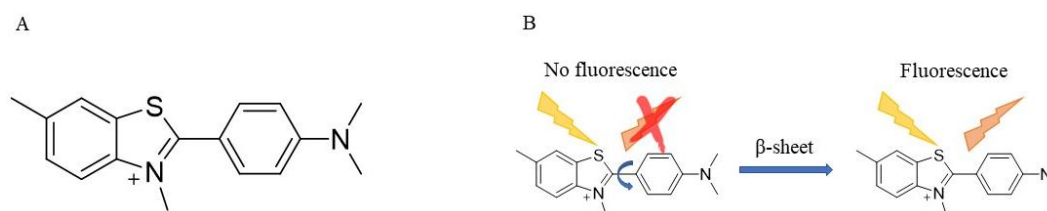


Figure 47 (A) Structure of Thioflavin-T dye, (B) Mechanism of its fluorescence emission

The aggregation process of hIAPP, followed by ThT spectroscopy, is characterized by a curve displaying the classical sigmoidal shape that can be divided into 3 different sections (Figure 48) (see paragraph 1.1.1 page 1):

- 1) The lag phase, which is quite short for hIAPP (about 2 h) and during this phase no fluorescence is detected because of the absence of β -sheets;
- 2) The elongation phase corresponding to a fast increasing of fluorescence which is detected because of the appearance of the β -sheet rich species;
- 3) The final plateau which is reached for hIAPP almost 10 h after the beginning of the aggregation.

Every time that an aggregation curve is collected either for hIAPP alone or in the presence of an inhibitor/modulator, it is possible to gather 2 important parameters:

- 1) F , representing the maximal value reached by the fluorescence at the plateau and it could be considered proportional to the quantity of formed fibrils;
- 2) $t_{1/2}$, which is the time needed to record the half of the maximal fluorescence reached at end of the experiment (Figure 48).

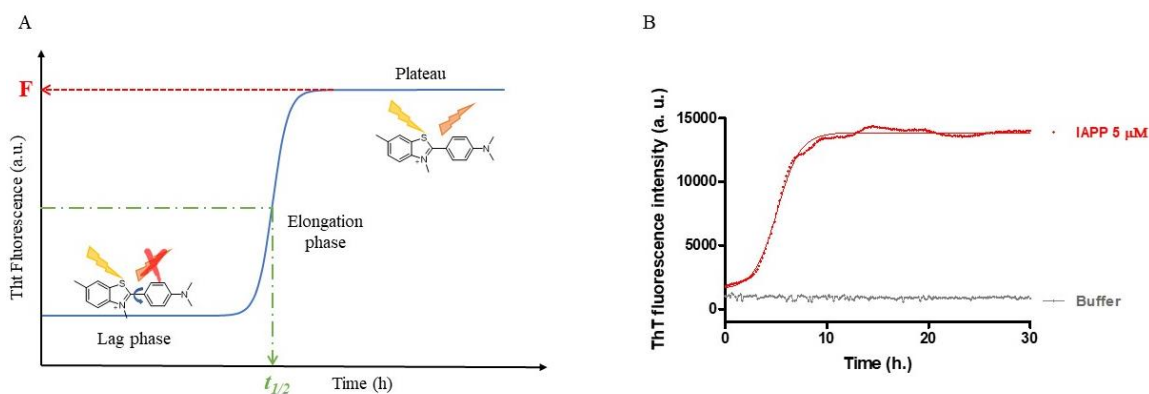


Figure 48(A) Drawn sigmoidal curve of hIAPP aggregation with graphical representation of F and $t_{1/2}$ (B) experimental curve of hIAPP aggregation (red) and the baseline of the buffer (grey).

Comparing F and $t_{1/2}$ values for hIAPP alone *versus* hIAPP co-incubated with an inhibitor, at several ratios, it is possible to build a rational scale of potency. Indeed, the more is potent an inhibitor, the lower is the ratio at which the inhibitory effect is observed. That is reflected in lower F value and in longer $t_{1/2}$ delay. Noteworthy from this experiment it is also possible to identify aggregation promoters, which could represent a valid strategy to prevent the formation and the toxicity of the oligomeric intermediate species.

Transmission electron microscopy (TEM)

TEM analysis is a complementary technique to ThT which provides images of the amyloid fibrillar network (Figure 49 A and B).^{121,122,124} TEM represents a powerful tool for the acquisition of highly resolved images of thin samples at high grade of magnification. Essentially TEM acquisition takes advantage of beam of a high energy electrons (up to 300kV) accelerated to almost the speed of the light to hit the samples. The impact of the beam on the surface of the sample results in a scattering

of the electrons, which are converted into an image through electromagnetic lens. Thanks to this process it is possible to observe objects in the scale of few Angström.¹²⁸

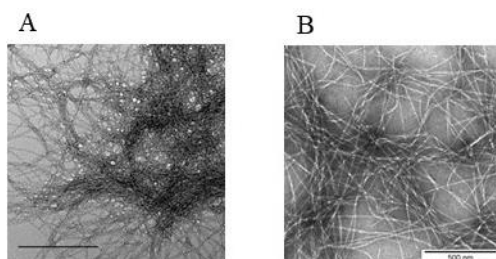


Figure 49 TEM images of hIAPP (A) and A β ₁₋₄₂ (B)

Membrane permeability assay

Because hIAPP has been demonstrated to be able to modify the membrane permeability through the formation of pores, it is essential to have a technique able to evaluate this permeability modification. The membrane permeability assay is an easy technique which provides information about the effect of hIAPP on the integrity of the membrane, that can be carried out in the presence of inhibitors.¹²⁹ This assay measures the increase of the fluorescence over the time in the presence of calcein (Figure 50), a dye able to self-quenches its fluorescence at high concentration (over 70 mM). This technique can be considered as a ThT test in which the dye is encapsulated in DOPC/DOPS membranes (LUVs) at self-quenching concentration (> 70 mM) and the enhancement of the fluorescence, over the time, is related to the membrane damage and not proportional to the formed fibrils. Indeed, the fluorescence is observed when hIAPP is added leading to the disruption of the membranes and, as a consequence, the leak of the calcein from LUVs. When the kinetics is completed, before to end the experiment, a detergent is added and an additional measure is collected, which correspond to the maximal leakage.

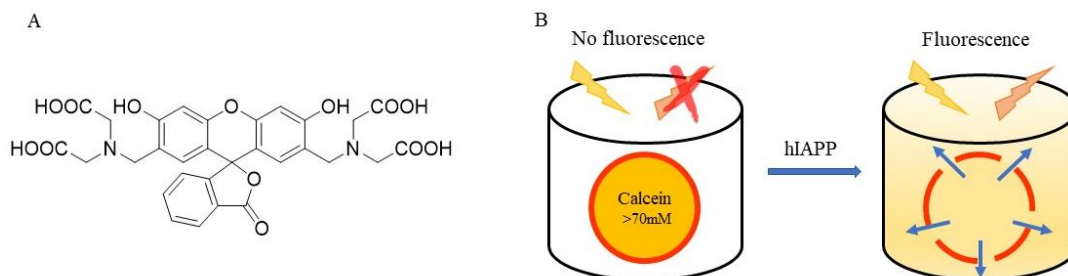


Figure 50 (A) Structure of calcein dye and (B) Scheme of its fluorescence mechanism

As for the ThT experiment, the curve of this leakage kinetics follows the classical “S” shape pattern and it is possible to gather the same two important parameters (Figure 51): F and $t_{1/2}$ (already explained for ThT).

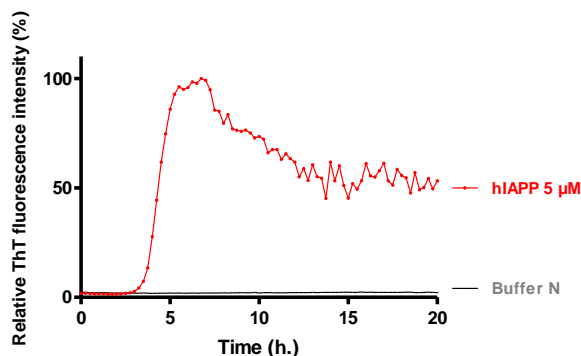


Figure 51 Example of membrane permeability assay curves for hIAPP (red) and the baseline of the buffer (grey).

Two other parameters that can be collected or calculated:

- 1) F_{100} , representing the maximal fluorescence collected only prior addition of detergent. It is function of the maximum quantity of dye that can leak from the LUVs;
- 2) L , being the fraction of dye released at time t .

Ion mobility spectroscopy-mass spectroscopy (IMS-MS):

The techniques described until now provide important information about the fibrillization and an overview of the aggregation process. However, nowadays it is widely proved that the most toxic species are the oligomers so, analytical techniques able to separate and characterize different oligomers are required. The separation performed with the ion mobility spectroscopy (IMS) coupled with the fine mass measure obtained by mass spectroscopy (MS) is of particular interest in the amyloid field because it provides a zoom insight of the early stages of the aggregation. The IMS-MS apparatus, which scheme is reported in figure 52, allows the separation and the identification of different oligomeric species from a complex mixture.¹³⁰

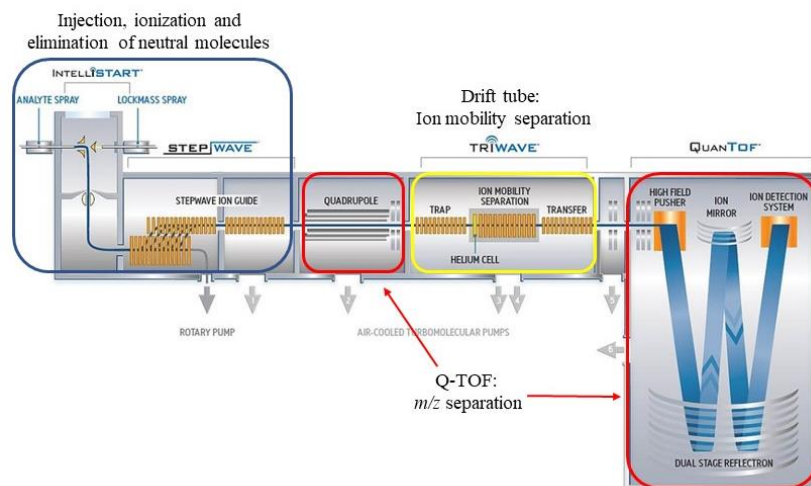


Figure 52 Scheme of the IMS-Q-TOF apparatus Synapt G2-Si (Waters)

The separation of the ionized oligomers, at the gaseous state, is based on their mobility in a drift tube when an electric field is applied. The ions, under the electric field influence, undergo to an acceleration that differs for each oligomeric species. The faster is the displacement, the smaller is the hydrodynamic volume and the higher is the charge density. Thus, after the separation in the drift tube, the different oligomeric species, up to the hexamer, are detected by mass spectrometry (Figure 53).¹³¹ IMS-MS is not only a powerful tool for the identification of the oligomeric species formed during hIAPP aggregation, indeed it is also possible to employ this technique to study how the inhibitors influence the oligomerization process just by analysing a co-incubated solution of hIAPP/inhibitors. Moreover, this technique being able to discriminate among different ions, it is thus possible to determine the ratio of the different monomeric/oligomeric formed species and to observe how an inhibitor is influencing this ratio.^{131–133} Complexes hIAPP/inhibitor can be also detected.¹²⁴

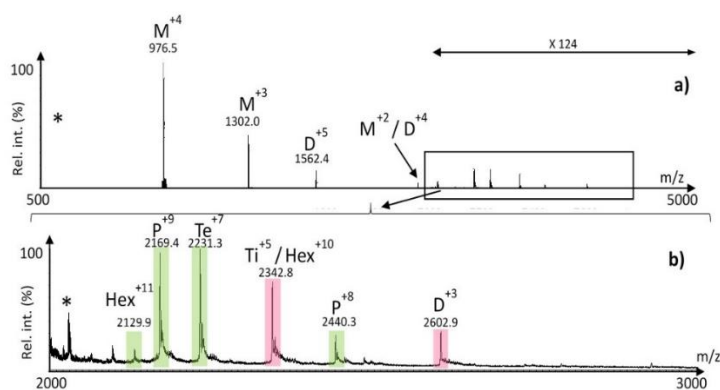


Figure 53 MS spectrum of hIAPP alone. **Legends:** M= hIAPP monomer, D = hIAPP dimer, Ti = hIAPP trimer, Te = hIAPP tetramer, P = hIAPP pentamer, Hex = hIAPP hexamer; * = contaminant

Capillary electrophoresis (CE):

Over the last years, the capillary electrophoresis has been successfully employed by us to study the oligomerization of amyloidogenic proteins like $A\beta_{1-42}$,^{117,121,122,134} however this powerful technique had not been yet widely employed to monitor hIAPP oligomerization. Thus, the lack of CE protocol for hIAPP oligomerization study led some of us to develop the first CE analysis able to monitor the *in vitro* hIAPP oligomerization over the time.^{131,135} Electrophoretic separations are conducted in a capillary (internal diameter 20-100 μm) filled with an electrolytic solution at constant ionic strength and pH (Figure 54) which allows the separation of analytes of several sizes and charges. The application of a potential difference, up to 30kV, between the two ends of the capillary generates a different migration for each analyte in solution, which are finally detected by a spectrophotometric detector (UV). The differential mobility under the effect of an electric field is directly related to the electroosmosis (depending on the analysis conditions) and to the electrophoretic migration (depending on the characteristics of the analytes).¹³⁶

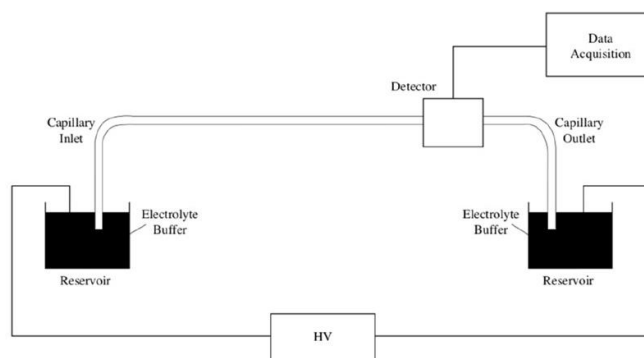


Figure 54 Scheme of a CE apparatus

The typical electrophoretic profile of hIAPP over the time is presented in figure 55. Over 20 hours of experiment, 3 different peaks of soluble species are detected. The intensity of peaks 1 (migrating with the electroosmotic flow) and 2 progressively increases because of the advancement of the oligomerization. The characterization of these peaks, made through a combination of membrane filtration and Capillary electrophoresis mass, revealed a composition of mainly large oligomeric species heavier than 100 kDa, which correspond to species up to the 25-mers. In contrast the intensity of peak 3, mainly composed of monomers with a small amount of dimers and trimers, gradually decreases until almost complete disappearance after 10 hours.¹³⁵

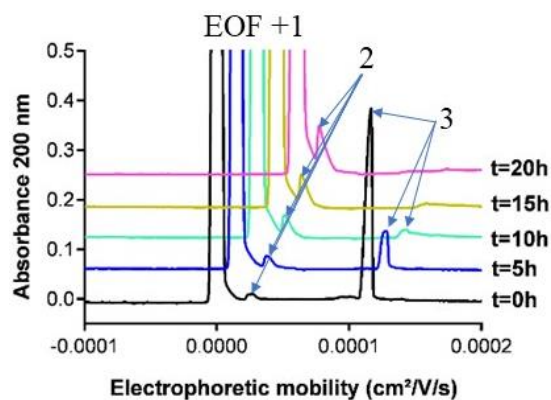


Figure 55 hIAPP electropherogram. **Legend:** EOF = electroosmotic flow; 1 and 2 = oligomers up to 25-mers; 3 monomers

This new and very recent CE methodology has already been successfully employed to evaluate the impact of the helical foldamers (see paragraph 2.1.1 page 47) on the early stages of the aggregation process.¹²⁴

Cell viability assay:

The biophysical evaluations can be completed with a cell viability assay that assesses the metabolic activity of the cells. This test is used to evaluate the ability of the inhibitors to reduce hIAPP toxicity on rat INS-1 cells⁵⁴ (provided by Professor Movassat and Dr. Tourrel-Cuzin, Equipe de Biologie et Pathologie du Pancréas Endocrine, UMR 8251, Université PARIS-DIDEROT). In this test, the viability of the INS-1 cells is detected by incubating the cells with the yellow MTT tetrazolium salt (3-(4,5-dimethylthiazol-2-yl)-2,5-diphenyltetrazolium bromide), which is internalized and reduced by a mitochondrial reductase in its insoluble purple metabolite formazan. At the end of the experiment, the formazan is solubilized and the absorbance values are collected at 570 nm. In accordance with the Lambert-Beer law, the absorbance is directly proportional to the concentration of the formazan, so it is directly proportional to the number of the viable cells. By comparison of the gathered values of cells incubated alone and cells incubated in the presence of hIAPP or hIAPP/inhibitor it is possible to estimate the inhibitors protective effect (Figure 56).¹³⁷⁻

139

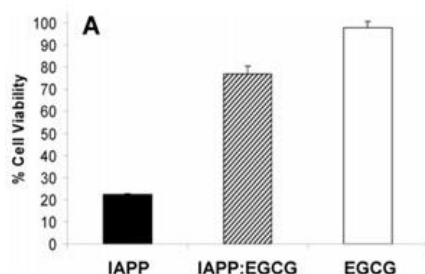


Figure 56 EGCG (30 μ M) restore INS-1 cells viability in the presence of hIAPP (30 μ M)¹³⁹

The employment of all these complementary techniques allows us to study the entire aggregation process of hIAPP protein in the presence of our inhibitors. Thioflavin-T fluorescence (ThT) spectroscopy represents the easiest analysis suitable to study hIAPP aggregation kinetics and the fastest methodology to screen a series of compounds. However, it does not provide information about the fibrils shape and the density of the fibrillar network, gathered acquiring TEM images. Even though these two techniques provide lots of useful information, to go deeper it is necessary to employ more sophisticated analyses. The capillary electrophoresis allows to follow the aggregation kinetics monitoring the monomeric/oligomeric species concentration over the time. However to know more about the formed species it is necessary to rely on the ion mobility

spectroscopy-mass spectroscopy, which is able to discriminate between different non covalent complexes (oligomers). Finally, the membrane permeability assay provides preliminary information about the protective effect of our compounds on the cellular membranes. In order to completely evaluate the ability of the inhibitors to reduce hIAPP toxicity it is necessary to perform the cell viability assay on INS-1 cells.

2.1.3 Conformational studies

As previously reported in this chapter, our team is specialized in the design of pre-structured PPIs inhibitors involved in amyloidoses. In the light of the expertise of the team, during my PhD, all the final and active synthesized compounds have been conformationally characterized in order to determine their structuration. The conformational studies have been planned and carried out employing analytical techniques such as circular dichroism, nuclear magnetic resonance and molecular dynamics.

Circular dichroism (CD):

CD employs polarized light to provide structural information about solubilized peptides or proteins. This technique employs a planar polarized light, which can be decomposed in two circularly polarized components of equal magnitude but of opposite direction of rotation (L and R). When the polarized light is passed through a sample, three different situations can occur:

- 1) L and R are not absorbed: their recombination results in the original planarly polarized light (Figure 57A);
- 2) L and R are absorbed in equal extent: same results of point 1;
- 3) L and R are absorbed not in equal extent: their recombination results in an elliptically polarized light, generating a CD signal. This situation happens when the sample is chiral (Figure 57B).

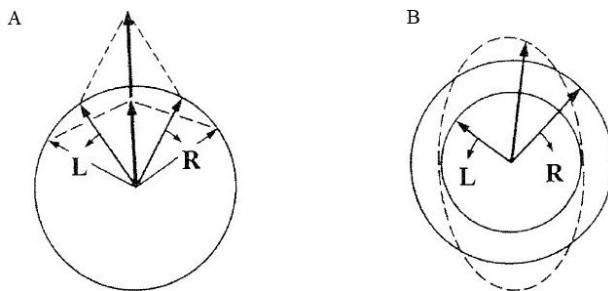


Figure 57 Origin of the CD effect¹⁴⁰

Since peptides and proteins are rich in chromophores allowing them to absorb the polarized light, their CD signals can provide useful information about the secondary structure. Because a particular secondary structure (e.g. α -helix or β -sheet) is characterized by a peculiar CD spectra (Figure 58), it is possible to deduce the secondary structure of a given peptide/protein from its CD spectrum. Moreover, when a peptide presents more than one secondary structure, it is possible to estimate the % of each one.¹⁴⁰

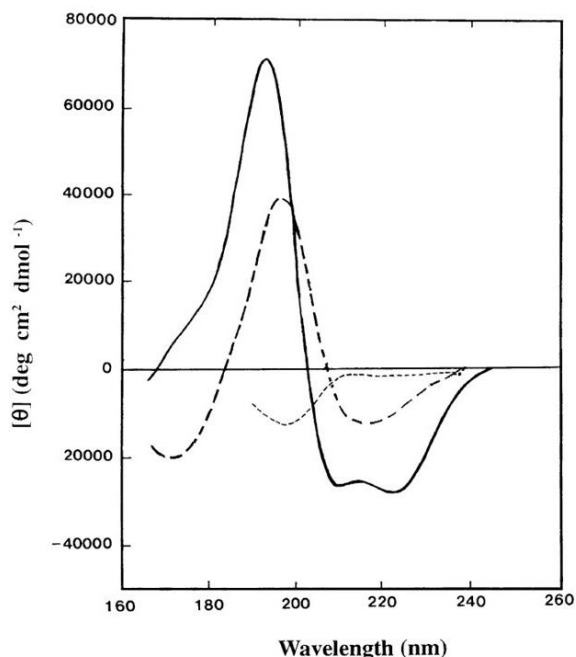


Figure 58 Examples of CD spectra for: α -helix (solid line), anti-parallel β -sheet (long dashed line) and random coil (short dashed line). Approximative value for: α -helix (Min = 208, 222 nm and Max = 192 nm) β -sheet (Min = 216 nm and Max = 195 nm)¹⁴⁰

Nuclear magnetic resonance (NMR):

The nuclear magnetic resonance spectroscopy is a powerful analytical technique that over the last decades has become the first choice, as alternative to the crystallography, in the determination of macromolecules three-dimensional structure at the atomic level. In contrast with crystallography, which provides essentially a photography of a “frozen” structure, liquid-state NMR provides dynamic structural information.

Nowadays, thanks to the development of more and more potent NMR spectrometers coupled with the development of new acquisition sequences, it is even possible to study entire proteins and go further inside their structures. Indeed, the secondary structure of specific small segment in a polypeptide or protein can be determined at atomic level.

In the conformational studies, the structural information source is given by the chemical shift and by the magnetization transfer between pairs of protons which can be through-bond (scalar or *J coupling*) or through-space (Nuclear Overhauser Effect *NOE*).

Through-bond magnetization transfer: J coupling

Given a system of two protons linked through three bonds, it is possible to measure the coupling constant (3J) between them, which depends on the dihedral angle Φ defined by the rotation around the middle bond of the system. It has been demonstrated that between the 3J magnitude and the angle Φ there is a correlation which is represented by the Karplus curve (Figure 59).

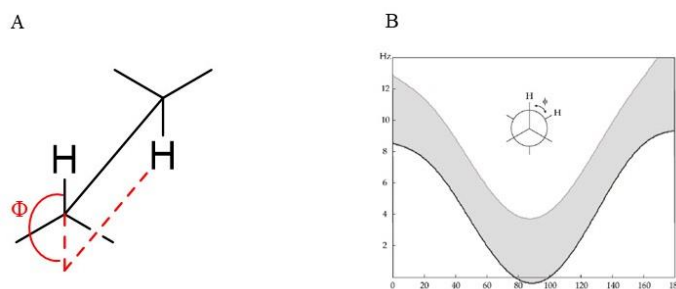


Figure 59 (A) Schematic representation of Φ -angle for a generic structure and (B) generic representation of a Karplus curve

In the case of a peptide, the main through-bond structural information comes from the correlation between the 3J value measured among the H^α and its H^N (Figure 60) in the backbone and their Φ -angle. Indeed, it is reported that for a peptide structured in α -helix, in which the Φ -angle is in the range of -60° , the coupling constant is around 4 Hz; while for a β -sheet, which angle is around -120° , the J coupling constant is between 8 Hz and 12 Hz.¹⁴¹



Figure 60 General peptide structure in which the atoms and the bonds involved in the 3J have been highlighted

Chemical shift analysis

The NMR techniques provide also useful information not only through the magnetization transfer but also through the analysis of the proton's chemical shifts. Over the years, different correlations between chemical shift and secondary structures have been identified. First of them is the correlation between the H^α chemical shift of an amino acid and the secondary structure. Considering a generic amino acid, inserted in a generic amino acidic sequence, there are marked

differences in its H^{α} chemical shift linked to the secondary structure. On this evidence Wishart *et al.* have introduced a simple methodology for the determination of the secondary structures employing the chemical shift deviations (CSD). For a given atom in an amino acid, the chemical shift deviation is defined as the difference between the experimental chemical shift and the corresponding reported random coil value. Despite the H^{α} CSD is the most employed, it is also possible to use the CSD of ^{13}CO , $^{13}\text{C}^{\alpha}$ and $^{13}\text{C}^{\beta}$ (Table 1).¹⁴²

Resonance	α -Helix	β -Sheet
H^{α}	Upfield (-0.38)	Downfield (+0.38)
H^{β}	0	Upfield (-0.1)
H^{N}	Upfield (-0.19)	Downfield (+0.29)
C^{α}	Downfield (+2.6)	Upfield (-1.4)
C^{β}	Upfield (-0.4)	Downfield (+2.2)
CO	Downfield (+1.7)	Upfield (-1.4)
N	Upfield (-1.7)	Downfield (+1.2)

Table 1 Average secondary structure shifts relative to random coil values

The second correlation between the chemical shift and the secondary structure is the one that involves the amide proton chemical shift (H^{N}). From the H^{N} chemical shift it is possible to establish which amide protons are engaged in hydrogen bonds. When a peptide is solubilized in aqueous or alcoholic solvent, the H^{N} chemical shifts typically show a marked temperature dependency, however when the H^{N} are engaged in a hydrogen bonds this dependence is reduced ($\Delta\delta_{\text{NH}}/\Delta T > -4.5$ ppb K^{-1}).¹⁴² The temperature dependency is useful to establish which amide protons are involved in hydrogen bond, nevertheless it does not provide a distinction between inter and intramolecular hydrogen bond. The distinction is achieved by acquisition of spectrum at different concentrations (usually one more and one less concentrated than the one used for attribution) observing the changes in the chemical shift and linewidth.

Through-space magnetization transfer: NOE

Other additional information for the conformational study comes from the magnetization transfer through-space. Given two nearby protons in the space, there is a through-space dipole-dipole coupling between them called *NOE*. It is known that a correlation between the intensity of the NOE and the distance between the two considered protons exists. More in detail, the NOE intensity is inversely proportional to the sixth power of the distance, thus the lower is the distance, the higher is the NOE intensity. Considering that the NOE is usually observed for protons separated by a

distance lower than 5 Å, it is a powerful tool for the measurement of the distance of two nuclei in peptides/proteins that provides information about their secondary structures.

Molecular dynamics (MD):

The β -hairpin mimics, prepared during my PhD project and studied by NMR techniques, were often found to be in equilibrium between two major conformers. The conformational analysis of such conformers was a real challenge. Sometimes, the small differences in the chemical shift between the two conformers made almost impossible an univocal interpretation of the NOE signals; for that reason we have also used molecular modelling for the secondary structure attribution.

Molecular modelling of the inhibitors developed during my PhD project was performed with techniques of molecular dynamics, a powerful tool that allows to follow the evolution of a molecular system, under influence of kinetics energy, over the time.

In molecular dynamics, molecules are considered as an ensemble of spheres (atoms) connected by springs (bonds) and their motion is modelled using classical mechanics. In a simple way, molecular dynamics consists of a series of successive configurations (trajectory) generated by the solution of the Newtonian equation of the motion at regular intervals. The behaviour of interacting atoms is governed by a set of rules imposed by the force field.¹⁴³

2.2 Objective of the thesis

For several years, our team has been involved in the development of compounds able to inhibit the PPIs, focusing on the PPIs involved in the amyloidoses. My PhD research project is part of a larger work which aims to develop new ligands able to interact with hIAPP in order to modulate its aggregation process.

As previously reported in the introduction, the aggregation process of peptides or proteins is a common feature of all the amyloidoses. Despite differences in the amyloidogenic sequences of peptides involved in the different pathologies, their aggregation follows a common process. The strategy pursued in my project is similar to that employed for A β ₁₋₄₂ peptide (described in part 2.1.1) synthesizing pre-structured inhibitors rationally designed to recognize and interfere with the aggregation of the amyloid target.

The similarity between A β ₁₋₄₂ and hIAPP aggregation and toxicity^{12,101} and the actual evidence about their cross-amyloid interaction^{55,56} led us to take advantage of our best class of A β ₁₋₄₂ inhibitors,^{121,122} in order to conceive effective β -hairpin mimics able to selectively target hIAPP.

At the beginning of my PhD we postulated few important questions to which we would like to answer with the research work developed in these 3 years:

- Are the β -hairpin mimics, rationally designed suitable for the inhibition of hIAPP aggregation?
- After the development of the first generation of peptidic inhibitors, will it be possible to reduce the peptidic character without affecting their activity?
- How does the addition of fluorinated groups affect the pre-structuration and activity of the hairpins?

Moreover, being conscious of the limited time of the PhD, we postulated two additional questions to which we would like to start to answer:

- Could the peptidomimetic molecules developed during my PhD project represent a potential T2D treatment?
- Could these hairpins, especially the fluorinated ones, be innovative investigation/diagnostic tools?

2.2.1 General structure of the hairpins

Keeping in mind the questions we wanted to answer, while designing the β -hairpin mimics we defined few crucial points that must be respected as much as possible:

- The β -turn inducer structure must induce a β -hairpin conformation and meanwhile ensure enough flexibility to promote inhibitor/hIAPP interaction;
- The two arms of the hairpins should be responsible of (1) recognition and binding to hIAPP target (self-recognition element or SRE) and (2) impeach intramolecular interactions and intermolecular interactions (see paragraph 1.3.5 page 22) between hIAPP peptides (blocking sequence), in order to block hIAPP aggregation (Figure 61)
- The evolution of the hairpins should lead to compounds with a reduced peptidic character;

- The hairpin design should allow easy introduction of fluorine atoms in different positions;
- An optimal hydrophilic/lipophilic equilibrium is necessary to ensure β -hairpin structuration and interaction with hIAPP. In addition, it is mandatory for the solubility in a medium compatible with the biological environment, in order to allow biophysical evaluations.

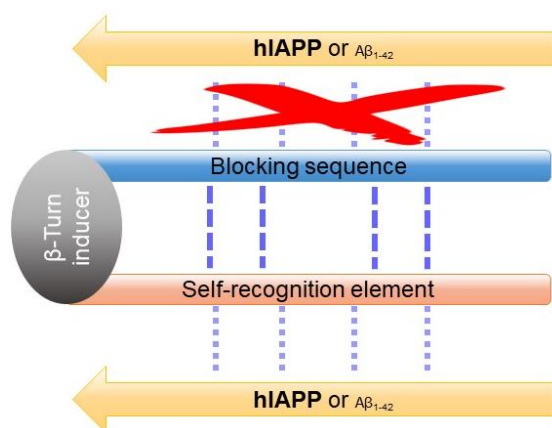


Figure 61 General scheme representing the design of our inhibitors

2.2.2 Overview of the investigated structures

All the inhibitors reported in this manuscript are based on a piperidine-pyrrolidine semirigid β -turn inducer. In some of them the scaffold is exactly the same as the one already successfully employed for our $A\beta_{1-42}$ inhibitors, while in other cases it carries some modifications which will be explained case by case.

In order to be clear as much as possible, we decided to divide the presentation of the work in 3 different chapters:

- 1) Non-fluorinated β -hairpin mimics: in this first macro-chapter the design, the synthesis and the evaluation of: (1) hairpins bearing two peptidic arms (pentapeptide and tripeptide) and (2) hairpin bearing one di-aza-tripeptide arm will be presented (Figure 62);
- 2) Fluorinated β -hairpin mimics: in this second part the importance of fluorine in medicinal chemistry will be briefly presented. Then the design, the synthesis and the evaluation of either hairpins bearing fluorinated peptidomimetic arms (F-benzhydrazide or *N*-

difluoromethyl-triazole) or hairpins fluorinated on the β -turn inducer will be discussed (Figure 62).

- 3) The last chapter will include an overall conclusion of the work and the perspectives for the future.

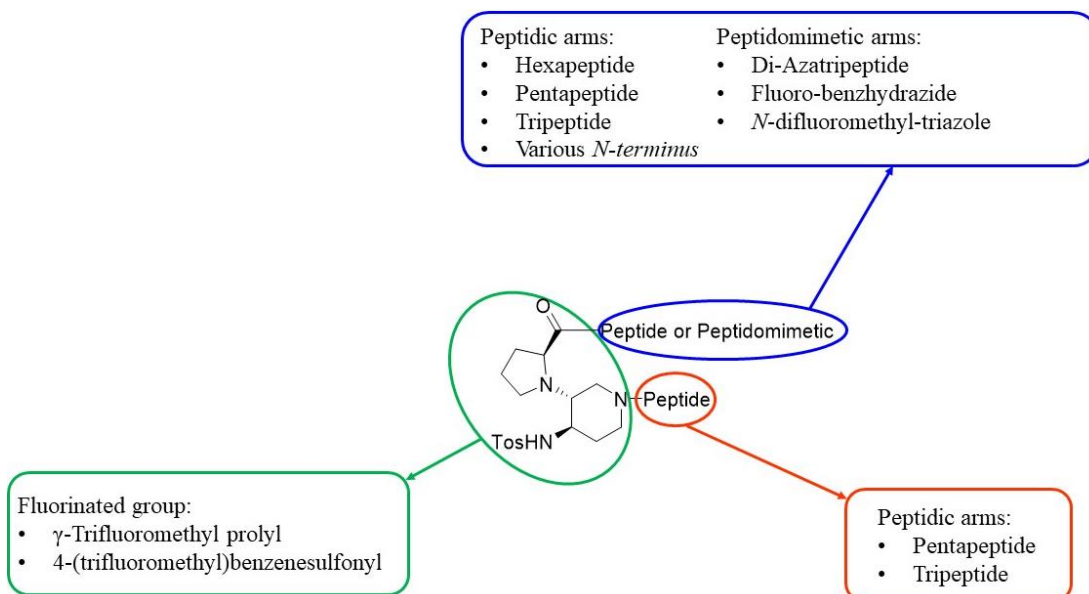


Figure 62 Overview of the structures presented in chapter 3 and 4

Chapter 3

Non-fluorinated β -hairpin mimics structure: β -hairpin mimics as protein-protein interaction inhibitors in T2D

3.1 Peptidic and aza-peptidomimetic β -hairpins

In the previous chapter 2, we explained that to target hIAPP aggregation we designed compounds taking advantage of the best class of $A\beta_{1-42}$ inhibitors (see sections 2.2.1 and 2.2.2 page 61-62). Thus, we developed our molecules on the piperidine-pyrrolidine β -turn inducer which is the core of the most active β -hairpins toward the β amyloid peptide aggregation.^{121,122} In chapter 3, we are reporting the design, the synthesis and the evaluation of non-fluorinated β -hairpin mimics bearing two peptidic arms or one peptidic arm and one di-aza-tripeptide arm.

3.1.1 Choice of the sequences

As for $A\beta_{1-42}$, the first step was to design and synthesize compounds whose arms were composed by peptides derived directly from hIAPP primary sequence. Since the selectivity was one of the primary objective, the selection of an appropriate SRE was mandatory. So, the choice turned on the amyloidogenic sequence N₂₂FGAIL₂₇ because this region is strongly involved in hIAPP aggregation process (see chapter 1.3.5) and because this sequence has been reported to be able to promote hIAPP fibrillization⁹⁶ and to inhibit its aggregation when inserted in a structure able to prevent the interactions between two hIAPP peptides.¹⁰⁶ Once chosen the SRE, the second step was the selection of the complementary sequence, which should be able to interact with the sequence NFGAIL and also to mimic and recognize hIAPP. Thus, as for the hairpins active on $A\beta_{1-42}$, aggregation, at first our research group opted for the peptidic sequence which was in face of the amyloidogenic one.¹²¹ As previously reported in chapter 1 (see paragraph 1.3.5 page 22), several models of hIAPP structures have been reported. Although these models are very close in amyloidogenic sequence, they differ significantly in complementary sequences. Faustine Bizet, in her PhD,¹⁴⁴ presented three different structures whose arms have been designed in accordance with some of the models reported in the literature.

More in detail, the first two structures **3.0** and **3.1** (Figure 63) were based on the models of the monomeric form reported by Mirecka *et al.*⁷¹ (sequences involved in the β -sheet: N₂₂FGAIL₂₇ and A₈TQRLANFLVH₁₈) and Kajava *et al.*⁶⁸ (sequences involved in the β -sheet: N₂₂FGAIL₂₇ and A₁₃NFLVH₁₈, see fig. 22, chapter 1), whose facing sequence were fitting with the experimental model described by Andretto *et al.*¹⁰⁹ (sequences involved in the β -sheet: N₂₂FGAILS₂₈ and L₁₂ANFLVH₁₈). Compounds **3.0** and **3.1** differed in the positioning of the arms. Indeed, in the case of **3.0**, the amyloidogenic sequence (NFGAIL) was linked to the piperidine ring and the facing sequence VLFNA was linked to the carboxylic group of proline; while **3.1** presented the amyloidogenic sequence on the proline and the VLFNA on the piperidine ring. In order to maintain the same *N* to *C* term direction of hIAPP, the peptidic sequences sense were inverted in the case of **3.1**.¹⁴⁴

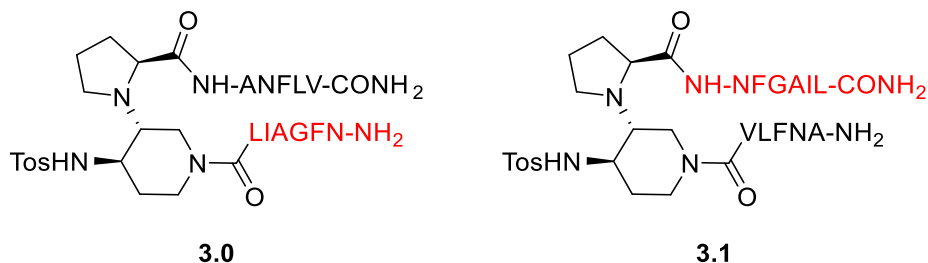


Figure 63 Structures of the compounds **3.0** (left) and **3.1** (right) reported by Bizet.¹⁴⁴ In red the SRE

The third compound **3.2** (Figure 64), which presented the amyloidogenic sequence FGAIL on the proline and the complementary sequence SHVLF on the piperidine ring, was designed on the *in silico* models reported by Zheng *et al.*⁷⁵ (sequences involved in the β -sheet: N₂₂FGAIL₂₇ and F₁₅LVHSS₂₀), Wu *et al.*⁷⁶ (sequences involved in the β -sheet: F₂₃GAILSSTNVG₃₃ and R₁₁LANFLVHS₁₉) and Eisenberg *et al.*⁷³ (sequences involved in the β -sheet: F₂₃GAILSSTNV₃₂ and L₁₂ANFLVH₁₈). A comparison with the previous structures **3.0** and **3.1** highlighted the shift of the sequences faced to the amyloidogenic one (2 to 3 residues). The shift allowed to study how the alignment of the arms could influence the activity of the compounds.

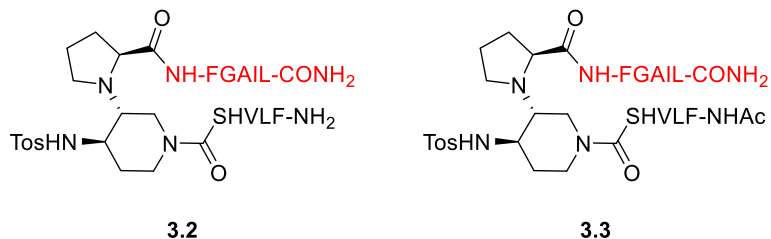


Figure 64 Structures of compounds **3.2** (left)¹⁴⁴ and **3.3** (right). In red the SRE

The presence of a C-terminal amide in these three compounds was justified because the carboxylic group, at physiological pH, would be under the form of carboxylate reducing the passive absorbance through membranes. Moreover, hIAPP does not present basic residues in or close to the amyloidogenic sequences with which the carboxylic group would engage interesting interactions. Last but not least, an amide could mimic the peptidic bond and *in vivo* it would be more stable than an ester.

Since hIAPP does not present acidic residue with which the terminal amine of the inhibitor would establish interesting ionic interactions, during my PhD, in order to determine if the terminal amine was necessary for the activity, we planned the synthesis of the *N*-acetyl derivative **3.3** (Figure 64) starting from the most active compound of the series. All the compounds bearing the long peptidic arms **3.0-3.3** were prepared in collaboration with the team of Prof. Maria Luisa Gelmi (Istituto A. Marchesini, Università degli Studi di Milano).

Moreover, one of the main objective of my work being the synthesis of compounds with a lower peptidic character in order to improve their metabolic stability and druggability, we decided to reduce the length of the peptidic arms. Because the sequences A₂₅IL₂₇ and F₁₅LV₁₇ were always present in the compounds **3.0-3.3** bearing the long peptidic arms, we exploited them to design smaller molecules **3.4**, **3.5**, **3.6** and **3.7** (Figure 65). In all these compounds the SRE AIL was linked to the piperidine ring (*N*-terminus of the hairpin) and the complementary sequence FLV was linked to the pyrrolidine ring (C-terminus of the hairpin). The terminal NH₂ was either free or protected by 3 different groups: Boc, acetyl or trifluoroacetyl. As for compounds **3.2**, the free amine was selected with the aim to prepare compound that is soluble as much as possible. As we observed that the acetyl derivative **3.3** was also effective as hIAPP aggregation inhibitor, we decided to prepare the acetyl and trifluoroacetyl derivatives in order to study if the same behavior was maintained also by the smaller compounds. Moreover, the trifluoroacetyl group was selected

to examine how the presence of the fluorine could influence the activity thanks to its unique characteristics (see chapter 4, paragraph 4.1, page 71).

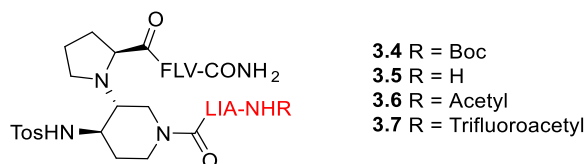


Figure 65 Structures of the designed compounds with shorter peptidic arms. In red the SRE.

In light with the reduction of the peptidic character, the last compound presented in this chapter is the one whose peptidic blocking sequence Phe-Leu-Val-CONH₂ (FLVCONH₂) has been replaced by the di-aza-tripeptide Phe-azaLeu-azaValCOCH₃ (FaFaV-Ac) in compound **3.8** (Figure 66). In this compound, mainly developed by Faustine Bizet,¹⁴⁴ phenylalanine was maintained while leucine and valine amide of the blocking sequence (C-terminal arm) have been replaced by the corresponding aza-amino acids. This choice was taken in order to simplify the synthesis as Faustine Bizet, synthesizing other di-azatripeptides,¹⁴⁴ noticed a certain grade of difficulty in the coupling between proline's carboxylic group and the hydrazine moiety (bulkiness and low nucleophilicity of the substituted hydrazino compounds).

The aza-amino acids are amino acids whose CH_α have been substituted by nitrogen atoms. This substitution, that is gaining great importance in medicinal chemistry,^{145–148} could provide particular conformational features due to the loss of stereogenicity and the reduction of flexibility.^{149,150} Moreover, maintaining the natural later chain, the introduction of aza-amino acids allows to preserve the selectivity. In addition, the formed urea bond reduces the proteolytic degradation enhancing the metabolic stability.^{151,152} At the best of our knowledge only few groups,^{153–156} including us,^{146,150,157} have reported the synthesis of peptides in which two or more consecutive aza-amino acids were inserted. Thus, we decided to exploit this scarcely explored structure to design innovative inhibitors, beginning from the di-aza amino acid unit.

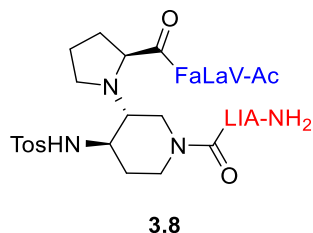
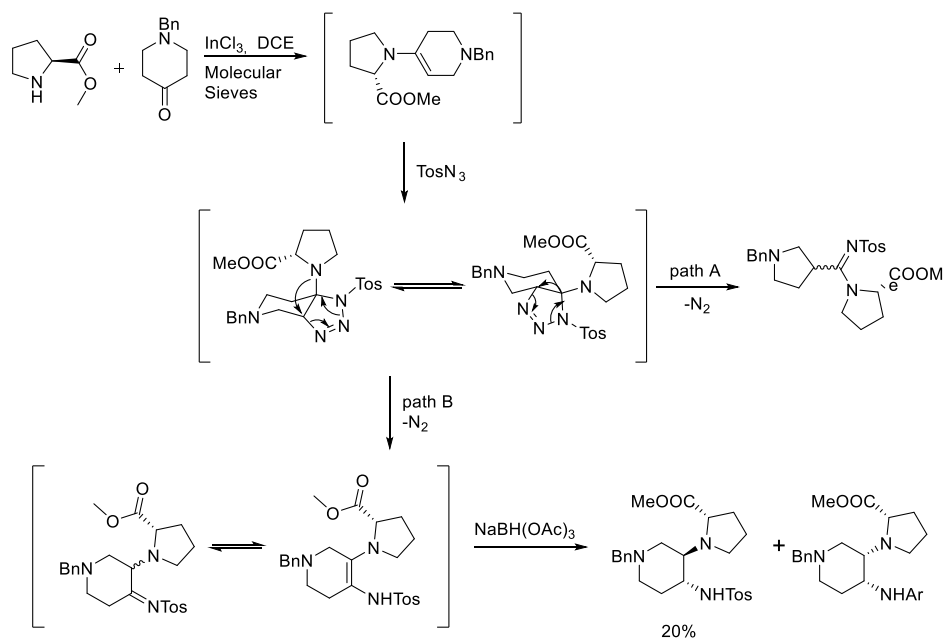


Figure 66 Structure of the designed compound **3.8** bearing the di-aza-tripeptide FaLaV.¹⁴⁴ In red the SRE

The following pages, that describe all the work about the designed compounds **3.0-3.8**, are a copy of the draft of the paper that is currently in preparation and will be submitted at the end of this year in the special issue : Amyloid-Membrane Interactions in Protein Misfolding Disorders: from Basic Mechanisms to Therapy, hosted by Dr(s) Neville Vassallo, Celine Galvagnion, Eva Y. Chi in Frontiers in Cell and Developmental Biology – section Molecular Medicine (under invitation).

3.1.2 β -Turn inducer synthesis

The tosyl β -turn inducer was produced in 20% yield starting from the commercially available material (Scheme 1). More in detail, one equivalent of proline methyl ester hydrochloride was suspended in 1,2-dichloroethane and the free secondary amine was obtained by addition of an equimolar amount of TEA. Subsequently, one equivalent of *N*-benzyl-piperidone was added followed by molecular sieves and 10% of indium trichloride. When the proline was completely consumed, the reaction was cooled down at 0° C and a solution of Tosyl azide (prepared in accordance with the literature)¹²⁰, was added dropwise. After one hour, sodium triacetoxy borohydride was added to the mixture in order to reduce the formed dienamine to afford the tosyl scaffold.



Scheme 1 Multicomponent synthesis of the Tosyl scaffold

3.1.3 Draft paper

β -Hairpin peptide mimics decrease human Islet Amyloid Polypeptide (hIAPP) Aggregation

Jacopo Lesma,¹ Faustine Bizet,¹ Corentin Berardet,^{1,2} Nicolo Tonali,¹ Sara Pellegrino,³ Myriam Taverna,² Lucie Khemtemourian,⁴ Jean-Louis Soulier,¹ Carine van Heijenoort,⁵ Frédéric Halgand,⁶ Tap Ha-Duong,¹ Julia Kaffy,^{*1} and Sandrine Ongeri ^{*1}

¹BioCIS, Université Paris-Saclay, CNRS, 92290 Châtenay-Malabry, France.

²Université Paris Saclay, CNRS, Institut Galien de Paris Sud, 92290 Châtenay-Malabry, France

³ DISFARM-Sez. Chimica Generale e Organica “A. Marchesini”, Università degli Studi di Milano, via Venezian 21, 20133 Milano, Italy

⁴ Institute of Chemistry & Biology of Membranes & Nanoobjects (CBMN), CNRS UMR 5248, Université de Bordeaux, Institut Polytechnique Bordeaux, 33600 Pessac, France.

⁵ Université Paris Saclay, CNRS, ICSN, Equipe Biologie et Chimie Structurales, Dept Chimie et Biologie Structurales et Analytiques, 91190 Gif sur Yvette France.

⁶ Université Paris-Saclay, CNRS, Institut de Chimie Physique, 91405, Orsay, France.

*** Correspondence:**

sandrine.ongeri@universite-paris-saclay.fr and julia.kaffy@universite-paris-saclay.fr

Keywords: amyloid, type 2 Diabetes, peptidomimetics, β -Hairpin, oligomerization, fibrillization

Introduction

Over the past decades, the field of amyloidosis research has gained increasing interest due to its relationship to at least 20 serious human diseases. Most of them are related to aging and they are all related to improper folding and assembly of proteins into various aggregate structures which can interact with membranes and lead to the death of cells (Ke et al., 2017; Ke et al., 2020). Among the pathologies most in the spotlight are neurodegenerative diseases like Alzheimer’s Disease (AD), Parkinson’s Disease (PD), Huntington’s Disease, Prion Disease or Amyotrophic Lateral Sclerosis (ALS), nevertheless other organs can be affected such as pancreas in Type 2 Diabetes (T2D). Type 2 diabetes (T2D) is a major public health issue, affecting nearly 420 million people in the world, value that is expected to increase to 600 million in 2045 (Chaundury et al., 2017). The actual treatments aim to reduce hyperglycemia, but the disease continues to progress, and the loss of function and the death of pancreatic β -cells requires a gradual transition to insulin therapy. Although the mechanism responsible for β -cell dysfunction and death is partially understood, amyloid deposits of human islet amyloid polypeptide (hIAPP, also known as amylin) are found in more than 95% of T2D patients, and more and more findings suggest an important role in pancreatic damage of the accumulation of misfolded β -sheet rich aggregates of hIAPP in the islets of Langerhans (Jeong et al., 2015; Akter et al., 2016; Kiriya et al., 2018). The cell toxicity is closely linked to membrane disruption characterized by pore formation and aggregate formation-

induced detergent-like mechanism (Brender et al., 2012; Terawaka et al., 2018; Bram et al., 2014). Cardiovascular complications affect around 65% of T2D patients despite medication, and it has been recently shown that glucose and LDL interact with hIAPP, resulting in β -sheet rich oligomers with increased β -cell toxicity and hemolytic activity suggesting a direct link between T2D and cardiovascular diseases (Rodriguez Camargo et al., 2018). Furthermore, T2D has been acknowledged as a risk factor for Alzheimer's disease (AD) and cross-amyloid interactions between hIAPP and amyloid- β peptide ($A\beta_{1-42}$) have been recently shown as playing a critical role in AD due to an increased toxicity of $A\beta$ -IAPP hetero-oligomerization on neuronal cell membranes (Roriz-Filho et al., 2009; Bharadwaj et al., 2020).

Thus, inhibiting the aggregation of hIAPP in order to prevent both the presence of large aggregates but also of highly toxic soluble oligomers has proven to be a therapeutic avenue to be further explored to find a viable therapeutic strategy against T2D, and also to decrease the risk factor of cardiovascular complications and AD in T2D patients (Kiriya et al., 2018; Bram et al., 2014; Brender et al., 2012).

Much fewer compounds have been reported as efficient inhibitors of hIAPP aggregation compared to $A\beta_{1-42}$ inhibitors for AD. Small molecules such as polyphenols (Pithadia et al. 2016), and few peptide derivatives (Armiento et al., 2020; Yan et al., 2013; Gilead et al., 2004; Paul et al., 2017; Cheng et al., 2012) have been mainly reported.

We recently demonstrated that peptide derivatives mimicking acyclic β -hairpin structures were able to decrease $A\beta_{1-42}$ aggregation and to preserve $A\beta_{1-42}$ monomers (Pellegrino et al., 2017; Tonali et al., 2018). These compounds were built on a piperidine-pyrrolidine β -turn inducer and due to the fact that their design was based on self-recognition elements (SRE), i.e. selected sequences of $A\beta_{1-42}$, they were selective for $A\beta_{1-42}$ and not active on hIAPP aggregation. The next step is to demonstrate that this strategy can be generalized and applied to the inhibition of the aggregation of other amyloid proteins. This work presents the synthesis and biophysical evaluations of new β -hairpin mimics designed to inhibit hIAPP aggregation. SRE based on hIAPP were selected and new compounds bearing peptidic sequences were proposed in combination with a novel strategy to decrease the peptidic character using α /aza/aza/ pseudotriptides.

RESULTS

Design

Our choice, for the first SRE to link to the piperidine-pyrrolidine β -turn inducer, turned on the amyloidogenic sequence $N_{22}FGAIL_{27}$ because this region is strongly involved in hIAPP aggregation process and in the folding of hIAPP described in experimental and in silico models of monomers and aggregates found in the literature (Sumner et al., 2004; Kajava et al. 2005; Luca et al., 2007; Wiltzius et al., 2008; Bedrood et al., 2012; Liang et al., 2013; Röder et al., 2020; Wu et al., 2013, Tran et al., 2016). Furthermore, this sequence has been reported to be able to promote hIAPP fibrillization (Porat et al., 2004) and to inhibit its aggregation when inserted in a macrocycle β -sheet mimic (Buchanan et al., 2013). Selecting the second SRE was trickier because the sequences facing $N_{22}FGAIL_{27}$ vary from one model to another being a little shifted. The selection of the complementary SER in compounds **1** and **2** was based on models reported by Kajava et al. in 2005, Mirecka et al. in 2016 and Andreetto et al. in 2015, where $A_{13}NFLV_{17}$ is facing $N_{22}FGAIL_{27}$. The only difference lies in the inversion of the SRE position with NFGAIL at the *N*-terminus in **1** or at the *C*-terminus in **2** (Fig. 1). Compounds **3** and **4** (Fig. 1) were based on models reported by Wu et al in 2013, Wiltzius in 2008 and Liang et al in 2013 where $F_{15}LVHSS_{20}$ is facing

N₂₂FGAIL₂₇. We kept 5 residues in each sequence, as pentapeptide sequences were sufficient in our hairpin mimics inhibiting A β ₁₋₄₂ (Pellegrino et al., 2017). On the contrary to A β ₁₋₄₂, hIAPP does not present acidic residue in the amyloidogenic region with which the terminal amine of the inhibitor would establish interesting ionic interactions. Thus, we introduced in compound **4** an *N*-acetyl group. The isolated SREs F₁₅LVHS₁₉ **5** and F₂₃GAIL₂₇ **6** (Fig. 1) were also prepared to demonstrate the interest of inserting the SREs in β -hairpin mimics. The next step was to decrease the peptidic character in the β -hairpin mimics. We kept the sequences A₂₅IL₂₇ and F₁₅LV₁₇ that were present in compounds **1-3**. The terminal amine was either free or protected by 3 different groups: Boc, acetyl or trifluoroacetyl (compounds **7-10**). The free amine should increase the water solubility but is probably not mandatory for the interaction with hIAPP, as described above for **4**. The trifluoroacetyl group was selected to examine how the presence of fluorine atoms could influence the activity. Fluorine possesses the unique capacity to increase the local hydrophobicity, to strengthen hydrogen bonds and to increase metabolic stability, that have been exploited in more than 300 approved drugs but not yet in peptide pharmaceuticals (Inoue et al., 2020). Fluorine has been also recently demonstrated as a useful probe for studying biological events by ¹⁹F-NMR spectroscopy (Dalvit et al., 2019). The shorter compounds **11** and **12** were also evaluated to validate the interest of linking two peptide arms to the piperidine-pyrrolidine β -turn inducer. Finally, one α /aza/aza/ pseudotriptide, F-azaL-azaV-Ac mimicking FLV, was inserted in compounds **13** and **14** and evaluated alone (compound **15**). The introduction of one aza-aminoacid in peptides has shown significant success in providing biologically active peptides (see the references cited in Tonali et al, 2020). However, to our knowledge, only scarce example of biologically active peptide mimics having two consecutive aza-amino acids have been reported (Gante et al, 1995; Han et al, 1998) and one by us, using two azaGly (Dufau et al., 2012), while here we should be able to evaluate if they can retain the selectivity of natural peptides due to the lateral chains.

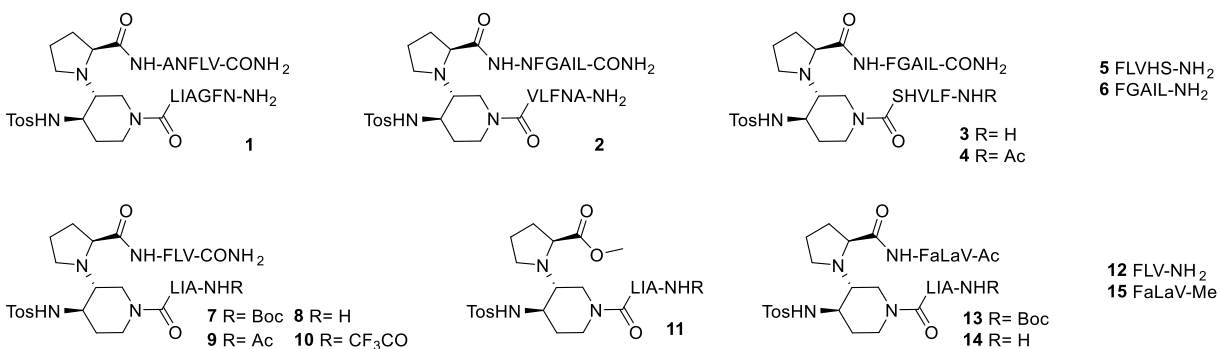


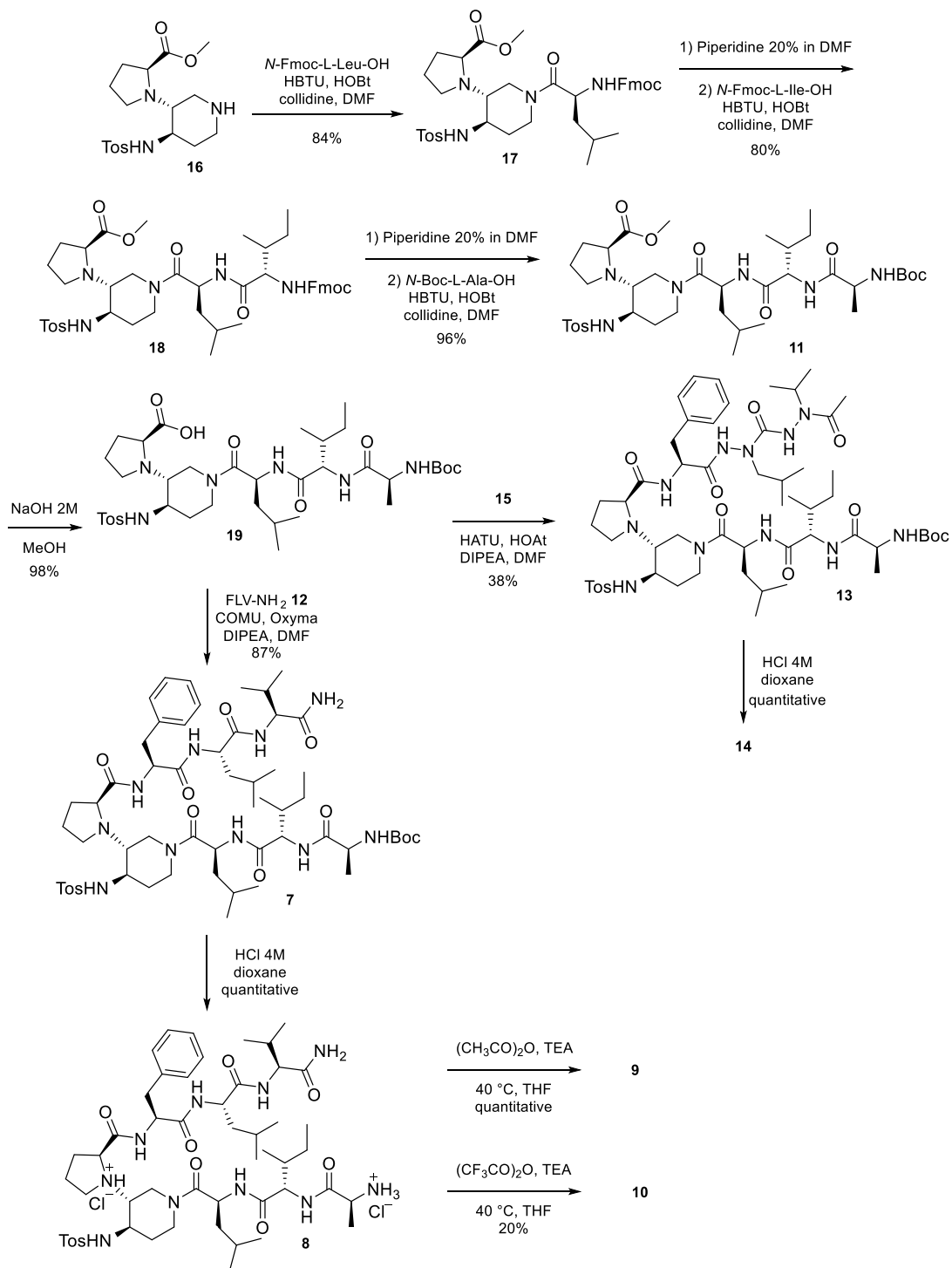
Figure. 1 Structure of the synthesized compounds

Synthesis

The preparation of the β -hairpin mimics **1-4** and of the SREs **5** and **6**, was performed by solid phase peptide synthesis, using the Fmoc strategy on a rink amide resin, as previously reported by our group (Pellegrino et al., 2017). The solution synthesis, outlined in Scheme 1, allowed the preparation of the target compounds **7-14**. Scaffold **16** was prepared in accordance with our

published procedure and using commercially available materials (Pellegrino et al., 2017). To the *N*-terminus of **16** appropriate amino acids were successively added to form the tripeptide AIL, using a classical mixed Fmoc/Boc strategy, in order to obtain the key intermediate **11**. The coupling of *N*-Fmoc-L-Leu-OH and **16**, using HOBt and HBTU, in the presence of collidine in dry DMF, led to intermediate **17** in a good yield (84 %). After the Fmoc cleavage of **17** using a solution of 20% piperidine in DMF, the free amine obtained was directly coupled with *N*-Fmoc-L-Ile-OH using the same coupling conditions as for **17**, to afford **18** in a good yield (80%). Similarly, the cleavage of the Fmoc group of **18**, followed by the coupling with the third amino acid (*N*-Boc-L-Ala-OH) led to compound **11** in an excellent yield (96 %). The saponification of the methyl ester of **11**, using NaOH 2M in MeOH, afforded **19** in an excellent yield (96 %). Its coupling with the tripeptide FLV-NH₂ **12** (synthesized in good yield, using the coupling conditions HBTU/HOBt/DIPEA in DMF in solution, see experimental section), using COMU/Oxyma as coupling agent, in the presence of DIPEA in dry DMF, led to **7** in a very good yield (87 %). Then, a classical acidic cleavage of the Boc moiety of **7** gave the hydrochloride salt **8** in quantitative yield. *N*-acylation of **8** using acetic anhydride, provided **9** in a quantitative yield while *N*-acylation of **8** with trifluoroacetic anhydride led to **10** in a poor yield (20%). The coupling between the intermediate **19** and the peptidomimetic arm FaLaV-CH₃ **15** was trickier than in the case of the coupling with the peptide FLV-NH₂ **12**. Using HATU, HOAt as coupling agents in the presence of DIPEA in dry DMF, the desired compound **13** was obtained in a poor yield (38%), together with a compound resulting from the intramolecular cyclization between the carboxylic group and the NH of the sulphonamide of 50% of **19** (Fig. 2). The formation of the cyclized by-product only observed in the coupling with the di-aza-tripeptide could be due to its steric hindrance and/or lower reactivity. Finally, the acid cleavage of the Boc moiety of **13** afforded the final hydrochloride salt **14** in quantitative yield.

The preparation of the di-aza-tripeptide FaLaV-CH₃ **15**, reported in Scheme 2, requires the combination of hydrazine chemistry and peptide synthesis. As recently reported by our group (Bizet et al., 2018), the introduction of two sequential aza-amino acids is really challenging because of the capricious reactivity of the alkyl-hydrazine. In our case, it was possible to prepare the di-aza-tripeptide arm **15** by elongating the peptidomimetic from the *C*-terminus to the *N*-terminus. Acetylation of Boc-2-isopropyl-hydrazine (**20**) prepared according to our reported procedure (Bizet et al., 2018), afforded **21** in a good yield (85%). The classical cleavage of the Boc moiety of **21** using 4 M HCl in dioxane gave the hydrochloride salt **22** in a quantitative yield. The activation of **22** using 4-nitrophenyl chloroformate, followed by the reaction with Boc-2-isobutyl-hydrazine led to Boc-protected intermediate **23** in a very satisfactory yield (85%). The acidic cleavage of the Boc moiety of **23** followed by the coupling reaction of the intermediate **24** with *N*-Cbz-L-Phe-OH using HBTU and HOBt as coupling agents in the presence of DIPEA in dry DMF, gave **25** in very good yield (80%). The cleavage of the Cbz moiety of **25** to afford the desired FaLaV-CH₃ **15** failed using classical hydrogenolysis with hydrogen in the presence of Pd/C, but was successively achieved employing McMurray's hydrogenolysis (triethylsilane in the presence of Pd/C in MeOH, Mandal et al., 2007).



Scheme. 1 Synthesis of compounds 7-14

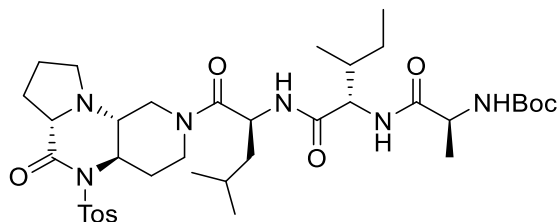
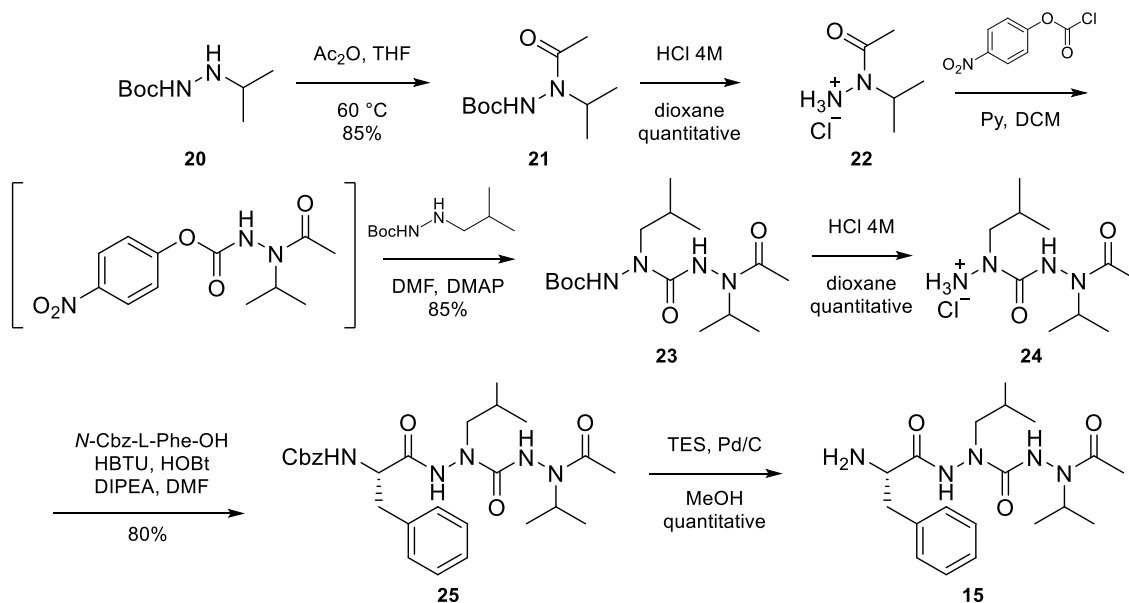


Figure. 2 Structure of the cyclized by-product



Scheme. 2 Synthesis of the peptidomimetic arm FaLaV-CH₃ **15**

Conformational studies

The most active inhibitors of hIAPP aggregation in the ThT fluorescence assays (see below) **4**, **8**, **9** and **14** were subjected to conformational studies by NMR in CD₃OH, a protic solvent that most closely approximates an aqueous environment. Methanol was used instead of water because of the low solubility in water of some compounds. An important advantage of CD₃OH is the possibility to record NMR spectra at low temperatures (248–273 K range), thus allowing to better characterize slowly interconverting conformers, as in the case of acyclic β -hairpin compounds based on a piperidine-pyrrolidine β -turn inducer (Pellegrino et al., 2017). When signals were sufficiently resolved and disperse, vicinal $^3J_{\text{HN-H}\alpha}$ coupling constants, H $^{\alpha}$ -HN ROE correlations, temperature coefficient ($\Delta\delta_{\text{HN}}/\Delta T$) of the amide protons and $^1\text{H}_{\alpha}$ and $^{13}\text{C}_{\alpha}$ chemical shift deviations (CSD), were examined to analyze backbone conformational propensities.

^1H -NMR experiments were performed on acetylated compound **4** in CD₃OH (6.5 mM, Tables 1). A good dispersion of the NH chemical shifts was observed indicating the presence of a

predominant conformation of the peptide. On the other hand, several overlapping among the H α and H β signals was detected. ROESY experiments suggested the presence of a turn structure around the piperidine-pyrrolidine scaffold as already reported for similar compounds (Pellegrino et al., 2017; Pellegrino et al., 2014; Tonali et al., 2018). In particular, a significant Roe proximity was present between H2 scaffold and H β Phe7. Regarding the FGAIL arm, a series of sequential NH- H α Overhauser effects was observed, suggesting an extended configuration of this part of the molecule. On the other hand, in the FLVHS sequence, the NH- H α Roe effect was only present between His and Val, hampering the definition of a specific conformation of the peptide fragment. Unfortunately, due to the several overlapping of the signals it is not possible to unequivocally assign interstrand spatial proximities. The variable temperature experiments showed that NH Gly8 is characterized by a $\Delta\delta/\Delta T$ of around 3.5 ppb/K, indicating its involvement in medium strength hydrogen bonds that probably stabilize the turn structure around the non natural scaffold.

Residue	δ NH (ppm)	δ H α (ppm)	δ H β (ppm)	δ other protons (ppm)	Roesy ^a
-COCH ₃	/	2.08	/	/	/
Phe-1	8.76	4.80 (overlapped)	3.40, 3.22 (overlapped)	Ar: 7.32-7.10 (overlapped)	/
Leu-2	8.07	4.31	1.84 (overlapped)	0.97 (overlapped)	/
Val-3	7.94	4.09	2.07 (overlapped)	0.97 (overlapped)	/
His-4	8.33	4.89 (overlapped)	3.40, (overlapped) 3.02	8.75, 7.32	NH: H α Val
Ser-5	7.99	4.85 (overlapped)	3.70, 3.65	/	/
Scaffold	7.48	/	H-2: 4.08, H-2': 3.84 H-3: 3.57; H-4: 2.73 H-5: 2.00, 1.29 H-6: 4.54, H-6': 2.85 Arom: 7.85 _o , 7.42 _m ; Me: 2.47		H2': H α Phe7 H2: H β Phe7
Pro-6		3.90	H-5: 3.02, H-5': 2.56; H-4: 1.58, 1.46; H-3: 2.06, 1.89		H5:H2' scaffold
Phe-7	8.66	4.80 (overlapped)	3.40, 3.22 (overlapped)	Ar: 7.32-7.10 (overlapped)	/
Gly-8	8.44	4.04, 3.85	/	/	/
Ala-9	8.17	4.44	1.36	/	NH: H α Gly
Ile-10	8.09	4.25	2.08 (overlapped)	1.90, 0.94 (overlapped)	NH: H α Ile
Leu-11	8.12	4.41	1.84 (overlapped)	0.97 (overlapped)	NH: H α Ile
NH ₂	7.52, 6.97	/	/	/	/

Table 1 ¹H NMR chemical shifts of **4**. ^aOnly significant ROEs are reported.

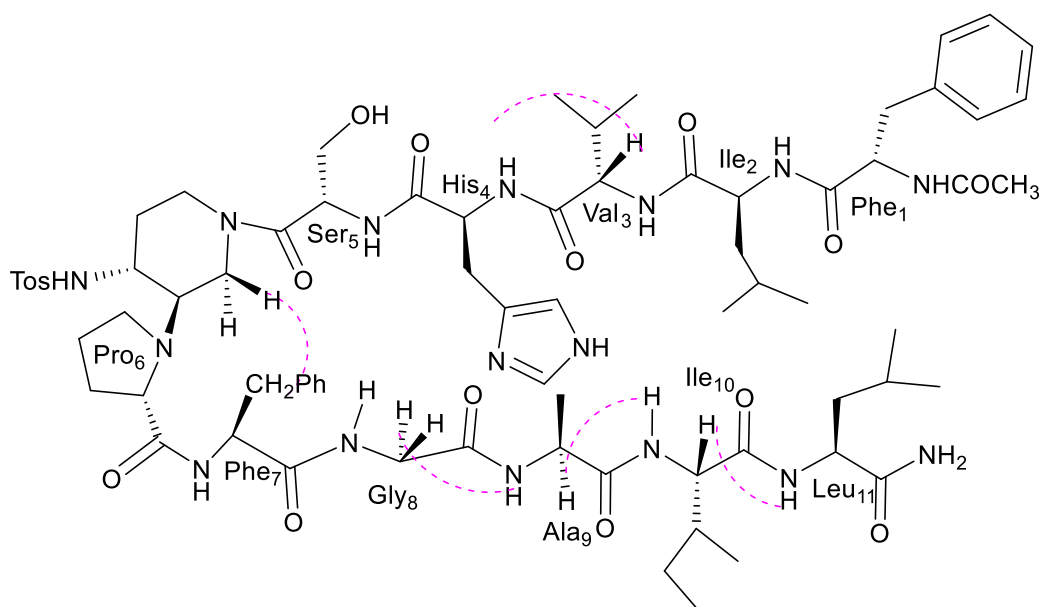


Figure. 3 Structure of compound **4** showing the significant ROEs

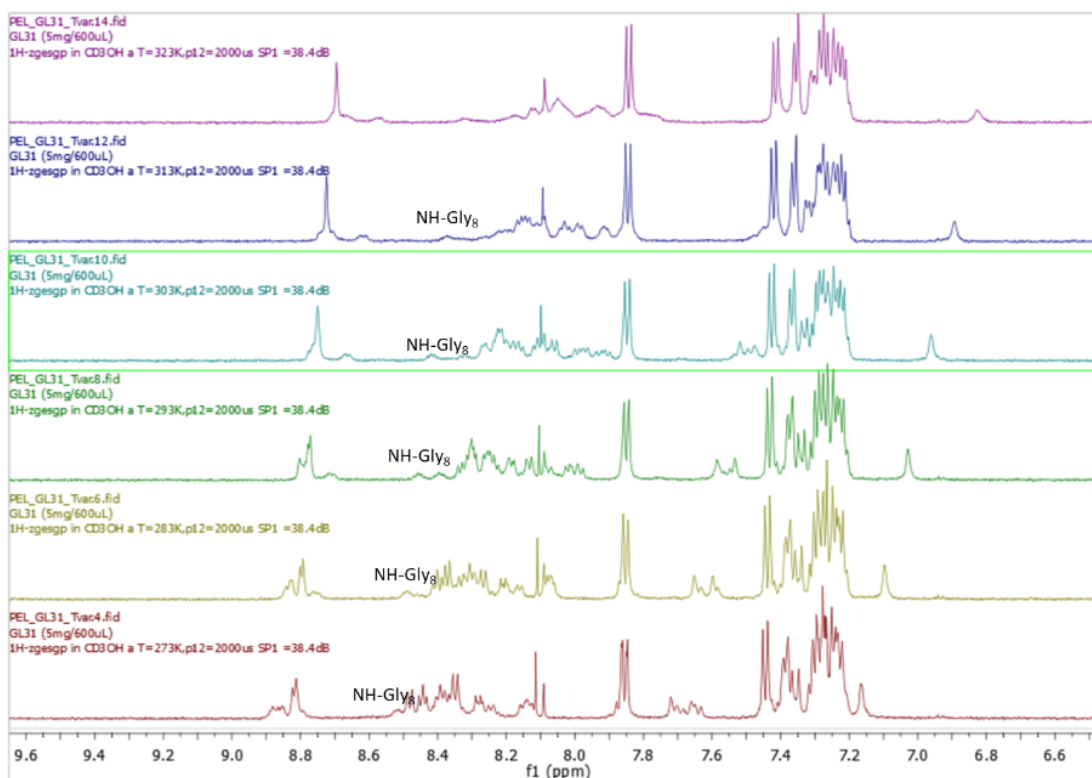


Figure. 4 Variable temperature $^1\text{H-NMR}$ experiments on compound **4** (amide protons region).

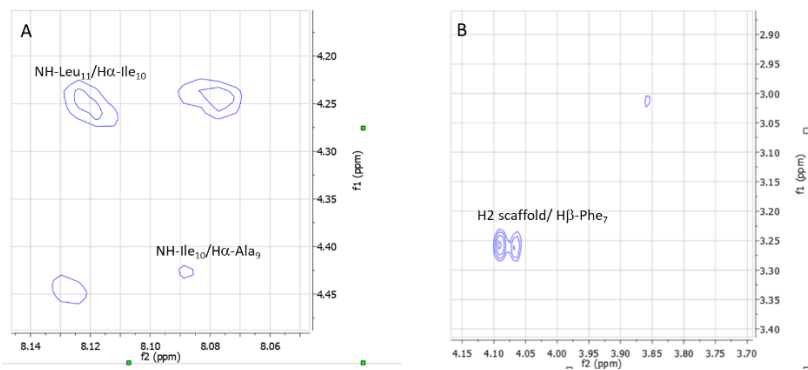


Figure. 5 Significant ROE proximities observed for compound **4** in the NH-Ha region (A) and Ha/Hb region

Conversely, compounds **8** and **9**, bearing two shorter tripeptide arms, displayed the presence of at least two major conformers in dynamic equilibrium. Complete assignment of the ^1H and ^{13}C signals was performed for the two conformers of compound **9** at 278 K (Tables 2 and 3). At this temperature, an equilibrium between two major conformers (ratio 1:1, **9a/9b**) was observed. We hypothesized that we were faced with two different β -hairpin structures, characterized by a different alignment of the two peptide arms. First, we tried to determine the secondary structures of both conformers, by taking structural information coming from through-bond (J coupling) or through space (ROE) magnetization transfer. Large vicinal $^3\text{J}_{\text{NH-H}\alpha}$ constants (>8.0 Hz) were observed in both cases, suggesting the presence of dihedral angles typical of peptide segments in extended conformation. Several sequential $\text{CH}\alpha_i/\text{NH}_{i+1}$ ROEs, indicating β -conformations, were found for both **9a** and **9b** conformers. The extended conformation of the two peptide arms was definitively confirmed by the positive difference between experimental $\text{H}\alpha$ and HN chemical shift values (CSDs) and “random ones” (Tables 4 and 5). Pro-5 in both conformers was characterized by a negative $\text{H}\alpha$ CSD value, thus confirming the folding in a β -hairpin conformation, induced by the piperidine-pyrrolidine β -turn mimic. The very slight differences in values of $^3\text{J}_{\text{NH-H}\alpha}$ and of CSD let consider that the peptide arms are similarly extended in both conformers **9a** and **9b**. ROESY experiments confirmed the presence of the β -turn in both conformers. Spatial proximities were found between the $\text{H}\alpha$ of Pro-5 and the H3 and H2 diastereotopic protons of the piperidine ring and between the H3 of Pip-4 with the HN of Phe-6. These ROEs showed that a β -turn conformation occurs in both conformers and that the dihedral angle between the two rings of the turn mimetic remains unchanged, thus rejecting the possible hypothesis of an equilibrium due to the free rotation of the $\text{C}_{3\text{pip}}\text{-N}_{\text{Pro}}$ single bond. We also hypothesized that the equilibrium could be ruled by a different chair conformation of the piperidine ring, which might affect the hairpin architecture. This hypothesis has been excluded because in both conformers the same ROEs pattern between the diastereotopic protons have been found (Table 6 Fig 6), confirming the trans and axial configuration of H3 and H4. The large ^3J value (25.8 Hz for **9a** and 26.8 Hz for **9b**) of H3 and H4, reflecting a large dihedral angle between the two protons, corroborates that in both

conformers the Pro-5 and the Tosyl group are in equatorial position. We could detect β -hairpin diagnostic ROEs only for 9b isomer (Fig 9 and 10). We observed spatial proximity between the two peptide arms and in particular between the H α of Ile-2 and the aromatic ring of Phe-6 and the CH₃ of Leu-7, between the H α of Leu-7 and the CH₃ of Ile-2 and, finally, between the side chains of Ile-2 and Leu-7. This difference let us hypothesize a dynamic equilibrium between two different β -hairpin architectures, with only one of them allowing the spatial proximity between the peptide arms.

Residue	δ NH (ppm)	δ H $^{\alpha}$ (ppm) 3J (Hz)	δ H $^{\beta}$ (ppm)	δ other protons (ppm)	δ CO (ppm)	δ C $^{\alpha}$ (ppm)	δ C $^{\beta}$ (ppm)	δ other carbons (ppm)
Ala-1	8.33	4.33 (6.9 Hz)	1.28	/	173.8	49.2	16.8	/
Ile-2	8.08	4.15 (10.7 Hz)	1.71	γ_{CH_3} 0.83 γ_{CH_2} 1.06 δ_{CH_3} 0.73	172.1	57.4	36.9	γ_{CH_3} 10.2 γ_{CH_2} 24.6 δ_{CH_3} 14.9
Leu-3	8.37	4.80 (9.1 Hz)	1.29/1.59	γ_{CH} 1.45 δ_{CH_3} 0.87	170.7	46.7	40.6	γ_{CH} 24.6 δ_{CH_3} 20.1
Pip.-4	/	/	/	H _{2/2'} 2.75/4.45 H ₃ 2.22 H ₄ 3.63 H _{5/5'} 1.24/1.66 H _{6/6'} 3.03/3.79	/	/	/	C _{2/2'} 39.6 H ₃ 59.3 H ₄ 53.9 H _{5/5'} 32.7 H _{6/6'} 44.2
Pro-5	/	3.34	1.30/1.93	γ 1.56 δ 2.61/3.09	176.0	63.4	30.8	γ 40.6 δ 44.5
Phe-6	8.59	4.76 (9.6 Hz)	3.17	H _o 7.36 H _m 7.26 H _p 7.20	173.4	54.1	37.3	C _q 137.5 C _o 129.2 C _m 128.1 C _p 126.4
Leu-7	8.74	4.54 (10.2 Hz)	1.58/1.66	γ_{CH} 1.60 δ_{CH_3} 0.95	173.5	51.8	40.6	γ_{CH} 24.6 δ_{CH_3} 20.1
Val-8	8.27	4.14 (8.2 Hz)	2.06	γ_{CH} 0.96 amide 7.14 or 7.18 and 7.76	174.7	58.7	30.7	18.47
Tosyl	7.69	/	/	H _o 7.82 H _m 7.41 CH ₃ 2.45	/	/	/	C _{qs} 139.7 C _o 126.6 C _m 129.8 C _{qm} 143.5 CH ₃ 20.2
Acetyl	/	/	/	CH ₃ 1.95	171.7	/	/	CH ₃ 21.1

Table. 2 ¹H and ¹³C NMR chemical shifts for the conformer **9a** (37.5 mM) in CD₃OH at 278K

Residue	δ NH (ppm)	δ H $^{\alpha}$ (ppm) 3J (Hz)	δ H $^{\beta}$ (ppm)	δ other protons (ppm)	δ CO (ppm)	δ C $^{\alpha}$ (ppm)	δ C $^{\beta}$ (ppm)	δ other carbons (ppm)
Ala-1	8.31	4.39 (6.5 Hz)	1.28	/	173.8	46.1	16.8	/
Ile-2	8.09	4.15 (10.7 Hz)	1.77	γ_{CH_3} 0.87 γ_{CH_2} 1.12	171.6	57.4	36.6	γ_{CH_3} 10.2 γ_{CH_2} 24.6

				δ_{CH_3} 0.73				δ_{CH_3} 14.9
Leu-3	8.34	4.86 (8.09 Hz)	1.46/1.53	γ_{CH} 1.67 δ_{CH_3} 0.86	171.3	47.3	40.5	γ_{CH} 24.6 δ_{CH_3} 20.8
Pip.-4	/	/	/	H _{2/2'} 3.26/4.23 H ₃ 2.49 H ₄ 3.57 H _{5/5'} 1.19/1.52 H _{6/6'} 2.48/4.28	/	/	/	C _{2/2'} 43.9 H ₃ 60.2 H ₄ 54.0 H _{5/5'} 31.7 H _{6/6'} 40.9
Pro-5	/	3.34	1.30/1.93	γ 1.56 δ 2.61/3.09	176.0	62.6	30.8	γ 40.7 δ 44.5
Phe-6	8.67	4.91 (10.1 Hz)	3.12/3.21	H _o 7.36 H _m 7.26 H _p 7.20	172.8	54.1	37.3	C _q 137.5 C _o 129.2 C _m 128.1 C _p 126.4
Leu-7	8.50	4.54 (10.2 Hz)	1.66/1.58	γ_{CH} 1.60 δ_{CH_3} 0.91/0.97	173.3	51.8	40.6	γ_{CH} 24.6 δ_{CH_3} 20.1
Val-8	8.11	4.21 (9.1 Hz)	2.06	γ_{CH} 0.96 amide 7.14 or 7.18 and 7.76	173.3	58.7	30.8	18.47
Tosyl	7.87	/	/	H _o 7.82 H _m 7.41 CH ₃ 2.45	/	/	/	C _{qs} 139.7 C _o 126.6 C _m 129.8 C _{qm} 143.5 CH ₃ 20.2
Acetyl	/	/	/	CH ₃ 1.95	171.9	/	/	CH ₃ 21.1

Table 3 ¹H and ¹³C NMR chemical shifts for the conformer **9b** (37.5 mM) in CD₃OH at 278K

Residue	δ NH random coil	δ NH experimental	NH CSD	δ H ^{α} random coil	δ H ^{α} experimental	H ^{α} CSD
Ala-1	8.24	8.33	+ 0.09	4.32	4.33	- 0.01
Ile-2	8.00	8.08	+ 0.08	4.17	4.15	- 0.02
Leu-3	8.16	8.37	+ 0.21	4.34	4.80	+ 0.46
Pro-5	/	/	/	4.42	3.34	- 1.08
Phe-6	8.30	8.59	+ 0.29	4.62	4.76	+ 0.14
Leu-7	8.16	8.74	+ 0.58	4.34	4.54	+ 0.20
Val-8	8.03	8.27	+ 0.24	4.12	4.14	+ 0.02
Residue	δ C ^{α} random coil	δ C ^{α} experimental	C ^{α} CSD	δ C=O random coil	δ C=O experimental	C=O CSD
Ala-1	52.5	49.2	-3.3	177.8	173.8	-4.0
Ile-2	61.1	57.4	-3.7	176.4	172.1	-4.3
Leu-3	55.1	46.7	-8.4	177.6	170.7	-6.9
Pro-5	63.3	30.8	-32.5	177.3	176.0	-1.3
Phe-6	57.7	37.3	-20.4	175.8	173.4	-2.4
Leu-7	55.1	40.6	-14.5	177.6	173.5	-4.1
Val-8	62.2	30.7	-31.5	176.3	174.7	-1.6

Table 4 Chemical shift deviations (CSD) of HN, H ^{α} , C ^{α} and CO, for conformer **9a**

Residue	δ NH random coil	δ NH experimental	NH CSD	δ H ^{α} random coil	δ H ^{α} experimental	H ^{α} CSD
Ala-1	8.24	8.31	+ 0.07	4.32	4.39	+0.07
Ile-2	8.00	8.09	+ 0.09	4.17	4.15	- 0.02

Leu-3	8.16	8.34	+ 0.18	4.34	4.86	+ 0.52
Pro-5	/	/	/	4.42	3.75	- 0.67
Phe-6	8.30	8.67	+0.37	4.62	4.91	+ 0.29
Leu-7	8.16	8.50	+ 0.34	4.34	4.54	+ 0.20
Val-8	8.03	8.11	+ 0.08	4.12	4.21	+ 0.09
Residue	δC^α random coil	δC^α experimental	C^α CSD	$\delta C=O$ random coil	$\delta C=O$ experimental	$C=O$ CSD
Ala-1	52.5	46.1	-6.4	177.8	173.8	-4.0
Ile-2	61.1	57.4	-3.7	176.4	171.6	-4.8
Leu-3	55.1	47.3	-7.8	177.6	171.3	-6.3
Pro-5	63.3	62.6	-0.7	177.3	176.0	-1.3
Phe-6	57.7	54.1	-3.6	175.8	172.8	-3.0
Leu-7	55.1	51.8	-3.3	177.6	173.3	-4.3
Val-8	62.2	58.7	-3.5	176.3	173.3	-3.0

Table. 5 Chemical shift deviations (CSD) of HN, H $^\alpha$, C $^\alpha$ and CO, for conformer **9b**

Conformer 9a

Proton (ppm)	δCH_2 (2) (ppm)	δCH_2 (5)(ppm)	δCH_2 (6)(ppm)
CH (3) 2.22	4.45 (H ^{eq})	1.24 (H ^{ax})	3.79 (H ^{eq})
CH (4) 3.63	2.75 (H ^{ax})	1.66 (H ^{eq})	3.03 (H ^{ax})

Conformer 9b

Proton (ppm)	δCH_2 (2) (ppm)	δCH_2 (5)(ppm)	δCH_2 (6)(ppm)
CH (3) 2.49	4.23 (H ^{eq})	1.19 (H ^{ax})	4.28 (H ^{eq})
CH (4) 3.57	3.26 (H ^{ax})	1.52 (H ^{eq})	2.48 (H ^{ax})

Table. 6 Piperidine diastereotopic protons with which H³ or H⁴ establish ROEs in conformers a and b of hairpin **9**.

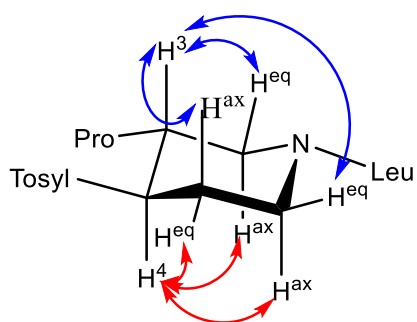


Figure. 6 Structure of the piperidine ring showing the common ROE of **9a** and **9b**. In blue the ROEs of H³ and in red the ROEs of H⁴

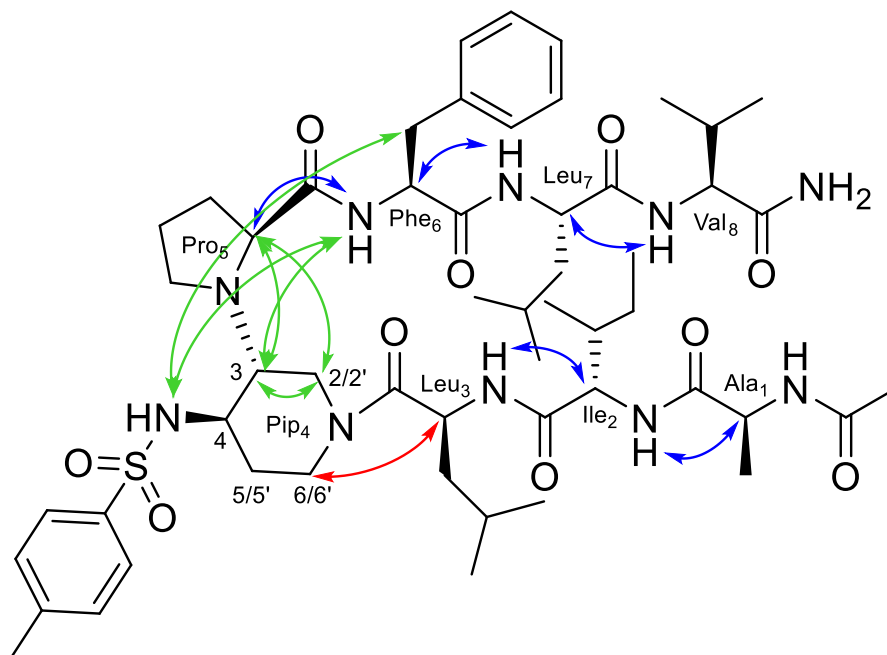


Figure 7 Structure of hairpin **9a** showing the assigned ROEs: in blue the sequential $\text{CH}\alpha_i/\text{NH}_{i+1}$ ROEs, in green the common ROEs with **9b** in red the differences.

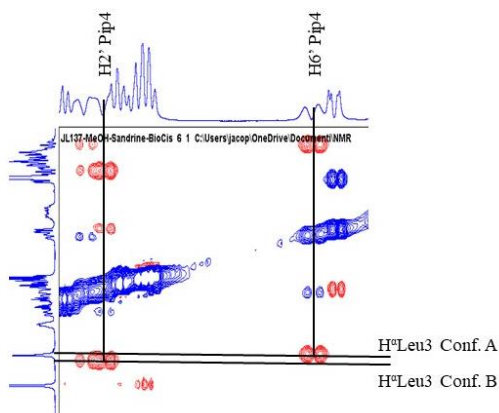


Figure 8 Expansion of the 2D ^1H - ^1H ROESY of compound **9** showing the different ROEs between Leu3 and Pip4 for both conformers a and b.

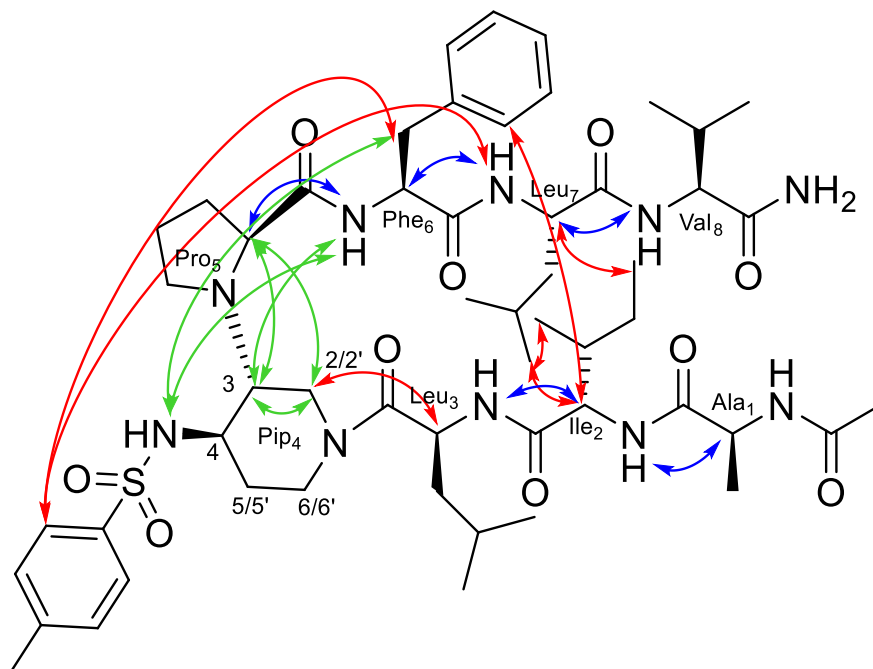


Figure. 9 Structure of hairpin **9b** showing the assigned ROEs: in blue the sequential $\text{CH}\alpha_i/\text{NH}_{i+1}$ ROEs, in green the common ROEs with **9a** in red the differences.

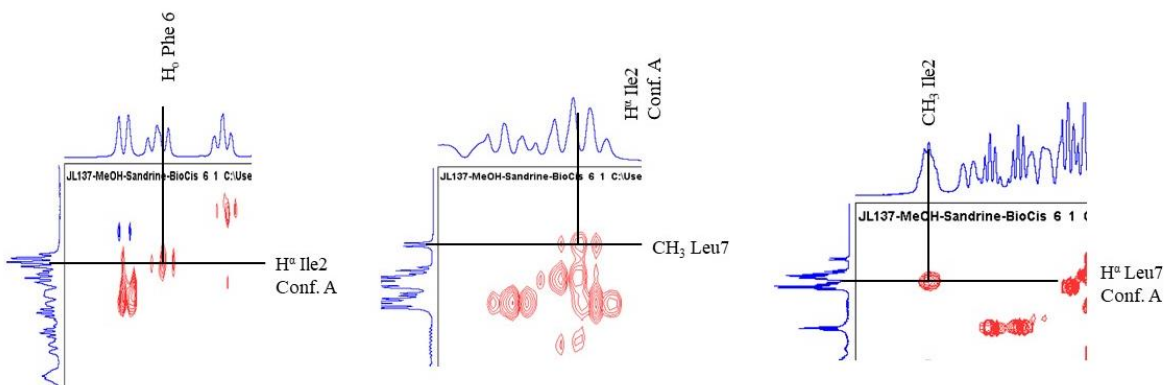


Figure. 10 Expansion of the 2D ^1H - ^1H ROESY of compound **9b** showing the inter-strand ROEs

The different alignment of the peptide chains between the two conformers might be explained by a different ROE between the $\text{H}\alpha$ of Leu-3 and the diastereotopic protons H2 or H6 of the Pip-4. In **9a**, Leu-3 $\text{H}\alpha$ can see H6, while in **9b** the same Leu-3 $\text{H}\alpha$ provides a ROE with H2 (Fig 6, 7 and 8). In that regard, we decided to perform a molecular dynamics (MD) study to investigate if different rotations of the amide bond between Leu-3 and Pip-4 could account for the two observed different β -hairpin architectures.

We performed 200 ns-MD simulations of both conformers **9a** and **9b** in explicit MeOH solvent at 280 K to be as close as possible to experimental conditions. Both initial structures have their piperidine ring in a chair conformation with axial orientation of H3 and H4 protons (torsion angle H3-C3-C4-H4 close to 180°). In both initial structures, the torsion angle between the piperidine

and proline rings were also identical with proline H α pointing toward piperidine H2 (torsion angle C α -N-C3-C2 around -60°). The main difference between the two initial structures was the torsion angle around the amide bond between Leu-3 and Pip-4 (Figs. 6 and 8): The C α -C-N-C2 angle was equal to -170° and -5° in the initial structures **9a** and **9b**, respectively. Before analyzing the spatial proximity between the two peptide arms in each conformer, we first checked the stability of the piperidine-proline local structure during the dynamic simulations. As displayed in Fig. 10, the probability distributions of the three torsion angles H3-C3-C4-H4, C α -N-C3-C2, and C α -C-N-C2 are unimodal and centered around their initial values, indicating that the piperidine-proline local structure is maintained and no conformational transition of the torsion angle C α -C-N-C2 between Leu-3 and Pip-4 occurs in MD simulations, for both conformers **9a** and **9b**.

We also calculated the $^3J_{\text{HN-H}\alpha}$ coupling constants of the two peptidic arms during simulations and compared them with NMR measurements (Table 7). Overall, the computed $^3J_{\text{HN-H}\alpha}$ coupling constants have lower values than NMR data, indicating that the two peptide arms are less extended in MD simulations than in NMR experiments. This is particularly striking for the **9b** peptide arms which exhibit local bent conformations at residues Ile-2 and Phe-6 as indicated by their low J-coupling values (4.9 and 3.3 Hz, respectively) whereas both NMR values are above 10 Hz. These discrepancies (which are also observed but in a lesser extent for conformer **9a**) might be due to the imperfections of the Generalized Amber Force Field (GAFF) used here for the non-purely peptide solute (in particular Pro-Pip residues) and/or the methanol solvent.

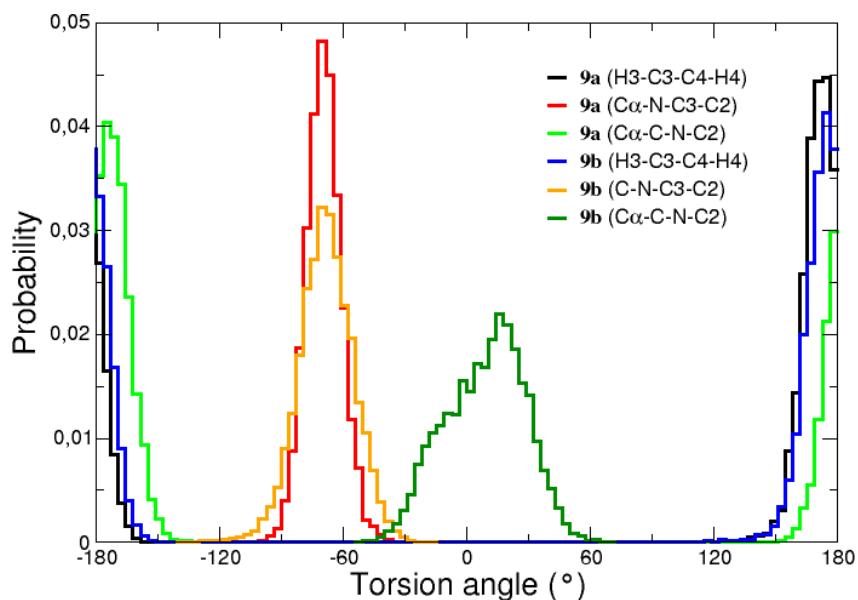


Figure. 11 MD-derived probability distribution of the torsion angles H3-C3-C4-H4 of the piperidine cycle, (Pro-5) C α -N-C3-C2 between the piperidine and proline rings, and (Leu-3) C α -C-N-C2 connecting Leu-3 to piperidine

	9a		9b	
	NMR	MD	NMR	MD
Ala-1	6.9	5.5	6.5	5.7

Ile-2	10.7	5.7	10.7	4.9
Leu-3	9.1	8.2	8.1	8.0
Phe-6	9.6	5.8	10.1	3.3
Leu-7	10.2	5.7	10.2	5.7
Val-8	8.2	7.2	9.1	8.5

Table. 7 Comparison between NMR-measured and MD-derived $^3J_{\text{HN-H}\alpha}$ coupling constants of the 6 amino acids of the two peptidic arms

Despite these discrepancies, significant differences in the spatial proximity of the two peptide arms were observed between conformers **9a** and **9b**. Indeed, when analyzing the probability distribution of the distances between protons for which ROEs were detected (Fig. 11), the distance between Ile-2 H α and Phe-6 aromatic ring as well as that one between Ile-2 side chain CH3 and Leu-7 H α are clearly lower in **9b** than in **9a**. This indicates that the two peptide arms are closer in conformer **9b** than in **9a** (Fig. 11). Altogether, our results confirm that the conformation of the torsion angle C α -C-N-C2 between Leu-3 and Pip-4 impacts the spatial proximity of the two peptide arms and the global β -hairpin architecture: When Leu-3 H α is oriented toward piperidine H6 (**9a**), this favors a separation of the two peptide arms, whereas when it is oriented toward piperidine H2 (**9b**), the two arms can come close each to other.

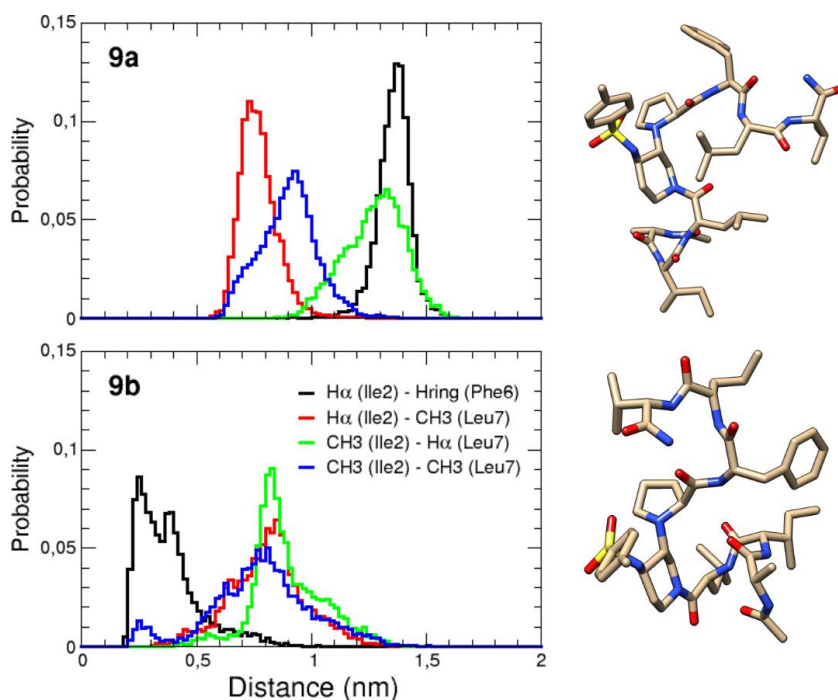


Figure. 12 MD-derived probability distribution of distances between protons in each of the two peptide arms. On the right are displayed representative structures of the most populated clusters of **9a** and **9b**.

This conformational analysis by NMR and molecular dynamics, performed on the acetylated hairpin mimic **9**, allowed us to establish some general guidelines, useful for the structural characterization of similar compounds based on our β -turn inducer when NMR assignment is not as precise as for compound **9**.

In the case of the free N-terminal compound **8**, it was not possible to perform a complete assignment of the two major conformers in equilibrium, even by lowering the temperature at 278 K. Increasing the temperature at 313 K, we could approach an approximately complete coalescence of the two conformers, allowing to the attribution of an average conformation.

The complete ^1H and ^{13}C assignment of the average conformer of **8** was performed (Table 8). The good dispersion of the NH chemical shifts indicated the presence of a single and major conformation whose turn structure was confirmed by ROESY experiments. Several sequential $\text{CH}\alpha_i/\text{NH}_{i+1}$ ROEs, large $^3J_{\text{NH-H}\alpha}$ coupling constants and positive ^1H CSD values (Table 9) for most of the amino acids (less remarkable for the more dynamic N-terminal Ala and C-terminal Val), confirmed the extended conformation of the two peptide arms. Diagnostic inter-strand ROEs were observed between the HN of Leu-3 and the H^α and H^β of Phe-6 and were in favor of a β -hairpin architecture (Fig. 12 and 13). Unfortunately, the characteristic ROEs of the β -turn inducer (Pip4/Pro5) observed for compound **9** were not all detected and only the diagnostic ROE $\text{H}\alpha_{\text{Pro5}}/\text{H}2_{\text{Pip4}}$ could be observed. In order to study the eventually presence of intramolecular hydrogen-bond, we analyzed the temperature dependence of amide proton chemical shifts, as it can provide information about the hydrogen bond network. No one of the amide protons showed a low temperature coefficient (Table 10). However, Ile-2, Leu-3 and Leu-7 values fell within intermediate values, suggesting their partial involvement in hydrogen-bond. Taking together all these experimental results, it is possible to conclude that two different hairpin architectures, reflecting the same equilibrium of compound **9**, are possible for compound **8**. At 313 K, we can assert that the average conformation of **8** adopts a partial β -hairpin conformation, with the N-terminal Ala residue not in contact with the C-terminal acetyl amide group, thing that would have allowed to form a more extended β -hairpin.

Residue	δ NH (ppm)	δ H^α (ppm) 3J (Hz)	δ H^β (ppm)	δ other protons (ppm)	δ CO (ppm)	δ C^α (ppm)	δ C^β (ppm)	δ other carbons (ppm)
Ala-1	8.16	3.98	1.47	/	169.7	48.9	16.5	/
Ile-2	8.28	4.24 (8.0 Hz)	1.81	γ_{CH_3} 0.92 γ_{CH_2} 1.18 δ_{CH_3} 0.86	171.9	58.3	36.5	γ_{CH_3} 14.4 γ_{CH_2} 24.6 δ_{CH_3} 9.9
Leu-3	8.37 8.52	4.46 (10.5 Hz)	1.64	γ_{CH} 1.66 δ_{CH_3} 0.94/0.90	174.7	52.4	40.6	γ_{CH} 24.6 δ_{CH_3} 20.1
Pip.-4	/	/	/	$\text{H}_{2/2'}$ 3.15/3.79 H_3 3.53 H_4 3.65 $\text{H}_{5/5'}$ 1.17/1.54 $\text{H}_{6/6'}$ 2.48/4.28	/	/	/	$\text{C}_{2/2'}$ 43.4 H_3 71.4 H_4 51.6 $\text{H}_{5/5'}$ 24.6 $\text{H}_{6/6'}$ 40.7
Pro-5	/	4.80	1.29/1.96	γ 1.63 δ 2.96/3.10	173.3	47.2	41.8	γ 40.6 δ 39.0
Phe-6	8.28 8.77	4.77 (11.3 Hz)	2.97/3.24	H_o 7.29 H_m 7.26	171.7	55.2	37.6	C_q 137.0 C_o 129.1

		4.77 (16.3 Hz)		H _p 7.18				C _m 128.2 C _p 126.7
Leu-7	8.29	4.48 (11.6 Hz)	1.64	γ _{CH} 1.66 δ _{CH₃} 0.94/0.90	173.3	52.4	40.6	γ _{CH} 24.6 δ _{CH₃} 20.1
Val-8	7.79	4.21 (11.8 Hz)	2.06	0.92/0.96	174.6	53.2	30.9	20.8
Tosyl	7.74	/	/	H _o 7.83 H _m 7.45 CH ₃ 2.45	/	/	/	C _{qs} 137.9 C _o 126.9 C _m 129.9 C _{qm} 144.4 CH ₃ 20.2

Table 8 ¹H-NMR and ¹³C-NMR chemical shifts for the mean conformer of hairpin **8** (14.6 mM) in CD₃OH at 313K

Residue	δ NH random coil	δ NH experimental	NH CSD	δ H ^α random coil	δ H ^α experimental	H ^α CSD
Ala-1	8.24	8.16	- 0.08	4.32	3.98	- 0.34
Ile-2	8.00	8.28	+ 0.28	4.17	4.24	+ 0.07
Leu-3	8.16	8.37 8.52	+ 0.21 + 0.36	4.34	4.46 4.46	+ 0.12 + 0.12
Pro-5	/	/	/	4.42	4.80	+ 0.38
Phe-6	8.30	8.28 8.77	- 0.02 + 0.47	4.62	4.77 4.77	+ 0.15 + 0.15
Leu-7	8.16	8.29	+ 0.13	4.34	4.48	+ 0.14
Val-8	8.03	7.79	- 0.24	4.12	4.21	+ 0.09
Residue	δ C ^α random coil	δ C ^α experimental	C ^α CSD	δ C=O random coil	δ C=O experimental	C=O CSD
Ala-1	52.5	48.9	-3.6	177.8	169.7	-8.1
Ile-2	61.1	58.3	-2.8	176.4	171.9	-4.5
Leu-3	55.1	52.4	-2.7	177.6	174.7	-2.9
Pro-5	63.3	47.2	-16.1	177.3	173.3	-4.0
Phe-6	57.7	55.2	-2.5	175.8	171.7	-4.1
Leu-7	55.1	52.4	-2.7	177.6	173.3	-4.3
Val-8	62.2	53.2	-9.0	176.3	174.6	-1.7

Table 9 Chemical shift deviations (CSD) of HN, H^α, C^α and CO for compound **8**

Residue	δ HN (ppm 313K)	δ HN (ppm 278K)	Δδ/ΔT
Ala1	8.16	/	/
Ile2	8.28	8.50	-6.29
Leu3	8.37 8.52	8.58 8.75	-6.00 -6.57
Pro5	/	/	/
Phe6	8.28 8.77	8.61 9.07	-9.43 -8.57
Leu7	8.29	8.47	-5.14
Val8	7.79	8.18	-11.14
Tos	7.75	7.94	-5.43

Table 10 Temperature coefficients of HN (Δδ/ΔT) for compound **8**

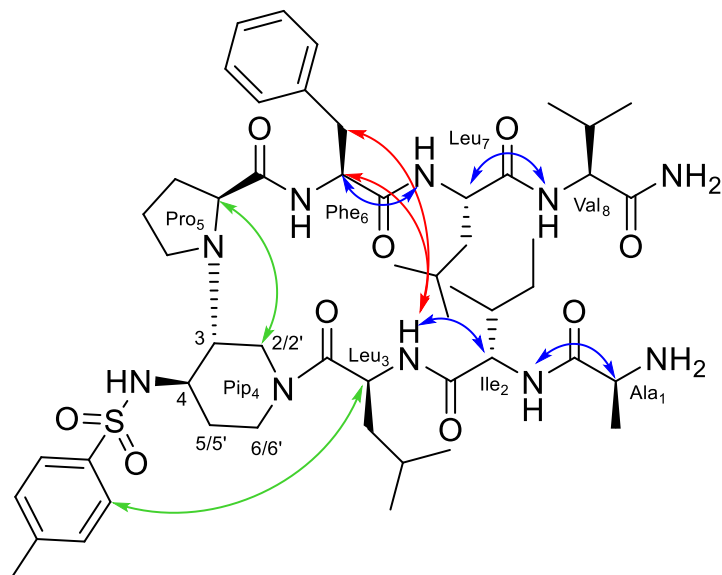


Figure. 13 Structure of hairpin **8** showing the assigned ROEs: in blue the sequential $\text{CH}\alpha_i/\text{NH}_{i+1}$ ROEs; in red the inter-strand ROEs, in black the β -turn inducer ROEs and in green other significant ROEs

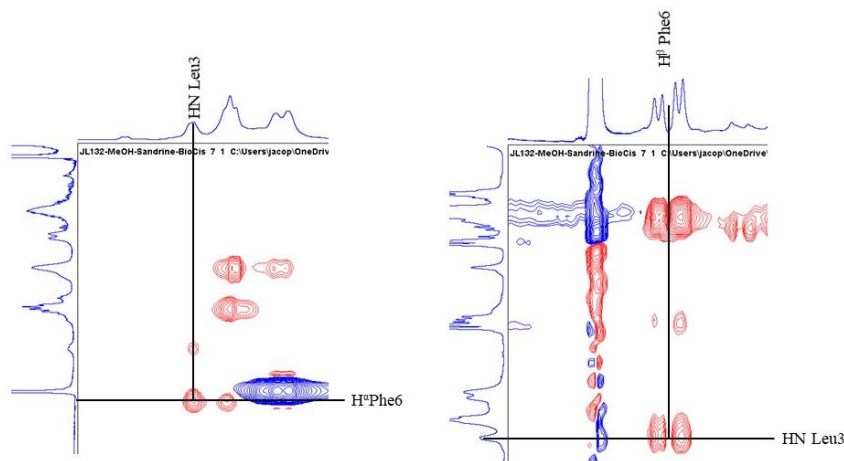


Figure. 14 Expansion of the 2D ^1H - ^1H ROESY of compound **8** showing the inter-strand ROEs

The ^1H and ^{13}C assignment of compound **14** was tricky even performed on a spectrometer operating at 800 MHz and equipped with a TCI cryoprobe. A dispersion of NH chemical shifts and poor resolution of the signals indicated the presence of different conformers whatever the temperature from 278K to 313K. Some signals and $^3J_{\text{NH-H}\alpha}$ coupling constants of the natural amino acids could not be determined with certainty (Tables 11 and 12). The temperature dependence of amide proton chemical shifts of Ile-2 was intermediate (-4.5 ppb K^{-1}), suggesting its partial involvement in hydrogen-bond. Several sequential $\text{CH}\alpha_i/\text{NH}_{i+1}$ ROEs and large and positive ^1H CSD values (Table 13) for Ile, Leu and Phe confirmed the extended conformation of the natural

amino acids in the two arms (Fig. 14). No typical spatial proximities were found between Pro-5 and Pip-4 and between the Pip-4 and Phe-6 to confirm the turn structure. However, both ROE between the H α of Leu-3 and the diastereotopic protons H2 and H6 of the Pip-4 were visible, indicating an equilibrium between an “open” hairpin structure and a structure where the arms are closer (see discussion for conformers **9a** and **9b**). Numerous intra-strands ROEs were identified, in particular in the diaza-tripeptide arm (Fig. 15). A very weak inter-strand ROE was observed and attributed to H δ PHE and H δ LEU or H γ ILEU which chemical shifts are identical (0,91 ppm, Fig. 15). Overall, **14** seems to adopt more flexible β -hairpin structure than the peptide analogues **8** and **9**.

Residue	δ NH (ppm)	δ H $^{\alpha}$ (ppm)	δ H $^{\beta}$ (ppm)	δ other protons (ppm)	δ CO (ppm)	δ C $^{\alpha}$ (ppm)	δ C $^{\beta}$ (ppm)	δ other carbons (ppm)
Ala-1	8.22 8.25 8.28	3.96	1.45	/	169.6	48.7	16.5	
Ile-2	8.44	4.22	1.79	γ_{CH_3} 0.91 γ_{CH_2} 1.17, 1.55 δ_{CH_3} 0.89	171.9	57.85	36.5	γ_{CH_3} 14.4 γ_{CH_2} 24.4 δ_{CH_3} 9.9
Leu-3	8.55	4.76	1.61	γ_{CH} 1.29 δ_{CH_3} 0.91	/	47.3	40.0	γ_{CH} 40.2 δ_{CH_3} 14.5
Pip-4	/	/	/	H $_{2/2'}$ 4.30/2.53 H $_3$ 3.42 H $_4$ 3.63 H $_{5/5'}$ 1.32/1.50 H $_{6/6'}$ 3.82/3.15	/	/	/	C $_{2/2'}$ 40.4 H $_3$ 63.3 H $_4$ 51.1 H $_{5/5'}$ 29.91 H $_{6/6'}$ 43.31
Pro-5	/	4.40	2.70/2.18	γ 1.94 δ 3.20/3.08	/	54.7	30.5	γ 26.95 δ 48.0
Phe-6	/	4.56	3.21	Ho 7.35 Hm 7.31 Hp 7.28	/	48.0	36.6	Cq 135.4 Co 128.5 Cm 129.2 Cp 127.0
Aza-Leu-7	10.65	/	2.48, 3.37	γ_{CH} 1.13 δ_{CH_3} 0.72	/	/	55.1	γ_{CH} 24.4 δ_{CH_3} 19.6
Aza-Val-8	/		4,65	δ 1.05	174.1		48.1	18.2
Tosyl	7.88	/	/	H $_o$ 7.83, H $_m$ 7.44 CH $_3$ 2.44	/	/	/	Cqs 144.0 Cqc 137.6 Co 126.8 Cm 129.7 CH $_3$ 20.0
CH$_3$(Ac)	/	/	/	CH $_3$ 1.99	169.6	/	/	CH $_3$ 20.1

Table 11 ^1H -NMR and ^{13}C -NMR chemical shifts for the mean conformer of hairpin 14 (10 mM) in CD $_3$ OH at 278K

Residue	δ HN (ppm 278K)	δ HN (ppm 313K)	$\Delta\delta/\Delta T$ (ppb K ⁻¹)
Ile-2 NH	8.44	8.28	-4.5
Leu-3 NH	8.55	8.28	-7.7

Table. 12 Temperature coefficients for the NH of the major conformer of **14** in CD₃OH between 278K and 313K

Residue	δ NH random coil	δ NH experimental	NH CSD	δ H ^{α} random coil	δ H ^{α} experimental	H ^{α} CSD
Ala-1	8.24	8.22/8.25/8.28	/	4.32	3.96	-0.36
Ile-2	8.00	8.44	+ 0.44	4.17	4.22	+ 0.05
Leu-3	8.16	8.55	+ 0.39	4.34	4.76	+ 0.42
Pro-5	/	/	/	4.42	4.40	-0.02
Phe-6	8.30	8.81	+0.51	4.62	4.56	- 0.06
Residue	δ C ^{α} random coil	δ C ^{α} experimental	C ^{α} CSD	δ C=O random coil	δ C=O experimental	C=O CSD
Ala-1	52.5	48.7	-3.8	177.8	169.6	-8.2
Ile-2	61.1	57.8	-3.3	176.4	171.9	-4.5
Leu-3	55.1	47.3	-7.8	177.6		
Pro-5	63.3	54.7	-8.6	177.3	/	/
Phe-6	57.7	48	-9.7	175.8	/	/

Table. 13 Chemical shift deviations (CSD) of HN, H ^{α} , C ^{α} and CO, for compound **14**

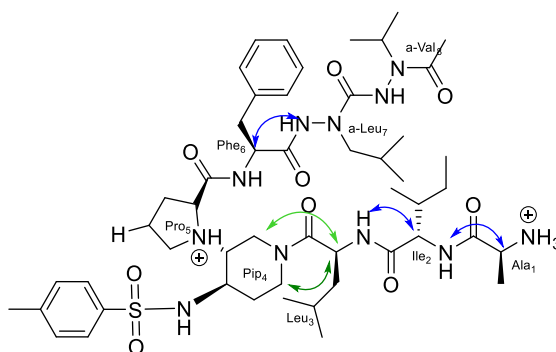


Figure. 15 Structure of hairpin **14** showing the assigned ROEs: in blue the sequential CH _{α} _{*i*}/NH_{*i*+1} ROEs, and in green other significant ROEs (light green/weak ROE; dark green/strong ROE).

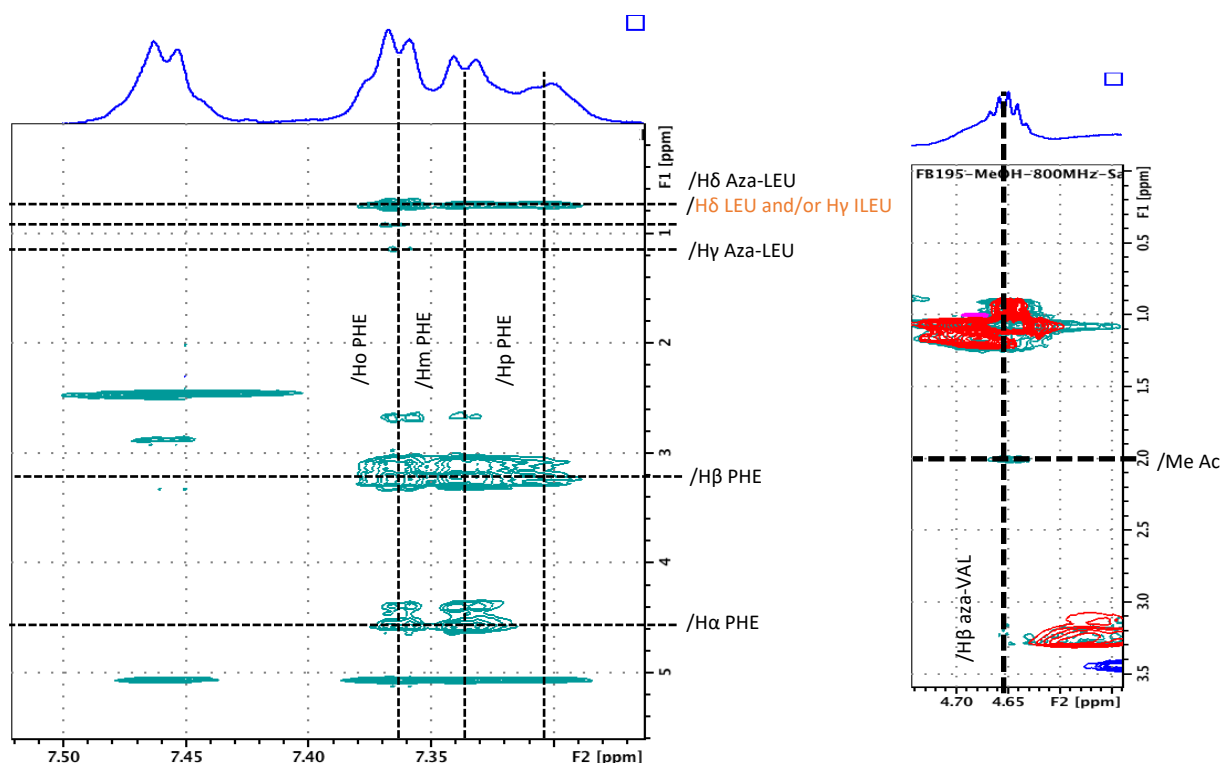


Figure. 16 Expansion of the 2D ^1H - ^1H ROESY of compound **14** showing the intra-strand ROEs involving the diaza-tripeptide arm and the weak inter-strand ROE (in light orange)

Evaluation of the effect of the synthesized compounds on hIAPP aggregation

Inhibition of hIAPP fibrillization

The evaluation on hIAPP fibrillization was performed for the hairpin **1-4**, **7-10**, **13-14**, the intermediate **11** and the arms **5-6**, **12**, **15** employing Thioflavin-T (ThT) fluorescence assay. ThT is a dye able to fluoresce upon binding to β -sheet rich structures (LeVine, H., 1999) and it is the standard dye used to study the aggregation kinetics of amyloidogenic proteins. The aggregation curve of hIAPP alone displays the classical sigmoidal pattern, characterized by 3 different portions: an initial lag phase of about 1h, followed by a rapid elongation phase which ends to a final plateau reached after about 5h. From the curve it is possible to collect two parameters: (1) F, maximal fluorescence measured at the plateau which is related to the highest amount of the formed fibrils (2) $t_{1/2}$, the time at which the fluorescence has reached the half of F. The inhibitory activity was evaluated at 3 different compound/peptide ratios: 10/1, 1/1 and 0.1/1; the calculated F and $t_{1/2}$ are summarized in table 14.

The longer hairpins **1-4** displayed significant and similar inhibitory effect on hIAPP fibrillization at the 3 tested ratios with a dose-dependent effect. Hairpin **1** showed only a slightly more pronounced activity on the fluorescence plateau compared to **2** ($\Delta F = -89, -49, -57\%$ vs $-76, -44, +22\%$ for **1** and **2** respectively, at 10/1, 1/1 and 0.1/1 ratios), however hairpin **2** exhibited a

significant higher activity in delaying aggregation, in particular at the highest ratio 10/1 ($\Delta t_{1/2} = +441\%$ for **2** vs $+230\%$ for **1**). For both hairpins **1** and **2**, the activity on $t_{1/2}$ was more modest at 1/1 and 0.1/1 ratios ($+15\% < \Delta t_{1/2} < +37\%$). Hairpin **3**, bearing the two pentapeptidic arms F₁₅LVHS₁₉ facing F₂₃GAIL₂₇, showed a comparable activity to **1** at a 10-fold excess ($\Delta t_{1/2} = +280\%$ vs $+230\%$ and $\Delta F = -87\%$ vs -89% for **3** and **1** respectively). Remarkably, hairpin **3** has proven to be the most potent inhibitor in this series since its activity on fibrillization kinetics was still significant at the low 1/1 and 0.1/1 ratios ($\Delta t_{1/2} = +166, +88\%$ and $\Delta F = -72, -78\%$ at the low 1/1 and 0.1/1 ratios respectively). Hairpin **4** which is the *N*-acetylated analogue of **3**, was significantly less active in particular in delaying the fibrillization ($+72\% < \Delta t_{1/2} < +56\%$ for **4** compared to $+280\% < \Delta t_{1/2} < +88\%$ for **3** at the three tested ratios). These results suggested that the position of the sequence F₂₃GAIL₂₇ at the C-terminus, its alignment with the sequence F₁₅LVHS₁₉, and the free N-terminus in hairpin **3** are three beneficial elements to reach a good effect even at low ratio 1/1 and 0.1/1 (**3**/hIAPP) on delaying the aggregation kinetics and decreasing the amount of fibrils of hIAPP. Minimal to no activity was observed for the isolated SREs, FGAIL (**5**) and FLVHS (**6**), demonstrating that these SREs are effective only when they are inserted in the whole β -hairpin structure.

Pleasantly, the hairpin **8**, bearing two shorter tripeptidic arms, retained most of the activity. Indeed, the free amine **8** significantly delayed the fibrillization at 10/1 ratio ($\Delta t_{1/2} = +147\%$, $\Delta F = -72\%$) but to a lesser extent than hairpins **1-3**. Nevertheless, at the low 1/1 and 0.1/1 ratios, the activity on hIAPP fibrillization was maintained and comparable to slightly better than for hairpins **1** and **2** ($\Delta t_{1/2} = +45\%, +27\%, +27\%$ for **8, 1** and **2** respectively; $\Delta F = -62\%, -49\%, -44\%$ for **8, 1** and **2** respectively, at 1/1 ratio). Here also the protection of the *N*-terminal amine was deleterious. Even if Boc-protected (**7**), acetylated (**9**) and trifluoroacetylated (**10**) compounds retained some activity on the fluorescence plateau comparable to the free amine hairpin **8** ($-57\% < \Delta F < -67\%$ at 10/1 ratio and $-60\% < \Delta F < -70\%$ at 1/1 ratio), however they were totally not efficient on the kinetics of hIAPP fibrillization. The Boc protected analogue **7** induced a very slight acceleration of the aggregation process ($\Delta t_{1/2} = -10\%$ and -13% respectively at 10/1 and 1/1 ratios). The lower efficiency of the three protected hairpins **7, 9** and **10** could be linked to their tendency to self-aggregate.

Interestingly, the hairpin of lower peptidic character **14**, bearing one diaza-tripeptide arm exceeded the activity of its peptide analogue **8** at the highest ratio 10/1 ($\Delta t_{1/2} = +186\%$ vs $+160\%$ for respectively **14** and **8**) but no effect was detected on the fibrillization rate at 1/1 and 0.1/1 ratios. Nevertheless, an important reduction of the fluorescence plateau was observed whatever the concentration tested ($\Delta F = -93, -85, -60\%$ for 10/1, 1/1 and 0.1/1 ratios), this reduction being more pronounced compared to the peptide analogue **8** ($\Delta F = -72, -62, -36\%$ for 10/1, 1/1 and 0.1/1 ratios). As observed for the peptide analogues **7** and **8**, the activity of the *N*-terminal Boc-protected hairpin **13** was lower; no effect was observed on the $t_{1/2}$ while the effect on the fluorescence plateau was maintained but slightly lower than for **14** at each ratio ($\Delta F = -88, -76, -48\%$ vs $-93, -85, -60\%$ for respectively **13** and **14** at 10/1, 1/1 and 0.1/1 ratios). Finally, to confirm that the entire β -hairpin structure was essential to modulate hIAPP fibrillization, the truncated molecule **11**, the peptide arm FLV **12** and the diaza-pseudo-peptide arm **15** were also evaluated by the Tht-fluorescence assay. The intermediate **11**, composed of the scaffold linked to only one tripeptide arm AIL, retained some activity ($\Delta t_{1/2} = +55\%$, $\Delta F = -52, -44\%$ for 10/1 and 1/1 ratios), but nevertheless much weaker than the full peptide (**8**) and peptidomimetic (**14**) hairpins. The peptide (**12**) and the diaza-tripeptide (**15**) arms were no to almost inactive.

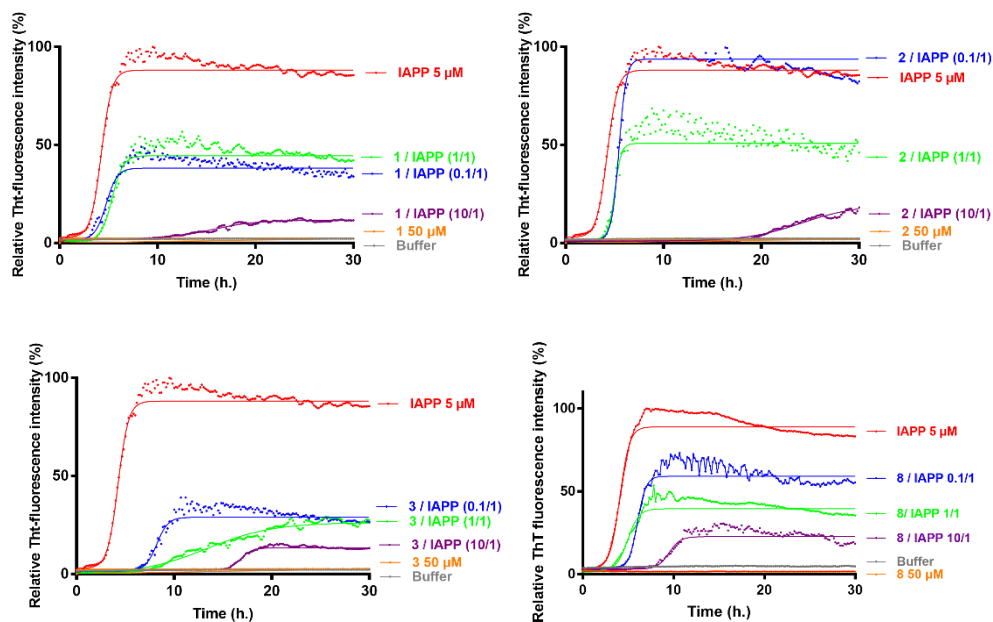
These results indicate that the peptide character can be lowered by decreasing the length of the peptide arms and by inserting an α /aza/aza/ pseudotriptide without compromising the inhibition of hIAPP fibrillization.

In order to evaluate the relative selectivity on hIAPP peptide, the ability of the most active compounds **1-3**, **8** and **14** to interact with $A\beta_{1-42}$, an amyloid protein involved in Alzheimer's disease and characterized by other amyloidogenic sequences, was also tested by the ThT-fluorescence assay. The longer peptide hairpins **1-3** were much less active on $A\beta_{1-42}$ than on hIAPP fibrillization (Table 15), and much less active than our reported hairpins **G1b** and **G2b** based on specific SREs from $A\beta_{1-42}$ (Pellegrino et al., 2017). No significant effect on the fibrillization kinetics of $A\beta_{1-42}$ was observed for the shorter tripeptidic hairpin **8**. On the contrary to its activity on hIAPP, this hairpin displayed no effect on $A\beta_{1-42}$ fluorescence plateau at 1/1 and 0.1/1 ratios, however it showed a comparable effect at high concentration. The diaza-pseudopeptide analogue **14** displayed no activity on the fluorescence plateau but slightly delayed the kinetics of fibrillization of hIAPP at 10/1 ratio ($\Delta t_{1/2} = +51\%$ on $A\beta_{1-42}$ vs $+186\%$ on hIAPP). These results confirm that our design based on specific hIAPP SREs is relevant, and also suggest that shortening the peptide or inserting diaza-pseudopeptide maintain the selectivity hIAPP/ $A\beta_{1-42}$.

Compound	Compound/hIAPP ratio ^[a]	$t_{1/2}$ extension/reduction (%) ^[b]	F extension/reduction (%) ^[c]
1	(10/1)	+230±20%	-89±2%
	(1/1)	+27±14%	-49±28%
	(0.1/1)	+15±8%	-57±18%
2	(10/1)	+441±64%	-76±5%
	(1/1)	+27±14%	-44±8%
	(0.1/1)	+37±9%	+22±13%
3	(10/1)	+280±65%	-87±2%
	(1/1)	+166±32%	-72±3%
	(0.1/1)	+88±47%	-78±8%
4	(10/1)	+72±16%	-73±3%
	(1/1)	+82±4%	-54±7%
	(0.1/1)	+56±25%	-46±5%
5	(10/1) ^[d]	ne ^[e]	-59±10%
	(1/1) 5	ne	-44±31%
	(0.1/1) 0.5	ne	-48±9%
6	(10/1)	ne	-46±10%
	(1/1)	ne	ne
	(0.1/1)	ne	ne
7	(10/1) ^[d]	-10±3%	-57±12%
	(1/1)	-13±1%	-70±5%
	(0.1/1)	ne	-37±9%
8	(10/1)	+147±24%	-72±8%
	(1/1)	+45±6%	-62±6%
	(0.1/1)	+64±2%	-36±2%
9	(10/1)	ne	-65±6%
	(1/1)	ne	-67±14%
	(0.1/1)	ne	-51±3%
10	(10/1) ^[d]	ne	-67±5%
	(1/1)	ne	-60±10%

	(0.1/1)	ne	ne
11	(10/1)	+55±6%	-52±8%
	(1/1)	ne	-44±1%
	(0.1/1)	nd ^[f]	nd
12	(10/1)	+25±9%	-19±4%
	(1/1)	ne	-58±9%
	(0.1/1)	-13±2%	+27±10%
13	(10/1) ^[d]	ne	-88±1%
	(1/1)	ne	-76±4%
	(0.1/1)	ne	-48±7%
14	(10/1)	+186±11%	-93±2%
	(1/1)	ne	-85±1%
	(0.1/1)	ne	-60±2%
15	(10/1)	ne	ne
	(1/1)	ne	ne
	(0.1/1)	ne	ne

Table. 14 Table summarizing the effects of compounds 1-15 on hIAPP fibrillization assessed by ThT-fluorescence spectroscopy at 10/1, 1/1 and 0.1/1 ratios of compound/hIAPP. Parameters are expressed as mean ± SE, n=3. ^[a] Unless otherwise indicated, compounds were dissolved in DMSO; the final concentration kept constant at 3 % (v). The concentration of hIAPP was 5 μM ^[b] See supporting information for the calculation of the $t_{1/2}$ extension/reduction. ^[c] See supporting information for the calculation of the F extension/reduction. ^[d] compounds 5, 10 and 13 self-aggregate at 50 μM, ^[e] ne = no effect, ^[f] nd = not determined.



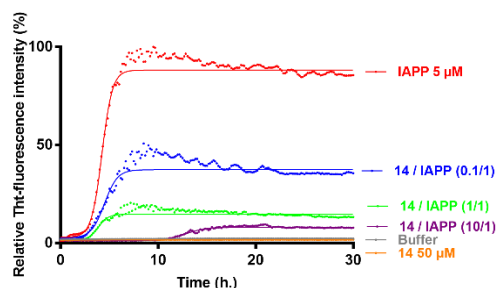


Figure. 17 Representative curves of ThT fluorescence assays over time showing hIAPP aggregation (5 μM) in presence of compounds **1-3**, **8** and **14** at compound/hIAPP peptide ratios = 0/1, 0.1/1, 1/1 and 10/1

Compound	Compound/ $\text{A}\beta_{1-42}$ ratio ^[a]	$t_{1/2}$ extension/reductio n (%) ^[b]	F extension/reductio n (%) ^[c]
G1b Pellegrino et al., 2017	(10/1) 100	NA	-97 \pm 1%
	(1/1) 10	NA	-90 \pm 1%
G2b Pellegrino et al., 2017	(10/1) 100	NA	-95 \pm 1%
	(1/1) 10	>+356 \pm 12%	-73 \pm 3%
1	(10/1) 100	+99 \pm 32%	-29 \pm 3%
	(1/1) 10	+28 \pm 4%	ne
	(0.1/1)1	ne	ne
2	(10/1) 100	+102 \pm 22%	+84 \pm 23%
	(1/1) 10	ne	ne
	(0.1/1)1	ne	-35 \pm 6%
3	(10/1) 100	+75 \pm 21%	-14 \pm 5%
	(1/1) 10	+43 \pm 13%	-27 \pm 8%
	(0.1/1)1	ne	ne
8	(10/1) 100	-13 \pm 4%	-61 \pm 7%
	(1/1) 10	+13 \pm 7%	ne
	(0.1/1)1	ne	ne
14	(10/1) 100	+51 \pm 19%	+8 \pm 2%
	(1/1) 10	ne	ne
	(0.1/1)1	ne	ne

Table. 15 Table summarizing the effects of compounds **1-3**, **8** and **14** on $\text{A}\beta_{1-42}$ fibrillization assessed by ThT-fluorescence spectroscopy at 10/1, 1/1 ratios of compound/ $\text{A}\beta_{1-42}$. Parameters are expressed as mean \pm SE, n=3. ^[a] Unless otherwise indicated, compounds were dissolved in DMSO; the final concentration kept constant at 0.5 % (v). The concentration of $\text{A}\beta_{1-42}$ was 10 μM ^[b] See supporting information for the calculation of the $t_{1/2}$ extension/reduction. ^[c] See supporting information for the calculation of the F extension/reduction. ^[d] compounds **1** and **2** self-aggregate at 100 μM , ^[e] ne = no effect, ^[f] nd = not determined, ^[g] NA = no aggregation.

Fibrils imaging by TEM

To evaluate the impact of the hairpins on the morphology of the hIAPP fibrillar material, Transmission electron microscopy (TEM) images were acquired for the three hairpins **3**, **8** and **14**. These analyses were performed after 17 h of incubation, corresponding to the time needed to reach the complete conversion of hIAPP monomer into fibrils in the ThT assay. hIAPP control sample showed the usual extremely dense network of long and tangled fibrils (Fig. 18a). The compounds were tested at the inhibitor/hIAPP ratio of 10/1. In the presence of hairpin **3** bearing pentapeptide sequences, a drastic reduction in the density of network formed by very shorter fibers was observed compared to the control sample (Fig. 18b versus 18a). For both compounds **8** and **14** (Fig. 18c and 18d) bearing two tripeptide sequences and one diaza-tripeptide sequence respectively, the amount of fibers remained significantly less important and shorter than in the control grid but longer than for the sample **3**. The comparable density of the fibers in samples **3**, **8** and **14** was in accordance with the similar reduction of the fluorescence plateau in the ThT experiment. The fibers of the grid of **14** appeared less tangled compared to the other grids. Thus, these results were consistent with the ThT-fluorescence data and confirmed the efficiency of hairpins **3**, **8** and **14** in disrupting and reducing the fibrillization process of hIAPP amyloid peptide.

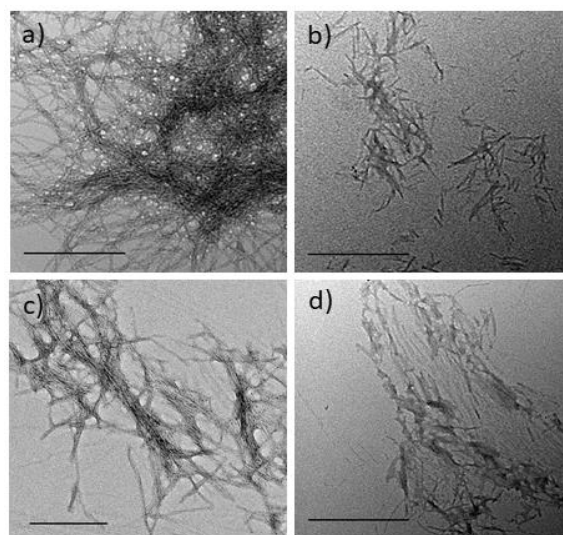


Figure. 18 Effect of hairpins on the fibrillization of hIAPP visualized by TEM (scale bars 500 nm). Negatively stained images recorded after 17 h of incubation of a 5 μ M solution of hIAPP alone (a) or in the presence of a 50 μ M solution of inhibitor: **3** (b), **8** (c), **14** (d)

Effect of the hairpins on membrane permeability and on membrane fibril formation

Considering that hIAPP is known to modify the properties of membranes, by modulating the membrane structure and by altering the permeability, the ability of the hairpins to reduce hIAPP-induced membrane damage was tested in DOPC/DOPS membranes (LUVs). The fluorescence signal of the encapsulated fluorophore was measured using calcein, a highly fluorescent molecule whose fluorescence is self-quenched at high concentrations. High concentrations of calcein were thus encapsulated into LUVs, and upon membrane disruption by hIAPP, the dye is released, and

the subsequent dilution leads to enhanced fluorescence. The fluorescence in the presence of the hairpins is then compared to the one in the absence of the hairpins to validate their efficacy.

The leakage kinetics is shown in Fig. 19A for hIAPP alone (grey) and in the presence of the hairpin **3** (green) in DOPC/DOPS vesicles at 25°C. The spontaneous calcein leakage through lipid membranes in the absence of hIAPP was found to be negligible. Our data indicate that 5 μM of hIAPP induces significant leakage in DOPC/DOPS vesicles to about 57% of the total vesicle content, in agreement with previous report. (Hoffmann et al., 2018) The process of hIAPP-induced membrane leakage is characterized by an S-shaped curve with a $t_{1/2}$ of approximately 4.5 h. The same experiments were done for hIAPP in the presence of the three most active hairpins **3**, **8** and **14** and compared with an experiment in the presence of the slightly less active hairpin **10**. The compounds were evaluated at 1/1 ratio and similar sigmoidal curves were obtained but were more or less shifted. The kinetics data obtained from the sigmoidal curves are given in Fig. 19B and indicate that the presence of **10** only slightly delay the kinetics of membrane damage from 4.5 h for hIAPP alone to 5.6 h while hairpins **3**, **8** and **14** have a more drastic effect in the lag phase increase. Indeed, the $t_{1/2}$ increases from 4.5 h for hIAPP alone to 10.5 h, 8.7 h and 8.0 h for **3**, **8** and **14** respectively. Altogether, these results demonstrate that the hairpins **3**, **8** and **14** not only decrease the kinetics of hIAPP fibril formation but also delay hIAPP-induced membrane damage even at a low ratio 1/1 hairpin/hIAPP.

Afterwards, we decided to study the characteristics and morphology of hIAPP in the presence of the hairpins using transmission electron microscopy. The hIAPP fibrils exhibited the typical morphology of long and twisted amyloid fibrils (Fig. 19C). Similar fibrils were observed in the presence of hairpins **3**, **8**, **10** and **14**, however the network of the fibrils was less dense and had a lower frequency compared to the fibrils formed by hIAPP alone (Fig. 19D-G). It is interesting to note that for the hairpins **3**, **8** and **10**, a few vesicles are surrounded by the fibrils and that those vesicles in contact with the fibrils somehow show distorted shapes. Altogether, the membrane leakage and the TEM indicated that the hairpins interacted strongly with hIAPP in the presence of membrane but are not able to totally inhibit hIAPP-fibril formation.

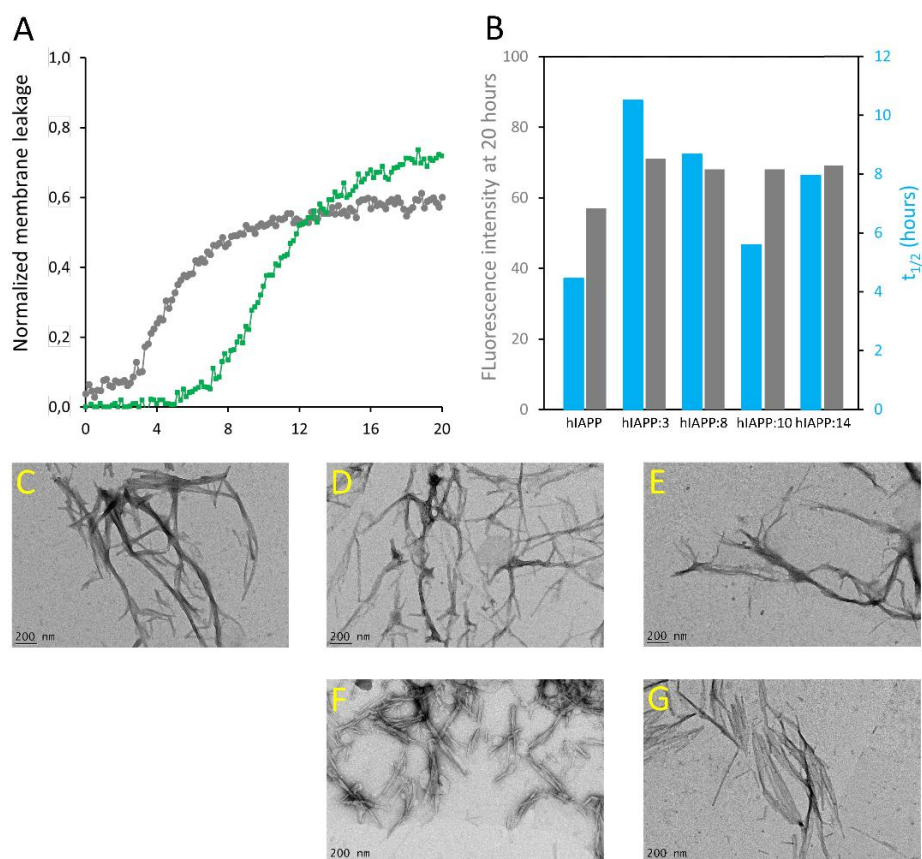


Figure. 19 (A) Kinetics of membrane disruption induced by 5 μ M hIAPP in the absence (grey) and in the presence (green) of the hairpin 3 (ratio 1:1) in 10 mM Tris-HCl, 100 mM NaCl buffer at pH 7.4. hIAPP and the hairpin were added to the calcein-containing DOPC/DOPS LUVs (100 μ M) at time zero (B) The value of the intensity of the final plateau (grey) and the average half-time ($t_{1/2}$, blue) are reported for each hairpin tested in the same condition (5 μ M hIAPP, 5 μ M hairpin, 100 μ M LUVs). Negatively stained microscopy images of mature hIAPP (C) alone and in the presence of the hairpins **3** (D), **8** (E), **10** (F) and **14** (G) at a ratio 1:1 after 24 hour of incubation with vesicles composed of DOPC/DOPS (7:3) (scale bars 200 nm).

Effect on the oligomerization process: capillary electrophoresis (CE)

We then evaluated the effect of the three hairpins **3**, **8** and **14** on the oligomerization process of hIAPP peptide using a CE method. Recently some of us have developed a CE technique able to monitor the soluble oligomeric species formed during the early hIAPP aggregation process. (Berardet et al., 2018; Berardet et al., 2020) The control electropherogram of hIAPP, shown in Fig. 18a), displayed over time the typical profile, showing three groups of soluble species : peak 3 is mainly composed by monomers with a small amount of dimers and trimers and peaks 1 and 2 are assigned to oligomeric aggregates larger than 25-mers (with peak 1 co-migrating with the electroosmotic flow EOF). (Berardet et al., 2018) Over time, the monomer peak 3 decreased steadily to almost disappear at 10h and in the meantime, the oligomeric peak 2 regularly increased

(Fig. 18a). The CE evaluations were conducted at 3 different compound/hIAPP ratios: 10/1, 1/1 and 0.5/1. In the presence of hairpin **3** bearing two pentapeptide arms, at 1/1 ratio, the quantity of monomeric species (peak 3) was significantly preserved until 5 h while in the control sample more than half of it disappeared (93% vs 43% of monomer maintained) (Fig. 18a) and c)). After 5 h, the kinetics of disappearance of the monomer was similar to the one observed for the control sample. Hairpin **3** was also tested at a 10-fold excess, but at this high concentration, the peak 4 corresponding to **3** itself (see control of **3**, Fig. 18e)) was very intense and partially merged with the monomer peak 3, preventing its monitoring (Fig. 18b)). Surprisingly, in contrast with the Tht results, the hairpin **3**, displayed the stronger activity on hIAPP oligomerization at the substoichiometric ratio of 0.5/1 (**3**/hIAPP, Fig. 18d)); the monomer being maintained up to 26% until 20 h while it almost disappeared in the control hIAPP experiment at 10h (Fig. 18a)), and at 15 h at 1/1 ratio (Fig. 18c)). Concerning the control electrophoretic profile of hairpin **3** at 50 μ M, an enlargement of its peak 4 was observed during the kinetics, and an additional peak 4' migrating close to the EOF was observed and increased over the time. (Figures 18e)). We attributed this peak to self-aggregated species that might explain the lack of activity of hairpin **3** at the highest ratio 10/1 (we also suspected self-aggregation of hairpin **3**, as peak 4 was more intense at t0 in the experiment at 0.5/1 ratio than in at the 1/1 ratio). Insert the results of **8** (Figure 19). As for hairpin **3**, the monitoring of **14** was not possible at 10-fold excess because of the strong intensity of the peak 4 corresponding to **14** itself very closed to the monomer peak (see control of **3**, Fig. 20b)). On the contrary to **3**, the peptidomimetic hairpin **14** displayed no activity at 1/1 ratio; the intensity of the monomer peak being comparable to what was observed for the control experiment (Figure 20d) and f)). However, hairpin **14** displayed a strong and significative activity at the substoichiometric ratio of 0.5/1 (**14**/hIAPP) (Figure 20e)); the monomer being significantly preserved until 5 h while in the control sample its amount was reduced by more than half (82% vs 35% of monomer maintained). Its activity was maintained at 10 h with a monomer quantity being twice more important than for the control (21% vs 11% of monomer maintained). Unlike the longer peptidic hairpin **3** which maintained the monomeric species, especially at the end on the kinetics, the di-aza-peptidomimetic hairpin **14** was more active at the beginning of the kinetics. This result could be related to the weaker recognition surface between **14** and the amyloid peptide (reconsider this hypothesis based on the results obtained with **8**).

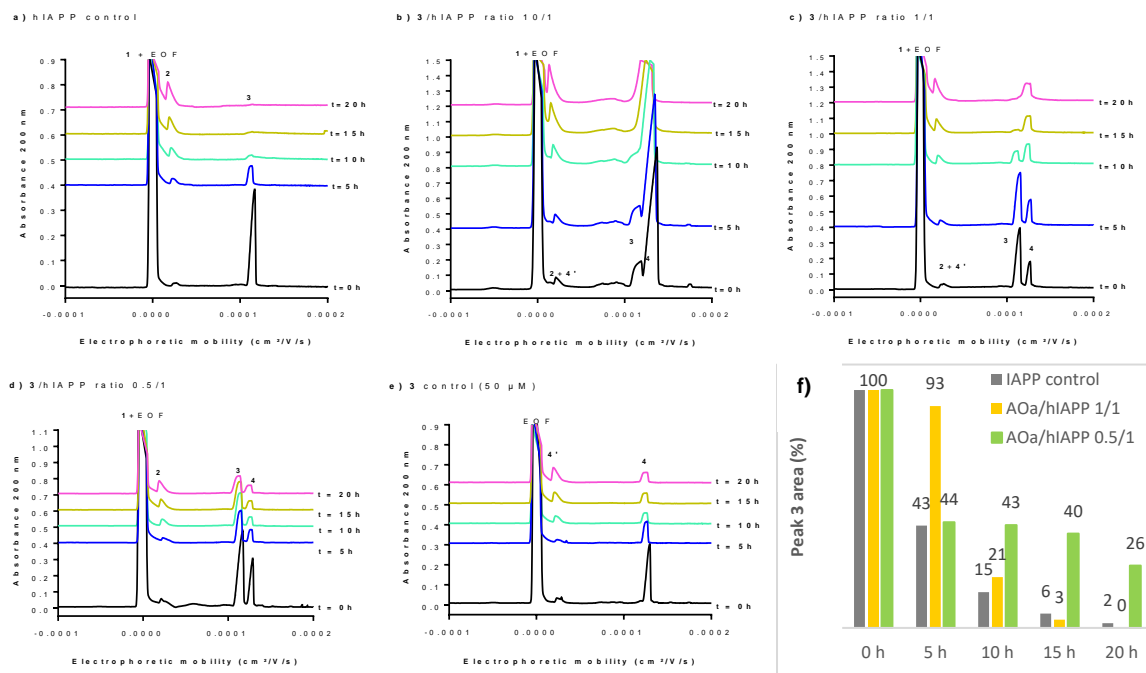


Figure. 20 Electrophoretic profiles over time (0 to 20h) of control samples of **a)** hIAPP (100 μ M) and **e)** hairpin **3** (50 μ M). EOF: electroosmotic flow; Peaks **1** and **2**: large hIAPP oligomer species; Peak **3**: monomer of hIAPP; Peak **4**: hairpin **3**; Peak **4'**: self-aggregated species of hairpin **3**. Electrophoretic profile over time (0 to 20 h) of hIAPP peptide (100 μ M) incubated with **3** at **3**/hIAPP ratio of: **b)** 10/1, **c)** 1/1, **d)** 0.5/1, **f)** Evolution of the hIAPP monomer area (peak 3) over time in the absence or in the presence of **3** (at 1/1 and 0.5/1 ratios) relative to hIAPP monomer peak area at t = 0 h

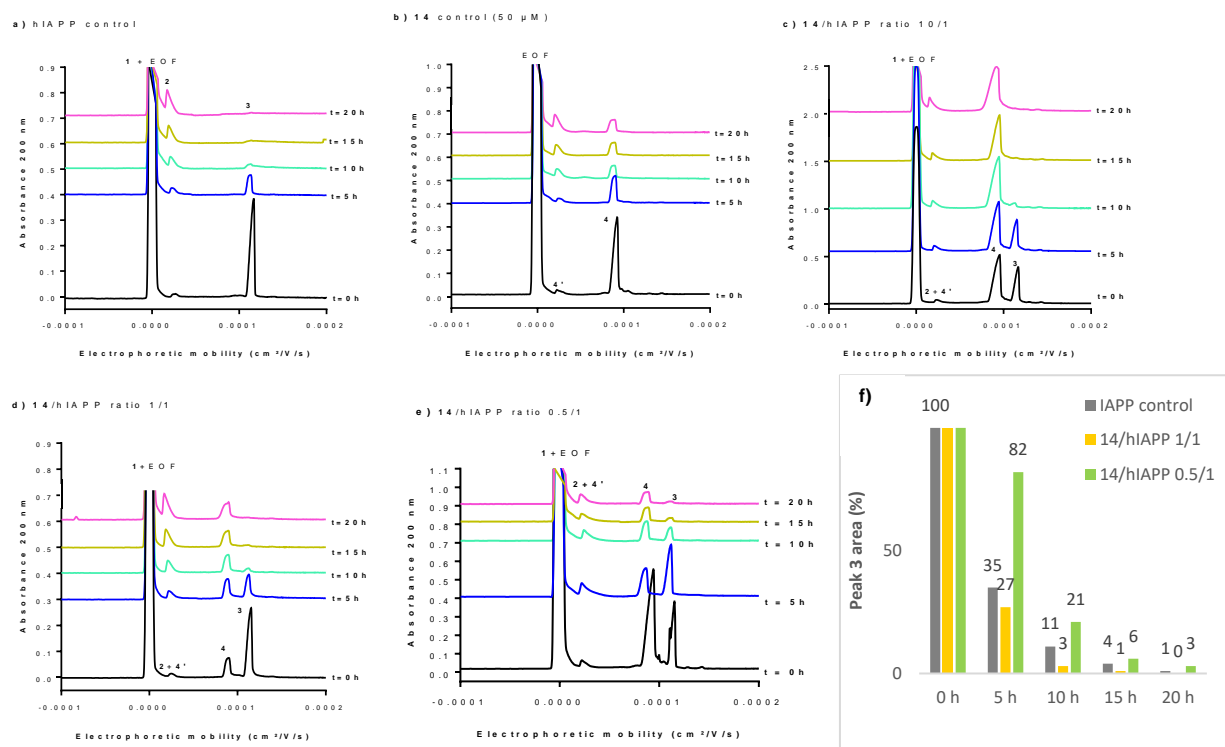


Figure 21 Electrophoretic profiles over time (0 to 20h) of control samples of **a)** hIAPP (100 μ M) and **b)** hairpin 14 (50 μ M). EOF: electroosmotic flow; Peaks 1 and 2: large oligomer species; Peak 3: monomer of hIAPP; Peak 4: hairpin **14**; Peak 4': self-aggregated species of hairpin **14**. Electrophoretic profile over time (0 to 20 h) of hIAPP peptide (100 μ M) incubated with **14** at compound/hIAPP ratio of : **c)** 10/1, **d)** 1/1, **e)** 0.5/1. **f)** Evolution of the hIAPP monomer area (peak 3) over time in the absence or presence of **14** (at 1/1 and 0.5/1 ratios) relative to hIAPP monomer peak area at t = 0 h.

Effect on the oligomerization process: ion mobility spectroscopy-mass spectrometry (IMS-MS)

Over the last years, mass spectrometry (MS) and ion mobility coupling (IMS-MS) have been reported as a pertinent tool for the identification of the oligomeric species formed during the aggregation process. This was exemplified with the detection of prion oligomers using SEC and ion mobility coupled with mass spectrometry under “native” detection for the first time (Van der Rest and Halgand, 2017). A similar approach was used to characterize beta-amyloid oligomer-aggregates properties (Iuraşcu et al, 2009). In addition, they also have been reported as powerful methods for studying the mechanism of hIAPP aggregation inhibitors (Berardet et al, 2020; Young et al, 2014; Young et al., 2015; Riba et al., 2015; Li et al., 2015; Young et al., 2016). Using the same buffer as for CE experiments allowed us to study the effect of the hairpins **3**, **8** and **14** on the oligomerization process of hIAPP at 3 different hairpin/hIAPP ratios (10/1, 5/1 and 1/1).

The MS spectrum of hIAPP control presents the classical sets of multicharged monomeric and oligomeric species; dimers to pentamers are visible on the mass spectrum (Fig. 22a). In the presence of hairpin **3** at the three different ratios, high mass oligomer species such as dimers and trimers, decreased to finally nearly totally disappear at ratio 10/1 (Fig. 22d). At ratio of 5/1 (Fig. 22 c) the formation of dimers and trimers was also strongly inhibited with the disappearance of

trimers and the remaining of only small amounts of dimers. Finally, at the ratio 1/1 (Fig. 22 b), dimers and trimers were the only oligomers that were observed. We can conclude that hairpin **3** has an anti-oligomerization activity on hIAPP preventing the formation of the small oligomeric species, and that it preferentially interacts with the monomer and the dimer to form non-covalent complexes $[M + 3]$ and $[2M + 3]$ of several natures.

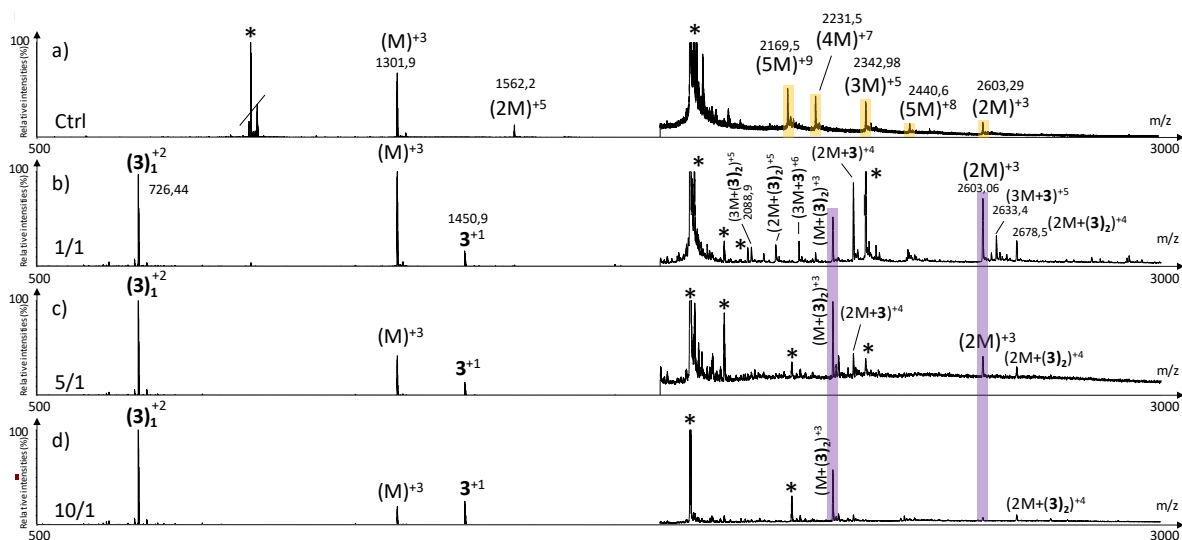


Figure. 22 Mass spectra for the 500-3000 m/z range of hIAPP control **a**) (IAPP oligomers are labeled in orange) and hIAPP in the presence of hairpin **3** at three different ratios of **3**/hIAPP : **b**) 1/1, **c**) 5/1 and **d**) 10/1. The different species are labeled with the number of IAPP monomer, the addition of n molecules of hairpin **3** and the charge state of the ion corresponding to this complex (e.g. $(2M+(3)_2)^{+5}$, is the dimer complexed with two molecules of hairpin **3** and refers to the ion of m/z 2142.9 having a +5 charge state). Peaks labeled with an asterisk belong to contaminants. Regions labeled in purple illustrate relevant changes.

Addition of tripeptidic hairpin **8** at a 10/1 ratio led to the inhibition of all oligomeric species; monomeric hIAPP being the only visible species ($[M]^{+3}$, $[M]^{+2}$, Fig. 23d). This inhibition is slightly less efficient at ratio 5/1; monomers remaining the major species with a very small quantity of dimer $[2M]^{+3}$ (Fig. 23c). At a 1/1 ratio, trimer of hIAPP $[3M]^{+5}$ are also formed. As hairpin **3**, hairpin **8** has an anti-oligomerization activity on hIAPP preventing the formation of the small oligomeric species (Fig. 23b). Moreover, it binds preferentially to the monomer and the pentamer of hIAPP, forming non-covalent complexes of several natures ($[M + 8]$ and $[5M + 8]$); the pentameric complex being mainly form at the lowest 1/1 ratio and decreasing when the concentration of **8** increases.

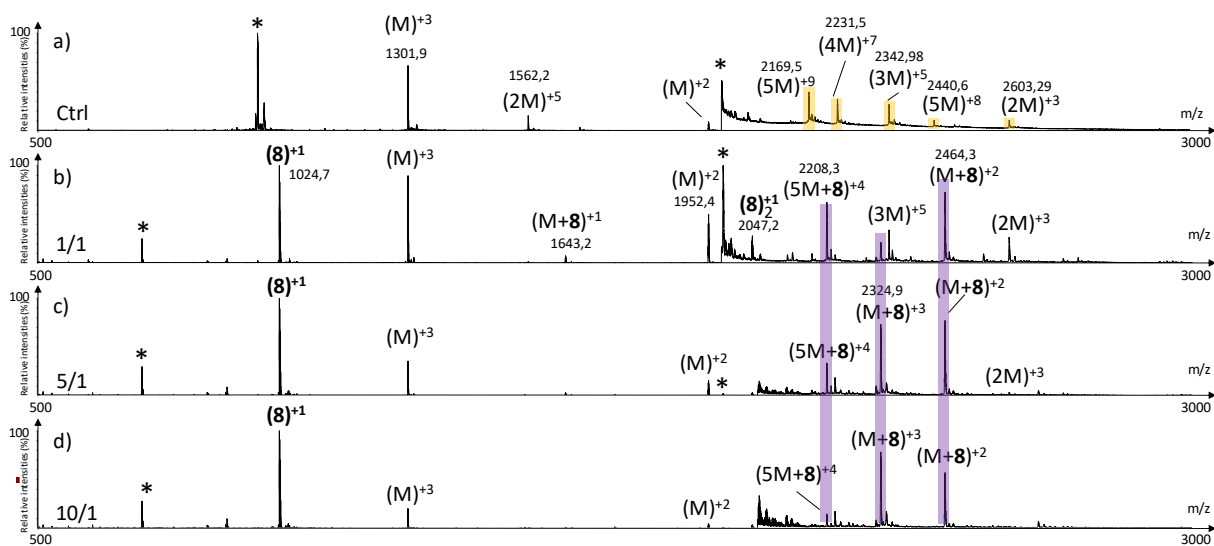


Figure 23 Mass spectra for the 500-3000 m/z range of hIAPP control **a**) (IAPP oligomers are labeled in orange) and hIAPP in the presence of hairpin **8** at three different ratios of **8**/hIAPP : **b**) 1/1, **c**) 5/1 and **d**) 10/1. The different species are labeled with the number of IAPP monomer, the addition of n molecules of hairpin **8** and the charge state of the ion corresponding to this complex (e.g. $(5M+8)^{+4}$). Peaks labeled with an asterisk belong to contaminants. Regions labeled in purple illustrate relevant changes.

Like for the hairpins **3** and **8**, the mass spectra in the presence of **14** (Fig. 24) showed the disappearance of the high mass oligomer species observed on the IAPP control. The effect on the formation of small oligomers (dimer and trimer) was dose dependent: almost none formed at the ratio 10/1 (Fig. 24d), a very small amount at the ratio 5/1 (Fig. 24c) and presence of dimers and trimers for the ratio 1/1 (Fig. 24b). Non-covalent complexes formed between hairpin **14** and monomers of hIAPP $(M+14)^{+2}$ and between **14** and dimers $(2M+14)^{+4}$ for 1/1 and 5/1 ratios were also detected; the only complex detected at 10 fold excess being with the monomeric form of hIAPP $(M+14)^{+2}$.

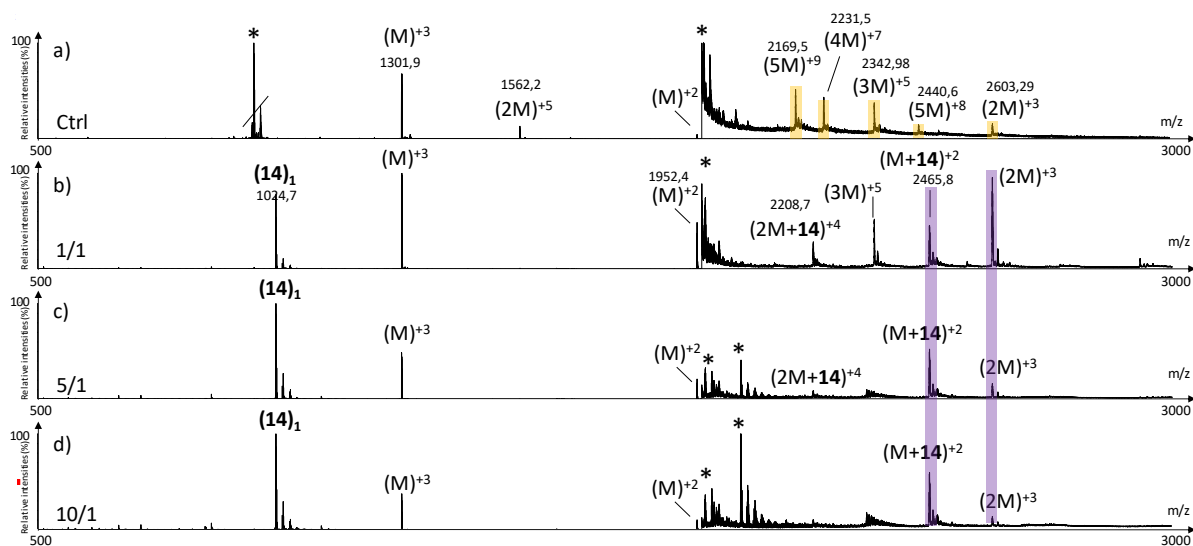


Figure 24 Mass spectra for the 500-3000 m/z range of hIAPP control **a**) (IAPP oligomers are labeled in orange) and hIAPP in the presence of hairpin **14** at three different ratios of **14**/hIAPP : **b**) 1/1, **c**) 5/1 and **d**) 10/1. The different species are labeled with the number of IAPP monomer, the addition of n molecules of hairpin **14** and the charge state of the ion corresponding to this complex (e.g. $(2M+(14)_2)^{+4}$). Peaks labeled with an asterisk belong to contaminants. Regions labeled in purple illustrate relevant changes.

Among the different hairpin/hIAPP peptide ratios, we decided to make a comparison between the 3 hairpins at the lower ratio of 1/1. We observed that the pentamers and tetramers have disappeared for the 3 hairpins. The trimer ($3M^{+5}$) was not detectable for the longer hairpin **3** but still visible for **8** and **14**. Whereas the dimer ($2M^{+3}$) was still formed in presence of the three hairpins. Indeed, it appeared that compound **3** formed non covalent complexes with various oligomers ($[2M+3]$, $[3M+3]$) and no complexes with the monomer of hIAPP whereas compounds **8** and **14** formed the same non-covalent complex with monomeric hIAPP ($[M+8/14]$) and only one complex with an oligomer for each hairpin ($[5M+8]$ $[2M+14]$). These observations allow us to conclude that hairpins **3**, **8** and **14** exhibit an efficient anti-oligomeric activity; and that the shorter hairpins **8** and **14** bind more preferentially to the monomeric form of hIAPP than the longer hairpin **3**.

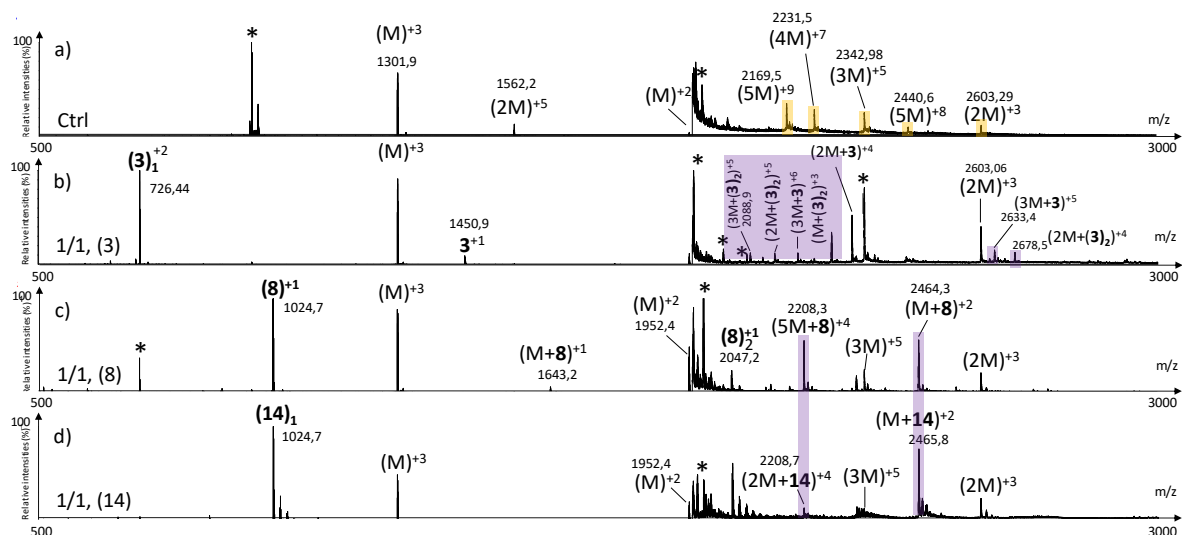


Figure. 25 Mass spectra for the 500-3000 m/z range of hIAPP control a) (IAPP oligomers are labeled in orange) and hIAPP in the presence of hairpin 3 (b), 8 (c) and 14 (d) for 1/1 ratio. The different species are labeled with the number of IAPP monomer, the addition of n molecules of dedicated hairpin and the charge state of the ion corresponding to this complex (e.g. $(2M+(\text{hairpin})_2)^{+4}$). Peaks labeled with an asterisk belong to contaminants. Highlighted regions show regions of interest. Regions labeled in purple illustrate relevant changes.

DISCUSSION

Nowadays, the reduction of blood glycemic level is still the standard therapy in T2D, although it does not represent an etiological treatment. Over the last decades, mounting evidences about the link between hIAPP peptide deposits and pancreatic β -cells loss have made that hIAPP peptide has become a promising target in the development of new T2D treatments. Only very few inhibitors of hIAPP aggregation and mainly natural compounds such as polyphenols (Pithadia et al. 2016), have been reported to date. Furthermore, they are generally described as non selective because they have been reported as inhibitors of other amyloid proteins such as $A\beta_{1-42}$ involved in AD, but also as potential other therapeutic agents to combat other many diseases.

The recent dramatic increased of peptides approved or in active development in various therapeutic areas corroborates that peptides are reasonable alternatives to small molecule pharmaceuticals and to biologics (Henninot et al. 2018; Lau et al. 2018). Greater efficacy, selectivity, and a reduced risk of unforeseen side-reactions compared to small organic molecules, combined with strategies to improve their pharmacokinetics properties explain this revival of interest of peptides in pharmaceutical science. Only few peptide or pseudopeptide derivatives (Armiento et al., 2020; Yan et al., 2013; Gilead et al., 2004; Paul et al., 2017; Cheng et al., 2012) have been reported as hIAPP aggregation inhibitors.

We previously reported that designing specific acyclic β -hairpin peptidomimetics built on a piperidine-pyrrolidine β -turn inducer and on self-recognition elements (SRE), selected from $A\beta_{1-42}$, were able to decrease $A\beta_{1-42}$ aggregation and to preserve $A\beta_{1-42}$ monomers (Pellegrino et al., 2017; Tonali et al., 2018). These compounds were selective for $A\beta_{1-42}$ and not active on hIAPP

aggregation. In the present work we hypothesized that this strategy can be generalized and applied to the selective inhibition of the aggregation of hIAPP.

By carefully selecting SREs derived from hIAPP amyloidogenic sequence and by modifying the length of the peptide sequences, the N-terminus or by incorporating a diaza-peptide motif, this study allowed us to explore the inhibitory behaviour in relation with the structural modifications introduced in our compounds.

The selection of the most active compounds was performed by ThT fluorescence spectroscopy, that is a technique exploring the kinetics of aggregation but more informative on the late fibrillization process. Hairpins **3** and **4** based on models reported by Wu et al in 2013, Wiltzius in 2008 and Liang et al in 2013 are bearing two SREs : the amyloidogenic sequence F₂₃GAIL₂₇ at their C-terminus and F₁₅LVHS₁₉ at their N-terminus. They were more active than compounds **1** and **2** based on models reported by Kajava et al. in 2005, Mirecka et al. in 2016 and Andreetto et al. in 2015, where the amyloidogenic sequence N₂₂FGAIL₂₇ was facing A₁₃NFLV₁₇. Although **3** was slightly more active than **4**, we suggest that a free terminal amine is not mandatory for the activity but is helpful to increase the solubility.

Shortening the peptidic sequence, we observed that three amino acids per arm in compounds **7-10** were sufficient to maintain the activity against hIAPP aggregation, although slightly lower than that for compound **3** bearing pentapeptides. Also in this series the compound characterized by the free terminal amine (**8**) was more active than the differently N-protected analogues **7**, **9** and **10** (Boc, acetyl and trifluoroacetyl) that have the tendency to self-aggregate. Finally, the replacement of the tripeptidic blocking sequence by a α /aza/aza/ pseudotriptide led to compound **14** whose inhibitory activity was even higher in decreasing the fluorescence plateau than the one displayed by its peptidic analogue **8**. The evaluation of truncated molecule **11** and arms **5**, **6**, **12** and **15**, corroborates the necessity of a whole hairpin to inhibit hIAPP aggregation. The ability of the best compounds **3**, **8** and **14** to disrupt and reduce the late fibrillization of hIAPP was confirmed by TEM imaging. The lack of activity of the best compounds **3**, **8** and **14** on A β ₁₋₄₂, compared with their efficiency on hIAPP fibrillization, and compared with our reported hairpins **G1b** and **G2b** designed for A β ₁₋₄₂ (Pellegrino et al., 2017) was next proven. This result validate our selection of SREs from hIAPP sequences.

The ability of compounds **3**, **8** and **10** to modulate hIAPP aggregation reflects in a strong delay of membrane damage induced by the presence of hIAPP peptide, as evaluated by calcein leakage through lipid membranes mimicked by DOPC/DOPS vesicles. However, in the presence of membranes, these three compounds were not able to totally prevent the fibrils formation.

The next step was to evaluate the ability of our compounds to decrease the presence of toxic oligomers and to maintain the presence of non toxic monomers, as it is now well established that oligomers of hIAPP are toxic species (Bram et al, 2014; Rodriguez et al. 2018; Kiriya et al, 2018). The very early steps of the oligomerization process overtime and the analysis the effect of our hairpins on these challenging first stages was thus performed by our reported methods CE and IMS-MS (Berardet et al., 2018; Berardet et al. 2020). The most promising compounds **3**, **8** and **14** as inhibitors of hIAPP fibrillization possess also a strong anti-oligomeric activity, and are able to stabilize the less toxic monomer species. .Even at low ratio (hairpin/hIAPP 0.5/1 or 1/1), they were able to preserve the monomer species in the CE and IMS-MS assays. A slightly superior activity of the longer hairpin **3** was observed. Interestingly, we observed by IMS-MS that compound **3** formed non covalent complexes with hIAPP oligomers (dimers and trimers) and no complex with monomers whereas compounds **8** and **14** formed non-covalent complexes with monomeric hIAPP and with pentamers for **8** and dimers for **14**.

The NMR conformational studies performed for the most active compounds of the series **3**, **8** and **10**, as well as for the two acetyl derivatives **4** and **9** allowed us to confirm their β -hairpin structure. However, a dynamic equilibrium between two different β -hairpin architectures was generally observed and was explained thanks to MD simulations, which suggest that conformation of the torsion angle $C\alpha-C-N-C2$ between Leu-3 and Pip-4 impacts the spatial proximity of the two peptide arms. The presence of the semi-rigid piperidine-pyrrolidine scaffold allows flexibility that might be important for the activity. Indeed this has been already suggested in our previous studies to inhibit $A\beta_{1-42}$ in which hairpins based on this piperidine-pyrrolidine scaffold (Pellegrino et al., 2017) were much more efficient than very stable hairpins based on diketopiperazine scaffold (Vahdati et al, 2017). Our results corroborate the hypothesis that compounds possessing several kinetically and thermodynamically accessible local minima representing conformations might be much more powerful inhibitors with respect to rigid ones in modulating protein-protein interactions (Li et al, 2015; Ko et al, 2012).

CONCLUSION

The work reported in this paper is the proof of concept that our inhibitory strategy represents a versatile approach for the development of compounds able to inhibit different amyloidogenic peptides. We also demonstrated that our hairpins are able not only to delay hIAPP fibrillization process but also to delay the membrane damage. This effect on the membrane damage could be linked to the effect that our inhibitors exert on the oligomeric species formations. Finally, with a view to develop a new treatment for T2D, we demonstrated that it is possible to prepare a more druggable compound with lower peptidic character maintaining an excellent inhibitory activity. Furthermore, the deeper structural analysis that we performed allowed us to draw some guidelines to better characterize the dynamic equilibrium between conformers of the hairpin compounds. Our compounds based on a semi-rigid piperidine-pyrrolidine β -turn mimic, and on specific small peptide arms selected from hIAPP, corroborate that they can be selective drug candidates to inhibit hIAPP aggregation involved in T2D. They also attest that flexible β -hairpin mimics might adapt to different conformations and to different monomer or oligomer species of amyloid proteins to prevent the presence of toxic oligomers and to impact the fibrils formation. We strongly believe that flexible small acyclic β -hairpins represent also valuable bio-chemical tools to further elucidate the interaction of amyloid proteins with membranes and lipids and with other components of cells, and to better understand the mechanism of toxicity of these proteins on membranes and on cells. We also strongly deem that these flexible small β -hairpin mimics could be used to study and to combat other diseases associated with protein-protein interactions involving β -sheet structures, that are far to be understood or even discovered, such as in cancer, in neurodegenerative diseases, or in infections (Laxio et al, 2019).

CONFLICT OF INTEREST

The authors declare that the research was conducted in the absence of any commercial or financial relationships that could be construed as a potential conflict of interest.

ACKNOWLEDGMENTS AND FUNDING

The Laboratory of Excellence LERMIT is thanked for financial support for F. Bizet (LERMIT is supported by a Grant from ANR, ANR-10-LABX-33). The Ministère de l'Enseignement Supérieur et de la Recherche (MESR) is thanked for financial support for J. Lesma. Karine Leblanc (BioCIS, UMR 8076) is thanked for her help with the HPLC analysis. Agostino Oliva ((BioCIS, UMR 8076, Erasmus student from the Università degli Studi di Milano) is thanked for his help in the preparation of β -hairpin compounds. Ghislaine Frébourg (Institut de Biologie Paris Seine (IBPS)/FR 3631, Service de Microscopie Electronique, Université Pierre et Marie Curie (UPMC), France) and Sandra Casale (Institut des Matériaux de Paris Centre, Sorbonne Université, France) are thanked for their contribution to electron microscopy. The laboratory PNAS is a member of the Laboratory of Excellence Nanosacly supported by a Grant from ANR (ANR-10-LABX-0035).

REFERENCES

Akter, R., Cao, P., Noor, H., Ridgway, Z., Tu, L.-H., Wang, H., Wong, A.-G., Zhang, X., Abedini, A., Schmidt, A.-M., Raleigh, D.-P. (2016). Islet Amyloid Polypeptide: Structure, Function, and Pathophysiology. *J Diabetes Res*, 2016, 2798269. doi.org/10.1155/2016/2798269

Andreetto, E., Malideli, E., Yan, L.-M., Kracklauer, M., Farbiarz, K., Taterek-Nossol, M., Rammes, G., Prade, E., Neumüller, T., Caporale, A., Spanopoulou, A., Bakou, M., Reif, B., Kapurniotu, A. (2015). A Hot-Segment-Based Approach for the Design of Cross-Amyloid Interaction Surface Mimics as Inhibitors of Amyloid Self-Assembly. *Angew. Chem. Int. Ed.* 54, 13095–13100. doi.org/10.1002/anie.201504973

Armiento, V., Spanopoulou, A., Kapurniotu, A. (2020). Peptide-Based Molecular Strategies To Interfere with Protein Misfolding, Aggregation, and Cell Degeneration. *Angew. Chem. Int. Ed.* 59, 3372 – 3384. doi.org/10.1002/anie.201906908.

Bedrood, S., Li, Y., Isas, J. M., Hegde, B. G., Baxa, U., Haworth, I. S., Langen, R. (2012). Fibril Structure of Human Islet Amyloid Polypeptide. *J. Biol. Chem.*, 287 (8), 5235–5241. Bedrood, S., Li, Y., Isas, J. M., Hegde, B. G., Baxa, U., Haworth, I. S., Langen, R. (2012). Fibril Structure of Human Islet Amyloid Polypeptide. *J. Biol. Chem.* 287, 5235–5241. doi.org/10.1074/jbc.M111.327817.

Bharadwaj, P., Solomon, T., Sahoo, B.R. et al. (2020). Amylin and beta amyloid proteins interact to form amorphous heterocomplexes with enhanced toxicity in neuronal cells. *Sci. Rep.* 10, 10356. doi.org/10.1038/s41598-020-66602-9.

Berardet, C., Kaffy, J., Ongeri, S., Taverna, M. (2018). A Capillary Zone Electrophoresis Method to Investigate the Oligomerization of the Human Islet Amyloid Polypeptide Involved in Type 2 Diabetes. *J. Chromatogr. A* 1578, 83–90. doi.org/10.1016/j.chroma.2018.10.006

Berardet, C., Kaffy, J., Halgand, F., Van der Rest, G., Ongeri, S., Taverna, M. (2020). Evidence for Different in Vitro Oligomerization Behaviors of Synthetic HIAPP Obtained from Different Sources. *Anal. Bioanal. Chem.* 412, 3103–3111. doi.org/10.1007/s00216-020-02560-5

Bizet, F., Tonali, N., Soulier, J.-L., Oliva, A., Kaffy, J., Crousse, B., Onger, S. (2018). Towards a General Synthesis of Di-Aza-Amino Acids Containing Peptides. *New J. Chem.* 42, 17062–17072. doi.org/10.1039/C8NJ03635G

Bram, Y., Frydman-Marom, A., Yanai, I., Gilead S., Shaltiel-Karyo, R., Amdursky, N., Gazit, E. (2014). Apoptosis induced by islet amyloid polypeptide soluble oligomers is neutralized by diabetes-associated specific antibodies. *Sci. Rep.* 4, 4267. doi.org/10.1038/srep04267

Brender, J. R., Salamekh, S., Ramamoorthy, A. (2012). Membrane Disruption and Early Events in the Aggregation of the Diabetes Related Peptide IAPP from a Molecular Perspective. *Acc. Chem. Res.* 45, 3, 454–462. doi.org/10.1021/ar200189b

Buchanan, L. E., Dunkelberger, E. B., Tran, H. Q., Cheng, P.-N., Chiu, C.-C., Cao, P., Raleigh, D. P., de Pablo, J. J., Nowick, J. S., Zanni, M. T. (2013). Mechanism of IAPP Amyloid Fibril Formation Involves an Intermediate with a Transient β -Sheet. *Proc. Natl. Acad. Sci.* 110, 19285–19290. doi.org/10.1073/pnas.1314481110

Chaundury, A., Duvoor, C., Dendi, V.S.R., Kraleti, S., Chada, A., Ravilla, R., Marco, A., Shekhawat, N. S., Montales, M. T., Kuriakose, K. et al. (2017). Clinical Review of Antidiabetic Drugs: Implications for Type 2 Diabetes Mellitus Management. *Front. Endocrinol.*, 8, 6. doi.org/10.3389/fendo.2017.00006

Cheng, P.-N., Liu, C., Zhao, M., Eisenberg, D., Nowick, J. S. (2012). Amyloid β -Sheet Mimics that Antagonize Amyloid Aggregation and Reduce Amyloid Toxicity. *Nat. Chem.* 4, 927–933. doi.org/10.1038/nchem.1433

Dalvit, C., Vulpetti, A. (2019). Ligand-Based Fluorine NMR Screening: Principles and Applications in Drug Discovery Projects. *J. Med. Chem.* 62, 2218–2244. doi.org/10.1021/acs.jmedchem.8b01210

Dufau, L., Marques Ressurreição, A. S., Fanelli, R., Kihal, N., Vidu, A., Milcent, T., Soulier, J.-L., Rodrigo, J., Desvergne, A., Leblanc, K., Bernadat, G., Crousse, B., Reboud-Ravaux, M. and Onger, S. (2012). Carbonylhydrazide-Based Molecular Tongs Inhibit Wild-Type and Mutated HIV-1 Protease Dimerization. *J. Med. Chem.* 55, 6762–6775. doi.org/10.1021/jm300181j

Gante, J.; Krug, M.; Lauterbach, G.; Weitzel, R.; Hiller, W. (1995). Synthesis and Properties of the First All-Aza Analogue of a Biologically Active Peptide. *J. Pept. Sci.* 1 (3), 201–206. doi.org/10.1002/psc.310010307.

Gilead, S., Gazit, E. (2004). Inhibition of amyloid fibril formation by peptide analogues modified with alpha-aminoisobutyric acid. *Angew. Chem. Int. Ed.* 43, 4041–4044. doi.org/10.1002/anie.200353565.

Han, H.; Yoon, J.; Janda, K. D. (1998). Investigations of Azapeptides as Mimetics of Leu-Enkephalin. *Bioorg. Med. Chem. Lett.* 8 (1), 117–120. doi.org/10.1016/S0960-894X(97)10198-6.

Henninot, A., Collins, J.C., Nuss, J.M. (2018) The Current State of Peptide Drug Discovery: Back to the Future? *J. Med. Chem.* 61, 1382–1414 DOI: 10.1021/acs.jmedchem.7b00318

Hoffmann, A.R.F., Saravanan, M.S., Lequin, O., Killian, J.A., Khemtémourian, L. (2018). A single mutation on the human amyloid polypeptide modulates fibril growth and affects the mechanism of amyloid-induced membrane damage, *Biochim.Biophys.Acta Biomembranes* 1860, 1783-1792. doi.org/10.1016/j.bbamem.2018.02.018

Inoue M., Sumii, Y., Shibata, N. (2020). Contribution of Organofluorine Compounds to Pharmaceuticals. *ACS Omega* , 5, 19, 10633–10640. doi.org/10.1021/acsomega.0c00830.

Iuraşcu M. I., Cozma C., Tomczyk N., Rontree J., Desor M., Drescher M., Przybylski M. (2009). Structural characterization of beta-amyloid oligomer-aggregates by ion mobility mass spectrometry and electron spin resonance spectroscopy. *Anal. Bioanal. Chem.*, 395, 2509-2519. doi: 10.1007/s00216-009-3164-3.

Jeong, H. R., An, S. S. A. (2015). Causative factors for formation of toxic islet amyloid polypeptide oligomer in type 2 diabetes mellitus. *Clin Interv Aging.* 10, 1873–1879. doi.org/10.2147/CIA.S95297

Kajava, A. V., Aebi, U., Steven, A. C. (2005). The Parallel Superpleated Beta-Structure as a Model for Amyloid Fibrils of Human Amylin. *J. Mol. Biol.* 348, 247-252. doi.org/10.1016/j.jmb.2005.02.029

Ke, P. C., Sani, M.-A., Ding, F., Kakinén, A., Javed, I., Separovic, F., Davis, T. P., and Mezzenga, R. (2017). Implications of peptide assemblies in amyloid diseases. *Chem. Soc. Rev.* 46, 6492–6531. doi.org/10.1039/c7cs00372b

Ke, P. C., Zhou R., Serpell, L. C., Riek, R., Knowles T. P J., Lashuel H. A., Gazit E., Hamley, I. W., Davis, T. P., Fändrich, M., Otzen, D. E., Chapman, M. R., Dobson, C. M., Eisenberg, D. S., Mezzenga, R. (2020). Half a century of amyloids: past, present and future. *Chem. Soc. Rev.* 49, 5473-5509. doi.org/10.1039/c9cs00199a.

Kiriyama, Y., Nochi, H. (2018). Role and Cytotoxicity of Amylin and Protection of Pancreatic Islet β -Cells from Amylin Cytotoxicity. *Cells* 7, 95. doi.org/10.3390/cells7080095

Ko, E., Raghuraman, A., Perez, Ioerger, L. M., T. R., Burgess, K. (2013). Exploring Key Orientations at Protein–Protein Interfaces with Small Molecule Probes. *J. Am. Chem. Soc.* 135, 167-173. doi.org/10.1021/ja3067258

Lau, J. L., Dunn, M. K. (2018). Therapeutic peptides: Historical perspectives, current development trends, and future directions. *Bioorg. Med. Chem.* 26, 2700–2707. Doi.org/10.1021/acs.jmedchem.7b00318

Laxio Arenas, J., Kaffy, J., Onger, S., (2019) Peptides and Peptidomimetics as Inhibitors of Protein–Protein Interactions Involving β -Sheet Secondary Structures. *Curr. Opin. Chem. Biol.* 52, 157–167. doi.org/10.1016/j.cbpa.2019.07.008

LeVine, H. (1999). Quantification of β -Sheet Amyloid Fibril Structures with Thioflavin T. In *Methods in Enzymology* 309, 274–284. doi.org/10.1016/S0076-6879(99)09020-5

Li, H., Ha, E., Donaldson, R. P., Jeremic, A. M., Vertes, A. (2015). Rapid Assessment of Human Amylin Aggregation and Its Inhibition by Copper(II) Ions by Laser Ablation Electrospray Ionization Mass Spectrometry with Ion Mobility Separation. *Anal. Chem.* 87, 9829–9837. doi.org/10.1021/acs.analchem.5b02217.

Li, X., Taechalertpaisarn, J., Xin, D., Burgess, K. (2015) Protein-Protein Interface Mimicry by an Oxazoline Piperidine-2,4-dione. *Org. Lett.* 17, 632–635. Doi.org/10.1021/ol5036547

Liang, G., Zhao, J., Yu, X., Zheng, J. (2013) Comparative Molecular Dynamics Study of Human Islet Amyloid Polypeptide (IAPP) and Rat IAPP Oligomers. *Biochemistry* 52, 1089–1100. doi.org/10.1021/bi301525e

Luca, S., Yau, W.-M., Leapman, R., Tycko, R. (2007). Peptide Conformation and Supramolecular Organization in Amylin Fibrils: Constraints from Solid-State NMR. *Biochemistry*, 46 (47), 13505–13522. doi.org/10.1021/bi701427q

Mandal, P. K., McMurray, J. S. (2007). Pd–C-Induced Catalytic Transfer Hydrogenation with Triethylsilane. *J. Org. Chem.* 72, 6599–6601. doi.org/10.1021/jo0706123

Mirecka, E. A., Feuerstein, S., Gremer, L., Schröder, G. F., Stoldt, M., Willbold, D.; Hoyer, W. (2016). β -Hairpin of Islet Amyloid Polypeptide Bound to an Aggregation Inhibitor. *Sci. Rep.* 6, 33474. doi.org/10.1038/srep33474

Paul, A.; Kalita, S.; Kalita, S.; Sukumar, P.; Mandal, B. (2017). Disaggregation of Amylin Aggregate by Novel Conformationally Restricted Aminobenzoic Acid containing α/β and α/γ Hybrid Peptidomimetics. *Sci. Rep.* 7, 40095. doi.org/10.1038/srep40095

Pellegrino, S., Contini, A., Gelmi, M. L., Lo Presti, L., Soave, R., Erba, E. (2014). Asymmetric Modular Synthesis of a Semirigid Dipeptide Mimetic by Cascade Cycloaddition/Ring Rearrangement and Borohydride Reduction. *J. Org. Chem.* 79, 3094–3102. doi.org/10.1021/jo500237j

Pellegrino, S., Tonali, N., Erba, E., Kaffy, J., Taverna, M., Contini, A., Taylor, M., Allsop, D., Gelmi, M. L., Onger, S. (2017). β -Hairpin Mimics Containing a Piperidine–Pyrrolidine Scaffold Modulate the β -Amyloid Aggregation Process Preserving the Monomer Species. *Chem. Sci.* 8, 1295–1302. doi.org/10.1039/C6SC03176E

Pithadia, A., Brender, J. R., Fierke, C. A., Ramamoorthy, A. (2016). Inhibition of IAPP Aggregation and Toxicity by Natural Products and Derivatives. *J. Diabetes Res.* 2016, 1-12. doi.org/10.1155/2016/2046327

Porat, Y., Mazor, Y., Efrat, S., Gazit, E. (2004). Inhibition of Islet Amyloid Polypeptide Fibril Formation: A Potential Role for Heteroaromatic Interactions. *Biochemistry* 43, 14454–14462. doi.org/10.1021/bi048582a

Sumner Makin, O., Serpell, L. C. (2004). Structural Characterisation of Islet Amyloid Polypeptide Fibrils. *J. Mol. Biol.* 335, 1279–1288. doi.org/10.1016/j.jmb.2003.11.048

Riba, I., Barran, P. E., Cooper, G. J. S., Unwin, R. D. (2015). On the Structure of the Copper–Amylin Complex. *Int. J. Mass Spectrom.* 391, 47–53. doi.org/10.1016/j.ijms.2015.09.001

Röder, C., Kupreichyk, T., Gremer, L., Schäfer, L. U., Pothula, K. R., Ravelli, R. B. G., Willbold, D., Hoyer, W., Schröder, G. F. (2020). Amyloid fibril structure of islet amyloid polypeptide by cryo-electron microscopy reveals similarities with amyloid beta. *Nat. Struct. Mol. Biol.*, 27 (7), 660–667. doi.org/10.1101/2020.02.11.944546.

Rodriguez Camargo D.C., Garg D., Buday K., Franko A., Rodriguez Camargo A., Schmidt F., Cox S.J., Suladze S., Haslbeck M., Mideksa Y.G., Gemmecker G., Aichler M., Mettenleiter G., Schulz M., Walch A.K., Hrabě de Angelis M., Feige M.J., Sierra C.A., Conrad M., Tripsianes K., Ramamoorthy A., Reif B. (2018). hIAPP forms toxic oligomers in plasma. *Chem. Commun.* 54, 5426-5429. doi.org/10.1039/C8CC03097A

Rouser, G., Fkeischer, S., Yamamoto, A. (1970). Two dimensional thin layer chromatographic separation of polar lipids and determination of phospholipids by phosphorus analysis of spots, *Lipids* 5, 494–496. doi.org/10.1007/BF02531316

Roriz-Filho, J. S., Sá-Roriz, T. M., Rosset, I., Camozzato, A. L., Santos, A. C., Chaves, M. L. F., Moriguti, J. C., Roriz-Cruz, M. (2009). (Pre)diabetes, brain aging, and cognition. *Biochim. Biophys. Acta BBA - Mol. Basis Dis.* 1792, 432–443. doi.org/10.1016/j.bbadis.2008.12.003.

Terakawa, M.S., Lin, Y., Kinoshita, M., Kanemura, S., Itoh, D., Sugiki, T., Okumura, M., Ramamoorthy, A. Lee, Y.H. (2018). Impact of membrane curvature on amyloid aggregation. *Biochim. Biophys. Acta*, 1741-1764. doi.org/10.1016/j.bbamem.2018.04.012

Tonali, N., Correia, I., Lesma, J., Bernadat, G., Ongeri, S., Lequin, O. (2020). Introducing sequential aza-amino acids units induces repeated β -turns and helical conformations in peptides. *Org. Biomol. Chem.* 18, 3452-3458. doi.org/10.1039/C9OB02654A

Tonali, N., Kaffy, J., Soulier, J.-L., Gelmi, M. L., Erba, E., Taverna, M., Van Heijenoort, C., Ha-Duong, T., Ongeri, S. (2018). Structure-Activity Relationships of β -Hairpin Mimics as Modulators of Amyloid β -Peptide Aggregation. *Eur. J. Med. Chem.* 154, 280–293. doi.org/10.1016/j.ejmech.2018.05.018

Tran, L., Ha-Duong, T. (2016). Insights into the Conformational Ensemble of Human Islet Amyloid Polypeptide from Molecular Simulations. *Curr. Pharm. Des.* 22, 3601–3607. doi.org/10.2174/1381612822666160414142538

Vahdati, L.; Kaffy, J.; Brinet, D.; Bernadat, G.; Correia, I.; Panzeri, S.; Fanelli, R.; Lequin, O.; Taverna, M.; Onger, S.; Piarulli, U. (2017). Synthesis and Characterization of Hairpin Mimics That Modulate the Early Oligomerization and Fibrillization of Amyloid β -Peptide: Synthesis and Characterization of Hairpin Mimics That Modulate the Early Oligomerization and Fibrillization of Amyloid β -Peptide. *Eur. J. Org. Chem.* 2017 (20), 2971–2980. <https://doi.org/10.1002/ejoc.201700010>.

Van der Rest G., Halgand F. (2017). Size Exclusion Chromatography-Ion Mobility-Mass Spectrometry Coupling: a Step Toward Structural Biology. *J. Am. Soc. Mass Spectrom.* 28, 2519–2522. doi: 10.1007/s13361-017-1810-0.

Wiltzius, J. J. W., Sievers, S. A., Sawaya, M. R., Cascio, D., Popov, D., Riek, C., Eisenberg, D. (2008). Atomic Structure of the Cross- β Spine of Islet Amyloid Polypeptide (Amylin). *Protein Sci.*, 17 (9), 1467–1474. doi.org/10.1110/ps.036509.108

Wu, C., Shea, J.-E. (2013). Structural Similarities and Differences between Amyloidogenic and Non-Amyloidogenic Islet Amyloid Polypeptide (IAPP) Sequences and Implications for the Dual Physiological and Pathological Activities of These Peptides. *PLoS Comput. Biol.* 9, e1003211. doi.org/10.1371/journal.pcbi.1003211

Yan, L.-M., Velkova, A., Taterek-Nossol, M., Rammes, G., Sibae, A., Andreetto, E., Kracklauer, M., Bakou, M., Malideli, E., Göke, B., Schirra, J., Storr, M., Kapurniotu, A. (2013). Selectively N-Methylated Soluble IAPP Mimics as Potent IAPP Receptor Agonists and Nanomolar Inhibitors of Cytotoxic Self-Assembly of Both IAPP and A β 40. *Angew. Chem. Int. Ed.* 52, 10378–10383. doi.org/10.1002/anie.201302840

Chapter 4

Fluorinated β -hairpin mimics in T2D: new protein-protein interaction inhibitors and potential tools for early diagnosis

4.1 Fluorine in medicinal chemistry

Small organic compounds have played a primary role as drugs since the beginning of the 20th century. However, during the last decades biopharmaceuticals have progressively gained in importance because of their advantages in terms of selectivity, side effects and toxicity. Over the last 50 years, beside biopharmaceutical compounds, the number of fluorinated drugs approved has gradually increased to represent approximatively 50% of the small molecules for the biennium 2018-2019. Nowadays, almost 70 years after the commercialization of the first fluoropharmaceutical (fludrocortisone), there are 340 fluorinated drugs on the market and this number is set to increase more in the near future.¹⁵⁸

4.1.1 Fluorine as bioisoster

The great success of fluorine in medicinal chemistry is due to its unique properties. In term of size, the fluorine is the smallest of the halogens, with a van der Waals radius of 1.47 Å, which is an intermediate value between those of hydrogen (1.20 Å) and oxygen (1.52 Å). Considering the similar size among F and H atoms, it is easy to understand why enzymes are not often able to discriminate between the natural substrate and the analogue wherein a proton has been replaced by a fluorine atom. Furthermore, according to the Pauling electronegativity scale, fluorine is the most electronegative element of the periodic table (3.98)¹⁵⁹ and this results in a highly polarized C-F bond¹⁶⁰ characterized by an interatomic distance within 1.39 and 1.32 Å (for respectively CH₃F and CF₄), representing a distance that is in average only 0.26 Å longer than the C-H bond. Fluorinated structures have also been largely explored as bioisosters of different functional groups containing oxygen (Figure 67). Indeed, from a structural point of view, fluorine and oxygen can be considered almost isosteres and their bond length (C-F vs C-O) differs by only 5%.^{161,162} Of particular interest in the field of the biopharmaceuticals are the fluoromethylene (C=CHF) and the

difluoromethylene (C=CF₂) groups which have been employed as bioisosters of the peptidic bond¹⁶³ Over the last twenty years, the trifluoroethyl amino group has emerged as new fluorinated peptide bond isostere because of its properties.^{164–166} Indeed, it has been proved that the presence of a trifluoromethyl in the α position of an amine reduces its basicity at similar level of an amide. Moreover, its backbone angle close to 120° is very similar to that of a peptide bond. The trifluoroethyl amino group low basicity and geometry together with the substantial isopolarity of C-CF₃ with the C=O make it an effective peptide bond isostere.

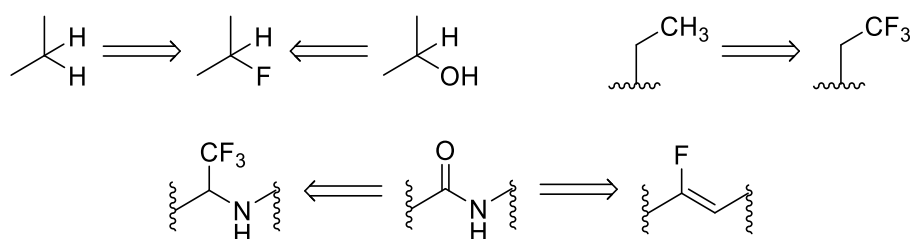


Figure 67 Examples of fluorine and fluorinated groups as bioisosters¹⁶²

4.1.2 Influence on the ADME

The introduction of a fluorinated group in a drug implies a strong influence on the pharmacokinetic and the pharmacodynamic properties through the modulation of electronic, lipophilic and steric parameters.^{160,167,168} The presence of a fluorine atom, because of its electron withdrawing nature, exerts a strong effect on the neighboring functional groups whose pKa can be impacted depending on the position of fluorine substitution. As general rule, the presence of fluorine atoms increases their acidity.¹⁶⁸ Considering a generic drug, a perfect balance between its lipophilicity and hydrophilicity is required to generate optimal absorption and distribution leading to a pharmacological *in vivo* effect. Often, for example, the pKa shift obtained by introducing a fluorinated group has been exploited to modulate the drug lipophilicity in order to enhance the BBB permeability. The *in vivo* metabolism of a biologically active compound is one of the problematics to take into account in drug discovery process. Actually, it is widely known that the insertion of fluorine atoms in strategic positions can increase the half-life, preventing the metabolic inactivation of the drug.¹⁶⁹

4.1.3 Fluorine in weak interactions

Despite inorganic fluorides are known to be able to form strong hydrogen bonds, the involvement of organic fluorides in hydrogen bonds has been debated for a long time. However, recently it has been demonstrated that a fluorine atom covalently bound to a carbon is able to act as a weak hydrogen bond acceptor.¹⁷⁰ The presence of C-F bonds in drugs have been reported to play a crucial role in the stabilization of the drug-protein complexes, which takes place through interactions between C-F bonds and polar amino acidic side chains such as those containing carbonyl or guanidinium ion.¹⁷¹ As mentioned above, a neighboring fluorine enhances the acidity of hydroxylic and amine groups and therefore makes them better hydrogen bond donors.^{160,168,172}

4.1.4 Fluorinated compounds as diagnostic tools

Over the last decades many lives have been saved thanks to the employment of several new non-invasive diagnostic techniques. Diagnostic imaging is one of the fields that has emerged and medicine takes advantage from many different imaging techniques. However, in some cases, as for the amyloidoses, an early diagnosis is still difficult. Indeed, these pathologies are often diagnosed when the symptoms arise and it is too late for a treatment able to prevent or slow down the course of the diseases. The fluorine, with its unique characteristics, represents a versatile tool for the development of new markers for the magnetic resonance imaging (MRI) and the positron emission tomography (PET) applicable for diagnostic and research scopes.

MRI:

In MRI, strong magnetic field and low-energy radiofrequency are used to visualize in real time specific anatomical and physiological information (Figure 68). The first MRI technique developed was the ¹H-MRI in which the instruments have been used to track the protons of the body (e.g. protons of water).^{173,174} As research progresses, new MR procedures have been introduced in order to increase resolution and specificity. As recently reviewed by Wahsner *et al.*,¹⁷⁵ the number of available MRI contrast agents is enormous, however most of them exploit gadolinium (III) ion to enhance the signals. The presence of Gd as well as others metal ions has recently arisen the problem of the long-term safety which pushed the researchers to find more suitable contrast agents. The best answer to this problem seems to be in the heteronuclear ¹⁹F-MRI which provides

information through ^{19}F nuclei covalently bound to the probe. The advantage of this nucleus lies in its natural abundance (100%) and in the negligible quantity of endogenous ^{19}F .¹⁷⁴

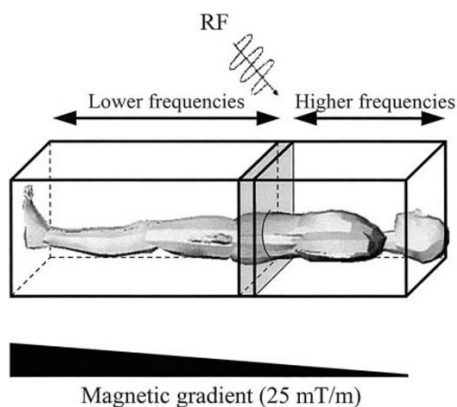


Figure 68 Schematic representation of MRI operation.¹⁷³ Superimposition the main magnetic field with a small magnetic gradient allow to select the image of a single slice

PET:

Since a long time, radioisotopes have been employed as tracker for non-invasive imaging techniques. In the case of positron emission tomography, the radiotracers are organic compounds analogues (usually biological substrates like glucose) in which an atom, in a specific position, has been replaced by a radioisotope characterized by a short half-life. The most common radioactive elements are ^{11}C ($t_{1/2} = 20.4$ min), ^{13}N ($t_{1/2} = 10$ min), ^{15}O ($t_{1/2} = 2$ min) and ^{18}F ($t_{1/2} = 110$ min) which are all positron emitters (β^+). After a specific time (half-life) the radioisotope decays emitting β^+ , that collides with the electron of a neighboring atom. The consequent annihilation releases two gamma rays in opposite directions (approximately 180°). The two γ rays hit the detector and the gathered signals are converted in an image (Figure 69).^{176,177}

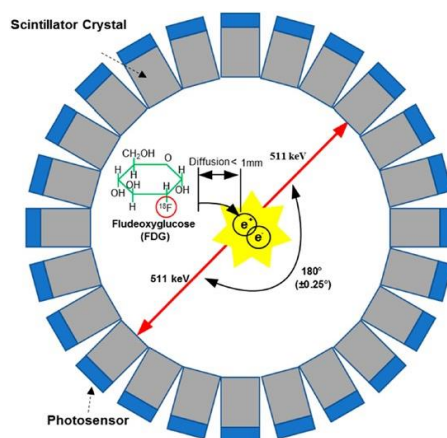


Figure 69 Schematic representation of PET functioning¹⁷⁷

4.1.5 Fluorinated compounds as NMR screening tools in FAXS experiment

Fluorine chemical shift Anisotropy and eXchange for Screening (FAXS) binding assay is a NMR technique that allows the binding affinity measurement.¹⁷⁸ Its high sensitivity to protein binding makes it an excellent technique for the identification of low binding affinity ligands in direct and competition mode (Figure 70).

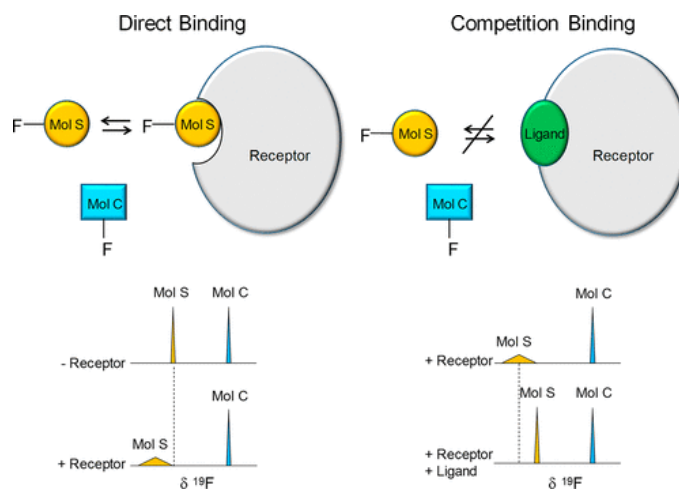


Figure 70 Schematic representation of FAXS experiments in direct (left) and competition mode (right)¹⁷⁸

In the direct mode it is possible to evaluate if a fluorinated compound is binding or not to the protein through the acquisition of ¹⁹F spectra. Indeed, if the compound binds to the protein, its

fluorine signal becomes broad and sometimes changes in chemical shift (Figure 70, left, Mol S); while in the case it does not bind, the signal remains sharp and does not change in chemical shift (Figure 70, left, Mol C). In the competition mode two compounds (Figure 70, right, Mol S and Mol C) are used as reporter and internal reference respectively. When a ligand (not necessarily fluorinated) is added to the NMR tube, the reporter signal becomes sharp and returns to the chemical shift of the free state when the ligand has a higher affinity for the protein.

4.2 Fluorinated peptidomimetics

Since the first fluorinated drug appeared on the market almost 70 years ago, fluorine has aroused a strong interest in medicinal chemistry. However, despite the large number of approved fluorinated drugs, no fluorinated peptides/peptidomimetics have yet been introduced in clinics. On the other hand, in the academic field, the introduction of fluorinated moiety into peptides/proteins and the synthesis of fluorinated peptidomimetics have gained lot of interest. One of the most exploited strategy to introduce fluorine in a peptide is the replacement of a natural amino acid by a fluorinated analogue. Salwiczek *et al.* first and Berger *et al.* later, in their reviews, tried to rationally summarize the effects of a fluorinated amino acid when incorporated in a peptide (impact on the protein conformation, stability and function).^{179,180} Despite the increasing number of publications, establishing general rules is still challenging and needs further investigation.

As previously mentioned in the chapter 1 (see paragraph 1.3.6 page 39), small acyclic β -hairpins have been scarcely investigated as hIAPP aggregation inhibitors and to the best of our knowledge fluorinated analogues, have not yet been reported in the literature.

Considering this lack, most of my PhD work focused on the development of novel fluorinated acyclic β -hairpins able to selectively interact with hIAPP in order to modulate its aggregation.

4.2.1 β -hairpin mimics containing the 3-fluoro-5-benzamido-2-hydroxybenzohydrazide peptidomimetic

Design of the compounds bearing a blocking sequence based on the 3-fluoro-5-benzamido-2-hydroxybenzohydrazide

Few years ago, our group began to study peptidomimetic derivatives based on the 5-amino-2-methoxybenzohydrazide (Amb) motif as potential inhibitors of amyloidogenic peptides such as A β ₁₋₄₂.

42. The first inhibitor bearing the Amb derivative **4.0** (Figure 71), whose design has been already described in chapter 2 (see paragraph 2.1.1, page 44, figure 42), was the glycopeptidomimetic reported by our team in 2016.¹¹⁷

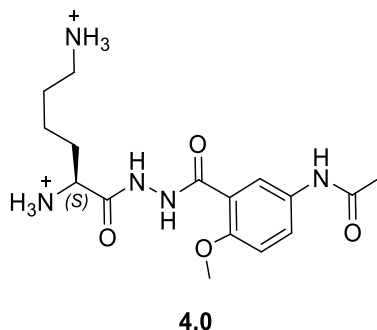


Figure 71 Structure of the first benzhydrazone derivatives **4.0** based on the Amb motif and inspired by the A β ₁₋₄₂ amyloidogenic sequence

Only two years later, the same structure inspired by A β ₁₋₄₂ amyloidogenic sequence was exploited as blocking sequence in β -hairpin **4.1** (Figure 72) published by Tonali *et al.* and already described in chapter 2 (see paragraph 2.1.1 page 46).¹²²

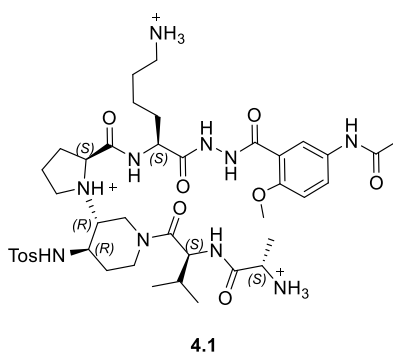


Figure 72 Structure of the inhibitor **4.1** reported by Tonali¹²²

In line with the group's continue interest in the synthesis of fluorinated peptidomimetics, in his PhD manuscript,¹⁸¹ Nicolò Tonali began to report the development of a fluorinated structure based on the β -hairpin of **4.1**. More in detail, it has been planned to replace the original benzhydrazone arm **4.0** by a fluorinated analogue which found its origins in Dimitri Brinet¹⁸² and Leila Vahdati¹⁸³ PhD works (Figure 73).

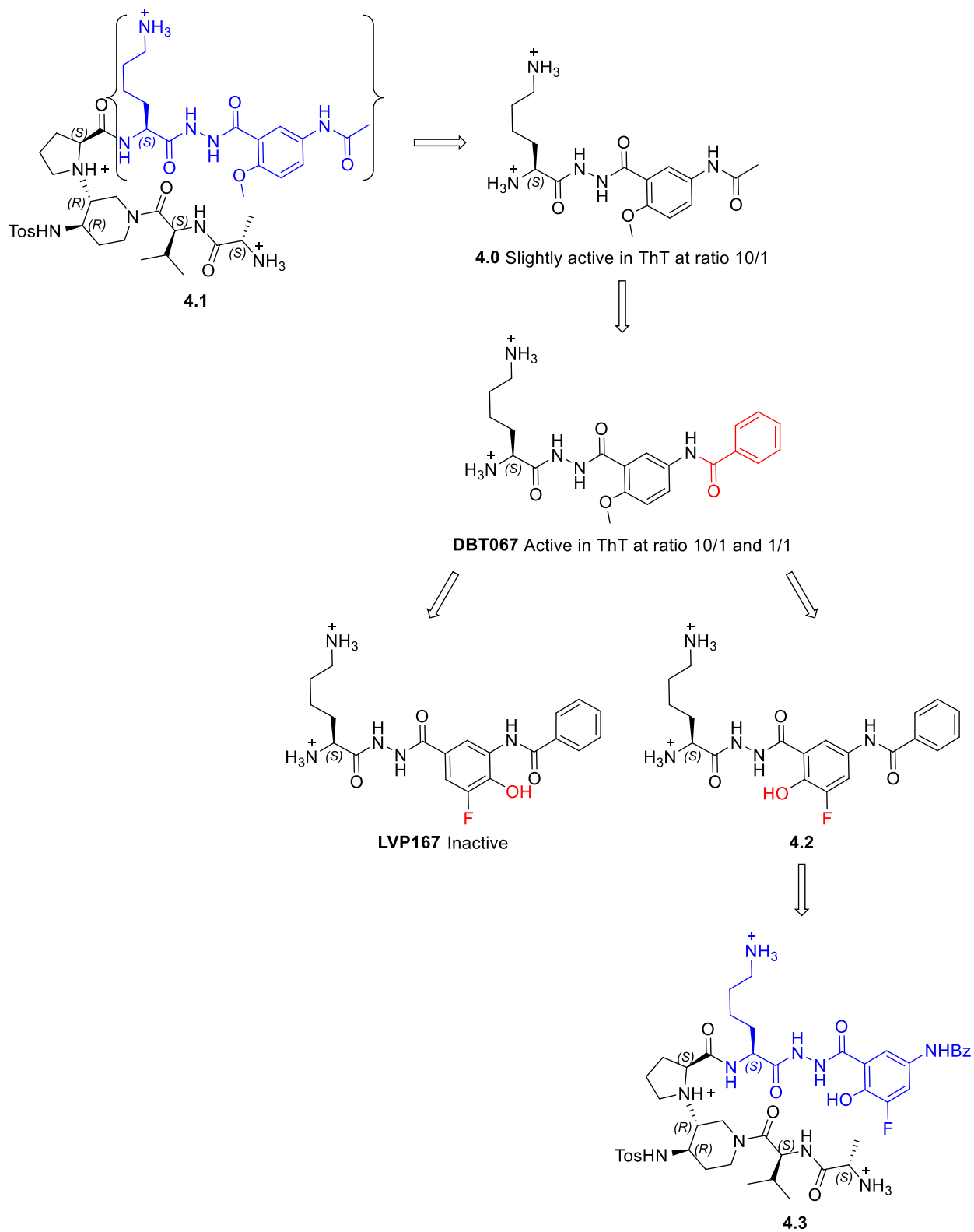


Figure 73 Design of the compound bearing the fluorinated 5-amino-2-methoxybenzhydrazone motif. In red the modifications

In order to improve the activity of the original benzhydrazide mimic **4.0**, during his PhD work,¹⁸² Dimitri Brinet was involved in the development of better mimic of KLVF sequence based on the 5-amino-2-methoxybenzhydrazide. He replaced the original acetyl group by an aromatic group in order to simulate the phenylalanine side chain. The mimic which was bearing the phenyl carbonyl group (**DBT067**, Figure 73) showed a good activity against A β ₁₋₄₂ aggregation in ThT assay (total suppression at inhibitor/peptide ratio 10/1).

Encouraged by the excellent activity showed by compound **DBT067**, our group decided to take advantage of its expertise in fluorine chemistry to develop fluorinated derivatives of **DBT067**. This work was initially carried out by Leila Vahdati who, in her PhD thesis,¹⁸³ presented the first fluorinated benzhydrazide analogue **LVP167** (Figure 73), which presented the fluorine atom in position 3 of the aromatic ring. Moreover, the methoxy group was replaced with a hydroxyl group placed in position 4 (in *ortho* position related to the fluorine and the amide). Unfortunately, this compound was totally inactive in the ThT assay.

More recently, our team has turn its attention on the development of the fluorinated benzhydrazide derivative **4.2** (Figure 73) with the aim to insert it as blocking sequence in a structure designed to mimic a β -hairpin (**4.3**, Figure 73). This new fluorinated benzhydrazide, whose synthesis has been explored by Nicolò Tonali¹⁸¹ first and then by myself, was characterized by 3 different chemical groups fixed on the benzhydrazide motif:

- 1) a **phenyl carbonyl group** present on the amine in position 5, which can mimic the side chain of a phenylalanine. As happened with Dimitri Brinet's inhibitors, its presence could enhance the anti-aggregation activity probably by stabilizing the peptide/inhibitor complex with the establishment of hydrophobic interactions;
- 2) a **hydroxyl group** in position 2: the rationale behind the position of this group was double. First, we were interested in studying the relation between its position and the activity of the arm. Indeed, as previously demonstrated (Leila Vahdati's work), the strand was totally inactive when the hydroxyl group was inserted in position 4 of the benzhydrazide moiety. Secondly, we wanted to study the impact on the hydrogen bond network when the methoxy group (hydrogen bond acceptor) is replaced by a hydroxyl one (hydrogen bond donor), that is furthermore influenced by a neighboring fluorine. In this case the hydroxyl group might

form hydrogen bond either with the fluorine atom (Figure 74A) or with the carbonyl group of the Lysine (Figure 74B), influencing the peptidomimetic conformation;

- 3) a **fluorine atom** in position 3: as previously reported in this chapter, a fluorine atom can strongly influence the properties of other functional groups and the whole molecule. So, we decided to prepare an *ortho* fluoro phenol in order to investigate first the effect that fluorine exerts on the activity of our hairpin and secondly, as mentioned just above, to study its influence on the conformation.

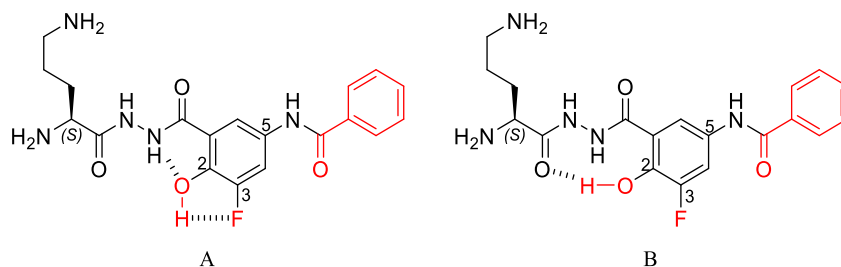


Figure 74 Structure of the new fluorinated benzhydrazide analogue **4.2** with the 2 possible hydrogen bonds

Meanwhile, our research group began to develop hIAPP inhibitors in collaboration with the team of Prof. Maria Luisa Gelmi (Istituto A. Marchesini, Università degli Studi di Milano) (refer to chapter 3). In light with the interest towards this new target, Faustine Bizet¹⁴⁴ synthesized compound **4.4** (Figure 75), a benzhydrazide containing hairpin based on Nicolò Tonali's work but rationally designed to interact selectively with hIAPP. This new inhibitor has been developed from the hairpin bearing the two tripeptide arms already described in chapter 3 (see paragraph 3.1.1 page 64). The tripeptide A₂₅IL₂₇ derived from the hIAPP amyloidogenic sequence was maintained as SRE, while the blocking sequence was replaced by the peptidomimetic **4.5** (Figure 75) inspired by the tripeptide F₁₅LV₁₇ and based on the 5-amino-2-methoxybenzhydrazide motif. The replacement of lysine, already employed by Tonali, the hydrophobic valine residue was justified by the fact that hIAPP does not present acid residues in the amyloidogenic sequence.

Synthesis of the compounds bearing the fluorinated benzhydrazide arm

The preparation of compounds **4.3**, **4.5** and **4.6** followed a common synthetic pathway (Figure 77) that will be presented in two parts. In the first one, the synthesis of the 3 fluorinated peptidomimetic arms **4.7**, **4.8** and **4.9** will be presented. The second one will describe the preparation of the precursors **4.10** and **4.11** starting from the common scaffold **4.12**, synthesized in accordance with the literature.¹²⁰

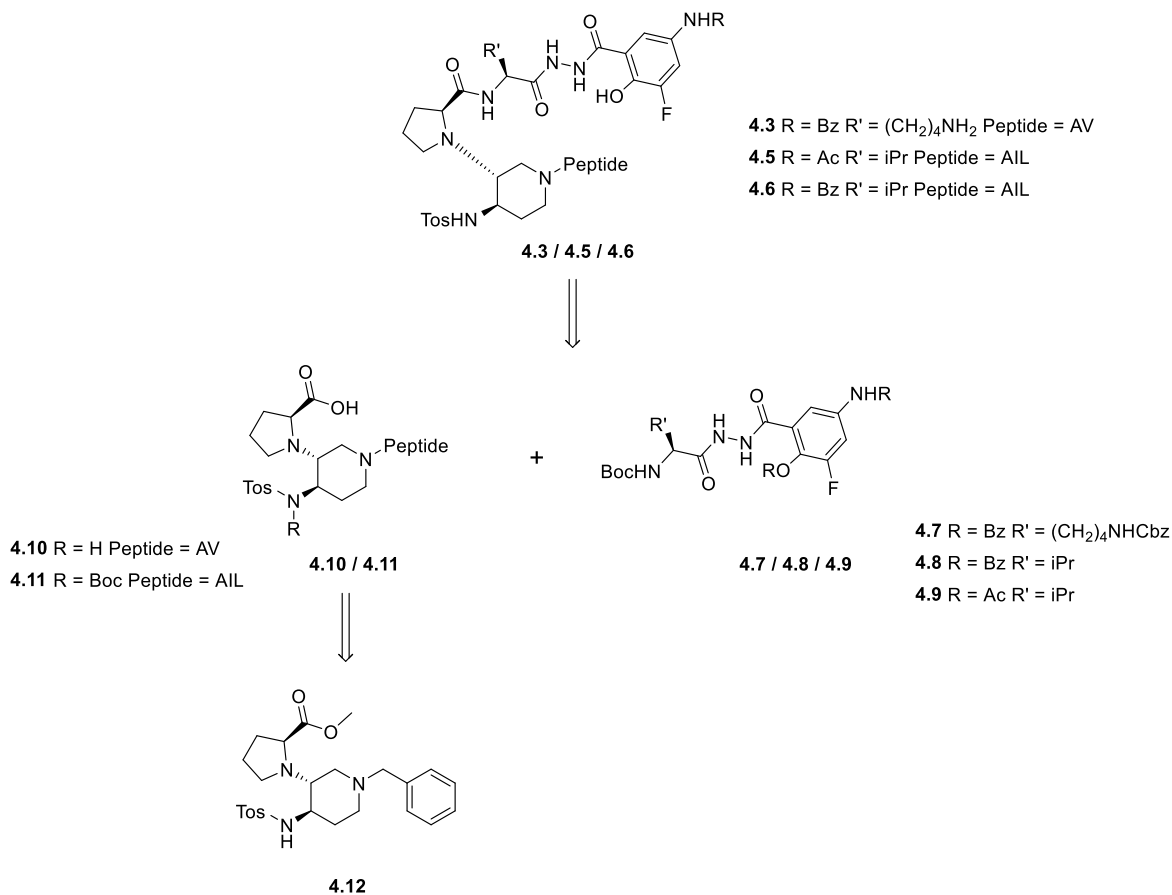
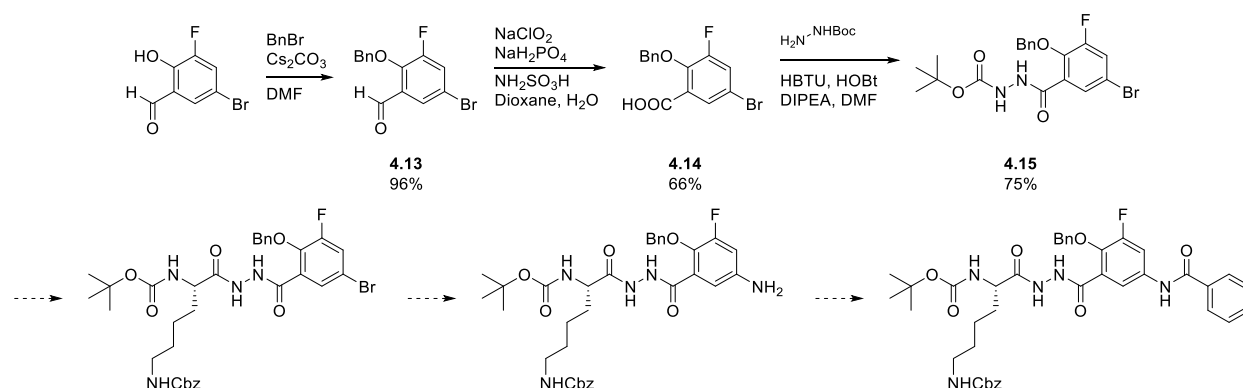


Figure 77 Retrosynthetic approach for obtaining the fluorinated hairpins **4.3**, **4.5** and **4.6**

Synthesis of the lysine-F-benzhydrazide- **4.7**

The preparation of the fluorinated strand required several trials to find the optimal synthetic pathway. This work was initiated by Nicolò Tonali¹⁸¹ who, in a first attempt, planned to start the synthesis from the commercially available 5-bromo-3-fluorosalicylaldehyde (Scheme 2). The strategy involved primarily a protection of the hydroxylic group in position 2 (**4.13**), followed by

the oxidation of the aldehydic group by a Pinnick oxidation. The obtained compound **4.14** was subsequently coupled with the *tert*-butyl carbazate to yield compound **4.15**.



Scheme 2 First synthetic strategy proposed by Tonali

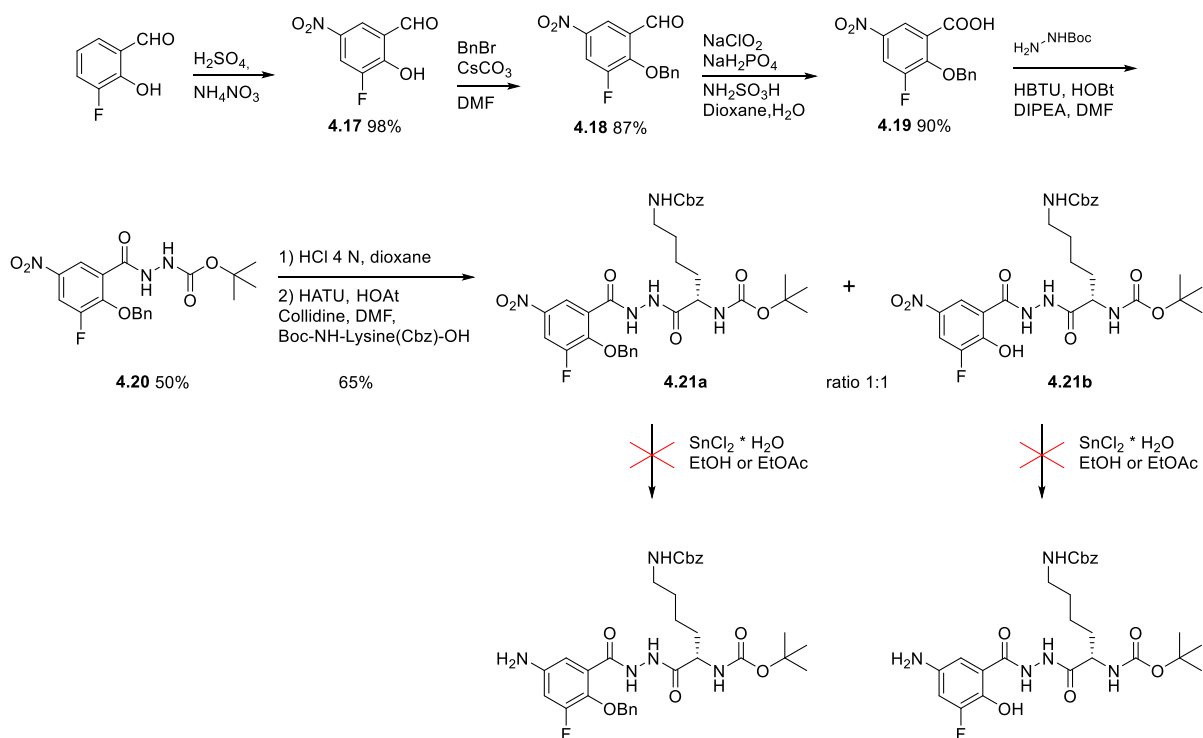
This strategy was not pursued and the following passages were not accomplished because a parallel study, conducted on a model substrate similar to **4.15** already available in the laboratory (Figure 78), showed the impossibility to replace the bromine atom in position 5 with an amine. As reported by Nicolò Tonali, neither Pd-catalyzed nor Cu-catalyzed amination led to the desired product. Indeed, when **4.15** and benzophenone imine (ammonia surrogate) were subjected to the Buchwald-Hartwig cross-coupling, only the starting bromine was recovered. Same results were obtained converting **4.15** in the corresponding aryl boronic ester (Miyaura boration) that would be theoretically use as intermediate for the Pd-catalyzed amination. Even worst results were obtained synthesizing the amine through the corresponding aryl azide employing copper as catalyst; in this case the starting material underwent to degradation.



Figure 78 Comparison between the structures of compound **4.15** and the model substrate **4.16** used by Tonali¹⁸¹ to study the bromine substitution. In red the difference

Because of the impossibility to convert the bromine in a primary aniline, Nicolò Tonali designed a new synthetic pathway in which the amino group will be inserted starting from an aromatic nitro

group. This second strategy is depicted in scheme 3. The regioselective nitration of 3-fluorosalicylaldehyde in position 5 was operated at 0°C in sulfuric acid, in the presence of ammonium nitrate. The reaction led to the desired product **4.17** in almost quantitative yield (98%). Product **4.17** was subsequently benzylated in the presence of Cs₂CO₃ in good yield (87%). The aldehyde intermediate **4.18** was oxidized by a Pinnick oxidation to obtain the carboxylic acid **4.19** in 90% yield. Compound **4.20** was obtained in good yield (50%) by coupling **4.19** with *tert*-butyl carbazate using HBTU and HOBT as coupling reagents in the presence of DIPEA.

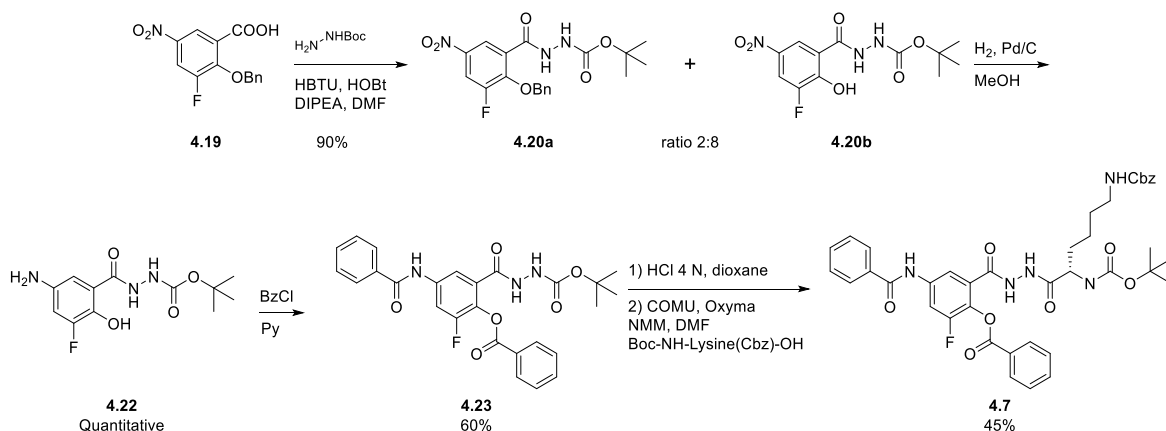


Scheme 3 Second synthetic strategy proposed by Nicolò Tonali

After Boc cleavage of **4.20**, the coupling reaction with Boc-NH-Lysine(Cbz)-OH was performed using HATU and HOAt in the presence of collidine. Interestingly, Nicolò Tonali obtained two different products **4.21a** and **4.21b** (global yield approximately 65%) in ratio 1:1 instead of the only desired **4.21a**. The formation of the deprotected compound **4.21b** was probably due to the electron-withdrawing effect of the fluorine in *ortho* position which made labile the bond between the oxygen and the carbon of the aromatic ring, allowing the OBn substitution by an hydroxyl group. Unfortunately, the selective reduction of both nitro-intermediates **4.21a** and **4.21b** using stannous chloride in EtOH or EtOAc always led to complex mixtures of products that were

impossible to purify (the more classical method using H₂/Pd/C could not be used because of the presence of the CBz group).

During my PhD work, I continued the development of the third strategy (Scheme 4) initially started by Nicolò Tonali, which exploited the same reactions used to synthesize the product **4.20** (Scheme 3). Since the coupling between **4.20** and Boc-NH-Lysine(Cbz)-OH led to the formation of two different products, we hypothesized that the same could happen in the previous passage. Further studies of the coupling between compound **4.19** and *tert*-butyl carbazate revealed the formation of two products which differed by the presence (**4.20a**) or not (**4.20b**) of the benzylic group (ratio 2:8). The isolation of the more polar free hydroxylic containing product improved the yield to a global value of 90%.



Scheme 4 Third strategy proposed by Tonali and optimized during my PhD

Because the second strategy led to two different products almost impossible to purify, being conscious to sacrifice the benzyl group, we decided to perform a catalytic hydrogenation on a mixture of both products **4.20a** and **4.20b**. Operating in this way, we were able to isolate compound **4.22** in quantitative yield with an high purity grade. Once obtained compound **4.22**, we subsequently performed a benzylation, with the double scope to correctly functionalize the amino group and to protect the hydroxyl group as benzoyl ester. This reaction required few optimization steps which are summarized in table 2. The initial trials, carried out in the presence of benzoic anhydride, always led to a complex mixture of products. In order to find better condition to obtain pure compound **4.23**, we decided to test other reagents. Thus, we first investigated the more reactive benzoic-(*tert*-butyl carbonic) anhydride generated reacting isobutyl chloroformate (IBCF)

with benzoic acid at low temperature.¹⁸⁴ Unfortunately, this condition only led to a partial degradation of the starting material. As last reagent, we tested the benzoyl chloride (BzCl) in the presence of pyridine as solvent and base. When the reaction was carried out at 25 °C and 40 °C in the presence of an excess of BzCl, the analysis revealed the formation of di and tri benzoyl derivatives. Finally, by lowering the temperature (to 0°C) and reducing the quantity of BzCl (to 2.1 eq.), we were able to isolate the desired product **4.23** in satisfactory yield (60%), after a simple purification.

Entry	Reagent	Eq.	Solvent	Base	Time	Temperature	Yield
1	Benzoic anhydride	4	THF	/	4 h	60 °C	45%
2	Benzoic anhydride	3	THF	/	6 h	0 °C	54%
3	Benzoic-(<i>tert</i> -butyl carbonic anhydride)	3	THF	NMM	o.n.	From -20 °C to 45 °C	Partial degradation of 4.22
4	Benzoyl chloride	4	Pyridine	Pyridine	4 h	40 °C	Poly-benzoylation
5	Benzoyl chloride	4	Pyridine	Pyridine	3 h	25 °C	Poly-benzoylation
6	Benzoyl chloride	2.1	Pyridine	Pyridine	45 min	0 °C	60%
7	Benzoyl chloride	2.1	Pyridine	Pyridine	45 min	-10 °C	55%

Table 2 Different conditions tested to obtain compound **4.23**

After the Boc cleavage in acidic condition (HCl 4N in dioxane) of **4.23**, the coupling of the resulting hydrazide with Boc-NH-Lysine(Cbz)-OH was performed using COMU and oxyma in anhydrous DMF in the presence of NMM as base in 45% of yield and 87% of purity. All the coupling conditions tested to obtain compound **4.7** are summarized in table 3. As it can be seen from the high number of entries, this coupling reaction was not easy to achieve. The difficulty to obtain **4.7** in good amount with a high grade of purity was probably due to the bulkiness of the starting material. In addition, the fluorine made the neighboring ester very labile. Indeed, high resolution mass spectrometry analysis of the basic washing revealed the presence of products whose molecular mass corresponded to the free hydroxylic derivatives of **4.23** and **4.7**.

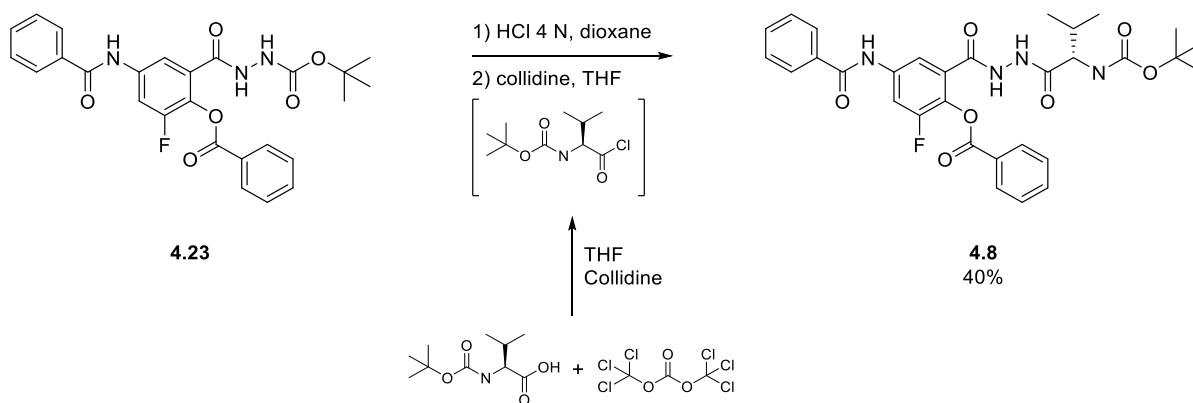
Entry	Eq Lys	Coupling reagent 1	Coupling reagent 2	base	time	Yield	LC-MS Purity
1	1,1	DMTMM (1.1 eq.)	\	NMM (2 eq.)	24 h	26%	80%
2	1,1	DMTMM (1.1 eq.)	\	NMM (2 eq.)	7 days	51%	71%
3	1,1	HBTU (1.1 eq.)	HOBt (1.1 eq.)	DIPEA (4 eq.)	24 h	Product trace + trace free OH	
4	1,1	HBTU (1.1 eq.)	HOBt (1.1 eq.)	DIPEA (2 eq.)	24 h	Product trace + trace free OH	
5	1,1	HOBt (1.1 eq.)	HBTU (1.1 eq.)	DIPEA (2 eq.)	3 days	40%	70%

6	2	HATU (2 eq.)	HOAt (2 eq.)	Collidine (6 eq.)	o.w.	22%	71%
7	1,1	EDC*HCl (1.1 eq.)	Oxyrna (1.1 eq.)	DIPEA (3.1 eq.)	o.n.	No product	/
8	1,1	EDC*HCl (1.1 eq.)	Oxyrna (1.1 eq.)	DIPEA (3.1 eq.)	o.w.	Product trace	
9	1	COMU (1 eq.)	\	NMM (2 eq.)	o.n.	45%	77%
10	1	COMU (1 eq.)	\	DIPEA (2 eq.)	o.n.	35%	73%
11	1,1	COMU (1 eq.)	Oxyrna (1 eq.)	NMM (2 eq.)	1h+23h	45%	87%

Table 3 Coupling conditions tested to obtain **4.7**

Synthesis of the valine-F-benzhydrazide-N-benzoyl **4.8**

In the case of benzoyl fluorinated benzhydrazide **4.8**, we planned to exploit the optimized synthetic pathway of **4.7** until the Boc cleavage of compound **4.23**. Being aware of the problems encountered during the final step of **4.7** synthesis, we decided to try the coupling with Boc-NH-Valine-OH by generating the acyl chloride of the amino acid. To avoid the employment of strong reagents like SOCl_2 , we used the Bis(trichloromethyl) carbonate (BTC), a reagent that have been reported for the *in situ* generation of amino acid chloride.^{185,186} Pleasantly, the trial operated on a small amount (50 mg) of compound **4.23** led to the desired product **4.8** (Scheme 5) which was easily isolated in satisfactory yield (40%).



Scheme 5 Scheme for the synthesis of **4.8** generating *in situ* the acyl chloride

Unfortunately, during the reaction scale-up from 0.1 mmol to 1.7 mmol, instead of compound **4.8** we mainly obtained a byproduct for which, after NMR analysis, the dimeric structure reported in figure 79 has been hypothesized.

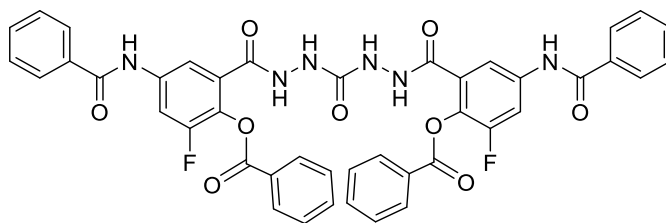


Figure 79 Hypothesized structure of the byproduct obtained operating the coupling in the presence of BTC

In order to confirm our hypothesis, we performed a crystallographic analysis which led to a model that correspond to the oxadiazolone whose structure is reported in figure 80. A fast bibliographic research allowed us to find other cases in which similar oxadiazolone were obtained employing the BTC.^{187,188}

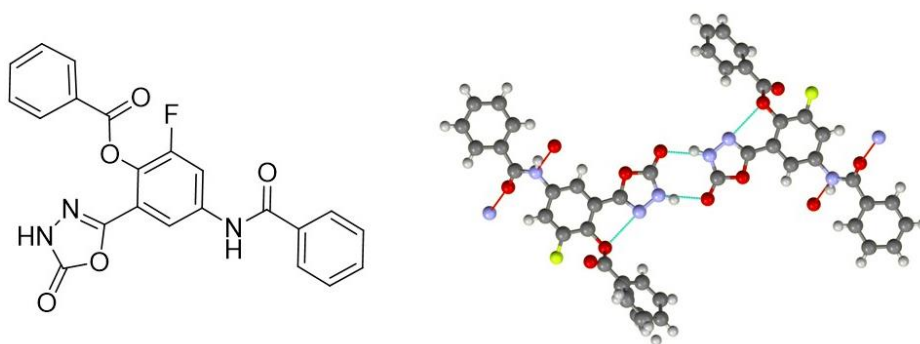
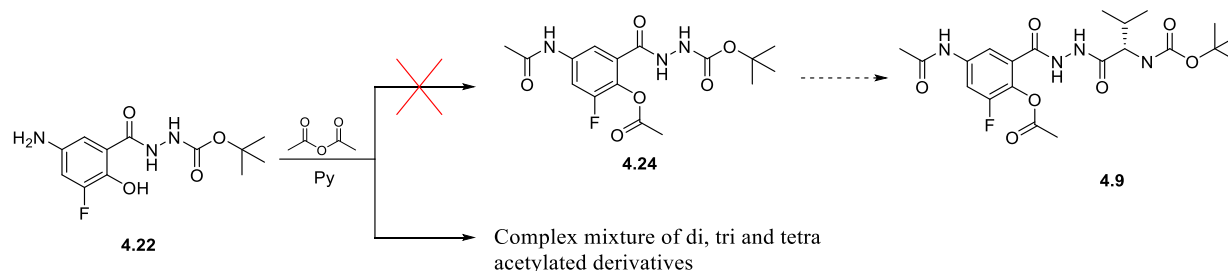


Figure 80 Structure of the obtained oxadiazolone (left) and model of crystallized dimeric form (right)

Finally, because of the coupling non-reproducibility performed with BTC, we decided to exploit the best coupling condition founded for **4.7**: COMU, oxyma in anhydrous DMF in the presence of NMM as base. The employment of this coupling condition allowed the preparation of compound **4.8** in large scale, up to 40% of yield.

Synthesis of the valine-F-benzhydrazide-N-acetyl 4.9

The synthesis of **4.9** was designed starting from intermediate **4.22** (Scheme 6). The employment of acetic anhydride, either at room temperature and low temperature (0°C), always led to a complex mixture of di, tri and tetra acetyl derivatives. In both cases, the fraction containing the desired product (confirmed by HRMS) was representing less than 20%.

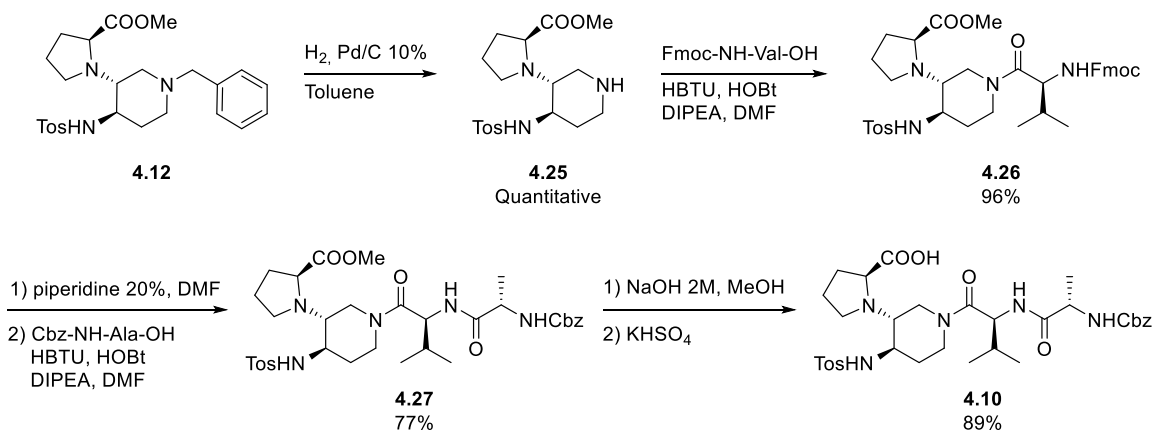


Scheme 6 Proposed synthetic pathway for compound **4.9**

Considering the low yields of the final coupling reactions for obtaining **4.7** and **4.8**, we decided to give up the synthesis of **4.9**.

Synthesis of intermediate 4.10: introduction of the SRE Alanine-Valine on the tosyl scaffold

The intermediate **4.10** was prepared in satisfactory yield following the procedure reported by Nicolò Tonali (Scheme 7),¹²² which started from the β -turn inducer **4.12**, synthesized from commercially available materials in accordance with the procedure reported in the literature.¹²⁰ After hydrogenolysis of **4.12**, performed in toluene in the presence of 10% Pd/C, the dipeptide Alanine-Valine was introduced on **4.25** amino acid by amino acid (intermediates **4.26** and **4.27**) employing the classical peptide synthesis conditions in solution: HBTU, HOBT, in the presence of DIPEA in anhydrous DMF, and in good yields. The methyl ester of compound **4.27** was then saponified with NaOH 2M in MeOH operating at 60°C leading to compound **4.10**.



Scheme 7 Synthetic scheme for the preparation of intermediate **4.10**

Synthesis of intermediate 4.11: introduction of the SRE Alanine-Isoleucine-Leucine on the β -turn inducer

During the coupling between the carboxylic group of proline and the amine of bulky blocking sequence, Faustine Bizet¹⁴⁴ and I often observed the formation of the cyclized by-product represented in Figure 81. This by-product results from the coupling between proline's carboxylic acid and the sulfonamide function and its quantity depended on the used coupling reagents.

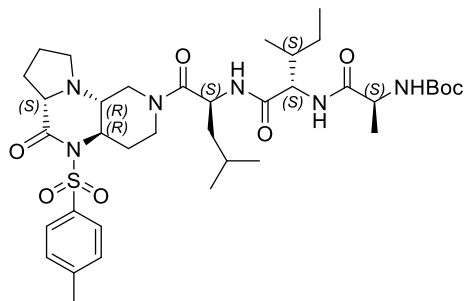
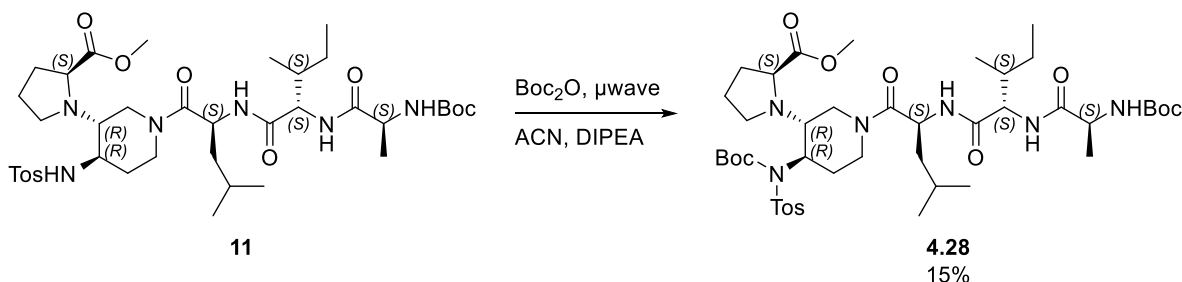


Figure 81 Structure of the cyclized by-product

In order to avoid the cyclization we decided to protect the sulfonamide function. We initially planned to introduce a *tert*-butyloxycarbonyl group directly on the sulfonamide function of compound **11** (see paragraph 3.1.3 page 70), already available in the laboratory (Scheme 8).



Scheme 8 Introduction of *tert*-butyloxycarbonyl group on the sulfonamide of **11**

Although the sulfonamide easily reacted with the free carboxylic group to form the cyclized by-product, the reaction to add the *tert*-butyloxycarbonyl on compound **11** resulted in **4.28** only in low yield (Table 4).

Entry	Reagent	Base	Solvent	DMAP	Temperature	μ wave	Time	Yield
1	Boc ₂ O	DIPEA	CH ₃ CN	Yes	From 30 to 70 °C	No	4 days	7% + Starting material
2	Boc ₂ O	DIPEA	CH ₃ CN	Yes	70 °C	Yes	4h	Starting material
3	Boc ₂ O	DIPEA	CH ₃ CN	Yes	100 °C	Yes	2h	15% + Degradation products
4	Boc ₂ O	\	HFIP	Yes	100 °C	Yes	6h	Ala Boc cleavage

Table 4 Conditions tested to introduce the *tert*-butyloxycarbonyl group on **11**

Thus, we designed a new synthesis for compound **4.11** (Scheme 9) in which the sulfonamide protection of intermediate **4.12** was the first step. Tonali *et al.* previously published a simple way for the introduction of a *tert*-butyloxycarbonyl group on the nosyl β -turn inducer.¹²² So, we started our investigation from these conditions. As reported in table 5, the employment of sodium hydride as base, in the presence of DMAP allowed the preparation of Boc protected sulfonamide **4.29** in a very good yield. Knowing that the cyclization was possible under mild conditions (DIPEA and coupling reagents), we wanted to find a milder way for this sulfonamide protection. We found that by using DIPEA instead of sodium hydride, it was possible to synthesize compound **4.29** (Table 5 entries 3 and 4). However, the presence of DMAP was necessary, otherwise the reaction did not take place (Table 5 entry 2). Since it is often necessary to have an orthogonal protecting group, we also investigated the possibility to protect the sulfonamide with a benzyloxycarbonyl group. Unfortunately, the reaction between benzyl chloroformate and **4.12** did not lead to the desired product (Table 5 entries 6 and 7).

Entry	Reagent	Base	Solvent	DMAP	Temperature	Time	Yield
1	Boc ₂ O	NaH	DMF	Yes	RT	o.n.	88%
2	Boc ₂ O	DIPEA	DMF	No	RT	o.n.	Starting material
3	Boc₂O	DIPEA	DMF	Yes	RT	o.n.	93%
4	Boc ₂ O	DIPEA	ACN	Yes	RT	o.n.	83%
5	Cbz-Cl	DIPEA	DMF	Yes	From RT to 50 °C	o.n.	Starting material
6	Cbz-Cl	TEA	DCM	Yes	From RT to 60 °C	o.n.	Starting material

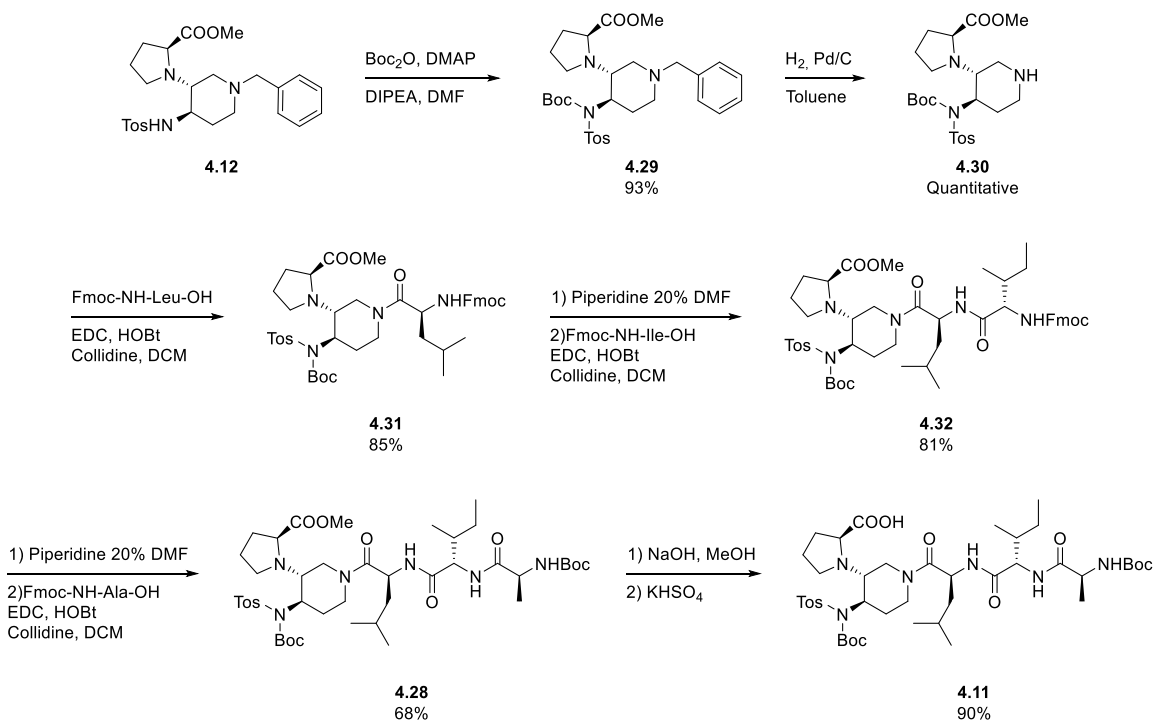
Table 5 Conditions tested for the protection of sulfonamide **4.12**

The following hydrogenolysis of **4.29** was performed in toluene in the presence of 10% Pd/C (scheme 9). The three amino acids Alanine, Isoleucine and Leucine were then successively inserted exploiting the solution peptide synthesis. In table 6 the different conditions tested for the coupling between the **4.30** and the carboxylic group of Fmoc-NH-Leu-OH are reported. We found that the

couple EDC hydrochloride/HOBt in DCM in the presence of collidine as base were the best conditions for the synthesis of intermediate **4.31** (Table 6 entry 7). These best conditions were used for the two subsequent coupling and intermediates **4.32** and **4.28** were obtained in 81% and 68% of yield respectively (Scheme 9). Finally, an easy saponification of **4.28** with sodium hydroxide in methanol led to the free carboxylic acid **4.11** needed for the following final coupling in good yield (90%).

Entry	Coupling Reagent 1	Coupling Reagent 2	Solvent	Base	Yield
1	Tosyl-Cl	\	DMF	TEA	24%
2	HATU	HAOt	DMF	Collidine	52%
3	DMTMM	\	DMF	NMM	53%
4	COMU	Oxyma	DMF	DIPEA	65%
5	COMU	Oxyma	DMF	Collidine	68%
6	BTC	/	THF	Collidine	71%
7	EDC*HCl	HOBt	DCM	Collidine	85%

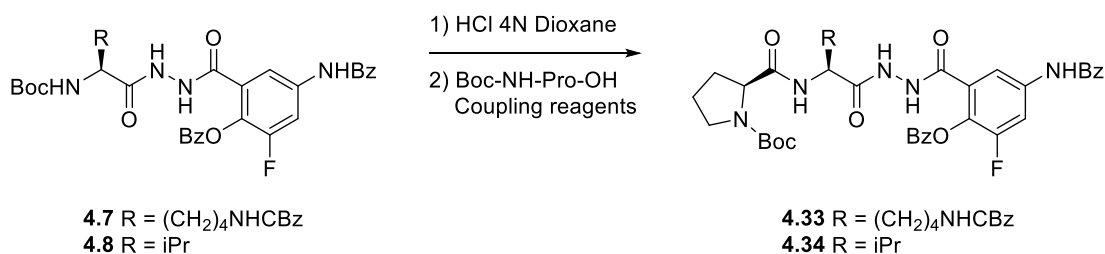
Table 6 Coupling reagents tested for the synthesis of **4.31**



Scheme 9 Synthesis of compound **4.11**

Synthesis of the complete hairpin mimics 4.3 bearing the lysine F-benzhydrazide and 4.6 bearing the valine F-benzhydrazide-N-benzoyl

As previously showed in the retrosynthetic scheme (Figure 77, page 80), we planned to synthesize compound **4.3** reacting the free carboxylic group of **4.10** with the free amine of intermediate **4.7**. Initially, we used the classical coupling conditions for solution peptide synthesis: HBTU, HOBt, in the presence of DIPEA. After complete consumption of the starting material, the analysis revealed the formation of only degradation products. So, to avoid the waste of **4.10** and **4.7**, we decided to use the Boc-NH-Proline-OH as model to study and to optimize this delicate coupling reaction (Scheme 10).



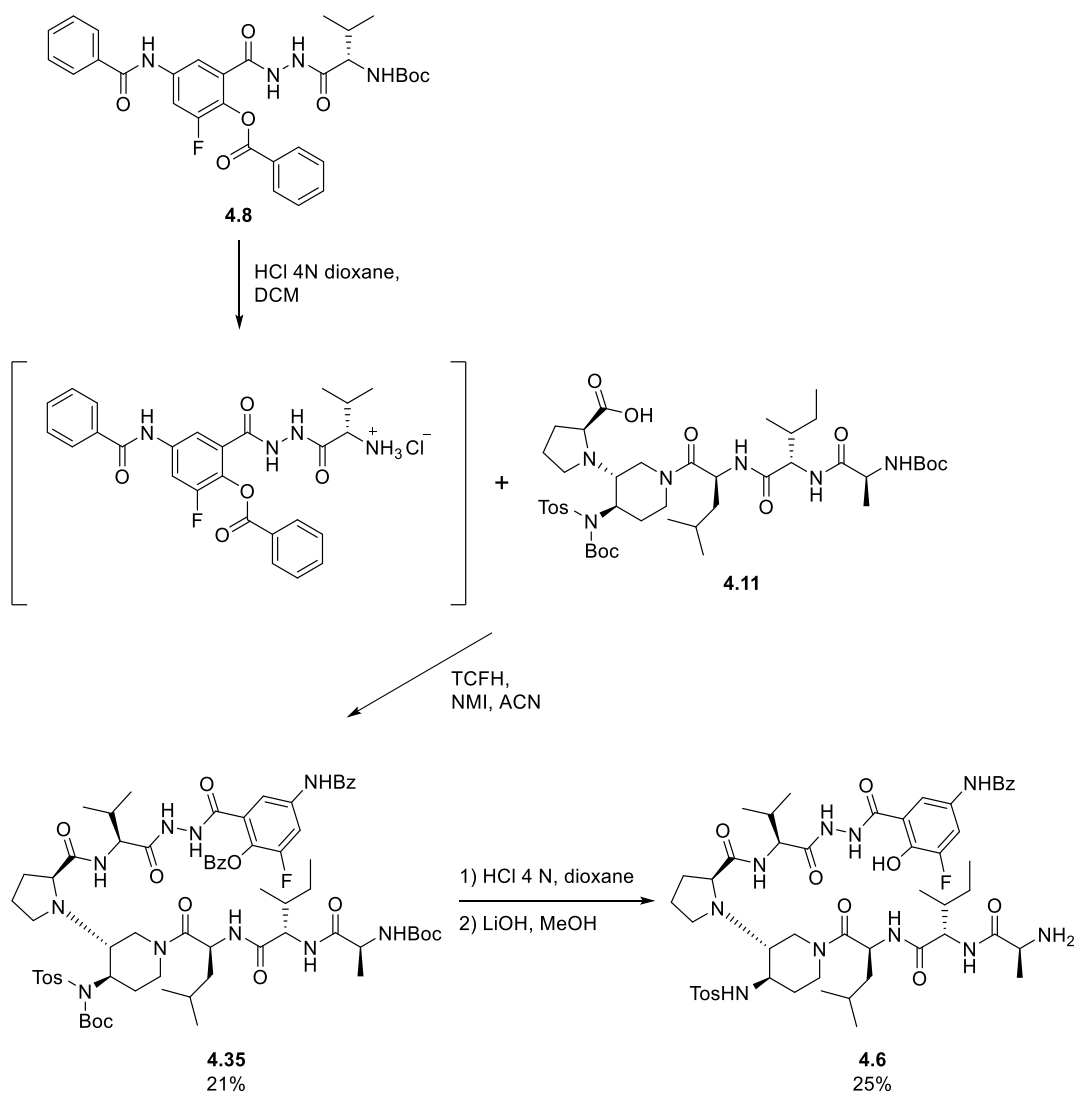
Scheme 10 Model reaction used to study the coupling reaction between the fluorinated benzhydrazide arm and the intermediate **4.7**

To try to understand what happened in the previous coupling, we first used the proline model to study the reaction with the coupling reagents HBTU and HOBt in the presence of DIPEA. As for the preparation of the complete hairpin, the reaction led to a mixture of starting material and degradation products. Among the degradation products, we observed the presence of the fluorinated benzhydrazide strand without the lysine. Thinking that the coupling failed because of the bulkiness of the arm, we decided to test COMU and Oxyma, two reagents that are often employed for difficult coupling reactions. In this case, we were able to isolate the desired product **4.33** but in a really low yield (<15%). Moreover, due to the degradation of the starting material, it was impossible to isolate pure **4.33** from the complex reaction mixture. Being sure that the Boc protected intermediate **4.7** was stable over time and supposing that the instability was to ascribe to the free amine, we tried a different coupling strategy to avoid the lysine cleavage. In 2014 Suppo *et al.* reported an innovative strategy to prepare a peptide via activated α -amino esters.¹⁸⁹ In accordance with this strategy, the free amine of an amino acid was rapidly converted in the reactive

species using carbonyl diimidazole (CDI) and then coupled with the carboxylic group of another amino acid. However, when we tried the activation with the CDI, we immediately observed the formation of several degradation products.

Taking in account the difficulty to perform this final coupling and the fact that the main biological target of my PhD project was hIAPP peptide, we decided to stop the synthesis of compound **4.3** and to focus our efforts to obtain **4.6** designed to inhibit hIAPP.

For this purpose, we started the investigation on the reaction model with proline (Scheme 10). As Valine is less bulky than lysine, we decided to test COMU and Oxyma as coupling reagents in the presence of collidine as base. In this case, 35% of the starting material **4.8** was converted to the final product **4.34** in 24 hours. Thus, we decided to transfer these conditions to the synthesis of the full hairpin **4.35** (Scheme 11). In contrast to the model reaction, **4.35** was obtained in only 20% yield over 3 days of reaction and the formation of side products made the purification a real challenge. Being not completely satisfied by the results, we decided to try a microwave assisted coupling reaction. However, because COMU is not very stable in the presence of microwaves, we replaced it with DIC. Disappointingly, instead of improving the yield, the employment of the microwaves led to a total degradation of the fluorinated benzhydrazide. Recently, Beutner *et al.* reported the use of *N,N,N',N'*-tetramethylchloroformamidinium hexafluorophosphate (TCFH) and *N*-methyl imidazole (NMI) for the preparation of challenging amide bond.¹⁹⁰ This reaction proceeds via *in situ* generation of highly reactive *N*-acyl imidazolium, which rapidly reacts with amine generating the desired amide bond. So, we decided to generate the *N*-acyl imidazolium of intermediate **4.11** employing TCFH and NMI and then to react it with freshly deprotected **4.8** (Scheme 11) After 4 hours, we were able to recover the desired product **4.35** in 21% yield after HPLC purification. Longer reaction time (3 days) led to an increased degradation of the benzhydrazide and a lower yield. Having in hand the intermediate **4.35**, we tried the total deprotection in aqueous acidic conditions. Unfortunately, the benzoyl cleavage did not occur, after removal of the volatile, the benzoyl group was removed using lithium hydroxide to yield the final compound **4.6** in modest yield (27% for two steps of deprotection and after final HPLC purification).



Scheme 11 Synthetic scheme for compound **4.6**

Conformational studies

In this subsection, we should report the conformational studies of compound **4.6**. Since the experiments are still ongoing, the preliminary attribution at 313K is reported in the experimental part at the end of the manuscript.

Biophysical evaluations

In this subsection, we report the inhibitory activity of hIAPP fibrillization for compound **4.6** and its *N*-Boc protected precursor **4.35** by Thioflavin-T (ThT) fluorescence assay. For each compound

the evaluation was carried out in triplicate and for every curve obtained, $t_{1/2}$ and F were calculated (For more detail see the experimental part).

Entry	Compound	Compound/hIAPP ratio	$t_{1/2}$ extension/reduction (%)	F extension/reduction (%)
1	4.35	10/1	ne	-37±8
		1/1	ne	-32±11
		0.1/1	ne	ne
2	4.6	10/1	+25±14	-82±0
		1/1	+30±17	-48±7
		0.1/1	ne	ne
3	4.4 (reference)	10/1	ne	-79±7
		1/1	ne	-45±6
		0.1/1	ne	-42±5

Table 7 Table summarizing the effect of the compounds **4.35**, **4.6** and **4.4** (reference compound) on $\Delta t_{1/2}$ and ΔF . Parameters are expressed as mean \pm SE, n=3. ^[a] ne = no effect

As summarized in table 7, both the *N*-Boc protected **4.35** and the free amine **4.6** were tested in ThT at the three different compound/hIAPP ratios 10/1, 1/1 and 0.1/1 and compared to the non fluorinated benzhydrazide compound **4.4** previously synthesised and studied by Faustine Bizet (Figure 75, page 81), Compound **4.35** did not show any significant effect on the $t_{1/2}$, while it displayed a very moderate activity on the fluorescence plateau at 10-fold excess and 1/1 ratio (Figure 81). In contrast, with its *N*-Boc precursor, the free amine **4.6** was able to affect either the $t_{1/2}$ and the fluorescence plateau (Figure 82). Although modest, the effect that **4.6** exerted on the $t_{1/2}$ at the two highest tested ratios 10/1 and 1/1, was higher than that of the reference compound **4.4**, which did not affect the $t_{1/2}$ ($\Delta t_{1/2} = +25$ and $+30\%$ vs ne, for **4.6** and **4.4** respectively). Much more pronounced was the effect on the fluorescence plateau, indeed, at 10-fold excess, **4.6** reduced the fluorescence plateau by 82% and at stoichiometric ratio by 48%. This dose-dependent effect, was comparable to the reference non fluorinated compound, **4.4** at the 2 higher ratios 10/1 and 1/1 ($\Delta F = -79$ and -45% respectively for 10/1 and 1/1 ratios). On the contrary, the reference compound **4.4** was more active at the substoichiometric ratio 0.1/1 ($\Delta F = -42\%$ vs ne respectively for **4.4** and **4.6**). On the whole, **4.6** displayed a slightly better activity than its non-fluorinated analogue **4.4**, except at the lowest ratio. This result confirms the beneficial effects on hIAPP anti-fibrillization of the 3 structural elements: OH, F and phenyl carbonyl which were discussed in the design (paragraph 4.2.1, page 80). However, **4.4** and **4.6** were tested in two different plaque thus, in order

to confirm these results and to be able to effectively compare the two compounds we will repeat the test.

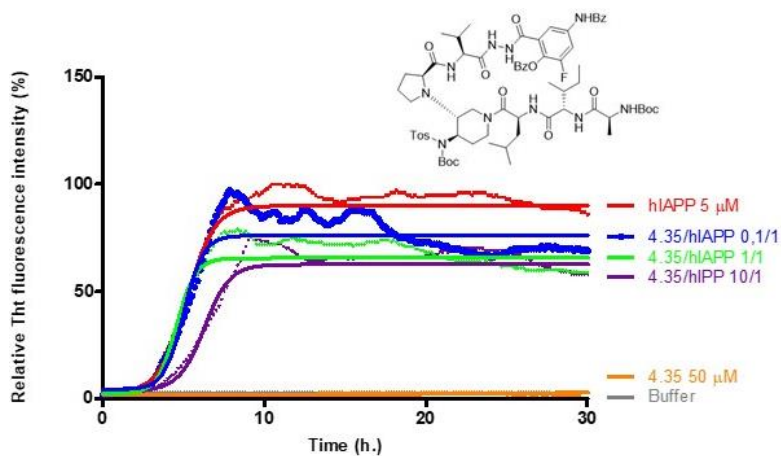


Figure 82 Representation of the mean curves of Tht fluorescence assays over time showing hIAPP aggregation (5 μM) in the presence of compound **4.35** (mean curve of the triplicate)

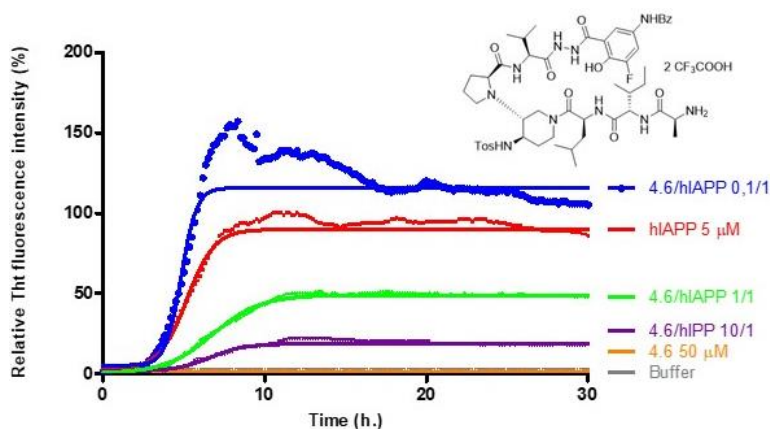


Figure 83 Representation of the mean curves of Tht fluorescence assays over time showing hIAPP aggregation (5 μM) in the presence of compound **4.6** (mean curve of the triplicate)

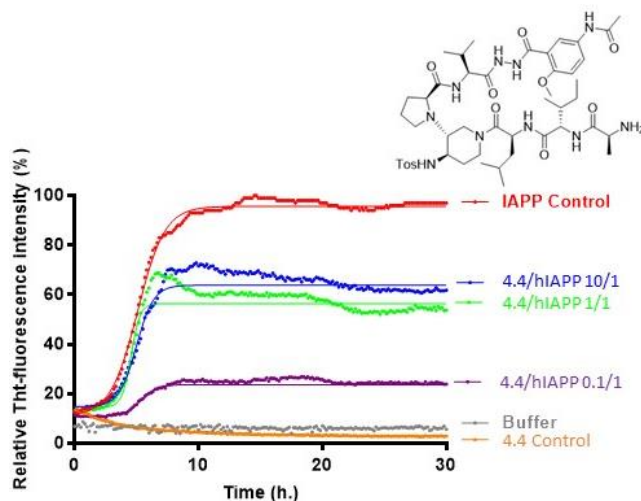


Figure 84 Representation of the mean curves of ThT fluorescence assays over time showing hIAPP aggregation (5 μ M) in the presence of compound **4.4** (mean curve of the triplicate)

Conclusion

In this subchapter we presented the design, synthesis and biophysical evaluation of a new acyclic β -hairpin peptidomimetic bearing the 3-fluoro-5-benzamido-2-hydroxybenzohydrazide blocking sequence, which was the first example of fluorinated hairpin. Compound **4.6**, whose peptidomimetic arm was designed following the information gathered from the work of previous PhD students, showed a marked inhibitory activity against hIAPP peptide aggregation. In contrast, its totally protected precursor **4.35** displayed only a modest inhibitory activity. This difference could probably be ascribed to the free hydroxylic group in *ortho* position to the fluorine atom and the terminal free amine.

The excellent results obtained during the preliminary evaluation by Thioflavin-T (ThT) fluorescence assay demonstrated that the structural modifications (OH, F and phenyl carbonyl) we introduced on the inhibitor **4.4** previously reported by Faustine Bizet¹⁴⁴ (See page 81) had a positive impact on the activity, especially at high inhibitor/peptide and 1/1 ratio. Indeed, the fact that our fluorinated inhibitor **4.6**, in contrast with compound **4.4**, did not self-aggregate at high concentration could be related to the different hydrogen bond network probably imposed by the presence of *ortho* fluoro phenol. Unfortunately, we could not confirm this hypothesis because at this moment the analyses are still in progress.

With the data in our possession we can affirm that our compound **4.6** could be a good candidate as hIAPP aggregation inhibitor. However, before to draw definitive conclusion these results need to be confirmed by repeating the Thioflavin-T (ThT) fluorescence assay and by performing other complementary biophysical experiments like TEM, CE and IMS-MS, in order to evaluate its effect on the morphology of the fibers and on the early oligomerization process (see chapter 2 and 3 for details on these experiments). Moreover, thanks to the NMR experiments in course, we will be able to evaluate if **4.6** is adopting a β -hairpin structure and how the presence of the *ortho* fluoro-phenol is influencing the overall conformation and hydrogen-bond network and its activity as a consequence.

4.2.2 β -hairpin mimics containing the *N*-difluoromethyltriazolyl peptidomimetic arm

*Design of the compounds bearing the *N*-difluoromethyltriazolyl peptidomimetic arm*

In the context of the development of new fluorinated β -hairpins able to modulate hIAPP aggregation, one of the explored strategies was to design compounds characterized by the presence of fluorinated pseudopeptides as blocking sequence. As previously seen in chapter 3 with the inhibitor bearing the di-aza-tripeptide **3.8** (See page 68) and in the previous paragraph 4.2.1 with the inhibitor bearing the Amb arm **4.4** (See page 81), the introduction of a peptidomimetic blocking sequence could represent the optimal balance between the activity and the desired reduced peptidic character.

Historically, our group has shown a strong interest in the development of fluorinated building blocks for pseudopeptides preparation. Recently, our team began the study of *N*-difluoromethyl-1,4-triazole amino acid as scaffold for the synthesis of peptidomimetics.¹⁹¹ The 1,4-triazole unit has been recognized as a *trans*-amide surrogate, extremely stable to hydrolysis, and even if its size and dipole moment are larger, triazolyl amino acids can mimic dipeptides.¹⁹² Interestingly, this new difluorinated unit, that can be considered as an analogue of Gly-difluoroGly dipeptide (Figure 85), is able to induce or stabilize β -strand conformation when inserted in a peptide.¹⁹¹

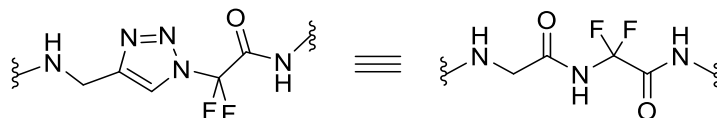


Figure 85 Structures of the new *N*-difluoromethyl-1,4-triazole amino acid unit (left) and its analogue Gly-difluoroGly dipeptide¹⁹¹

This feature has been linked to the presence of the *gem* difluoro group which can engage interactions with neighbouring protons (both the CH of the triazole ring and the NH of the successive amino acid) stabilizing the extended conformation (Figure 86).

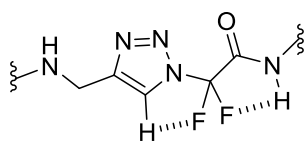


Figure 86 *N*-difluoromethyl-1,4-triazole amino acid unit showing the *gem* difluoro group interactions that stabilize the extended conformation

This is also supported by the fact that, on the contrary, a non-fluorinated 1,4 disubstituted 1,2,3-triazole analogues, inserted in a linear peptide, is rather able to induce a β -turn.¹⁹³ The *N*-difluoromethyl triazole, with its interesting characteristics, could represent a powerful tool for the synthesis of restrained peptidomimetic structures. PhD colleagues of my group are currently using this scaffold to build foldamers (triazolamers) but it has never been inserted into a pseudopeptide designed to fold into β -hairpin mimics. As previously reported in the first chapter, one of the main problems in the development of small acyclic β -hairpins is the difficulty in the design of structures capable to maintain a stable β -hairpin folding. Thus, we decided to design pseudopeptides containing our *N*-difluoromethyl-1,4-triazole amino acid in order to study its effect on the conformation and as a consequence on the inhibitory activity on the aggregation of hIAPP. Indeed, we supposed that the presence of a structure able to impose a β -strand conformation to one arm could positively influence the β -hairpin folding.

While planning the work for the synthesis of this new class of hIAPP fluorinated inhibitors, we decided to maintain the same tripeptide alanine-isoleucine-leucine as SRE and to design novel pseudopeptide containing the *N*-difluoromethyl-1,4-triazole amino acid motif as blocking sequence. As made in chapter 3 (See page 68) for the hairpin which bears the di-aza-tripeptide, we

took inspiration from hIAPP sequence and we planned the synthesis of two different structures (Figure 87):

- the first one (**4.36**) bears a blocking sequence inspired by the tripeptide phenylalanine-leucine-valinamide already successfully employed in chapter 3. Here, we replaced the central leucine by the *N*-difluoromethyl-1,4-triazole amino acid in order to exploit its ability to induce the extended conformation;
- As the first sequence is longer than the original tripeptide, we decided to investigate how the length of the pseudopeptidic blocking sequence can influence the inhibitory activity. So we designed a second inhibitor (**4.37**) bearing a truncated blocking sequence in which the terminal valinamide was removed.

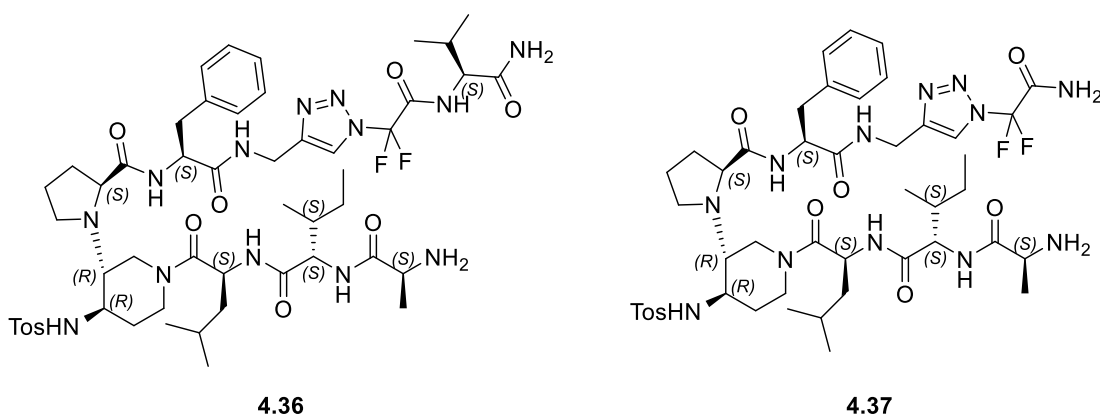


Figure 87 Structures of the hairpins **4.36** and **4.37** bearing the *N*-difluoromethyl-1,4-triazolyl blocking sequence

*Synthesis of the hairpins bearing the *N*-difluoromethyl-1,4-triazolyl peptidomimetic arms*

Compounds **4.36** and **4.37** were prepared following a synthetic strategy (Figure 88) similar to the one previously described for compounds bearing the fluorinated benzhydrazone arms (Figure 77, page 82). We prepared separately the two building blocks **4.38** and **4.39** which were then coupled with the intermediate **4.11**, whose synthesis has already been described (see paragraph 4.2.1, Scheme 10, page 93).

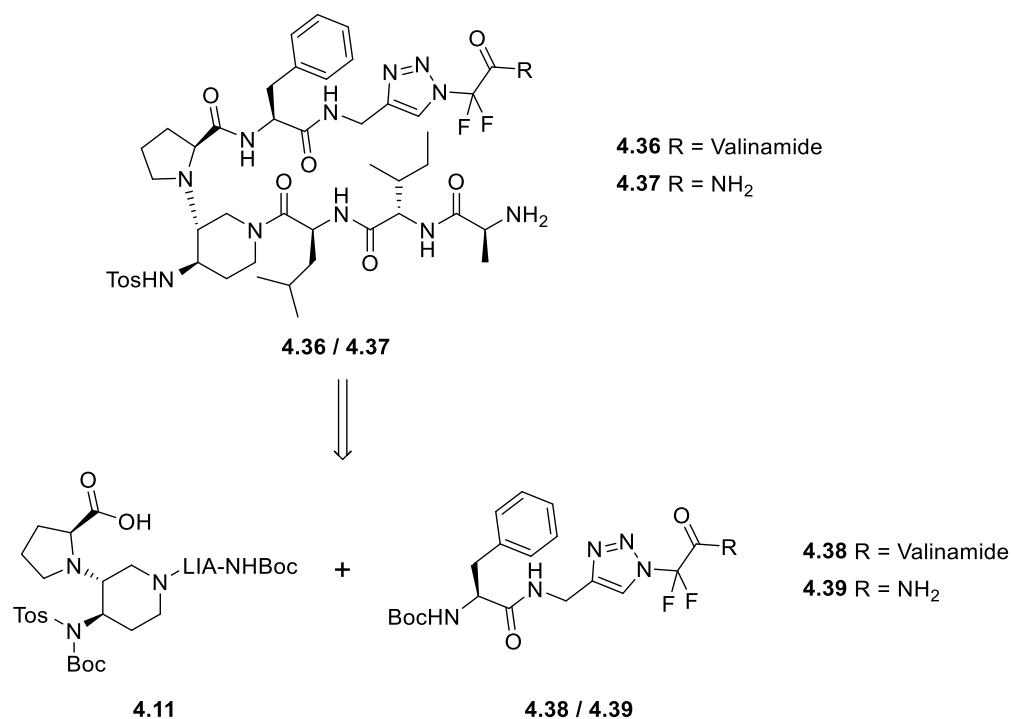
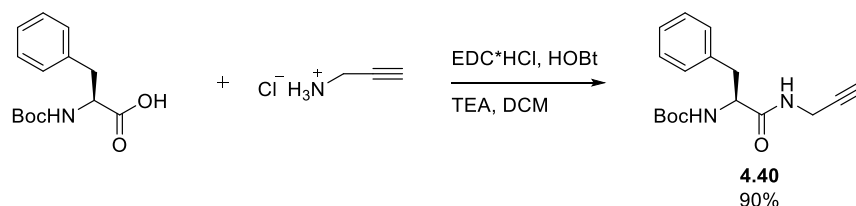


Figure 88 Retrosynthetic scheme for the preparation of compounds **4.36** and **4.37**

*Synthesis of the N-difluoromethyl-1,4-triazolyl blocking sequences **4.38** and **4.39***

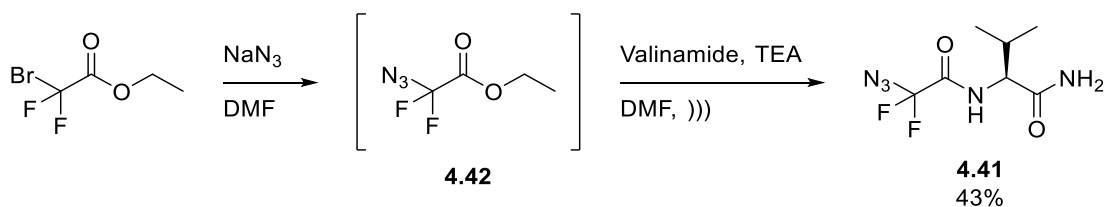
Following the methodology previously published by our group,¹⁹¹ pseudopeptides **4.38** and **4.39** were prepared using Huisgen 1,3 dipolar cycloaddition between appropriate propargylamides and azidodifluoroacetamides. The common propargylamide **4.40** was synthesized in very good yield, from the commercially available Boc-NH-Phenylalanine-OH and propargylamine hydrochloride, using EDC hydrochloride and HOBT as coupling agents, in DCM, and in the presence of TEA as base (Scheme 12).



Scheme 12 Synthesis of the common Phe-propargylamide intermediate **4.40**

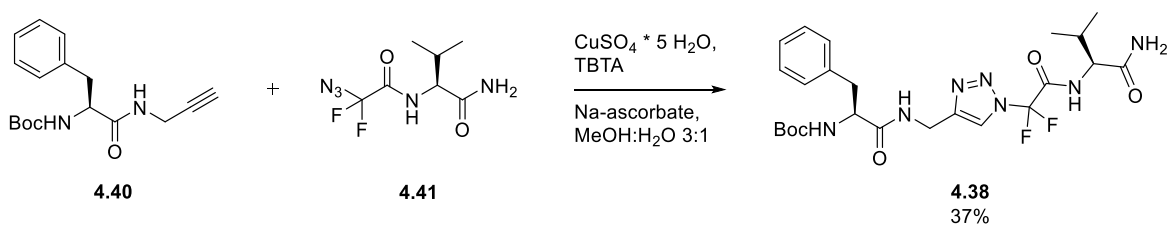
The synthesis of the azidodifluoroacetamide **4.41** was carried out starting from commercial ethyl 2-bromo-2,2-difluoroacetate, which reacted with sodium azide to form intermediate **4.42**. This

non-isolated azide underwent to a transamidification with valinamide, performed in an ultrasonic bath in the presence of TEA, to lead to the azidodifluoroacetamide **4.41** in 43% yield (Scheme 13).



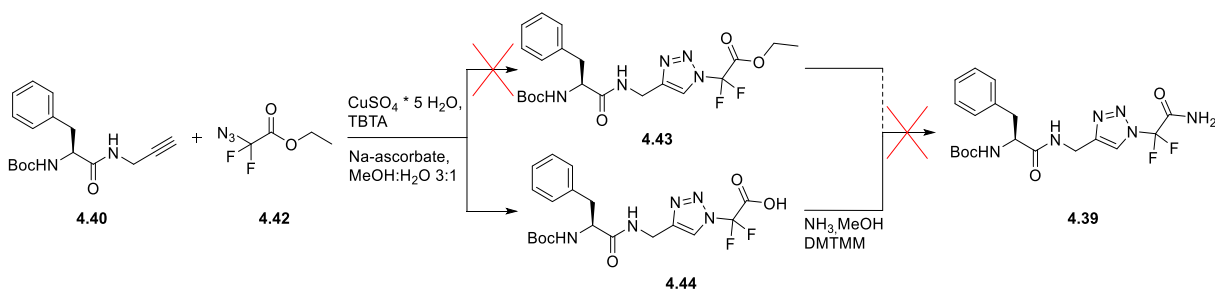
Scheme 13 Synthesis of the azidodifluoroacetamide **4.41**

Having in hand both intermediates **4.40** and **4.41**, it was possible to perform the 1,3-dipolar cycloaddition (Scheme 14). The reaction was carried out in a mixture of MeOH and water (ratio 3:1) in the presence of copper(II) sulfate (10%), sodium ascorbate (20%) and tris(benzyltriazolymethyl)amine (TBTA, 10%) to yield the desired pseudo-tetrapeptide **4.38** in 37% yield (that is almost two times and half less than what is reported in the literature for similar compounds).¹⁹¹



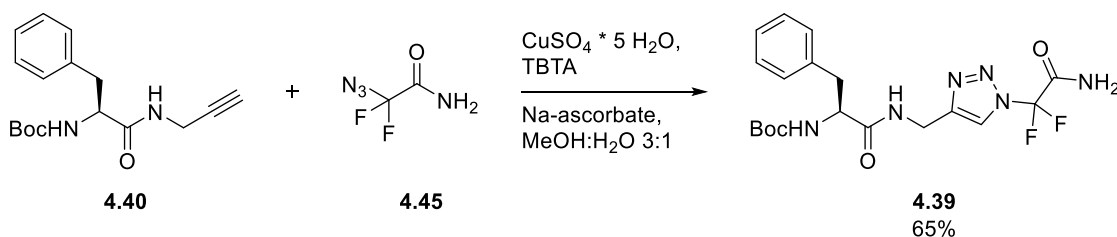
Scheme 14 Synthesis of pseudo-peptide **4.38**

To prepare the pseudo-peptide **4.39**, we initially planned the cycloaddition between Phe-propargylamide **4.40** and 2-azido-2,2-difluoroacetate **4.42** followed by a transamidification (Scheme 15). However, after the cycloaddition, instead of the desired ethyl ester **4.43**, we isolated the free carboxylic acid **4.44**. Thus, we decided to transform the carboxylic acid into the corresponding amide by reaction with ammonia in the presence of DMTMM.¹⁹⁴ Unfortunately, this methodology led to a complete degradation of compound **4.44**. Hypothesizing that the ethyl ester hydrolysis took place during the purification step, we planned to perform the transamidification directly on the crude of the cycloaddition. However, only the carboxylic acid **4.44** was recovered.



Scheme 15 First proposed synthesis for pseudopeptide **4.39**

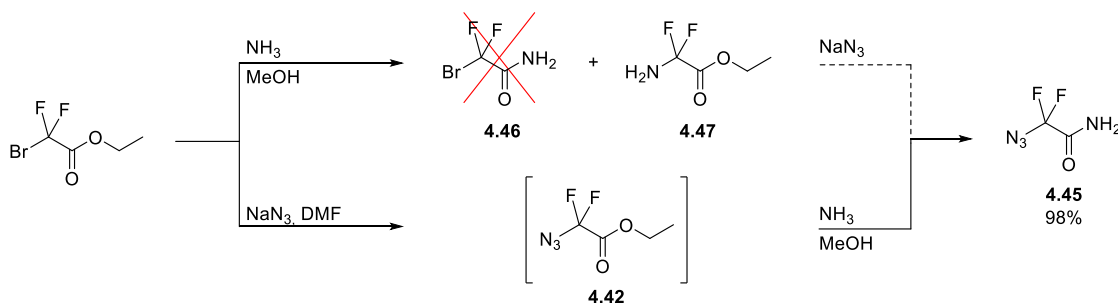
Because it was impossible to obtain **4.39** following the strategy reported above, we designed a new synthesis (Scheme 16) in which the amide **4.45** was prepared before the cycloaddition on the 2-azido-2,2-difluoroacetate **4.42**.



Scheme 16 Synthesis of intermediate **4.39**

In order to prepare azidodifluoroacetamide **4.45**, we thought of a synthesis whose steps can be theoretically invertible (Scheme 17). As **4.46** was already described in the literature, we tried first the transamidification on ethyl 2-bromo-2,2-difluoroacetate. According to what was reported by Tarui *et al.*, the transamidification should occur simply employing a methanolic solution of ammonia without the use of metal catalyst such as lanthanum trifluoromethanesulfonate.¹⁹⁵ However, after 3 hours of reaction we were able to recover only the byproduct **4.47**, because, instead of the transamidification reported by Tarui, we observed the nucleophilic substitution on the bromine. Thus, we decided to follow the inverse pathway already employed for the preparation of intermediate **4.41**. We first reacted the ethyl 2-bromo-2,2-difluoroacetate with sodium azide to prepare the intermediate **4.42**. Then, the non-isolated azide underwent a transamidification with ammonia, carried out in an ultrasonic bath. Pleasantly, the use of a methanolic solution of ammonia gave the desired product **4.45** in excellent yield (Scheme 17). Having in hand the appropriate propargylamides **4.40** and the azide **4.45**, it was then possible to carry out the Huisgen cycloaddition in a mixture of MeOH and water (ratio 3:1) in the presence of copper(II) sulfate

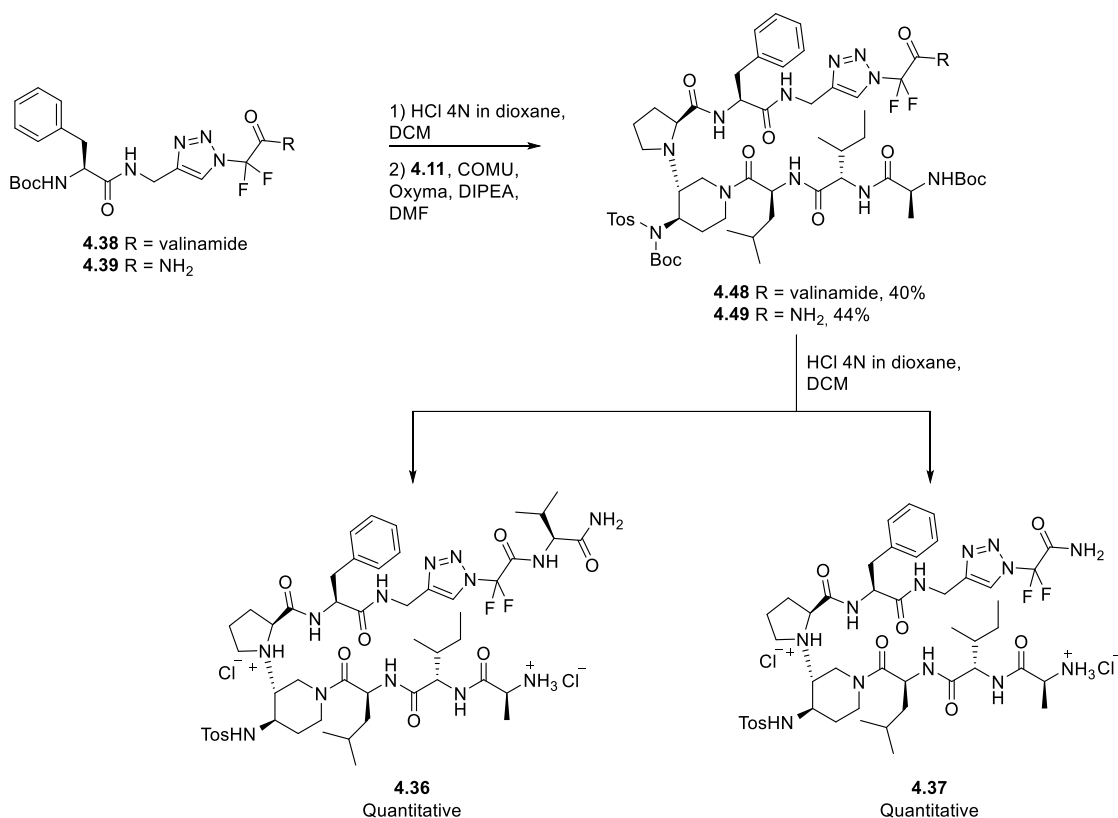
(10%), sodium ascorbate (20%) and tris(benzyltriazolylmethyl)amine (TBTA, 10%) to obtain the pseudotetrapeptide **4.39** in satisfactory yield (65%, Scheme 16).



Scheme 17 Synthesis of azidodifluoroacetamide **4.45**

*Synthesis of compounds **4.36** and **4.37** bearing the N-difluoromethyl-1,4-triazolyl blocking sequence*

Having in hand both pseudopeptide arms **4.38** and **4.39**, we could think to the final coupling with the intermediate **4.11** (Scheme 18). The tert-butyl carbamate was removed in acidic condition from both compounds **4.38** and **4.39**. The obtained hydrochloride salts were then coupled with intermediate **4.11** using COMU and Oxyma in the presence of collidine giving intermediates **4.48** and **4.49** in good yields. The following deprotection in acidic conditions led to the desired hairpin targets **4.36** and **4.37**.



Scheme 18 Synthesis of the final compounds **4.36** and **4.37** bearing the the *N*-difluoromethyl-1,4-triazolyl blocking sequence

Conformational studies

In this subsection, we report the conformational studies of compounds **4.36** and **4.37**. The analyses were performed in a protic solvent, which is more challenging for the hydrogen bond formation in comparison with an aprotic organic solvent such as chloroform. Since these two compounds are poorly soluble in water, we decided to perform all the analyses in CD₃OH. The aim of these studies was to determine if our compounds were adopting a β -hairpin pre-structuration similar to our previous compounds bearing other peptide or peptidomimetic sequences (see chapters 3 and 4.2.1). NMR spectra were recorded on a spectrometer operating at 600 MHz equipped with a cryoprobe (ICSN, Institute de Chimie des Substance Naturelles, Gif-sur-Yvette). ¹H and ¹³C resonances were completely assigned using 1D ¹H WATERGATE, 2D ¹H-¹H COSY (30 ms mixing time), 2D ¹H-¹H DIPSII (30 ms mixing time), 2D ¹H-¹H ROESY (500 ms mixing time), 2D ¹H-¹³C HSQC, 2D ¹H-¹³C HMBC and 2D ¹⁹F-¹H HOESY spectra. The resonances were assigned using spectrum acquired at 278K, other supplementary spectra were recorded respectively at 300K or 313K. ¹H

and ^{13}C chemical shifts were calibrated on the solvent residual peak (CD_3OH). The chemical shift deviations were calculated as the differences between the measured chemical shift and random coil value reported by Wishart *et al.*¹⁴² The vicinal coupling constants (3J) were extracted from 1D ^1H and 2D ^1H - ^1H COSY spectrum at 278K. To evaluate the presence of intramolecular hydrogen bonds, we examined amide proton coefficient temperature.

Hairpin 4.36 bearing the Phe-N-difluoromethyl-1,4-triazolyl-Val-CONH₂ blocking sequence

Working at 278K allowed the observation of two different conformers in dynamic equilibrium in ratio 3:1. However, in contrast with **4.37** (see the following pages of this chapter), despite the low temperature some protons and carbons displayed the same chemical shift in both conformers. Their ^1H -NMR and ^{13}C -NMR chemical shifts are reported in tables 7 and 8 respectively for conformers A and B.

Residue	δ NH (ppm)	δ H $^\alpha$ (ppm)	δ H $^\beta$ (ppm)	δ other protons (ppm)	δ CO (ppm)	δ C $^\alpha$ (ppm)	δ C $^\beta$ (ppm)	δ other carbons (ppm)
Ala-1	8.24	4.22	1.47	/	169.7	48.9	16.6	/
Ile-2	8.52	4.24	1.84	γ_{CH_3} 0.93 γ_{CH_2} 1.55 δ_{CH_3} 0.88	172.1	57.8	36.6	γ_{CH_3} 14.5 γ_{CH_2} 24.4 δ_{CH_3} 9.9
Leu-3	8.70	4.91	1.62	γ_{CH} 1.67 δ_{CH_3} 0.93/0.95	171.4	46.8	40.1	γ_{CH_2} 24.6 δ_{CH_3} 21.4/22.1
Piperidine Ring-4	/	/	/	H _{2/2'} 3.48/4.57 H ₃ 3.08 H ₄ 3.67 H _{5/5'} 1.36/1.53 H _{6/6'} 3.21/4.29	/	/	/	C _{2/2'} 43.6 C ₃ 63.0 C ₄ 50.8 C _{5/5'} 29.8 C _{6/6'} 40.4
Pro-5	/	4.45	2.18/2.58	γ 1.92/2.12 δ 3.55/3.86	167.8	66.3	30.0	γ 23.9 δ 51.3
Phe-6	9.13	4.64	2.98/3.11	H _o 7.23 H _m 7.22 H _p 7.19	171.5	56.0	37.8	C _q 136.1 C _o 129.1 C _m 128.4 C _p 126.9
Tzl-7	8.82	/	/	CH ₂ 4.43 CH 8.15	158.7	/	/	CH ₂ 34.1 C _q 145.7 CH 121.1
Val-8	9.33	4.31	2.18	γ_{CH_3} 1.01/1.02 CONH ₂ 7.88/7.91	173.5	59.8	30.5	17.5/18.4
Tosyl	7.96	/	/	H _o 7.84 H _m 7.45 CH ₃ 2.45	/	/	/	C _{qs} 137.2 C _o 127.0 C _m 130.

Residue	δ NH A (ppm)	J (Hz)	δ NH B (ppm)	J (Hz)
Ala-1	/	/	/	/
Ile-2	8.52	8.8	8.44	8.7
Leu-3	8.70	6.9	8.57	7.6
Phe-6	9.13	7.5	9.08	6.6
NH_{T21}	8.82	/	8.82	/
Val-8	9.33	8.9	9.33	8.9

Table 10 $^3J_{NH-H\alpha}$ coupling constants for both conformers A and B of compound **4.36**

In both conformations (Table 10) the $^3J_{NH-H\alpha}$ coupling constant assumed values systematically higher than the average value of 4 Hz found in the coil library. However, only Ile-2 and Val-8 values of both conformers fell within the range 8-12 Hz that correspond to the dihedral angles associated with peptide segments in extended conformation as expected for β -hairpin arms.¹⁴¹ These evidence suggested that compound **4.36** was not fully structured. Thus, to further investigate we next examined the chemical shift deviation since it could provide other useful information about the secondary structure. The calculated values of each amino acid of both conformers are reported in tables 11 and 12.

Residue	δ NH random coil	δ NH experimental	NH CSD	δ H $^{\alpha}$ random coil	δ H $^{\alpha}$ experimental	H $^{\alpha}$ CSD
Ala-1	8.24	/	/	4.32	4.22	-0.1
Ile-2	8.00	8.52	+0.52	4.17	4.24	+0.07
Leu-3	8.16	8.70	+0.54	4.34	4.91	+0.57
Pro-5	/	/	/	4.42	4.45	+0.03
Phe-6	8.30	9.13	+0.83	4.62	4.64	+0.02
Val-8	8.03	9.33	+1.03	4.12	4.31	+0.19
Residue	δ C $^{\alpha}$ random coil	δ C $^{\alpha}$ experimental	C $^{\alpha}$ CSD	δ C=O random coil	δ C=O experimental	C=O CSD
Ala-1	52.5	48.9	-3.6	177.8	169.7	-8.1
Ile-2	61.1	57.8	-3.3	176.4	172.1	-4.3
Leu-3	55.1	46.8	-8.3	177.6	171.4	-6.2
Pro-5	63.3	66.3	+6.0	177.3	167.8	-9.5
Phe-6	57.7	56.0	-1.7	175.8	171.5	-4.3
Val-8	62.2	59.8	-2.4	176.3	173.5	-2.8

Table 11 Chemical shift deviation (CSD) of each amino acid of compound **4.36** conformer A

Residue	δ NH random coil	δ NH experimental	NH CSD	δ H $^{\alpha}$ random coil	δ H $^{\alpha}$ experimental	H $^{\alpha}$ CSD
Ala-1	8.24	/	/	4.32	3.96	-0.36
Ile-2	8.00	8.44	+0.44	4.17	4.24	+0.07
Leu-3	8.16	8.57	+0.41	4.34	4.74	+0.4
Pro-5	/	/	/	4.42	4.45	+0.03
Phe-6	8.30	9.08	+0.78	4.62	4.64	+0.02
Val-8	8.03	9.33	+1.30	4.12	4.31	+0.19

Residue	δC^α random coil	δC^α experimental	C^α CSD	$\delta C=O$ random coil	$\delta C=O$ experimental	$C=O$ CSD
Ala-1	52.5	48.9	-3.6	177.8	169.9	-7.9
Ile-2	61.1	57.8	-3.3	176.4	172.1	-4.3
Leu-3	55.1	47.6	-7.5	177.6	171.4	-6.2
Pro-5	63.3	66.3	+6.0	177.3	167.8	-9.5
Phe-6	57.7	56.6	-1.1	175.8	171.5	-4.3
Val-8	62.2	59.8	-2.4	176.3	173.5	-2.8

Table 12 Chemical shift deviation (CSD) of each amino acid of compound **4.36** conformer B

In both conformers NH-CSD generally showed positive values as expected for the extended arms of a β -hairpin. Noteworthy were the high values of Val-8 (+1.0 and +1.3 respectively for conformers A and B), that could be hypothetically ascribe to the presence of the vicinal CF_2 group. Indeed, the CF_2 could enhance the CSD by either de-shielding the amide (down fielded) thanks to its electron withdrawing effect or stabilizing the extended conformation because of its electronic properties. The borderline H^α -CSD values for almost all the amino acids fitted with the hypothesis of a non-fully structured β -hairpin. Anyway, the general C-CSDs up-fielding (negative values of both conformers confirmed the presence of extended conformations of the arms. While the positive C^α -CSD of Pro-5 was the only evidence of the presence of a β -turn inducer in both conformations. In order to complete the conformational studies, we finally examined the ROE network. In both conformers the presence of sequential CH_{α_i}/NH_{i+1} ROEs for the tripeptide FLV and for the segment from Pro-5 to Tzl-7 confirmed the extended conformation of the arms (Figure 89, blue arrow). Concerning the ROEs network usually observed for similar compounds (see draft paper chapter 3, page 68) we observed only the ROEs between H^α -Pro-5 and proton in position 3 of the piperidine ring. More interesting were the two different ROEs displayed by the H^α -Leu-3 with the piperidine ring. Indeed, in conformer A we observed a ROE signal of H^α -Leu-3 with proton in position 2 while in conformer B the ROE was between H^α -Leu-3 and proton in position 6. As we recently demonstrated (see draft paper chapter 3, page 68), these signals are diagnostic of two different β -hairpin conformations: one more closed (conformer A) and one more open (conformer B). Although only for conformer A we observed spatial proximities between the lateral chains of Leu-3 and Phe-6, reflecting the interaction between the two arms, as expected for the more closed hairpin. Thus, we can conclude that compound **4.36** is adopting a β -hairpin secondary structure even though it is not well defined as for other similar compounds bearing two peptidic sequences (see draft paper chapter 3, 68).

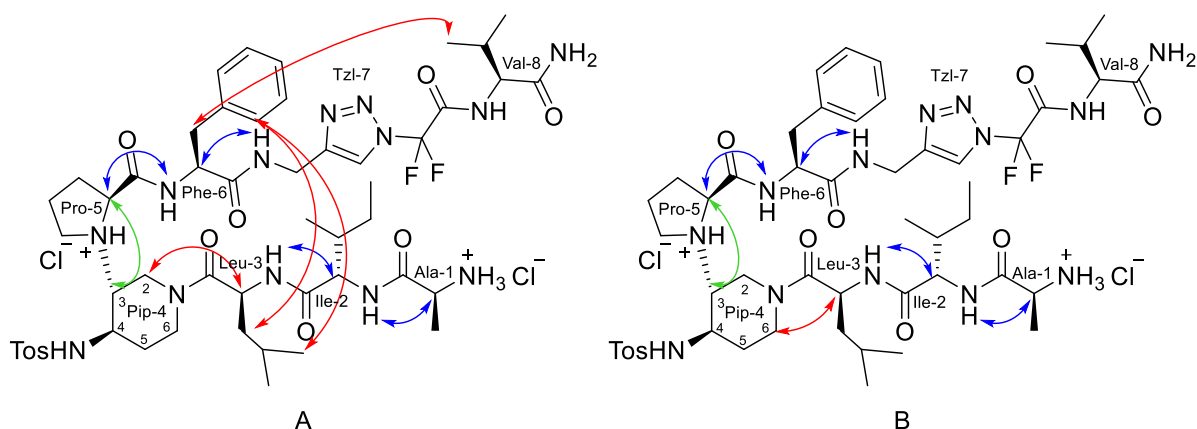


Figure 89 In green the common ROEs, in blue the common sequential ROEs and in red the differences between conformers A and B of compound **4.36**

Hairpin 4.37 bearing the Phe-N-difluoromethyl-1,4-triazolyl amide blocking sequence

Working at 278K, as for compound **4.36**, made possible an optimal resolution, which allowed the complete attribution of two conformers A and B. Indeed, as proved by the splitting of some peaks, compound **4.37** was present as mixture of two different conformers in ratio 1:1. Their $^1\text{H-NMR}$ and $^{13}\text{C-NMR}$ chemical shifts are reported in tables 13 and 14 respectively for conformers A and B.

Residue	δ NH (ppm)	δ H $^\alpha$ (ppm)	δ H $^\beta$ (ppm)	δ other protons (ppm)	δ CO (ppm)	δ C $^\alpha$ (ppm)	δ C $^\beta$ (ppm)	δ other carbons (ppm)
Ala-1	/	3.74	1.33	/	173.0	49.5	18.3	/
Ile-2	8.23	4.18	1.70	γ_{CH_3} 0.77 γ_{CH_2} 1.05 δ_{CH_3} 0.81	171.6	57.4	36.9	γ_{CH_3} 14.7 γ_{CH_2} 24.8 δ_{CH_3} 10.0
Leu-3	8.37	4.82	1.43	γ_{CH_2} 1.60 δ_{CH_3} 0.84/0.85	171.9	46.8	40.1	γ_{CH_2} 24.5 δ_{CH_3} 20.5
Piperidine Ring-4	/	/	/	H $_{2/2'}$ 3.29/4.16 H $_3$ 2.63 H $_4$ 3.57 H $_{5/5'}$ 1.17/1.51 H $_{6/6'}$ 2.48/4.28	/	/	/	C $_{2/2'}$ 43.8 C $_3$ 60.1 C $_4$ 54.0 C $_{5/5'}$ 31.8 C $_{6/6'}$ 40.8
Pro-5	/	3.73	1.34/1.92	γ 1.32/1.57 δ 2.71/3.11	176.4	62.8	30.3	γ 24.3 δ 44.5
Phe-6	8.80	4.77	3.14/3.24	H $_o$ 7.32 H $_m$ 7.26 H $_p$ 7.21	173.1	54.0	37.5	C $_q$ 137.5 C $_o$ 129.4 C $_m$ 128.1 C $_p$ 126.1
Tzl-7	8.87	/	/	CH $_2$ 4.54 CH 8.36	/	/	/	CH $_2$ 34.2 C $_q$ 145.5 CH 121.1
CF$_2$CONH$_2$	8.53	/	/	/	/	/	/	/

Tosyl	7.70	/	/	H _o 7.83 H _m 7.41 CH ₃ 2.45	/	/	/	C _{qs} 139.2 C _o 126.7 C _m 129.8 C _{qm} 143.6 CH ₃ 20.3
--------------	------	---	---	--	---	---	---	--

Table 13 ¹H-NMR and ¹³C-NMR chemical shifts for conformer A. **Legend:** C_{qs} = carbon bearing the sulfonamide, C_{qm} = carbon bearing the methyl of tosyl.

Residue	δ NH (ppm)	δ H ^α (ppm)	δ H ^β (ppm)	δ other protons (ppm)	δ CO (ppm)	δ C ^α (ppm)	δ C ^β (ppm)	δ other carbons (ppm)
Ala-1	/	3.70	1.33	/	173.4	49.5	18.3	/
Ile-2	8.23	4.19	1.78	γ _{CH3} 0.89 γ _{CH2} 1.14 δ _{CH3} 0.88	172.1	57.7	36.6	γ _{CH3} 14.6 γ _{CH2} 24.5 δ _{CH3} 10.0
Leu-3	8.37	4.82	1.43	γ _{CH} 1.60 δ _{CH3} 0.87/0.90	171.9	46.8	40.1	γ _{CH2} 24.5 δ _{CH3} 22.1
Piperidine Ring-4	/	/	/	H _{2/2'} 2.77/4.42 H ₃ 2.35 H ₄ 3.59 H _{5/5'} 1.32/1.64 H _{6/6'} 3.05/3.81	/	/	/	C _{2/2'} 39.8 C ₃ 59.5 C ₄ 54.0 C _{5/5'} 32.5 C _{6/6'} 43.9
Pro-5	/	3.38	1.34/1.94	γ 1.32/1.57 δ 2.64/3.05	176.4	63.4	30.3	γ 24.3 δ 44.5
Phe-6	8.67	4.69	3.16/3.27	H _o 7.32 H _m 7.26 H _p 7.21	173.2	54.3	37.5	C _q 137.5 C _o 129.4 C _m 128.1 C _p 126.1
Tzl-7	8.94	/	/	CH ₂ 4.56 CH 8.31	/	/	/	CH ₂ 34.2 C _q 145.6 CH 121.1
CF₂CONH₂	8.53	/	/	/	/	/	/	/
Tosyl	7.56	/	/	H _o 7.83 H _m 7.41 CH ₃ 2.45	/	/	/	C _{qs} 139.2 C _o 126.7 C _m 129.8 C _{qm} 143.6 CH ₃ 20.3

Table 14 ¹H-NMR and ¹³C-NMR chemical shifts for conformer B. **Legend:** C_{qs} = carbon bearing the sulfonamide, C_{qm} = carbon bearing the methyl of tosyl.

Having in hand the complete attribution of both conformers, we then turned our attention on the study of their conformations. Thus, we examined the chemical shift deviation for each natural amino acid present in the structures (Tables 15 and 16). In both conformers the residues Ile-2, Leu-3 and Phe-6 showed a general down-fielding for α hydrogens and amides, while Ala-1 and Pro-5 displayed an opposite tendency. The positive values are compatible with an extended conformation, as expected for the arms of a β-hairpin. The negative value of Pro-5 was indicative

of a β -turn presence, while in the case of Ala-1 it suggested a certain grade of flexibility at the N-terminal. C-CSDs further confirmed what have been observed for the H-CSDs. Indeed, C α and carbonyl of both conformers were found upfield shielded (negative CSD) for each amino acid compatible with extended conformation. Moreover, Pro-5 had very small C α and carbonyl CSD values when compared to those of the other residues, confirming its involvement in a β -turn (see paragraph 2.1.3 page 58).

Residue	δ NH random coil	δ NH experimental	NH CSD	δ H $^\alpha$ random coil	δ H $^\alpha$ experimental	H $^\alpha$ CSD
Ala-1	8.24	/	/	4.32	3.74	-0.58
Ile-2	8.00	8.23	+0.23	4.17	4.18	+0.01
Leu-3	8.16	8.37	+0.21	4.34	4.82	+0.48
Pro-5	/	/	/	4.42	3.73	-0.69
Phe-6	8.30	8.80	+0.50	4.62	4.77	+0.15
Residue	δ C $^\alpha$ random coil	δ C $^\alpha$ experimental	C $^\alpha$ CSD	δ C=O random coil	δ C=O experimental	C=O CSD
Ala-1	52.5	49.5	-3	177.8	173.4	-4.4
Ile-2	61.1	57.4	-3.7	176.4	172.1	-4.3
Leu-3	55.1	46.8	-8.3	177.6	171.9	-5.7
Pro-5	63.3	62.8	-0.5	177.3	176.4	-0.9
Phe-6	57.7	54.0	-3.7	175.8	173.1	-2.7

Table 15 Chemical shift deviation (CSD) of each amino acid of compound **4.37** conformer A

Residue	δ NH random coil	δ NH experimental	NH CSD	δ H $^\alpha$ random coil	δ H $^\alpha$ experimental	H $^\alpha$ CSD
Ala-1	8.24	/	/	4.32	3.70	-0.62
Ile-2	8.00	8.23	+0.23	4.17	4.19	+0.02
Leu-3	8.16	8.37	+0.21	4.34	4.82	+0.48
Pro-5	/	/	/	4.42	3.38	-1.04
Phe-6	8.30	8.67	+0.37	4.62	4.69	+0.07
Residue	δ C $^\alpha$ random coil	δ C $^\alpha$ experimental	C $^\alpha$ CSD	δ C=O random coil	δ C=O experimental	C=O CSD
Ala-1	52.5	49.5	-3	177.8	173.4	-4.4
Ile-2	61.1	57.7	-3.4	176.4	172.1	-4.3
Leu-3	55.1	46.8	-8.3	177.6	171.9	-5.7
Pro-5	63.3	63.4	-0.1	177.3	176.4	-0.9
Phe-6	57.7	54.3	-3.4	175.8	173.1	-2.7

Table 16 Chemical shift deviation (CSD) of each amino acid of compound **4.37** conformer B

Encouraged by the good data gathered from the CSD, we then focused our attention to the analysis of the vicinal $^3J_{NH-H\alpha}$ coupling constants, which are another source of information about the backbone conformation (see paragraph 2.1.3 page 58). The measurable $^3J_{NH-H\alpha}$ displayed large values systematically higher than average values of 4 Hz found in the coil library¹⁴¹ (Table 17), which reflected in extended arms, further confirming the existence of a β -hairpin.

Residue	δ NH A (ppm)	J (Hz)	δ NH B (ppm)	J (Hz)
Leu-3	8.37	8.9	8.37	8.9
Phe-6	8.80	9.7	8.67	9.3
NH_{T21}	8.87	13.1	8.94	/

Table 17 $^3J_{NH-H\alpha}$ coupling constants for both conformers A and B

We next examined the ROE network. The arms of both conformers showed the characteristic pattern of sequential $CH\alpha_i/NH_{i+1}$ ROEs typical of extended peptides (Figure 92, blue arrow). This sequence was interrupted only for the terminal Ala-1, further confirming the two β -strands and the more flexible N -terminus. Moreover, both conformers had the typical ROE pattern of a β -turn inducer. In similar compounds previously studied in our group, as well as in compounds reported in chapter 3, it has been proved that the presence of this network is diagnostic of a β -hairpin conformation.^{120–122} A deeper analysis of the ROESY spectrum revealed a huge difference in term of inter-strand signals. Indeed, conformer A presented numerous spatial proximity signals between the upper and the lower arms, unlike conformer B, suggesting that one conformer was more compact than the second one. The difference was probably due to a rotation around a single bond. As observable in figure 90 (red arrow), in the two conformers, H^α Leu-3 had ROE signal with protons in two different positions (2 and 6 respectively for conformers A and B) of piperidine ring (Figure 91). As we recently demonstrated (see draft paper chapter 3, page 68), this difference lied in the rotation around the amidic bond between Leu-3 and Pip-4. This rotation allowed a different spatial arrangement that explained the different ROE networks.

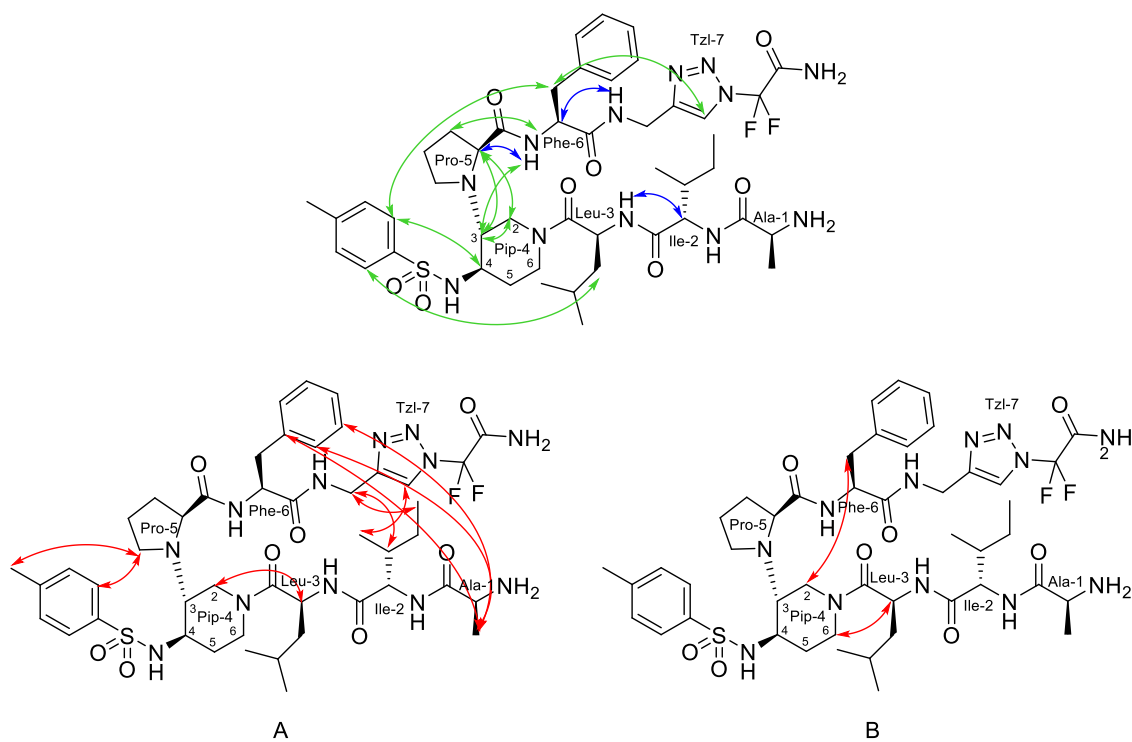


Figure 90 Structure of compound **4.37** showing the ROE networks. In green the common ROEs, in blue the common sequential ROEs and in red the differences between conformers A and B.

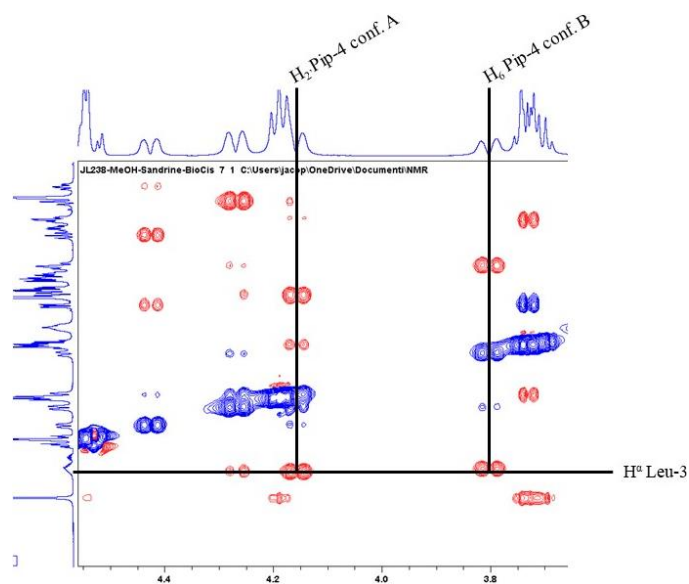


Figure 91 2D ^1H - ^1H ROESY expansion of compound **4.37** showing the two different ROEs between H^α Leu-3 and the piperidine ring in the two conformers A and B

Biophysical evaluations

As for the other compounds reported in chapter 3 and 4, the hairpins bearing the *N*-difluoromethyl-1,4-triazolyl blocking sequence **4.36** and **4.37**, as well as their corresponding *N*-Boc protected precursors **4.48** and **4.49**, were preliminary evaluated by Thioflavin-T (ThT) fluorescence assay. In table 18 the effect of compounds **4.36**, **4.37**, **4.48**, **4.49** and resveratrol on $t_{1/2}$ and F during hIAPP fibrillization are summarized.

Entry	Compound	Compound/hIAPP ratio	$t_{1/2}$ extension/reduction (%)	F extension/reduction (%)
1	4.36	10/1	+77±33	-65±6
		1/1	ne	-30±17
		0.1/1	ne	ne
2	4.37	10/1	ne	-46±1
		1/1	-14±6	-14±5
		0.1/1	-12±5	ne
2	4.48	10/1	ne	-71±1
		1/1	ne	-65±10
		0.1/1	ne	-51±5
4	4.49	10/1	ne	-64±10
		1/1	ne	-64±14
		0.1/1	ne	-35±22
5	Resveratrol (reference)	10/1	+26±18	-94±1
		1/1	ne	-86±7
		0.1/1	ne	-68±4

Table 18 Table summarizing the effect of the compounds **4.36**, **4.37**, **4.48**, **4.49** and Resveratrol on $\Delta t_{1/2}$ and ΔF . Parameters are expressed as mean \pm SE, n=3. ^[a] ne = no effect

Among the 4 tested hairpins, only **4.36** showed a significant effect on the $t_{1/2}$ at compound/hIAPP ratio 10/1 ($\Delta t_{1/2} = +77\%$). However, all the compounds showed a some effect on the fluorescence plateau at the 3 tested ratios (10/1, 1/1 and 0.1/1). A marked fluorescence reduction was detected for both *N*-Boc protected precursors **4.48** and **4.49** that was almost the same at the two higher compound/hIAPP ratios 10/1 and 1/1 ($\Delta F = -71, -65\%$ vs $-64, -64\%$ respectively for **4.48** and **4.49**, Figure 93 and 94). Even at the lowest ratio 0.1/1 they displayed a significant reduction of the fluorescence plateau, although in this case the activity of **4.48** was slightly more pronounced than for **4.49** ($\Delta F = -51\%$ vs -35% respectively for **4.48** and **4.49**). We can note that these two Boc-protected compounds had the similar behavior as the reference compound (Resveratrol), in the sense that they only affected the fluorescence plateau without modifying the kinetic parameter $t_{1/2}$. The free amines **4.36** and **4.37** demonstrated also to be able to reduce the fluorescence plateau at the two compound/hIAPP ratios 10/1 and 1/1 ($\Delta F = -65\%, -30\%$ and $-46\%, -14$ respectively for

4.36 and 4.37). But the reduction was more modest than for the *N*-Boc protected analogues 4.48 and 4.49. However, we can notice that this F reduction was more pronounced for 4.36 compared to 4.37. This result, associated with the effect of 4.36 on the delay of the fibrillization kinetics ($\Delta t_{1/2} = +77\%$), highlights the positive effect of a longer valinamide *C*-term arm in interacting with hIAPP and delaying its fibrillization.

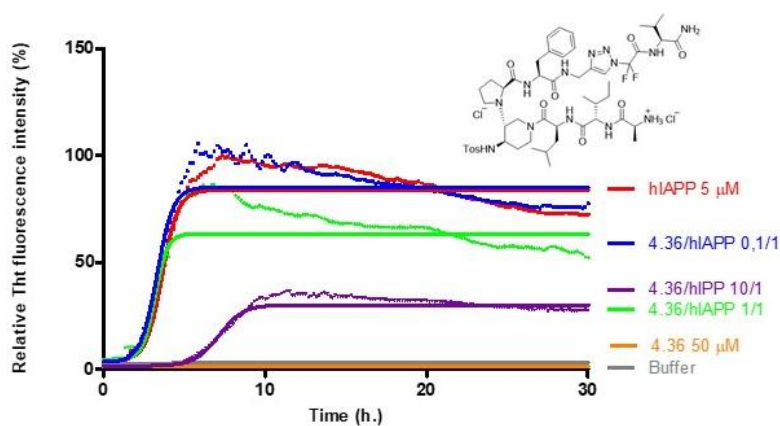


Figure 92 Representation of the mean curves of ThT fluorescence assays over time showing hIAPP aggregation (5 μM) in the presence of compound 4.36 (mean curve of the triplicate)

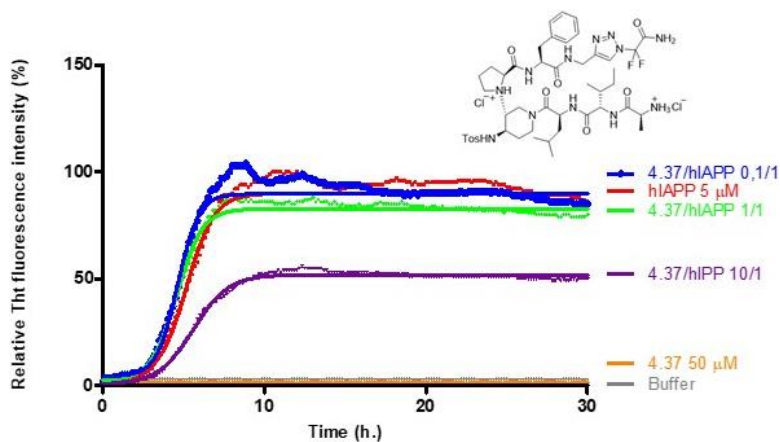


Figure 93 Representation of the mean curves of ThT fluorescence assays over time showing hIAPP aggregation (5 μM) in the presence of compound 4.37 (mean curve of the triplicate)

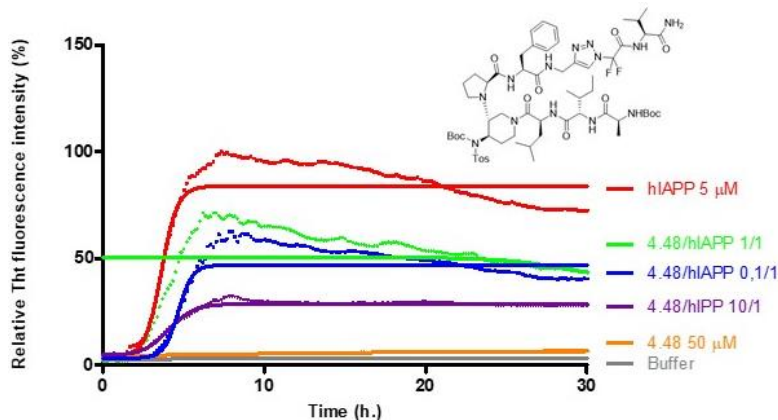


Figure 94 Representation of the mean curves of ThT fluorescence assays over time showing hIAPP aggregation (5 μ M) in the presence of compound **4.48** (mean curve of the triplicate)

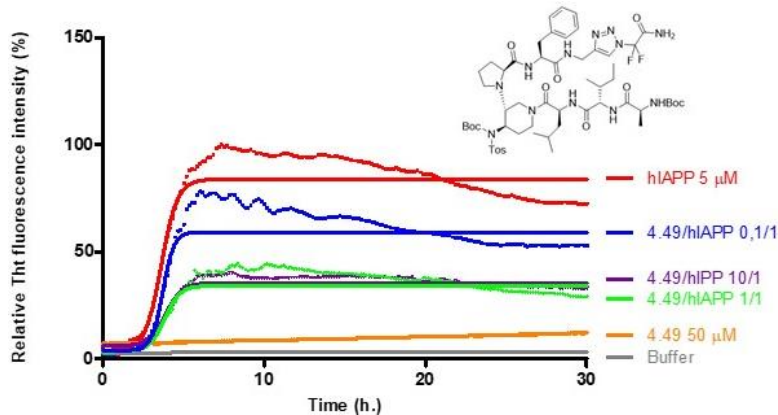


Figure 95 Representation of the mean curves of ThT fluorescence assays over time showing hIAPP aggregation (5 μ M) in the presence of compound **4.49** (mean curve of the triplicate)

Conclusion

In this subchapter, we presented two different β -hairpin mimics bearing a *N*-difluoromethyltriazolyl peptidomimetic arms as blocking sequence. As we said at the beginning of this chapter, *N*-difluoromethyltriazolyl moiety have never been inserted in structure designed to fold in β -hairpin. So, thanks to the work here reported we were able to study the impact of this dipeptide mimic on the secondary structure. Both compounds **4.36** and **4.37** were present in solution as a mixture of two conformers in dynamic equilibrium. However only compound **4.37**, which was bearing the shorter peptidomimetic arm, was found to be completely structured in β -hairpin. Thus we can hypothesize that the different conformational behavior could come from the different

length of the blocking sequence. Further NMR analysis (2D NMR ^{19}F - ^1H HOESY experiment) that at this moment are still on going, will shed light on the role of the *gem* difluoro group on the structuration.

Furthermore, thanks to the Tht fluorescence spectroscopy we were able to evaluate their inhibitory activity and to start to draw some conclusion concerning the relation between the structure and the activity. First of them, we demonstrate that the free amine was not necessary for the activity, indeed the *N*-Boc protected precursor **4.48** and **4.49** were able to reduce the fluorescence plateau and at some ratios they were even better than the corresponding free amine. We also noticed that the less structured hairpin **4.36** was slightly more active than **4.37** suggesting a possible correlation between the activity and the length of the *N*-difluoromethyltriazoly arm. However, we were not able to establish if the different activity was simply due to the presence of one more amino acids that could help the interaction with the target or to the fact that the longer hairpin was less structured and as a consequence more prone to adopt itself the secondary structure adopted by hIAPP. In order to better elucidate this point, it could be interesting the synthesis of another derivative in which the phenylalanine will be removed and its later chain will be inserted directly on the CH_2 of the triazolyl moiety.

In light with the results reported in this chapter, we can conclude that the presence of a *N*-difluoromethyltriazolyl moiety could positively influence the folding of a β -hairpin mimic, although its presence does not always correspond to a better structuration. This moiety can replace peptidic sequences, however, considering the global modest activity on hIAPP fibrillization of these specific prepared fluorinated β -hairpin mimic, we can not affirm that they will be candidate for future deeper investigation.

4.2.3 β -hairpin mimics fluorinated on the β -turn inducer

Design of the compounds based on the fluorinated β -turn inducer

Until now, among the compounds developed during my PhD work, only structures with fluorinated self-recognition elements (see chapter 3, page 67, compound **3.7**) or fluorinated blocking sequences (see the previous chapter 4.2) have been reported. With the aim to explore deeper the effect that fluorine exerts on the activity of our hairpins as inhibitors of hIAPP aggregation and on the conformation, we planned the synthesis of structures fluorinated on the β -turn inducer. The

development of this new class of peptidomimetics required a preliminary choice of the fluorinated group that we wanted to insert. Thinking to a possible application as a probe for ligand-hIAPP interactions by ^{19}F NMR studies or even eventually as MRI probe, in order to have a good sensitivity, we opted for the trifluoromethyl group. Then we turned our attention on the position where to add it. Looking at the structure of compound **4.12** (see chapter 4, page 87,), we identified two different possible positions. We first planned to replace the tosyl group by the 4-(trifluoromethyl)benzenesulfonyl group (compound **4.50**, Figure 96). Then, by questioning ourselves about the insertion on the proline or on the piperidine ring, we tried to select the position which, in our opinion, could have affected the reactivity of the starting material and the final β -turn the least. Thus, our selection fell on the proline, more precisely on its γ position (compound **4.51**, Figure 96). Pleasantly, in the literature a methodology to produce in large scale the γ -(S)- CF_3 -proline was reported.¹⁹⁶ In order to evaluate if the presence of the trifluoromethyl turn was influencing positively or negatively the activity, we planned to build a structure based on peptidic hairpins reported in chapter 3. Because synthesizing compounds bearing two peptidic arms was easier and faster than synthesizing peptidomimetic structures and since two tripeptidic arms were sufficient to have a good activity (see chapter 3, page 67, compounds **3.4-3.7**), we designed the two analogues **4.50** and **4.51** (Figure 96) of the inhibitor **3.5** reported in chapter 3.

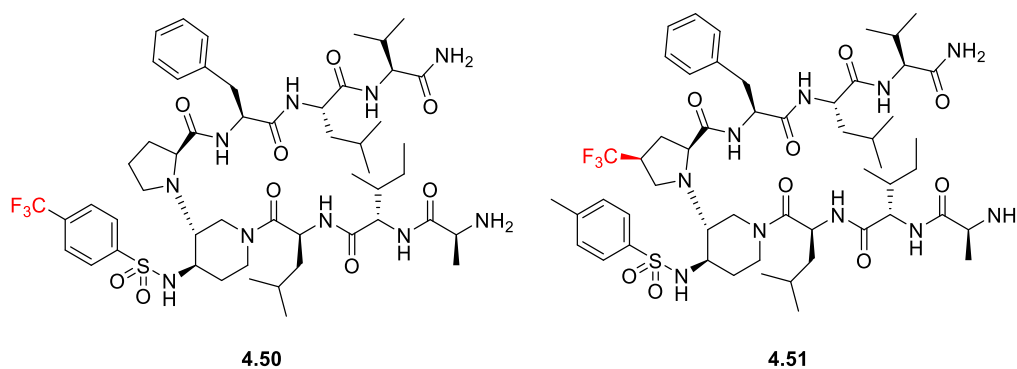


Figure 96 Structures of the two fluorinated hairpins on the β -turn inducer.

Synthesis of the hairpins having fluorinated β -turn inducer

In order to go straight to the final compounds **4.50** and **4.51** having two peptidic arms, we planned to use the solid phase peptide synthesis (SPPS). Thus, synthetic pathways for the preparation of appropriate *N*-Fmoc protected β -turn inducers **4.52** and **4.53** (Figure 97) have been designed.

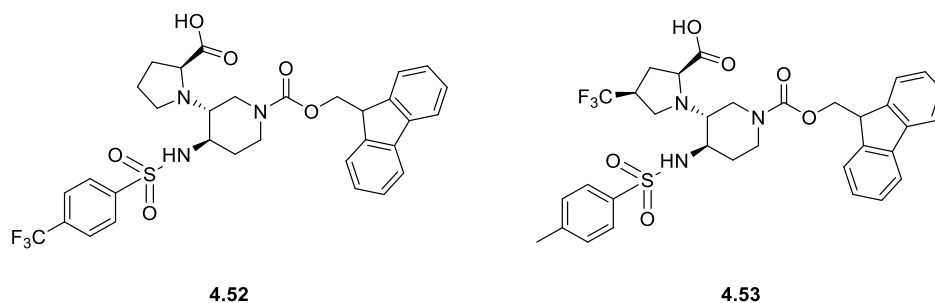


Figure 97 Structures of the Fmoc protected β -turns **4.52** and **4.53**

Synthesis of the N-Fmoc-4-(trifluoromethyl)benzenesulfonyl-COOH β -turn 4.52

As previously reported, it is possible to synthesize the β -turn inducer **4.12** (Figure 98) through a multicomponent reaction developed by the team of Prof. Maria Luisa Gelmi (Istituto A. Marchesini, Università degli Studi di Milano).¹²⁰ More recently, Nicolò Tonali from our group demonstrated that the same multicomponent reaction can be used to prepare a scaffold in which the tosyl group is replaced by a nosyl group (**4.54**).¹²² Moreover, he reported a strategy to convert the nosyl scaffold into the Boc scaffold **4.55** (Figure 98 and Scheme 19), that can also be deprotected to lead the free amine **4.56**, which could represent the key intermediate for the synthesis of our turn **4.57** (Figure 98).

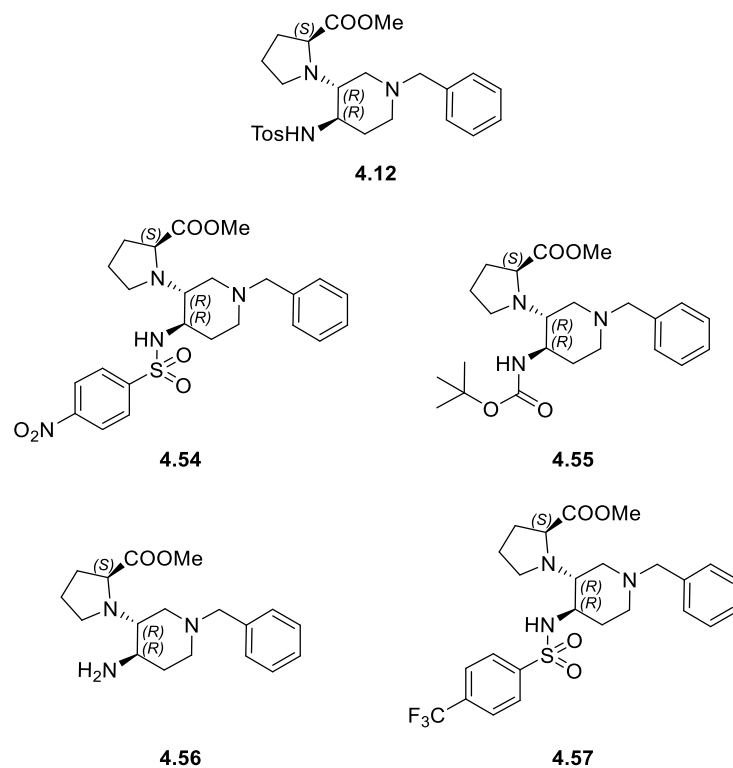


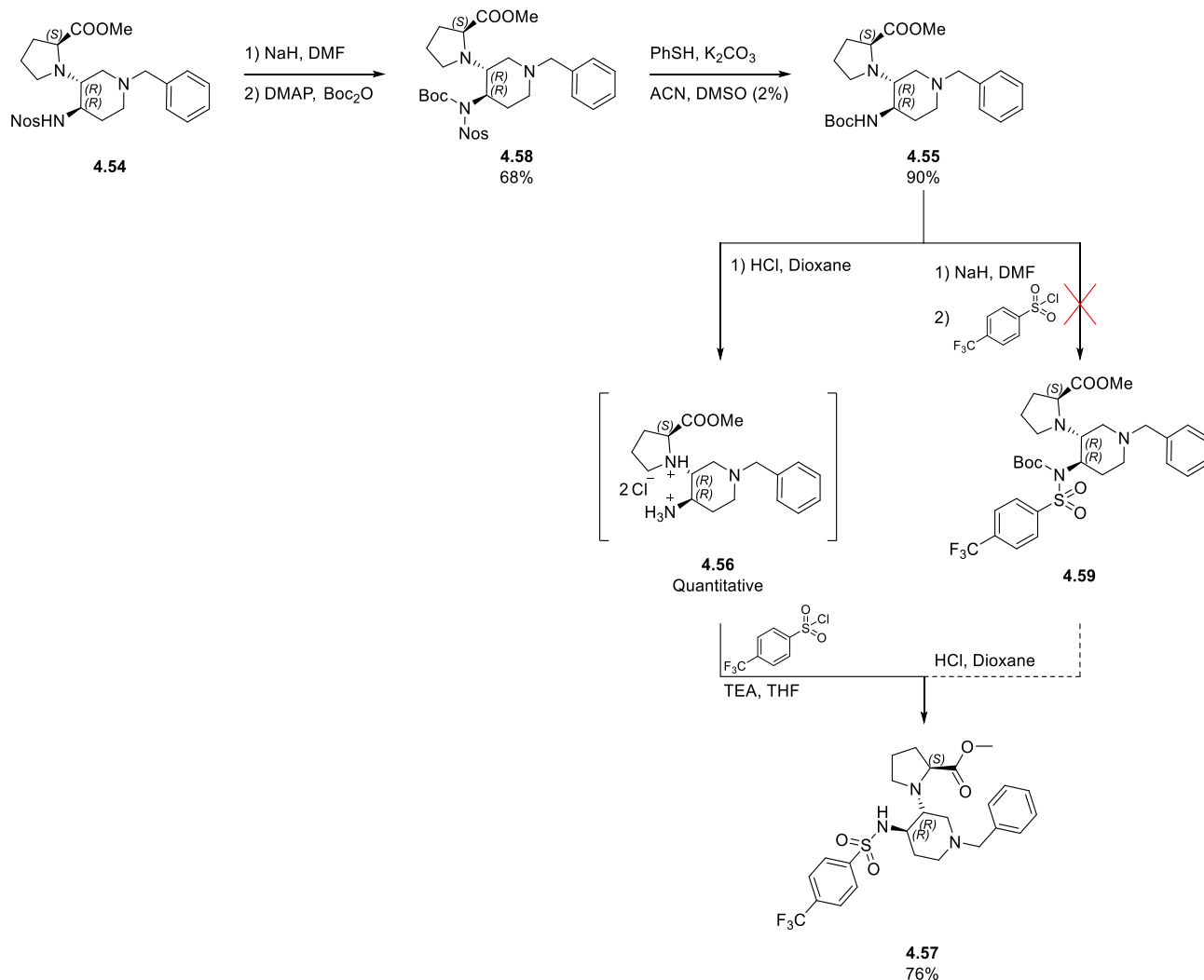
Figure 98 Structures of the Tosyl (**4.12**), Nosyl (**4.54**), Boc (**4.55**) and -NH₂ (**4.56**) scaffolds prepared by Tonali¹²² and the new 4-(trifluoromethyl)benzenesulfonyl scaffold **4.57**

Thus, to prepare the trifluoromethyl scaffold **4.57** (Figure 98), we were faced to two possible synthetic strategies to choose from:

- through the multicomponent reaction;
- exploit the Boc scaffold as building block.

Because with the multicomponent reaction it was theoretically possible to obtain a mixture of 4 diastereomers and 2 amidines, in order to have a reference of **4.57**, we first followed the second strategy. As reported in scheme 19, in a first attempt, we tried to deprotonate **4.55** with NaH and then to react the corresponding anion with the 4-(trifluoromethyl)benzenesulfonyl chloride. However, maybe because NaH was not enough strong to deprotonate the carbamate or rather because of the presence of traces of water in the solvent or of HCl in the 4-(trifluoromethyl)benzenesulfonyl chloride, we recovered only the starting material and not the desired intermediate **4.59**. Being worried that a stronger base could cause a racemization of the

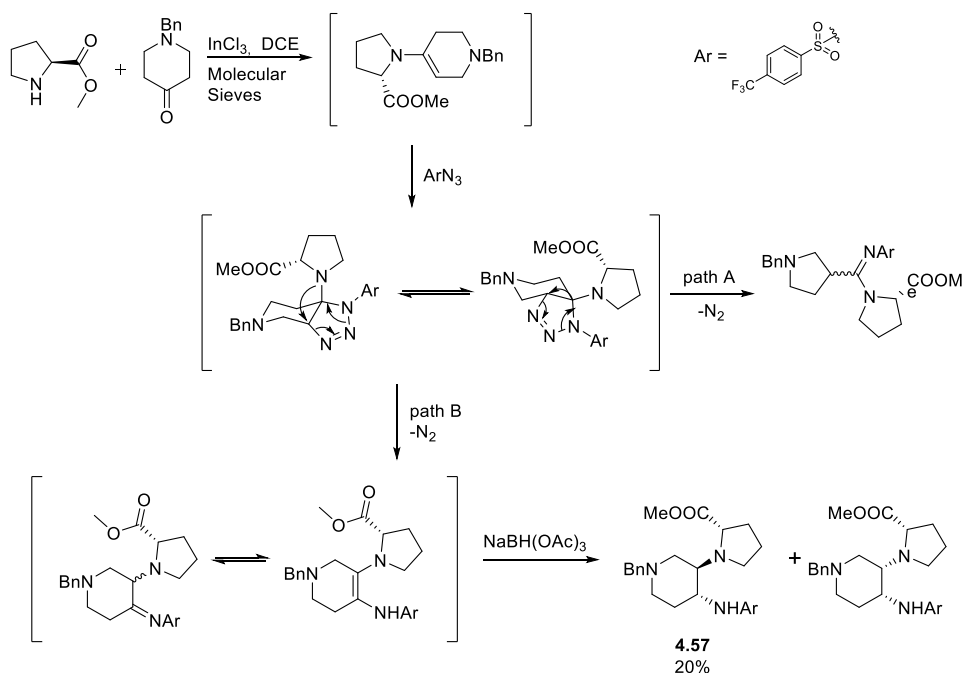
proline, we decided to carry out the synthesis through the intermediate **4.56**. Thus, **4.55** was deprotected using acidic conditions and the obtained amine was subsequently employed as nucleophile for the reaction with 4-(trifluoromethyl)benzenesulfonyl chloride. It is important to underline that, because the stereocenter involved in the substitution is the nucleophile, the stereochemistry of the turn has been maintained, allowing the preparation of the desired scaffold **4.57** in good yield (76%).



Scheme 19 Synthetic pathway employed to prepare the reference of the 4-trifluoromethylbenzenesulfonyl scaffold **4.57**

Despite the synthesis above mentioned is an effective methodology for the preparation of **4.57**, it is hard to imagine its employment in a large scale synthesis because of the large number of steps

required just to prepare the Boc-tern 4.55. Thus, having in hand the reference for the desired scaffold 4.57, we turned our attention on the multicomponent reaction. Following the same procedure already successfully employed for the synthesis of the tosyl and the nosyl scaffolds, we were able to produce 4.57 in 20% yield (almost two times superior to the usual yield for Nosyl and Tosyl scaffolds) starting from the commercially available material (Scheme 20). More in detail, one equivalent of proline methyl ester hydrochloride was suspended in 1,2-dichloroethane and the free secondary amine was obtained by addition of an equimolar amount of TEA. Subsequently, one equivalent of *N*-benzyl-piperidone was added followed by molecular sieves and 10% of indium trichloride. When the proline was completely consumed, the reaction was cooled down at 0° C and a solution of 4-(trifluoromethyl)benzenesulfonyl azide (prepared in accordance with the literature),¹⁹⁷ was added dropwise. After one hour, sodium triacetoxy borohydride was added to the mixture in order to reduce the formed dienamine to afford the corresponding final product 4.57.



Scheme 20 Multicomponent synthesis of the 4-(trifluoromethyl)benzenesulfonyl scaffold 4.57

In order to confirm that we obtained the same product synthesized from the Boc scaffold, we performed a chiral HPLC analysis of both products, using the same conditions. The retention time being the same for the two products (Figure 99), we were able to confirm that we isolated the same diastereoisomer.

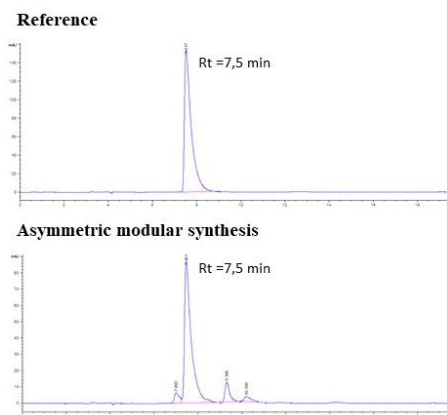


Figure 99 Chiral HPLC of **4.57** produced obtained from the Boc scaffold building block (Reference) and through the multicomponent reaction

Moreover, being able to prepare **4.57** in large amount, we produced a crystal that was analyzed by X-ray to confirm the R configuration for both new stereocenters (Figure 100).

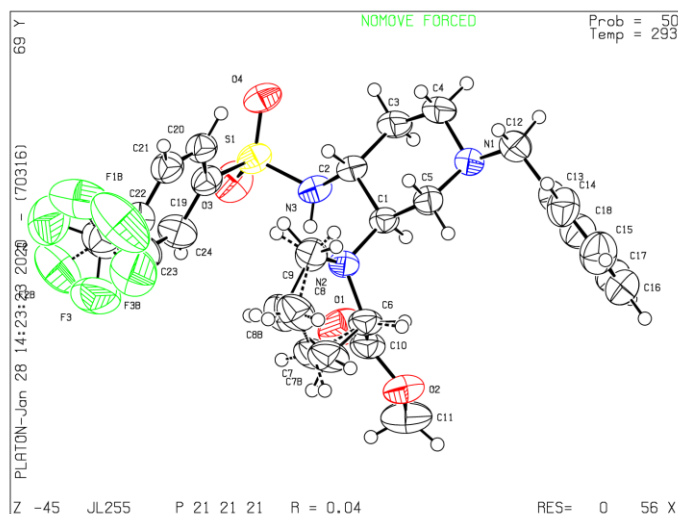
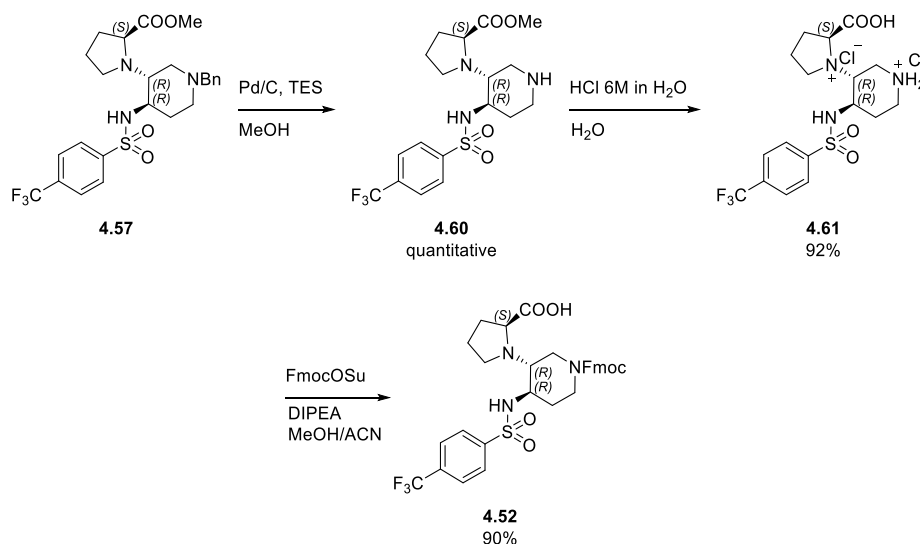


Figure 100 X-ray structure of the 4-(trifluoromethyl)benzenesulfonyl scaffold **4.57**

Having achieved the synthesis of the β -turn **4.57**, the next step was the preparation of its *N*-Fmoc protected derivative **4.52** (Schema 20). Precisely, **4.57** underwent McMurray's hydrogenolysis. The reaction between triethyl silane and MeOH (used as solvent) generated *in situ* H₂, allowing the hydrogenolysis. Subsequently, the methyl ester hydrolysis of **4.60**, performed at high temperature using acid condition, led to the completely unprotected compound **4.61**. Finally, by

reacting **4.61** with FmocOSu in the presence of DIPEA in a mixture 4:1 of MeOH and ACN, we were able to isolate the desired compound **4.52** in excellent yield.



Scheme 21 Synthesis of the *N*-Fmoc-4-(trifluoromethyl)benzenesulfonyl-COOH turn **4.52**

Synthesis of the N-Fmoc-(trifluoromethyl)prolyl-COOH β -turn 4.53

In order to prepare the Fmoc protected compound **4.53** we designed the synthesis from the parent compound **4.62** (Figure 101) that could be theoretically prepared employing the same multicomponent reaction already used.

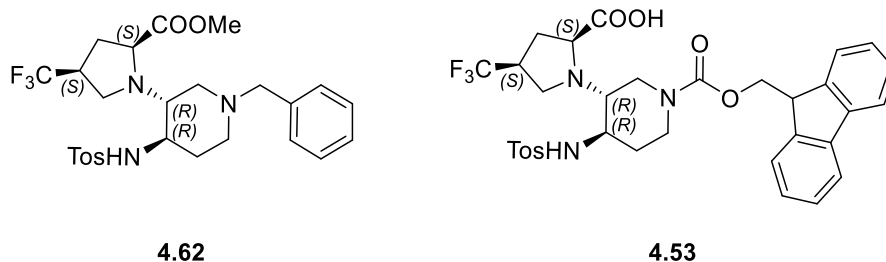
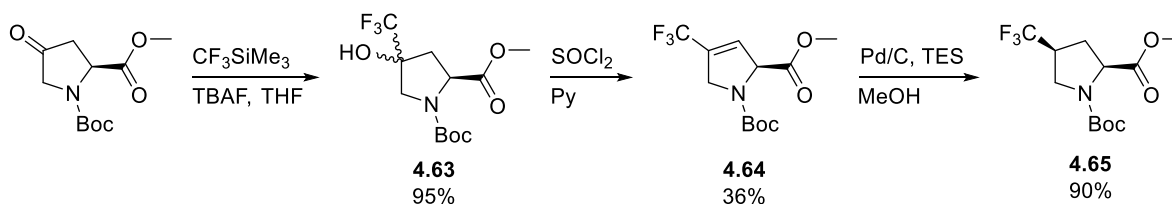


Figure 101 Structures of the parent (trifluoromethyl)prolyl scaffold **4.62** (left) and the desired *N*-Fmoc derivative **4.53** (right)

Thus, we planned to study the multicomponent reaction employing the corresponding γ -(*S*)-CF₃-proline methyl ester. As mentioned at the beginning of this paragraph, we found that a methodology for the large scale synthesis of γ -(*S*)-CF₃-proline was reported in literature by Kubyshkin *et al.*¹⁹⁶ So, following this protocol, γ -(*S*)-CF₃-proline was prepared from the

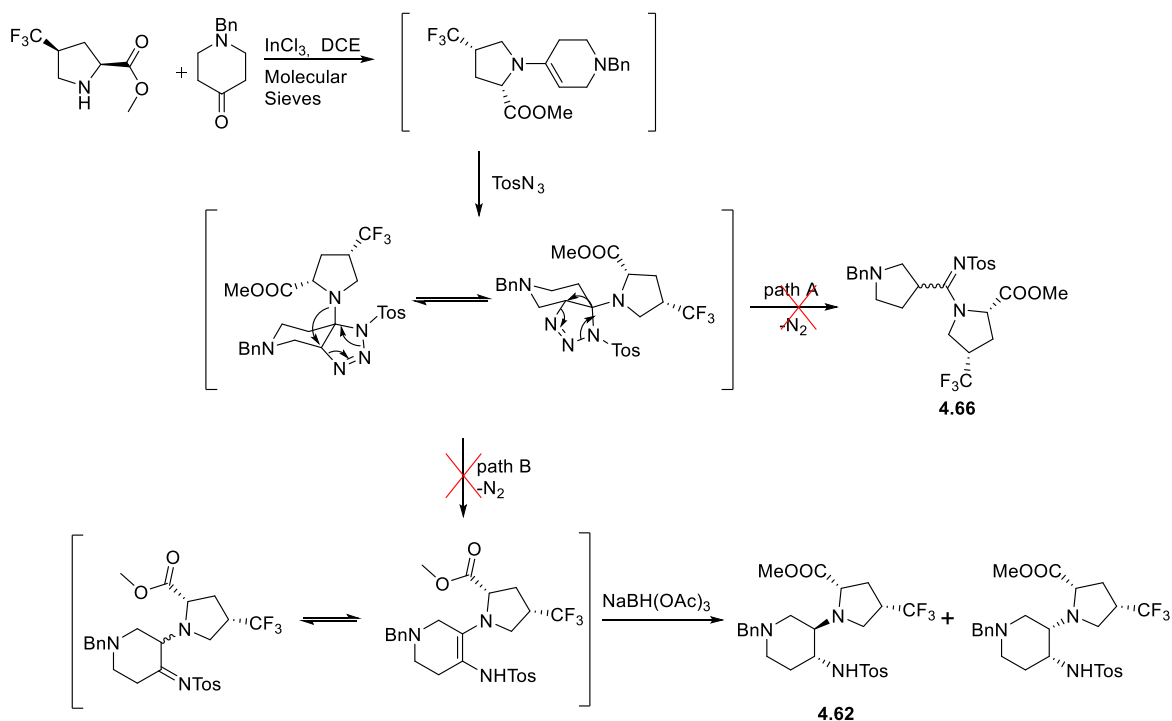
commercially available *N*-Boc-4-oxo-*L*-proline methyl ester. As reported in scheme 22, the treatment of the starting material with trimethyl(trifluoromethyl)silane in the presence of TBAF led to the intermediate **4.63** in excellent yield (95%). Unfortunately, the subsequent dehydration operated using thionyl chloride in pyridine gave **4.64** only in modest yield (36%). The modest yield could be ascribed to the formation of a strong emulsion that made the purification step really challenging. To reduce the double bond in a stereoselective manner, Kubyshkin *et al.* used H₂ and Pd/C in methanol. However, in contrast with the fast reaction reported by the authors (5 hours), we observed that after 6 hours **4.64** had still only partially reacted. Thus, in order to push the reaction, we added triethyl silane to generate H₂ *in situ*. Finally, after a short filtration through silicagel, the desired γ -(*S*)-CF₃-proline **4.65** was recovered in very good yield (90%).



Scheme 22 Synthesis of the γ -(*S*)-CF₃-proline **4.65**

Having in hand the *N*-Boc- γ -(*S*)-CF₃-proline methyl ester, we could think to the multicomponent reaction, which was tempted following the same procedure as the one previously reported for the synthesis of 4-(trifluoromethyl)benzenesulfonyl scaffold **4.57**. Being needed a free amine, the *N*-Boc- γ -(*S*)-CF₃-proline methyl ester was deprotected in acidic condition. The obtained hydrochloric salt was directly suspended in 1,2-dichloroethane without any further purification and an equimolar amount of TEA was added. Subsequently, one equivalent of *N*-benzylpiperidone was added followed by molecular sieves and 10% of indium trichloride. When the CF₃-proline was completely consumed (monitored by TLC and ¹⁹F NMR), the reaction mixture was cooled down at 0° C and a solution of tosyl azide was added dropwise. After one hour, sodium triacetoxy borohydride was added to the mixture. In contrast with the synthesis of 4-(trifluoromethyl)benzenesulfonyl scaffold **4.57**, we obtained a complex mixture of products. The column chromatography allowed the identification of the fractions that were containing fluorinated products but unfortunately none of their HRMS analysis corresponded to the desired product. However, one of the fraction had a molecular weight corresponding to that of the amidine **4.66**. In order to confirm the amidine formation, we performed a NMR analysis. Surprisingly we noticed

the NMR spectrum did not correspond to the structure we supposed to have. Being at the end of my PhD, and the COVID crisis starting, we were forced to stop the synthesis of the (trifluoromethyl)prolyl scaffold. However, it could be interesting to repeat the synthesis investigating it step by step in order to understand why the multicomponent reaction didn't work.



Scheme 23 Multicomponent synthesis of the trifluoromethyl-prolyl scaffold **4.62**

Synthesis of the hairpin 4.50 containing the 4-trifluoromethylbenzenesulfonyl scaffold

As reported at the beginning of this paragraph, we decided to synthesize this hairpin **4.50** employing the SPPS and following our procedure described in chapter 3 for the non-fluorinated analogue **3.0-3.3** (see draft paper chapter 3, page 68). Since our design is characterized by a terminal amide, the synthesis was carried out on a rink amide resin (loading 0.64 mmol). The peptidic chain was elongated by adding the appropriate *N*-Fmoc amino acids. The unique exception was the terminal *N*-Boc-alanine, which was used in order to be deprotected during the cleavage step. All the coupling steps were performed using HBTU and HOBt in the presence of DIPEA and followed by a capping step with acetic anhydride. Finally, the peptide was cleaved from the resin with a cleavage cocktail (TFA/ H_2O /Phenol/TIPS) and precipitated in cold Et_2O (9% yield).

Conformational studies

In this subsection, we report the conformational studies of compound **4.50**. Since our compound was well soluble in methanol, we decided to perform the entire conformational studies of **4.50** in CD₃OH, getting as close as possible to an aqueous environment. Moreover, the employment of this solvent would allow a structural comparison with other similar compounds already reported in chapters 3 and 4. Specifically, we were interested in comparing **4.50** with its non-fluorinated analogue **3.5** (see draft chapter 3, page 17) in order to evaluate how the tosyl replacement (**3.5**) by the 4-(trifluoromethyl)benzenesulfonyl group (**4.50**) influenced the secondary structure.

To find the best temperature at which perform the characterization, a preliminary series of ¹H-NMR spectra was acquired from 278K to 313K. An improvement in resolution was observed when the temperature was increased to 303K (Figure 102). Unlike for **3.5**, at high temperature we did not observe any coalescence of the amide signals, so we hypothesized to be faced with only one conformer. Taking in account this hypothesis we did not consider a low temperature characterization necessary but rather at 303K which was closer to the physiological one.

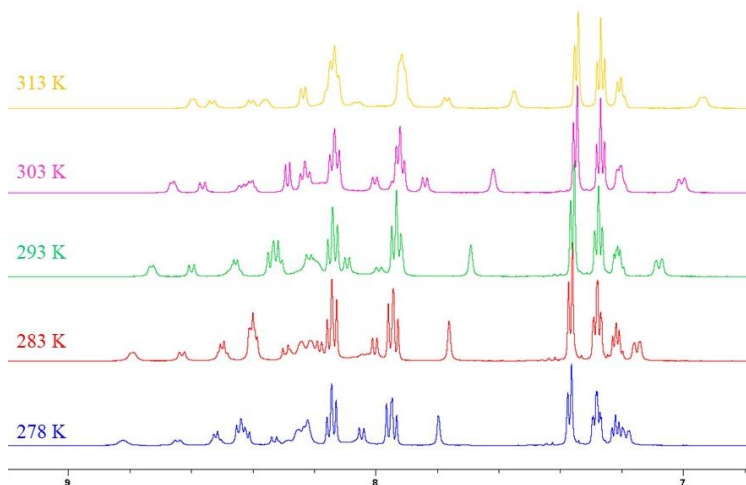


Figure 102 ¹H-NMR amide region spectra at different temperatures from 278K to 313K

Nevertheless, as we can see from the data reported in table 19, our initial hypothesis of the single conformer was refuted. Indeed, at 303K compound **4.50** was present in solution as a mixture of two conformers at 1:1 ratio. The occurrence of splitting for all the amide protons of the tripeptide FLV, as well as some H^α (Pro-5, Phe-6, Val-8), along with their negative ROEs, confirmed the presence of two different conformers.

Unfortunately, an unambiguous assignment for both conformers was impossible due to different issues. First of them, in both conformations Ala-1, Ile-2, Leu-3 and Leu-7 presented the same chemical shift with the exception of the CH₃ on Ile-2 lateral chain and NH of Leu-7. Concerning the β -turn inducer, it was possible the complete assignment of the piperidine ring and the proline. However, the absence of the univocal diagnostic ROEs between H ^{α} Pro-5 and the piperidine ring usually detected for similar compounds (see chapter 3 and 4) made impossible to establish which Pip-4 and Pro-5 signals belonged to the same conformers. Moreover, the fact that the C=O of Pro-5 was not detected and the H ^{α} chemical shift of Leu-3 (4.88 ppm) was very similar to those of Phe-6 (4.79 and 4.87 ppm), eliminated any other possibility to complete the system of the β -turn inducer employing the ROEs.

Residue	δ NH (ppm)	δ H ^{α} (ppm)	δ H ^{β} (ppm)	δ other protons (ppm)	δ CO (ppm)	δ C ^{α} (ppm)	δ C ^{β} (ppm)	δ other carbons (ppm)
Ala-1	8.19	3.96	1.45	/	169.6	48.8	16.6	/
Ile-2	8.28	4.21	1.75	γ CH ₃ 0.77 (γ CH ₃ 0.89) γ CH ₂ 1.09/1.12 δ CH ₃ 0.84 (δ CH ₃ 0.88)	171.2	58.1	36.8	γ CH ₃ 14.9 (γ CH ₃ 14.6) γ CH ₂ 24.8 δ CH ₃ 10.3 (δ CH ₃ 9.9)
Leu-3	8.22	4.88	1.46/1.55	γ CH 1.68 δ CH ₃ 0.87/0.88	nd	46.7	40.5	γ CH ₂ 24.7 δ CH ₃ 20.8/22.1
Piperidine Ring-4	/	/	/	H _{2/2'} 3.28/4.24 (H _{2/2'} 2.77/4.46) H ₃ 2.46 (H ₃ 2.26) H ₄ 3.65 (H ₄ 3.71) H _{5/5'} 1.25/1.59 (H _{5/5'} 1.36/1.77) H _{6/6'} 2.52/4.31 (H _{6/6'} 3.10/3.83)	/	/	/	C _{2/2'} 43.9 (C _{2/2'} 39.8) C ₃ 60.6 (C ₃ 59.8) C ₄ 48.8 (C ₄ 54.3) C _{5/5'} 31.7 (C _{5/5'} 33.1) C _{6/6'} 40.9 (C _{6/6'} 44.0)
Pro-5	/	3.76 (3.34)	1.31/1.93 (1.31/1.96)	γ 1.42/1.50 (γ 1.38/1.58) δ 2.71/3.14 (δ 2.64/3.08)	nd	62.8	30.3	γ 24.6 (γ 24.3) δ 44.7 (δ 44.6)
Phe-6	8.43 (8.56)	4.79 (4.87)	3.15/3.22	H _o 7.35 H _m 7.27 H _p 7.20	173.1 (173.5)	54.0 (54.1)	37.8	C _q 137.4 C _o 129.2 C _m 128.1 C _p 126.5
Leu-7	8.40 (8.66)	4.51	1.66/1.63	γ CH ₂ 1.68 δ CH ₃ 0.92/0.95	173.0 (173.4)	51.9	40.5	γ CH ₂ 24.7 δ CH ₃ 20.9/22.1
Val-8	7.84 (8.00)	4.21 (4.13)	2.03	γ CH ₃ 0.91/0.95 CONH ₂ 7.00/7.61	174.6	58.1 (58.8)	30.9	γ CH ₃ 17.5/18.4
CF₃Tos	7.93 (8.13)	/	/	H _o 8.13 H _m 7.93	/	/	/	C _{qs} 133.8 C _o 127.4 C _m 126.4 C _{qm} 146.5

Table 19 ¹H-NMR and ¹³C-NMR chemical shifts for compounds **4.50**; in brackets the chemical shift of the second conformer. **Legend:** C_{qs} = carbon bearing the sulfonamide, C_{qm} = carbon bearing the CF₃.

Despite the impossibility to establish which residues belonged to which conformations, we tried to gather some general information about the secondary structure of compound **4.50**. Thus, first we examined the chemical shift deviation for each amino acid present in the structure (Table 20). The general down-fielding (positive CSDs) for α hydrogens and amides suggested an extended conformation of the arms, as expected for β -hairpin. Conversely, the negative values for both H $^\alpha$ of Pro-5 were indicative of the β -turn presence, while in the case of Ala-1 and Val-8 they suggested a certain grade of flexibility at the *N*- and *C*- termini. The same structural behavior of the arms was confirmed by the C-CSDs. Indeed, as normally observed in β -hairpin, C $^\alpha$ and carbonyl of each amino acid presented negative CSD even for Ala-1 and Val-8. Moreover, Pro-5 had very small C $^\alpha$ value when compared to those of the other residues, confirming its involvement in a β -turn (see paragraph 2.1.3 page 58).

Residue	δ NH random coil	δ NH experimental	NH CSD	δ H $^\alpha$ random coil	δ H $^\alpha$ experimental	H $^\alpha$ CSD
Ala-1	8.24	/	/	4.32	3.96	-0.36
Ile-2	8.00	8.28	+0.28	4.17	4.21	+0.04
Leu-3	8.16	8.22	+0.06	4.34	4.88	+0.54
Pro-5	/	/	/	4.42	3.36 3.76	-1.06 -0.66
Phe-6	8.30	8.43 8.56	+0.13 +0.26	4.62	4.79 4.87	+0.17 +0.25
Leu-7	8.16	8.40 8.66	+0.24 +0.50	4.34	4.51	+0.17
Val-8	8.03	7.84 8.00	-0.19 -0.03	4.12	4.13 4.21	+0.01 +0.09
Residue	δ C $^\alpha$ random coil	δ C $^\alpha$ experimental	C $^\alpha$ CSD	δ C=O random coil	δ C=O experimental	C=O CSD
Ala-1	52.5	48.8	-3.7	177.8	169.6	-8.2
Ile-2	61.1	58.1	-3.0	176.4	171.2	-5.2
Leu-3	55.1	46.7	-8.4	177.6	nd	/
Pro-5	63.3	62.8	-0.5	177.3	nd	/
Phe-6	57.7	54.0 54.1	-3.7 -3.6	175.8	173.1 173.5	-2.7 -2.3
Leu-7	55.1	51.9	-3.2	177.6	173.0 173.4	-4.6 -4.2
Val-8	62.2	58.1 58.8	-4.1 -3.4	176.3	174.6	+0.3

Table 20 Chemical shift deviation (CSD) of each amino acid of compound **4.37**

The analysis of the vicinal $^3J_{NH-H\alpha}$ coupling constants, which are another source of information about the backbone conformation (see paragraph 2.1.3, page 58), further confirmed the presence of extended arms. As visible from the $^3J_{NH-H\alpha}$ reported in table 21, constants systematically higher than 6-7 Hz (average values for random coil¹⁴¹) were found, as expected for peptide adopting a β -hairpin structure.

Residue	δ NH (ppm)	J (Hz)
Ala-1	/	/
Ile-2	8.28	8.7
Leu-3	8.22	8.1
Pro-5	/	/
Phe-6	8.43	9.4
	8.56	9.8
Leu-7	8.40	7.4
	8.66	7.5
Val-8	7.84	8.8
	8.00	8.2

Table 21 $^3J_{NH-H\alpha}$ coupling constants for compound **4.50**

We next analyzed the temperature dependence of amide proton chemical shifts, as it can provide information about the hydrogen bond network. As reported in table 22, some amide protons showed a low temperature coefficient (both conformers of Phe-6 and one conformer of Leu-7), indicating their involvement in hydrogen-bond. Moreover Ile-2 and Leu-7 (second conformer) values fell within intermediate values, suggesting their partial involvement in hydrogen-bond.

Residue	δ HN (ppm 313K)	δ HN (ppm 278K)	$\Delta\delta/\Delta T$
Ala1	/	/	
Ile2	8.23	8.41	-5.14
Leu3	8.14 (?)	8.43	-8.28
Pro5	/	/	/
Phe6	8.40	8.51	-3.14
	8.53	8.64	-3.14
Leu7	8.36	8.51	-4.28
	8.59	8.81	-6.28
Val8	7.77	8.04	-7.71
	7.91	8.22	-8.85
Tos	/	/	/

Table 22 Temperature coefficients of HN ($\Delta\delta/\Delta T$) for compound **4.50**

Thus, encouraged by the information gathered from the CSDs, $^3J_{NH-H\alpha}$ and the HN ($\Delta\delta/\Delta T$), we finally turned our attention to the ROEs network. The arms showed the characteristic pattern of sequential $CH\alpha_i/NH_{i+1}$ ROEs typical of extended peptides (Figure 103, blue arrow). Unfortunately, no more information could be gathered from the ROESY spectrum because of the presence of protons characterized by the same chemical shift. For instance, the CH_3 of Leu-7 and Ile-2 presented ROEs signal with a proton at 4.21 ppm, whose corresponded to the H^α of both Ile-2 and Val-8.

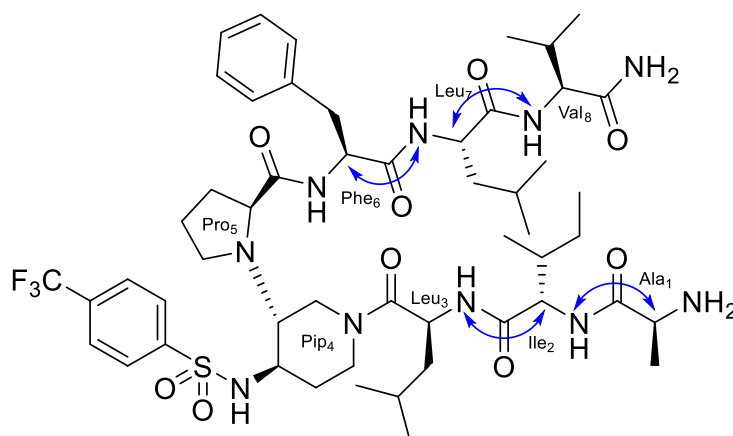


Figure 103 Structure of compound **4.50** showing the sequential $CH\alpha_i/NH_{i+1}$ ROEs

Biophysical evaluations

The effect of compound **4.50** on hIAPP fibrillization process was primarily evaluated by Thioflavin-T (ThT) fluorescence assay. The results are summarized in table 23 as well as the data concerning the non trifluoromethylated compound **3.5** used as a reference compound (see draft paper chapter 3, page 68).

Entry	Compound	Compound/hIAPP ratio	t $_{1/2}$ extension/reduction (%)	F extension/reduction (%)
1	4.50	10/1	+102±31	-85±48
		1/1	+62±14	-79±2
		0.1/1	ne	-50±23
2	3.5 (reference)	10/1	+147±24	-72±8
		1/1	+45±6	-62±6
		0.1/1	+64±2	-36±2

Table 23 Table summarizing the effect of the compounds **4.50** on $\Delta t_{1/2}$ and ΔF . Parameters are expressed as mean \pm SE, n=3. ^[a] ne = no effect

Compound **4.50**^[a] showed a strong inhibitory effect on hIAPP fibrillization (Table 23 and Figure 104) and comparable to the effect of its non-fluorinated analogues **3.5** presented in chapter 3 (see draft paper chapter 3, page 68). Indeed, at 10-fold excess, the $t_{1/2}$ extension was slightly lower for **4.5** compared to **3.5** ($\Delta t_{1/2} = +102$ vs $+147$ % respectively for **4.50** and **3.5**) but the fluorescence plateau reduction was greater ($\Delta F = -85\%$ vs -72% respectively for **4.50** and **3.5**). At 1/1 ratio, the anti-fibrillization activity was better for **4.5** compared to **3.5**, both for $t_{1/2}$ and F ($\Delta t_{1/2} = +62\%$ vs $+45$ % and $\Delta F = -79\%$ vs -62% respectively for **4.50** and **3.5**). At substoichiometric ratio, as at 10-fold excess, the $t_{1/2}$ extension was lower for **4.5** compared to **3.5** ($\Delta t_{1/2} = \text{ne}$ vs $+64$ % respectively for **4.50** and **3.5**) but the fluorescence plateau reduction was greater ($\Delta F = -50\%$ vs -36% respectively for **4.50** and **3.5**). On the whole, we can conclude that this compound, based on a trifluoromethylated beta-turn inducer, displayed a similar activity as its non trifluoromethylated analogue. Interestingly, it even showed a more significative effect at the low ratio 1/1. If this effect is confirmed by other techniques (TEM, CE and IMS-MS), this compound will allow us to use it as a probe for ligand-hIAPP interactions by ^{19}F NMR studies or even eventually as MRI probe.

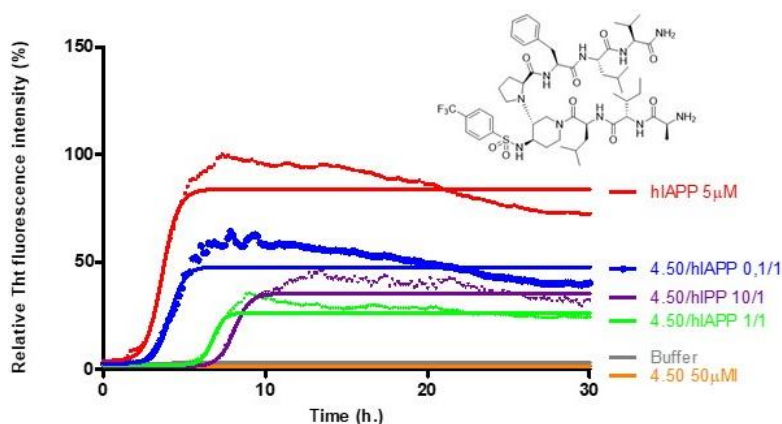


Figure 104 Representation of the mean curves of ThT fluorescence assays over time showing hIAPP aggregation (5 μM) in presence of compound **4.50** (mean curve of the triplicate)

Conclusion

In this subchapter we presented the design of 2 different β -hairpin mimics fluorinated on the β -turn inducer. Because of the COVID crisis the synthesis, the conformational studies and the biophysical evaluation were achieved for only one of them. Despite an unambiguous attribution of each conformer of **4.50** was not possible, we gathered numerous evidences that compound **4.50**

was adopting a β -hairpin secondary structure in both conformers. As seen for other compounds, further NMR analysis (2D NMR ^{19}F - ^1H HOESY experiment), that at this moment are still on going, will probably shed light on the folding of compound **4.50**. However, to overcome the lack of information due to protons characterized by the same chemical shift, it would be helpful to generate a model of **4.50** by molecular dynamics in order to well elucidate its conformational behavior. The ThT evaluation of **4.50** highlighted its strong ability to delay hIAPP fibrillization process and to reduce the fluorescence plateau even at low ratio 1/1. These promising results by ThT fluorescence assay allowed us to suggest that while the tosyl group was essential for the activity of hairpins inhibiting A β 1-42 aggregation (4-aminophenyl)sulfonyl (Boc or free amino were deleterious)¹²⁰, it can be replaced by a 4-(trifluoromethyl)benzenesulfonyl group in hairpins modulating hIAPP fibrillization. In the future it will be necessary to further investigate the activity of **4.50** by other biophysical evaluations such as TEM, CE and IMS-MS. Next to the biophysical assays, it will be very interesting to determine if this compound, thanks to the trifluoromethyl group, would be a good probe for FAXS experiment first and MRI experiments later. The peptidic arms might also be replaced by peptidomimetic arms in order to try to improve the activity and decrease the peptidic character.

General conclusion and perspectives

The work carried out during my PhD, as well as the bigger project of which is part, had the aim to develop new β -hairpins able to selectively interact and inhibit hIAPP peptide aggregation process. To pursue this objective, we designed, synthesised and evaluated different acyclic β -hairpin mimics based on differently substituted piperidine-pyrrolidine β -turn inducers bearing peptidic and peptidomimetic arms.

As reported in chapter 2, at the beginning of the PhD we postulated the following questions:

- Are the β -hairpin mimics, rationally designed suitable for the inhibition of hIAPP aggregation?
- After the development of the first generation of peptidic inhibitors, will it be possible to reduce the peptidic character without affecting their activity?
- How does the addition of fluorinated groups affect the pre-structuration and activity of the hairpins?
- Could the peptidomimetic molecules developed during my PhD project represent a potential T2D treatment?
- Could these hairpins, especially the fluorinated ones, be innovative investigation/diagnostic tools?

In chapter 3, we presented the first generation of peptidic β -hairpin mimics proving that, exploiting our architecture originally designed to inhibit $A\beta_{1-42}$ and the correct SREs, it is possible to selectively inhibit hIAPP aggregation process. This work brings the demonstration that this strategy can be generalized and applied to the inhibition of the aggregation of other amyloid proteins.

We explored the correlation between the activity and the length of the peptidic arms observing that hairpins bearing arms of equal number of amino acids were much more active, whether they were pentapeptides or tripeptides. The synthesis of peptidic hairpin mimics characterized by different *N-termini* led us to the conclusion that even if acetylated or trifluoroacetylated compounds present similar activity, the free amine is helpful for the solubility, in particular to avoid self-aggregation, that might explain its superior activity. Furthermore, the introduction of a peptidomimetic blocking

sequence, inspired by the natural peptide and constituted by a diaza-tripeptide, led to a theoretically more druggable compound. However, diaza-tripeptides are probably not the best peptidomimetic to use to replace tripeptides adopting extended sequences. Indeed, while we previously observed that azaGly-azaGly was compatible with extended structures,¹⁵⁷ we recently observed that diaza-peptide bearing lateral chains inserted in tripeptides rather promotes double turn and helical conformation.¹⁵⁰

Finally, NMR analyses and molecular dynamics allowed us to investigate the conformational preferences: all the active compounds were characterized by a dynamic equilibrium meaning that they were flexible. This flexibility potentially made them more adaptable to the several conformations adopted by hIAPP over the aggregation process.

In chapter 4, we reported the design and the synthesis of fluorinated β -hairpin mimics, allowing us to examine the effect that a fluorinated group exerts on the activity and the conformation of these compounds. Fluorine atoms were introduced either on the β -turn inducer, either on peptidomimetic arms. Original hairpins bearing 4-(trifluoromethyl)benzenesulfonyl group on the piperidine-pyrrolidine turn or 3-fluoro-5-benzamido-2-hydroxybenzhydrazide peptidomimetic arm or N-difluoromethyl-1,4-triazolyl peptidomimetic arm were designed and synthesized. Since some of these compounds were fluorinated analogues of compounds already reported either in chapter 3 or in Faustine Bizet's manuscript, we had the opportunity to directly compare the activity and thus getting direct evidences on the effect of the fluorine atoms. In these cases, a positive effect of fluorine was observed with a slightly better activity of the fluorinated hairpins compared to their non-fluorinated analogues. More details about the effect of the fluorine on the structure will come from NMR analyses that are still on going, allowing probably the design and the synthesis of more powerful fluorinated compounds. This new class of fluorinated β -hairpin mimics could potentially allow for more in-depth knowledge in future assays. In particular, they might prove to be good candidates as probes for ¹⁹F-NMR FAXS experiments in the presence of hIAPP, in order to evaluate the interaction over the kinetics of oligomerization of hIAPP, in solution or in the presence of membrane. These fluorinated spies can be used also to screen libraries of compounds in order to find ligands having a better affinity for hIAPP and for different species (monomers or various soluble oligomers). We can also imagine to use these fluorinated probes in MRI experiments to follow their behavior in cells, in tissues or even in vivo. We can even go further and imagine that they could be used as diagnostic tools to detect early toxic oligomers or more aggregated and late

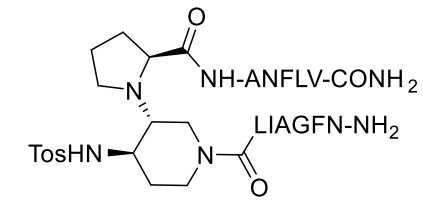
species according if they show a better affinity for soluble oligomers or for insoluble aggregated forms of hIAPP.

Drawing the conclusion, we can now affirm that acyclic β -hairpin mimics are suitable as hIAPP aggregation process modulator/inhibitors. Although β -hairpin mimics bearing peptidic arms were an excellent starting point for the design and the synthesis of inhibitors, the necessity to develop more druggable compounds led us to design and synthesize acyclic β -hairpin mimics bearing peptidomimetic arms. Now, we can conclude that pursuing this strategy has rewarded our efforts giving us very promising compounds.

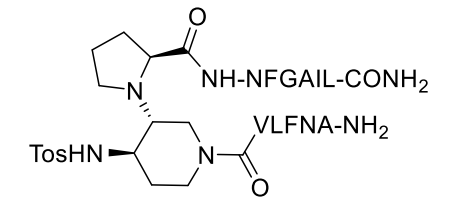
Of course, lots remains to understand about hIAPP aggregation process and its influence on the development of type 2 Diabetes.

Even if in this thesis we begin to demonstrate that β -hairpins are able to inhibit *in vitro* hIAPP aggregation, the way forward to demonstrate their applicability as type 2 Diabetes treatment and or diagnostic remains long and requires further investigations and efforts. However, they can become tools to better understand the toxicity of hIAPP, its aggregation process and the cross-interactions of hIAPP with other amyloid proteins such as $A\beta_{1-42}$, Tau, TTR or synuclein involved in other pathologies studied in our laboratory (Alzheimer's and Parkinson diseases).

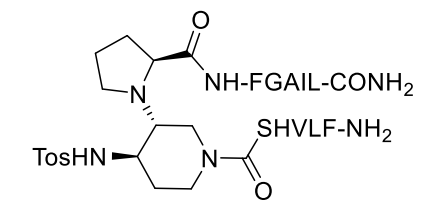
Annex 1: hairpins chapter 3



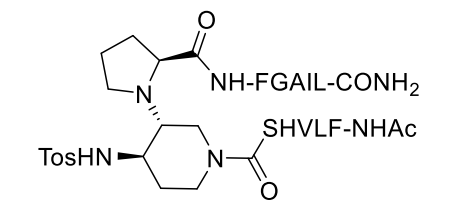
3.0 (1)



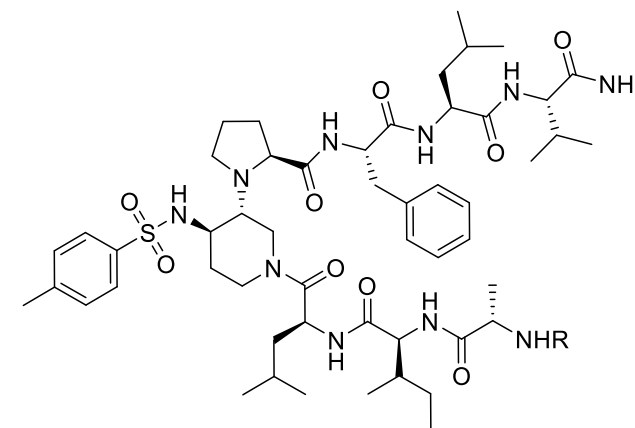
3.1 (2)



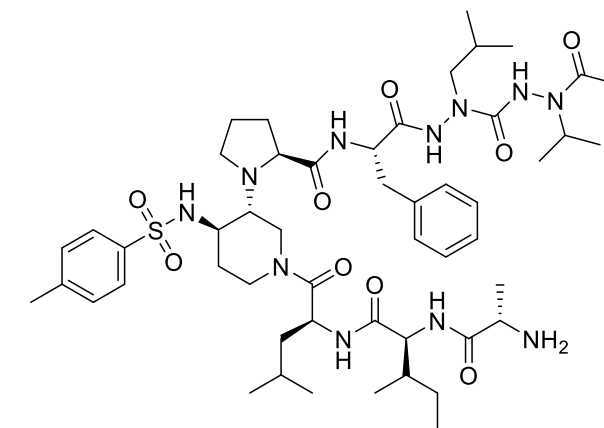
3.2 (3)



3.3 (4)

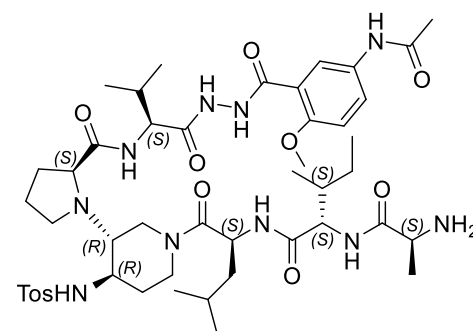


3.4 (7) R = Boc
3.5 (8) R = H
3.6 (9) R = Acetyl
3.7 (10) R = Trifluoroacetyl

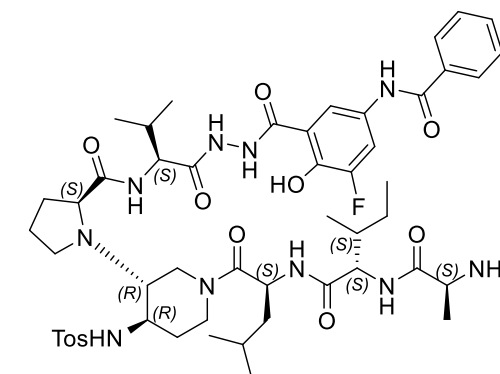


3.8 (14)

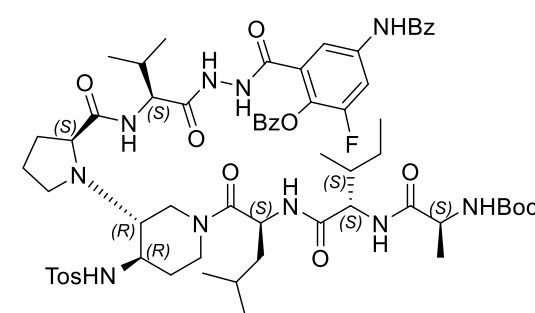
Annex 2: hairpins chapter 4



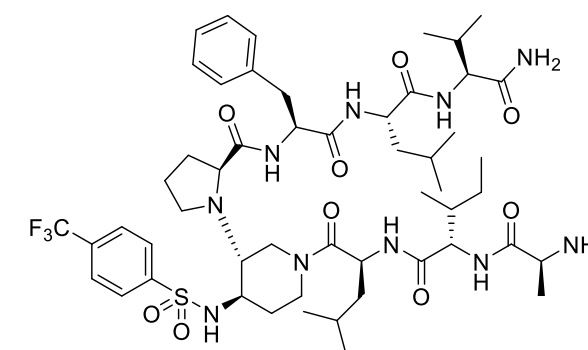
4.4



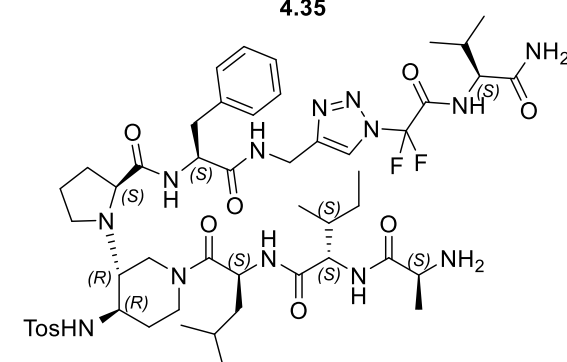
4.6



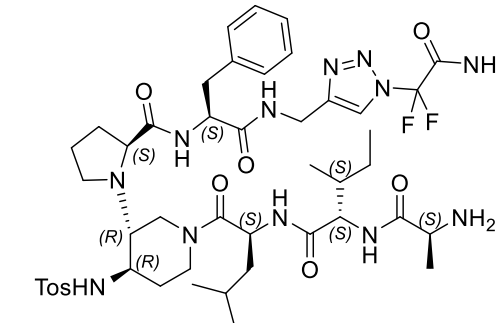
4.35



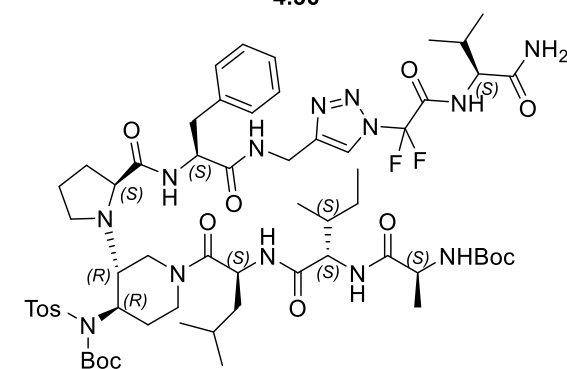
4.50



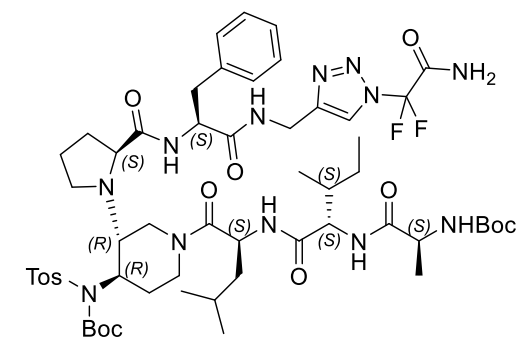
4.36



4.37



4.48



4.49

Experimental part

General experimental methods

NMR, HPLC, Mass

Usual solvents were purchased from commercial sources, dried and distilled by standard procedures. Pure compounds were obtained after liquid chromatography using Merck silical gel 60 (40–63 μm). TLC analyses were performed on silica gel 60 F250 (0.26 mm thickness) plates. The plates were visualized with UV light ($\lambda = 254 \text{ nm}$) or revealed with a 4 % solution of phosphomolybdic acid or ninhydrin in EtOH. NMR spectra were recorded on an Ultrafield Bruker AVANCE 300 (^1H , 300 MHz, ^{13}C , 75 MHz) or on a Bruker AVANCE 400 (^1H , 400 MHz, ^{13}C , 100 MHz) or on a Bruker AVANCE 600 equipped with a cryoprobe (^1H , 600 MHz, ^{13}C , 150 MHz) or on a Bruker AVANCE 800 (^1H , 800 MHz, ^{13}C , 200 MHz). Chemical shifts δ are in ppm and the following abbreviations are used: singlet (s), doublet (d), doublet of doublet (dd), triplet (t), quadruplet (q), multiplet (m) and broad singlet (bs). Mass spectra were obtained using a Bruker Esquire electrospray ionization apparatus. HRMS were obtained using a TOF LCT Premier apparatus (Waters), with an electrospray ionization source. The purity of compounds was determined by HPLC using a WATERS gradient system (pump + controller E 600, UV detector PDA 2996, autosampler 717) on a Xselect column (C18, 2.1 x150mm-3.5 μm), mobile phase, MeCN/H₂O + 0.1% formic acid (gradient 5-100% in 20 min), detection at 257 nm. Melting points were determined on a Kofler melting point apparatus. Preparative HPLC were performed on Agilent Infinity II.

Fluorescence-Detected ThT Binding Assay (hIAPP)

hIAPP, purchased from Bachem, was dissolved in pure hexafluoro-isopropanol (HFIP) at a concentration of 1 mM and incubated for 1 hour at room temperature to dissolve any preformed aggregates. Next, HFIP was evaporated with dry nitrogen gas followed by vacuum desiccation for at least 3 hours. The resulting peptide film was then dissolved in DMSO to obtain stock solutions of hIAPP (0.2 mM) and stock solutions of compounds to test were dissolved in DMSO (10, 1 and 0.1 mM). The concentration of DMSO was kept constant at 3% (v/v) in the final volume of 200 μL . Thioflavin-T binding assays were used to measure the formation of fibrils over time. A plate

reader (Fluostar Optima, BmgLabtech) and standard 96-wells flat-bottom black microtiter plates in combination with a 440 nm excitation and 480 nm emission filters were used. The ThT assay was started by adding 5 μ L of a 0.2 mM hIAPP stock solution to a mixture of 10 μ M ThT and 10 mM Tris/HCl, 100 mM NaCl at pH 7.4 containing 1 μ L of stock solutions of compound to test. The concentration of IAPP was held constant at 5 μ M and inhibitors were added to yield compound/IAPP ratios of 10/1, 1/1 and 0.1/1. The ThT assays were performed in triplicate and between 2 and 4 times on different days, with the same batch of peptide. The ability of compounds to inhibit IAPP aggregation was assessed considering the time of the half-aggregation ($t_{1/2}$) and the intensity of the experimental fluorescence plateau (F), both values were obtained by fitting the obtained kinetic data to a Boltzmann sigmoidal curve using GraphPad Prism 5. The relative extension/reduction of $t_{1/2}$ is defined as the experimental $t_{1/2}$ in the presence of the tested compound relative to the one obtained without the compound and is evaluated as the following percentage: $[t_{1/2}(\text{hIAPP} + \text{compound}) - t_{1/2}(\text{hIAPP})] / t_{1/2}(\text{hIAPP}) \times 100$. The relative extension/reduction of the experimental plateau is defined as the intensity of experimental fluorescence plateau observed with the tested compound relative to the value obtained without the compound and is evaluated as the following percentage: $(F_{\text{hIAPP} + \text{compound}} - F_{\text{hIAPP}}) / F_{\text{hIAPP}} \times 100$. The curves of the tested compounds are fitted to a Boltzmann sigmoidal model, normalized to the control experiment and represented in supporting information.

Fluorescence-Detected ThT Binding Assay ($A\beta_{1-42}$)

$A\beta_{1-42}$ was purchased from Bachem and ThT was obtained from Sigma. The peptide was dissolved in an aqueous 1% ammonia solution to a concentration of 1 mM and then, just prior to use, was diluted to 0.2 mM with 10 mM Tris-HCl and 100 mM NaCl buffer (pH 7.4). Stock solutions of compounds to test were dissolved in DMSO with the final concentration kept constant at 0.5% (v/v). ThT fluorescence was measured to evaluate the development of $A\beta_{1-42}$ fibrils over time using a fluorescence plate reader (Fluostar Optima, BMG labtech) with standard 96-well black microtiter plates (final volume in the wells of 200 μ L). Experiments were started by adding the peptide (final $A\beta_{1-42}$ concentration equal to 10 μ M) into a mixture containing 40 μ M ThT in 10 mM Tris-HCl and 100 mM NaCl buffer (pH 7.4) with and without the compounds at different concentrations (100, 10, 1 μ M) at room temperature. The ThT fluorescence intensity of each sample (performed in triplicate) was recorded with 440/480 nm excitation/emission filters set for 42 h performing a double orbital shaking of 10 s before the first cycle. The fluorescence assays were performed

between 2 and 4 times on different days, with the same batch of peptide. The ability of compounds to inhibit A β ₁₋₄₂ aggregation was assessed considering the time of the half-aggregation ($t_{1/2}$) and the intensity of the experimental fluorescence plateau (F), both values were obtained by fitting the obtained kinetic data to a Boltzmann sigmoidal curve using GraphPad Prism 5. The relative extension/reduction of $t_{1/2}$ is defined as the experimental $t_{1/2}$ in the presence of the tested compound relative to the one obtained without the compound and is evaluated as the following percentage: $[t_{1/2} (\text{A}\beta + \text{compound}) - t_{1/2} (\text{A}\beta)] / t_{1/2} (\text{A}\beta) \times 100$. The relative extension/reduction of the experimental plateau is defined as the intensity of experimental fluorescence plateau observed with the tested compound relative to the value obtained without the compound and is evaluated as the following percentage: $(\text{FA}\beta + \text{compound} - \text{FA}\beta) / \text{FA}\beta \times 100$. Curves of the tested compounds are fitted to a Boltzmann sigmoidal model, normalized to the control experiment and represented in supporting information.

Transmission Electron Microscopy

Samples were prepared under the same conditions as in the ThT-fluorescence assay. Aliquots of hIAPP (5 μ M in 10 mM Tris-HCl, 100 mM NaCl, pH 7.4 in the presence and absence of hairpins 3, 8, 13 and 14 were adsorbed onto 300-mesh carbon grids for 2 min, washed and dried. The samples were negatively stained for 45 s. on 2 % uranyl acetate in water. After draining off the excess of staining solution and drying, the grids were observed using a JEOL 2100HC TEM operating at 200 kV with a LaB6 filament. Images were recorded in zero-loss mode with a Gif Tridiem energy-filtered-CCD camera equipped with a 2k x 2k pixel-sized chip (Gatan inc., Warrendale, PA). Acquisition was accomplished with the Digital Micrograph software (versions 1.83.842, Gatan inc., Warrendale, PA).

Preparation of large unilamellar vesicles

The LUVs were composed of a mixture of DOPC/DOPS in a 7:3 molar ratio. Stock solutions of DOPC and DOPS in chloroform at concentrations of 20-30 mM were mixed in a glass tube. The solvent was evaporated with dry nitrogen gas yielding a lipid film that was subsequently kept in a vacuum desiccator for 1 h. Lipid films were hydrated during at least 30 minutes in a solution containing 70 mM calcein and 10 mM Tris (pH 7.4). The lipid suspensions were subjected to 10 freeze-thaw cycles, at temperatures of approximately -190°C and 50°C, respectively, and subsequently extruded 19 times through a mini-extruder (Avanti Alabaster, AL) equipped with

polycarbonate membranes (at 200 nm cut-off). Free calcein was separated from the calcein-filled unilamellar vesicles using size-exclusion chromatography (Sephadex G50-fine) and elution with 10 mM Tris/HCl, 100 mM NaCl (pH 7.4). The phospholipid content of lipid stock solutions and vesicle preparations was determined by assessing inorganic phosphate according to Rouser.

Membrane permeability assay

Leakage experiments were performed in standard 96-wells transparent microtiter plates using a plate reader (Spectrafluor, Tecan, Salzburg, Austria). Aliquots of 2.5 μ L of molecules solution in DMSO at the desired concentration were added to 192.5 μ L of 100 μ M lipid vesicles in 10 mM Tris-HCl, 100 mM NaCl buffer at pH 7.4. The assay was then started by adding 5 μ L of a 0.2 mM IAPP solution in DMSO or 2.5 μ L DMSO only as control. Directly after addition of all components, the microtiter plate was shaken for 10 s. The plate was not shaken during the measurement. Fluorescence was measured from the top, every 5 min, using a 485 nm excitation filter and a 535 nm emission filter. The temperature during the measurement was $25 \pm 3^\circ\text{C}$. The maximum leakage at the end of each measurement was determined by adding 2 μ L of 10% Triton X-100 to a final concentration of 0.1% (v/v). The release of fluorescent dye was calculated according to the following equation:

$$L(t) = (F_t - F_0)/(F_{100} - F_0)$$

$L(t)$ is the fraction of dye released (normalized membrane leakage) at time t , F_t is the measured fluorescence intensity at time t , and F_0 and F_{100} are the fluorescence intensities at times $t=0$ and after addition of Triton X-100, respectively. All membrane leakage assays were performed three times, each in triplicate, on different days, using different IAPP stock solutions.

Capillary electrophoresis protocol (hIAPP)

Sample preparation: commercial hIAPP was dissolved upon reception in pure HFIP at 1 mM and incubated for 1 hour at room temperature, followed by an aliquoting and an immediate evaporation under nitrogen, then under vacuum and storage at -20°C . Just before performing real time kinetics, the dried peptide was reconstituted in 50 mM ammonium acetate buffer pH 3.7 at 100 μ M. Hexamer 6 was dissolved in DMSO and added to the peptide solution to reach final concentration of 100 μ M and DMSO/ammonium acetate buffer ratio of 1%.

CE-UV experiments were carried out with a MDQ Instrument (SCIEX, Framingham, MA, USA) equipped with a UV detector. Detection was performed at 200 nm. Fused silica capillaries (50 μ m id x 365 μ m od) were purchased from Polymicro Technologies (Phoenix, AZ, USA). Silica capillaries were coated with a 0.2% polybrene solution. Briefly, solid polybrene was dissolved in water under heating at 50°C. The capillary was preconditioned with MeOH, NaOH 1M, NaOH 0.1M and with H₂O. All flushings were done at 20 psi for 15 min. The capillary was then coated with the 0.2% polybrene solution for 15 min at 20 psi. The coated capillary was then flushed with the background electrolyte (BGE) at 20 psi for 45 min and equilibrated under -25 kV for 2 hours. Polybrene-coated capillaries were 60 cm total length (49.8 cm to the detector). The BGE was a 50 mM ammonium acetate buffer, pH 3.7. The separation was carried out under -25 kV at 25°C. Samples were injected from the inlet by hydrodynamic injection at 0.8 psi for 10 s. After each run, the capillary was rinsed for 5 min with 1 M NaOH, 5 min with water, recoated for 10 min with 0.2% polybrene, and finally equilibrated with the running buffer for 5 min at 20 psi.

ESI-MS experiments

were carried out with a Synapt G2-SⁱQ-TOF instrument (Waters, Manchester, UK) equipped with an ESI interface. Positive ion mode was used. Samples of hIAPP (as previously described for the CE-UV experiments) were injected by direct infusion through a syringe at 5 μ L/min. Main MS parameters are detailed the following: the capillary voltage was set at 2.4 kV, with the sampling cone and source offset at 70V. Source and desolvation temperatures were respectively 40 °C and 75°C. Data were processed with MassLynx.

Cell viability assay

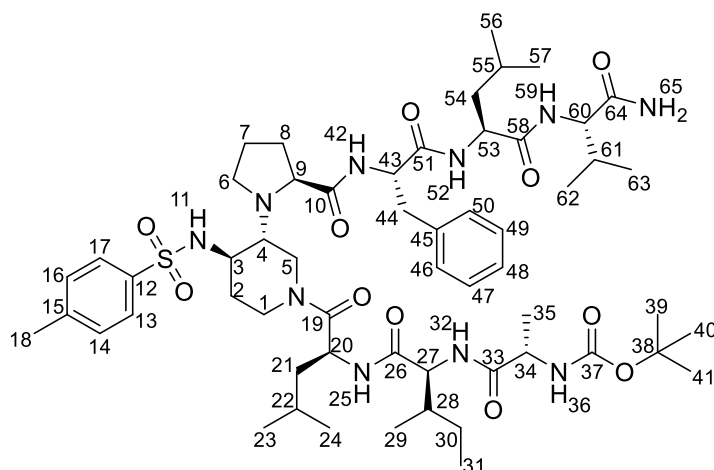
Sample preparation : commercial hIAPP (Bachem batch 3016548) was dissolved in pure hexafluoro-isopropanol (at 1 mM) and incubated for 1 hour at room temperature. Next; HFIP was evaporated with dry nitrogen followed by a vacuum desiccation for 3 hours. The dry sample was stored at -20 °C until use.

Rat INS-1 cells (given by Pr MOVASSAT / Dr TOURREL-CUZIN, Unité Biologie Fonctionnelle et Adaptative, Equipe: Biologie et Pathologie du Pancréas Endocrine, UMR 8251 Université PARIS-DIDEROT (UP7)) were used for cell viability measurement. Cells were grown in 50 μ L of medium (RPMI-1640 supplemented with 50 μ M of β -mercaptoethanol, 1 μ M of pyruvate, P/S 0.5 %, FBS 10 %) for 24 hours at 37 °C, 5% CO₂ in a 96 well plate at 30 000 cells per well. 50 μ L

of the previously prepared peptide, dissolved in fresh medium at 40 μM with or without compounds to test (compounds and EGCG as reference) were immediately added to individual well (dilution one to two; 20 μM hIAPP final concentration). The cells were then incubated for an additional 24 hours at 37 $^{\circ}\text{C}$ and the cell viability was determined using a MTT toxicity assay with an addition of 10 μL of 5 mg/mL MTT to each well. After incubation for 1 h at 37 $^{\circ}\text{C}$, the medium was removed and 200 μL of DMSO were added to dissolve formazan crystals. The absorbance at 570 nm was measured with Multiskan MS microplate reader (Labsystems). Averages from 3 to 6 replicates wells were done for each sample and control, and each experiment was repeated 3 times.

Compounds chapter 3

Compound [7 or 3.4]



To a stirred solution of **19** (232 mg, 0.303 mmol, 1.0 eq.) in dry DMF (5 mL), cooled at 0 $^{\circ}\text{C}$, COMU (130 mg, 0.303 mmol, 1.0 eq) and oxyma (43 mg, 0.303 mmol, 1.0 eq.) were added. The reaction mixture was stirred for 30 min at 0 $^{\circ}\text{C}$, at that moment **12** (125 mg, 0.303 mmol, 1.0 eq.) and DIPEA (82 μL , 0.606 mmol, 2.0 eq.) were added. The solution was stirred at room temperature overnight under argon atmosphere and the volatile was removed under reduced pressure. The crude oil obtained was taken up with EtOAc, washed with saturated solution of NaHCO_3 , water and brine, dried over Na_2SO_4 , filtered and concentrated under reduced pressure. The residue obtained was purified by column chromatography on silica gel, eluting with $\text{CH}_2\text{Cl}_2/\text{MeOH}$ 95:5 to afford **7** (297 mg, 0.264 mmol, 87%) as a white solid.

Molecular weight = 1123.47 g mol^{-1}

R_f = 0.4 ($\text{CH}_2\text{Cl}_2/\text{MeOH}$ 95:5)

HRMS: Calcd. for $[C_{57}H_{90}N_{10}O_{11}S + H]^+$: m/z 1123.6590, found: 1123.6576 $g\ mol^{-1}$

1H NMR (CD_3OH , 600 MHz): two conformers δ 8.74 (0.5H, m, NH52); 8.69 (0.5H, d, $J = 10$ Hz, NH42); 8.60 (0.5H, d, $J = 9.5$ Hz, NH42); 8.46 (0.5H, m, NH52); 8.39 (0.5H, d, $J = 7.6$ Hz, NH25); 8.35 (0.5H, d, $J = 8.2$ Hz, NH25); 8.27 (0.5H, d, $J = 8.5$ Hz, NH59); 8.14 (0.5H, d, $J = 9.0$ Hz, NH59); 7.96 (0.5H, d, $J = 9.2$ Hz, NH32); 7.95-7.87 (1H, m, NH32, NH11); 7.83 (2H, m, H17, H13); 7.77 (1H, d, $J = 7.9$ Hz, NH65); 7.72 (0.5H, d, $J = 9.8$ Hz, NH11); 7.41 (2H, d, $J = 8.9$ Hz, H16, H14); 7.36 (2H, m, H50, H46); 7.26 (2H, m, H49, H47); 7.23-7.17 (1.5H, m, NH65, H48); 7.15 (0.5H, bs, NH65); 6.97 (0.5H, d, $J = 7.3$ Hz, NH36); 6.91 (0.5H, d, $J = 7.5$ Hz, NH36); 4.86 (1H, bs, H43, H20); 4.78 (1H, bs, H43, H20); 4.57 (1H, bs, H53); 4.44 (1H, d, $J = 14.1$ Hz, H5); 4.28 (1H, d, $J = 14.6$ Hz, H1); 4.25-4.00 (3.5H, m, H60, H34, H27, H5); 3.83-3.70 (1H, m, H9, H1); 3.68-3.50 (1H, m, H3); 3.39-2.98 (4.5H, m, H44, H9, H6, H5, H1); 2.80-2.66 (1H, m, H6, H5); 2.61 (0.5H, m, H6); 2.52-2.41 (1H, m, H4, H1); 2.44 (3H, s, H18); 2.22 (0.5H, m, H4); 2.05 (1H, m, H61); 1.93 (1H, m, H8); 1.80-1.04 (16H, m, H55, H54, H35, H30, H28, H22, H21, H8, H7, H2); 1.43 (9H, s, H43, H42, H41); 1.01-0.80 (21H, m, H63, H62, H57, H56, H31, H23, H24); 0.74 (3H, d, $J = 7.0$ Hz, H29) ppm

^{13}C NMR (CD_3OH , 150 MHz, 278K): two conformers δ 176.0 (C10); 174.7 (C64); 174.5 (C33); 173.4 (C51); 173.3 (C58); 172.0 (C26); 171.5 (C26); 171.3 (C19); 143.5 (C15); 139.6 (C12); 137.5 (C45); 129.7 (C16, C14); 129.2 (C50, C46); 128.1 (C49, C47); 126.7 (C17, C13); 126.4 (C48); 79.2 (C38); 63.4 (C9); 62.8 (C9); 60.3 (C4); 59.5 (C4); 58.8 (C60); 58.5 (C60); 57.6 (C27); 57.2 (C27); 54.3 (C43); 54.1 (C3); 53.8 (C3); 51.8 (C53); 50.3 (C34); 47.4 (C20); 46.7 (C20); 44.5 (C6); 44.2 (C1); 43.8 (C5); 41.0 (C1); 40.8 (C54); 40.7 (C7); 40.6 (C21); 40.4 (C21); 40.3 (C54); 39.8 (C5); 37.4 (C44); 36.9 (C28); 31.6 (C2); 30.9 (C61); 30.8 (C8); 27.4 (C41, C42, C43); 24.6 (C30); 24.5 (C55, C22); 24.1 (C2); 21.0 (C23, C24); 20.3 (C18); 18.0 (C62, C63); 17.7 (C57, C56); 17.0 (C35); 14.9 (C31); 10.1 (C29); ppm

IR: 3300 (ν N-H); 2963 (ν C-H); 1643 (ν C=O); 1523 (δ N-H); 1453 (δ C-N) cm^{-1}

HPLC purity: XBridge C18 3.5 μm ; H₂O + 0:2 % form. ac./ACN, gradient 5–100 % in 20 min; $R_t = 18.68$ min, 100 %

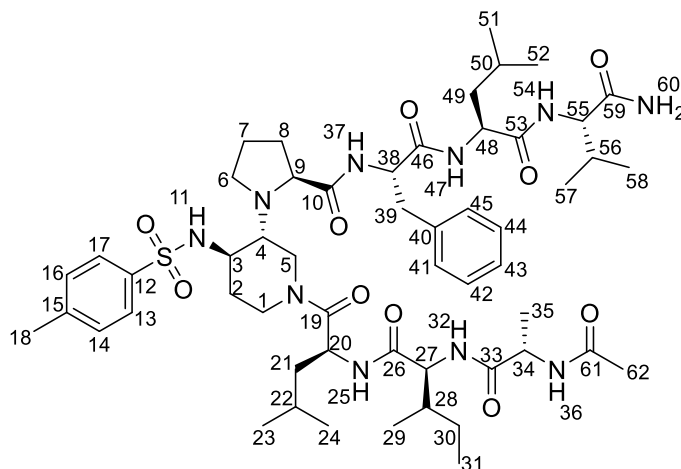
Compound [8 or 3.5]

(C49, C21, C7); 37.6 (C39); 36.5 (C28); 30.9 (C56); 24.6 (C50, C30, C22, C2); 20.8 (C58, C57); 20.2 (C18); 20.1 (C52, C51, C24, C23); 16.5 (C35); 14.4 (C29); 9.9 (C31) ppm

IR: 3251 (ν N-H); 2963 (ν C-H); 1647 (ν C=O); 1546 (δ N-H); 1456 (δ C-N) cm^{-1}

HPLC purity: XBridge C18 3.5 μm ; H₂O + 0:2 % form. ac./ACN, gradient 5–100 % in 20 min; $R_t = 13.16$ min, 92 %

Compound [9 or 3.6]



To a stirred solution of **8** (40 mg, 39 μmol , 1 eq.) in dry THF (2 mL) TEA (28 μL , 199 μmol , 5.0 eq.) and acetic anhydride (11 μL , 0.117 μmol , 3.0 eq.) were successively added. The reaction mixture was stirred at 40°C for 6 h. After concentration under reduced pressure, the residue obtained was purified by column chromatography on silica gel eluting with CH₂Cl₂ up to CH₂Cl₂/MeOH (90:10) to afford compound **9** (41.5 mg, 39 μmol , quant.).

Molecular weight = 1064.61 g mol^{-1}

R_f = 0.2 (CH₂Cl₂ /MeOH 95:5)

HRMS: Calcd. for [C₅₄H₈₄N₁₀O₁₀S + H]⁺: m/z 1065.6126, found: 1065.6184 g mol^{-1}

¹H NMR (CD₃OH, 600 MHz, 278K): two conformers δ 8.74 (0.5H, m, NH47); 8.67 (0.5H, d, $J = 10.1$ Hz, NH37); 8.59 (0.5H, d, $J = 9.6$ Hz, NH37); 8.50 (0.5H, m, NH47); 8.37 (0.5H, d, $J = 9.1$ Hz, NH25); 8.34 (0.5H, d, $J = 8.1$ Hz, NH25); 8.33-8.25 (1.5H, m, NH54, NH36); 8.1 (0.5H, d, $J = 9.1$ Hz, NH54); 8.08 (1H, m, NH32); 7.87 (0.5H, d, $J = 9.7$ Hz, NH11); 7.82 (2H, m, H17, H13); 7.76 (1H, m, NH60); 7.69 (0.5H, d, $J = 9.8$ Hz, NH11); 7.41 (2H, d, $J = 8.5$ Hz, H16, H14); 7.36 (2H, m, H45, H41); 7.27 (2H, m, H44, H42); 7.20 (1H, d, $J = 7.6$ Hz, H43); 7.18 (0.5H, bs, NH60); 7.14 (0.5H, bs, NH60); 4.91 (0.5H, m, H38); 4.88-4.72 (1.5H, m, H38, H20); 4.54 (1H, m, H48)

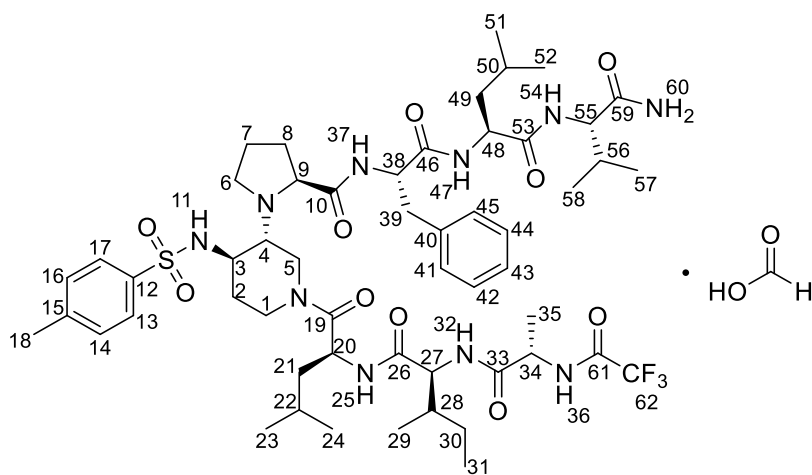
4.45 (0.5H, d, $J = 13.5$ Hz, H5); 4.39 (0.5H, m, H34); 4.33 (0.5H, m, H34); 4.30-4.12 (3H, m, H55, H27, H5, H1); 3.84-3.72 (1H, m, H9, H1); 3.60 (1H, m, H3); 3.34 (0.5H, m, H9); 3.29-3.01 (4H, m, H39, H6, H5, H1); 2.75 (0.5H, m, H5); 2.67 (0.5H, m, H6); 2.61 (0.5H, m, H6); 2.52-2.46 (1H, m, H6, H4); 2.45 (3H, s, H18); 2.22 (0.5H, m, H4); 2.06 (1H, m, H56); 1.95 (3H, m, H62); 1.93 (1H, m, H8); 1.80-1.49 (9.5H, m, H50, H49, H28, H22, H21, H7, H2); 1.45 (0.5H, m, H22); 1.39-1.17 (5.5H, m, H35, H22, H8, H2); 1.12 (0.5H, m, H30); 1.06 (0.5H, m, H30); 1.01-0.80 (21H, m, H58, H57, H52, H51, H31, H24, H23); 0.73 (3H, d, $J = 7.0$ Hz, H31) ppm

^{13}C NMR (CD₃OH, 150 MHz, 278K): two conformers δ 176.0 (C10); 174.7 (C59); 173.8 (C33); 173.5 (C53); 173.4 (C46); 173.3 (C55, C53); 172.8 (C46); 172.1 (C26); 171.7 (C61); 171.6 (C26); 171.3 (C19); 170.7 (C19); 143.5 (C15); 139.7 (C12); 137.5 (C40); 129.8 (C16, C14); 129.2 (C45, C41); 128.1 (C44, C42); 126.6 (C17, C13); 126.4 (C43); 63.4 (C9); 62.6 (C9); 60.2 (C4); 58.7 (C55); 57.4 (C27); 54.1 (C38); 54.0 (C3); 53.9 (C3); 51.8 (C48); 49.2 (C34); 47.3 (C20); 46.7 (C20); 46.1 (C34); 44.5 (C6); 44.2 (C1); 43.9 (C5); 40.9 (C1); 40.7 (C7); 40.6 (C49, C21, C7); 40.5 (C20); 39.6 (C5); 37.3 (C39); 36.9 (C28); 36.6 (C28); 32.7 (C2); 31.7 (C2); 30.8 (C56, C8); 30.7 (C56); 24.6 (C50, C30, C22); 21.1 (C18); 20.8 (C24, C23); 20.2 (C15); 20.1 (C52, C51, C24, C23); 18.5 (C58, C57); 16.8 (C35); 14.9 (C31); 10.2 (C29) ppm

IR: 3273 (ν N-H); 2959 (ν C-H); 1640 (ν C=O); 1519 (δ N-H); 1454 (δ C-N) cm⁻¹

HPLC purity: XBridge C18 3.5 μm ; H₂O + 0:2 % form. ac./ACN, gradient 5–100 % in 20 min; $R_t = 16.33$ min, 100 %

Compound [10 or 3.7]



To a stirred solution of **8** (60 mg, 54 μmol , 1 eq.) in dry THF (2mL) at 0°C, TEA (31 μL , 222 μmol , 4.0 eq.) and trifluoroacetic anhydride (11 μL , 0.117 μmol , 3.0 eq.) were successively added.

The reaction mixture was then stirred for 6 h at 0°C. After concentration under reduced pressure, the residue was purified by preparative HPLC eluting with H₂O + 0.2% formic acid/CH₃CN (gradient 50 to 100% in 20 min) on a Sunfire column (C18, 4.6 x150mm-5µm) to afford **10** (11 mg, 9.4 µmol, 5%) as a white powder.

Molecular weight = 1165.38 g mol⁻¹; free amine 1119.36 g mol⁻¹

R_f = 0.3 (CH₂Cl₂/MeOH 95:5)

HRMS: Calcd. for [C₅₄H₈₁F₃N₁₀O₁₀S + H]⁺: m/z 1119.5888, found: 1119.5898 g mol⁻¹

¹H NMR (CD₃OH, 600 MHz, 278K): two conformers δ 9.46 (1H, m, NH36); 8.74 (0.5H, m, NH47); 8.69 (0.5H, d, *J* = 10.4 Hz, NH37); 8.60 (0.5H, d, *J* = 10.4 Hz, NH37); 8.45-8.35 (1.5H, m, NH47, NH25); 8.27-8.22 (1H, m, NH54, NH32); 8.11 (0.5H, d, *J* = 9.2 Hz, NH54); 7.91 (0.5, d, *J* = 10.0 Hz, NH11); 7.82 (2H, m, H17, H13); 7.77 (1H, m, NH60); 7.70 (0.5H, d, *J* = 9.8 Hz, NH54); 7.42 (2H, d, *J* = 8.4 Hz, H16, H14); 7.37 (2H, m, H45, H41); 7.27 (2H, m, H44, H42); 7.21 (1H, d, *J* = 7.6 Hz, H43); 7.18 (0.5H, bs, NH60); 7.14 (0.5H, bs, NH60); 4.90 (0.5H, m, H38); 4.87 (0.5H, m, H20); 4.79 (0.5H, m, H20); 4.76 (0.5H, m, H38); 4.53 (0.5H, m, H48); 4.49-4.39 (1.5H, m, H34, H5); 4.32-4.10 (3H, m, H55, H27, H5, H1); 3.83-3.73 (1H, m, H9, H1); 3.66-3.57 (1H, m, 3); 3.34-3.01 (4.5H, m, H39, H9, H6, H5, H1); 2.76 (0.5H, m, H5); 2.69 (0.5H, m, H6); 2.62 (0.5H, m, H6); 2.53-2.46 (1H, m, H4, H1); 2.45 (3H, s, H18); 2.23 (0.5H, m, H4); 2.05 (1H, m, H56); 1.93 (1H, m, H8); 1.81-1.48 (8.5H, m, H50, H49, H28, H22, H21, H7, H2); 1.47-1.06 (7.5, m, H35, H30, H21, H8, H2); 1.01-0.81 (21H, m, H58, H57, H52, H51, H31, H24, H23); 0.73(3H, d, *J* = 6.9 Hz, H29) ppm

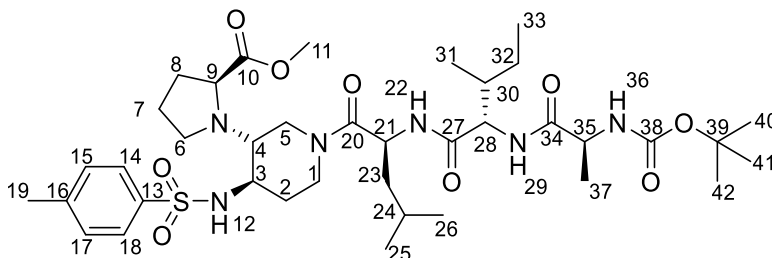
¹³C NMR (CD₃OH, 150 MHz, 278K): two conformers δ 176.0 (C10); 174.7 (C59); 173.4 (C46); 173.2 (C53); 172.9 (C46); 172.3 (C33); 172.0 (C26); 171.4 (C26); 171.3 (C19); 157.4 (C61); 143.5 (C15); 139.6 (C12); 137.5 (C40); 129.7 (C16, C14); 129.3 (C45, C41); 128.1 (C44, C42); 126.6 (C17, C13); 126.4 (C43); 63.4 (C9); 60.3 (C4); 59.5 (C4); 58.8 (C55); 58.5 (C55); 57.6 (C27); 57.2 (C27); 54.1 (C3); 54.0 (C38); 53.8 (C3); 51.8 (C48); 49.6 (C34); 47.3 (C20); 46.7 (C20); 44.5 (C6); 44.0 (C1); 43.8 (C5); 41.0 (C1); 40.7 (C49); 40.6 (C21); 40.5 (C7); 40.3 (C21); 39.7 (C5); 37.4 (C39); 36.9 (C28); 36.6 (C28); 31.6 (C2); 30.8 (C56, C8); 29.5 (C8); 24.6 (C30); 24.5 (C50, C22); 24.1 (C2); 21.0 (C24, C23); 20.3 (C18); 18.0 (C58, C57); 17.5 (C52, C51); 16.3 (C35); 14.9 (C31); 10.1 (C29) ppm

¹⁹F NMR (CD₃OD, 188 MHz, 298K): two conformers δ -77.1; -77.0 ppm

IR: 3291 (ν N-H); 2961 (ν C-H); 1642 (ν C=O); 1541 (δ N-H); 1456 (δ C-N) cm⁻¹

HPLC purity: XBridge C18 3.5 μm ; H₂O + 0:2 % form. ac./ACN, gradient 5–100 % in 20 min;
 R_t = 13.45 min, 97 %

Methyl((3*R*,4*R*)-1-((*tert*-butoxycarbonyl)-*L*-alanyl-*L*-isoleucyl-*L*-leucyl)-4-((4-methylphenyl)sulfonamido)piperidin-3-yl)-*L*-prolinate [11]



To a stirred solution of **18** (590 mg, 0.72 mmol, 1 eq.) in dry DMF (5 mL) piperidine (2 mL, 20%/vol. DMF) was added under argon atmosphere. The reaction was let under stirring 2 h and then the volatile were removed under reduced pressure. The crude free amine obtained was kept aside without further purification before peptic coupling. To a solution of *L*-Boc-NH-Ala-OH (272 mg, 1.44 mmol, 2 eq.) in dry DMF (4 mL) were added successively HBTU (547 mg, 1.44 mmol, 2 eq.) and HOBt (196 mg, 1.44 mmol, 2 eq.) at 0°C. At this time, a solution of the previous free amine (438 mg, 0.72 mmol, 1 eq.) and DIPEA (0.50 mL, 2.88 mmol, 4 eq.) in DMF (4 mL) was added dropwise at 0°C on the previous one and the reaction was let stirring overnight. After removal of the solvent under reduced pressure, the crude oil obtained was taken up with EtOAc and successively washed with distilled water, 100% aqueous solution of NaHCO₃ and brine. The organic phase was dried over Na₂SO₄, filtered and the volatile was then removed under reduced pressure. The crude residue obtained was purified by column chromatography with silica gel eluting with *c*-Hex/EtOAc 4:6 to afford **11** as a white powder (414 mg, 0.53 mmol, 74%).

Molecular weight = 779.01 g mol⁻¹

R_f = 0.43 (*c*-Hex/EtOAc 4:6)

HRMS: Calcd. for [C₃₈H₆₂N₆O₉S + H]⁺: *m/z* 779.4361, found: 779.4364 Calcd. for [C₃₈H₆₂N₆O₉S + Na]⁺: *M/z* 801.4182, found: 801.4188

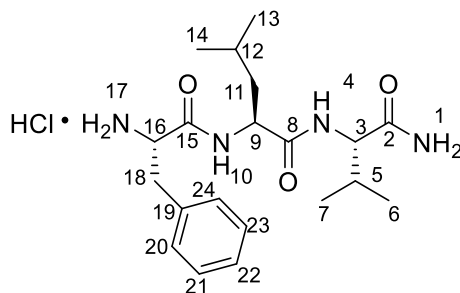
¹H NMR (CDCl₃, 400 MHz): δ 7.79 (2H, d, J = 7.9 Hz, H14, H18); 7.30 (2H, d, J = 7.8 Hz, H15, H17); 7.32 (1H, bs, NH12); 6.72 (1H, bs, NH22); 6.69 (1H, bs, NH29); 5.05 (1H, bs, NH36); 4.92 (1H, m, H21); 4.47 (1H, m, H1); 4.28 (1H, m, H28); 4.16 (1H, m, H35); 3.76 (3H, s, H11); 3.81 (1H, m, H6); 3.55 (1H, m, H9); 3.54 (1H, m, H8); 2.97 (1H, m, H6); 2.85 (1H, m, H3); 2.56 (1H,

m, H7); 2.46 (1H, m, H1); 2.42 (3H, s, H19); 2.31 (1H, m, H4); 2.28 (1H, m, H2); 2.05 (1H, m, H5), 1.88 (1H, m, H30); 1.86 (1H, m, H5); 1.62 (1H, m, H2); 1.55 (2H, m, H7, H24); 1.51 (3H, m, H23, H8); 1.42 (9H, s, H40, H41, H42); 1.41 (1H, m, H32), 1.32 (3H, d, $J = 6.7$ Hz, H37); 1.09 (1H, m, H32); 0.93 (3H, m, H26); 0.88 (3H, m, H25); 0.86 (3H, m, H33); 0.84 (3H, m, H31) ppm
 $^{13}\text{C NMR}$ (CDCl_3 , 100 MHz): δ 175.5 (C10); 172.6 (C20); 172.3 (C34); 170.4 (C27); 143.4 (C16); 137.2 (C13); 129.7 (C15, C17); 127.2 (C14, C18); 80.7 (C39); 58.0 (C28, C4); 53.5 (C3); 52.8 (C11); 52.6 (C9); 50.5 (C35); 47.5 (C21); 44.0 (C2); 43.7 (C6); 43.1 (C8); 42.8 (C23); 40.7 (C1); 37.2 (C30); 33.4 (C7); 30.0 (C5); 28.4 (C40, C41, C42); 24.8 (C3, C24); 24.6 (C32); 21.7 (C19, C26); 17.6 (C37); 15.6 (C31, C25); 11.5 (C33) ppm

Melting point = 118–120°C

IR: 3284 (ν N-H); 2961 (ν C-H); 1721, 1632 (ν C=O); 1519, 1447 (ν C=C); 1213 (ν C-N); 1162 (ν C-O) cm^{-1}

(S)-1-(((S)-1-(((S)-1-amino-3-methyl-1-oxobutan-2-yl)amino)-4-methyl-1-oxopentan-2-yl)amino)-1-oxo-3-phenylpropan-2-aminium chloride [12]



To a stirred solution of **Boc-NH-Phe-Leu-Val-CONH₂** (200 mg, 0.42 mmol, 1.0 eq.) in dioxane (10 mL) under argon atmosphere, at 0°C, HCl 4M in dioxane (6.3 mL, 25.2 mmol, 60.0 eq.) was added. The reaction was let stirring 4 h at room temperature. After removal of the volatile under reduced pressure, the hydrochloride salt **12** was yielded as a white solid (174 mg, 0.42 mmol, quant.)

Molecular weight = 412.22 g mol^{-1} ; free amine 376.50 g mol^{-1}

R_f = 0 (c-Hex/EtOAc 1:1)

HRMS: Calcd. for $[\text{C}_{20}\text{H}_{32}\text{N}_4\text{O}_3 + \text{H}]^+$: m/z 377.2508, found: 377.2545

$^1\text{H NMR}$ ($\text{DMSO}-d_6$, 400 MHz): δ 8.80 (1H, d, $J = 8.4$ Hz, NH10); 8.21 (2H, bs, NH17); 7.99 (1H, bs, NH4); 7.44 (1H, bs, NH1); 7.32 (5H, bs, H20, H21, H22, H23, H24); 7.07 (1H, bs, NH1);

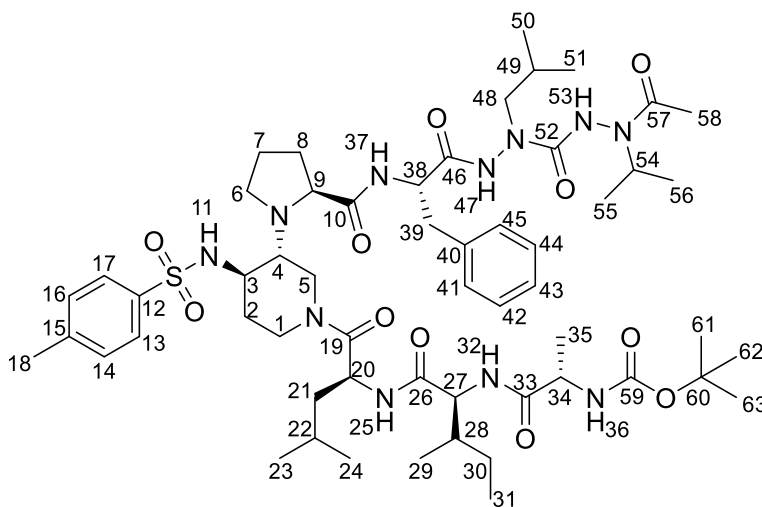
4.48 (1H, m, H9), 4.19-4.09 (2H, m, H3, H16); 3.20 (1H, dd, $J = 14.1, 5.4$ Hz, H18); 2.98 (1H, dd, $J = 14.1, 7.7$ Hz, H18); 2.00 (1H, m, H5); 1.69 (1H, m, H12); 1.52 (2H, m, H11), 0.95-0.88 (12H, m, H6, H7, H13, H14) ppm

^{13}C NMR (DMSO- d_6 , 100 MHz): δ 173.6 (C2); 172.1 (C8); 168.5 (C15); 135.7 (C19); 130.6, 129.3, 128.0 (C20, C21, C22, C23, C24); 58.3 (C3); 53.9 (C16); 52.3 (C9); 41.9 (C11); 37.6 (C18); 31.4 (C5); 25.0 (C12); 24.0, 22.6 (C13, C14); 20.2, 19.0 (C6, C7) ppm

Melting point = 80-83°C

IR: 3272 (v N-H); 2954 (v C-H); 1675-1637 (v C=O); 1547 (v C=C) cm^{-1}

Compound [13]



To a solution of compound **19** (0.19 g, 0.25 mmol, 1 eq.) in dry DMF were successively added under argon atmosphere HATU (0.19 g, 0.5 mmol, 2 eq.) and HOAt (0.07 g, 0.5 mmol, 2 eq.) were added at 0°C. A solution of compound **15** (0.10 g, 0.25 mmol, 1 eq.) and DIPEA (0.75 mL, 1.25 mmol, 5 eq.) in dry DMF was added dropwise to the previous mixture at 0°C. Then, the reaction was let 2 days at 60°C under argon atmosphere. After removal of the volatile under reduced pressure, the crude oil was taken up with EtOAc, washed with distilled water, saturated NaHCO_3 and brine, dried over MgSO_4 , filtered and concentrated under reduced pressure. The crude residue obtained was purified by column chromatography on silica gel eluting with EtOAc as eluent to afford **13** as a white powder (0.16 g, 0.15 mmol, 59 %).

Molecular weight = 1124.44 g mol^{-1}

R_f = 0.45 (EtOAc)

HRMS: Calcd. for $[\text{C}_{56}\text{H}_{89}\text{N}_{11}\text{O}_{11}\text{S}+\text{H}]^+$: M/z 1124.6542, found: 1124.6511

¹H NMR (DMSO-*d*₆, 400 MHz, 298 K): δ 10.44 (1H, bs, NH47); 8.78 (1H, bs, NH54); 8.40 (1H, bs, NH37); 8.04 (1H, bs, NH25); 7.74 (2H, m, H17, H13); 7.50 (1H, bs, NH32); 7.46 (1H, bs, NH11); 7.39 (2H, m, H16, H14); 7.26 (4H, m, H45, H44, H42, H41); 7.20 (1H, m, H43); 7.00 (1H, bs, NH36); 4.66 (1H, bs, H20); 4.54 (1H, m, H54); 4.50 (1H, m, H38); 4.48 (1H, m, H29); 4.25 (2H, m, H5); 4.16 (1H, m, H27); 3.96 (1H, bs, H34); 3.27 (1H, m, H9); 3.69 (1H, m, H1); 3.26 (1H, m, H3); 3.16 (1H, m, H39), 3.01 (1H, m, H48), 3.00 (1H, m, H39); 2.98 (1H, m, H1); 2.97 (1H, m, H48), 2.69 (1H, m, H4); 2.54 (2H, m, H6); 2.39 (3H, s, H18); 1.96 (1H, m, H8), 1.76 (1H, m, H22); 1.73 (3H, s, H58); 1.65 (1H, m, H28); 1.46 (2H, m, H8, H7); 1.55 (1H, m, H7); 1.38 (1H, m, H30); 1.36 (9H, s, H63, H62, H61); 1.26 (2H, m, H21); 1.23 (2H, m, H2); 1.12 (3H, m, H35); 1.05 (1H, m, H30); 1.02 (3H, d, $J = 6.3$ Hz, H55); 0.95 (3H, d, $J = 6.7$ Hz, H56); 0.90 (6H, d, $J = 6.9$ Hz, H51, H50); 0.84 (3H, m, H24); 0.82 (3H, m, H23); 0.78 (3H, m, H29); 0.77 (3H, m, H31) ppm

¹³C NMR (DMSO-*d*₆, 100 MHz, 298 K): δ 175.0 (C10); 172.7 (C33); 172.2 (C52); 172.0 (C57); 170.2 (C26); 170.8 (C46); 162.2 (C19), 142.8 (C15); 139.1 (C59); 138.1 (C12); 136.7 (C40); 129.6 (C16, C14); 129.3 (C45, C41); 128.1 (C44, C42); 126.5 (C43, C17, C13); 78.0 (C60); 62.6 (C9); 56.4 (C27); 53.0 (C3, C38); 49.7 (C34); 46.8 (C29); 46.4 (C54, C20); 44.7 (C6); 43.2 (C48), 43.0 (C1); 40.5 (C21); 39.5 (C5); 38.1 (C4); 36.9 (C28); 36.8 (C39); 30.4 (C7, C8); 28.9 (C2); 28.1 (C63, C62, C61); 24.1 (C30); 23.1 (C24); 21.5 (C23); 21.0 (C18); 20.9 (C22); 20.8 (C58); 19.5 (C55); 19.1 (C51, C50); 19.0 (C56); 17.7 (C35); 15.2 (C49); 10.9 (C31) ppm

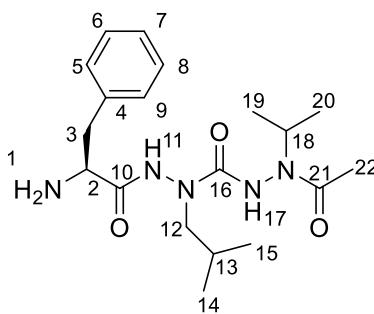
Melting point = 164-168°C

IR: 3277 (ν N-H); 2962 (ν C-H); 1639 (ν C=O); 1518, 1444 (ν C=C); 1251 (ν C-N); 1159 (ν C-O) cm^{-1}

^{13}C NMR (CD₃OH, 800 MHz): δ 174.3 (C57); 172.0 (C19); 169.8 (C26); 169.7 (C33); 144.4 (C15); 136.2 (C40); 129.5 (C16, C14); 129.2 (C44, C42); 128.6 (C45, C41); 127.1 (C43); 126.9 (C17, C13); 66.6 (C4); 57.9 (C27); 55.1 (C48); 54.5 (C38); 53.5 (C9); 51.2 (C3); 48.5 (C34); 47.9 (C54); 47.5 (C20); 43.1 (C1); 40.6 (C6); 40.4 (C2); 40.0 (C21); 36.8 (C39); 36.4 (C28); 29.6 (C7); 25.7 (C49); 24.6 (C5); 24.5 (C22, C30); 20.8 (C58); 20.4 (C24, C23); 20.2 (C18); 18.8 (C51, C50); 18.3 (C56, C55); 16.6 (C35); 14.6 (C29); 10.0 (C31) ppm

HPLC purity: XBridge C18 3.5 μm ; H₂O + 0:2 % form. ac./ACN, gradient 5–100 % in 20 min; R_t = 12.38 min, 100 %

N'-(*L*-phenylalanyl)-*N'*-acetyl-*N*-isobutyl-*N'*-isopropylmethanedihydrazide [15]



To a solution of **25** (94 mg, 0.184 mmol, 1.0 eq.) in CH₂Cl₂ and MeOH under argon atmosphere, Pd/C (19 mg, 20 % mass) and triethyl silane (294 μL , 1.84 mmol, 10 eq.) were added. The reaction mixture was stirred for 20 minutes at room temperature and filtered on a Celite pad. After concentration of the filtrate under reduced pressure, **15** (70 mg, 0.184 mmol, quant.) was afforded as a white solid.

Molecular weight = 377.48 g mol⁻¹

R_f = 0 (c-Hex/EtOAc 3:7)

HRMS: Calcd. for [C₁₉H₃₁N₅O₃ + H]⁺: m/z 378.2505, found: 378.2501

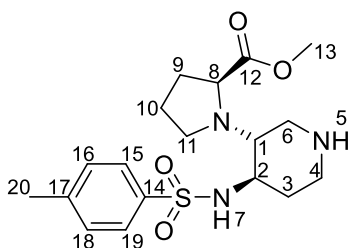
^1H NMR (CD₃OD, 400 MHz): δ 7.23-7.31 (5H, m, H5, H6, H7, H8, H9); 4.63 (1H, m, H18); 3.59 (1H, m, H2); 3.28 (1H, m, H12), 3.41 (1H, m, H12); 2.98 (2H, m, H3); 1.96 (3H, s, H22); 1.23 (1H, m, H13); 1.07 (6H, m, H19, H20); 0.73 (6H, m, H14, H15) ppm

^{13}C NMR (CD₃OD, 100 MHz): δ 176.0 (C21); 175.1 (C10); 158.9 (C16); 130.1 (C6,C8); 129.6 (C5, C9); 127.7 (C7); 138.2 (C4); 56.4 (C12); 56.1 (C2); 48.8 (C18); 42.6 (C3); 26.8 (C13); 21.0 (C22); 19.64(C14, C15); 19.2 (C19, C20) ppm

Melting point = 244-246°C

IR: 3318 (ν N-H); 2928 (ν C-H); 1691 (ν C=O); 1495 (ν N-H); 1351 (ν C-H); 1213 (ν C-N); 1167 (ν C-O) cm⁻¹

S)-Methyl-1-((3R,4R)-4-(4-methylphenylsulfonamido)piperidin-3-yl)pyrrolidine-2-carboxylate [16]



To a solution of compound piperidine pyrrolidine β-turn inducer (1 g, 2.12 mmol, 1 eq.) in toluene (30 mL) was added Pd/C 10% (0.45 g, 4.24 mmol, 2 eq.). The mixture was kept under stirring at 30 °C overnight under hydrogen atmosphere. After filtration through a pad of Celite with MeOH, the solvent was evaporated under reduced pressure to yield a colorless oil with a quantitative yield (0.81 g, 2.12 mmol).

Molecular weight = 381.17 g mol⁻¹

R_f = 0.20 (DCM/MeOH 20:1)

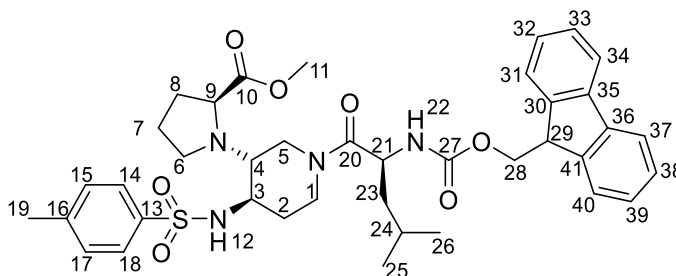
HRMS: Calcd. for [C₁₈H₂₇N₃O₄S + H]⁺: M/z 382.1801, found: 382.1800

¹H NMR (CDCl₃, 300 MHz, 298 K): δ 7.76 (2H, d, J = 7.6 Hz, H15, H19); 7.26 (2H, d, J = 7.6 Hz, H16, H18); 6.79 (1H, bs, NH7); 3.74 (3H, s, H13); 3.45 (2H, m, H8, NH5); 2.97 (2H, m, H2, H4); 2.74 (2H, m, H6); 2.49 (6H, m, H1, H4, H11, H20); 2.24 (1H, m, H11); 1.99 (1H, m, H9); 1.77 (2H, m, H3, H9); 1.39 (3H, m, H3, H10) ppm

¹³C NMR (CDCl₃, 75 MHz, 298 K): δ 176.3 (C12); 143.0 (C17); 37.5 (C14); 129.9 (C16,C18); 127.4 (C15, C19); 62.3 (C1); 59.9 (C8); 54.2 (C2); 52.6 (C13); 45.1 (C4); 44.9 (C6); 44.3 (C3); 35.3 (C9); 30.0 (C11); 24.6 (C10); 21.7 (C20) ppm

IR: 3206 (ν N-H); 2951, 2849 (ν C-H); 1727 (ν C=O); 1669 (δ N-H bend); 1438 (ν C=C); 1209, 1161 (ν C-N) cm⁻¹

Methyl((3*R*,4*R*)-1-(((9*H*-fluoren-9-yl)methoxy)carbonyl)-*L*-leucyl)-4-((4-methylphenyl)sulfonamido)piperidin-3-yl)-*L*-prolinate [17]



To a solution of *L*-Fmoc-NH-Leu-OH (757 mg, 2.14 mmol, 2 eq.) in dry DMF under argon atmosphere HATU (814 mg, 2.14 mmol, 2 eq.) and HOAt (292 mg, 2.14 mmol, 2 eq.) were added at 0°C. The mixture was let 40 min at 0°C under stirring. Meanwhile a solution of compound **16** (408 mg, 1.07 mmol, 1 eq.) and collidine (0.85 mL, 6.43 mmol, 6 eq.) in dry DMF was prepared and added dropwise at 0°C on the previous mixture. The reaction was let stirring overnight at room temperature. After removal of the volatile under reduced pressure, the crude oil was taken up with EtOAc and washed with distilled water, 100% aqueous solution of NaHCO₃ and brine, dried over MgSO₄, filtered and concentrated under reduced pressure. The crude residue obtained was purified by column chromatography on silica gel eluting with *c*-Hex/EtOAc 6:4 to afford **17** as a white powder (645 mg, 0.9 mmol, 84%).

Molecular weight = 716.32 g mol⁻¹

R_f = 0.4 (*c*-Hex /EtOAc 6:4)

HRMS: Calcd. for [C₃₉H₄₈N₄O₇S + H]⁺: *m/z* 717.3322, found: 717.3317

¹H NMR (CDCl₃, 400 MHz): δ 7.84-7.72 (4H, m, H14, H18, H31, H40); 7.56 (2H, m, H34, H37); 7.39 (2H, m, H33, H38); 7.31 (2H, m, H15, H17); 7.28 (2H, m, H32, H39); 7.01 (1H, bs, NH12); 5.46 (1H, bs, NH22); 4.65 (1H, m, H21); 4.34 (2H, m, H28); 4.19 (1H, m, H29); 4.13 (2H, m, H1); 3.78 (3H, s, H11), 3.76 (1H, m, H9); 3.60 (1H, m, H4); 3.05 (2H, m, H8); 2.95 (1H, m, H3); 2.48 (3H, s, H19); 2.47 (2H, m, H6); 2.43 (2H, m, H5); 2.09 (1H, m, H2); 1.92 (1H, m, H2); 1.64 (1H, m, H24); 1.53 (2H, m, H7); 1.49 (2H, m, H23); 0.96 (3H, d, *J* = 6.2 Hz, H26); 0.86 (3H, d, *J* = 6.5 Hz, H25) ppm

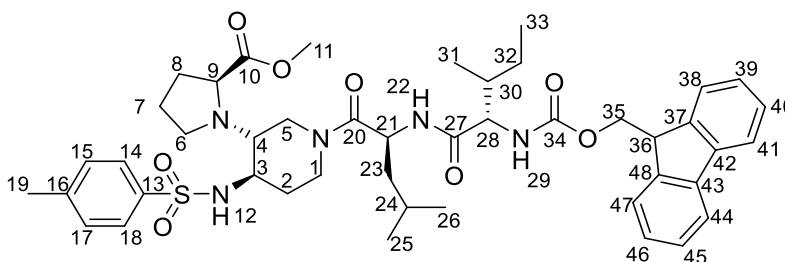
¹³C NMR (CDCl₃, 100 MHz): δ 175.8 (C10); 171.2 (C20); 156.4 (C27); 143.9 (C30, C41); 143.3 (C16); 141.4 (C35, C36); 129.6 (C15, C17); 127.7 (C34, C37); 127.2 (C14, C18); 127.1 (C13, C32, C39); 125.1 (C33, C38); 119.9 (C31, C40); 67.0 (C28); 60.4 (C1); 52.8 (C9); 52.6 (C4, C11);

52.5 (C3); 49.4 (C21); 47.2 (C29); 44.0 (C8); 42.6 (C23); 42.4 (C7); 41.2 (C6); 41.0 (C5); 29.8 (C2); 24.6 (C24); 21.8 (C25, C26); 21.5 (C19) ppm

Melting point = 90-92°C

IR: 3201 (ν N-H); 2954 (ν C-H); 1721, 1635 (ν C=O); 1448 (ν C=C); 1212 (ν C-N); 1162 (ν C-O) cm^{-1}

Methyl((3*R*,4*R*)-1-(((9*H*-fluoren-9-yl)methoxy)carbonyl)-*L*-isoleucyl)-*L*-leucyl)-4-((4-methylphenyl)sulfonamido)piperidin-3-yl)-*L*-prolinate [18]



To a stirred solution of **17** (640 mg, 0.894 mmol, 1 eq.) in dry DMF (10 mL) piperidine (2 mL, 20% vol in DMF) was added. The reaction was let under stirring 2 h and then the volatile were removed under reduced pressure. The crude free amine was kept aside without further purification before peptidic coupling. Meanwhile, to a solution of *L*-Fmoc-NH-Ile-OH (632 mg, 1.79 mmol, 2 eq.) in dry DMF at 0°C HBTU (678 mg, 1.79 mmol, 2 eq.) and HOBt (243 mg, 1.79 mmol, 2 eq.) were added. At this time, a solution of the previous free amine (442 mg, 0.894 mmol, 1 eq.) in dry DMF and DIPEA (0.63 mL, 3.58 mmol, 4 eq.) was added at 0°C. The reaction was stirred overnight under argon atmosphere at room temperature. After concentration under reduced pressure, the remaining crude oil was taken up with EtOAc, and washed successively with distilled water, 100% aqueous solution of NaHCO_3 and brine. The organic layer was dried over Na_2SO_4 , filtered and the volatile was removed under reduced pressure. The crude residue obtained was purified by column chromatography on silica gel eluting with *c*-Hex/EtOAc 6:4 to afford **18** as a white powder. (590 mg, 0.702 mmol, 79%).

Molecular weight = 829.41 g mol^{-1}

R_f = 0.2 (*c*-Hex/EtOAc 6:4)

HRMS: Calcd. for $[\text{C}_{45}\text{H}_{59}\text{N}_5\text{O}_8\text{S} + \text{H}]^+$: m/z 830.4163, found: 830.4171

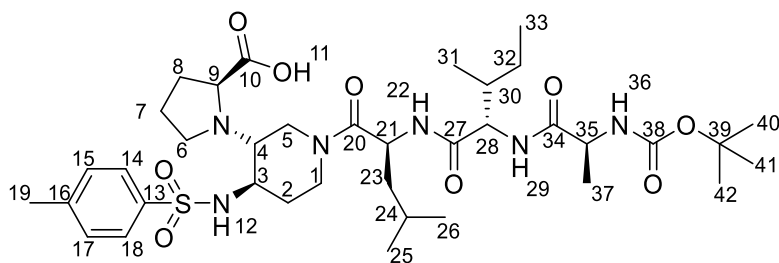
$^1\text{H NMR}$ (CDCl_3 , 300 MHz): δ 7.84-7.81 (4H, m, H14, H18, H38, H47); 7.60 (2H, m, H40, H45); 7.39 (2H, m, H41, H44); 7.34-7.24 (4H, m, H15, H17, H39, H47); 6.99 (1H, bs, NH12); 6.47 (1H,

bs, NH29); 5.38 (1H, bs, NH22); 4.93 (1H, m, H36); 4.65 (1H, m, H21); 4.43 (2H, m, H6); 4.25 (2H, m, H35); 4.06 (1H, m, H28); 3.78 (1H, m, H9); 3.58 (3H, s, H11); 3.55 (1H, m, H4); 3.10-2.80 (3H, m, H3, H8); 2.42 (2H, m, H5); 2.60-2.35 (6H, m, H1, H19, H30); 1.83 (2H, m, H2); 1.54 (4H, m, H7, H32); 1.43 (3H, m, H23, H24); 0.97 (3H, s, H31); 0.89 (9H, m, H25, H26, H33) ppm
 $^{13}\text{C NMR}$ (CDCl_3 , 300 MHz): δ 170.8 (C10); 165.4 (C21); 161.4 (C27); 156.3 (C34); 141.4 (C16); 141.3 (C42, C43); 129.7 (C14, C18); 127.8 (C13, C41, C44); 127.4 (C15, C17); 127.2 (C39, C46); 125.2 (C40, C45); 120.1 (C38, C47); 67.2 (C35); 61.5 (C28); 59.9 (C1); 53.4 (C3); 52.7 (C9, C11); 52.6 (C4); 48.3 (C36); 47.4 (C21); 42.9 (C8); 41.2 (C23, C6); 40.7 (C7); 37.8 (C5, C30); 25.1 (C2); 25.0 (C32); 24.6 (C24); 21.6 (C25, C26); 15.6 (C19); 14.3 (C31); 11.7 (C33) ppm

Melting point = 104–106°C

IR: 3285 (ν N-H); 2959 (ν C-H); 1722, 1629 (ν C=O); 1523, 1449 (ν C=C); 1213 (ν C-N); 1163 (ν C-O) cm^{-1}

((3R,4R)-1-((tert-butoxycarbonyl)-L-alanyl-L-isoleucyl-L-leucyl)-4-((4-methylphenyl)sulfonamido)piperidin-3-yl)-L-proline [19]



To a solution of **11** (260 mg, 0.33 mmol, 1 eq.) in MeOH (10 mL) NaOH 2M (0.84 mL, 1.65 mmol, 5 eq.) was added. After stirring for 3 h at 60°C, the volatile was removed under reduced pressure and the obtained oil was dissolved in distilled water, acidified until pH 4 with 10% aqueous solution of KHSO_4 . The precipitate which was formed at this time was dissolved in CH_2Cl_2 . The organic layer was separated and let aside. Meanwhile, the aqueous phase was extracted several times with CH_2Cl_2 . The combined organic phase were dried over Na_2SO_4 , filtered and the volatile was removed under vacuum to afford **19** as a white powder (239 mg, 0.31 mmol, 94%).

Molecular weight = 764.97 g mol^{-1}

Rf = 0.3 (EtOAc/MeOH 9:1)

HRMS: Calcd. for $[C_{37}H_{60}N_6O_9S + H]^+$: m/z 765.4221, found: 765.4222; Calcd. for $[C_{37}H_{60}N_6O_9S + Na]^+$: M/z 787.4048, found: 787.4045

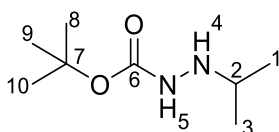
1H NMR (DMSO-*d*₆, 400 MHz): δ 12.55 (1H, bs, OH11); 8.02 (1H, bs, NH22); 7.70 (2H, m, H14, H18); 7.52 (1H, bs, NH29); 7.41 (2H, m, H15, H17); 7.00 (1H, bs, NH36); 4.70 (1H, m, H21); 4.18 (1H, m, H28); 4.17 (1H, m, H5); 3.97 (1H, m, H35); 3.72 (1H, m, H1); 3.41 (1H, m, H9); 3.06 (1H, m, H1); 3.00 (1H, m, H3); 2.73 (1H, m, H5); 2.39 (3H, s, H19); 2.41 (1H, m, H6); 2.26 (1H, m, H4); 2.15 (1H, m, H2); 2.01 (1H, m, H8); 1.85 (1H, m, H6); 1.77 (1H, m, H8); 1.66 (1H, m, H30); 1.56 (1H, m, H24); 1.50 (1H, m, H7); 1.46 (1H, m, H23); 1.37 (9H, s, H40, H41, H42); 1.35 (1H, m, H2); 1.34 (1H, m, H23); 1.29 (1H, m, H32); 1.28 (1H, m, H7); 1.13 (3H, d, $J = 6.9$ Hz, H37); 1.03 (1H, m, H32); 0.86 (3H, m, H26); 0.83 (3H, m, H25); 0.78 (3H, m, H33); 0.77 (3H, m, H31) ppm

^{13}C NMR (DMSO-*d*₆, 100 MHz): δ 176.1 (C10); 171.8 (C34); 169.9 (C27); 169.3 (C20); 154.3 (C38); 142.3 (C16); 136.5 (C13); 129.7 (C15, C17); 126.4 (C14, C18); 77.4 (C39); 61.4 (C9); 58.0 (C4); 56.0 (C28); 52.2 (C3); 49.5 (C35); 46.0 (C21); 44.1 (C6); 43.2 (C1); 40.2 (C23); 39.5 (C5); 36.6 (C30); 32.3 (C2); 29.1 (C8); 27.7 (C40, C41, C42); 23.9 (C24); 23.7 (C32); 23.3 (C7); 22.6 (C25); 21.6 (C26); 20.6 (C19); 17.4 (C37); 14.9 (C31); 10.6 (C33) ppm

Melting point = 144-148°C

IR: 3292 (ν N-H); 2962 (ν C-H); 1636 (ν C=O); 1521, 1450 (ν C=C); 1225 (ν C-N); 1160 (ν C-O); cm^{-1}

***Tert*-butyl 2-isopropylhydrazine-1-carboxylate [20]**



To a stirred solution of *tert*-butylcarbazate (2 g, 15.1 mmol, 1 eq.) in dry THF (20 mL) under argon atmosphere, acetone (3.3 mL, 45.3 mmol, 3 eq.) and acetic acid (1.05 mL, 13.6 mmol, 0.9 eq.) were added. After 3 h, volatile were removed under reduced pressure and the remaining oil was taken up with dry THF (100 mL). To this solution, under argon atmosphere, $NaBH_3CN$ (1.56 g, 22.7 mmol, 1.5 eq.) was added with some seeds of bromocresol green. At that time, a solution of 4-toluene-sulfonic acid (2.86 g, 16.6 mmol, 1.1 eq.) in dry THF (4 mL) was added dropwise and the mixture became yellow. After 1 h the volatile were removed under reduced pressure. The remaining powder was dissolved in a mixture of EtOAc and brine and then taken up again with

CH₂Cl₂. The organic layer was washed with a mixture of 10% aqueous solution of NaCl/NaHCO₃ 1/1, dried over Na₂SO₄, filtered, and concentrated under reduced pressure. The crude material obtained was then dissolved in MeOH (10 mL) and NaOH 1 M (18 mL, 18.1 mmol, 1.2 eq.) was added. After stirring for 1 h at room temperature, volatile was removed under reduced pressure and the crude oil obtained was taken up with EtOAc, washed with brine, dried over Na₂SO₄ and filtered. After concentration under reduced pressure, the residue obtained was purified by column chromatography on silica gel eluting with CH₂Cl₂/MeOH 98:2 to yield **20** (1.37 g, 7.86 mmol, 52%) as an oil that crystallized in the fridge.

Molecular weight = 174.24 g mol⁻¹

R_f = 0.5 (CH₂Cl₂/MeOH 98:2)

HRMS: Calcd. for [C₈H₁₈N₂O₂ + Na]⁺: m/z 197.1266, found: 197.1266

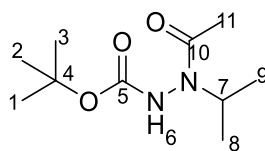
¹H NMR (CDCl₃, 300 MHz): δ 5.31 (2H, bs, NH₄, NH₅); 3.28 (1H, m, H₂); 1.47 (9H, s, H₈, H₉, H₁₀); 1.12 (6H, d, *J* = 6.4 Hz, H₁, H₃) ppm

¹³C NMR (CDCl₃, 75 MHz): δ 156.9 (C₆); 80.3 (C₇); 50.8 (C₂); 28.3 (C₈, C₉, C₁₀); 20.6 (C₁, C₃) ppm

Melting point = 177-179°C

IR: 3197 (ν N-H); 2988, 2938, 2901 (ν C-H); 1737 (ν C=O); 1340, 1320 (ν CH₃); 1199, 1149 (ν C-N, ν C-C(O)) cm⁻¹

***Tert*-butyl 2-acetyl-2-isopropylhydrazine-1-carboxylate [21]**



To a solution of **20** (1.37 g, 7.86 mmol, 1 eq.) in dry THF was added under argon atmosphere acetic anhydride (4.4 mL, 47.16 mmol, 6 eq.). The reaction was stirred overnight at 60°C. After removal of the volatile under reduced pressure, the crude residue was purified by column chromatography on silica gel eluting with CH₂Cl₂/MeOH 98:2 to yield **21** (1.63 g, 7.53 mmol, 96%) as a white powder.

Molecular weight = 216.28 g mol⁻¹

R_f = 0.4 (CH₂Cl₂/MeOH 98:2)

HRMS: Calcd. for $[C_{10}H_{20}N_2O_3 + H]^+$: m/z 217.1552, found: 217.1549; Calcd. for $[C_{10}H_{20}N_2O_3 + Na]^+$: M/z 239.1372, found: 239.1374

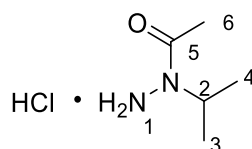
1H NMR ($CDCl_3$, 400 MHz): δ 6.47 (1H, bs, NH6); 4.80 (1H, m, H7); 2.05 (3H, s, H11); 1.48 (9H, s, H1, H2, H3); 1.09 (6H, d, $J = 6.8$ Hz, H8, H19) ppm

^{13}C NMR ($CDCl_3$, 100 MHz): δ 173.4 (C10); 155.2 (C5); 82.2 (C4); 47.6 (C7); 28.7 (C1, C2, C3); 21.6 (C11); 19.8 (C8, C9) ppm

Melting point = 79-81°C

IR: 3255 (ν N-H); 2979 (ν C-H); 1738 (ν C=O); 1411 (ν , N-H); 1367 (ν , C-H); 1242 (ν C-N); 1158 (ν C-O) cm^{-1}

***N*-isopropylacetohydrazide hydrochloride [22]**



To a solution of **21** (0.58 g, 2.69 mmol, 1 eq.) in dioxane under argon atmosphere, HCl 4 M in dioxane (20 mL, 80.6 mmol, 30 eq) was added at 0°C. After stirring overnight at room temperature, a precipitate appeared. The solvent was removed with a Pasteur pipette, and the white solid obtained was washed carefully with diethyl ether twice, dried under reduced pressure to afford the hydrochloride salt **22** (0.411 g, 2.69 mmol, quant.) as a white powder.

Molecular weight = 152.62 $g\ mol^{-1}$; free amine = 116.16 $g\ mol^{-1}$

R_f = 0 ($CH_2Cl_2/MeOH$ 98/2)

HRMS: Calcd. for $[C_5H_{12}N_2O + H]^+$: m/z 117.1028, found: 117.1023

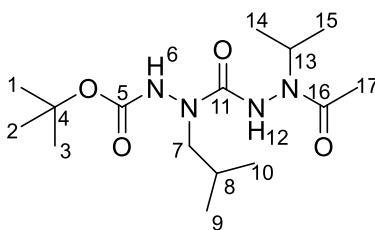
1H NMR (CD_3OD , 400 MHz): δ 4.51 (1H, m, H2); 2.24 (3H, s, H6); 1.33 (6H, d, $J = 6.8$ Hz, H3, H4)

^{13}C NMR (CD_3OD , 100 MHz): δ 52.3 (C2); 20.3 (C6); 19.8 (C3, C4) ppm

Melting point = 174-176°C

IR: 3359 (ν N-H); 2993 (ν C-H); 1657 (ν C=O); 1371 (ν C-N) 1157 (ν C-O) cm^{-1}

Tert-butyl 2-(2-acetyl-2-isopropylhydrazine-1-carbonyl)-2-isobutylhydrazine-1-carboxylate [23]



To a stirred solution of **22** (142 mg, 0.93 mmol, 1.2 eq.) in dry CH₂Cl₂ under argon atmosphere at 0°C, pyridine (0.34 mL, 4.22 mmol, 6 eq.) was added. After a period 10 min, 4-nitrophenyl chloroformate (184 mg, 0.92 mmol, 1.3 eq.) in dry CH₂Cl₂ (0.5 mL) was added dropwise. The reaction was stirred overnight at room temperature and the volatile were then removed under reduced pressure. To the crude residue, dissolved in dry DMF (2 mL), a solution of **azaLeu** (132 mg, 0.71 mmol, 1.0 eq.) in dry DMF (0.7 mL) and DMAP (129.2 mg, 1.05 mmol, 1.5 eq.) were added under argon atmosphere. After stirring overnight at 40°C and concentration under reduced pressure, the crude residue afforded was purified by column chromatography on silica gel eluting with EtOAc to yield **23** (170 mg, 0.52 mmol, 74%) as a white powder.

Molecular weight = 330.42 g mol⁻¹

R_f = 0.4 (EtOAc)

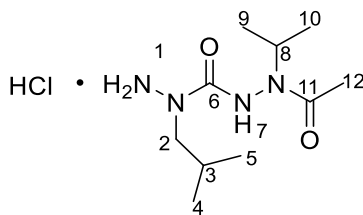
HRMS: Calcd. for [C₁₅H₃₀N₄O₄ + Na]⁺: M/z 353.2165, found: 353.2174

¹H NMR (CDCl₃, 400 MHz): δ 7.47 (1H, bs, NH6); 6.94 (1H, bs, NH12); 4.72 (1H, m, H13); 2.09 (3H, s, H17); 1.80 (1H, m, H8); 1.43 (9H, s, H1, H2, H3); 1.01 (6H, m, H14, H15); 0.84 (6H, m, H9, H10) ppm

¹³C NMR (CDCl₃, 100 MHz): δ 173.2 (C11); 169.7 (C16); 156.7 (C5); 82.7 (C4); 55.8 (C7); 47.0 (C17); 27.9 (C1, C2, C3); 26.12(C8); 21.0 (19); 19.7 (C9, C10); 18.8 (C14, C15) ppm

Melting point = 79-81°C

***N'*-Acetyl-*N*-isobutyl-*N'*-isopropylmethanedihydrazide hydrochloride [24]**



To a solution **23** (305 mg, 0.93 mmol, 1 eq.) in dioxane under argon atmosphere HCl 4 M in dioxane (9.3 mL, 37.2 mmol, 40 eq) was added at 0°C. The mixture was stirred 3 h at room temperature. After removal of the volatile under reduced pressure, the hydrochloride salt **24** (248 mg, 0.93 mmol, quant.) was afforded as a white powder.

Molecular weight = 266.77 g mol⁻¹; free amine = 230:31 g mol⁻¹

R_f = 0 (EtOAc)

HRMS: Calcd. for [C₁₀H₂₂N₄O₂ + H]⁺: m/z 231.1821, found: 231.1818; Calcd. for [C₁₀H₂₂N₄O₂ + Na]⁺: m/z 253.1640, found: 253.1631

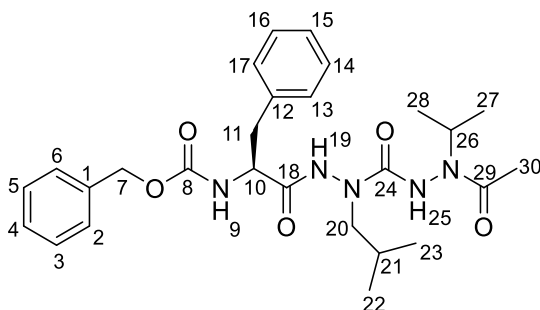
¹H NMR (CD₃OD, 400 MHz): δ 4.74 (1H, m, H8); 3.70 (2H, m, H2); 2.16 (3H, s, H12); 2.06 (1H, m, H3); 1.17 (6H, m, H9, H10); 1.00 (3H, m, H4, H5) 0.92 (3H, m, H4, H5) ppm

¹³C NMR (CD₃OD, 100 MHz): δ 173.3 (C6), 170.2 (C11); 54.7 (C2); 49.0 (C8); 27.4 (C3); 20.7 (C12); 19.8 (C4, C5); 19.5 (C9, C10) ppm

Melting point = 72-74°C

IR: 3186 (ν N-H); 2962 (ν C-H); 1685 (ν C=O); 1529 (ν N-H); 1468 (ν C-H); 1282 (ν C-N) cm⁻¹

Benzyl (*S*)-(1-(2-(2-acetyl-2-isopropylhydrazine-1-carbonyl)-2-isobutylhydrazinyl)-1-oxo-3-phenylpropan-2-yl)carbamate [25]



To a solution of *L*-Cbz-NH-Phe-OH (154 mg, 0.514 mmol, 1 eq.) in dry DMF, HBTU (399 mg, 1.03 mmol, 2 eq.) and HOBt (139 mg, 1.03 mmol, 2 eq.) were successively added at 0°C. The reaction mixture was stirred for 40 min at 0°C under argon atmosphere. At this moment, a solution of compound **24** (137 mg, 0.514 mmol, 1 eq.) and DIPEA (0.54 mL, 3.08 mmol, 6 eq.) in dry DMF was added dropwise. The reaction was let stirring for 2 days at room temperature under argon atmosphere. The volatile was removed under reduced pressure and the crude oil taken up with EtOAc, washed with distilled water, 100% aqueous solution of NaHCO₃ and brine, dried over Na₂SO₄, filtered and concentrated under vacuum. The crude residue obtained was purified by column chromatography on silica gel eluting with *c*-Hex/EtOAc 7:3 to afford **25** (110 mg, 0.215 mmol, 42%) as a white powder.

Molecular weight = 511.62 g mol⁻¹

R_f = 0.4 (*c*-Hex/EtOAc 3:7)

HRMS: Calcd. for [C₂₇H₃₇N₅O₅ + Na]⁺: m/z 534.2692, found: 534.2688

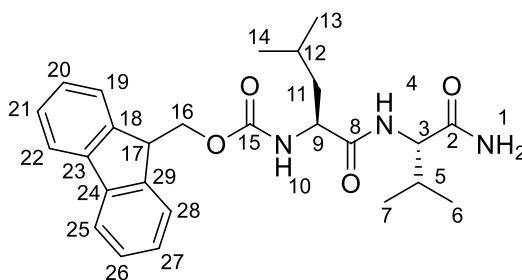
¹H NMR (CD₃OD, 400 MHz): δ 7.37-7.29 (10H, m, H13, H14, H15, H16, H17, H2, H3, H4, H5, H6); 5.11 (2H, m, H7); 4.70 (1H, m, H26); 4.15 (1H, m, H10); 3.34 (1H, m, H20); 3.08 (1H, m, H11); 2.91 (1H, m, H11); 2.45 (1H, m, H20); 1.76 (3H, s, H30); 1.06 (1H, m, H21); 1.03, 1.14 (6H, m, H27, H28); 0.68 (6H, m, H22, H23) ppm

¹³C NMR (CD₃OD, 100 MHz): δ 176.0 (C29); 173.7 (C18); 158.7 (C8); 136.8 (C12); 136.8 (C1); 130.6 (C13, C14, C15, C16, C17); 128.9 (C2, C3, C4, C5, C6); 67.7 (C7); 56.8 (C10); 56.4 (C20); 48.7 (C26); 37.8 (C11); 27.1 (C21); 21.3 (C30); 19.9 (C22, C23); 19.5 (C27, C28) ppm

Melting point = 86-88°C

IR: 3312 (ν N-H); 2926 (ν C-H); 1692 (ν C=O); 1495 (ν N-H); 1351 (ν C-N); 1213 (ν C-O) cm⁻¹

(9H-fluoren-9-yl)methyl((S)-1-(((S)-1-amino-3-methyl-1-oxobutan-2-yl)amino-4-methyl-1-oxopentan-2-yl)carbamate



To a stirred solution of Fmoc-NH-Leu-OH (500 mg, 1.41 mmol, 1.0 eq.) in dry DMF (10 ml) were added successively under argon atmosphere at 0°C, HOBt (209 mg, 1.55 mmol, 1.1 eq.), HBTU (586 mg, 1.55 mmol, 1.1 eq.), DIPEA (0.74 mL, 4.23 mmol, 3.0 eq.) and *L*-Valinamide hydrochloride (215 mg, 1.41 mmol, 1.0 eq.). The reaction mixture was stirred overnight at room temperature. After filtration of the suspension formed, the solid obtained was dried to yield **Fmoc-NH-Leu-Val-CONH₂** (620 mg, 1.37 mmol, 97%).as a white powder.

Molecular weight = 451.57 g mol⁻¹

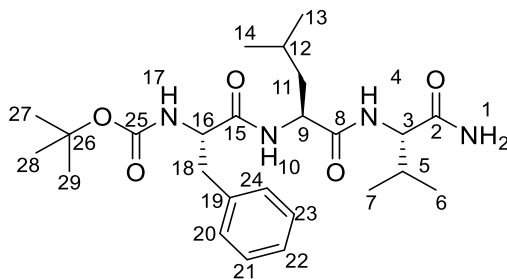
R_f = 0.5 (EtOAc)

HRMS: Calcd. for [C₂₆H₃₃N₃O₄ + H]⁺: m/z 452.2505, found: 452.2731

¹H NMR (DMSO-*d*₆, 400 MHz): δ 8.00-7.25 (10H, m, H1, H18, H20, H21, H22, H25, H26, H27, H28); 7.60 (1H, m, NH4); 7.07 (1H, bs, NH10); 4.34 (2H, m, H16); 4.26 (1H, m, H17); 4.18-4.07 (2H, m, H3, H9); 1.96 (1H, m, H5); 1.62 (1H, m, H12); 1.49 (2H, m, H11); 0.98-0.84 (12H, m, H6, H7, H13, H14) ppm

¹³C NMR (DMSO-*d*₆, 100 MHz): δ 173.4 (C2); 144.6 (C18, C29); 141.6 (C23, C24); 128.5 (C21, C26); 128.0 (C22, C25); 126.1 (C20, C27); 120.9 (C19, C28); 66.3 (C16); 57.9 (C3); 54.3 (C9); 47.7 (C17); 41.6 (C11); 31.7 (C5); 25.1 (C12); 24.0 (C13), 22.3 (C14); 20.1 (C6); 18.8 (C7) ppm

***tert*-butyl ((*S*)-1-(((*S*)-1-(((*S*)-1-amino-3-methyl-1-oxobutan-2-yl)amino)-4-methyl-1-oxopentan-2-yl)amino)-1-oxo-3-phenylpropan-2-yl)carbamate**



To a solution of **Fmoc-NH-Leu-Val-CONH₂** (600 mg, 1.33 mmol, 1.0 eq.) in dry DMF (10 mL) piperidine (12 mL, 20% v/DMF) was added. The solution was let under stirring for 3h and then the volatile was then removed under reduced pressure to afford the crude free amine which was used for the following coupling reaction without further purification. Precisely, to a solution of this crude free amine in DMF (10mL), under argon atmosphere and cooled to 0°C HOBt (360 mg, 2.66 mmol, 2.0 eq.), HBTU (1.0 g, 2.66 mmol, 2.0 eq.), DIPEA (0.93 mL, 5.32 mmol, 4.0 eq.) and *L*-

Boc-NH-Phe-OH (706 mg, 2.66 mmol, 2.0 eq) were successively added. The reaction mixture was stirred at room temperature overnight. The volatile was removed under reduced pressure and after addition of EtOAc to the crude residue, **Boc-NH-Phe-Leu-Val-CONH₂** precipitated as a white solid (550 mg, 1.16 mmol, 87%).

Molecular weight = 476.62 g mol⁻¹

R_f = 0.7 (EtOAc)

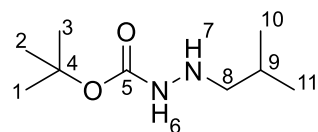
HRMS: Calcd. for [C₂₅H₄₀N₄O₅ + H]⁺: m/z 477.3032, found: 477.3034; Calcd. for [C₂₅H₄₀N₄O₅ + NH₄]⁺: M/z 494.2999, found: 494.3334

¹H NMR (DMSO-*d*₆, 400 MHz): δ 8.07 (1H, d, *J* = 8.2 Hz, NH10); 7.68 (1H, d, *J* = 8.8 Hz, NH4); 7.38 (1H, bs, NH1); 7.30, 7.29 (4H, s, H20, H21, H23, H24); 7.21 (1H, m, H22); 7.07 (1H, bs, NH1); 6.98 (1H, d, *J* = 8.81 Hz, NH17); 4.41 (1H, m, H9); 4.24-4.11 (2H, m, H3, H16); 2.99 (1H, dd, *J* = 13.8, 3.8 Hz, H18); 2.77 (1H, dd, *J* = 13.8, 10.6 Hz, H18); 1.98 (1H, m, H5); 1.68 (1H, m, H12); 1.52 (2H, m, H11), 1.33 (9H, s, H27, H28, H29); 0.98-0.82 (12H, m, H6, H7, H13, H14) ppm

¹³C NMR (DMSO-*d*₆, 100 MHz): δ 173.6 (C2, C15); 172.5 (C8); 139.2 (C19); 130.1, 128.9 (C20, C21, C23, C24); 127.0 (C22); 79.1 (C26); 58.1 (C3); 56.6 (C9); 52.0 (C16); 41.7 (C11); 38.0 (C18); 31.6 (C5); 29.0 (C27, C28, C29); 25.0 (C12); 24.1, 22.5 (C13, C14); 20.2, 18.8 (C6, C7) ppm

IR: 3312 (ν N-H); 2966 (ν C-H); 1692-1676 (ν C=O); 1632-1531 (ν C=C) cm⁻¹

***Tert*-butyl 2-isobutylhydrazine-1-carboxylate [azaLeu]**



To a solution of *tert*-butylcarbazate (1 g, 7.6 mmol, 1 eq.) in dry THF (15 mL), under argon atmosphere isobutyraldehyde (1.0 mL, 11.4 mmol, 1.5 eq.) and acetic acid (0.524 mL, 6.81 mmol, 0.9 eq.) were successively added. After 5 h, the volatile were removed under reduced pressure and the crude oil was dissolved in dry THF (15 mL). At that time, NaBH₃CN (0.714 g, 11.4 mmol, 1.5 eq.) and acetic acid (0.866 mL, 15.1 mmol, 2 eq.) were added. The mixture was let under stirring overnight. The volatile was removed under reduced pressure. The remaining powder was dissolved in a mixture of EtOAc and brine and then taken up again with EtOAc. The organic layer was washed with a mixture of 10% aqueous solution of NaCl/NaHCO₃ 1/1, dried over Na₂SO₄, filtered,

and concentrated under reduced pressure. The crude residue obtained was then dissolved in MeOH (10 mL) and NaOH 1 M (9 mL, 9 mmol, 1.2 eq.) was added. The solution was let 1 h at room temperature under stirring. After removal of the volatile under reduced pressure, the obtained oil was taken up with EtOAc, washed with brine, dried over Na₂SO₄ and filtered. After concentration under reduced pressure, the residue obtained was purified by column chromatography on silica gel eluting with CH₂Cl₂ to afford **azaLeu** (0.95 g, 5.1 mmol, 67%) as a colorless oil.

Molecular weight = 188.15 g mol⁻¹

R_f = 0.11 (CH₂Cl₂)

HRMS: Calcd. for [C₉H₂₀N₂O₂ + H]⁺: m/z 189.1603, found: 189.1600

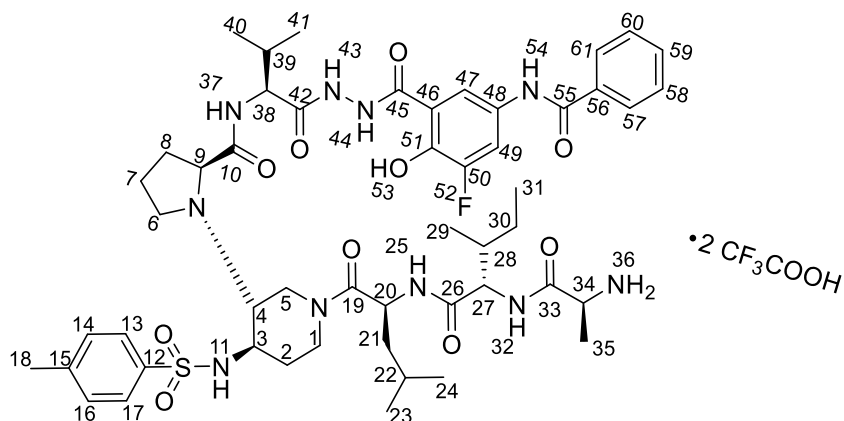
¹H NMR (CDCl₃, 300 MHz): δ 7.3 (1H, bs, NH6); 5.25 (1H, bs, NH7); 2.65 (2H, d, *J* = 6.8 Hz, H8); 1.73 (1H, m, H9); 1.44 (9H, s, H1, H2, H3); 0.91 (6H, d, *J* = 6.7 Hz, H10, H11) ppm

¹³C NMR (CDCl₃, 75 MHz): δ 157.3 (C5); 81.0 (C4); 60.4 (C8); 28.8 (C1, C2, C3); 27.1 (C9); 21.1 (C10, C11) ppm

IR: 3312 (ν N-H); 2920 (ν C-H); 1719 (ν C=O); 1259 (ν C-N) 1157 (ν C-O) cm⁻¹

Compounds chapter 4

Compound [4.6]



To a stirred solution of **4.35** (31 mg, 0.023 mmol, 1.0 eq.) in dioxane (1.5mL) under argon atmosphere, at 0°C, HCl 4M in dioxane (50 μL, 0.23 mmol, 10.0 eq.) was added. The reaction was let stirring 6 h at room temperature. After removal of the volatile under reduced pressure, the hydrochloride salt was dissolved in MeOH (1mL) and LiOH (2.41 mg, 0.058 mmol, 2.5 eq.) was added. The reaction mixture was let stirring at room temperature for 5 h, concentrated under reduced pressure and purified by preparative HPLC eluting with H₂O + 0.2% TFA/CH₃CN

(gradient 30 to 60% in 15 min), on an Xselect column (4.6x150mm-5 μ m) to afford the hydrochloride salt **4.6** (5.6 mg, 0.021 mmol, 27%) as a pale pink powder.

Molecular weight = 1262.49 g mol⁻¹; free amine = 1034.51 g mol⁻¹

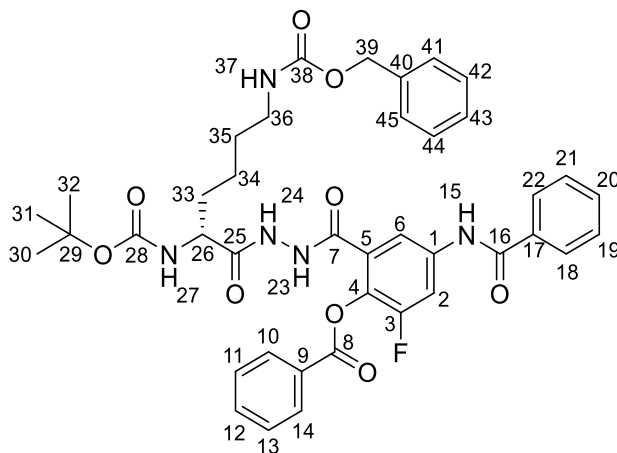
R_f = 0 (c-Hex /EtOAc 6:4)

HRMS: Calcd. for [C₅₁H₇₁FN₁₀O₁₀S + H]⁺: m/z 1035.5093, found: 1035.5097 g mol⁻¹

¹H NMR (CD₃OH, 600 MHz, 313K): two conformers δ 10.75-10.43 (2H, m, NH54, NH43); 10.13 (1H, d, *J* = 28.8 Hz, NH44); 8.65 (0.5H, d, *J* = 8.9 Hz, NH37); 8.58 (0.5H, bs, NH37); 8.22 (0.5H, d, *J* = 7.7 Hz, NH37); 8.15 (1H, bs, NH25); 8.08 (0.5H, bs, NH32); 8.02 (0.5, bs, H49); 7.99-7.86 (2.5H, m, H61, H57, H49); 7.80 (2H, m, H17, H13); 7.73 (1H, m, H47); 7.58 (1H, m, H59); 7.50 (2H, m, H60, H58); 7.34 (2H, m, H16, H14); 7.29 (1H, m, NH11); 4.85 (0.5H, m, H20); 4.80 (0.5H, m, H20); 4.47 (1H, m, H5); 4.33-4.14 (2H, m, H27, H5, H1); 4.45 (0.5H, m, H38); 4.42-4.32 (1.5H, m, H38, H9); 4.07 (0.5H, bs, H34); 3.96 (0.5H, bs, H34); 3.82 (0.5H, d, *J* = 15.8 Hz, H1); 3.66-3.48 (1 H, m, H3); 3.31 (0.5H, m, H5); 3.20-3.08 (3.5H, m, H6, H1); 2.81 (1H, m, H4); 2.55 (0.5H, m, H1); 2.44-2.15 (2H, m, H39, H7); 2.38 (3H, s, H18); 1.97 (1H, bs, H7); 1.91-1.63 (3H, m, H28, H8); 1.63-1.11 (9.5H, m, H35, H30, H22, H21, H2); 1.11-0.96 (6.5H, m, H41, H40, H30); 0.96-0.67 (12H, m, H31, H29, H24, H23) ppm (OH53, NH36 undetected)

¹³C NMR (CD₃OH, 600 MHz, 313K): two conformers δ 169.7 (C33); 167.5 (C55); 164.8 (C_qfluorinated ring); 143.6 (C_qfluorinated ring); 142.6 (C_qfluorinated ring); 137.7 (C59); 134.6 (C56); 128.3 (C60, C58); 127.3 (C61, C57); 117.4 (C49); 116.8 (C49); 113.6 (C47); 60.5 (C4); 57.9 (C27); 57.3 (C38); 53.9 (C3); 53.7 (C9); 49.2 (C34); 48.9 (C34); 47.4 (C20); 47.0 (C20); 43.9 (C5); 43.8 (C1); 41.2 (C1); 40.8 (C21); 40.2 (C21, C6); 39.7 (C5); 37.0 (C28); 36.6 (C28); 31.7 (C2); 30.7 (C7); 30.6 (C39); 29.3 (C2); 24.7 (C30); 24.5 (C22, C8); 22.1 (C23); 21.7 (C24); 21.1 (C24); 20.7 (C23); 20.2 (C18); 18.6 (C41, C40); 17.7 (C41, C40); 16.6 (C35); 14.5 (C29); 9.9 (31) ppm (C45, C42, C26, C19, C10, undetected)

(S)-4-benzamido-2-(2-(6-(((benzyloxy)carbonyl)amino)-2-((tert-butoxycarbonyl)-amino)hexanoyl)hydrazinecarbonyl)-6-fluorophenyl benzoate [4.7]



To a solution of **4.23** (50 mg, 0.10 mmol, 1.0 eq.) in dry dioxane (5 mL) under argon atmosphere, at 0°C, HCl 4M in dioxane (1.52 mL, 6.1 mmol, 60.0 eq.) was added. The reaction was let stirring 4 h at room temperature. After evaporation of the volatile under reduced pressure, the obtained hydrochloride salt was used in the following peptide coupling reaction step without further purification. Precisely, the hydrochloride salt was dissolved in dry DMF (2 mL) under argon atmosphere, the solution was cooled to 0°C and then *L*-Boc-NH-Lys(Z)-OH (42.2 mg, 0.11 mmol, 1.1 eq.), COMU (42.8 mg, 0.10 mmol, 1.0 eq.), Oxyma (18.0 mg, 0.10 mmol, 1.0 eq.), NMM (22.0 μ L, 0.20 mmol, 2.0 eq.) were added at the same time. The reaction mixture was let stirring overnight at room temperature. After concentration under reduced pressure, the crude residue obtained was taken up with EtOAc and successively washed with 10% aqueous solution of KHSO₄, 100% aqueous solution of NaHCO₃ and brine. The organic phase was then dried over Na₂SO₄, filtered and concentrated under reduced pressure. The crude residue obtained was purified by column chromatography on silica gel eluting with *c*-Hex/EtOAc 7:3 to afford **4.7** as a white solid (34 mg, 0.045 mmol, 45%).

Molecular weight = 755.80 g mol⁻¹

R_f = 0.4 (*c*-Hex/EtOAc 4:6)

HRMS: Calcd. for [C₄₀H₄₂FN₅O₉ + Na]⁺: m/z 778.2864, found: 778.2866

¹H NMR (DMSO-*d*₆, 300 MHz): δ 10.68 (1H, s, NH15); 10.41 (1H, s, NH23); 10.0 (1H, s, NH24); 8.11 (1H, d, J = 7.6 Hz, H2); 7.92 (1H, d, J = 7.6 Hz, H6); 7.99, 7.64, 7.60 (5H, m, H22, H21,

with EtOAc and successively washed with 10% aqueous solution of KHSO₄, 100% aqueous solution of NaHCO₃ and brine. The organic phase was then dried over Na₂SO₄, filtered and concentrated under reduced pressure. The crude residue obtained was purified by column chromatography on silica gel eluting with CH₂Cl₂/EtOAc 9:1 to afford compound **4.8** as a white solid (140 mg, 0.24 mmol, 40%).

Molecular weight = 592.62 g mol⁻¹

R_f = 0.6 (CH₂Cl₂/EtOAc 7:3)

HRMS: Calcd. for [C₃₁H₃₃FN₄O₇ + H]⁺: m/z 593.2367, found: 593.2397

¹H NMR (DMSO-*d*₆, 400 MHz): δ 10.70 (1H, s, NH₁₅); 10.42 (1H, s, NH₂₃); 10.05 (1H, s, NH₂₄); 8.21-8.12 (3H, m, H₂, H₁₀, H₁₄); 8.04 (2H, m, H₁₈, H₂₂); 7.96 (1H, s, H₆); 7.80 (1H, m, H₁₂); 7.72-7.55 (5H, m, H₁₁, H₁₃, H₁₉, H₂₀, H₂₁); 6.69 (1H, d, *J* = 8.8 Hz, NH₂₇); 3.90 (1H, t, *J* = 8.1 Hz, H₂₆); 1.96 (1H, m, H₃₃); 1.40 (9H, s, H₃₀, H₃₁, H₃₂); 0.92 (3H, d, *J* = 6.8 Hz, H₃₄); 0.88 (3H, d, *J* = 6.7 Hz, H₃₅) ppm

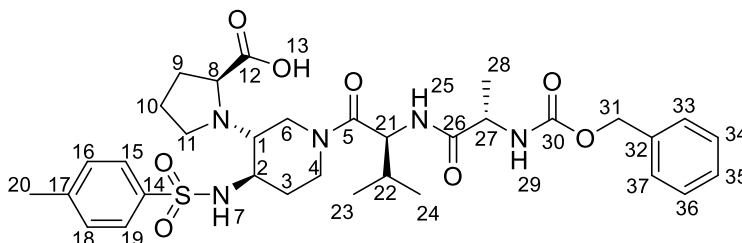
¹³C NMR (DMSO-*d*₆, 100 MHz): δ 171. (C₂₅); 166.9 (C₁₆); 164.4 (C₈); 164.1 (C₇); 156.2, 155.7 (C_q_{benzoyl}); 153.7 (C₂₈); 138.8 (*J*_{C-F} = 227.3 Hz, C₃); 135.2 (C₁₂); 135.1 (C₄); 132.8 (C₂₀); 131.7, 129.8 (C₁, C₅); 131.1 (C₁₀, C₁₄); 129.5 (C₁₁); 128.8 (C₁₉, C₂₁); 128.7 (C₁₈, C₂₂); 116.8 (C₆); 110.8 (*J*_{C-F} = 24.0 Hz, C₂); 78.8 (C₂₉); 59.1 (C₂₆); 31.5 (C₃₃); 29.1 (C₃₀, C₃₁, C₃₂); 20.0 (C₃₄); 19.1 (C₃₅) ppm

¹⁹F NMR (DMSO-*d*₆, 376 MHz): δ -126.65 ppm

Melting point = 90-92°C

IR: 3294 (ν N-H); 3252 (ν C-H); 2961 (ν C-H); 1755-1687-1671 (ν N-H); 1593 (δ N-H); 153-1473 (ν C=C); 1299 (ν C-O) cm⁻¹

(S)-1-((3R,4R)-1-((S)-2-(((benzyloxy)carbonyl)amino)propanamido)-3-methylbutanoyl)-4-(4-methylphenylsulfonamido)piperidin-3-yl)pyrrolidine-2-carboxylic acid [4.10]



Compound **4.27** (150 mg, 0.22 mmol, 1.0 eq.) was dissolved in MeOH (8.0 mL) and NaOH 2 M (0.6 mL, 1.1 mmol, 5.0 eq.) was added dropwise to the solution. The reaction was stirred at 60°C for 2 h. The solvent was evaporated and the solid obtained was solubilized in water. The mixture was acidified with 10 % solution of KHSO₄ until pH = 2-3. A part of the product was extracted from the water phase with EtOAc and an another part of the desired compound was recuperated by solving the solid residue of the water phase with MeOH. The two combined organic phases were dried over Na₂SO₄ and concentrated under vacuum to yield compound **4.10** (134 mg, 0.20 mmol, Yield 91 %) as a white solid.

Molecular weight = 671.80 g mol⁻¹

R_f = 0 (Cyclo/EtOAc 6:4)

HRMS: Calcd. for [C₃₃H₄₅N₅O₈S + H]⁺: M/z 672.3067, found: 672.3065

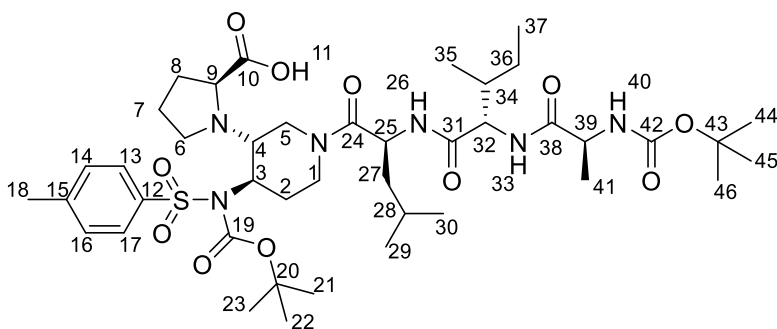
¹H NMR (DMSO-*d*₆, 400 MHz): δ 7.75 (1H, bp, NH25); 7.72 (2H, m, H15, H19); 7.41 (2H, m, H16, H18); 7.35, 7.23 (5H, m, H33, H34, H35, H36, H37); 7.23 (1H, bp, NH29); 7.02 (1H, bp, NH7); 5.01 (2H, s, H31); 4.48 (1H, m, H21); 4.24 (1H, m, H6); 4.07 (1H, m, H27); 4.03 (1H, m, H4); 3.42 (1H, m, H8); 3.10 (1H, m, H4); 3.01 (1H, m, H2); 2.75 (1H, m, H6); 2.40 (1H, m, H11); 2.38 (3H, s, H20); 2.26 (1H, m, H1); 2.12 (1H, m, H9); 2.03 (1H, m, H3); 1.92 (1H, m, H22); 1.89 (1H, m, H11); 1.74 (1H, m, H3); 1.50 (1H, m, H10); 1.30 (1H, m, H9); 1.24 (1H, m, H10); 1.15 (3H, s, H28); 0.81, 0.78 (6H, m, H23, H24) ppm

¹³C NMR (DMSO-*d*₆, 100 MHz): δ 176.6 (C12); 172.2 (C26); 171.9 (C5); 155.6 (C30); 142.6 (C17); 137.1 (C14); 136.9 (C32); 129.2 (C16, C18); 127.7, 126.3 (C33, C34, C35, C36, C37); 126.4 (C15, C19); 65.1 (C31); 61.8 (C8); 58.3 (C1); 52.7 (C21); 52.3 (C2); 49.7 (C27); 44.4 (C11); 43.8 (C4); 39.5 (C6); 32.5 (C9); 29.9 (C22); 29.3 (C3); 23.6 (C10); 20.7 (C20); 19.2; 17.8 (C23, C24); 18.1 (C28) ppm

Melting point = 163–165°C

IR: 3302 (ν N-H; ν O-H); 2962, 2927, 2874 (ν C-H); 1712, 1631 (ν C=O); 1524 (δ N-H); 1452 (ν C=C); 1331, 1226 (δ C-O-H, ν C-O); 1185 (ν C-N) cm⁻¹

((3*R*,4*R*)-4-((*N*-(*tert*-butoxycarbonyl)-4-methylphenyl)sulfonamido)-1-((*tert*-butoxycarbonyl)-*L*-alanyl-*L*-isoleucyl-*L*-leucyl)piperidin-3-yl)-*L*-proline [4.11]



To a solution of **4.28** (250 mg, 0.28 mmol, 1.0 eq.) in MeOH (3 mLmmol, 5 eq.) was added NaOH 2M (0.71 mL, 1.42 mmol, 5 eq.). The reaction was stirred for 3 h at 40°C and the volatile was then removed under reduced pressure. The crude oil obtained was dissolved in distilled water, acidified until pH 4 with 10% aqueous solution of KHSO₄. The precipitate which appeared was immediately dissolved in EtOAc and extracted from the aqueous phase with EtOAc. The organic layer was dried over Na₂SO₄, filtered and the volatile was removed under vacuum to afford **4.11** as a white powder (219 mg, 0.25 mmol, 90%).

Molecular weight = 865.10 g mol⁻¹

R_f = 0.3 (c-Hex/EtOAc 7:3)

HRMS: Calcd. for [C₄₂H₆₈N₆O₁₁S + H]⁺: m/z 865.4700, found: 865.4749

¹H NMR (DMSO-*d*₆, 400 MHz): δ 11.95 (1H, bs, H11); 8.12 (1H, d, *J* = 8.1 Hz, NH26); 8.05 (2H, d, *J* = 8.0 Hz, H17, H13); 7.56 (1H, d, *J* = 8.6 Hz, NH33); 7.41 (2H, d, *J* = 8.0 Hz, H16, H14); 7.05 (1H, d, *J* = 7.1 Hz, NH40); 4.76 (1H, m, H25); 4.62 (1H, m, H3); 4.50 (2H, d, *J* = 12.0 Hz, H5); 4.38 (2H, d, *J* = 11.4.0 Hz H1); 4.24 (1H, m, H32); 4.01(1H, m, H39); 3.55 (1H, m, H9); 3.50 (1H, m, H4); 3.07 (1H, m, H6); 2.87 (1H, m, H6); 2.43 (3H, s, H18); 2.30 (1H, m, H2); 2.10 (1H, m, H8); 2.01-1.84 (2H, m, H2, H8); 1.82-1.67 (2H, m, H34, H7); 1.62 (1H, m, H28); 1.53 (1H, m, H27); 1.47-1.33 (3H, m, H36, H27); 1.41 (19H, s, H46, H45, H44, H23, H22, H21); 1.19 (3H, m, H41); 1.08 (1H, m, H7); 0.96-0.79 (12H; m, H37, H35, H30, H29) ppm

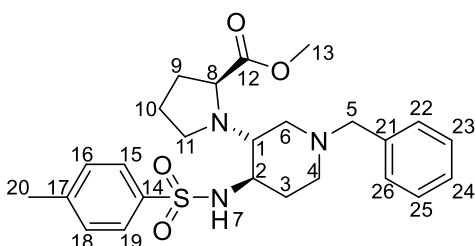
¹³C NMR (DMSO-*d*₆, 100 MHz): δ 176.2 (C10); 173.1 (C24); 171.3 (C38); 170.6 (C31); 155.8 (C42, C19); 144.2 (C15); 139.3 (C12); 130.0 (C16, C14); 127.7 (C17, C13); 79.0 (C43, C20); 62.2 (C9); 57.7 (C3); 56.9 (C32); 56.7 (C4); 50.3 (C39); 47.2 (C25); 46.5 (C6); 41.6 (C27); 40.8 (C5); 37.6 (C34); 30.8 (C2); 30.7 (C8); 28.8 (C41); 25.2 (C36); 25.0 (C7); 24.8 (C28); 23.8 (C37, C35,

C30, C29); 22.9 (C46, C45, C44, C23, C22, C21); 22.1 (C37, C35, C30, C29); 21.7 (C18); 15.9 and 11.7 (C37, C35, C30, C29) ppm

Melting point = 132-133°C

IR: 3286 (ν N-H); 2962 (ν C-H); 1726-1633 (ν C=O); 1519-1453 (ν C=C); 1366 (ν C-N); 1279 (ν C-O) cm⁻¹

Methyl ((3*R*,4*R*)-1-benzyl-4-((4-methylphenyl)sulfonamido)piperidin-3-yl)-*L*-prolinate [4.12]



To a solution of *L*-proline methyl ester hydrochloride (5 g, 30.2 mmol, 1 eq.) in 1,2 dichloroethane (20 mL), triethylamine (4.3 mL, 30.2 mmol, 1 eq.) was added. After 30 min at room temperature, 4-benzylpiperidone (5.6 mL, 30.2 mmol, 1 eq.) was added under argon atmosphere with molecular sieves (3 Å), followed after a period of 45 min by a catalytic amount of InCl₃ (668 mg, 3.02 mmol, 0.1 eq.). The reaction mixture was let stirring 45 min, cooled down to 0°C and a solution of tosyl azide prepared as reported in the literature¹⁹⁷ (5.95 g, 30.2 mmol, 1 eq.) in 1,2 dichloroethane (25 mL) was added dropwise to the mixture while maintaining the temperature at 0°C. After 45 min at room temperature, the mixture became orange and at this moment NaBH(OAc)₃ (16 g, 75.5 mmol, 2.5 eq.) was added and the mixture was let under stirring at room temperature overnight. The reaction mixture was then filtered through a Celite pad with CH₂Cl₂, the filtrated solution was successively washed with distilled water and dried over Na₂SO₄. After concentration under reduced pressure, the expected compound was precipitated with MeOH, filtered, washed with MeOH to yield **4.12** (1.37 g, 2.9 mmol, 15%) as a light pink powder.

Molecular weight = 471.61 g mol⁻¹

R_f = 0.7 (CH₂Cl₂/MeOH 20:1)

HRMS: Calcd. for [C₂₅H₃₃N₃O₄S + H]⁺: m/z 472.2270, found: 472.2262

¹H NMR (CD₃OD, 400 MHz): δ 7.77 (2H, d, *J* = 8.2 Hz, H15, H19); 7.46, 7.44 (5H, m, H22, H23, H24, H25, H26); 7.40 (2H, d, *J* = 8.0 Hz, H16, H18); 6.83 (1H, bs, NH7); 4.19, 4.07 (2H, m, H5);

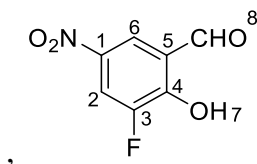
3.74 (3H, s, H13); 3.53 (1H, m, H8); 3.29 (1H, m, H6); 3.01 (1H, m, H2); 3.21 (1H, m, H4); 2.87 (1H, m, H1); 2.83 (1H, m, H6); 2.74 (1H, m, H4); 2.46 (1H, m, H3); 2.43 (3H, s, H20); 2.33 (2H, m, H11); 2.05 (1H, m, H9); 1.82 (1H, m, H9); 1.70 (1H, m, H3); 1.55, 1.33 (2H, m, H10) ppm

^{13}C NMR (CD₃OD, 100 MHz): δ 145.8 (C21), 145.2 (C21); 138.1 (C14); 131.9, 130.9, 130.2 (C22, C23, C24, C25, C26), 129.9 (C16, C18); 128.4 (C15, C19); 77.9 (C12); 63.0 (C8); 62.3 (C5); 58.1 (C1); 52.9 (C13); 52.8 (C2); 51.7 (C6); 51.3 (C4); 45.5 (C11); 31.7 (C3); 30.8 (C9); 25.3 (C10); 21.4 (C20) ppm

Melting point = 177-179°C

IR: 3197 (ν N-H); 2988, 2938, 2901 (ν C-H); 1737 (ν C=O); 1340, 1320 (ν CH₃); 1199, 1161, 1149 (ν C-N and C-C(O)-C) cm⁻¹

3-fluoro-2-hydroxy-5-nitrobenzaldehyde [4.17]



To a stirred solution of 3-fluoro-2-hydroxybenzaldehyde (1.0 g, 7.14 mmol) in concentrated H₂SO₄ (17 mL) and cooled to -10°C NH₄NO₃ (740 mg 9.2 mmol, 1.1 eq.) was added. The solution was stirred at -10°C for 2h. After completion of the reaction, ice was added and the mixture was poured in distilled water. A precipitate was formed to give after filtration **4.17** as a white solid (1.28 g, 6.9 mmol, 89%)

Molecular weight = 185.11 g mol⁻¹

R_f = 0,40 (EtOAc/MeOH 9:1 + 10 μ L AcOH)

HRMS: Calcd. for [C₇H₄NO₄F + H]⁺: m/z 184.0046, found: 184.0042

^1H NMR (CDCl₃, 300 MHz): δ 11.63 (1H, s, OH7); 10.03 (1H, d, J = 1.7 Hz, H8); 8.42 (1H, dd, J = 2.6, 1.5 Hz, H6); 8.25 (1H, dd, J = 9.9, 2.6 Hz, H2) ppm

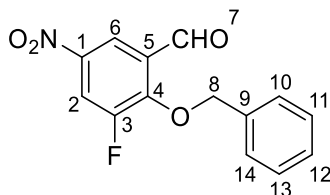
^{13}C NMR (CDCl₃, 75 MHz): δ 195.1 (C8); 155.2 ($J_{\text{C-F}}$ = 12.6 Hz, C4); 152.2 (C3); 148.8 (C1); 124.2 (C5); 120.6 (C6); 117.6 ($J_{\text{C-F}}$ = 22.0 Hz, C2) ppm

^{19}F NMR (CDCl₃, 188 MHz): δ -130.83 ppm

Melting point = 89-91°C

IR: 3098-3052 (ν C-H and CHO + broad peak for OH); 1667 (ν C=O); 1517 (ν NO₂); 1472, 1447 (ν C=C); 1396 (ν OH); 1366 (ν C-H of CHO); 1342 (NO₂) cm⁻¹

2-(benzyloxy)-3-fluoro-5-nitrobenzaldehyde [4.18]



To a solution of **4.17** (1.26 g, 6.81 mmol, 1.0 eq.) in dry DMF, Cs₂CO₃ (3.54g, 10.9 mmol, 1.6 eq.) and benzyl bromide (1.71 mL, 14.30 mmol, 2.1 eq.) were successively added. The reaction mixture was stirred overnight at room temperature. After removal of the volatiles under reduced pressure, the residue obtained was taken up with EtOAc and successively washed twice with water and brine, dried over Na₂SO₄, filtered and concentrated to obtain a yellow solid. The crude product was purified by column chromatography on a silica gel using c-Hex/EtOAc from 9:1 to 8:2 as eluent to yield **4.18** as a white solid (1.67 g, 6.07 mmol, 89%)

Molecular weight = 275.23 g mol⁻¹

R_f = 0.30 (c-Hex /EtOAc 9:1)

HRMS: Calcd. for [C₁₄H₉NO₄F + H]⁺: m/z 274.0516, found: 274.0511

¹H NMR (CDCl₃, 300 MHz): δ 10.26 (1H, s, H7); 8.47 (1H, dd, *J* = 2.8, 1.4 Hz, H6); 8.22 (1H, dd, *J* = 11.5, 2.8 Hz, H2); 7.40 (5H, s, H10, H11, H12, H13, H14); 5.48 (2H, d, *J* = 2.2 Hz, H8)

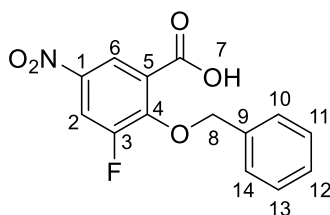
¹³C NMR (CDCl₃, 75 MHz): δ 186.7 (C7); 155.7 (C4); 152.3 (C3); 142.5 (C1); 134.6 (C9); 129.7 (C5); 129.4, 129.0, 128.6 (C10, C11, C12, C13, C14); 119.3 (C6); 117.6 (*J*_{C-F} = 24.8 Hz, C2); 77.4 (C8)

¹⁹F NMR (CDCl₃, 188 MHz): δ -123.32 ppm

Melting point = 97-99°C

IR: 3098-2870 (ν C-H aromatic and CHO); 1686 (ν C=O); 1613-1600 (ν C=C); 1527 (ν NO₂); 1498-1452 (ν C=C); 1340 (ν NO₂) cm⁻¹

2-(benzyloxy)-3-fluoro-5-nitrobenzoic acid [4.19]



NaClO₂ (705 mg, 7.8 mmol, 1.3 eq.) was dissolved in water (5 mL) and let aside. During this time, compound **4.18** (1.65 g, 6.0 mmol, 1.0 eq.) was dissolved in 1,4-dioxane (15 mL) and water (5 mL). Sulfamic acid (874 mg, 9.0 mmol, 1.5 eq.) and NaH₂PO₄ H₂O (2.81 g, 23.4 mmol, 3.9 eq.) were added to the stirring reaction mixture. The mixture was cooled to 0°C for 15 min and the NaClO₂ solution was then added dropwise to the mixture. Once addition was complete, the solution was stirred for an additional 15 min. At this moment, Na₂SO₄ (906 mg, 7.2 mmol, 1.2 eq.) was added in one portion and stirring was continued for an additional 15 min. The solution was then acidified to pH 1 by dropwise addition of concentrated aqueous HCl. After concentration under reduced pressure the crude residue obtained was taken up in 5% aqueous NaOH solution, and concentrated aqueous HCl was added dropwise to the solution until pH 1 was reached. The solid formed was collected by filtration on a Buchner funnel and dried overnight in the open air to afford **4.19** as a white solid (1.76 g, 6.0 mmol, quant.).

Molecular weight = 291.23 g mol⁻¹

R_f = 0 (c-Hex /EtOAc 8:2)

HRMS: Calcd. for [C₁₄H₉NO₅F + H]⁺: m/z 290.0465, found: 290.0463; Calcd. for [C₁₄H₁₀NO₅F + Na]⁺: M/z 314.0441, found: 314.0448

¹H NMR (CDCl₃, 300 MHz): δ 8.71 (1H, dd, *J* = 2.8, 1.6 Hz, H6); 8.21 (1H, dd, *J* = 11.0, 2.8 Hz, H2); 7.51-7.39 (6H, m, H7, H10, H11, H12, H13, H14); 5.45 (2H, d, *J* = 2.1 Hz, H8) ppm

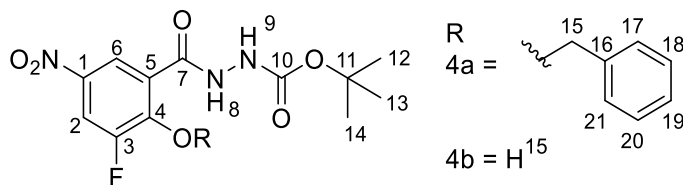
¹³C NMR (CDCl₃, 75 MHz): δ 164.6 (C7); 156.1 (C4); 152.7 (C3); 142.5 (C1); 134.2 (C9); 129.7 (C5); 129.2, 129.0, 128.8 (C10, C11, C12, C13, C14); 123.4 (C6); 116.8 (*J*_{C-F} = 24.8 Hz, C2); 77.9 (C8) ppm

¹⁹F NMR (CDCl₃, 188 MHz): δ -122.30 ppm

Melting point = 100-102°C

IR: 3431 (ν O-H); 3095, 2890 (ν C-H); 1682 (ν C=O); 1616 (ν C=C); 1525 (ν NO₂); 1454-1410 (ν O-H); 1345 (ν C-O), 1266 (ν NO₂) cm⁻¹

***tert*-butyl 2-(2-(benzyloxy)-3-fluoro-5-nitrobenzoyl)hydrazine-1-carboxylate [4.20a] and *tert*-butyl 2-(3-fluoro-2-hydroxy-5-nitrobenzoyl)hydrazine-1-carboxylate [4.20b]**



To a stirred solution of **4.19** (1.23 g, 4.23 mmol, 1.0 eq.) in dry DMF cooled to 0°C, and under argon atmosphere, *tert*-butyl carbazate (6156 mg, 4.66 mmol, 1.1 eq.), HBTU (1.77 g, 4.66 mmol, 1.1 eq.), HOBT (630 mg, 4.66 mmol, 1.1 eq.) and DIPEA (1.48 mL, 8.46 mmol, 2.0 eq) were successively added. The reaction mixture was let stirring overnight at room temperature. After removal of the volatile under reduced pressure, the crude residue obtained was taken up with EtOAc and successively washed with 100% aqueous solution of citric acid, water, 100% aqueous solution of K₂CO₃ and brine, dried over Na₂SO₄, filtered and concentrated under vacuum. The crude product obtained was purified by column chromatography on silica gel using *c*-Hex/EtOAc from 9:1 to 8:2 as eluent to afford first **4.20a** as a pale yellow solid (140 mg, 0.35 mmol) and secondly pure EtOAc as eluant to afford **4.20b** as a yellow solid (1.08 g, 3.45 mmol) for a total yield of 90%.

Molecular weight 4.20a = 405.38 g mol⁻¹

R_f 4.20a = 0.30 (*c*-Hex/EtOAc 8:2)

HRMS 4.20a: Calcd. for [C₁₉H₂₀N₃O₆F + Na]⁺: m/z 428.1234, found: 428.1231

¹H NMR 4.20a (CDCl₃, 300 MHz): δ 9.29 (1H, bs, NH₈); 8.82 (1H, dd, *J* = 2.8, 1.6 Hz, H₆); 8.14 (1H, dd, *J* = 11.0, 2.8 Hz, H₂); 7.57-7.35 (5H, m, H₁₇, H₁₈, H₁₉, H₂₀, H₂₁); 6.81 (1H, bs, NH₉); 5.45 (2H, dd, *J* = 1.9 Hz, H₁₅); 1.48 (9H, s, H₁₂, H₁₃, H₁₄) ppm

¹³C NMR 4.20a (CDCl₃, 75 MHz): δ 161.4 (C₇); 155.9 (C₁₀); 154.7 (C₃); 152.5 (C₄); 142.9 (C₁); 134.1 (C₁₆); 129.7, 129.3, 129.1 (C₁₇, C₁₈, C₁₉, C₂₀, C₂₁); 126.1 (C₅); 122.9 (C₆); 115.7 (*J*_{C-F} = 15.9 Hz, C₂); 82.2 (C₁₁); 77.9 (C₁₅); 28.1 (C₁₂, C₁₃, C₁₄) ppm

¹⁹F NMR 4.20a (CDCl₃, 188 MHz): δ -122.58 ppm

Melting point 4.20a = 120-122°C

IR 4.20a: 3390, 3258 (ν N-H); 3072, 2988 (ν C-H); 1717, 1682 (ν C=O); 1615 (ν C=C); 1536 (ν NO₂); 1498-1458 (ν N-H); 1395-1302 (ν C-O); 1279 (ν NO₂) cm⁻¹

Molecular weight 4.20b = 315.26 g mol⁻¹

Rf 4.20b = 0.2 (EtOAc)

HRMS 4.20b: Calcd. for [C₁₂H₁₄FN₃O₆ – H]⁻: m/z 314.0867, found 314.0776

¹H NMR 4.20b (DMSO-*d*₆, 400 MHz): δ 11.92 (1H, s bs, NH₈); 8.90 (1H, bs, NH₉); 8.55 (1H, dd, *J* = 3.15, 1.00 Hz, H₆); 7.76 (1H, dd *J* = 11.02, 3.15 Hz, H₂); 3.34 (1H, bs, OH₁₅); 1.46 (9H, s, H₁₂, H₁₃, H₁₄) ppm

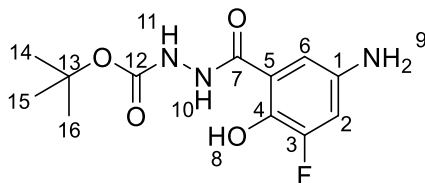
¹³C NMR 4.20b (DMSO-*d*₆, 100 MHz): δ 167.7 (C₇); 166.7 (C₁₀); 156.1 (C₁); 153.7 (C₅); 128.7 (C₄); 124.9 (C₆); 119.2 (C₃); 112.0 (*J*_{C-F} = 24.0 Hz, C₂); 80.2 (C₁₁); 28.9 (C₁₂, C₁₃, C₁₄) ppm

¹⁹F NMR 4.20b (DMSO-*d*₆, 376MHz): δ 134.53 ppm

Melting point 4.21b = 158-160°C

IR 4.20b: 3254 (ν O-H); 1681 (ν C=O); 1633 (δ N-H); 1500 (ν NO₂); 1477 (ν C=C); 1342 (ν NO₂); 1240 (ν C-O) cm⁻¹

tert-butyl 2-(5-amino-3-fluoro-2-hydroxybenzoyl)hydrazine-1-carboxylate [4.22]



To a stirred solution of **4.20a** and **4.20b** (1.22 g, 3.8 mmol, 1.0 eq.) in MeOH, (15 mL) under argon atmosphere, Pd/C (244 mg, 20% mass) was added. The reaction mixture was stirred two hours under hydrogen atmosphere at room temperature. Once the reaction was finished, the mixture was filtered on a Celite pad and the volatile was removed under reduced pressure to afford **4.22** as a purple solid (1.08 g, 3.8 mmol, quant.).

Molecular weight = 285.27 g mol⁻¹

Rf = 0 (c-Hex/EtOAc 8:2)

HRMS: Calcd. for [C₁₂H₁₆N₃O₄F+Na]⁺: m/z 308.1023, found: 308.1020

¹H NMR (DMSO-*d*₆, 300 MHz): δ 10.80 (1H, bs, OH₈); 10.20 (1H, bs, NH₁₀); 9.00 (1H, bs, NH₁₁); 6.82 (1H, s, H₆); 6.67 (1H, d, *J* = 12.8 Hz, H₂); 4.94 (2H, bs, NH₉); 1.30 (9H, s, H₁₄, H₁₅, H₁₆) ppm

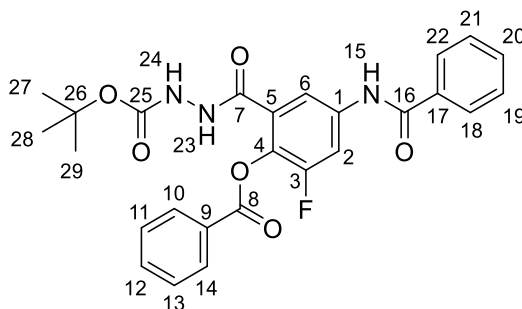
^{13}C NMR (DMSO-*d*₆, 75 MHz): δ 168.2 (C7); 155.6 (C12); 153.6 - 150.4 ($J_{\text{C-F}} = 239.4$ Hz, C3); 141.4 (C1); 137.6 (C4); 118.1 (C5); 108.0 (C6); 107.1 ($J_{\text{C-F}} = 20.4$ Hz, C2); 79.9 (C13); 28.5 (C14, C15, C16) ppm

^{19}F NMR (DMSO-*d*₆, 188 MHz): δ -133.58 ppm

Melting point = 197-199°C

IR: 3455 (v N-H); 3300 (v broad peak for OH); 2976 (v C-H); 1735 (v C=O); 1625 (v C=C aromatic); 1590-1497 (v N-H); 1385-1307 (v C-O); 1270-1214 (v C-N) cm^{-1}

tert-butyl 2-(5-benzamido-2-(benzoyloxy)-3-fluorobenzoyl)hydrazine-1-carboxylate [4.23]



To a stirred solution of **4.22** (30 mg, 0.105 mmol, 1.0 eq.) in pyridine (1.5 mL), cooled to 0°C, benzoyl chloride (24 μL , 0.210 mmol, 2.1 eq.) was added dropwise. After agitation for 45 minutes at 0°C, the volatiles were removed under reduced pressure. The obtained residue was taken up with EtOAc and successively washed with 100% aqueous solution of citric acid and brine, dried over Na_2SO_4 , filtered and concentrated under reduced pressure. The crude solid afforded was purified by column chromatography on silica gel using *c*-Hex/EtOAc 7:3 as eluent to yield **4.23** (30.2 mg, 0.062 mmol, 60%) as white powder.

Molecular weight = 493.48 g mol^{-1}

R_f = 0.50 (*c*-Hex/EtOAc 1:1)

HRMS: Calcd. for $[\text{C}_{26}\text{H}_{24}\text{N}_3\text{O}_6\text{F} + \text{H}]^+$: m/z 494.172, found: 494.1732; Calcd. for $[\text{C}_{26}\text{H}_{24}\text{N}_3\text{O}_6\text{F} + \text{Na}]^+$: M/z 516.1547, found: 516.1547

^1H NMR (DMSO-*d*₆, 300 MHz): δ 10.67 (1H, bs, NH15); 10.18 (1H, bs, NH23); 8.98 (1H, bs s, NH24); 8.10 (1H, d, H2); 8.13 (2H, d, 8.0 Hz, H10, H14); 7.99 (2H, d, 8.0 Hz, H18, H22); 7.90 (1H, bs, H6); 7.76 (2H, t, H12); 7.68-7.52 (5H, m, H11, H14, H19, H20, H21) 1.38 (9H, s, H27, H28, H29) ppm

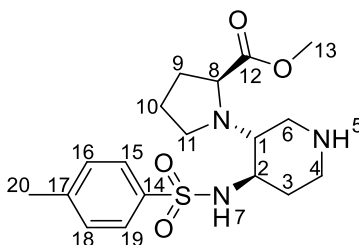
¹³C NMR (DMSO-*d*₆, 75 MHz): δ 166.0 (C16); 164.0 (C7); 163.6 (C8); 154.8 (C25); 155.5 (C3); 152.4 (C9); 138.5, 138.4, 134.6 (C1, C5, C17); 134.3, 130.2, 128.9 (C10, C11, C12, C13, C14); 132.1, 127.8, 125.6 (C18, C19, C20, C21, C22); 128.4 (C4); 115.8 (C6); 109.8 ($J_{\text{C-F}} = 23.4$ Hz, C2); 79.3 (C26); 28.5 (C27, C28, C29) ppm

¹⁹F NMR (DMSO-*d*₆, 188 MHz): δ -124.74 ppm

Melting point = 125–127°C

IR: 3287 (ν N-H); 2981 (ν C-H); 1726 (ν C=O); 1662 (ν C=C); 1602-1541 (ν N-H); 1203-1157 (ν C-C(O)-C) cm⁻¹

Methyl((3*R*,4*R*)-4-((4-methylphenyl)sulfonamido)piperidin-3-yl)-*L*-prolinate [4.25]



To a stirred solution of **4.12** (1 g, 2.12 mmol, 1.0 eq.) in toluene (20 mL) under argon atmosphere, Pd/C 10 % (452 mg, 4.24 mmol, 2.0 eq.) was added. The reaction mixture was stirred at 30°C under hydrogen atmosphere for 6 h. Once the reaction was over, the mixture was filtered on a Celite pad and volatile was removed under reduced pressure to afford **4.25** as a white solid (444.7 mg, 1.06 mmol, quant.).

Molecular weight = 381.17 g mol⁻¹

R_f = 0.20 (CH₂Cl₂/MeOH 20:1)

HRMS: Calcd. for [C₁₈H₂₇N₃O₄S + H]⁺: m/z 382.1801, found: 382.1801

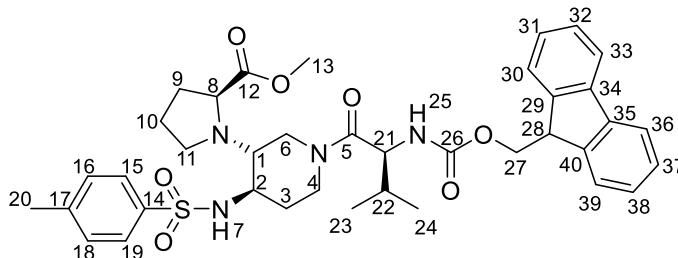
¹H NMR (CDCl₃, 300 MHz): δ 7.76 (2H, d, $J = 7.6$ Hz, H15, H19); 7.26 (2H, d, $J = 7.6$ Hz, H16, H18); 6.79 (1H, bs, NH7); 3.74 (3H, s, H13); 3.45 (2H, m, H8, NH5); 2.97 (2H, m, H2, H4); 2.74 (2H, m, H6); 2.49 (6H, m, H1, H4, H11, H20); 2.24 (1H, m, H11); 1.99 (1H, m, H9); 1.77 (2H, m, H3, H9); 1.39 (3H, m, H3, H10) ppm

¹³C NMR (CDCl₃, 75 MHz): δ 176.3 (C12); 143.0 (C17); 137.5 (C14); 129.9 (C16, C18); 127.4 (C15, C19); 62.3 (C1); 59.9 (C8); 54.2 (C2); 52.6 (C13); 45.1 (C4); 44.9 (C6); 44.3 (C3); 35.3 (C9); 30.0 (C11); 24.6 (C10); 21.7 (C20) ppm

Melting point = 122-124°C

IR: 3206 (ν N-H); 2951-2849 (ν C-H); 1727 (ν C=O); 1669 (ν N-H); 1438 (ν C=C); 1209-1161 (ν C-N) cm^{-1}

(S)-methyl 1-((3R,4R)-1-((S)-2-(((9H-fluoren-9-yl)methoxy)carbonyl)amino)-3-methylbutanoyl)-4-(4-methylphenylsulfonamido)piperidin-3-yl)pyrrolidine-2-carboxylate [4.26]



To a solution of **4.25** (500 mg, 1.31 mmol, 1.0 eq.) in dry DMF (7.0 mL) under a nitrogen atmosphere DIPEA (0.91 mL, 5.24 mmol, 4.0 eq) was added. This solution was let aside. Meanwhile, to a solution of FmocNH-Val-OH (889 mg, 2.62 mmol, 2.0 eq.) in dry DMF (10.0 mL) under a nitrogen atmosphere and cooled at 0°C, HBTU (994 mg, 2.62 mmol, 2.0 eq.) and HOBT (354 mg, 2.62 mmol, 2.0 eq.) were added. The reaction was let stirring at 0°C for 1 h and finally added dropwise to the previous solution **4.25**. The reaction was stirred at room temperature overnight. After concentration under vacuum, the residue obtained was taken up with EtOAc, washed with water, saturated aqueous solution of NaHCO₃, brine, dried over Na₂SO₄ and concentrated under reduced pressure. The crude residue obtained was purified by column chromatography on silica gel, using *c*-Hex /EtOAc 6:4 as eluent to afford compound **4.26** (493 mg, 0.70 mmol, 53 %) as a white solid.

Molecular weight = 702.86 g mol^{-1}

R_f = 0.35 (Cyclo/EtOAc 6:4)

HRMS: Calcd. for [C₃₈H₄₆N₄O₇S + H]⁺: M/z 703.3165, found: 703.3170

¹H NMR (DMSO-*d*₆, 400 MHz): δ 7.88 (4H, m, H15, H19, H33, H36); 7.72 (2H, m, H16, H18); 7.69 (2H, m, H30, H39); 7.67 (1H, bp, NH25); 7.39 (2H, m, H32, H37); 7.32 (2H, m, H31, H38); 7.00 (1H, bp, NH7); 4.18 (2H, m, H27); 4.16 (1H, m, H4); 4.14 (1H, m, H21); 4.11 (1H, m, H28); 4.08 (1H, m, H6); 3.80 (1H, m, H2); 3.66 (1H, m, H8); 3.48 (3H, s, H13); 3.05 (1H, m, H6); 2.92 (1H, m, H1); 2.75 (1H, m, H4); 2.37 (3H, s, H20); 2.34 (1H, m, H11); 2.17 (1H, m, H9); 2.02 (1H,

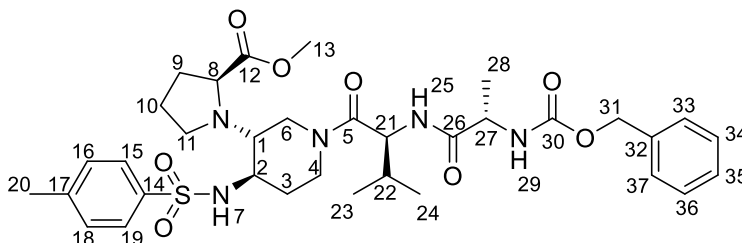
m, H3); 1.92 (1H, m, H22); 1.70 (1H, m, H3); 1.64 (1H, m, H11); 1.48 (1H, m, H10); 1.23 (1H, m, H10); 1.13 (1H, m, H9); 0.85, 0.75 (6H, m, H23, H24) ppm

¹³C NMR (DMSO-*d*₆, 100 MHz): δ 176.5 (C12); 175.8 (C5); 170.0 (C26); 143.8 (C29, C40); 142.6 (C17); 140.7 (C14); 140.6 (C34, C35); 127.6 (C32, C37); 127.1 (C31, C38); 125.5 (C16, C18); 125.4 (C30, C39); 120.2 (C15, C19, C33, C36); 65.5 (C27); 60.6 (C2); 55.4 (C21); 55.3 (C28); 52.8 (C1); 51.9 (C8); 51.8 (C13); 44.2 (C6); 44.1 (C11); 39.9 (C4); 32.7 (C9); 29.8 (C22); 29.3 (C3); 24.0 (C10); 21.0 (C20); 19.2, 18.5 (C23, C24) ppm

Melting point = 113-115°C

IR: 3200 (ν N-H); 2959, 2926, 2872 (ν C-H); 1721, 1634 (ν C=O); 1524 (δ N-H); 1449 (ν C=C); 1220 (ν C=O); 1164 (ν C-N) cm⁻¹

(S)-methyl-1-((3R,4R)-1-((S)-2-((S)-2-(((benzyloxy)carbonyl)amino)propionamido)-3-methylbutanoyl)-4-(4-methylphenylsulfonamido)piperidin-3-yl)pyrrolidine-2-carboxylate [4.27]



The N-protected compound **4.26** (880 mg, 1.25 mmol, 1.0 eq.) was dissolved in a 20 % solution of piperidine in DMF (10 mL) and the reaction mixture was let stirring at room temperature for 2 h. The solvent was evaporated under vacuum to give the Fmoc deprotected amine that was used for the next coupling reaction without any further purification. The N-deprotected compound was dissolved in DMF (7.0 mL) under a nitrogen atmosphere and DIPEA (0.87 mL, 5.0 mmol, 4.0 eq) was added. This solution was let aside. Meanwhile CbzNH-Ala-OH (558 mg, 2.50 mmol, 2.0 eq.) was dissolved in DMF (10.0 mL) under a nitrogen atmosphere and the solution was cooled at 0°C. At this moment, HBTU (948 mg, 2.50 mmol, 2.0 eq.) and HOBT (338 mg, 2.50 mmol, 2.0 eq.) were then added at 0°C. The reaction was let stirring at 0°C for 1 h. Finally, the previous solution of compound **4.26** was added dropwise. The reaction was stirred at room temperature overnight. After concentration of the solvent under vacuum, the residue was taken up with EtOAc, washed successively with water, saturated aqueous NaHCO₃, brine, dried over Na₂SO₄ and the solvent

evaporated under reduced pressure. The crude product obtained was purified by column chromatography on silica gel using Cyclo/EtOAc 1:1 as eluent to afford compound **4.27** (656 mg, 0.96 mmol, Yield 77 %) as a white solid.

Molecular weight = 685.83 g mol⁻¹

R_f = 0:15 (Cyclo/EtOAc 6:4)

HRMS: Calcd. for [C₃₄H₄₇N₅O₈S + H]⁺: M/z 686.3224, found: 686.3221

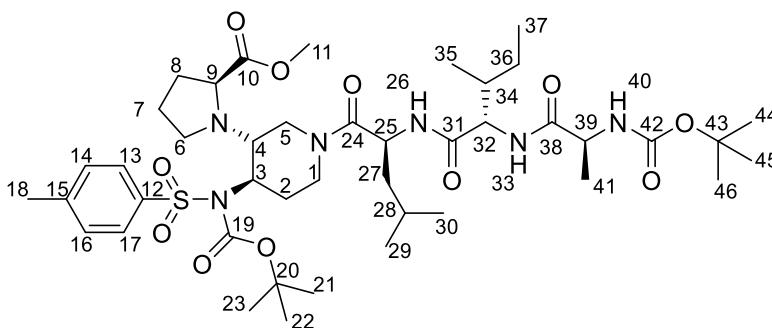
¹H NMR (DMSO-*d*₆, 400 MHz): δ 7.91 (1H, bp, NH25); 7.70 (2H, m, H15, H19); 7.44 (1H, bp, NH29); 7.41 (2H, m, H16, H18); 7.36, 7.27 (5H, m, H33, H34, H35, H36, H37); 7.18 (1H, bp, NH7); 5.01 (2H, s, H31); 4.45 (1H, m, H21); 4.24 (1H, m, H6); 4.06 (1H, m, H27); 4.05 (1H, m, H4); 3.83 (1H, m, H8); 3.64 (3H, s, H13); 3.07 (1H, m, H4); 3.01 (1H, m, H2); 2.52 (1H, m, H6); 2.38 (3H, s, H20); 2.37 (1H, m, H11); 2.35 (1H, m, H1); 2.15 (1H, m, H9); 2.03 (1H, m, H3); 1.92 (1H, m, H22); 1.73 (1H, m, H3); 1.65 (1H, m, H11); 1.50 (1H, m, H10); 1.24 (1H, m, H10); 1.14 (3H, s, H28); 1.13 (1H, m, H9); 0.81, 0.76 (6H, m, H23, H24) ppm

¹³C NMR (DMSO-*d*₆, 100 MHz): δ 175.6 (C12); 172.3 (C26); 169.4 (C5); 155.5 (C30); 142.8 (C17); 136.9 (C14); 136.8 (C32); 129.6 (C16, C18); 127.7 (C33, C34, C35, C36, C37); 126.6 (C15, C19); 65.2 (C31); 60.3 (C8); 58.1 (C1); 52.7 (C21); 51.9 (C2); 51.6 (C13); 49.8 (C27); 43.8 (C11); 43.7 (C4); 39.5 (C6); 32.4 (C9); 29.7 (C22); 29.1 (C3); 23.6 (C10); 20.8 (C20); 18.2 (C23, C24); 17.7 (C28) ppm

Melting point = 123-125°C

IR: 3294 (ν N-H); 2963, 2929, 2874 (ν C-H); 1720, 1665, 1625 (ν C=O); 1519 (δ N-H); 1452 (ν C=C); 1220 (ν C=O); 1184 (ν C-N) cm⁻¹

Methyl((3*R*,4*R*)-4-((*N*-(*tert*-butoxycarbonyl)-4-methylphenyl)sulfonamido)-1-((*tert*-butoxycarbonyl)-*L*-alanyl-*L*-isoleucyl-*L*-leucyl)piperidin-3-yl)-*L*-prolinate [4.28]



To a stirred solution of **4.32** (2.62 g, 2.82 mmol, 1.0 eq.) in dry DMF (10 mL), under argon atmosphere, a solution of piperidine in DMF (29 mL, 20%/vol) was added. The reaction was let under stirring 4 h and then the volatiles were removed under reduced pressure to afford the crude free amine which was used for the following coupling reaction without further purification. Precisely, to a solution of this crude free amine in CH₂Cl₂ (20 mL) cooled to 0°C, HOBT (0.46 g, 3.38 mmol, 1.2 eq.), EDC·HCl (0.65 g, 3.38 mmol, 1.2 eq.), *L*-Boc-NH-Ala-OH (0.64 g, 3.38 mmol, 1.2 eq.) and Collidine (0.94 mL, 7.05 mmol, 2.5 eq.) were successively added under argon atmosphere. The reaction mixture was then stirred overnight at room temperature. Then, the solution was washed with distilled water, 100 % aqueous solution of NaHCO₃, brine, dried over Na₂SO₄, filtered and concentrated under reduced pressure. The crude residue obtained was purified by column chromatography on silica gel eluting with *c*-Hex/EtOAc 8:2 to afford **4.28** as a white powder (1.67 g, 1.90 mmol, 67%).

Molecular weight = 879.12 g mol⁻¹

R_f = 0.3 (*c*-Hex/EtOAc 7:3)

HRMS: Calcd. for [C₄₃H₇₀N₆O₁₁S + H]⁺: m/z 879.4857, found: 879.4904

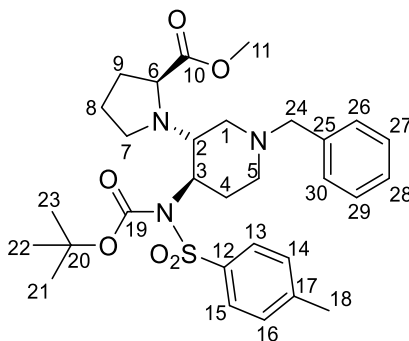
¹H NMR (DMSO-*d*₆, 400 MHz): 2 conformers δ 8.12 (0.5 H, d, *J* = 8.0 Hz, H26); 8.00 (0.5 H, d, *J* = 8.0 Hz, NH26); 7.71 (2H, m, H13, H17); 7.52 (0.5 H, d, *J* = 8.9 Hz, NH33); 7.40 (2H, d, *J* = 8.1, H14, H16); 7.33 (0.5 H, d, *J* = 8.9 Hz, H33); 7.01 (1H, m, NH40); 4.70 (1H, m, H25); 4.23-4.13 (3H, m, H32, CH₂scaff); 4.06 (1H, m, CH₂scaff); 4.02-3.91 (3H, m, CH₂scaff, H39); 3.79 (0.5H, m, H9); 3.68 (1H, m, CH₂scaff); 3.52 (0.5H, m, H9); 3.30 (3H, s, H11); 3.10 (1H, m, CH₂scaff); 3.01 (0.5H, m, H3); 2.94 (0.5H, m, H3); 2.82 (1H, m, CH₂scaff); 2.53 (1H, m, CH₂scaff); 2.43-2.24 (3H, m, H4, CH₂scaff); 2.38 (3H, 1s, H18); 2.15 (1H, m, CH₂scaff); 1.98 (1H, m, CH₂scaff); 1.84 (1H, m, CH₂scaff); 1.80-1.19 (9H, m, H36, H34, H28, H27, CH₂scaff); 1.39, (18H, s, H46, H45, H44, H23, H22, H21); 1.14 (3H, d, *J* = 6.3 Hz, H41); 1.10 (1H, m, CH₂scaff); 0.88-0.72 (12H, m, H37, H35, H30, H29) ppm

¹³C NMR (DMSO-*d*₆, 100 MHz): δ 176.3 (C10); 175.8 (C24); 172.1 (C38); 170.4 (C31); 169.9 (C19); 169.6 (C42); 142.8 (C15); 137.1 (C12); 129.8 (C14, C16); 126.6 (C17,C13); 77.8 (C43, C20); 61 (C9); 58.4 (C4); 56.4 (C32); 52.5 (C3); 49.7 (C39); 46.2 (C25); 45.0 (C_{scaff}); 44.1 (C_{scaff}); 43.8 (C_{scaff}); 42.4 (C_{scaff}); 40.4 (C27); 39.6 (C_{scaff}); 36.9 (C34); 32.3 (C_{scaff}); 29.3 (C_{scaff}); 28.0 (C46, C45, C44, C23, C22, C21); 24.0 (C28); 23.5 (C36); 20.9 (C18); 17.7 (C41); 22.9, 21.6, 15.2, 10.7 (C37, C35, C30, C29) ppm

Melting point = 115-116°C

IR: 3284 (ν N-H); 2961 (ν C-H); 1729-1632 (ν C=O); 1521-1449 (ν C=C); 1341 (ν C-N); 1278 (ν C-O) cm⁻¹

Methyl ((3*R*, 4*R*)-1-benzyl-4-((*N*-(*tert*-butoxycarbonyl)-4-methylphenyl)sulfonamido)piperidin-3-yl)-*L*-prolinate [4.29]



To a solution of **4.12** (2.0 g, 4.37 mmol, 1 eq.) in dry DMF (17 mL) under argon atmosphere DIPEA (1.88 mL, 10.9 mmol, 2.5 eq.), Boc₂O (2.38 g, 10.9 mmol, 2.5 eq.) and DMAP (1.33 g, 10.9 mmol, 2.5 eq.) were added. The reaction was stirred overnight at room temperature. After concentration under reduced pressure, the crude residue was taken up with EtOAc. The organic layer was successively washed with water, 100% aqueous solution of NaHCO₃ and brine, dried over Na₂SO₄, filtered and concentrated under reduced pressure. The crude solid obtained was purified using column chromatography on silica gel eluting with *c*-Hex/EtOAc from 8:2 to 7:3 affording compound **4.29** as white powder (2.25 g, 3.93 mmol, 90%).

Molecular weight = 571.73 g mol⁻¹

R_f = 0.7 (*c*-Hex/EtOAc 6:4)

HRMS: Calcd. for [C₃₀H₄₁N₃O₆S + H]⁺: *m/z* 572.2794, found: 572.2795

¹H NMR (DMSO-*d*₆, 400 MHz): δ 7.98 (2H, d, *J* = 8.4 Hz, H13, H15), 7.38 (2H, m, H14, H16), 7.33 (2H, m, H27, H29), 7.30 (2H, m, H26, H30), 7.25 (1H, m, H28), 4.28 (1H, td, *J* = 10.9, 3.6 Hz, H6), 3.77 (1H, m, H2), 3.58 (1H, m, H24), 3.63-3.51 (4H, m, H3, H11), 3.44 (1H, m, H24), 3.04 (1H, m, H1), 2.97 (1H, m, H8), 2.77 (1H, m, H5), 2.75 (1H, m, H8), 2.40 (3H, s, H18), 2.36 (1H, m, H7), 2.03 (1H, m, H1), 1.95 (1H, m, H5), 1.94 (1H, m, H4), 1.85 (1H, m, H4), 1.71 (2H, m, H9), 1.70 (1H, m, H7), 1.16 (9H, s, H21, H22, H23) ppm

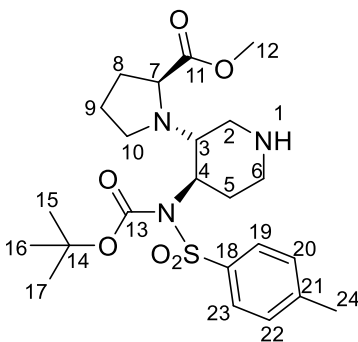
¹³C NMR (DMSO-*d*₆, 100 MHz): δ 178.3 (C19); 174.6 (C10); 143.3 (C17); 138.8 (C12); 138.3 (C25); 129.2 (C14, C16); 128.5 (C26, C30); 128.2 (C27, C29); 126.9 (C28); 126.8 (C13, C15);

83.4 (C20); 61.6 (C24); 60.9 (C11); 57.5 (C6); 55.4 (C2); 52.2 (C5); 51.9 (C1); 51.4 (C3); 45.8 (C8); 29.5 (C7, C4); 27.3 (C21, C22, C23); 24.2 (C9); 21.0 (C18) ppm

Melting point = 56-58°C

IR: 2926 (ν C-H); 1727 (ν C=O); 1368 (ν C-N); 1278 (ν C-H); 1151 (ν C-O) cm^{-1}

Methyl ((3*R*,4*R*)-4-((*N*-(*tert*-butoxycarbonyl)-4-methylphenyl)sulfonamido-piperidin-3-yl)-*L*-prolinate [4.30]



To a solution of **4.29** (2.39 g, 4.18 mmol, 1.0 eq.) in toluene (30 mL) Pd/C 10% (478 mg, 4.18 mmol, 1.0 eq.) was added. The reaction was stirred at 30°C for 24 h under hydrogen atmosphere. Once the reaction was over, the mixture was filtered on a Celite pad and the volatile was removed under reduced pressure to afford **4.30** (2.01 g, 4.18 mmol, quant.) as a white powder.

Molecular weight = 481.61 g mol^{-1}

R_f = 0 (c-Hex/EtOAc 1:1)

HRMS: Calcd. for $[\text{C}_{23}\text{H}_{35}\text{N}_3\text{O}_6\text{S} + \text{H}]^+$: m/z 482.2280, found 482.2315

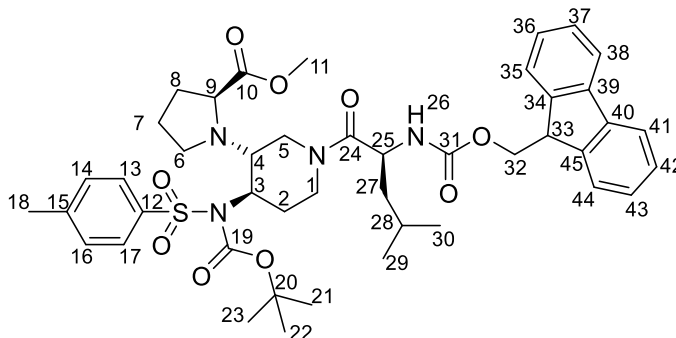
¹H NMR (CDCl_3 , 400 MHz): δ 8.05 (2H, d, $J = 8.5$ Hz, H19, H23); 7.28 (2H, d, $J = 8.5$ Hz, H20, H22); 4.55 (1H, td, $J = 11.4, 4.51$ Hz, H3); 3.83 (1H, m, H4); 3.66 (1H, dd, $J = 8.2, 5.3$ Hz, H7); 3.61 (3H, s, H12); 3.30 (1H, m, H5); 3.16 (2H, m, H10); 2.80 (1H, m, H6); 2.73-2.59 (2H, m, H6, H5); 2.50 (1H, m, H2); 2.42 (3H, s, H24); 2.10-1.83 (4H, m, H2, H8, H9); 1.75 (1H, m, H9), 1.22 (9H, s, H15, H16, H17) ppm

¹³C NMR (CDCl_3 , 100 MHz): δ 175.6 (C11); 143.6 (C21); 139.8 (C18); 129.5 (C20, C22); 128.5 (C13); 127.6 (C19, C23); 84.5 (C14); 61.8 (C7); 58.1 (C3); 57.3 (C4); 52.1 (C12) 46.7 (C6); 46.4 (C10); 45.5 (C5); 32.2 (C2); 30.4 (C8); 28.4 (C15, C16, C17); 25.0 (C9); 22.2 (C24) ppm

Melting point = 72-75°C

IR: 3399 (ν N-H); 2953 (ν C-H); 1726 (ν C=O); 1436 (ν C=C); 1338 (ν C-N); 1280 (ν C-O) cm^{-1}

Methyl ((3*R*,4*R*)-1-(((9*H*-fluoren-9-yl)methoxy)carbonyl)-*L*-leucyl)-4-((*N*-*tert*-butoxycarbonyl)-4-methylphenyl)sulfonamido)piperidin-3-yl)-*L*-prolinate [4.31]



To a solution of **4.30** (1.90 g, 3.93 mmol, 1.0 eq.) in CH₂Cl₂ (20 mL), under argon atmosphere, HOBt (0.64 g, 4.72 mmol, 1.2 eq.), EDC·HCl (0.90 g, 4.72 mmol, 1.2 eq.), *L*-Fmoc-NH-Leu-OH (1.67 g, 4.72 mmol, 1.2 eq.) and Collidine (1.30 mL, 9.82 mmol, 2.5 eq.) were added at 0°C. The reaction mixture was let under stirring overnight at room temperature and successively washed with distilled water, 100% aqueous solution of NaHCO₃ and brine, dried over Na₂SO₄, filtered and concentrated under reduced pressure. The crude residue obtained was purified by column chromatography on silica gel eluting *c*-Hex/EtOAc 8:2 to afford **4.31** (2.35 g, 2.88 mmol, 73%) as a white powder.

Molecular weight = 817.01 g mol⁻¹

R_f = 0.6 (*c*-Hex/EtOAc 6:4)

HRMS: Calcd. for [C₄₄H₅₆N₄O₉S + H]⁺: *m/z* 817.3802, found 817.3846

¹H NMR (DMSO-*d*₆, 400 MHz): two conformers δ 7.97 (2H, m, H17, H13); 7.88 (2H, d, *J* = 7.4 Hz, H41, H38); 7.71 (2H, m, H44, H35); 7.62 (1H, m, NH26); 7.45-7.28 (6H, m, H43, H42; H37, H36, H16, H14); 4.63-4.42 (3H, m, H25, H9, CH₂scaff.); 4.40-4.13 (5H, m, H33, H32, CH₂scaff.); 3.93 (1H, m, CH₂scaff.); 3.73 (0.5H, m, CH_{scaff}); 3.60 (1H, m, CH_{scaff}); 3.52 (2H, s, H11); 3.46 (0.5H, m, CH_{scaff}); 3.39 (1H, s, H11); 3.21 (1H, m, CH_{scaff}); 3.00 (1H, m, CH_{scaff}); 2.83 (1H, m, CH_{scaff}); 2.67 (1H, m, CH_{scaff}); 2.39 (3H, m, H18); 2.05 (1H, m, CH_{scaff}); 1.94-1.50 (5H, m, H28, H27, CH_{scaff}); 1.32 (1H, m, H27); 1.15 (6H, s, H23, H22, H21); 1.09 (3H, s, H23, H22, H21); 0.89 (6H, m, H30, H29) ppm

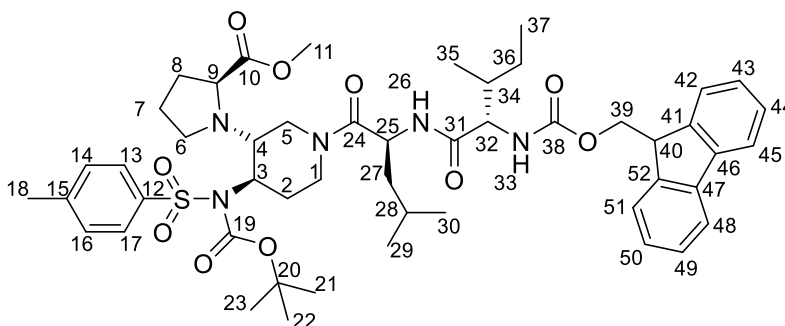
¹³C NMR (DMSO-*d*₆, 100 MHz): two conformers δ 174.4 (C10); 170.3 (C24); 143.8 (C45, C34); 143.3 (C15); 140.7 (C40, C39); 138.4 (C12); 129.3 (C16, C14); 127.6 (C42, C37); 127.0 (C17,

C13); 126.9 (C43, C36); 125.3 (C44, C35); 120.1 (C41, C38); 83.8 (C20); 65.5 (C32); 61.2 (C4, C3); 56.8 (C9); 55.9 (C4, C3); 51.5 (C11); 48.8 (C25); 46.8 (C33); 45.7 (CH₂scaff.); 43.9 (CH₂scaff.); 40.9 (CH₂scaff.); 40.5 (C27); 40.0 (CH₂scaff.); 29.3 (CH₂scaff.); 27.6 (C21, C22, C23); 24.2 (C28); 23.9 (CH₂scaff.); 23.1 (C30, C29); 21.2 (C30, C29); 21.0 (C18) ppm

Melting point = 84-86°C

IR: 2954 (v C-H); 1724-1636 (v C=O); 1449 (v C=C); 1339 (v C-N); 1253 (v C-O) cm⁻¹

Methyl ((3*R*,4*R*)-1-(((9*H*-fluoren-9-yl)methoxy)carbonyl)-*L*-isoleucyl)-*L*-leucyl)-4-((*N*-(*tert*-butoxycarbonyl)-4-methylphenyl)sulfonamido)piperidin-3-yl)-*L*-pro-linate [4.32]



To a stirred solution of **4.31** (2.83 g, 3.46 mmol, 1.0 eq.) in dry DMF (10 mL), under argon atmosphere, a solution of piperidine in DMF (35 mL, 20%/vol) was added. The reaction was let under stirring 4 h and then the volatiles were removed under reduced pressure to afford the crude free amine which was used for the following coupling reaction without further purification. Precisely, to a solution of this crude free amine in CH₂Cl₂ (25 mL) cooled to 0°C, HOBT (0.56 g, 4.15 mmol, 1.2 eq.), EDC·HCl (0.80 g, 4.15 mmol, 1.2 eq.), *L*-Fmoc-NH-Ile-OH (1.47 g, 4.15 mmol, 1.2 eq.) and Collidine (1.14 mL, 8.65 mmol, 2.5 eq.) were successively added under argon atmosphere. The reaction mixture was then stirred overnight at room temperature. Then, the solution was washed with distilled water, 100 % aqueous solution of NaHCO₃, brine, dried over Na₂SO₄, filtered and concentrated under reduced pressure. The crude residue obtained was purified by column chromatography on silica gel eluting with *c*-Hex/EtOAc 7:3 to afford **4.32** as a white powder (2.62 g, 2.82 mmol, 81%).

Molecular weight = 930.17 g mol⁻¹

R_f = 0.2 (*c*-Hex/EtOAc 7:3)

HRMS: Calcd. for [C₅₀H₆₇N₅O₁₀S + H]⁺: m/z 930.4642, found: 930.4697

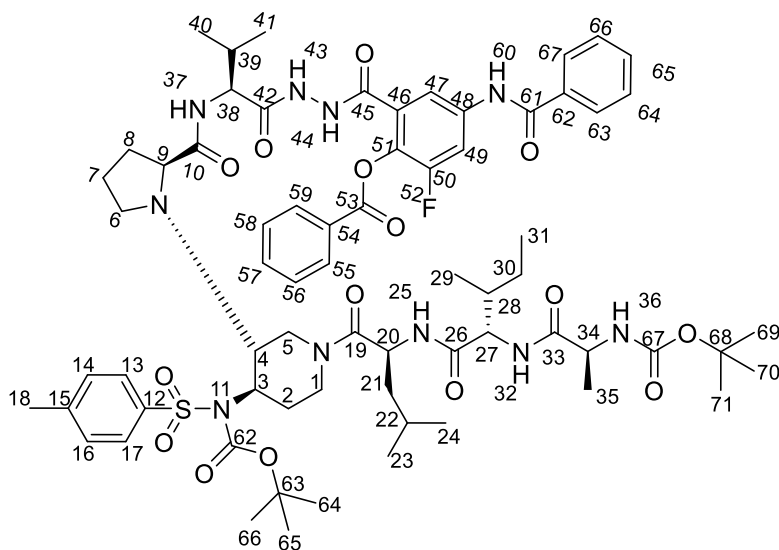
¹H NMR (CDCl₃, 400 MHz): δ 7.97 (2H, d, $J = 8.30$ Hz, H17, H13); 7.90 (2H, d, $J = 7.49$ Hz, H_{Fmoc}); 7.79-7.70 (3H, m, NH26, H_{Fmoc}); 7.49-7.31 (7H, m, NH33, H16, H14, H_{Fmoc}); 4.88 (1H, m, H25); 4.60 (1H, m, H32); 4.34 (2H, m, H39); 4.26 (1H, m, H40); 3.98 (1H, m, H10); 3.79-3.51 (6H, m, H11, H4, CH₂scaff); 3.10-3.01 (H3, CH₂scaff); 2.90 (2H, m, CH₂scaff); 2.45 (3H, s, H18); 2.33 (1H, m, CH₂scaff); 2.12 (1H, m, CH₂scaff); 1.94 (1H, m, CH₂scaff); 1.87-1.60 (2H, m, H34, H28); 1.60-1.43 (3H, m, H36, H27); 1.29-1.12 (4H, m, H36, H23, H22, H21); 1.00-0.83 (12H, m, H37, H35, H30, H29) ppm (some CH₂ of the scaffold are missed)

¹³C NMR (CDCl₃, 100 MHz): δ 174.6 (C10); 144.2 (C52, C41); 143.5 (C15); 138.1 (C12); 136.8 (C_{aromFmoc}); 129.4 (C16, C14); 129.0 (C_{aromFmoc}); 127.9 (C_{aromFmoc}); 127.4 (C17, C13); 120.2 (C_{aromFmoc}); 84.7 (C20); 65.8 (C39); 61.4 (C4); 59.8 (C3); 59.1 (C9); 51.5 (C11); 57.4 (C32); 47.3 (C40); 46.6 (C25); 41.8 (C27); 38.4 (C34); 28.0 (C23, C22, C21); 24.6 (C28); 24.4 (C36); 23.2 (C30); 22.1 (C29); 21.2 (C18); 16.0 (C35); 11.5 (C37) ppm (C38, C31, C24, C19, C9, C8, C7, C5, C2, C1 undetected)

Melting point = 98-101°C

IR: 3304 (v N-H); 2959 (v C-H); 1727-1634 (v C=O); 1533-1450 (v C=C); 1341 (v C-N); 1244 (v C-O) cm⁻¹

Compound [4.35]



To a solution of **4.8** (170 mg, 0.286 mmol, 1.0 eq.) in dry CH₂Cl₂ (3 mL) at 0°C, HCl 4M in dioxane (1.43 mL, 5.7 mmol, 20.0 eq.) was added under argon atmosphere. The reaction was let stirring 4 h at room temperature. After evaporation of the volatile under reduced pressure, the

obtained hydrochloride salt was dissolved in dry CH₃CN (2 mL), **4.11** (247.6 mg, 0.286 mmol, 1.0 eq.) and TCFH (53.9 mg, 0.315 mmol, 1.1 eq.) were added successively. At this precise moment, *N*-methylimidazole (70.6 μL, 0.886 mmol, 3.1 eq.) was added dropwise. The solution was stirred at room temperature for 2 days. After concentration under reduced pressure, the crude residue obtained was taken up with EtOAc and successively washed with water, 100% aqueous solution of NaHCO₃ and brine. The organic layer was dried over Na₂SO₄, filtered and concentrated under reduced pressure. Half of the afforded crude oil was purified by preparative HPLC eluting with H₂O + 0.1% TFA/ CH₃CN (gradient 50 to 80%) in 20 min on an Xselect column (4.6x150mm-5μm) to yield **4.35** (40.2 mg, 0.03 mmol, 10%) as a white solid.

Molecular weight = 1338.64 g mol⁻¹

R_f = 0.5 (EtOAc)

HRMS: Calcd. for [C₆₈H₉₁FN₁₀O₁₅S + H]⁺: m/z 1339.6404, found: 1339.6410 g mol⁻¹

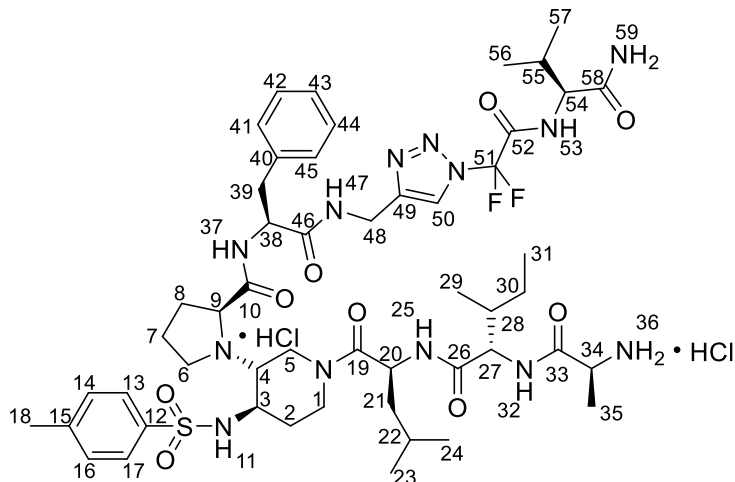
¹H NMR (CD₃OH, 600 MHz, 313K): δ 10.42-10.24 (2H, m, NH60, NH43); 10.08 (1H, bs, NH44); 8.17 (2H, d, *J* = 8.23 Hz, H59, H55); 8.15 (1H, bs, NH25); 8.00-7.90 (6H, m, *J* = 8.52, 7.92 Hz, H67, H63, H49, H47, H17, H13); 7.70-7.64 (3H, m, H57, NH37, NH32); 7.59 (1H, m, H65); 7.56-7.49 (4H, m, H66, H64, H53, H56); 7.42 (2H, d, *J* = 8.52 Hz, H16, H14); 6.79 (1H, bs, NH36); 4.82 (1H, m, H20); 4.50 (1H, m, H5); 4.27-3.96 (4H, m, H38, H34, H22, H1); 3.82 (1H, m, H9); 3.49-3.23 (3H, m, H6, H1); 2.73 (1H, m, H5); 2.47-2.22 (2H, m, H8, H2); 2.44 (3H, s, H18); 2.21-1.95 (3H, m, H39, H8, H2); 1.94-1.72 (5H, m, H28, H21, H7); 1.68-1.07 (24 H, m, H71, H70, H69, H66, H65, H64, H35, H30, H22); 1.03-0.70 (18H, m, H40, H41, H31, H29, H24, H23) ppm (H4, H3, undetected)

¹³C NMR (CD₃OH, 150 MHz, 313K): δ 174.5 (C10); 173.4 (C33); 171.8 (C26); 167.5 (C61); 166.9 (C45); 164.2 (C53); 155.3 (C50); 153.6 (C46); 137.5 (C51, C48); 144.9 (C15); 137.2 (C12); 134.6 (C62); 134.4 (C54); 133.8 (C57); 131.9 (C65); 130.3 (C59, C55); 129.6 (C16, C14); 128.5 (C66, C64, C58, C56); 127.8 (C17, C13); 127.5 (C67, C63); 116.3 (C47); 111.5 (C49); 85.8 (C68 or C63); 79.4 (C68 or C63); 58.9 (C9); 58.3 (C38, C27); 57.2 (C20); 50.3 (C34); 48.8 (C6); 44.4 (C1); 41.5 (C5); 37.0 (C28); 30.5 (C39); 30.4 (C8); 29.7 (C2); 24.4 (C7); 27.6 (C71, C70, C69 or C66, C65, C64); 26.9 (C71, C70, C69 or C66, C65, C64); 24.7 (C30); 24.6 (C22); 24.2 (C21); 21.6 (C24, C23); 20.2 (C18); 18.9 (C41, C40); 16.8 (C35); 14.6 (C31); 9.93 (C29) ppm (C67, C62, C42, C19, C4, C3 undetected)

¹⁹F NMR(CD₃OH, 376 MHz, 313K): -127.38 ppm

HPLC purity: XBridge C18 3.5 μm ; H₂O + 0:2 % form. ac./ACN, gradient 5–100 % in 20 min;
 R_t = 20.33 min, 98 %

Compound [4.36]



To a solution **4.48** (44 mg, 0.034 mmol, 1.0 eq) in CH₂Cl₂ (1 mL) under argon atmosphere HCl 4 M in dioxane (170 μL , 0.68 mmol, 20.0 eq.). The mixture was stirred for 6 h at room temperature and Et₂O was added to the suspension formed. After decantation, the solvent was carefully removed with a Pasteur pipette. The obtained solid was washed twice with Et₂O, dried under reduced pressure to afford the hydrochloride salt **4.36** (38 mg, 0.033 mmol, 97%) as a white powder.

Molecular weight = 1157.22 g mol⁻¹; free amine 1084.30 g mol⁻¹

R_f = 0 (c-Hex/EtOAc 1:1)

HRMS: Calcd. for [C₅₁H₇₅F₂N₁₃O₉S + H]⁺: m/z 1084.5578, found: 1084.5576 g mol⁻¹

¹H NMR (CD₃OH, 600 MHz, 278K): two conformers δ 9.33 (1H, d, J = 8.86 Hz, NH53); 9.13 (0.5H, d, J = 7.46 Hz, NH37); 9.08 (0.5H, d, J = 6.63 Hz, NH37); 8.82 (1H, m, NH47); 8.70 (0.5H, d, J = 6.97 Hz, NH25); 8.57 (0.5H, d, J = 7.57 Hz NH25); 8.52 (0.5H, d, J = 8.80 Hz, NH32); 8.44 (0.5H, d, J = 8.70 Hz, NH32); 8.24 (2H, m, NH36); 8.15 (0.5H, s, H50); 8.05 (0.5H, s, H50); 7.96 (1H, d, J = 8.69 Hz, NH11); 7.93-7.81 (4H, m, NH59, H17, H13); 7.48-7.42 (2H, m, H16, H14); 7.28-7.17 (5H, H45, H44, H43, H42, H41); 4.91 (0.5H, m, H20); 4.74 (0.5H, m, H20); 4.64 (1H, m, H38); 4.57 (0.5H, m, H5); 4.51-4.39 (3.5H, m, H48, H9, H5); 4.38-4.19 (3H, m, H54, H34, H27, H1); 4.00-3.80 (1.5H, m, H34, H6); 3.78-3.60 (2H, m, H6, H3, H1); 3.59-3.41 (1H, m, H6, H5); 3.35-3.14 (2H, m, H39, H5, H4, H1); 3.14-2.94 (2H, H39, H4); 2.67-2.50 (1.5H, m, H8, H1);

2.46 (1.5H, s, H18); 2.45 (1.5H, s, H18); 2.23-2.01 (3.5H, m, H55, H8, H7); 1.92 (0.5H, m, H7); 1.87-1.75 (1H, m, H28); 1.72-1.50 (4H, m, H30, H21, H2); 1.47 (1.5H, d, $J = 7.36$ Hz, H35); 1.44 (1.5H, d, $J = 7.18$ Hz, H35); 1.39-1.12 (2H, m, H30, H2); 1.04-0.98 (6H, H57, H56); 0.97-0.84 (12H, H31, H29, H24, H23) ppm

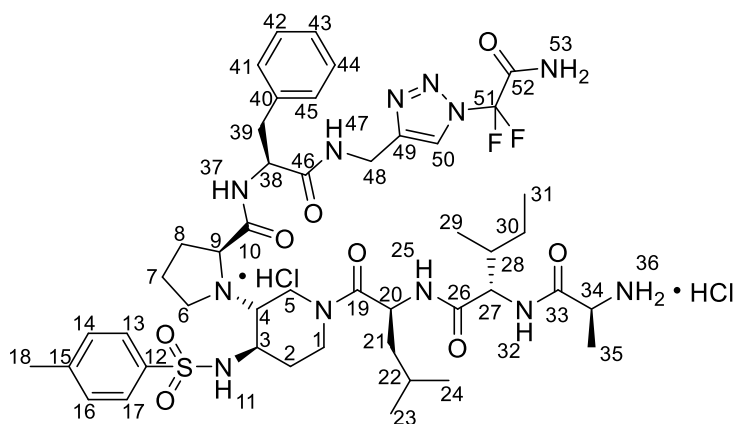
^{13}C NMR (CD₃OH, 150 MHz, 303K): two conformers δ 173.5 (C58); 172.1 (C26); 171.5 (C46); 171.4 (C19); 169.9 (C33); 169.7 (C33); 167.8 (C10); 158.7 (C52); 145.7 (C49); 143.6 (C15); 137.2 (C12); 136.1 (C40); 130.0 (C16, C14); 129.1 (C45, C41); 128.4 (C44, C42); 127.0 (C17, C13); 126.9 (C43); 121.1 (C50); 66.3 (C9); 64.0 (C4); 63.0 (C4); 59.8 (C54); 57.8 (C27); 56.6 (C38); 56.0 (C38); 51.3 (C6, C3); 50.8 (C3); 48.9 (C34); 47.6 (C20); 46.8 (C20); 43.6 (C5); 42.9 (C1); 40.4 (C1); 40.1 (C21); 38.8 (C5); 38.4 (C39); 37.8 (C39); 36.6 (C28); 34.1 (C48); 30.5 (C55); 30.0 (C8); 29.8 (C2); 24.7 (C7); 24.6 (C22); 24.4 (C30); 23.9 (C7); 22.3 (C24 or C23); 22.1 (C24 or C23); 21.4 (C24 or C23); 20.3 (C24 or C23, C18); 18.4 (C57 or C56); 17.5 (C57 or C56); 16.6 (C35); 14.5 (C31); 9.9 (C29) ppm

^{19}F NMR (CD₃OH, 565 MHz, 278K): two conformers δ -88.2; -87.6 ppm

IR: 3190 (ν N-H); 2963 (ν C-H); 1655 (ν C=O); 1542 (δ N-H); 1454 (δ C-N) cm⁻¹

HPLC purity: XBridge C18 3.5 μm ; H₂O + 0:2 % form. ac./ACN, gradient 5–100 % in 20 min; $R_t = 13.07$ min, 97%

Compound [4.37]



To a solution of **4.49** (94 mg, 0.079 mmol, 1.0 eq) in CH₂Cl₂ (1 mL) HCl 4 M in dioxane (396 μL , 1.58 mmol, 20.0 eq.) was added under argon atmosphere at 0°C. The reaction mixture was stirred for 6 h at room temperature and to the suspension formed Et₂O was added. After decantation, the solvent was carefully removed with a Pasteur pipette. The obtained solid was purified by

preparative HPLC eluting with H₂O + 0.2% formic acid/CH₃CN (gradient 20 to 80% in 15 min) on an Xselect column (4.6x150mm-5 μ m) to afford the hydrochloride salt **4.37** (22 mg, 0.021 mmol, 27%) as a white solid.

Molecular weight = 1058.08 g mol⁻¹; free amine 985.17 g mol⁻¹

R_f = 0 (c-Hex/EtOAc 1:1)

HRMS: Calcd. for [C₄₆H₆₆F₂N₁₂O₈S + H]⁺: m/z 984.4815, found: 984.4817 g mol⁻¹

¹H NMR (CD₃OH, 600 MHz, 278K): two conformers δ 8.94 (0.5H, m, NH47); 8.87 (0.5H, m, NH47); 8.80 (0.5H, d, *J* = 8.7 Hz, NH37); 8.67 (0.5H, d, *J* = 9.3 Hz, NH37); 8.53 (1H, bs, NH53); 8.37 (1H, d, *J* = 8.0 Hz, NH25); 8.36 (0.5H, s, H50); 8.31 (0.5H, s, H50); 8.23 (1H, bs, NH32); 7.83 (2H, m, H17, H13); 7.70 (0.5H, bs, NH11); 7.56 (0.5H, bs, NH11); 7.41 (2H, m, H16, H14); 7.32 (2H, m, H45, H41); 7.26 (2H, m, H44, H42); 7.21 (1H, m, H43); 4.85-4.74 (1.5H, m, H38, H20); 4.69 (0.5H, m, H38); 4.63-4.49 (2H, m, H48); 4.42 (0.5H, d, *J* = 13.6 Hz, H5); 4.28 (0.5H, d, *J* = 14.4 Hz, H5); 4.21-4.12 (1.5H, m, H27, H5); 3.81 (0.5H, d, *J* = 17 Hz, H1); 3.76-3.68 (1.5H, m, H34, H9); 3.57 (1H, m, H3); 3.38 (0.5H, m, H9); 3.31-3.21 (1.5H, m, H39, H5); 3.18-3.01 (2.5H, m, H39, H6, H1); 2.81-2.60 (2H, m, H6, H5, H4); 2.48 (0.5H, m, H1); 2.45 (3H, s, H18); 2.35 (0.5H, m, H4); 1.94 (1H, m, H8); 1.78 (0.5H, m, H28); 1.73-1.24 (11H, m, H35, H28, H22, H21, H8, H7, H2); 1.20-1.10 (1.5H, m, H30, H2); 1.04 (1H, m, H30); 0.92-0.79 (10.5H, m, H31, H29, H24, H23); 0.77 (1.5H, d, *J* = 7.0 Hz, H29) ppm

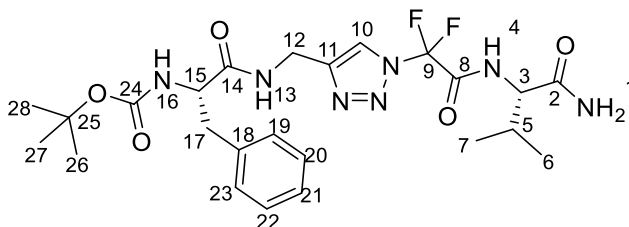
¹³C NMR (CD₃OH, 150 MHz, 278K): two conformers δ 176.4 (C10); 173.4 (C33); 173.2 (C46); 173.1 (C46); 173.0 (C33); 172.1 (C26); 171.9 (C19); 171.6 (C26); 145.5 (C49); 143.6 (C15); 137.5 (C40); 139.2 (C12); 129.8 (C16, C14); 129.4 (C45, C41); 128.1 (C44, C42); 126.7 (C17, C13); 126.1 (C43); 121.1 (C50); 63.4 (C9); 62.8 (C9); 60.1 (4); 59.5 (C4); 57.7 (C27); C 57.4 (C27); 54.3 (C38); 54.0 (C38, C3); 49.5 (C34); 46.8 (C20); 44.5 (C6); 43.9 (C1); 43.8 (C5); 40.8 (C1); 40.1 (C21); 39.8 (C5); 36.9 (C28); 37.5 (C39); 36.6 (C28); 34.2 (C48); 32.5 (C2); 31.8 (C2); 30.3 (C8); 24.8 (C30); 24.5 (C30, C22); 24.3 (C7); 22.1 (C24, C23); 20.5 (C24, 23); 20.3 (C18); 18.3 (C35); 14.6 (C29); 14.7 (C29); 10.0 (C31) ppm

¹⁹F NMR (CD₃OH, 565 MHz, 278K): two conformers δ -87.6; -87.50 ppm

IR: 3279 (ν N-H); 2961 (ν C-H); 1647 (ν C=O); 1524 (δ N-H); 1451 (δ C-N) cm⁻¹

HPLC purity: XBridge C18 3.5 μ m; H₂O + 0.2 % form. ac./ACN, gradient 5–100 % in 20 min; R_t = 12.41 min, 90 %

***tert*-butyl ((*S*)-1-(((1-(2-(((*S*)-1-amino-3-methyl-1-oxobutan-2-yl)amino)-1,1-difluoro-2-oxoethyl)-1*H*-1,2,3-triazol-4-yl)methyl)amino)-1-oxo-3-phenylpropan-2-yl)carbamate [4.38]**



To a solution of **4.41** (200 mg, 0.85 mmol, 1.0 eq.) and **4.40** (257 mg, 0.85 mmol, 1.0 eq.) in a mixture of MeOH and H₂O (3:1 v:v, 10 mL), TBTA (4.5 mg, 8.5 μmol, 0.01 eq.), sodium ascorbate (34 mg, 0.17 mmol, 0.2 eq.) and CuSO₄·5H₂O (21.2 mg, 0.085 mmol, 0.1 eq.) were added under argon atmosphere. The reaction mixture was stirred for 4 days at room temperature meanwhile the colour turned to light blue. After concentration under reduced pressure, the crude residue was taken up with H₂O (15 mL) and extracted with EtOAc. The organic layer was washed with H₂O, brine, dried over Na₂SO₄ and the volatile was removed under reduced pressure. The crude residue obtained was purified by column chromatography on silica gel eluting with *c*-Hex/EtOAc 7:3 to afford **4.38** as a white powder (168 mg, 0.31 mmol, 37%).

Molecular weight = 537.57 g mol⁻¹

R_f = 0.1 (*c*-Hex/EtOAc 7:3)

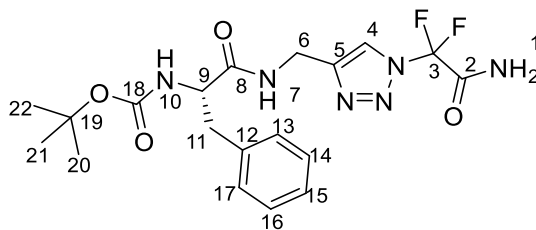
HRMS: Calcd. for [C₂₄H₃₃F₂N₇O₅ + H]⁺: *m/z* 538.2583, found: 538.2589; Calcd. for [C₂₄H₃₃F₂N₇O₅ + Na]⁺: *m/z* 560.2403, found: 560.2421; Calcd. for [C₂₄H₃₃F₂N₇O₅ + NH₄]⁺: *m/z* 555.2849, found: 555.2861

¹H NMR (CD₃OD, 400 MHz): δ 8.18 (1H, s, H10); 7.29-7.14 (5H, m, H19, H20, H21, H22, H23); 4.46 (2H, s, H12); 4.32 (1H, d, *J* = 7.5 Hz, H3); 4.26 (1H, m, H15), 3.18 (1H, m, H5); 3.05 (1H, dd, *J* = 6.6, 13.6 Hz, H17); 2.86 (1H, dd, *J* = 6.6 Hz, 13.6 Hz, H17); 1.37 (9H, bs, H26, H27, H28); 1.02 (3H, d, *J* = 6.9 Hz, H7); 1.00 (3H, d, *J* = 6.7 Hz)

¹³C NMR (CD₃OD, 100 MHz): δ 177.9 (C2); 174.6 (C14); 159.9 (*J*_{C-F} = 32.4 Hz, C8); 147.6 (C11); 147.4 (C24); 138.5 (C18); 130.6, 129.5, 127.9 (C19, C20, C21, C22, C23); 122.4 (C10); 112.6 (*J*_{C-F} = 267.7 Hz, C9); 80.7 (C25); 60.9 (C3); 57.6 (C15); 39.1 (C17); 35.5 (C12); 31.8 (C5); 28.6 (C26, C27, C28); 19.7 (C7), 18.7 (C6)

¹⁹F NMR (CD₃OD, 376 MHz): δ -87.61 (*J* = 206.5 Hz); -88.39 (*J* = 206.5 Hz)

***tert*-butyl (*S*)-(1-(((1-(2-amino-1,1-difluoro-2-oxoethyl)-1H-1,2,3-triazol-4-yl)-methyl)amino)-1-oxo-3-phenylpropan-2-yl)carbamate [4.39]**



To a solution of ethyl 2-bromo-2,2-difluoroacetate (0.63 mL, 4.92mmol, 1.0 eq.) in dry DMF (10 mL), NaN₃ (385 mg, 5.90 mmol, 1.2 eq.) was added. The reaction mixture was stirred overnight in a sealed tube at 35°C. After completion checked by ¹⁹F-NMR, NH₃ (3.5 mL, 7M in MeOH) was added at 0°C. The suspension was then let in an ultrasonic heated bath for 5 h and the crude was diluted with H₂O (20 mL) and extracted with Et₂O. The organic layer was then washed with H₂O, brine and dried over Na₂SO₄. After evaporation under reduced pressure, the obtained white powder was used without any further purification in the following reaction. Precisely, to a solution of the azide (329 mg, 2.41 mmol, 1.0 eq.) and compound **4.40** (729 mg, 2.41 mmol, 1.0 eq.) in a mixture of MeOH/H₂O (3:1 v:v 28 mL) under argon atmosphere, TBTA (12.8 mg, 24.1 μmol, 0.01 eq.), sodium ascorbate (96 mg, 0.482 mmol, 0.2 eq.) and CuSO₄·5H₂O (60 mg, 0.241 mmol, 0.1 eq.) were added. The reaction mixture was then stirred for 4 days at room temperature. The suspension was concentrated under reduced pressure, taken up with H₂O (20 mL) and extracted with EtOAc. The organic layer was washed with H₂O, brine, dried over Na₂SO₄ and the volatile was removed under reduced pressure. The obtained crude residue was purified by column chromatography eluting with *c*-Hex/EtOAc 8:2 up to 1:1 to afford **4.39** (677 mg, 1.54 mmol, 65%) as a white solid.

Molecular weight = 438.18 g mol⁻¹

R_f = 0.2 (CH₂Cl₂/MeOH 95:5)

HRMS: Calcd. for [C₁₉H₂₄F₂N₆O₄ + H]⁺: m/z 439.1861, found: 439.1905; Calcd. for [C₁₉H₂₃F₂N₆O₄ + Na]⁺: m/z 461.1719, found: 461.1735

¹H NMR (DMSO-*d*₆, 400 MHz): 8.56 (1H, t, *J* = 5.6 Hz, NH7); 8.35 (1H, s, H4); 7.35-7.17 (7H, m, H1, H13, H14, H15, H16, H17); 7.01 (1H, d, *J* = 8.5 Hz, NH10); 4.46 (1H, dd, *J* = 5.7, 15.6 Hz, H6); 4.39 (1H, dd, *J* = 5.5, 15.6 Hz, H6); 4.22-4.16 (1H, m, H9); 2.99 (1H, dd, *J* = 4.7, 13.8 Hz, H11); 2.80 (1H, dd, *J* = 9.8, 13.8, H11); 1.35 (9H, s, H20, H21, H22) ppm

^{13}C NMR (DMSO-*d*₆, 100 MHz): δ 172.9 (C8); 160.2 ($J_{\text{C-F}} = 30.4$ Hz, C2); 156.3 (C18); 147.3 (C5); 138.9 (C12); 130.1 (C13, C17); 128.8, 127.1 (C14, C15, C16); 122.2 (C4); 111.2 ($J_{\text{C-F}} = 269.9$ Hz, C3); 79.0 (C19); 56.8 (C9); 38.2 (C11); 34.9 (C6); 29.0 (C20, C21, C22) ppm

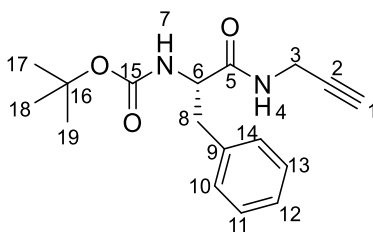
^{19}F NMR (DMSO-*d*₆, 376 MHz): δ -86.00 ppm

Melting point = 66-69°C

IR: 3332 (ν N-H); 1719-1660 (ν C=O); 1519 (δ C=C) cm^{-1}

***tert*-butyl (*S*)-(1-oxo-3-phenyl-1-(prop-2-yn-1-ylamino)propan-2-yl)carbamate**

[4.40]



To a stirred solution of *L*-Boc-NH-Phe-OH (1.0 g, 3.77 mmol, 1.0 eq.) in dry CH_2Cl_2 (20 mL) were successively added at 0°C under argon atmosphere HOBt (0.61 g, 4.52 mmol, 1.2 eq.), EDC·HCl (0.87 g, 4.52 mmol, 1.2 eq.), propargylamine·HCl (0.41 g, 4.52 mmol, 1.2 eq.) and NEt_3 (1.31 mL, 9.42 mmol, 2.5 eq.). The reaction mixture was stirred for 4 h at room temperature and then successively washed with 10% aqueous solution of citric acid, 10% aqueous solution of K_2CO_3 and brine, dried over Na_2SO_4 , filtered and concentrated under reduced pressure to give **4.40** as a white solid (1.02 g, 3.40 mmol, 90%).

Molecular weight = 302.37 g mol^{-1}

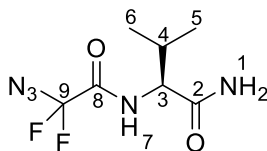
R_f = 0.5 (c-Hex/EtOAc 1:1)

HRMS: Calcd. for $[\text{C}_{17}\text{H}_{22}\text{N}_2\text{O}_3 + \text{H}]^+$: m/z 303.1664, found: 303.1691

^1H NMR (CDCl_3 , 300 MHz): δ 7.45-7.15 (5H, m, H10, H11, H12, H13, H14); 6.35 (1H, bs, NH7); 5.12 (1H, bs, NH4); 4.36 (1H, m, H6); 3.99 (2H, m, H3); 3.08 (2H, d, $J = 6.8$ Hz, H8); 2.20 (1H, t, $J = 2.4$ Hz, H1); 1.41 (9H, s, H17, H18, H19) ppm

Analysis are coherent with what it is reported in literature¹⁹¹

(S)-2-(2-azido-2,2-difluoroacetamido)-3-methylbutanamide [4.41]



To a solution of ethyl 2-bromo-2,2-difluoroacetate (0.63 mL, 4.92mmol, 1.0 eq.) in dry DMF (10 mL), NaN₃ (385 mg, 5.90 mmol, 1.2 eq.) was added. The reaction mixture was stirred overnight in a sealed tube at 35°C. After completion checked by ¹⁹F-NMR, *L*-Valinamide hydrochloride (751 mg, 4.92 mmol, 1.0 eq.) and NEt₃ (1.03 mL, 7.38 mmol, 1.5 eq.) were added at 0°C. The suspension was then let in an ultrasonic heating bath for 4 h, then diluted with H₂O (20 mL) and extracted with Et₂O. The organic layer was then washed with H₂O and brine, dried over Na₂SO₄, filtered and concentrated under reduced pressure, without heating to afford **4.41** (493 mg, 2.10 mmol, 43%) as a white solid.

Molecular weight = 235.15 g mol⁻¹

R_f = 0 (c-Hex/EtOAc 1:1)

HRMS: Calcd. for [C₇H₁₁F₂N₅O₂ + H]⁺: m/z 236.0914, found: 236.0975

¹H NMR (CDCl₃, 200 MHz): δ 7.15 (1H, bs, NH7); 5.97 (1H, bs, NH1); 5.84 (1H, bs, H1); 4.36 (1H, m, H3); 2.16 (1H, m, H4); 1.03 (3H, d, J = 4.8 Hz); 1.00 (3H, d, J = 4.8 Hz) ppm

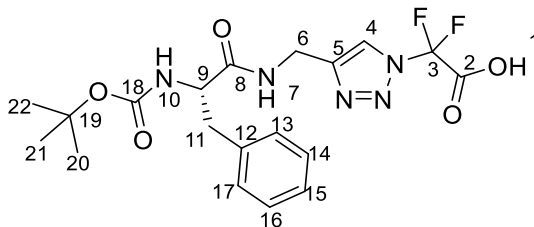
¹³C NMR (CDCl₃, 75 MHz): δ 171.9 (C2); 58.6 (C3); 31.8 (C4); 19.6 (5); 18.5 (C6) ppm

¹⁹F NMR (CDCl₃, 188 MHz): δ -83.02 (J = 21.5 Hz); -83.12 (J = 21.5 Hz) ppm

Melting point = 56-58°C

IR: 3383 (ν N-H); 1721-1670 (ν C=O); 1557 (δ C=C) cm⁻¹

(S)-2-(4-((2-((tert-butoxycarbonyl)amino)-3-phenylpropanamido)methyl)-1H-1,2,3-triazol-1-yl)-2,2-difluoroacetic acid [4.44]



To a solution of ethyl 2-bromo-2,2-difluoroacetate (0.200 mL, 4.92mmol, 1.0 eq.) in dry DMF (10 mL) was added NaN₃ (385 mg, 5.90 mmol, 1.2 eq.). The reaction mixture was stirred overnight in

a sealed tube at 35 °C. After completion checked by ^{19}F -NMR, the volatile was removed under reduced pressure and the azide obtained was used in the following reaction without further purification. Precisely, to a solution of the azide (200 mg, 1.21 mmol, 1.0 eq. and **4.40** (366 mg, 1.21 mmol, 1.0 eq.) in a mixture of MeOH/H₂O (3:1 v:v, 12 mL) under argon atmosphere TBTA (6.4 mg, 21 μmol , 0.01 eq.), sodium ascorbate (48 mg, 0.24 mmol, 0.2 eq.) and CuSO₄·5H₂O (30.2 mg, 0.12 mmol, 0.1 eq.) were added. The reaction mixture was stirred for 2 days at room temperature. The suspension was concentrated under reduced pressure, taken up with H₂O (20 mL) and extracted with EtOAc. The organic layer was washed with H₂O, brine, dried over Na₂SO₄ and the volatile was removed under reduced pressure. The crude residue obtained was purified by column chromatography on silica gel eluting with CH₂Cl₂/MeOH 95:5 up to 80:20 to afford **4.44** (229 mg, 0.52 mmol, 43%) as a white powder.

Molecular weight = 439.42 g mol⁻¹

R_f = 0.1 (CH₂Cl₂/MeOH 95:5)

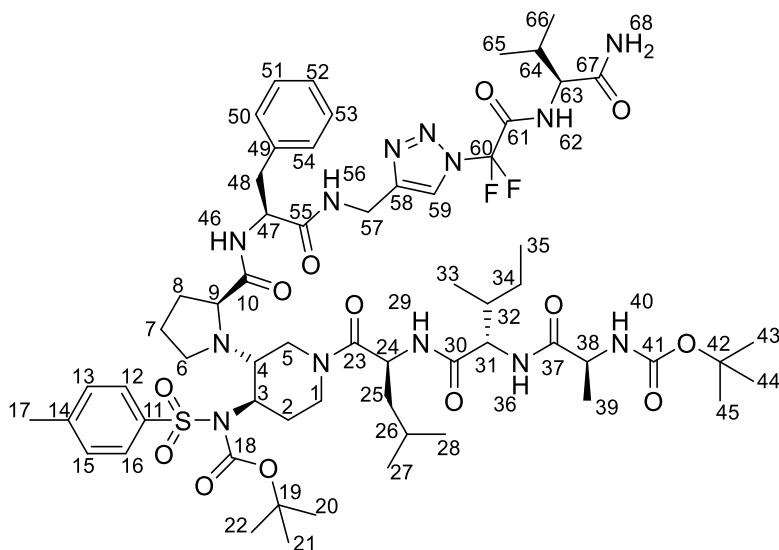
HRMS: Calcd. for [C₁₉H₂₃F₂N₅O₅ + H]⁺: m/z 440.1739, found: 440.1734; Calcd. for [C₁₉H₂₃F₂N₅O₅ + Na]⁺: m/z 462.1559, found: 462.1536

^1H NMR (CD₃OD, 400 MHz): δ 8.07 (1H, s, H4); 7.29-7.14 (5H, m, H13, H14, H15, H16, H17); 4.45 (2H, d, J = 3.46 Hz, H6); 4.27 (1H, m, H9); 3.06 (1H, d, J = 6.50 Hz, 13.6 Hz, H11); 2.85 (1H, d, J = 6.50 Hz, 13.6 Hz, H11); 1.37 (9H, s, H21, H22, H23) ppm

^{13}C NMR (CD₃OD, 100 MHz): δ 174.6 (C8); 163.5 (C2); 157.6 (C3); 146.5 (C5); 138.4 (C12); 130.5, 129.5, 127.8 (C13, C14, C15, C16, C17); 122.6 (C4); 80.7 (C19); 57.6 (C9); 39.8 (C11); 35.3 (C6); 28.6 (C20, C21, C22) ppm

^{19}F NMR (CD₃OD, 376 MHz): δ -87.45 ppm

Compound [4.48]



To a stirred solution of **4.38** (110 mg, 0.25 mmol, 1.0 eq.) in dioxane (4mL), HCl 4M in dioxane (1.25 mL, 5 mmol, 20.0 eq.) was added under argon atmosphere, at 0°C. The reaction was let stirring 2 h at room temperature. After removal of the volatile under reduced pressure, the obtained hydrochloride salt was used for the following peptide coupling without further purification. Precisely, to a stirred solution of **4.11** (178 mg, 0.205 mmol, 1.0 eq.) in dry DMF (5 mL), cooled at 0°C, COMU (88 mg, 0.205 mmol, 1.0 eq) and oxyma (29 mg, 0.205 mmol, 1.0 eq.) were added. The reaction mixture was stirred for 30 min at 0°C, at that moment the hydrochloric salt of **4.38** (97 mg, 0.205 mmol, 1.0 eq.) and collidine (68 μ L, 0.512 mmol, 2.5 eq.) were added. The solution was stirred at room temperature overnight under argon atmosphere. The volatile was removed under reduced pressure and the obtained crude oil was taken up with EtOAc, washed with 100% aqueous solution of NaHCO₃, water and brine. The organic layer was dried over Na₂SO₄, filtered and concentrated under reduced pressure. The obtained residue was purified on silica gel, eluting with CH₂Cl₂/EtOAc 6/4 + 1% NH₃ 7N in MeOH to afford **4.48** (54 mg, 0.042 mmol, 21%) as a white solid.

Molecular weight = 1284.54 g mol⁻¹

R_f = 0.3 (EtOAc)

HRMS: Calcd. for [C₆₁H₉₁F₂N₁₃O₁₃S + H]⁺: m/z 1284.6626, found: 1284.6616 g mol⁻¹

¹H NMR 8.96 (1H, bs, NH62); 8.22 (1H, bs, NH29); 8.15 (0.5H, bs, H59); 8.08 (0.5H, bs, H59); 7.99 (0.5H, bs, NH36); 7.95-7.80 (2H, m, H16, H12); 7.68 (1.5H, m, NH36, NH?); 7.43 (2H, d, J

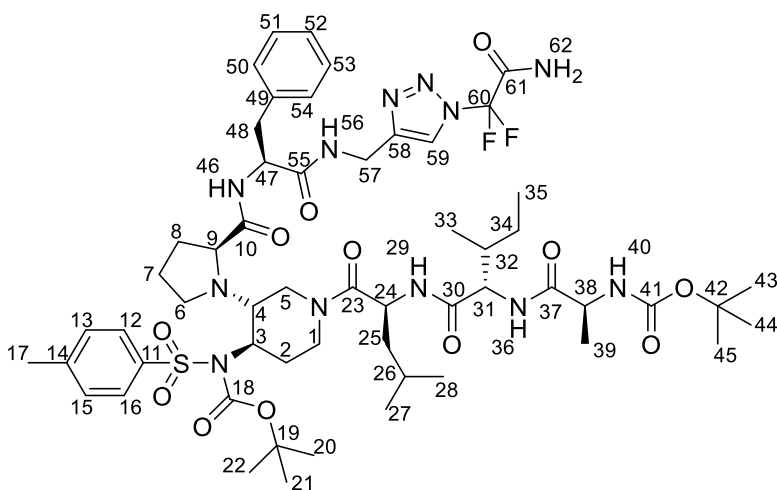
= 8.5 Hz, H15, H13); 7.29-7.14 7.27 (5H, m, H54, H53, H52, H51, H50); 6.79-6.56 (1H, NH40); 4.91 (1H, m, H24); 4.67 (1H, m, H47); 4.49 (3H, m, H57, H8); 4.33 (1H, bs, H63); 4.30-4.03 (3H, m, H38, H31, H1); 3.90 (1H, d, $J = 12.3$ Hz, H3); 3.64 (1H, d, $J = 12.0$ Hz, H4); 3.49 (1H, bs, H9); 3.31-3.14 (2H, m, H48, H1); 3.08 (0.5H, m, H48); 3.04-2.84 (1.5H, m, H48, H6); 2.83-2.67 (2H, m, H8, H6); 2.46 (3H, s, H17); 2.43 (1H, m, H2); 2.35 (2H, bs, H7); 2.26-2.07 (2H, H64, H2); 2.02-1.86 (1.5H, m, H32, H5); 1.82 (0.5H, bs, H32); 1.75 (1H, m, H5); 1.69-1.36 (12H, m, H26, H25, H22, H21, H20); 1.32-1.10 (14H, m, H45, H44, H43, H39, H34); 1.04-0.96 (6H, m, H66, H65); 0.96-0.79 (12H, m, H35, H33, H28, H27) ppm (NH46, NH56, NH68 undetected)

^{13}C NMR (CD₃OH, 150 MHz, 313K): two conformers δ 175.9 (C37); 175.2 (C67); 173.7 (C30); 148.0 (C58); 146.7 (C14); 140.2 (C11); 139.7 (C11); 139.6 (C49); 132.2 (C15, C13); 130.6 (C54, C50); 129.9 (C53, C51); 129.5 (C16, C12); 128.8 (C52); 122.8 (C59); 87.4 (C42); 81.2 (C19); 66.9 (C4); 66.5 (C3); 61.3 (C63, C9); 61.2 (C63); 59.4 (C31); 57.1 (C47); 52.1 (C38); 49.5 (C24); 48.7 (C6); 47.2 (C1); 43.9 (C2); 43.3 (C8); 42.9 (C25); 42.6 (C25); 39.4 (C48); 38.8 (C48); 37.1 (C32); 36.0 (C57); 33.0 (C5); 32.3 (C64); 31.0 (C7); 29.2 (C22, C21, C20); 28.7 (C45, C44, C43); 26.4 (C26); 24.7 (C34); 24.1 (C27); 22.8 (C28); 22.0 (C17); 20.2 (C66); 19.2 (C65); 18.7 (C39); 16.5 (C33); 11.7 (C35) ppm (C10, C18, C23, C41, C55, C60, C61 undetected)

^{19}F NMR (CD₃OH, 376 MHz, 313K): -88.58 ppm

HPLC purity: XBridge C18 3.5 μm ; H₂O + 0:2 % form. ac./ACN, gradient 5–100 % in 20 min; $R_t = 20.15$ min, 90 %

Compound [4.49]



To a stirred solution of **4.39** (94 mg, 0.214 mmol, 1.0 eq.) in dioxane (4mL), HCl 4M in dioxane (1.14 mL, 4.56 mmol, 20.0 eq.) was added under argon atmosphere, at 0°C. The reaction was let stirring 2 h at room temperature. After removal of the volatile under reduced pressure, the obtained hydrochloride salt was used for the following peptide coupling without further purification. Precisely, to a solution of **4.11** (185 mg, 0.214 mmol, 1.0 eq.) in dry DMF (5 mL), cooled at 0°C, COMU (92 mg, 0.214 mmol, 1.0 eq.) and oxyma (30 mg, 0.214 mmol, 1.0 eq.) were added. The reaction mixture was stirred for 30 min at 0°C, at that moment the hydrochloric salt of **4.39** (80 mg, 0.214 mmol, 1.0 eq.) and collidine (71 μ L, 0.535 mmol, 2.5 eq.) were added. The solution was stirred at room temperature overnight under argon atmosphere. After concentration under reduced pressure, the obtained crude oil was taken up with EtOAc, washed successively with 100% aqueous solution of NaHCO₃ water and brine. The organic layer was dried over Na₂SO₄, filtered and concentrated under reduced pressure. The afforded residue was purified on silica gel, eluting with c-Hex/EtOAc 3/7 + 1% NH₃ 7N in MeOH to give **4.49** (111 mg, 0.095 mmol, 44%) as a white solid.

Molecular weight = 1185.40 g mol⁻¹

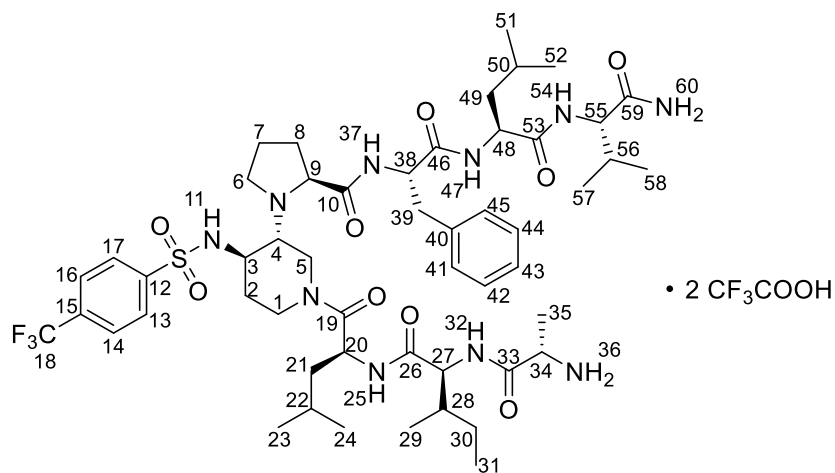
Rf = 0.2 (c-Hex/EtOAc 3/7 + 1% NH₃ 7N in MeOH)

HRMS: Calcd. for [C₅₆H₈₂F₂N₁₂O₁₂S + H]⁺: m/z 1185.5942, found: 1185.5933 g mol⁻¹

¹⁹F NMR (CD₃OH, 376 MHz): -87.80 ppm

HPLC purity: XBridge C18 3.5 μ m; H₂O + 0:2 % form. ac./ACN, gradient 5–100 % in 20 min; Rt = 19.87 min, 88 %

Compound [4.50]



4.50 was obtained in solid phase peptide synthesis using Rink-amide resin (300mg, loading 0.64 mmol g⁻¹). Fmoc-amino acid was coupled using standard conditions (AA/HOBt/HBTU/DIPEA 3:3:3:6) shaking for 1:30 h. Each coupling step was followed by a capping step operated with Ac₂O (1 eq.) and DIPEA (1 eq.). The complete peptide cleavage from the resin was performed using the cocktail (TFA/H₂O/Phenol/TIPS 90:5:2.5:2.5). After precipitation in cold Et₂O the peptide was washed several times with cold Et₂O and the crude peptide obtained was purified by preparative HPLC eluting with H₂O + 0.2 % TFA/CH₃CN (gradient 40 to 60% in 25 min) on an Xselect column (4.6x150mm-5μm) to afford **56** (22 mg, 0.017 mmol, 9%) as a white solid.

Molecular weight = 1304.57 g mol⁻¹; free amine = 1077.32 g mol⁻¹

R_f = 0.3 (c-Hex/EtOAc 3/7)

HRMS: Calcd. for [C₅₂H₇₉F₃N₁₀O₉S + H]⁺: m/z 1077.5738, found: 1077.5736 g mol⁻¹

¹H NMR (CD₃OH, 600 MHz, 303K): two conformers δ 8.66 (0.5H, d, *J* = 7.53 Hz, NH47); 8.56 (0.5H, d, *J* = 9.84 Hz NH37); 8.43 (0.5H, d, *J* = 9.37 Hz, NH37); 8.40 (0.5H, d, *J* = 7.37 Hz, NH47); 8.28 (1H, d, *J* = 8.65 Hz, NH 32); 8.22 (1H, m, NH25); 8.19 (2H, m, NH36); 8.13 (2.5H, m, H17, H23, NH11); 8.00 (0.5H, d, *J* = 8.23 Hz, NH54); 7.96-7.88 (2.5H, m, H16, H14, NH11); 7.84 (0.5H, d, *J* = 8.82 Hz NH54); 7.61 (1H, s, NH60); 7.35 (2H, d, *J* = 7.50 Hz, H45, H41); 7.27 (2H, m, H44, H42); 7.20 (1H, m, H43); 7.00 (1H, d, *J* = 10.80 Hz NH60); 4.88 (1H, m, H20); 4.87 (0.5H, m, H38); 4.79 (0.5H, m, H38); 4.56-4.42 (1.5H, m, H48, H5); 4.31 (0.5H, d, *J* = 15.73 Hz, H1); 4.28-4.17 (2H, m, H55, H27, H5); 4.13 (0.5H, m, H55); 3.96 (1H, m, H34); 3.83 (0.5H, d, *J* = 18.15 Hz, H1); 3.79-3.60 (1.5H, H9, H3); 3.38-3.02 (4H, m, H39, H9, H6, H5, H1); 2.80-2.59 (1.5H, m, H6, H5); 2.52 (0.5H, m, H1); 2.46 (0.5H, m, H4); 2.26 (0.5H, bs, H4); 2.10-1.87 (2H, m H56, H8); 1.84-1.71 (1.5H, m, H28, H2); 1.71-1.49 (6.5H, m, H50, H49, H22, H21, H2, H7); 1.49-1.22 (7H, m, H35, H21, H8, H7, H2); 1.12 (1H, m, H30); 1.09 (1H, m, H30); 0.99-0.81 (22.5H, m, H58, H57, H52, H51, H31, H29, H24, H23,); 0.77 (1.5H, d, *J* = 7.29 Hz H31) ppm

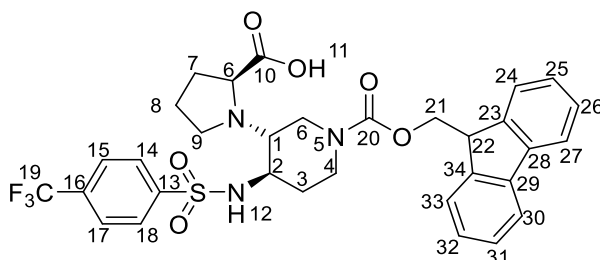
¹³C NMR (CD₃OH, 150 MHz, 303K): two conformers δ 174.6 (C59); 173.5 (C46); 173.4 (C53); 173.1 (C46); 173.0 (C53); 171.2 (C26); 169.9 (C33); 146.5 (C15); 137.4 (C40); 133.8 (C12); 129.2 (C45, C41); 128.1 (C44, C42); 127.4 (C17, C13); 126.5 (C43); 126.4 (C16, C14); 62.8 (C9); 60.6 (C4); 59.8 (C4); 58.8 (C55); 58.1 (C55, C27); 54.3 (C3); 54.1 (C38); 54.0 (C38); 51.9 (C48); 48.8 (C34, C3); 46.7 (C20); 44.7 (C6); 44.6 (C6); 44.0 (C1); 43.9 (C5); 40.9 (C1); 40.5 (C49, C21); 39.8 (C5); 37.8 (C39); 36.8 (C28); 33.1 (C2); 31.7 (C2); 30.9 (C56); 30.3 (C8); 24.8 (C30); 24.7 (C50, C22); 24.6 (C7); 24.3 (C7); 22.1 (C24 or C23, C52 or C51); 20.9 (C52 or C51); 20.8 (C24

or C23); 18.4 (C58 or C57); 17.5 (C58 or C57); 16.6 (C35); 14.9 (C31); 14.6 (C31); 10.3 (C29); 9.9 (C29) ppm (C19, C10 undetected)

^{19}F NMR (CD_3OH , 565 MHz, 278K): δ -64.7 ppm

HPLC purity: XBridge C18 3.5 μm ; H_2O + 0:2 % form. ac./ACN, gradient 5–100 % in 20 min; R_t = 20.33 min, 98 %

((3*R*,4*R*)-1-(((9*H*-fluoren-9-yl)methoxy)carbonyl)-4-((4-(trifluoromethyl)phenyl)sulfonamido)piperidin-3-yl)-*L*-proline [4.52]



To a solution of **4.61** (0.265 g, 0.536 mmol, 1 eq.) in $\text{CH}_3\text{CN}/\text{MeOH}$ (4:1, 5.5 mL) were added Fmoc-OSu (0.199 g, 0.590 mmol, 1.1 eq.) and DIPEA (145 μL , 1.07 mmol, 2.0 eq.). After 3 h under stirring, the volatiles were removed under reduced pressure. The crude was taken up with CH_2Cl_2 and successively washed 3 times with H_2O and brine, dried over Na_2SO_4 and concentrated under vacuum. After precipitation from EtOAc/*c*-Hex, **4.52** was afforded as a white solid (310.5 mg, 0.483 mmol, 90%).

Molecular weight = 643.68 g mol^{-1}

R_f = 0.4 ($\text{CH}_2\text{Cl}_2/\text{MeOH}$ 10:1) free amine

HRMS: Calcd. for $[\text{C}_{32}\text{H}_{32}\text{F}_3\text{N}_3\text{O}_6\text{S} + \text{H}]^+$: m/z 644.2042, found: 644.2039

^1H NMR (CDCl_3 , 400 MHz): δ 8,08 (2H, d, J = 7.3 Hz, H15, H17); 7,87 (2H, d, J = 7.3 Hz, H14, H18); 7,77 (2H, d, J = 7.0 Hz, H27, H30); 7,53 (2H, d, J = 7.7 Hz, H24, H33); 7,37 (2H, m, H26, H31); 7,29 (2H, m, H25, H32); 4,51 (2H, dd, J = 5.24 Hz, H21); 4,17 (1H, t, J = 5.24 Hz, H22); 3,58 (1H, m, H6); 3,03 (1H, m, H2); 2,66 (2H, $\text{CH}_{2\text{scaf.}}$); 2,56-2,35 (1H, m, H1, $\text{CH}_{2\text{scaf.}}$); 2,19-1.85 (4H, m, $\text{CH}_{2\text{scaf.}}$); 1,55 (1H, m, $\text{CH}_{2\text{scaf.}}$); 1,35 (1H, m, $\text{CH}_{2\text{scaf.}}$); 1,18 (1H, m, $\text{CH}_{2\text{scaf.}}$) ppm

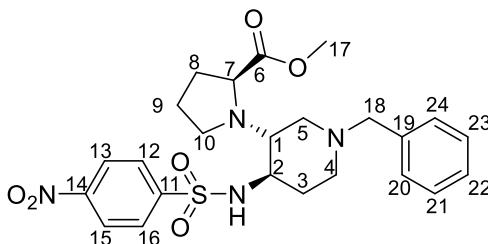
^{13}C NMR (CDCl_3 , 100 MHz): δ 180,2 (C10); 156,6 (C20); 145,5 (C13); 145,2 (C23, C34); 142,7 (C28, C29); 135,2 (C16, $J_{\text{C-F}}$ = 32.8 Hz); 129,3 (C15, C17); 128,8 (C26, C31); 128,2 (C25, C32); 127,4 (C14, C18); 125,8 (C24, C33); 121,1 (C27, C30); 68,0 (C21); 60,8 (C1); 54,0 (C2); 48,7 (C22); 46,9 ($\text{CH}_{2\text{scaf.}}$); 42,9 ($\text{CH}_{2\text{scaf.}}$); 33,6 ($\text{CH}_{2\text{scaf.}}$); 31,1 ($\text{CH}_{2\text{scaf.}}$); 25,5 ($\text{CH}_{2\text{scaf.}}$) ppm

^{19}F NMR (CDCl_3 , 376 MHz): δ -64.5 ppm

Melting point = 151-154°C

IR: 3507 (ν O-H); 1687 (ν C=O); 1562 (ν C=C); 1323 (ν C-O) cm^{-1}

Methyl ((3*R*,4*R*)-1-benzyl-4-((4-nitrophenyl)sulfonamido)piperidin-3-yl)-*L*-prolinate [4.54]



To a solution of *L*-proline methyl ester hydrochloride (5 g, 30.2 mmol, 1 eq.) in 1,2 dichloroethane (20 mL), TEA (4.3 mL, 30.2 mmol, 1 eq.) was added. After 30 min at room temperature, 4-benzylpiperidone (5.6 mL, 30.2 mmol, 1eq.) was added under argon atmosphere with molecular sieves (3 Å), followed after a period of 45 min by a catalytic amount of InCl_3 (668 mg, 3.02 mmol, 0.1 eq.). The reaction mixture was let stirring 45 min, cooled to 0°C and a solution of nosyl azide (prepared as reported in the literature) (6.9 g, 30.2 mmol, 1 eq.) in 1,2 dichloroethane (25 mL) was added dropwise, while maintaining the temperature at 0°C. After 45 min at room temperature $\text{NaBH}(\text{OAc})_3$ (16 g, 75.5 mmol, 2.5 eq.) was added and the mixture was let under stirring at room temperature overnight. The reaction mixture was filtered through a Celite pad with CH_2Cl_2 and the filtrate was washed with distilled water, dried over Na_2SO_4 and the volatile was removed under reduced pressure. The crude residue obtained was purified by column chromatography on silica gel eluting with *c*-Hex/EtOAc 6:4 which led to the good but not pure diastereoisomer (R,R,S) **4.54**. The not completely pure compound **4.54** was solubilized in CH_2Cl_2 and the impurity was precipitated with cyclohexane. After concentration of the volatile under reduced pressure pure compound **4.54** was afforded as a yellow powder (1.80 g, 3.58 mmol, 12%).

Molecular weight = 502.58 g mol^{-1}

*R*_f = 0.40 (*c*-Hex/EtOAc 1:1)

HRMS: Calcd. for $[\text{C}_{24}\text{H}_{30}\text{N}_4\text{O}_6\text{S} + \text{H}]^+$: m/z 503.1964, found: 503.1969

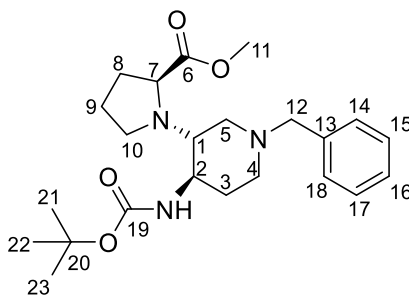
^1H NMR (Acetone-*d*₆, 400 MHz): δ 8.44 (2H, d, J = 8.9 Hz, H12, H16); 8.16 (2H, d, J = 8.9 Hz, H13, H15); 7.27-7.22 (5H, m, H20, H21, H22, H23, H24); 7.27 (1H, NH); 3.75 (3H, s, H17); 3.53-

3.43 (3H, m, H7, H18); 2.92-2.73 (3H, m, H5, H2, H4); 2.59 (1H, td, $J = 10.7, 3.9$ Hz, H1); 2.39-2.30 (2H, m, H10, H3); 2.04-1.78 (4H, m, H5, H4, H8); 1.75-1.31 (4H, m, H10, H3, H9) ppm
 ^{13}C NMR (Acetone- d_6 , 100 MHz): δ 177.6 (C6); 151.0 (C14); 147.4 (C11); 139.5 (C19); 129.6 (C12, C16); 129.5 (C20, C21, C23, C24); 127.45 (C22); 124.5 (C13, C15); 63.0 (C18); 62.5 (C7); 59.4 (C1); 54.5 (C2); 52.5 (C5); 52.4 (C17); 51.8 (C4); 44.9 (C10); 34.1 (C3); 29.9 (C8); 24.7 (C9) ppm

Melting point = 75-77°C

IR: 3168 (ν N-H); 2953-2820 (ν C-H); 1723 (ν C=O); 1527 (ν NO₂); 1347 (ν NO₂) cm⁻¹

Methyl ((3*R*,4*R*)-1-benzyl-4-((*tert*-butoxycarbonyl)amino)piperidin-3-yl)-*L*-prolinate [4.55]



To a stirred solution of **4.58** (1.23 g, 2.0 mmol, 1.0 eq.) in CH₃CN (30 mL) and DMSO (0.6 mL) under argon atmosphere K₂CO₃ (842 mg, 6.0 mmol, 3.0 eq.) and thiophenol (310 μ L, 3.0 mmol, 1.5 eq.) were added. The reaction was stirred at 70°C overnight. After concentration under vacuum the crude residue was taken up with EtOAc and successively washed with 100 % aqueous solution of NaHCO₃ and brine, dried over Na₂SO₄, filtered and concentrated under vacuum. The residue was purified by column chromatography on a silica gel eluting with *c*-Hex/EtOAc 6:4 to afford compound **4.55** as a pale-yellow oil (763 mg, 1.82 mmol, 90%).

Molecular weight = 417.54 g mol⁻¹

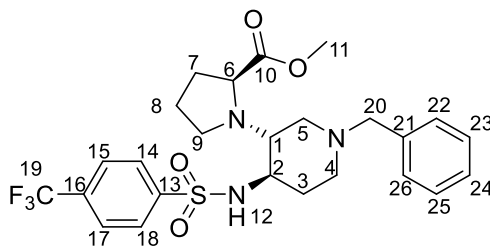
R_f = 0.50 (*c*-Hex/EtOAc 6:4)

HRMS: Calcd. for [C₂₃H₃₅N₃O₄ + H]⁺: m/z 418.2706, found: 418.2712

^1H NMR (Acetone- d_6 , 400 MHz): δ 7.45-7.24 (5H, m, H14, H15, H16, H17, H18); 5.98 (1H, bs, NH); 3.69 (3H, s, H11); 3.59-3.50 (3H, m, H12, H7,); 3.28 (1H, m, H2); 2.96-2.71 (5H, m, H4, H10, H1); 2.23 (2H, m, H3); 2.08-1.71 (6H, m, H5, H8, H9); 1.40 (9H, s, H21, H22, H23) ppm

^{13}C NMR (Acetone- d_6 , 100 MHz): δ 176.1 (C6); 155.8 (C19); 139.3 (C13); 129.5, 128.8, 127.6 (C14, C15, C16, C17, C18); 78.3 (C20); 63.2 (C12); 61.8 (C7); 59.5 (C1); 52.4 (C5); 52.2 (C4); 51.9 (C11); 51.8 (C2); 46.2 (C10); 32.4 (C3); 29.9 (C8); 28.4 (C21, C22, C23); 24.9 (C9) ppm
IR: 2927 (ν C-H); 1737-1708 (ν C=O); 1495-1453 (ν C=C); 1241-1170 (ν C-C(O)-C) cm^{-1}

Methyl **((3*R*,4*R*)-1-benzyl-4-((4-(trifluoromethyl)phenyl)sulfonamido)piperidin-3-yl)-*L*-prolinate [4.57]**



Procedure A: to a solution of **4.55** (96 mg, 0.229 mmol, 1.0 eq.) in dry dioxane (5 mL) under argon atmosphere, was added at 0°C HCl 4M in dioxane (1.72 mL, 6.87 mmol, 30.0 eq.). The reaction was let stirring 3 h at room temperature. After evaporation of the volatile under reduced pressure, the hydrochloride salt obtained from **4.55** was used in the following reaction step without further purification. Precisely, to a solution of this hydrochloride salt in dry THF under argon atmosphere, cooled to 0°C, was added NEt₃ (128 μL , 0.914 mmol, 4 eq.). After 20 minutes under stirring, a solution of 4-(trifluoromethyl)benzenesulfonyl chloride (56.0 mg, 0.229 mmol, 1 eq.) in dry THF (2 mL) was added dropwise. The reaction mixture was stirred for 3 h at room temperature. The white precipitate of triethylammonium chloride formed during the reaction was filtered and the volatile was removed under reduced pressure. The crude residue obtained was then purified by column chromatography on silica gel eluting with *c*-Hex/EtOAc 75:25 to yield **4.57** as white solid (90 mg, 0.171 mmol, 76%).

Procedure B: To a solution of *L*-proline methyl ester hydrochloride (2.98 g, 18 mmol, 1 eq.) in 1,2 dichloroethane (100 mL) was added NEt₃ (2.53 mL, 18 mmol, 1 eq.). After 15 min at room temperature, 4-benzylpiperidone (3.33 mL, 18 mmol, 1eq.) was added under argon atmosphere with molecular sieves (3 Å), followed after a period of 30 min by a catalytic amount of InCl₃ (398 mg, 1.8 mmol, 0.1 eq.). The reaction mixture was let stirring 45 min, cooled to 0°C and a solution of 4-(trifluoromethyl)benzenesulfonyl azide (prepared as reported in the literature¹⁹⁷) (4.52 g, 18 mmol, 1 eq.) in 1,2 dichloroethane (40 mL) was added dropwise to the mixture while maintaining

the temperature at 0°C. After 45 min at room temperature NaBH(OAc)₃ (9.5 g, 45 mmol, 2.5 eq.) was added and the mixture was let under stirring at room temperature overnight. After filtration through a Celite pad with CH₂Cl₂, the solution was washed with distilled water, dried over Na₂SO₄, and the volatile was removed under reduced pressure. The obtained crude was purified by column chromatography on neutral alumina eluting with c-Hex/EtOAc 85:15 to afford the pure diastereoisomer (R,R,S) **4.57**.

Molecular weight = 525.59 g mol⁻¹

R_f = 0.4 (c-Hex/EtOAc 7:3)

HRMS: Calcd. for [C₂₅H₃₀F₃N₃O₄S + H]⁺: m/z 526.1909, found: 526.1978

¹H NMR (CDCl₃, 400 MHz): δ 8.04 (2H, d, *J* = 8.1 Hz, H15, H17); 7.74 (2H, d, *J* = 8.1 Hz, H14, H18); 7.34-7.21 (5H, m, H22, H23, H24, H25, H26); 7.12 (1H, bs, NH12); 3.77 (3H, s, H11); 3.48 (2H, s, H20); 3.46 (0.5H, d, *J* = 4.9 Hz, H6); 3.44 (0.5H, d, *J* = 4.9 Hz, H6); 2.85-2.72 (3H, m, H2, H3); 2.6 (1H, m, H1); 2.36-2.25 (2H, m, H5, H9); 2.06 -1.70 (5H, m, H4, H7,H9); 1.67-1.45 (2H, m, H5, H8); 1.27 (1H, m, H8) ppm

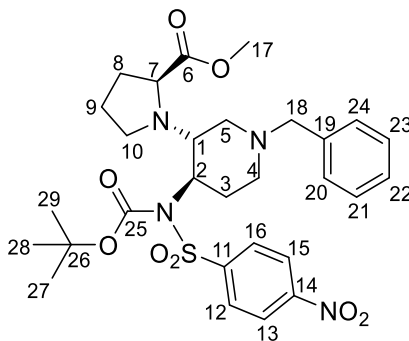
¹³C NMR (CDCl₃, 100 MHz): δ 176.8 (C10); 144.7 (C13); 137.8 (C21); 134.2 (C16, *J*_{C-F} = 33.1 Hz); 129.3, 128.7, 127.6 (C22, C23, C24, C25, C26); 128.1 (C14, C18); 126.2 (C15, C17 *J*_{C-F} = 8.3 Hz); 63.2 (C20); 62.3 (C6); 58.8 (C1); 54.1 (C2); 52.8 (C11); 52.3 (C3); 51.8 (C4); 44.6 (C9); 33.3 (C5); 30.1 (C7); 24.7 (C8) ppm

¹⁹F NMR (CDCl₃, 376 MHz): δ -63.1 (3F) ppm

Melting point = 165-168°C

IR: 3209 (ν C-H_{ar}); 2951 (ν C-H); 1733 (ν C=O); 1434-1403 (ν C=C); 1321 (ν C-O) cm⁻¹

Methyl((3*R*,4*R*)-1-benzyl-4-((*N*-(*tert*-butoxycarbonyl)-4-nitrophenyl)sulfonamido)piperidin-3-yl)-*L*-prolinate [4.58]



To a solution of **4.54** (1.51 g, 3.0 mmol, 1.0 eq.) in dry DMF (50 mL) NaH 60% in mineral oil (132 mg, 3.3 mmol, 1.1 eq.) was added. After the addition, the colour of the reaction turned from yellow to dark orange. At this moment Boc₂O (1.63 g, 7.5 mmol, 2.5 eq.) and DMAP (916 mg, 7.5 mmol, 2.5 eq.) were added and the reaction mixture was let stirring overnight at room temperature under argon atmosphere. After concentration under vacuum, the crude residue obtained was taken up with EtOAc and successively washed with water, 100% aqueous solution of NaHCO₃ and brine, dried over Na₂SO₄, filtered and concentrated under vacuum. The crude was purified by column chromatography on silica gel eluting with *c*-Hex/EtOAc 7:3 to afford compound **4.58** as a pale yellow solid (1.23 g, 2.03 mmol, 68%).

Molecular weight = 602.70 g mol⁻¹

R_f = 0.50 (*c*-Hex/EtOAc 7:3)

HRMS: Calcd. for [C₂₉H₃₈N₄O₈S + H]⁺: *m/z* 603.2489, found: 603.2496

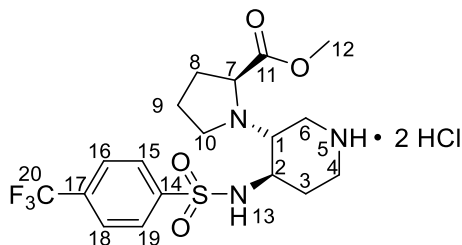
¹H NMR (Acetone-*d*₆, 400 MHz): δ 8.63 (2H, d, *J* = 8.9 Hz, H12, H16); 8.42 (2H, d, *J* = 8.9 Hz, H13, H15); 7.35-7.25 (5H, m, H20, H21, H22, H23, H24); 4.43 (1H, td, *J* = 11.6, 4.6 Hz, H2); 3.92 (1H, t, *J* = 9.0 Hz, H1); 3.62 (3H, s, H17); 3.60-3.53 (3H, m, H7, H18); 3.16 (1H, d, *J* = 9.0 Hz, H5); 3.05 (1H, m, H10); 2.91-2.88 (2H, m, H10, H4); 2.63 (1H, m, H3); 2.21 (1H, t, *J* = 10.7 Hz, H5); 2.07-1.86 (3H, m, H4, H8); 1.86-1.78 (3H, m, H9, H3); 1.24 (9H, s, H27, H28, H29) ppm

¹³C NMR (Acetone-*d*₆, 100 MHz): δ 176.4 (C6); 151.2 (C14); 150.8 (C25); 149.4 (C11); 139.9 (C19); 129.8 (C12, C16); 129.7 (C20, C24); 129.2 (C21, C23); 128.0 (C22); 125.1 (C13, C15); 85.6 (C26); 63.2 (C18); 62.8 (C7); 59.7 (C2); 57.1 (C1); 53.7 (C4); 52.8 (C5); 52.2 (C17); 46.6 (C10); 31.1 (C8); 31.0 (C3); 28.1 (C27, C28, C29); 25.7 (C9) ppm

Melting point = 61-63°C

IR: 3026-2953-2820 (ν C-H); 1737 (ν C=O); 1531 (ν NO₂); 1347 (ν NO₂) cm⁻¹

Methyl ((3*R*,4*R*)-4-((4-(trifluoromethyl)phenyl)sulfonamido)piperidin-3-yl)-*L*-prolinate hydrochloride [4.60]



To a stirred solution of **4.57** (343.3 mg, 0.65 mmol, 1.0 eq.) in MeOH under argon atmosphere .) were added Pd/C (69 mg, 20% mass) and triethyl silane (1.04 mL, 6.5 mmol, 10 eq. The reaction mixture was stirred at room temperature for 30 min. Once the reaction was over, the mixture was filtered on a Celite pad and HCl in dioxane was added to the filtrate until pH = 1. The volatile was removed under reduced pressure and the crude hydrochloride salt obtained was taken up with MeOH. By adding anhydrous Et₂O, the pure hydrochloride salt **4.60** precipitated as a white powder (85 mg, 0.181 mmol, 89%).

Molecular weight = 508.37 g mol⁻¹; free amine 435.46 g mol⁻¹

R_f = 0 (c-Hex/EtOAc 7:3)

HRMS: Calcd. for [C₁₈H₂₄F₃N₃O₄S + H]⁺: m/z 536.1518, found: 536.1512

¹H NMR (CD₃OD, 400 MHz): δ 8.21 (2H, d, *J* = 8.4 Hz, H16, H18); 7.99 (2H, d, *J* = 8.4 Hz, H15, H19); 4.55 (1H, m, H7); 4.02-3.80 (6H, m, H1, H2, H6, H12); 3.48 (2H, m, H10); 3.45 (1H, m, H6); 3.31 (1H, m, H4); 3.10 (1H, m, H4); 2.5 (1H, m, H8); 2.23 (1H, m, H8); 2.05 (2H, m, H9); 1.82 (1H, m, H3); 1.65 (1H, m, H3) ppm

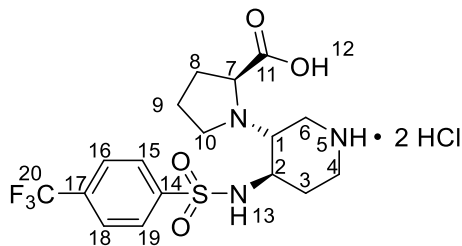
¹³C NMR (CD₃OD, 100 MHz): δ 171.6 (C11); 145.7 (C14); 136.6 (C17, *J*_{C-F} = 31.2 Hz); 129.8 (C16, C18), 128.8 (C15, C19); 66.2 (C7); 60.6 (C1); 54.1 (C12); 51.5 (C2); 50.6 (C10); 43.5 (C4); 42.0 (C6); 30.0 (C8); 29.2 (C3); 24.9 (C9) ppm

¹⁹F NMR (CD₃OD, 376 MHz): δ -64.6 ppm

Melting point = 184-187°C

IR: 2961 (ν C-H); 1742 (ν C=O); 1445-1404 (ν C=C); 1322 (ν C-O); 1166 (ν C-N) cm⁻¹

((3*R*,4*R*)-4-((4-(trifluoromethyl)phenyl)sulfonamido)piperidin-3-yl)-*L*-proline hydrochloride [4.61]



A solution of **4.60** (0.298 g, 0.585 mmol, 1 eq.) in aqueous HCl 6M (10 mL) was heated in a sealed tube at 110°C under stirring. After 6 h, the volatile were removed under reduced pressure and the

crude hydrochloride salt obtained was taken up with MeOH. By adding anhydrous Et₂O, the pure hydrochloride salt **4.61** precipitated as a white powder. (0.265 g, 0.536 mmol, 93%)

Molecular weight = 494.35 g mol⁻¹; Free amine 421.44 g mol⁻¹

Rf = 0 (CH₂Cl₂/MeOH 20:1) hydrochloride salt

HRMS: Calcd. for [C₁₇H₂₂F₃N₃O₄S + H]⁺: m/z 422.1361, found: 522.1359

¹H NMR (CD₃OD, 400 MHz): δ 8.17 (2H, d, *J* = 8.2 Hz, H16, H18); 7.96 (2H, d, *J* = 8.2 Hz, H15, H19); 4.53 (1H, m, H7); 3.97-3.71 (3H, m, H1, H2, H6); 3.60-3.37 (3H, m, H10, H10, H6); 3.30 (1H, m, H4); 3.08 (1H, m, H4); 2.51 (1H, m, H8); 2.25 (1H, m, H8); 2.02 (2H, m, H9); 1.81 (1H, m, H3); 1.65 (1H, m, H3) ppm

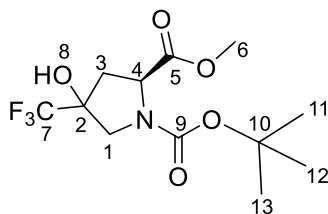
¹³C NMR (CD₃OD, 100 MHz): δ 172.1 (C11); 145.7 (C14); 135.7 (C17, *J*_{C-F} = 32.1 Hz); 129.2 (C16, C18), 127.9 (C15, C19); 66.1 (C7); 60.9 (C1); 51.8 (C2); 50.7 (C10); 43.7 (C4); 42.1 (C6); 29.8 (C8); 29.3 (C3); 24.5 (C9) ppm

¹⁹F NMR (CD₃OD, 376 MHz): δ -64.6 ppm

Melting point = 177-179°C

IR: 3356 (ν O-H); 1725 (ν C=O); 1454-1404 (ν C=C); 1323 (ν C-O); 1168 (ν C-N) cm⁻¹

1-(*tert*-butyl) 2-methyl (2*S*)-4-hydroxy-4-(trifluoromethyl)pyrrolidine-1,2-dicarboxylate[4.63]



To a stirred solution of Boc-4-oxo-Pro-OMe (2 g, 8.21mmol, 1.0 eq.) in dry THF was added within 5 minutes at 0°C TMSCF₃ (1.58 mL, 10.7 mmol, 1.3 eq, immediately followed by a solution of TBAF 1M in THF (0.37 mL, 0.37 mmol, 0.045 eq.). The reaction was left to return to room temperature and kept reacting for 22 h. After addition of a saturated aqueous solution of NH₄Cl (3.40 mL) and additional agitation for 4 h, a solution of TBAF 1M in THF (8.62 mL, 8.62 mmol, 1.05 eq.) was added again. The reaction mixture was let under stirring for an additional hour and the organic layer was separated. After extraction of the aqueous phase with Et₂O (3x20 mL), the combined organic layer was washed with water and brine, dried over Na₂SO₄, filtered and

concentrated under vacuum to afford a diastereomeric mixture of **4.63** (2.47 g, 7.89 mmol, 96%) as a brownish oil.

Molecular weight = 313.27 g mol⁻¹

R_f = 0.75 (c-Hex/EtOAc 7:3)

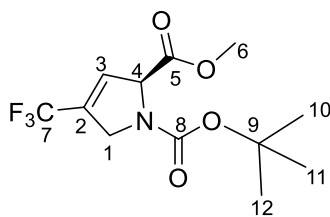
HRMS: Calcd. for [C₁₂H₁₈F₃NO₅ + H]⁺: m/z 314.1137, as reported in the literature the molecule is not stable in mass and only fragment are found.

¹H NMR (CDCl₃, 300 MHz): two diastereoisomer δ 4.49 (1H, m, H4); 4.37 and 4.25 (2H, 2 bs, H2); 3.78 and 3.75 (3H, 2 s, H6); 2.52 (1H, m, H3); 2.19 (1H, m, H3); 1.44 and 1.39 (9H, 2 s, H11, H12, H13) ppm

¹⁹F NMR (CDCl₃, 188 MHz): two diastereoisomer δ -81.1 and -81.2

Analysis are coherent with what it is reported in literature¹⁹⁶

1-(*tert*-butyl) 2-methyl (S)-4-(trifluoromethyl)-2,5-dihydro-1H-pyrrole-1,2-dicarboxylate [**4.64**]



To a solution of **4.63** (607.7 mg, 1.94 mmol, 1.0 eq.) in dry pyridine was slowly added SOCl₂ (1.7 mL, 23.3 mmol, 12 eq.), at this moment the solution was heated until reflux. After 20 minutes at reflux the reaction was cooled at room temperature and then ice was added (15 g). The mixture was extracted with Et₂O (2 x 30mL) and EtOAc (2 x 30mL). The combined organic phase were concentrated to approximately 20 mL. The resulting solution was washed with 5% aqueous solution of HCl, saturated aqueous solution of NaHCO₃, brine, dried on Na₂SO₄, filtered and concentrated under reduced pressure. The obtained crude oil was purified by filtration on a short column chromatography on silica gel eluting with c-Hex/EtOAc 2:1 to afford **4.64** as a yellowish powder (205 mg, 0.696 mmol, 36%).

Molecular weight = 295.26 g mol⁻¹

R_f = 0.8 (c-Hex/EtOAc 2:1)

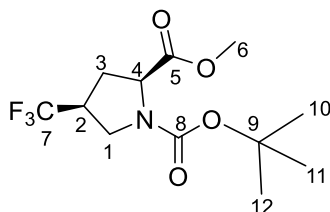
HRMS: Calcd. for [C₁₂H₁₆F₃NO₄ + H]⁺: m/z 296.1065, found fragmentation

¹H NMR (CDCl₃, 300 MHz): δ 6.19 (1H, m, H3); 5.08 (1H, m, H4); 4.33 (2H, m, H1); 3.71 (3H, H6); 1.44 and 1.38 (9H, 2 s, H11, H12, H13) ppm

¹⁹F NMR (CDCl₃, 188 MHz): δ -65.3 ppm

Analysis are coherent with what it is reported in literature¹⁹⁶

1-(*tert*-butyl) 2-methyl (2*S*,4*S*)-4-(trifluoromethyl)pyrrolidine-1,2-dicarboxylate [4.65]



To a stirred solution of **4.64** (205 mg, 0.69 mmol, 1.0 eq.) in MeOH were added under argon atmosphere Pd/C (47 mg, 20% mass) and triethyl silane (1.10 mL, 6.9 mmol, 10 eq.). The reaction mixture was stirred at room temperature for 3 h. Once the reaction was over, the mixture was filtered on a Celite pad. The volatile was removed under reduced pressure to afford the pure hydrochloride salt **4.65** (85 mg, 0.181 mmol, 89%) as a white powder.

Molecular weight = 297.27 g mol⁻¹

R_f = 0.6 (c-Hex/EtOAc 7:3)

HRMS: Calcd. for [C₁₂H₁₈F₃NO₄ + H]⁺: m/z 297.1188, as reported in the literature the molecule is not stable in mass and only fragment are found.

¹H NMR (CDCl₃, 300 MHz): δ 4.36 (1H, t, *J* = 7.9, H4); 3.92 (1H, t, *J* = 10 Hz, H1); 3.84 (1H, t, *J* = 10 Hz, H1); 3.76 (3H, s, H6); 2.96 (1H, m, H2); 2.56 (1H, m, H3); 2.14 (1H, m, H3); 1.48 and 1.43 (9H, 2 s, H11, H12, H13) ppm

¹⁹F NMR (CDCl₃, 188 MHz): two diastereoisomer δ -70.4

Analysis are coherent with what it is reported in literature¹⁹⁶

List of abbreviations

2DIR	Two dimensions infra-red
Abz	Aminobenzoic acids
ACN	Acetonitrile
AcOH	Acetic acid
AD	Alzheimer's Disease
ADME	Absorption, Distribution, Metabolism and Excretion
Aib	α -aminoisobutyric acid
Amb	5-amino-2-methoxybenzhydrazide
AMY	Amylin Receptors Y
ArN ₃	Aryl azide
ATC	4-amino(methyl)-1,3-thiazole-5-carboxylic acid
ATP	Adenosine triphosphate
BBB	Blood-Brain Barrier
Bn	Benzyl
BnBr	Benzyl bromide
Boc	<i>tert</i> -butyloxycarbonyl
Boc ₂ O	Di- <i>tert</i> -butyl dicarbonate
BTC	Bis(trichloromethyl) carbonate
Bz	Benzoyl
BzCl	Benzoyl chloride
Cbz	Carboxybenzyl
Cbz-Cl	Carboxybenzyl chloride
CD	Circular dichroism
CDI	Carbonyl diimidazole
CE	Capillary electrophoresis
CGRP	Calcitonin gene-related peptide
CHD	Coronary Heart Disease
c-Hex	Cyclo hexane
CNS	Central Nervous System

COMU	(1-Cyano-2-ethoxy-2-oxoethylidenaminoxy)dimethylamino-morpholino-carbenium hexafluorophosphate
COSY	Correlation spectroscopy
CPE	Carboxypeptidase E
CR	Congo Red
cryo-EM	Cryo-Electron Microscopy
cryo-ET	Cryo-Electron Tomography
CSD	Chemical shift deviation
CT	Calcitonin family
CTR	Calcitonin receptors
DCE	Dichloroethane
DCM	Dichlorometane
DIC	N,N'-Diisopropylcarbodiimide
DIPEA	N,N-Diisopropylethylamine
DIPSI	Decoupling In the Presence of Scalar Interactions
DMAP	4-Dimethylaminopyridine
DMF	N,N-diméthylformamide
DMSO	Dimethyl sulfoxide
DMTMM	4-(4,6-Dimethoxy-1,3,5-triazin-2-yl)-4-methylmorpholinium chloride
DOPC	1,2-dioleoyl-sn-glycero-3-phosphatidylcholine
DOPS	1,2-dioleoyl-sn-glycero-3-phosphatidylserine
DPP4	Dipeptidyl peptidase 4
EDC	1-Ethyl-3-(3-dimethylaminopropyl)carbodiimide
EGCG	Epigallocatechin Gallate
EM	Electron Microscopy
EMA	European Medicines Agency
EtOAc	Ethyl acetate
EtOH	Ethanol
F	Fluorescence at the plateau
FAXS	Fluorine chemical shift Anisotropy and eXchange for Screening
FBPase	Fructose-1,6-bisphosphatase

FDA	Food and Drug Administration
FFAR1	Free fatty acid receptor 1
Fmoc	Fluorenylmethyloxycarbonyl
Fmoc-Osu	Fmoc N-hydroxysuccinimide
GIP	Glucose-dependent insulinotropic polypeptide
GLP-1	Glucagon Like Peptide
GLUT-4	Glucose transporter type 4
GP	Glycogen phosphorylase
Hao	Hydrazine, 5-Amino-2-methoxybenzoic acid and Oxalic acid
HATU	1-[Bis(dimethylamino)methylene]-1H-1,2,3-triazolo[4,5-b]pyridinium 3-oxid hexafluorophosphate
HBTU	N,N,N',N'-Tetramethyl-O-(1H-benzotriazol-1-yl)uronium hexafluorophosphate
HFIP	1,1,1,3,3,3-Hexafluoro-2-propanol
hIAPP	human Islet Amyloid Polypeptide
HMBC	Heteronuclear multiple-bond correlation spectroscopy
HOAt	1-Hydroxy-7-azabenzotriazole
HOBt	Hydroxybenzotriazole
HPLC	High-performance liquid chromatography
HRMS	High resolution mass spectrometry
HSQC	Heteronuclear Single Quantum Coherence
IAC	Insulin chains A
IAPP	Islet amyloid polypeptide
IBC	Insulin chains B
IBCF	Isobutyl chloroformate
IDF	International Diabetes Federation
IMS-MS	Ion mobility spectroscopy-mass spectrometry
IR	Insulin receptors
LC-MS	Liquid chromatography-mass spectrometry
LUV	Large Unilamellar Vesicle
MD	Molecular dynamics

MeOH	Methanol
MRI	Magnetic resonance imaging
MS	Mass spectroscopy
MTT	3-(4,5-dimethylthiazol-2-yl)-2,5-diphenyltetrazolium bromide
NMI	N-methyl imidazole
NMM	N-Methylmorpholine
NMR	Nuclear Magnetic Resonance
NOE	Nuclear overhauser effect
oxyma	Ethyl cyano(hydroxyimino)acetate
PAM	Peptidylglycine- α -amidating monooxygenase
PC1/3	Prohormone convertase 1/3
PC2	Prohormone convertase 2
PD	Parkinson Disease
PET	Positron Emission Tomography
PhSH	Thiophenol
PPI	Protein-protein interactions
PTP1B	Protein Tyrosine Phosphatase 1 B
Py	Pyridine
RAMPs	Receptor Activity-Modifying Proteins
REMD	Replica Exchange Molecular Dynamics Simulations
rIAPP	rat Islet Amyloid PolyPeptide
ROE	Rotating-frame Overhauser Effect
ROESY	Rotating Frame Overhauser Enhancement Spectroscopy
ROS	Reactive Oxygen Species
SGLT-2	Sodium-Glucose cotransporter-2
SPPS	Solid Phase Peptide Synthesis
SRE	Self Recognition Element
ssNMR	solid state NMR spectroscopy
STD	Saturation-Transfer Difference
t1/2	Half time
T1D	Type 1 Diabetes

T2D	Type 2 Diabetes
TBAF	Tetrabutylammonium Fluoride
TBTA	Tris(benzyltriazolylmethyl)amine
TCFH	N,N,N',N'-tetramethylchloroformamidinium
TEA	Triethylamine
TEM	Transmission Electron Microscopy
TES	Triethyl Silane
TFA	Trifluoroacetic Acid
THF	Tetrahydrofuran
ThT	Thioflavin T fluorescence spectroscopy
TIPS	Tri isopropyl Silane
TLC	Thin-layer chromatography
TMSCF ₃	Trimethyl(trifluoromethyl)silane
Tos	Tosyl
TosN ₃	Tosyl azide
WHO	World Health Organization
ΔF	α,β-dehydrophenylalanine

Bibliography

- (1) Riek, R.; Eisenberg, D. S. The Activities of Amyloids from a Structural Perspective. *Nature* **2016**, *539* (7628), 227–235. <https://doi.org/10.1038/nature20416>.
- (2) Westermark, P.; Benson, M. D.; Buxbaum, J. N.; Cohen, A. S.; Frangione, B.; Ikeda, S.-I.; Masters, C. L.; Merlini, G.; Saraiva, M. J.; Sipe, J. D. A Primer of Amyloid Nomenclature. *Amyloid* **2007**, *14* (3), 179–183. <https://doi.org/10.1080/13506120701460923>.
- (3) Landreh, M.; Sawaya, M. R.; Hipp, M. S.; Eisenberg, D. S.; Wüthrich, K.; Hartl, F. U. The Formation, Function and Regulation of Amyloids: Insights from Structural Biology. *J. Intern. Med.* **2016**, *280* (2), 164–176. <https://doi.org/10.1111/joim.12500>.
- (4) Eisenberg, D.; Jucker, M. The Amyloid State of Proteins in Human Diseases. *Cell* **2012**, *148* (6), 1188–1203. <https://doi.org/10.1016/j.cell.2012.02.022>.
- (5) Ross, C. A.; Poirier, M. A. Protein Aggregation and Neurodegenerative Disease. *Nat. Med.* **2004**, *10* (S7), S10–S17. <https://doi.org/10.1038/nm1066>.
- (6) Nguyen, P. T.; Andraka, N.; De Carufel, C. A.; Bourgault, S. Mechanistic Contributions of Biological Cofactors in Islet Amyloid Polypeptide Amyloidogenesis. *J. Diabetes Res.* **2015**, *2015*, 1–13. <https://doi.org/10.1155/2015/515307>.
- (7) Anfinsen, C. B. Principles That Govern the Folding of Protein Chains. *Science* **1973**, *181* (4096), 223–230.
- (8) Anfinsen, C. B.; Scheraga, H. A. Experimental and Theoretical Aspects of Protein Folding. In *Advances in Protein Chemistry*; Anfinsen, C. B., Edsall, J. T., Richards, F. M., Eds.; Academic Press, 1975; Vol. 29, pp 205–300. [https://doi.org/10.1016/S0065-3233\(08\)60413-1](https://doi.org/10.1016/S0065-3233(08)60413-1).
- (9) Gazit, E. The “Correctly Folded” State of Proteins: Is It a Metastable State? *Angew. Chem. Int. Ed.* **2002**, *41* (2), 257–259. [https://doi.org/10.1002/1521-3773\(20020118\)41:2<257::AID-ANIE257>3.0.CO;2-M](https://doi.org/10.1002/1521-3773(20020118)41:2<257::AID-ANIE257>3.0.CO;2-M).
- (10) Baldwin, A. J.; Knowles, T. P. J.; Tartaglia, G. G.; Fitzpatrick, A. W.; Devlin, G. L.; Shammass, S. L.; Waudby, C. A.; Mossuto, M. F.; Meehan, S.; Gras, S. L.; Christodoulou, J.; Anthony-Cahill, S. J.; Barker, P. D.; Vendruscolo, M.; Dobson, C. M. Metastability of Native Proteins and the Phenomenon of Amyloid Formation. *J. Am. Chem. Soc.* **2011**, *133* (36), 14160–14163. <https://doi.org/10.1021/ja2017703>.
- (11) Knowles, T. P. J.; Vendruscolo, M.; Dobson, C. M. The Amyloid State and Its Association with Protein Misfolding Diseases. *Nat. Rev. Mol. Cell Biol.* **2014**, *15* (6), 384–396. <https://doi.org/10.1038/nrm3810>.
- (12) Ke, P. C.; Sani, M.-A.; Ding, F.; Kakinen, A.; Javed, I.; Separovic, F.; Davis, T. P.; Mezzenga, R. Implications of Peptide Assemblies in Amyloid Diseases. *Chem. Soc. Rev.* **2017**, *46* (21), 6492–6531. <https://doi.org/10.1039/C7CS00372B>.
- (13) Iadanza, M. G.; Jackson, M. P.; Hewitt, E. W.; Ranson, N. A.; Radford, S. E. A New Era for Understanding Amyloid Structures and Disease. *Nat. Rev. Mol. Cell Biol.* **2018**, *19* (12), 755–773. <https://doi.org/10.1038/s41580-018-0060-8>.
- (14) Benson, M. D.; Buxbaum, J. N.; Eisenberg, D. S.; Merlini, G.; Saraiva, M. J. M.; Sekijima, Y.; Sipe, J. D.; Westermark, P. Amyloid Nomenclature 2018: Recommendations by the International Society of Amyloidosis (ISA) Nomenclature Committee. *Amyloid* **2018**, *25* (4), 215–219. <https://doi.org/10.1080/13506129.2018.1549825>.
- (15) Sipe, J. D.; Cohen, A. S. Review: History of the Amyloid Fibril. *J. Struct. Biol.* **2000**, *130* (2), 88–98. <https://doi.org/10.1006/jsbi.2000.4221>.
- (16) Virchow, R. Zur Cellulose —Frage. *Arch. Für Pathol. Anat. Physiol. Für Klin. Med.* **1854**, *6* (3), 416–426. <https://doi.org/10.1007/BF02116546>.

- (17) Schmidt, C. Ueber Das Sogenannte „thierische Amyloid“ (Substanz Der Corpuscula Amylacea). *Justus Liebigs Ann. Chem.* **1859**, *110* (2), 250–254. <https://doi.org/10.1002/jlac.18591100220>.
- (18) Yakupova, E. I.; Bobyleva, L. G.; Vikhlyantsev, I. M.; Bobylev, A. G. Congo Red and Amyloids: History and Relationship. *Biosci. Rep.* **2019**, *39* (1). <https://doi.org/10.1042/BSR20181415>.
- (19) IDF_Atlas_9th_Edition_2019.Pdf.
- (20) Ndisang, J. F.; Vannacci, A.; Rastogi, S. Insulin Resistance, Type 1 and Type 2 Diabetes, and Related Complications 2017. *J. Diabetes Res.* **2017**, *2017*, 1–3. <https://doi.org/10.1155/2017/1478294>.
- (21) Gardner, A.; Duprez, W.; Stauffer, S.; Ayu Kencana Ungu, D.; Clauson-Kaas, F. *Labster Virtual Lab Experiments*; Springer Berlin / Heidelberg: Berlin, Heidelberg, 2019.
- (22) Foley, K.; Boguslavsky, S.; Klip, A. Endocytosis, Recycling, and Regulated Exocytosis of Glucose Transporter 4. *Biochemistry* **2011**, *50* (15), 3048–3061. <https://doi.org/10.1021/bi2000356>.
- (23) Ali, O. Genetics of Type 2 Diabetes. *World J. Diabetes* **2013**, *4* (4), 114–123. <https://doi.org/10.4239/wjd.v4.i4.114>.
- (24) Jiang, X.; Ma, H.; Wang, Y.; Liu, Y. Early Life Factors and Type 2 Diabetes Mellitus. *J. Diabetes Res.* **2013**, *2013*, 1–11. <https://doi.org/10.1155/2013/485082>.
- (25) Forbes, J. M.; Cooper, M. E. Mechanisms of Diabetic Complications. *Physiol. Rev.* **2013**, *93* (1), 137–188. <https://doi.org/10.1152/physrev.00045.2011>.
- (26) Chaudhury, A.; Duvoor, C.; Reddy Dendi, V. S.; Kraleti, S.; Chada, A.; Ravilla, R.; Marco, A.; Shekhawat, N. S.; Montales, M. T.; Kuriakose, K.; Sasapu, A.; Beebe, A.; Patil, N.; Musham, C. K.; Lohani, G. P.; Mirza, W. Clinical Review of Antidiabetic Drugs: Implications for Type 2 Diabetes Mellitus Management. *Front. Endocrinol.* **2017**, *8*. <https://doi.org/10.3389/fendo.2017.00006>.
- (27) Malm-Erfjält, M.; Bjørnsdottir, I.; Vanggaard, J.; Helleberg, H.; Larsen, U.; Oosterhuis, B.; van Lier, J. J.; Zdravkovic, M.; Olsen, A. K. Metabolism and Excretion of the Once-Daily Human Glucagon-Like Peptide-1 Analog Liraglutide in Healthy Male Subjects and Its In Vitro Degradation by Dipeptidyl Peptidase IV and Neutral Endopeptidase. *Drug Metab. Dispos.* **2010**, *38* (11), 1944–1953. <https://doi.org/10.1124/dmd.110.034066>.
- (28) Holst, J. J. Incretin Therapy for Diabetes Mellitus Type 2: *Curr. Opin. Endocrinol. Diabetes Obes.* **2020**, *27* (1), 2–10. <https://doi.org/10.1097/MED.0000000000000516>.
- (29) Gallwitz, B. Clinical Use of DPP-4 Inhibitors. *Front. Endocrinol.* **2019**, *10*, 389. <https://doi.org/10.3389/fendo.2019.00389>.
- (30) Brunton, L. L.; Lazo, J. S.; Buxton, I. L. O.; Blumenthal, D. K.; Akil, H.; Amrein, P. C.; Baldessarini, R. J.; Balser, J. R.; Bennett, W. M.; Bennett, J. E.; Bersot, T. P.; Bickers, D. R.; Bloom, F. E.; Braverman, L. E.; Brown, J. H.; Burke, A.; Catterall, W. A.; Chabner, B. A.; Chambers, H. F.; Charney, D. S.; Crowder, C. M.; Davis, S. N.; Druker, B.; Erdos, E. G.; Evers, A. S.; Fang, J. C.; Farwell, A. P.; FitzGerald, G. A.; Fleming, M. F.; Flexner, C.; Fox, L. P.; Friedman, P. A.; Giacomini, K. M.; Goldberg, D. E.; Gonzalez, F. J.; Goss, P. E.; Gutstein, H. B.; Harris, R. A.; Hayden, F. G.; Henderer, J. D.; Hoffman, B. B.; Hoogerwerf, W. A.; Hotez, P. J.; Isoherranen, N.; Jackson, E. K.; Johns, R. A.; Kaushansky, K.; Kipps, T. J.; Klaassen, C. D.; Krensky, A. M.; Loose, D. S.; Loukas, A.; Mackie, K.; Mahley, R. W.; Majerus, P. W.; Mayer, S. E.; McNamara, J. O.; Merk, H. F.; Michaelson, M. D.; Michel, T.; Mihic, S. J.; Mitsiades, C. S.; Moody, E. J.; Oates, J. A.; O'Brien, C. P.; Parker, K. L.; Pasricha, P. J.; Petri, W. A.; Phillips, M. A.; Ramachandra, S.; Rapuano, C. J.; Relling, M. V.; Richardson, P. G.; Rocco, T. P.; Roden, D. M.; Ryan, D. P.; Sanders-Bush, E.; Schimmer, B. P.; Sellin, J. H.; Shapiro, T. A.; Shen, D. D.; Simon, B. A.; Skidgel, R. A.; Smith, H. E.; Smyth, E. M.; Snyder, P. J.; Stancel, G. M.; Standaert, D. G.; Stanley, S. L.; Sugiyama, Y.; Supko, J. G.; Tarazi, F. I.; Taylor, P.; Thummel, K. E.; Tollefsen, D. M.; Tukey, R. H.; Undem, B. J.; Vincenti, F.; Westfall, T. C.; Westfall, D. P.; Wilson, W. H.; Young, A. B.; Brown, D.; Carethers, J. M.; Crowley, W. R.; Dillmann, W.; Egorin, M. J.; Fierer, J.; Gorin, M. B.; Hanson, G. R.; Harris, R.; Helderman, J. H.; James, C. L.; Movsesian, M. A.; Murri, N.; Ragan, P.; Reed, S. L.; Rodgers, G. M.; Rollins, D. E.; Roth, D. M.; Shelton, R.;

- Steinman, L.; Wasserman, S. I.; White, H. S.; Witztum, J. L.; Zone, J. J. *Goodman & Gilman's the Pharmacological Basis of Therapeutics.*; McGraw-Hill: New York, 2006.
- (31) Kerru, N.; Singh-Pillay, A.; Awolade, P.; Singh, P. Current Anti-Diabetic Agents and Their Molecular Targets: A Review. *Eur. J. Med. Chem.* **2018**, *152*, 436–488. <https://doi.org/10.1016/j.ejmech.2018.04.061>.
- (32) Belete, T. M. A Recent Achievement In the Discovery and Development of Novel Targets for the Treatment of Type-2 Diabetes Mellitus. *J. Exp. Pharmacol.* **2020**, *Volume 12*, 1–15. <https://doi.org/10.2147/JEP.S226113>.
- (33) Belete, T. M. <p>A Recent Achievement In the Discovery and Development of Novel Targets for the Treatment of Type-2 Diabetes Mellitus</p> <https://www.dovepress.com/a-recent-achievement-in-the-discovery-and-development-of-novel-targets-peer-reviewed-article-JEP> (accessed Mar 20, 2020). <https://doi.org/10.2147/JEP.S226113>.
- (34) Halban, P. A.; Polonsky, K. S.; Bowden, D. W.; Hawkins, M. A.; Ling, C.; Mather, K. J.; Powers, A. C.; Rhodes, C. J.; Sussel, L.; Weir, G. C. β -Cell Failure in Type 2 Diabetes: Postulated Mechanisms and Prospects for Prevention and Treatment. *J. Clin. Endocrinol. Metab.* **2014**, *99* (6), 1983–1992. <https://doi.org/10.1210/jc.2014-1425>.
- (35) Westermark, P.; Wernstedt, C.; Wilander, E.; Hayden, D. W.; O'Brien, T. D.; Johnson, K. H. Amyloid Fibrils in Human Insulinoma and Islets of Langerhans of the Diabetic Cat Are Derived from a Neuropeptide-like Protein Also Present in Normal Islet Cells. *Proc. Natl. Acad. Sci.* **1987**, *84* (11), 3881–3885. <https://doi.org/10.1073/pnas.84.11.3881>.
- (36) Andersson, A.; Bohman, S.; Borg, L. A. H.; Paulsson, J. F.; Schultz, S. W.; Westermark, G. T.; Westermark, P. Amyloid Deposition in Transplanted Human Pancreatic Islets: A Conceivable Cause of Their Long-Term Failure. *Exp. Diabetes Res.* **2008**, *2008*, 1–8. <https://doi.org/10.1155/2008/562985>.
- (37) Westermark, P.; Andersson, A.; Westermark, G. T. Islet Amyloid Polypeptide, Islet Amyloid, and Diabetes Mellitus. *Physiol. Rev.* **2011**, *91* (3), 795–826. <https://doi.org/10.1152/physrev.00042.2009>.
- (38) Akter, R.; Cao, P.; Noor, H.; Ridgway, Z.; Tu, L.-H.; Wang, H.; Wong, A. G.; Zhang, X.; Abedini, A.; Schmidt, A. M.; Raleigh, D. P. Islet Amyloid Polypeptide: Structure, Function, and Pathophysiology. *J. Diabetes Res.* **2016**, *2016*, 1–18. <https://doi.org/10.1155/2016/2798269>.
- (39) Kiriya, Y.; Nochi, H. Role and Cytotoxicity of Amylin and Protection of Pancreatic Islet β -Cells from Amylin Cytotoxicity. *Cells* **2018**, *7* (8), 95. <https://doi.org/10.3390/cells7080095>.
- (40) Hay, D. L.; Pioszak, A. A. Receptor Activity-Modifying Proteins (RAMPs): New Insights and Roles. *Annu. Rev. Pharmacol. Toxicol.* **2016**, *56* (1), 469–487. <https://doi.org/10.1146/annurev-pharmtox-010715-103120>.
- (41) Gebre-Medhin, S.; Mulder, H.; Pekny, M.; Westermark, G.; Törnell, J.; Westermark, P.; Sundler, F.; Ahrén, B.; Betsholtz, C. Increased Insulin Secretion and Glucose Tolerance in Mice Lacking Islet Amyloid Polypeptide (Amylin). *Biochem. Biophys. Res. Commun.* **1998**, *250* (2), 271–277. <https://doi.org/10.1006/bbrc.1998.9308>.
- (42) Åkesson, B.; Panagiotidis, G.; Westermark, P.; Lundquist, I. Islet Amyloid Polypeptide Inhibits Glucagon Release and Exerts a Dual Action on Insulin Release from Isolated Islets. *Regul. Pept.* **2003**, *111* (1), 55–60. [https://doi.org/10.1016/S0167-0115\(02\)00252-5](https://doi.org/10.1016/S0167-0115(02)00252-5).
- (43) Kahn, S. E.; D'Alessio, D. A.; Schwartz, M. W.; Fujimoto, W. Y.; Ensink, J. W.; Tabor, G. J.; Porte, D. Evidence of Cosecretion of Islet Amyloid Polypeptide and Insulin by β -Cells. *Diabetes* **1990**, *39* (5), 634. <https://doi.org/10.2337/diab.39.5.634>.
- (44) Caillon, L.; Hoffmann, A. R. F.; Botz, A.; Khemtouri, L. Molecular Structure, Membrane Interactions, and Toxicity of the Islet Amyloid Polypeptide in Type 2 Diabetes Mellitus. *J. Diabetes Res.* **2015**, *2016*, 5639875. <https://doi.org/10.1155/2016/5639875>.

- (45) Mukherjee, A.; Morales-Scheihing, D.; Butler, P. C.; Soto, C. Type 2 Diabetes as a Protein Misfolding Disease. *Trends Mol. Med.* **2015**, *21* (7), 439–449. <https://doi.org/10.1016/j.molmed.2015.04.005>.
- (46) Abedini, A.; Schmidt, A. M. Mechanisms of Islet Amyloidosis Toxicity in Type 2 Diabetes. *FEBS Lett.* **2013**, *587* (8), 1119–1127. <https://doi.org/10.1016/j.febslet.2013.01.017>.
- (47) Janson, J.; Ashley, R. H.; Harrison, D.; McIntyre, S.; Butler, P. C. The Mechanism of Islet Amyloid Polypeptide Toxicity Is Membrane Disruption by Intermediate-Sized Toxic Amyloid Particles. *Diabetes* **1999**, *48* (3), 491. <https://doi.org/10.2337/diabetes.48.3.491>.
- (48) Haataja, L.; Gurlo, T.; Huang, C. J.; Butler, P. C. Islet Amyloid in Type 2 Diabetes, and the Toxic Oligomer Hypothesis. *Endocr. Rev.* **2008**, *29* (3), 303–316. <https://doi.org/10.1210/er.2007-0037>.
- (49) Meier, J. J.; Kaye, R.; Lin, C.-Y.; Gurlo, T.; Haataja, L.; Jayasinghe, S.; Langen, R.; Glabe, C. G.; Butler, P. C. Inhibition of Human IAPP Fibril Formation Does Not Prevent β -Cell Death: Evidence for Distinct Actions of Oligomers and Fibrils of Human IAPP. *Am. J. Physiol.-Endocrinol. Metab.* **2006**, *291* (6), E1317–E1324. <https://doi.org/10.1152/ajpendo.00082.2006>.
- (50) Membrane Disruption and Early Events in the Aggregation of the Diabetes Related Peptide IAPP from a Molecular Perspective | Accounts of Chemical Research <https://pubs-acrs-org.proxy.scd.u-psud.fr/doi/full/10.1021/ar200189b> (accessed Mar 24, 2020).
- (51) Casas, S.; Novials, A.; Reimann, F.; Gomis, R.; Gribble, F. M. Calcium Elevation in Mouse Pancreatic Beta Cells Evoked by Extracellular Human Islet Amyloid Polypeptide Involves Activation of the Mechanosensitive Ion Channel TRPV4. *Diabetologia* **2008**, *51* (12), 2252–2262. <https://doi.org/10.1007/s00125-008-1111-z>.
- (52) Zraika, S.; Hull, R. L.; Verchere, C. B.; Clark, A.; Potter, K. J.; Fraser, P. E.; Raleigh, D. P.; Kahn, S. E. Toxic Oligomers and Islet Beta Cell Death: Guilty by Association or Convicted by Circumstantial Evidence? *Diabetologia* **2010**, *53* (6), 1046–1056. <https://doi.org/10.1007/s00125-010-1671-6>.
- (53) Zraika, S.; Hull, R. L.; Udayasankar, J.; Aston-Mourney, K.; Subramanian, S. L.; Kisilevsky, R.; Szarek, W. A.; Kahn, S. E. Oxidative Stress Is Induced by Islet Amyloid Formation and Time-Dependently Mediates Amyloid-Induced Beta Cell Apoptosis. *Diabetologia* **2009**, *52* (4), 626–635. <https://doi.org/10.1007/s00125-008-1255-x>.
- (54) Li, X.-L.; Xu, G.; Chen, T.; Wong, Y.-S.; Zhao, H.-L.; Fan, R.-R.; Gu, X.-M.; Tong, P. C. Y.; Chan, J. C. N. Phycocyanin Protects INS-1E Pancreatic Beta Cells against Human Islet Amyloid Polypeptide-Induced Apoptosis through Attenuating Oxidative Stress and Modulating JNK and P38 Mitogen-Activated Protein Kinase Pathways. *Int. J. Biochem. Cell Biol.* **2009**, *41* (7), 1526–1535. <https://doi.org/10.1016/j.biocel.2009.01.002>.
- (55) Messier, C. Impact of Impaired Glucose Tolerance and Type 2 Diabetes on Cognitive Aging. *Neurobiol. Aging* **2005**, *26* (1, Supplement), 26–30. <https://doi.org/10.1016/j.neurobiolaging.2005.09.014>.
- (56) Jayaraman, A.; Pike, C. J. Alzheimer's Disease and Type 2 Diabetes: Multiple Mechanisms Contribute to Interactions. *Curr. Diab. Rep.* **2014**, *14* (4), 476. <https://doi.org/10.1007/s11892-014-0476-2>.
- (57) Jackson, K.; Barisone, G. A.; Diaz, E.; Jin, L.; DeCarli, C.; Despa, F. Amylin Deposition in the Brain: A Second Amyloid in Alzheimer Disease? *Ann. Neurol.* **2013**, *74* (4), 517–526. <https://doi.org/10.1002/ana.23956>.
- (58) Oskarsson, M. E.; Paulsson, J. F.; Schultz, S. W.; Ingelsson, M.; Westermark, P.; Westermark, G. T. In Vivo Seeding and Cross-Seeding of Localized Amyloidosis: A Molecular Link between Type 2 Diabetes and Alzheimer Disease. *Am. J. Pathol.* **2015**, *185* (3), 834–846. <https://doi.org/10.1016/j.ajpath.2014.11.016>.
- (59) Fu, W.; Ruangkittisakul, A.; MacTavish, D.; Shi, J. Y.; Ballanyi, K.; Jhamandas, J. H. Amyloid β (A β) Peptide Directly Activates Amylin-3 Receptor Subtype by Triggering Multiple Intracellular Signaling Pathways. *J. Biol. Chem.* **2012**, *287* (22), 18820–18830. <https://doi.org/10.1074/jbc.M111.331181>.

- (60) Wang, E.; Zhu, H.; Wang, X.; Gower, A. C.; Wallack, M.; Blusztajn, J. K.; Kowall, N.; Qiu, W. Q. Amylin Treatment Reduces Neuroinflammation and Ameliorates Abnormal Patterns of Gene Expression In the Cerebral Cortex of an Alzheimer’s Disease Mouse Model. *J. Alzheimers Dis.* **2017**, *56* (1), 47–61. <https://doi.org/10.3233/JAD-160677>.
- (61) Zhu, H.; Wang, X.; Wallack, M.; Li, H.; Carreras, I.; Dedeoglu, A.; Hur, J.-Y.; Zheng, H.; Li, H.; Fine, R.; Mwamburi, M.; Sun, X.; Kowall, N.; Stern, R. A.; Qiu, W. Q. Intraperitoneal Injection of the Pancreatic Peptide Amylin Potently Reduces Behavioral Impairment and Brain Amyloid Pathology in Murine Models of Alzheimer’s Disease. *Mol. Psychiatry* **2015**, *20* (2), 252–262. <https://doi.org/10.1038/mp.2014.17>.
- (62) Miettlicki-Baase, E. G. Amylin in Alzheimer’s Disease: Pathological Peptide or Potential Treatment? *Neuropharmacology* **2018**, *136* (Pt B), 287–297. <https://doi.org/10.1016/j.neuropharm.2017.12.016>.
- (63) Akter, R.; Cao, P.; Noor, H.; Ridgway, Z.; Tu, L.-H.; Wang, H.; Wong, A. G.; Zhang, X.; Abedini, A.; Schmidt, A. M.; Raleigh, D. P. Islet Amyloid Polypeptide: Structure, Function, and Pathophysiology. *J. Diabetes Res.* **2015**, *2016*, 2798269. <https://doi.org/10.1155/2016/2798269>.
- (64) Westermark, P.; Engström, U.; Johnson, K. H.; Westermark, G. T.; Betsholtz, C. Islet Amyloid Polypeptide: Pinpointing Amino Acid Residues Linked to Amyloid Fibril Formation. *Proc. Natl. Acad. Sci.* **1990**, *87* (13), 5036.
- (65) Higham, C. E.; Jaikaran, E. T. A. S.; Fraser, P. E.; Gross, M.; Clark, A. Preparation of Synthetic Human Islet Amyloid Polypeptide (IAPP) in a Stable Conformation to Enable Study of Conversion to Amyloid-like Fibrils. *FEBS Lett.* **2000**, *470* (1), 55–60. [https://doi.org/10.1016/S0014-5793\(00\)01287-4](https://doi.org/10.1016/S0014-5793(00)01287-4).
- (66) Jaikaran, E. T. A. S.; Clark, A. Islet Amyloid and Type 2 Diabetes: From Molecular Misfolding to Islet Pathophysiology. *Biochim. Biophys. Acta BBA - Mol. Basis Dis.* **2001**, *1537* (3), 179–203. [https://doi.org/10.1016/S0925-4439\(01\)00078-3](https://doi.org/10.1016/S0925-4439(01)00078-3).
- (67) Sumner Makin, O.; Serpell, L. C. Structural Characterisation of Islet Amyloid Polypeptide Fibrils. *J. Mol. Biol.* **2004**, *335* (5), 1279–1288. <https://doi.org/10.1016/j.jmb.2003.11.048>.
- (68) Kajava, A. V.; Aebi, U.; Steven, A. C. The Parallel Superpleated Beta-Structure as a Model for Amyloid Fibrils of Human Amylin. *J. Mol. Biol.* **2005**, *348* (2), 247–252. <https://doi.org/10.1016/j.jmb.2005.02.029>.
- (69) Luca, S.; Yau, W.-M.; Leapman, R.; Tycko, R. Peptide Conformation and Supramolecular Organization in Amylin Fibrils: Constraints from Solid-State NMR [†]. *Biochemistry* **2007**, *46* (47), 13505–13522. <https://doi.org/10.1021/bi701427q>.
- (70) Bedrood, S.; Li, Y.; Isas, J. M.; Hegde, B. G.; Baxa, U.; Haworth, I. S.; Langen, R. Fibril Structure of Human Islet Amyloid Polypeptide. *J. Biol. Chem.* **2012**, *287* (8), 5235–5241. <https://doi.org/10.1074/jbc.M111.327817>.
- (71) Mirecka, E. A.; Feuerstein, S.; Gremer, L.; Schröder, G. F.; Stoldt, M.; Willbold, D.; Hoyer, W. β -Hairpin of Islet Amyloid Polypeptide Bound to an Aggregation Inhibitor. *Sci. Rep.* **2016**, *6* (1), 33474. <https://doi.org/10.1038/srep33474>.
- (72) Röder, C.; Kupreichyk, T.; Gremer, L.; Schäfer, L. U.; Pothula, K. R.; Ravelli, R. B. G.; Willbold, D.; Hoyer, W.; Schröder, G. F. Cryo-EM Structure of Islet Amyloid Polypeptide Fibrils Reveals Similarities with Amyloid- β Fibrils. *Nat. Struct. Mol. Biol.* **2020**, *27* (7), 660–667. <https://doi.org/10.1038/s41594-020-0442-4>.
- (73) Wiltzius, J. J. W.; Sievers, S. A.; Sawaya, M. R.; Cascio, D.; Popov, D.; Riek, C.; Eisenberg, D. Atomic Structure of the Cross- β Spine of Islet Amyloid Polypeptide (Amylin). *Protein Sci.* **2008**, *17* (9), 1467–1474. <https://doi.org/10.1110/ps.036509.108>.
- (74) Wang, L.; Middleton, C. T.; Singh, S.; Reddy, A. S.; Woys, A. M.; Strasfeld, D. B.; Marek, P.; Raleigh, D. P.; de Pablo, J. J.; Zanni, M. T.; Skinner, J. L. 2DIR Spectroscopy of Human Amylin Fibrils Reflects

- Stable β -Sheet Structure. *J. Am. Chem. Soc.* **2011**, *133* (40), 16062–16071. <https://doi.org/10.1021/ja204035k>.
- (75) Liang, G.; Zhao, J.; Yu, X.; Zheng, J. Comparative Molecular Dynamics Study of Human Islet Amyloid Polypeptide (IAPP) and Rat IAPP Oligomers. *Biochemistry* **2013**, *52* (6), 1089–1100. <https://doi.org/10.1021/bi301525e>.
- (76) Wu, C.; Shea, J.-E. Structural Similarities and Differences between Amyloidogenic and Non-Amyloidogenic Islet Amyloid Polypeptide (IAPP) Sequences and Implications for the Dual Physiological and Pathological Activities of These Peptides. *PLoS Comput. Biol.* **2013**, *9* (8), e1003211. <https://doi.org/10.1371/journal.pcbi.1003211>.
- (77) Tran, L.; Ha-Duong, T. Insights into the Conformational Ensemble of Human Islet Amyloid Polypeptide from Molecular Simulations. *Curr. Pharm. Des.* **2016**, *22* (23), 3601–3607. <https://doi.org/10.2174/1381612822666160414142538>.
- (78) Knight, J. D.; Hebda, J. A.; Miranker, A. D. Conserved and Cooperative Assembly of Membrane-Bound α -Helical States of Islet Amyloid Polypeptide[†]. *Biochemistry* **2006**, *45* (31), 9496–9508. <https://doi.org/10.1021/bi060579z>.
- (79) Zhao, J.; Yu, X.; Liang, G.; Zheng, J. Structural Polymorphism of Human Islet Amyloid Polypeptide (HIAPP) Oligomers Highlights the Importance of Interfacial Residue Interactions. *Biomacromolecules* **2011**, *12* (1), 210–220. <https://doi.org/10.1021/bm101159p>.
- (80) Zhao, J.; Yu, X.; Liang, G.; Zheng, J. Heterogeneous Triangular Structures of Human Islet Amyloid Polypeptide (Amylin) with Internal Hydrophobic Cavity and External Wrapping Morphology Reveal the Polymorphic Nature of Amyloid Fibrils. *Biomacromolecules* **2011**, *12* (5), 1781–1794. <https://doi.org/10.1021/bm2001507>.
- (81) Pithadia, A.; Brender, J. R.; Fierke, C. A.; Ramamoorthy, A. Inhibition of IAPP Aggregation and Toxicity by Natural Products and Derivatives. *J. Diabetes Res.* **2016**, *2016*, 1–12. <https://doi.org/10.1155/2016/2046327>.
- (82) Young, L. M.; Cao, P.; Raleigh, D. P.; Ashcroft, A. E.; Radford, S. E. Ion Mobility Spectrometry–Mass Spectrometry Defines the Oligomeric Intermediates in Amylin Amyloid Formation and the Mode of Action of Inhibitors. *J. Am. Chem. Soc.* **2014**, *136* (2), 660–670. <https://doi.org/10.1021/ja406831n>.
- (83) Mo, Y.; Lei, J.; Sun, Y.; Zhang, Q.; Wei, G. Conformational Ensemble of HIAPP Dimer: Insight into the Molecular Mechanism by Which a Green Tea Extract Inhibits HIAPP Aggregation. *Sci. Rep.* **2016**, *6* (1), 33076. <https://doi.org/10.1038/srep33076>.
- (84) Cao, P.; Raleigh, D. P. Analysis of the Inhibition and Remodeling of Islet Amyloid Polypeptide Amyloid Fibers by Flavanols. *Biochemistry* **2012**, *51* (13), 2670–2683. <https://doi.org/10.1021/bi2015162>.
- (85) Engel, M. F. M.; vandenAkker, C. C.; Schleegeer, M.; Velikov, K. P.; Koenderink, G. H.; Bonn, M. The Polyphenol EGCG Inhibits Amyloid Formation Less Efficiently at Phospholipid Interfaces than in Bulk Solution. *J. Am. Chem. Soc.* **2012**, *134* (36), 14781–14788. <https://doi.org/10.1021/ja3031664>.
- (86) Nedumpully-Govindan, P.; Kakinen, A.; Pilkington, E. H.; Davis, T. P.; Chun Ke, P.; Ding, F. Stabilizing Off-Pathway Oligomers by Polyphenol Nanoassemblies for IAPP Aggregation Inhibition. *Sci. Rep.* **2016**, *6* (1), 19463. <https://doi.org/10.1038/srep19463>.
- (87) Sparks, S.; Liu, G.; Robbins, K. J.; Lazo, N. D. Curcumin Modulates the Self-Assembly of the Islet Amyloid Polypeptide by Disassembling α -Helix. *Biochem. Biophys. Res. Commun.* **2012**, *422* (4), 551–555. <https://doi.org/10.1016/j.bbrc.2012.05.013>.
- (88) Cao, P.; Meng, F.; Abedini, A.; Raleigh, D. P. The Ability of Rodent Islet Amyloid Polypeptide To Inhibit Amyloid Formation by Human Islet Amyloid Polypeptide Has Important Implications for the Mechanism of Amyloid Formation and the Design of Inhibitors. *Biochemistry* **2010**, *49* (5), 872–881. <https://doi.org/10.1021/bi901751b>.

- (89) Abedini, A.; Meng, F.; Raleigh, D. P. A Single-Point Mutation Converts the Highly Amyloidogenic Human Islet Amyloid Polypeptide into a Potent Fibrillization Inhibitor. *J. Am. Chem. Soc.* **2007**, *129* (37), 11300–11301. <https://doi.org/10.1021/ja072157y>.
- (90) Young, A. A.; Vine, W.; Gedulin, B. R.; Pittner, R.; Janes, S.; Gaeta, L. S. L.; Percy, A.; Moore, C. X.; Koda, J. E.; Rink, T. J.; Beaumont, K. Preclinical Pharmacology of Pramlintide in the Rat: Comparisons with Human and Rat Amylin. *Drug Dev. Res.* **1996**, *37* (4), 231–248. [https://doi.org/10.1002/\(SICI\)1098-2299\(199604\)37:4<231::AID-DDR5>3.0.CO;2-M](https://doi.org/10.1002/(SICI)1098-2299(199604)37:4<231::AID-DDR5>3.0.CO;2-M).
- (91) Younk, L. M.; Mikeladze, M.; Davis, S. N. Pramlintide and the Treatment of Diabetes: A Review of the Data since Its Introduction. *Expert Opin. Pharmacother.* **2011**, *12* (9), 1439–1451. <https://doi.org/10.1517/14656566.2011.581663>.
- (92) Wang, H.; Ridgway, Z.; Cao, P.; Ruzsicska, B.; Raleigh, D. P. Analysis of the Ability of Pramlintide To Inhibit Amyloid Formation by Human Islet Amyloid Polypeptide Reveals a Balance between Optimal Recognition and Reduced Amyloidogenicity. *Biochemistry* **2015**, *54* (44), 6704–6711. <https://doi.org/10.1021/acs.biochem.5b00567>.
- (93) Tenidis, K.; Waldner, M.; Bernhagen, J.; Fischle, W.; Bergmann, M.; Weber, M.; Merkle, M.-L.; Voelter, W.; Brunner, H.; Kapurniotu, A. Identification of a Penta- and Hexapeptide of Islet Amyloid Polypeptide (IAPP) with Amyloidogenic and Cytotoxic Properties. *J. Mol. Biol.* **2000**, *295* (4), 1055–1071. <https://doi.org/10.1006/jmbi.1999.3422>.
- (94) Azriel, R.; Gazit, E. Analysis of the Minimal Amyloid-Forming Fragment of the Islet Amyloid Polypeptide: AN EXPERIMENTAL SUPPORT FOR THE KEY ROLE OF THE PHENYLALANINE RESIDUE IN AMYLOID FORMATION. *J. Biol. Chem.* **2001**, *276* (36), 34156–34161. <https://doi.org/10.1074/jbc.M102883200>.
- (95) Porat, Y.; Stepensky, A.; Ding, F.-X.; Naider, F.; Gazit, E. Completely Different Amyloidogenic Potential of Nearly Identical Peptide Fragments. *Biopolymers* **2003**, *69* (2), 161–164. <https://doi.org/10.1002/bip.10386>.
- (96) Porat, Y.; Mazor, Y.; Efrat, S.; Gazit, E. Inhibition of Islet Amyloid Polypeptide Fibril Formation: A Potential Role for Heteroaromatic Interactions[†]. *Biochemistry* **2004**, *43* (45), 14454–14462. <https://doi.org/10.1021/bi048582a>.
- (97) Knight, J. D.; Williamson, J. A.; Miranker, A. D. Interaction of Membrane-Bound Islet Amyloid Polypeptide with Soluble and Crystalline Insulin. *Protein Sci.* **2008**, *17* (10), 1850–1856. <https://doi.org/10.1110/ps.036350.108>.
- (98) Susa, A. C.; Wu, C.; Bernstein, S. L.; Dupuis, N. F.; Wang, H.; Raleigh, D. P.; Shea, J.-E.; Bowers, M. T. Defining the Molecular Basis of Amyloid Inhibitors: Human Islet Amyloid Polypeptide–Insulin Interactions. *J. Am. Chem. Soc.* **2014**, *136* (37), 12912–12919. <https://doi.org/10.1021/ja504031d>.
- (99) Gilead, S.; Wolfenson, H.; Gazit, E. Molecular Mapping of the Recognition Interface between the Islet Amyloid Polypeptide and Insulin. *Angew. Chem. Int. Ed.* **2006**, *45* (39), 6476–6480. <https://doi.org/10.1002/anie.200602034>.
- (100) Mirecka, E. A.; Gremer, L.; Schiefer, S.; Oesterhelt, F.; Stoldt, M.; Willbold, D.; Hoyer, W. Engineered Aggregation Inhibitor Fusion for Production of Highly Amyloidogenic Human Islet Amyloid Polypeptide. *J. Biotechnol.* **2014**, *191*, 221–227. <https://doi.org/10.1016/j.jbiotec.2014.06.006>.
- (101) Yan, L.-M.; Velkova, A.; Tatarek-Nossol, M.; Rammes, G.; Sibae, A.; Andreetto, E.; Kracklauer, M.; Bakou, M.; Malideli, E.; Göke, B.; Schirra, J.; Storr, M.; Kapurniotu, A. Selectively N-Methylated Soluble IAPP Mimics as Potent IAPP Receptor Agonists and Nanomolar Inhibitors of Cytotoxic Self-Assembly of Both IAPP and A β 40. *Angew. Chem. Int. Ed.* **2013**, *52* (39), 10378–10383. <https://doi.org/10.1002/anie.201302840>.

- (102) Gilead, S.; Gazit, E. Inhibition of Amyloid Fibril Formation by Peptide Analogues Modified With α -Aminoisobutyric Acid. *Angew. Chem. Int. Ed.* **2004**, *43* (31), 4041–4044. <https://doi.org/10.1002/anie.200353565>.
- (103) Paul, A.; Kalita, S.; Kalita, S.; Sukumar, P.; Mandal, B. Disaggregation of Amylin Aggregate by Novel Conformationally Restricted Aminobenzoic Acid Containing α/β and α/γ Hybrid Peptidomimetics. *Sci. Rep.* **2017**, *7* (1), 40095. <https://doi.org/10.1038/srep40095>.
- (104) Mishra, A.; Misra, A.; Sri Vaishnavi, T.; Thota, C.; Gupta, M.; Ramakumar, S.; Chauhan, V. S. Conformationally Restricted Short Peptides Inhibit Human Islet Amyloid Polypeptide (HIAPP) Fibrillization. *Chem. Commun.* **2013**, *49* (26), 2688. <https://doi.org/10.1039/c3cc38982k>.
- (105) Laxio Arenas, J.; Kaffy, J.; Onger, S. Peptides and Peptidomimetics as Inhibitors of Protein–Protein Interactions Involving β -Sheet Secondary Structures. *Curr. Opin. Chem. Biol.* **2019**, *52*, 157–167. <https://doi.org/10.1016/j.cbpa.2019.07.008>.
- (106) Buchanan, L. E.; Dunkelberger, E. B.; Tran, H. Q.; Cheng, P.-N.; Chiu, C.-C.; Cao, P.; Raleigh, D. P.; de Pablo, J. J.; Nowick, J. S.; Zanni, M. T. Mechanism of IAPP Amyloid Fibril Formation Involves an Intermediate with a Transient β -Sheet. *Proc. Natl. Acad. Sci.* **2013**, *110* (48), 19285–19290. <https://doi.org/10.1073/pnas.1314481110>.
- (107) Cheng, P.-N.; Liu, C.; Zhao, M.; Eisenberg, D.; Nowick, J. S. Amyloid β -Sheet Mimics That Antagonize Protein Aggregation and Reduce Amyloid Toxicity. *Nat. Chem.* **2012**, *4* (11), 927–933. <https://doi.org/10.1038/nchem.1433>.
- (108) Spanopoulou, A.; Heidrich, L.; Chen, H.-R.; Frost, C.; Hrle, D.; Malideli, E.; Hille, K.; Grammatikopoulos, A.; Bernhagen, J.; Zacharias, M.; Rammes, G.; Kapurniotu, A. Designed Macrocyclic Peptides as Nanomolar Amyloid Inhibitors Based on Minimal Recognition Elements. *Angew. Chem. Int. Ed.* **2018**, *57* (44), 14503–14508. <https://doi.org/10.1002/anie.201802979>.
- (109) Andreetto, E.; Malideli, E.; Yan, L.-M.; Kracklauer, M.; Farbiarz, K.; Tatarek-Nossol, M.; Rammes, G.; Prade, E.; Neumüller, T.; Caporale, A.; Spanopoulou, A.; Bakou, M.; Reif, B.; Kapurniotu, A. A Hot-Segment-Based Approach for the Design of Cross-Amyloid Interaction Surface Mimics as Inhibitors of Amyloid Self-Assembly. *Angew. Chem. Int. Ed.* **2015**, *54* (44), 13095–13100. <https://doi.org/10.1002/anie.201504973>.
- (110) Huggins, K. N. L.; Bisaglia, M.; Bubacco, L.; Tatarek-Nossol, M.; Kapurniotu, A.; Andersen, N. H. Designed Hairpin Peptides Interfere with Amyloidogenesis Pathways: Fibril Formation and Cytotoxicity Inhibition, Interception of the Preamyloid State. *Biochemistry* **2011**, *50* (38), 8202–8212. <https://doi.org/10.1021/bi200760h>.
- (111) Saraogi, I.; Hebda, J. A.; Becerril, J.; Estroff, L. A.; Miranker, A. D.; Hamilton, A. D. Synthetic α -Helix Mimetics as Agonists and Antagonists of Islet Amyloid Polypeptide Aggregation. *Angew. Chem. Int. Ed.* **2010**, *49* (4), 736–739. <https://doi.org/10.1002/anie.200901694>.
- (112) Kumar, S.; Schlamadinger, D. E.; Brown, M. A.; Dunn, J. M.; Mercado, B.; Hebda, J. A.; Saraogi, I.; Rhoades, E.; Hamilton, A. D.; Miranker, A. D. Islet Amyloid-Induced Cell Death and Bilayer Integrity Loss Share a Molecular Origin Targetable with Oligopyridylamide-Based α -Helical Mimetics. *Chem. Biol.* **2015**, *22* (3), 369–378. <https://doi.org/10.1016/j.chembiol.2015.01.006>.
- (113) Kumar, S.; Brown, M. A.; Nath, A.; Miranker, A. D. Folded Small Molecule Manipulation of Islet Amyloid Polypeptide. *Chem. Biol.* **2014**, *21* (6), 775–781. <https://doi.org/10.1016/j.chembiol.2014.05.007>.
- (114) Cunningham, A. D.; Qvit, N.; Mochly-Rosen, D. Peptides and Peptidomimetics as Regulators of Protein–Protein Interactions. *Curr. Opin. Struct. Biol.* **2017**, *44*, 59–66. <https://doi.org/10.1016/j.sbi.2016.12.009>.
- (115) Dorgeret, B.; Khemtémourian, L.; Correia, I.; Soulier, J.-L.; Lequin, O.; Onger, S. Sugar-Based Peptidomimetics Inhibit Amyloid β -Peptide Aggregation. *Eur. J. Med. Chem.* **2011**, *46* (12), 5959–5969. <https://doi.org/10.1016/j.ejmech.2011.10.008>.

- (116) Kaffy, J.; Brinet, D.; Soulier, J.-L.; Khemtémourian, L.; Lequin, O.; Taverna, M.; Crousse, B.; Ongeri, S. Structure–Activity Relationships of Sugar-Based Peptidomimetics as Modulators of Amyloid β -Peptide Early Oligomerization and Fibrillization. *Eur. J. Med. Chem.* **2014**, *86*, 752–758. <https://doi.org/10.1016/j.ejmech.2014.09.031>.
- (117) Kaffy, J.; Brinet, D.; Soulier, J.-L.; Correia, I.; Tonali, N.; Fera, K. F.; Iacone, Y.; Hoffmann, A. R. F.; Khemtémourian, L.; Crousse, B.; Taylor, M.; Allsop, D.; Taverna, M.; Lequin, O.; Ongeri, S. Designed Glycopeptidomimetics Disrupt Protein–Protein Interactions Mediating Amyloid β -Peptide Aggregation and Restore Neuroblastoma Cell Viability. *J. Med. Chem.* **2016**, *59* (5), 2025–2040. <https://doi.org/10.1021/acs.jmedchem.5b01629>.
- (118) Vahdati, L.; Fanelli, R.; Bernadat, G.; Correia, I.; Lequin, O.; Ongeri, S.; Piarulli, U. Synthesis and Conformational Studies of a Stable Peptidomimetic β -Hairpin Based on a Bifunctional Diketopiperazine Turn Inducer. *New J. Chem.* **2015**, *39* (5), 3250–3258. <https://doi.org/10.1039/C4NJ01437E>.
- (119) Vahdati, L.; Kaffy, J.; Brinet, D.; Bernadat, G.; Correia, I.; Panzeri, S.; Fanelli, R.; Lequin, O.; Taverna, M.; Ongeri, S.; Piarulli, U. Synthesis and Characterization of Hairpin Mimics That Modulate the Early Oligomerization and Fibrillization of Amyloid β -Peptide: Synthesis and Characterization of Hairpin Mimics That Modulate the Early Oligomerization and Fibrillization of Amyloid β -Peptide. *Eur. J. Org. Chem.* **2017**, *2017* (20), 2971–2980. <https://doi.org/10.1002/ejoc.201700010>.
- (120) Pellegrino, S.; Contini, A.; Gelmi, M. L.; Lo Presti, L.; Soave, R.; Erba, E. Asymmetric Modular Synthesis of a Semirigid Dipeptide Mimetic by Cascade Cycloaddition/Ring Rearrangement and Borohydride Reduction. *J. Org. Chem.* **2014**, *79* (7), 3094–3102. <https://doi.org/10.1021/jo500237j>.
- (121) Pellegrino, S.; Tonali, N.; Erba, E.; Kaffy, J.; Taverna, M.; Contini, A.; Taylor, M.; Allsop, D.; Gelmi, M. L.; Ongeri, S. β -Hairpin Mimics Containing a Piperidine–Pyrrolidine Scaffold Modulate the β -Amyloid Aggregation Process Preserving the Monomer Species. *Chem. Sci.* **2017**, *8* (2), 1295–1302. <https://doi.org/10.1039/C6SC03176E>.
- (122) Tonali, N.; Kaffy, J.; Soulier, J.-L.; Gelmi, M. L.; Erba, E.; Taverna, M.; van Heijenoort, C.; Ha-Duong, T.; Ongeri, S. Structure-Activity Relationships of β -Hairpin Mimics as Modulators of Amyloid β -Peptide Aggregation. *Eur. J. Med. Chem.* **2018**, *154*, 280–293. <https://doi.org/10.1016/j.ejmech.2018.05.018>.
- (123) Mathieu, L.; Legrand, B.; Deng, C.; Vezenkov, L.; Wenger, E.; Didierjean, C.; Amblard, M.; Averlant-Petit, M.-C.; Masurier, N.; Lisowski, V.; Martinez, J.; Maillard, L. T. Helical Oligomers of Thiazole-Based γ -Amino Acids: Synthesis and Structural Studies. *Angew. Chem. Int. Ed.* **2013**, *52* (23), 6006–6010. <https://doi.org/10.1002/anie.201302106>.
- (124) Ongeri, S.; Kaffy, J.; Berardet, C.; Mathieu, L.; Legrand, B.; Taverna, M.; Halgand, F.; Van Der Rest, G.; Maillard, L. T. Helical F-peptide Foldamers as Dual Inhibitors of Amyloid- β Peptide and Islet Amyloid Polypeptide Oligomerization and Fibrillization. *Chem. – Eur. J.* **2020**, *chem.202001716*. <https://doi.org/10.1002/chem.202001716>.
- (125) LeVine, H. [18] Quantification of β -Sheet Amyloid Fibril Structures with Thioflavin T. In *Methods in Enzymology*; Elsevier, 1999; Vol. 309, pp 274–284. [https://doi.org/10.1016/S0076-6879\(99\)09020-5](https://doi.org/10.1016/S0076-6879(99)09020-5).
- (126) Biancalana, M.; Koide, S. Molecular Mechanism of Thioflavin-T Binding to Amyloid Fibrils. *Biochim. Biophys. Acta BBA - Proteins Proteomics* **2010**, *1804* (7), 1405–1412. <https://doi.org/10.1016/j.bbapap.2010.04.001>.
- (127) Sulatskaya, A. I.; Kuznetsova, I. M.; Turoverov, K. K. Interaction of Thioflavin T with Amyloid Fibrils: Fluorescence Quantum Yield of Bound Dye. *J. Phys. Chem. B* **2012**, *116* (8), 2538–2544. <https://doi.org/10.1021/jp2083055>.

- (128) Reimer, L. *Transmission Electron Microscopy*; Springer Series in Optical Sciences; Springer Berlin Heidelberg: Berlin, Heidelberg, 1984; Vol. 36. <https://doi.org/10.1007/978-3-662-13553-2>.
- (129) Hoffmann, A. R. F.; Saravanan, M. S.; Lequin, O.; Killian, J. A.; Khemtémourian, L. A Single Mutation on the Human Amyloid Polypeptide Modulates Fibril Growth and Affects the Mechanism of Amyloid-Induced Membrane Damage. *Biochim. Biophys. Acta BBA - Biomembr.* **2018**, *1860* (9), 1783–1792. <https://doi.org/10.1016/j.bbamem.2018.02.018>.
- (130) Woods, L. A.; Radford, S. E.; Ashcroft, A. E. Advances in Ion Mobility Spectrometry–Mass Spectrometry Reveal Key Insights into Amyloid Assembly. *Biochim. Biophys. Acta BBA - Proteins Proteomics* **2013**, *1834* (6), 1257–1268. <https://doi.org/10.1016/j.bbapap.2012.10.002>.
- (131) Berardet, C.; Kaffy, J.; Halgand, F.; Van der Rest, G.; Ongerì, S.; Taverna, M. Evidence for Different in Vitro Oligomerization Behaviors of Synthetic HIAPP Obtained from Different Sources. *Anal. Bioanal. Chem.* **2020**. <https://doi.org/10.1007/s00216-020-02560-5>.
- (132) Young, L. M.; Saunders, J. C.; Mahood, R. A.; Revill, C. H.; Foster, R. J.; Tu, L.-H.; Raleigh, D. P.; Radford, S. E.; Ashcroft, A. E. Screening and Classifying Small-Molecule Inhibitors of Amyloid Formation Using Ion Mobility Spectrometry–Mass Spectrometry. *Nat. Chem.* **2015**, *7* (1), 73–81. <https://doi.org/10.1038/nchem.2129>.
- (133) Young, L. M.; Ashcroft, A. E.; Radford, S. E. Small Molecule Probes of Protein Aggregation. *Curr. Opin. Chem. Biol.* **2017**, *39*, 90–99. <https://doi.org/10.1016/j.cbpa.2017.06.008>.
- (134) Brinet, D.; Kaffy, J.; Oukacine, F.; Glumm, S.; Ongerì, S.; Taverna, M. An Improved Capillary Electrophoresis Method for in Vitro Monitoring of the Challenging Early Steps of A β 1–42 Peptide Oligomerization: Application to Anti-Alzheimer’s Drug Discovery. *ELECTROPHORESIS* **2014**, *35* (23), 3302–3309. <https://doi.org/10.1002/elps.201400271>.
- (135) Berardet, C.; Kaffy, J.; Ongerì, S.; Taverna, M. A Capillary Zone Electrophoresis Method to Investigate the Oligomerization of the Human Islet Amyloid Polypeptide Involved in Type 2 Diabetes. *J. Chromatogr. A* **2018**, *1578*, 83–90. <https://doi.org/10.1016/j.chroma.2018.10.006>.
- (136) Lim, C. K. S. F. Y. Li Capillary Electrophoresis—Principles, Practice and Applications, Journal of Chromatography Library, Vol. 52 Elsevier, Amsterdam, 1992; 582+XXVI Pp., Dfl. 395, ISBN 044-89433-0. *J. Appl. Toxicol.* **1993**, *13* (4), 305–305. <https://doi.org/10.1002/jat.2550130415>.
- (137) Riss, T. L.; Moravec, R. A.; Niles, A. L.; Duellman, S.; Benink, H. A.; Worzella, T. J.; Minor, L. Cell Viability Assays. In *Assay Guidance Manual*; Sittampalam, G. S., Grossman, A., Brimacombe, K., Arkin, M., Auld, D., Austin, C. P., Baell, J., Bejcek, B., Caaveiro, J. M. M., Chung, T. D. Y., Coussens, N. P., Dahlin, J. L., Devanaryan, V., Foley, T. L., Glicksman, M., Hall, M. D., Haas, J. V., Hoare, S. R. J., Inglese, J., Iversen, P. W., Kahl, S. D., Kales, S. C., Kirshner, S., Lal-Nag, M., Li, Z., McGee, J., McManus, O., Riss, T., Saradjian, P., Trask, O. J., Weidner, J. R., Wildey, M. J., Xia, M., Xu, X., Eds.; Eli Lilly & Company and the National Center for Advancing Translational Sciences: Bethesda (MD), 2004.
- (138) Hassanpour, A.; De Carufel, C. A.; Bourgault, S.; Forgione, P. Synthesis of 2,5-Diaryl-Substituted Thiophenes as Helical Mimetics: Towards the Modulation of Islet Amyloid Polypeptide (IAPP) Amyloid Fibril Formation and Cytotoxicity. *Chem. - Eur. J.* **2014**, *20* (9), 2522–2528. <https://doi.org/10.1002/chem.201303928>.
- (139) Meng, F.; Abedini, A.; Plesner, A.; Verchere, C. B.; Raleigh, D. P. The Flavanol (–)-Epigallocatechin 3-Gallate Inhibits Amyloid Formation by Islet Amyloid Polypeptide, Disaggregates Amyloid Fibrils, and Protects Cultured Cells against IAPP-Induced Toxicity. *Biochemistry* **2010**, *49* (37), 8127–8133. <https://doi.org/10.1021/bi100939a>.
- (140) Kelly, S. M.; Jess, T. J.; Price, N. C. How to Study Proteins by Circular Dichroism. *Biochim. Biophys. Acta BBA - Proteins Proteomics* **2005**, *1751* (2), 119–139. <https://doi.org/10.1016/j.bbapap.2005.06.005>.

- (141) Smith, L. J.; Bolin, K. A.; Schwalbe, H.; MacArthur, M. W.; Thornton, J. M.; Dobson, C. M. Analysis of Main Chain Torsion Angles in Proteins: Prediction of NMR Coupling Constants for Native and Random Coil Conformations. *J. Mol. Biol.* **1996**, *255* (3), 494–506. <https://doi.org/10.1006/jmbi.1996.0041>.
- (142) Wishart, D. S.; Bigam, C. G.; Holm, A.; Hodges, R. S.; Sykes, B. D. ¹H, ¹³C and ¹⁵N Random Coil NMR Chemical Shifts of the Common Amino Acids. I. Investigations of Nearest-Neighbor Effects. *J. Biomol. NMR* **1995**, *5* (1), 67–81. <https://doi.org/10.1007/BF00227471>.
- (143) Höltje, H.-D.; Folkers, G.; Beier, T. *Molecular Modeling: Basic Principles and Applications*; Methods and principles in medicinal chemistry; VCH: Weinheim ; New York, 1997.
- (144) Bizet, F. Mimes de Béta-Hairpin Inhibiteurs de l'agrégation de IAPP : Intérêt Pour Le Diabète de Type 2. These de doctorat, Université Paris-Saclay (ComUE), 2018.
- (145) Galibert, M.; Wartenberg, M.; Lecaille, F.; Saidi, A.; Mavel, S.; Joulin-Giet, A.; Korkmaz, B.; Brömme, D.; Aucagne, V.; Delmas, A. F.; Lalmanach, G. Substrate-Derived Triazolo- and Azapeptides as Inhibitors of Cathepsins K and S. *Eur. J. Med. Chem.* **2018**, *144*, 201–210. <https://doi.org/10.1016/j.ejmech.2017.12.012>.
- (146) Bizet, F.; Tonalì, N.; Soulier, J.-L.; Oliva, A.; Kaffy, J.; Crousse, B.; Ongeri, S. Towards a General Synthesis of Di-Aza-Amino Acids Containing Peptides. *New J. Chem.* **2018**, *42* (20), 17062–17072. <https://doi.org/10.1039/C8NJ03635G>.
- (147) Randolph, J. T.; Zhang, X.; Huang, P. P.; Klein, L. L.; Kurtz, K. A.; Konstantinidis, A. K.; He, W.; Kati, W. M.; Kempf, D. J. Synthesis, Antiviral Activity, and Conformational Studies of a P3 Aza-Peptide Analog of a Potent Macrocyclic Tripeptide HCV Protease Inhibitor. *Bioorg. Med. Chem. Lett.* **2008**, *18* (8), 2745–2750. <https://doi.org/10.1016/j.bmcl.2008.02.053>.
- (148) Proulx, C.; Sabatino, D.; Hopewell, R.; Spiegel, J.; García Ramos, Y.; Lubell, W. D. Azapeptides and Their Therapeutic Potential. *Future Med. Chem.* **2011**, *3* (9), 1139–1164. <https://doi.org/10.4155/fmc.11.74>.
- (149) Thormann, M.; Hofmann, H.-J. Conformational Properties of Azapeptides. *J. Mol. Struct. THEOCHEM* **1999**, *469* (1–3), 63–76. [https://doi.org/10.1016/S0166-1280\(98\)00567-3](https://doi.org/10.1016/S0166-1280(98)00567-3).
- (150) Tonalì, N.; Correia, I.; Lesma, J.; Bernadat, G.; Ongeri, S.; Lequin, O. Introducing Sequential Aza-Amino Acids Units Induces Repeated β -Turns and Helical Conformations in Peptides. *Org. Biomol. Chem.* **2020**, *18* (18), 3452–3458. <https://doi.org/10.1039/C9OB02654A>.
- (151) Adessi, C.; Soto, C. Converting a Peptide into a Drug: Strategies to Improve Stability and Bioavailability. *Curr. Med. Chem.* **2002**, *9* (9), 963–978. <https://doi.org/10.2174/0929867024606731>.
- (152) Vagner, J.; Qu, H.; Hruby, V. J. Peptidomimetics, a Synthetic Tool of Drug Discovery. *Curr. Opin. Chem. Biol.* **2008**, *12* (3), 292–296. <https://doi.org/10.1016/j.cbpa.2008.03.009>.
- (153) Gante, J.; Krug, M.; Lauterbach, G.; Weitzel, R.; Hiller, W. Synthesis and Properties of the First All-Aza Analogue of a Biologically Active Peptide. *J. Pept. Sci.* **1995**, *1* (3), 201–206. <https://doi.org/10.1002/psc.310010307>.
- (154) Hill, R. D.; Vederas, J. C. Azodicarboxamides: A New Class of Cysteine Proteinase Inhibitor for Hepatitis A Virus and Human Rhinovirus 3C Enzymes. *J. Org. Chem.* **1999**, *64* (26), 9538–9546. <https://doi.org/10.1021/jo9915123>.
- (155) Han, H.; Yoon, J.; Janda, K. D. Investigations of Azapeptides as Mimetics of Leu-Enkephalin. *Bioorg. Med. Chem. Lett.* **1998**, *8* (1), 117–120. [https://doi.org/10.1016/S0960-894X\(97\)10198-6](https://doi.org/10.1016/S0960-894X(97)10198-6).
- (156) Han, H.; Janda, K. D. Azatides: Solution and Liquid Phase Syntheses of a New Peptidomimetic. *J. Am. Chem. Soc.* **1996**, *118* (11), 2539–2544. <https://doi.org/10.1021/ja9535470>.
- (157) Dufau, L.; Marques Ressurreição, A. S.; Fanelli, R.; Kihal, N.; Vidu, A.; Milcent, T.; Soulier, J.-L.; Rodrigo, J.; Desvergne, A.; Leblanc, K.; Bernadat, G.; Crousse, B.; Reboud-Ravaux, M.; Ongeri, S.

- Carbonylhydrazide-Based Molecular Tongs Inhibit Wild-Type and Mutated HIV-1 Protease Dimerization. *J. Med. Chem.* **2012**, *55* (15), 6762–6775. <https://doi.org/10.1021/jm300181j>.
- (158) Inoue, M.; Sumii, Y.; Shibata, N. Contribution of Organofluorine Compounds to Pharmaceuticals. *ACS Omega* **2020**, *5* (19), 10633–10640. <https://doi.org/10.1021/acsomega.0c00830>.
- (159) Bondi, A. Van Der Waals Volumes and Radii. *J. Phys. Chem.* **1964**, *68* (3), 441–451. <https://doi.org/10.1021/j100785a001>.
- (160) Gillis, E. P.; Eastman, K. J.; Hill, M. D.; Donnelly, D. J.; Meanwell, N. A. Applications of Fluorine in Medicinal Chemistry. *J. Med. Chem.* **2015**, *58* (21), 8315–8359. <https://doi.org/10.1021/acs.jmedchem.5b00258>.
- (161) Muller, K.; Faeh, C.; Diederich, F. Fluorine in Pharmaceuticals: Looking Beyond Intuition. *Science* **2007**, *317* (5846), 1881–1886. <https://doi.org/10.1126/science.1131943>.
- (162) Meanwell, N. A. Fluorine and Fluorinated Motifs in the Design and Application of Bioisosteres for Drug Design. *J. Med. Chem.* **2018**, *61* (14), 5822–5880. <https://doi.org/10.1021/acs.jmedchem.7b01788>.
- (163) Zhao, K.; Lim, D. S.; Funaki, T.; Welch, J. T. Inhibition of Dipeptidyl Peptidase IV (DPP IV) by 2-(2-Amino-1-Fluoro-Propylidene)-Cyclopentanecarbonitrile, a Fluoroolefin Containing Peptidomimetic. *Bioorg. Med. Chem.* **2003**, *11* (2), 207–215. [https://doi.org/10.1016/S0968-0896\(02\)00384-X](https://doi.org/10.1016/S0968-0896(02)00384-X).
- (164) Volonterio, A.; Bellosta, S.; Bravin, F.; Bellucci, M. C.; Bruché, L.; Colombo, G.; Malpezzi, L.; Mazzini, S.; Meille, S. V.; Meli, M.; Ramírez de Arellano, C.; Zanda, M. Synthesis, Structure and Conformation of Partially-Modified Retro- and Retro-Inverso ψ [NHCH(CF₃)]Gly Peptides. *Chem. - Eur. J.* **2003**, *9* (18), 4510–4522. <https://doi.org/10.1002/chem.200304881>.
- (165) Black, W. C.; Bayly, C. I.; Davis, D. E.; Desmarais, S.; Falgueyret, J.-P.; Léger, S.; Li, C. S.; Massé, F.; McKay, D. J.; Palmer, J. T.; Percival, M. D.; Robichaud, J.; Tsou, N.; Zamboni, R. Trifluoroethylamines as Amide Isosteres in Inhibitors of Cathepsin K. *Bioorg. Med. Chem. Lett.* **2005**, *15* (21), 4741–4744. <https://doi.org/10.1016/j.bmcl.2005.07.071>.
- (166) Sani, M.; Volonterio, A.; Zanda, M. The Trifluoroethylamine Function as Peptide Bond Replacement. *ChemMedChem* **2007**, *2* (12), 1693–1700. <https://doi.org/10.1002/cmdc.200700156>.
- (167) Adejare, A. Chemistry of Organic Fluorine Compounds II: A Critical Review Edited by M. Hudlicky and A. E. Pavlath. American Chemical Society Monograph 187. American Chemical Society, Washington, D.C. 1995. Xxi + 1296 Pp. 16.0 × 23.5 Cm. ISBN 0-8412-2515-X. \$169.95. *J. Med. Chem.* **1996**, *39* (18), 3601–3601. <https://doi.org/10.1021/jm960422c>.
- (168) Swallow, S. Fluorine in Medicinal Chemistry. In *Progress in Medicinal Chemistry*; Elsevier, 2015; Vol. 54, pp 65–133. <https://doi.org/10.1016/bs.pmch.2014.11.001>.
- (169) Kirk, K. Selective Fluorination in Drug Design and Development: An Overview of Biochemical Rationales. *Curr. Top. Med. Chem.* **2006**, *6* (14), 1447–1456. <https://doi.org/10.2174/156802606777951073>.
- (170) Champagne, P.; Desroches, J.; Paquin, J.-F. Organic Fluorine as a Hydrogen-Bond Acceptor: Recent Examples and Applications. *Synthesis* **2014**, *47* (03), 306–322. <https://doi.org/10.1055/s-0034-1379537>.
- (171) Paulini, R.; Müller, K.; Diederich, F. Orthogonal Multipolar Interactions in Structural Chemistry and Biology. *Angew. Chem. Int. Ed.* **2005**, *44* (12), 1788–1805. <https://doi.org/10.1002/anie.200462213>.
- (172) O'Hagan, D. Understanding Organofluorine Chemistry. An Introduction to the C–F Bond. *Chem Soc Rev* **2008**, *37* (2), 308–319. <https://doi.org/10.1039/B711844A>.
- (173) van Geuns, R.-J. M.; Wielopolski, P. A.; de Bruin, H. G.; Rensing, B. J.; van Ooijen, P. M. A.; Hulshoff, M.; Oudkerk, M.; de Feyter, P. J. Basic Principles of Magnetic Resonance Imaging☆. *Prog. Cardiovasc. Dis.* **1999**, *42* (2), 149–156. [https://doi.org/10.1016/S0033-0620\(99\)70014-9](https://doi.org/10.1016/S0033-0620(99)70014-9).

- (174) Xie, D.; Yu, M.; Kadakia, R. T.; Que, E. L. ¹⁹F Magnetic Resonance Activity-Based Sensing Using Paramagnetic Metals. *Acc. Chem. Res.* **2020**, *53* (1), 2–10. <https://doi.org/10.1021/acs.accounts.9b00352>.
- (175) Wahsner, J.; Gale, E. M.; Rodríguez-Rodríguez, A.; Caravan, P. Chemistry of MRI Contrast Agents: Current Challenges and New Frontiers. *Chem. Rev.* **2019**, *119* (2), 957–1057. <https://doi.org/10.1021/acs.chemrev.8b00363>.
- (176) Saha, G. B. *Basics of PET Imaging*; Springer Science+Business Media: New York, NY, 2015.
- (177) Jiang; Chalich; Deen. Sensors for Positron Emission Tomography Applications. *Sensors* **2019**, *19* (22), 5019. <https://doi.org/10.3390/s19225019>.
- (178) Dalvit, C.; Vulpetti, A. Ligand-Based Fluorine NMR Screening: Principles and Applications in Drug Discovery Projects. *J. Med. Chem.* **2019**, *62* (5), 2218–2244. <https://doi.org/10.1021/acs.jmedchem.8b01210>.
- (179) Salwiczek, M.; Nyakatura, E. K.; Gerling, U. I. M.; Ye, S.; Kokschi, B. Fluorinated Amino Acids: Compatibility with Native Protein Structures and Effects on Protein–Protein Interactions. *Chem Soc Rev* **2012**, *41* (6), 2135–2171. <https://doi.org/10.1039/C1CS15241F>.
- (180) Berger, A. A.; Völler, J.-S.; Budisa, N.; Kokschi, B. Deciphering the Fluorine Code—The Many Hats Fluorine Wears in a Protein Environment. *Acc. Chem. Res.* **2017**, *50* (9), 2093–2103. <https://doi.org/10.1021/acs.accounts.7b00226>.
- (181) Tonali, N. Mimes Synthétiques de Feuilletés Bêta : Conception, Synthèse et Évaluation de Leur Capacité à Moduler l'agrégation Du Peptide Bêta-Amyloïde 1-42. These de doctorat, Université Paris-Saclay (ComUE), 2016.
- (182) Brinet, D. Développement d'outils Analytiques Pour l'étude de l'agrégation de Protéines Amyloïdes : Application à La Synthèse et à l'évaluation de Composés Anti-Maladie d'Alzheimer. These de doctorat, Paris 11, 2015.
- (183) Vahdati, L. Synthesis of Peptidomimetics Containing Bifunctional Diketopiperazine Scaffolds and Their Evaluation as Modulators of Amyloid-B Peptide Oligomerization. These de doctorat, Paris 11, 2015.
- (184) Shendage, D. M.; Fröhlich, R.; Haufe, G. Highly Efficient Stereoconservative Amidation and Deamidation of α -Amino Acids. *Org. Lett.* **2004**, *6* (21), 3675–3678. <https://doi.org/10.1021/ol048771l>.
- (185) Falb, E.; Yechezkel, T.; Salitra, Y.; Gilon, C. In Situ Generation of Fmoc-Amino Acid Chlorides Using Bis-(Trichloromethyl)Carbonate and Its Utilization for Difficult Couplings in Solid-Phase Peptide Synthesis. *J. Pept. Res.* **1999**, *53* (5), 507–517. <https://doi.org/10.1034/j.1399-3011.1999.00049.x>.
- (186) Roestamadji, J.; Mobashery, S.; Banerjee, A. Bis(Trichloromethyl) Carbonate. In *Encyclopedia of Reagents for Organic Synthesis*; John Wiley & Sons, Ltd, Ed.; John Wiley & Sons, Ltd: Chichester, UK, 2006; p rb200.pub2. <https://doi.org/10.1002/047084289X.rb200.pub2>.
- (187) Le Quement, S. T.; Flagstad, T.; Mikkelsen, R. J. T.; Hansen, M. R.; Givskov, M. C.; Nielsen, T. E. Petasis Three-Component Coupling Reactions of Hydrazides for the Synthesis of Oxadiazolones and Oxazolidinones. *Org. Lett.* **2012**, *14* (2), 640–643. <https://doi.org/10.1021/ol203280b>.
- (188) Zampieri, D.; Fortuna, S.; Calabretti, A.; Romano, M.; Menegazzi, R.; Schepmann, D.; Wunsch, B.; Collina, S.; Zanon, D.; Mamolo, M. G. Discovery of New Potent Dual Sigma Receptor/GluN2b Ligands with Antioxidant Property as Neuroprotective Agents. *Eur. J. Med. Chem.* **2019**, *180*, 268–282. <https://doi.org/10.1016/j.ejmech.2019.07.012>.
- (189) Suppo, J.-S.; Subra, G.; Bergès, M.; Marcia de Figueiredo, R.; Campagne, J.-M. Inverse Peptide Synthesis via Activated α -Aminoesters. *Angew. Chem. Int. Ed.* **2014**, *53* (21), 5389–5393. <https://doi.org/10.1002/anie.201402147>.

- (190) Beutner, G. L.; Young, I. S.; Davies, M. L.; Hickey, M. R.; Park, H.; Stevens, J. M.; Ye, Q. TCFH–NMI: Direct Access to *N*-Acyl Imidazoliums for Challenging Amide Bond Formations. *Org. Lett.* **2018**, *20* (14), 4218–4222. <https://doi.org/10.1021/acs.orglett.8b01591>.
- (191) Mamone, M.; Gonçalves, R. S. B.; Blanchard, F.; Bernadat, G.; Onger, S.; Milcent, T.; Crousse, B. *N*-Difluoromethyl-Triazole as a Constrained Scaffold in Peptidomimetics. *Chem. Commun.* **2017**, *53* (36), 5024–5027. <https://doi.org/10.1039/C7CC01298E>.
- (192) Kolb, H. C.; Sharpless, K. B. The Growing Impact of Click Chemistry on Drug Discovery. *Drug Discov. Today* **2003**, *8* (24), 1128–1137. [https://doi.org/10.1016/S1359-6446\(03\)02933-7](https://doi.org/10.1016/S1359-6446(03)02933-7).
- (193) Bag, S. S.; Jana, S.; Yashmeen, A.; De, S. Triazolo- β -Aza- ϵ -Amino Acid and Its Aromatic Analogue as Novel Scaffolds for β -Turn Peptidomimetics. *Chem. Commun.* **2015**, *51* (25), 5242–5245. <https://doi.org/10.1039/C4CC08414D>.
- (194) Mizuhara, T.; Hioki, K.; Yamada, M.; Sasaki, H.; Morisaki, D.; Kunishima, M. Direct Preparation of Primary Amides by Reaction of Carboxylic Acids and Ammonia in Alcohols Using DMT-MM. *Chem. Lett.* **2008**, *37* (12), 1190–1191. <https://doi.org/10.1246/cl.2008.1190>.
- (195) Huang, W.; Chen, W.; Wang, G.; Li, J.; Cheng, X.; Li, G. Thiyl-Radical-Catalyzed Photoreductive Hydrodifluoroacetamidation of Alkenes with Hantzsch Ester as a Multifunctional Reagent. *ACS Catal.* **2016**, *6* (11), 7471–7474. <https://doi.org/10.1021/acscatal.6b02420>.
- (196) Kubyshkin, V.; Afonin, S.; Kara, S.; Budisa, N.; Mykhailiuk, P. K.; Ulrich, A. S. γ -(*S*)-Trifluoromethyl Proline: Evaluation as a Structural Substitute of Proline for Solid State ¹⁹F-NMR Peptide Studies. *Org. Biomol. Chem.* **2015**, *13* (11), 3171–3181. <https://doi.org/10.1039/C5OB00034C>.
- (197) Ryu, T.; Min, J.; Choi, W.; Jeon, W. H.; Lee, P. H. Synthesis of 2-Aryl-2 *H*-Benzotriazoles from Azobenzenes and *N*-Sulfonyl Azides through Sequential Rhodium-Catalyzed Amidation and Oxidation in One Pot. *Org. Lett.* **2014**, *16* (11), 2810–2813. <https://doi.org/10.1021/ol501250t>.

Titre: Peptidomimétiques structurés en β -hairpin inhibiteurs de l'agrégation de la protéine amyloïde hIAPP: conception, synthèse, évaluation

Mots clés: Diabète de type 2, peptide hIAPP, amyline, peptidomimétiques, fluor, amyloïde

Résumé: Le diabète de type 2 (DT2), qui compte plus de 400 millions de cas dans le monde, représente 90 % du nombre total de cas de diabète. T2D est une maladie dégénérative associée à la résistance à l'insuline et à la mort des β -cellules pancréatiques liées aux dépôts de la protéine amyloïde hIAPP (également appelée amyline), qui sont observés dans le pancréas de plus de 95 % des patients atteints de DT2. Les traitements actuellement disponibles sont symptomatiques et caractérisés soit par des effets secondaires significatifs, soit par un faible impact sur l'incidence des pathologies associées et la réduction de la mortalité. Ainsi, pour trouver un traitement étiologique contre DT2, le ciblage de hIAPP est devenu une stratégie prometteuse à explorer. À ce jour, peu de classes de composés ont été proposées pour inhiber le processus d'agrégation de hIAPP. Cependant, à notre connaissance, seuls de très rares exemples de β -hairpin acycliques ont été décrits. Puisque l'agrégation hIAPP est un processus très complexe et dynamique, nous avons émis l'hypothèse que des β -hairpins flexibles pourraient mieux s'adapter aux différentes conformations de hIAPP formées au cours du processus d'agrégation. Notre conception a été basée sur différents β -turn flexibles constitué d'un motif pipéridino-pyrrolidine lié à deux bras différents inspirés de la séquence primaire du peptide hIAPP, avec un élément d'auto-reconnaissance peptidique (SRE) dérivé de la séquence amyloïdogène de hIAPP, et faisant face à une séquence de blocage peptidique ou peptidomimétique. Afin de confirmer la conformation en β -hairpin de nos inhibiteurs, la conformation de nos composés a été étudiée par RMN et dans quelques cas par une dynamique moléculaire. Ensuite, leur capacité à interférer avec le processus d'agrégation de hIAPP a été principalement évaluée par la spectroscopie de fluorescence à la thioflavine-T. Les composés les plus prometteurs de la série ont ensuite été étudiés par d'autres essais biophysiques comme la microscopie électronique à transmission (TEM), l'électrophorèse capillaire (CE) et l'IMS-MS. Les meilleurs composés de la série ont ensuite été étudiés pour déterminer leur capacité à réduire la toxicité du hIAPP sur les cellules pancréatiques INS-1 du rat.

Ayant prouvé la possibilité de moduler le processus d'agrégation de hIAPP par des petits mimes de β -hairpins acycliques portant à la fois des bras peptidiques et peptidomimétiques, nous avons ensuite concentré notre attention sur le développement de β -hairpins fluorés qui, jusqu'à présent, n'ont jamais été explorés ni comme inhibiteurs d'agrégation hIAPP, ni, à notre connaissance, plus largement en chimie médicinale. La préparation de ces analogues fluorés avait le double objectif d'étudier comment le fluor, avec ses caractéristiques uniques, pouvait influencer à la fois l'activité et la conformation de nos inhibiteurs.

En conclusion, les travaux présentés dans cette thèse fournissent des informations précieuses pour le développement de nouveaux mimes de β -hairpins acycliques comme modulateurs de hIAPP et potentiellement comme nouveaux outils fluorés pour approfondir son processus d'agrégation.

Title: β -Hairpin peptidomimetics as inhibitors of hIAPP amyloid protein aggregation: design, synthesis and evaluation

Keywords: Type 2 Diabetes, hIAPP peptide, amylin, peptidomimetics, fluorine, amyloid

Abstract: Type 2 Diabetes (T2D) with over 400 million cases worldwide represents 90% of total diabetes cases. T2D is a degenerative disease associated with insulin resistance and pancreatic β -cells death linked to deposits of the amyloid protein hIAPP (also called amylin), that are observed in the pancreas of over 95% of the T2D patients. The treatments currently available are symptomatic and characterized either by significant side effects or low impact on the incidence of related pathologies and mortality reduction. Thus, to find an etiological treatment for T2D, targeting hIAPP has become a promising strategy to explore. To date, few classes of compounds have been proposed to inhibit hIAPP aggregation process. However, to the best of our knowledge, only very scarce examples of acyclic β -hairpin have been described. Since hIAPP aggregation is a highly complex and dynamic process, we hypothesized that flexible β -hairpins could better adapt to different hIAPP conformations formed during the aggregation process. Our design was based on flexible piperidine pyrrolidine β -turn inducers linked to two different arms inspired by the primary sequence of hIAPP peptide, with a peptidic self-recognition element (SRE) derived from the hIAPP amyloidogenic sequence facing to a peptidic or peptidomimetic blocking sequence. In order to confirm β -hairpin conformation of our inhibitors, our compounds were conformationally studied by NMR and in few cases by molecular dynamics. Then, their ability to interfere with hIAPP aggregation process was primarily evaluated by thioflavin-T fluorescence spectroscopy. The most promising compounds of the series were then investigated by other biophysical assays such as transmission electron microscopy (TEM), capillary electrophoresis (CE) and IMS-MS. The best compounds of the series were then studied to determine their ability to reduce hIAPP toxicity on rat INS-1 pancreatic cells.

Having proved the possibility to modulate hIAPP aggregation process employing small acyclic β -hairpin mimics bearing both peptidic and peptidomimetic arms, we then focused our attention on the development of fluorinated hairpin peptidomimetics that, until now, have never been explored either as hIAPP aggregation inhibitors, nor, to our knowledge, more broadly in medicinal chemistry. The preparation of these fluorinated analogues had the double scope to investigate how fluorine, with its unique characteristics, could influence both the activity and the conformations of our inhibitors.

In conclusion, the work presented in this thesis provides valuable insight for the development of new acyclic β -hairpin mimics as modulators of hIAPP and potentially new fluorinated tools to further investigate its aggregation process.